RE-ORDER NO. 64-406

~~JPL DISCREET~~

GENERAL MOTORS CORPORATION

NASA CR 71260

Final Report

SURVEYOR LUNAR ROVING VEHICLE

Phase I — JPL Contract 950657

under NAS 7-100

VOL. II: APPENDIXES

Section III Mechanical Subsystems

FACILITY FORM 602

N66-19713	
(ACCESSION NUMBER)	(THRU)
462	/
(PAGES)	(CODE)
CR 71260	11
(NASA CR OR TMX OR AD NUMBER)	(CATEGORY)

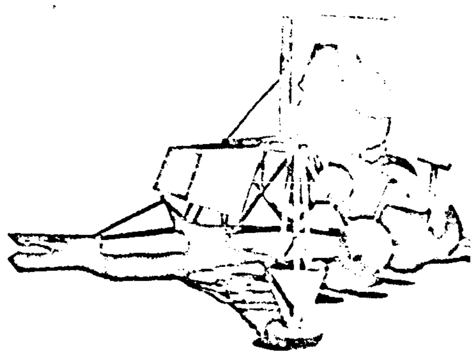

GPO PRICE $ ______

CFSTI PRICE(S) $ ______

Hard copy (HC) 7.62

Microfiche (MF) 2.25

ff 653 July 65

GM DEFENSE RESEARCH LABORATORIES SANTA BARBARA, CALIFORNIA

TR64-26

~~JPL DISCREET~~

April 23, 1964

108-430

Copy No 034

Sec. III

GENERAL MOTORS CORPORATION

Final Report

SURVEYOR LUNAR ROVING VEHICLE

Phase I — JPL Contract 950657

VOL. II: APPENDIXES
Section III Mechanical Subsystems

This work was performed for the Jet Propulsion Laboratory, California Institute of Technology, sponsored by the National Aeronautics and Space Administration under Contract NAS7-100.

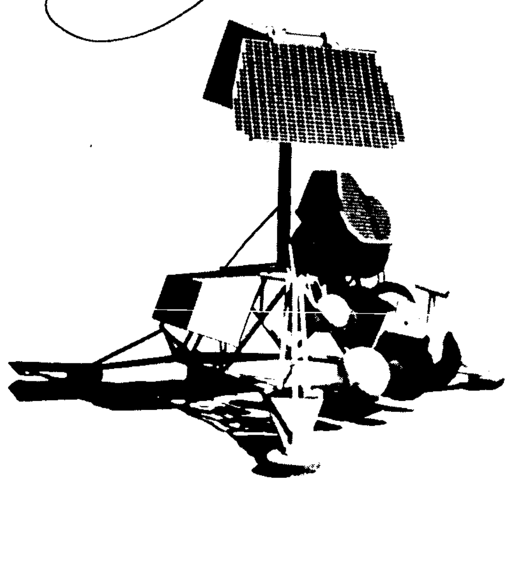

GM DEFENSE RESEARCH LABORATORIES SANTA BARBARA, CALIFORNIA

TR64-26

April 23, 1964

PREFACE

This report is one of a series of reports prepared under JPL Contract No. 950657 by GM Defense Research Laboratories, Santa Barbara, California, and its major subcontractor for electronics, Radio Corporation of America, Astro-Electronics Division, Princeton, New Jersey.

[redacted]

TABLE OF CONTENTS

RE-ORDER No. 64-406

APPENDIX I
MOBILITY

APPENDIX I
MOBILITY

D. VEHICLE SYSTEM

1. Introduction

The successful adaptation of any vehicle to an off-road environment, whether on Earth or on the Moon, depends not only on the vehicle characteristics, but also on the characteristics of the terrain over which it must travel.

Two sets of terrain factors influence the mobility performance of a vehicle:

1) The mechanical properties of the soil which relate to the stress-strain relationships existing between soil and vehicle, both in the vertical and horizontal directions; and
2) The surface geometry of the terrain

The vertical-deformation characteristics determine the ability of the vehicle to stay on or close to the surface (flotation), while the horizontal characteristics determine the ability of the vehicle to develop thrust for locomotion.

The surface geometry of the terrain affects mobility in that obstacles such as boulders and crevices may prevent or at least hinder vehicle movement, and rough ground may impart unacceptable shock and vibration to the vehicle and its payload.

Therefore, in order to evaluate vehicle performance in a rational manner, it is necessary to be able to describe quantitatively the terrain characteristics that affect performance, in addition to knowing pertinent vehicle characteristics such as weight, size and form of the loading area, power, etc. Mathematical models expressing the physico-geometric relationship between vehicle and soil can then be used either to evaluate performance characteristics, or, given a desired level of performance, to select vehicle design criteria. Laboratory and field tests of scale models can also be utilized, either to confirm calculated predictions or to help solve mobility problems that are not readily amenable to analytical treatment. This approach is illustrated schematically in Figure III. 1-1.

From a methodological point of view, this approach is identical to that used in solving problems associated with the design and performance of sea and air vehicles.

To further illustrate the nature of the problem, consider the case of a vehicle crossing a steel bridge or a soil mass (Fig. III. 1-2). To determine whether the steel bridge can safely support the vehicle, it is necessary to know the mechanical properties of the steel as well as the geometry of bridge and the load distribution on it. The problem is identical to that of crossing the soil "bridge"— the pertinent mechanical properties of the soil must be known.

MEASUREMENT & DERIVATION OF SOIL VALUES

It has been shown[(1, 2, 3)*] that the vertical stress-strain relationship which relates to sinkage, and thereby motion resistance, can be expressed by the following equation:

$$p = (k_c/b + k_\phi)\, z^n \qquad \text{(III. 1-1)}$$

where

- p = unit ground contact pressure (psi)
- b = width of the loading area (in.)
- z = sinkage (in.)
- k_c = cohesive modulus of soil deformation (lb/in.^{n+1})
- k_ϕ = frictional modulus of soil deformation (lb/in.^{n+2})
- n = exponent of sinkage (dimensionless)

* Raised numbers in parentheses refer to references listed on page III. 1-66.

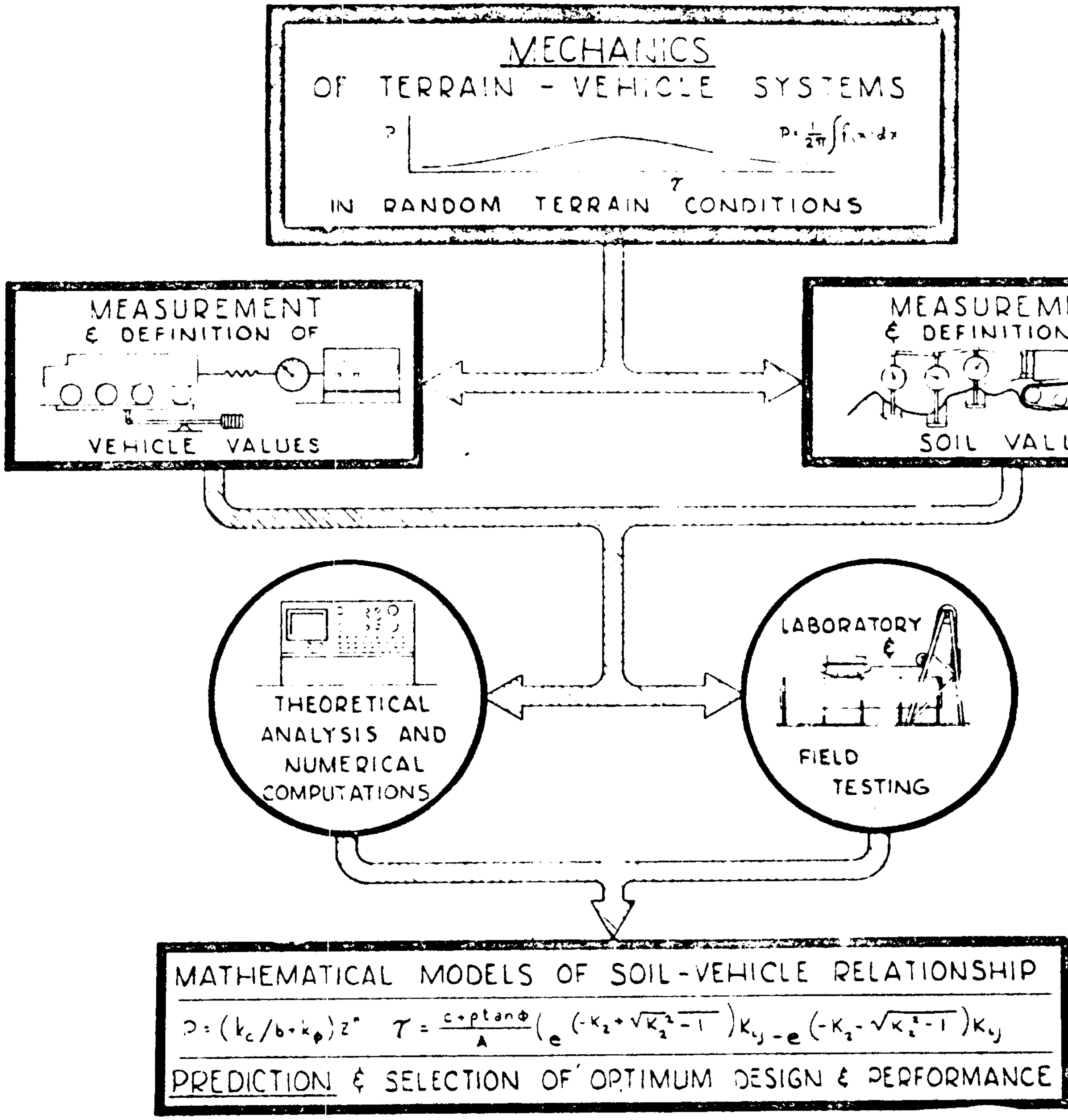

Fig. III. 1-1. Mechanics of Terrain-Vehicle Systems

64-406
VOL. II APP.
SEC. III

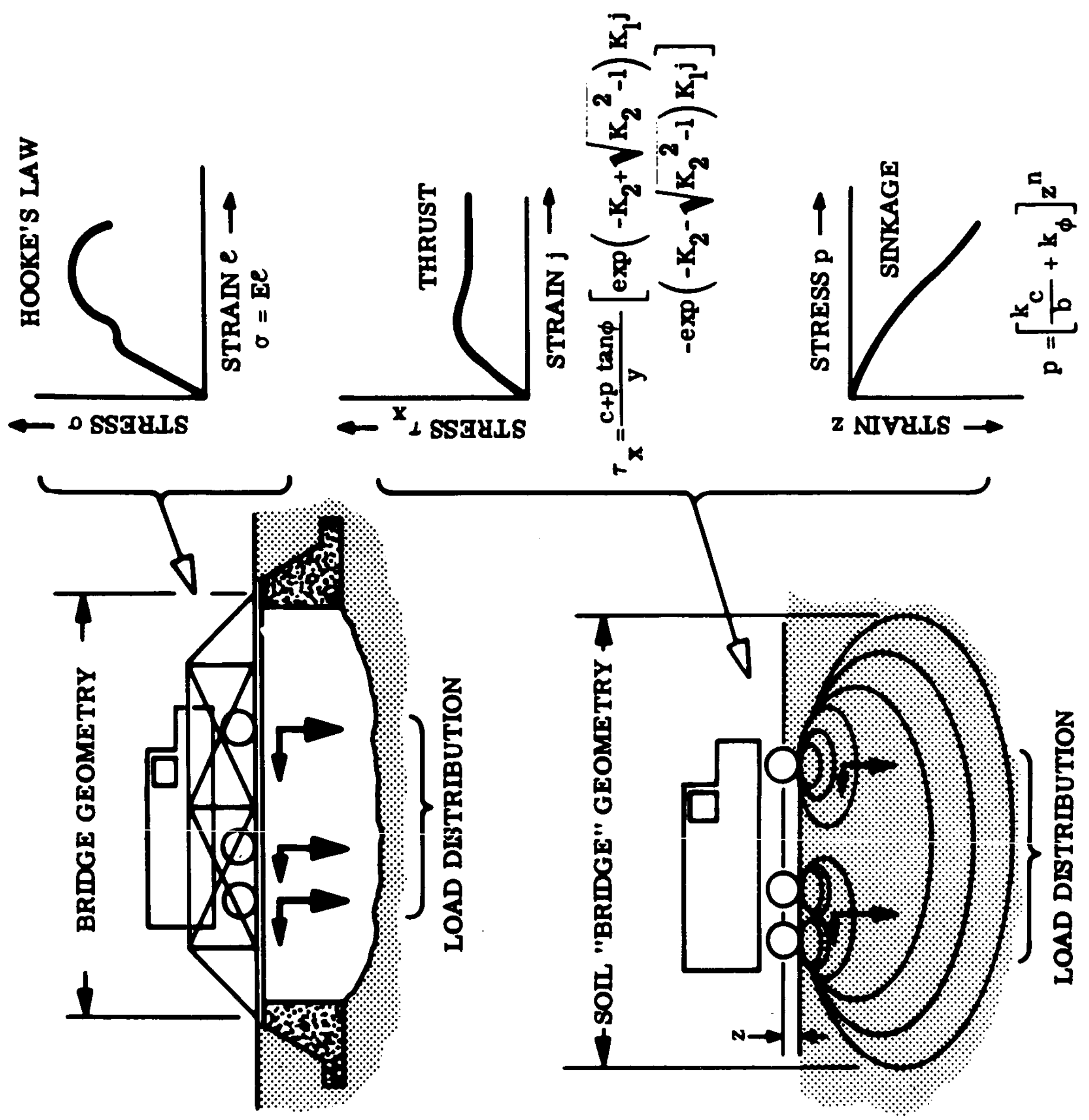

Fig. III. 1-2. Stress-Strain Functions for Bridge and Soft Ground Crossings

Thus, in order to define the relationship between load and sinkage, the soil values k_c, k_Φ and n have to be determined.

An instrument for this purpose is shown schematically in Figure III. 1-3.

Load W is applied first to plate I and next to wide plate II, while a motor M forces the respective footings down. The load is plotted as a function of sinkage z by recorder R. Thus, for each plate a separate curve is obtained, and their general equations may be written in accordance with Equation (III. 1-1) as follows:

$$p_1 = (k_c/b_1 + k_\Phi)\, z^n$$
$$p_2 = (k_c/b_2 + k_\Phi)\, z^n \qquad \text{(III. 1-2)}$$

Plotting Equations (III. 1-2) on a logarithmic scale will produce practically straight parallel lines which form angle α. It is evident that $\tan\alpha = n$. Thus the exponent of sinkage is easily determined. Abscissas a_1 and a_2 are identical with the respective quantities $(k_c/b + k_\Phi)$. As a result two equations may be obtained:

$$k_\Phi = (a_2 b_2 - a_1 b_1)/(b_2 - b_1)$$
$$k_c = \left[(a_1 - a_2) b_1 b_2 \right] / (b_2 - b_1) \qquad \text{(III. 1-3)}$$

from which the moduli of deformation k_c and k_Φ can be determined.

The horizontal stress-strain relationship which relates to the maximum thrust a vehicle can develop can be expressed [3, 4] by Coulomb's law:

$$s = c + p \tan\Phi \qquad \text{(III. 1-4)}$$

where
- s = soil shearing strength (psi)
- c = soil cohesion (psi)
- Φ = angle of friction (degrees)

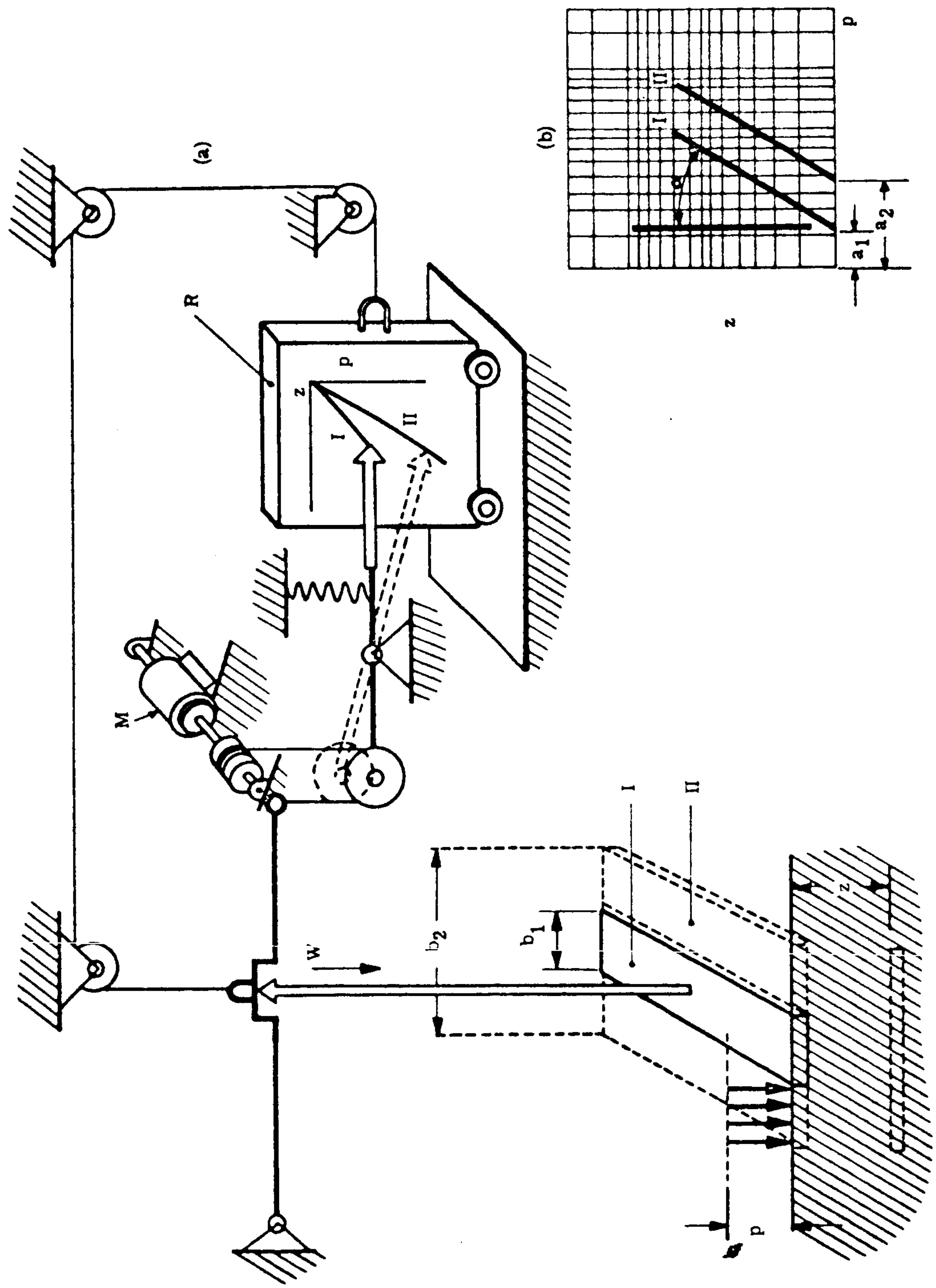

Fig. III. 1-3. Measurement and Derivation of Vertical Stress-Strain Parameters

Thus, if only the maximum traction a vehicle can develop is of interest, it is necessary to determine only the soil parameters c and Φ.

However, if it is desired to evaluate thrust in terms of slippage, say of a track or wheel, the soil shearing strength must be expressed in a more general form.

For a soil whose shear strength deformation curve exhibits a sharp peak, as in Fig. III. 1-4 Equation III. 1-5 will take a form similar to that of an aperiodically damped vibration:[3,4]

$$s = \left[(c + p \tan\Phi)/Y \right] \left[\exp\left(-K_2 + \sqrt{K_2^2 - 1}\right) K_1 j - \exp\left(-K_2 - \sqrt{K_2^2 - 1}\right) K_1 j \right] \qquad \text{(III. 1-5)}$$

where Y = the maximum value of the quantity in brackets

K_1 = slip or deformation coefficient (in.$^{-1}$)

K_2 = slip or deformation coefficient (dimensionless)

j = horizontal soil deformation (in.)

For a soil that does not exhibit a sharp peak, which is more usually the case (See Fig. III. 1-5), it has been determined[5] that the following equation is sufficient to define the shear strength deformation characteristics:

$$s = (c + p \tan\Phi) \left[1 - \exp(-j/K) \right] \qquad \text{(III. 1-6)}$$

where K - soil deformation modulus (in.)

Note that for large deformations, j, Equation (III. 1-6) approaches Coulomb's equation $s = c + p \tan\Phi$.

Thus it is seen that to fully evaluate the thrust capability of a vehicle, it is necessary to know the soil values c, Φ, K or c, Φ, K_1, K_2. These can be determined either by rotating a shear ring or annulus in the soil, or by moving a grouser plate through the soil. The principle of a horizontal displacement shear device is shown in Figure III. 1-6.

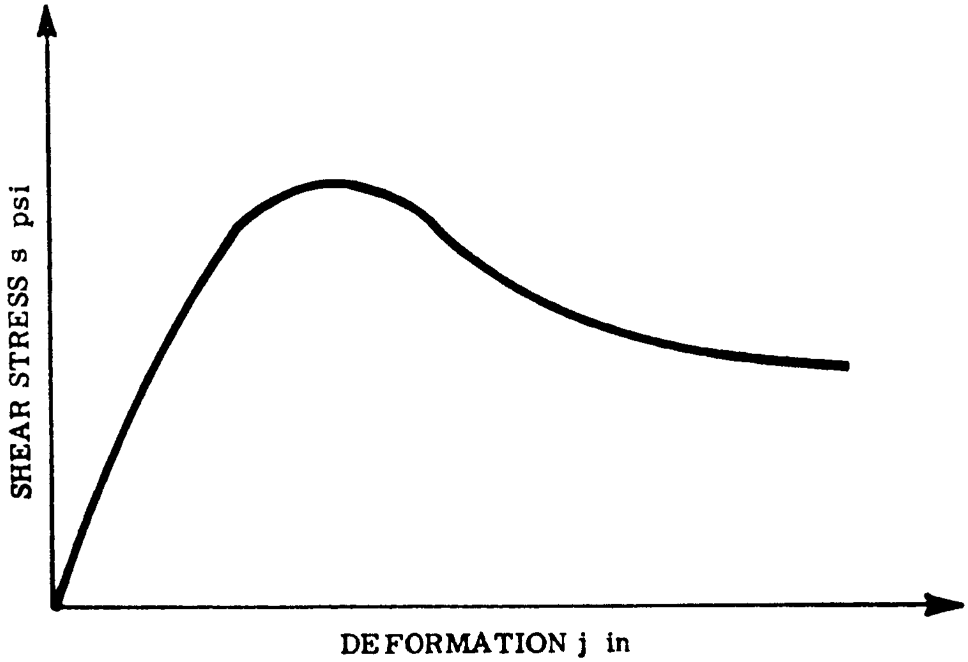

Fig.III.1-4. Typical Shear-Deformation Curve (With Peak)

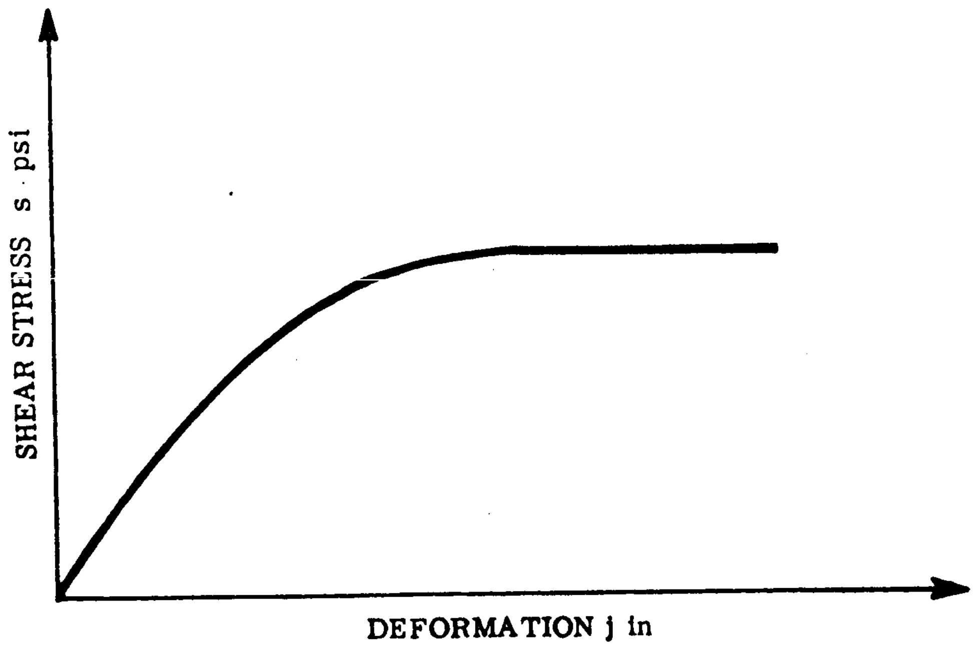

Fig. III.1-5. Typical Shear-Deformation Curve (Without Peak)

The device shown in Fig.III.1-6(a)utilizes a rectangular grouser plate. The grouser plate is loaded vertically with weights W and subsequently moved a distance j by means of a motor M or by a manually operated gear drive. The recording dynamometer R plots instantaneous force and deformation values on a chart.

If this operation is repeated for various loads W_1, W_2, W_3. . . . W_n, a number of curves will be obtained, all showing certain peak load values H_1, H_2, H_3. . . . H_n. (Fig.III.1-6(b).In order to make the readings independent of plate size, the H and W values are divided by the area of the plate so that the maximum shearing strength, s, of soil under corresponding unit pressure, p, can be determined.

The peak values of these curves, plotted on a linear scale, will fall on a straight line as shown in Fig.III.1-6(c).The resulting line represents the Coulomb function $s = c + p \tan\phi$, so that the distance Oc represents the cohesion, c, and the slope represents the angle of friction, ϕ.

Procedures for calculating the values K, K_1 and K_2 are described in References 1 and 4.

Thus, with a few relatively simple measurements, all the soil parameters necessary to evaluate a soil-vehicle system can be obtained. Many instruments for this purpose have been devised. Fig. III. 1-7 shows a soil-measuring instrument developed by GM-DRL for remote operation on the lunar surface. It consists essentially of two penetration plates identified as 1 and 2, and a shear ring, 3. Plate 4 is a sensing pad which, upon contacting the ground surface, starts the automatic operation of the instrument. Equipment for determining the discussed soil properties in the laboratory is shown in Figure III. 1-8.

SURFACE GEOMETRY CONSIDERATIONS

As was stated previously, the mobility of an off-road vehicle depends not only on its soft-ground-crossing ability but also on its ability to overcome obstacles

RE-ORDER No. 64-406

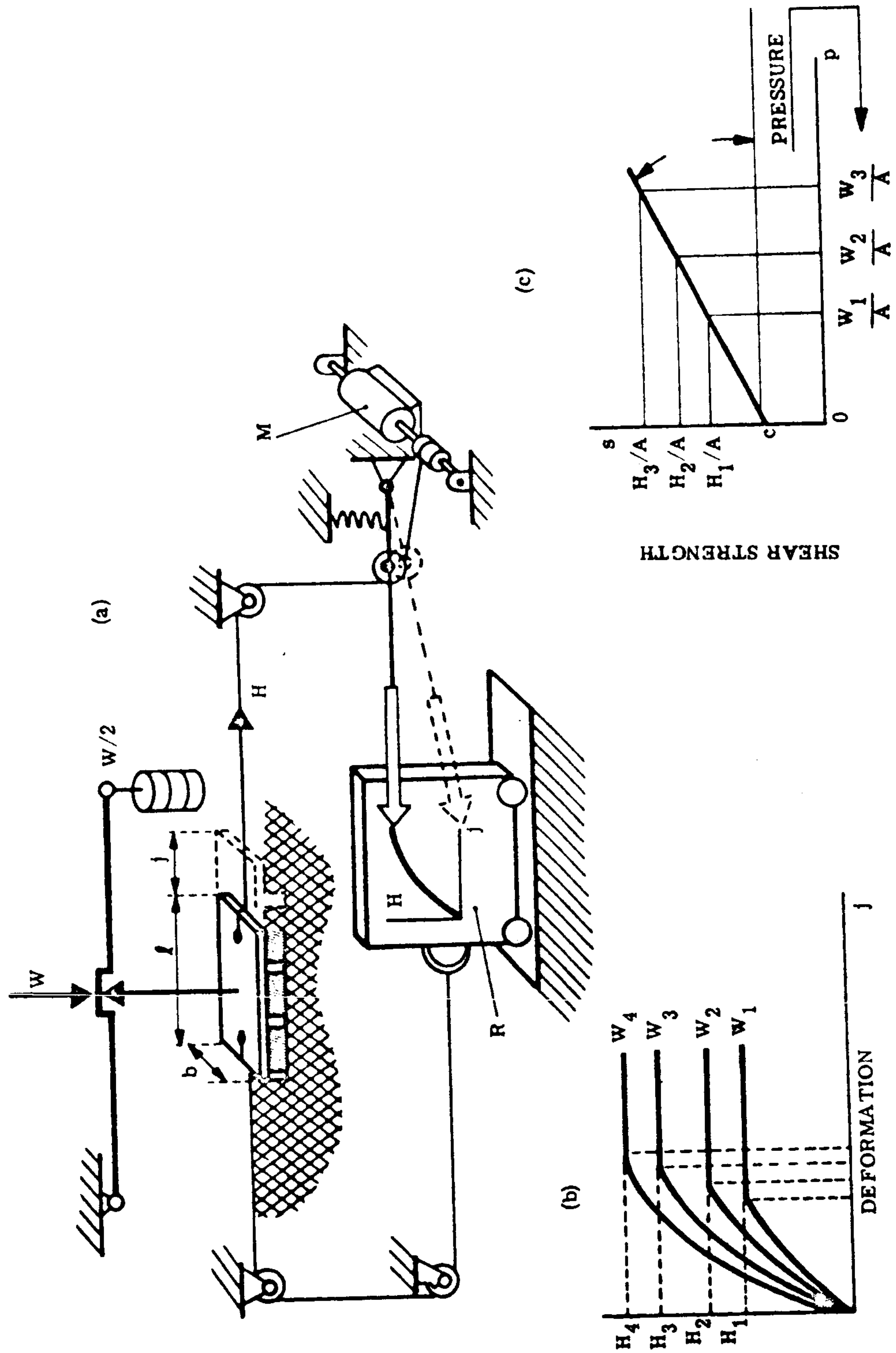

Fig. III. 1-6. Measurement and Derivation of Horizontal Stress-Strain Parameters

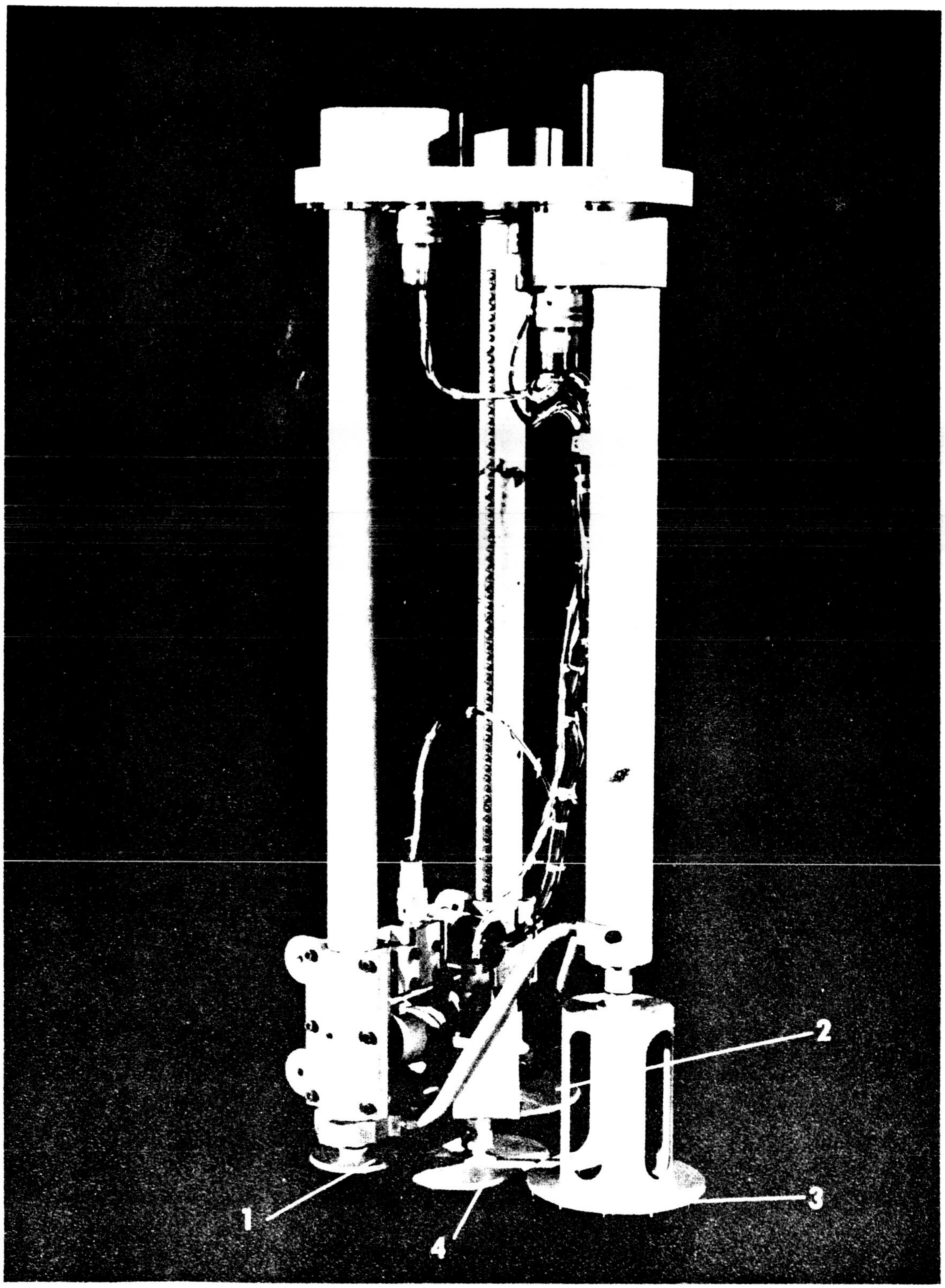

Fig. III. 1-7. Lunar Soil Properties Measuring Instrument

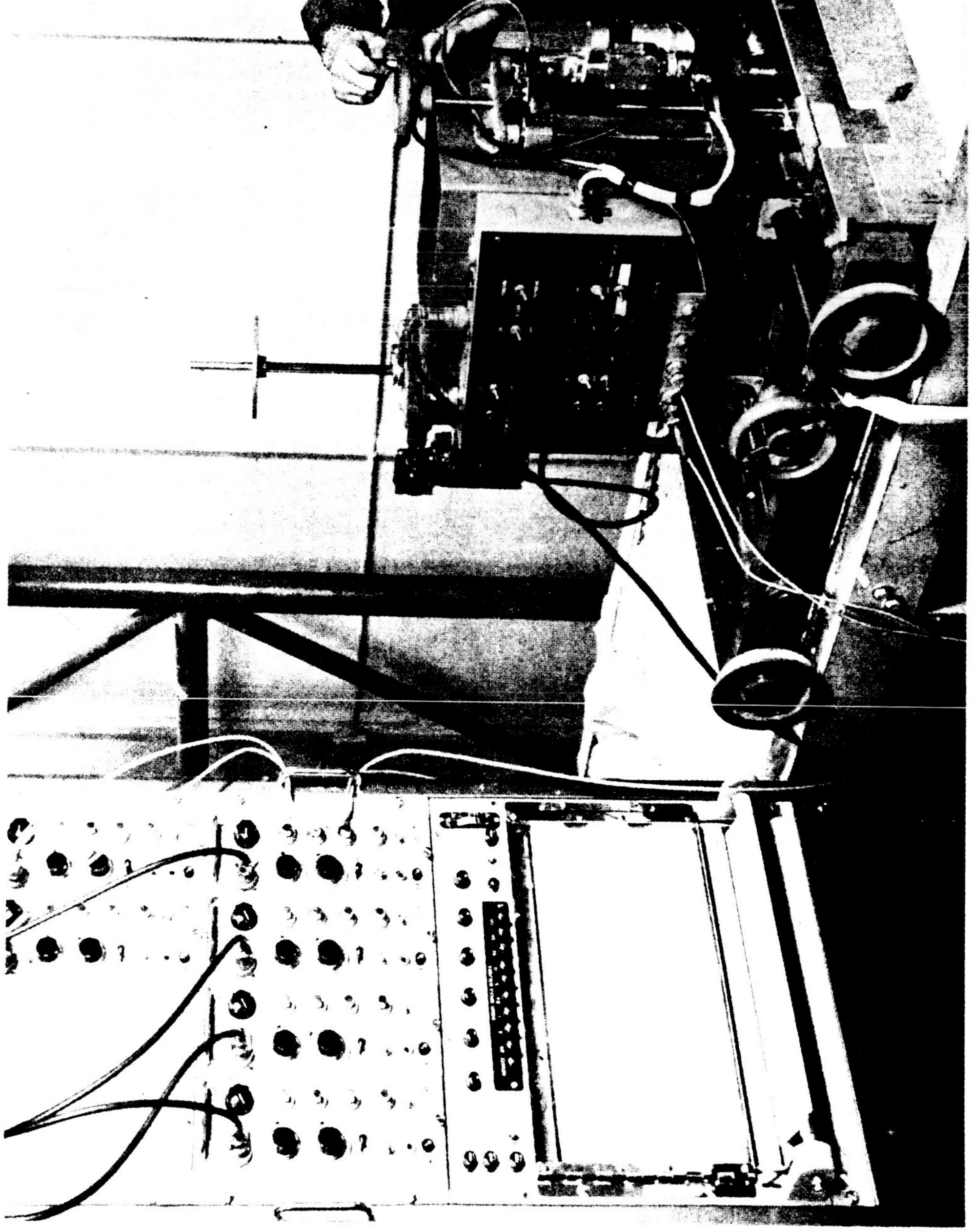

Fig. III. 1-7. Laboratory Soil Properties Measuring Instrument and respond to ground-surface unevenness with minimum shock and vibration to vehicle and payload.

For example, extremely low operational speeds occur not only when the ground is soft, but also when it is hard and strong if the surface is rough. The vehicle may then vibrate to such an extent that its speed must be radically reduced.

Since the response of the vehicle to surface roughness is related to its dynamic characteristics, no fully rational vehicle form or design is possible if appropriate characteristics of the ground surface are not considered.

Given characteristic terrain profiles, analytical and analog simulation methods are now available[6, 7, 8] that permit the vibrational responses of the vehicle to be evaluated. In addition, scale-model tests conducted in the laboratory and in the field over simulated rough terrain yield much valuable information regarding vehicle dynamics.

However, in the case of first-generation lunar surface vehicles, it is highly probable that operational speeds will be severely limited due to terrain-uncertainty considerations rather than terrain roughness. That being the case, it is then unlikely that vibrational and dynamic stability will be seriously affected by terrain micro-roughness on a scale that is small in relation to vehicle size.

On the other hand, obstacles such as boulders and crevices can seriously impede or even prevent locomotion. Ability of a vehicle to negotiate such obstacles may be just as important as its ability to cross soft ground.

This problem also can be studied by either analytical or scale-model techniques. Both methods have proven successful in the prediction of obstacle performance.[9, 10]

MATHEMATICAL MODELS OF SOIL-VEHICLE RELATIONSHIP

Knowing the pertinent terrain properties, it is possible to formulate mathematical expressions which enable one to compute any desired aspect of vehicle performance or design.

For example, the resistance due to soil compaction, which in soft soil is the major component of the external motion resistance of a vehicle, has been shown[4, 11] to be equal to

$$R_c = b\int_0^z p\,dz \qquad \text{(III. 1-7)}$$

The gross traction or thrust a vehicle can develop can be expressed by

$$H = b\int_0^{\ell} s\,dx \qquad \text{(III. 1-8)}$$

In the above equations, b and ℓ represent the width and length respectively of the vehicle ground-contact areas.

The capacity of a vehicle to do useful work is represented by the drawbar pull it can develop, which is equal to H - R_c. Thus

$$\text{Drawbar Pull} = DP = b\left[\int_0^{\ell} s\,dx - \int_0^z p\,dz\right] \qquad \text{(III. 1-9)}$$

Expressed as a proportion of vehicle weight (DP/W), it becomes a measure corresponding in concept to the drag/lift ratio of a ship or plane, denoting the vehicle's ability to perform such functions as climbing slopes and accelerating.

Other equations for determining vehicle performance criteria or design parameters can be established from the foregoing. Several examples follow:

Vehicle Thrust:

For soils whose shear-deformation curves exhibit a pronounced peak:

$$H = \frac{cA + W\tan\Phi}{Y}\left[\exp\left(-K_2 + \sqrt{K_2^2 - 1}\right) K_1 j - \exp\left(-K_2 - \sqrt{K_2 - 1}\;K_1 j\right)\right] \qquad \text{(III. 1-10)}$$

where A = ground contact area.

For soils whose shear-deformation curves exhibit no peak:

$$H = (cA + W\tan\Phi)\left[1 - \exp(-j/K)\right] \qquad \text{(III. 1-11)}$$

Maximum thrust in any soil:

$$H = cA + W\tan\Phi \qquad \text{(III. 1-12)}$$

Vehicle Sinkage:

For a flat loading area (track, high-deflection elastic tire):

$$z = \left[\frac{p}{k_c/b + k_\Phi}\right]^{1/n} \qquad \text{(III. 1-13)}$$

For a rigid wheel or low-deflection elastic tire:

$$z = \left[\frac{3W}{(3-n)(k_c + bk_\Phi)\sqrt{D}}\right]^{2/(2n+1)} \qquad \text{(III. 1-14)}$$

where D = wheel diameter.

Motion Resistance Due to Soil Compaction:

For a flat loading area (track, high-deflection elastic tire):

$$R_c = \frac{1}{(n+1)(k_c + bk_\Phi)^{1/n}} \left[\frac{W}{\ell}\right]^{(n+1)/n} \qquad \text{(III. 1-15)}$$

For a rigid wheel:

$$R_c = \frac{1}{(3-n)^{(2n+2)/(2n+1)}(n+1)(k_c + bk_\phi)^{1/(2n+1)}}\left[\frac{3W}{D}\right]^{(2n+2)/(2n+1)} \qquad \text{(III. 1-16)}$$

Drag/Lift or Drawbar Pull/Weight Ratio:

For a flat loading area (track, high-deflection elastic tire):

$$\frac{DP}{W} = \frac{c}{p} + \tan\phi - \frac{W^{1/n}}{(n+1)(k_c + bk_\phi)^{1/n}\,\ell^{(n+1)/n}} \qquad \text{(III. 1-17)}$$

For a rigid wheel or low-deflection elastic tire:

$$\frac{DP}{W} = \frac{c}{p} + \tan\phi - \left[\frac{3}{(3-n)\sqrt{D}}\right]^{(2n+2)/(2n+1)}\left[\frac{1}{n+1}\right]\left[\frac{W}{k_c + bk_\phi}\right]^{1/(2n+1)} \qquad \text{(III. 1-18)}$$

Maximum Negotiable Slope:

The slope climbing ability S can be expressed approximately in precent in terms of the drawbar pull/weight ratio:

$$S = \left(\frac{DP}{W}\right) 100\% \qquad \text{(III. 1-19)}$$

Power Required for Propulsion Over Flat Terrain at Negligible Slip

For a flat loading area (track, high-deflection elastic tire):

$$HP = \frac{v}{550\eta(n+1)(k_c + bk_\phi)^{1/n}}\left[\frac{W}{\ell}\right]^{(n+1)/n} \qquad \text{(III. 1-20)}$$

where η = drive train efficiency and v = speed (ft/sec)

For a rigid wheel:

$$HP = \frac{v}{550\eta\,(3-n)^{(2n+2)/(2n+1)}(n+1)\,(k_c + bk_\Phi)^{1/(2n+1)}} \left[\frac{3W}{\sqrt{D}}\right]^{(2n+2)/(2n+1)} \qquad \text{(III. 1-21)}$$

Energy Required for Propulsion Over Flat Terrain at Negligible Slip

For a flat loading area (track, high-deflection elastic tire):

$$E_{whr} = \frac{2\,M}{(n+1)\,(k_c + bk_\Phi)^{1/n}} \left[\frac{W}{l}\right]^{(n+1)/n} \qquad \text{(III. 1-22)}$$

For a rigid wheel:

$$E_{whr} = \frac{2\,M}{(3-n)^{(2n+2)/(2n+1)}(n+1)(k_c + bk_\Phi)^{1/(2n+1)}} \left[\frac{3W}{\sqrt{D}}\right]^{(2n+2)/(2n+1)} \qquad \text{(III. 1-23)}$$

where M = distance traveled (miles).

Motion Resistance Due to Slopes

$$R_s = W \sin \alpha \qquad \text{(III. 1-24)}$$

where α = angle of slope.

2. Vehicle Performance Characteristics

The expected ranges of the lunar terrain characteristics, both with regard to the mechanical properties of the soil and the surface geometry, have been listed as part of the exhibits accompanying JPL RFP No. 3146. Interpretation of the soft surface depicted in this RFP result in equivalent bearing strength constants of: $k_c = 0$, $k_\Phi = 0.083$ and $n = 1.0$, while shear strength constants are: cohesion, 0 to .5 psi, and internal friction as low as 20 degrees.

Having specified a range of possible lunar terrain characteristics, it is then possible, utilizing the analytical methods discussed previously, to evaluate and compare from the mobility viewpoint any desired mode of lunar locomotion.

Modes of locomotion usually considered for lunar surface vehicles are:

- Walking (running)
- Crawling (sliding)
- Rolling (wheels, tracks)
- Jumping (leaping)

In the following discussion only the first three modes will be considered. Locomotive mechanisms pertaining to jumping will not be discussed. Difficulties involved in that type of translation and the reasons supporting this course of action are discussed in References 11 and 12.

TENTATIVE EVALUATION OF A WALKING MACHINE

It has been suggested that walking is more economical than rolling because the motion resistance due to soil compaction may be freely reduced by applying a sufficiently long stride.[13] This theoretically correct assumption may be derived by reducing Equation (15) to the following form:

$$R_c = \frac{\ell}{\ell_s}\left(\frac{1}{(n-1)(k_c + bk_\phi)^{1/n}}\right)\left(\frac{W}{\ell}\right)^{(n+1)/n} \qquad \text{(III.1-25)}$$

where ℓ_s is the length of the stride and ℓ is the length of the foot. The above equation defines the amount of resistance reduction as being directly proportional to the ratio of foot length ℓ to stride length ℓ_s. Hence, by making the ratio ℓ/ℓ_s sufficiently small, R_c may be theoretically reduced to any desired extent.

In order to make a meaningful quantitative comparison between a foot and a wheel, their relative sizes must be so selected that they are comparable, at least from a design viewpoint. Although this may lead to a somewhat arbitrary choice of dimensions for both the wheeled and the walking machine, one must start at that very point before drawing any conclusion.

Let it be assumed that the envelope of the walking device must be able to be inscribed in the wheel under comparison. In other words, it is assumed that both mechanisms have similar space requirements. In trying to accomplish this task, it will be found that while one can accommodate legs in the space occupied by a comparable wheel size, it is practically impossible to fit legs and their actuating mechanisms in that space. This is illustrated in Fig. III. 1-9. At this point, it must be conceded that the designer must either reduce the body of the vehicle or extend the legs and their actuators beyond the size of the comparable wheeled vehicle in order to accommodate a walking mechanism.

This disadvantage becomes more evident when the absolute need of having at least two legs per one comparable wheel is considered.

Starting with these remarks, let the comparable wheel and the walking device with two feet be assumed as sketched in Fig. III. 1-9. To compare the motion resistances of the foot and rigid wheel devices, the ratio of their resistances (R_c) foot/ (R_c) wheel may be plotted as a function of load W for various soil values k_ϕ. Such a ratio may be obtained by dividing Equation (III. 1-15) by Equation (III. 1-16). This yields for $k_c = 0$ (dry, granular material):

64-406
VOL. II APP.
Sec. III

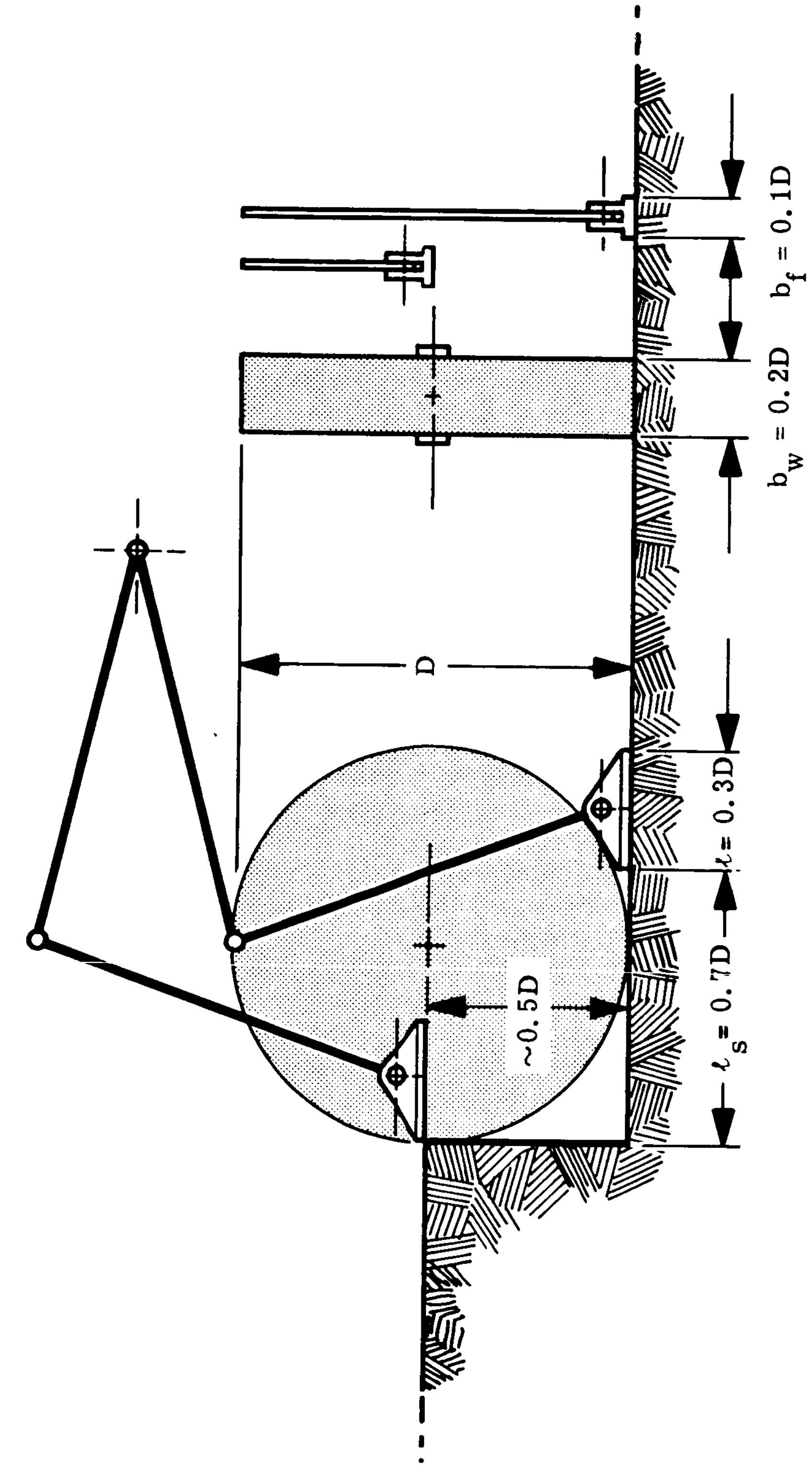

Fig. III. 1-9. Outline of a Walking Mechanism and a Comparable Wheel

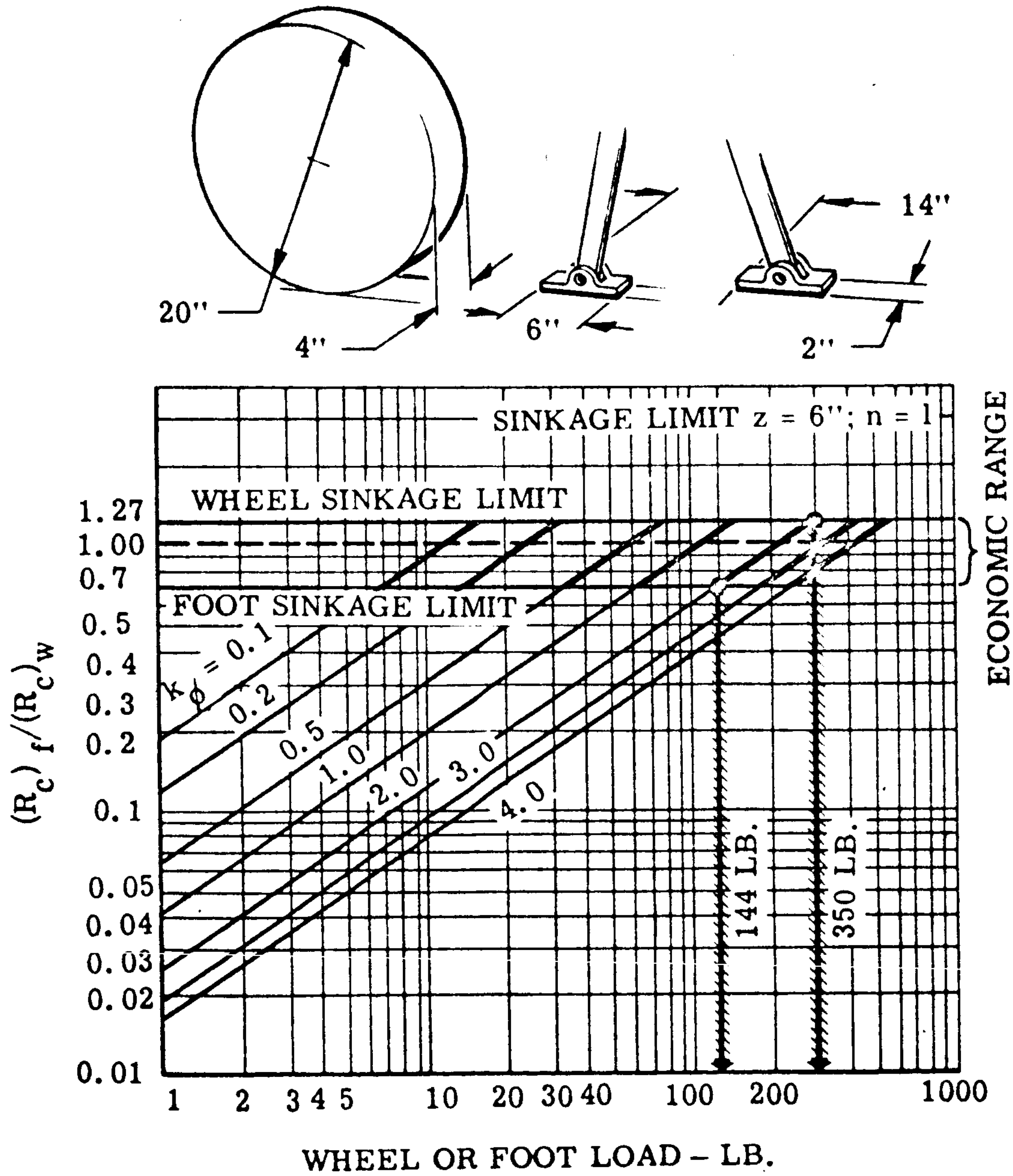

Fig. III. 1-10. Ratio of Motion Resistances of a Pair of Feet and a Comparable Wheel

$$\frac{(R_c)_f}{(R_c)_w} = \left[\frac{W^{1/n}D}{k_\phi^{1/n}}\right]^{\frac{n+1}{2n+1}} \left[\frac{3-n}{3}\right]^{\frac{2n+2}{2n+1}} \frac{b_w^{\frac{1}{2n+1}}}{b_f^{1/n}\ell^{1/n}\ell_s} \qquad \text{(III. 1-26)}$$

According to the previous remarks, width b_w of the wheel must be substituted by two feet each having half the width of the wheel if one is to avoid encroachment upon more space. Thus foot width b_f must equal $b_w/2$. Assuming further that within the proposed geometry $\ell_s = 0.7D$, $\ell = 0.3D$, $b_w = 0.2D$, and $n = 1$ Equation (III. 1-26) takes a more simple form.

$$\frac{(R_c)_f}{(R_c)_w} = \frac{16.2}{D^2} \left[\frac{W}{k_\phi}\right]^{2/3} \qquad \text{(III. 1-27)}$$

Function $\frac{(R_c)_f}{(R_c)_w}$ (W) plotted on log-log paper for various k_ϕ values and a constant D produces a series of parallel straight lines sloped at an angle whose tangent = 2/3. A graph computed for D=20 inches has been reproduced in Figure III. 1-10.

Sinkage due to load cannot increase indefinitely. Assume that the maximum load limit is defined by sinkage $z = 0.3D$, which is a conservative estimate. Then from Equations (III.1-13) and (III.1-14), for the foot and rigid wheel respectively, assumin again that $k_c = 0$, $n = 1$, and $p = W/\ell b_f$, it will be found that the limiting W-values plotted for various soil values k_ϕ limit foot performance at $(R_c)_f/(R_c)_w$ = 0.7; wheel performance is limited at higher loads corresponding to $(R_c)_f/(R_c)_w$ = 1.27.

The fact that the foot will be "bogged" down at lower loads than those which immobilize the wheel may be explained by the fact that the assumed rectangular area of the foot is constant and does not change with sinkage. The bearing area of the wheel, however, increases with sinkage up to $z = D/2$, and hence tends to support higher loads. From the viewpoint of acceptable sinkage limit, the wheel can be loaded more than the pair of feet.

It would be uneconomical to load the feet and the wheel far below the point of sinkage limit. This is, however, the price at which one may buy reduced compaction resistance for the foot. Fig. III.1-10 shows that the lower the load values the lower is the $(R_c)_f/(R_c)_w$ ratio, i.e., the greater is the advantage of walking. If, however, the vehicle operates at higher economic loads considered critical from the viewpoint of foot sinkage (0.7), but far enough from the critical loads of the corresponding wheel (1.27), which appears to be a more rational solution, then the gain in reducing soil compaction resistance by walking rapidly diminishes from some 30% to zero, i.e., to the point where $(R_c)_f/(R_c)_w$ is equal, or close to 1. For higher loads, which may be unacceptable for a walking machine but which may still be acceptable for a wheeled vehicle, walking produces more resistance than rolling.

Furthermore, it should be kept in mind that the above comparative analysis was made for a rigid wheel. As will be demonstrated later, an elastic tire is greatly superior to a rigid wheel in weak, deformable soils from the viewpoint of sinkage and motion resistance. That is to say, even the relatively minor advantages of the foot indicated above would greatly diminish or disappear when compared to an elastic tire.

To sum up, it may be stated that the gains of a walking mechanism in comparison to a wheel are not overwhelming, at least not from a low-resistance viewpoint, and the complexity of the device is rather staggering. If one considers the problems of leg stability in rough terrain, obstacle crossing, and the need for sensing the surface geometry in order to avoid traps into which a foot may fall more readily than a wheel, then a walking machine becomes still less attractive.

It also should be noted that on hard ground (higher k_Φ-values), even for very low ratios of $(R_c)_f/(R_c)_w$ which are advantageous for the foot, the amount of absolute gain may be small because of the insignificant ground deformation. Accordingly, the total absolute saving will not be appreciable, although percentagewise it may look impressive. Here the statistical distribution of k_Φ values would enter into the picture.

At this point, one may actually ask the basic question: What is the ultimate in locomotion evolution, the wheel or the foot? Attempts have been made to give the answer in favor of the wheel. (11, 14) After all, the wheel may be considered a kind of idealized walking mechanism as suggested in an earlier study. Professor Gray has independently produced a sketch to that effect in his admirable book in which he describes how animals move. (15) Gray's sketch has been reproduced in Fig. III.1-11 and dramatizes the fact that a rolling wheel is basically a series of motions of walking feet with the actuating mechanisms reduced to the utmost simplicity, and with reliability second to none.

COMPARISON BETWEEN TRACKED & SCREW-DRIVEN VEHICLES

It has been suggested that if lunar soil properties are such that no appreciable surface bearing capacity can develop, only a screw-driven type of vehicle may provide the necessary means of locomotion, because it would be unaffected by sinkage and would be able to operate even if totally buried in the ground.

While this assumption appears correct, the usefulness of a burrowing vehicle, at least during the earliest stages of lunar exploration, may be questionable. For this reason, the present discussion will be concerned only with an analysis of a screw vehicle and a comparable tracked vehicle, both moving on the surface with a relatively low sinkage. To this end, the thrust and motion resistance due to compaction will be evaluated.

The general similarity between the action of a track and that of a screw is shown in Fig. III.1-12. The difference between the two modes of operation lies in the curvature of the screw which produces cylindrical and circular forms in cross section with its thread, as opposed to the flat rectangular forms of the track shoe and its grouser (see thick lines in Fig. III.1-12. Otherwise, the processes of thrust production and sinkage are identical. Hence, the maximum

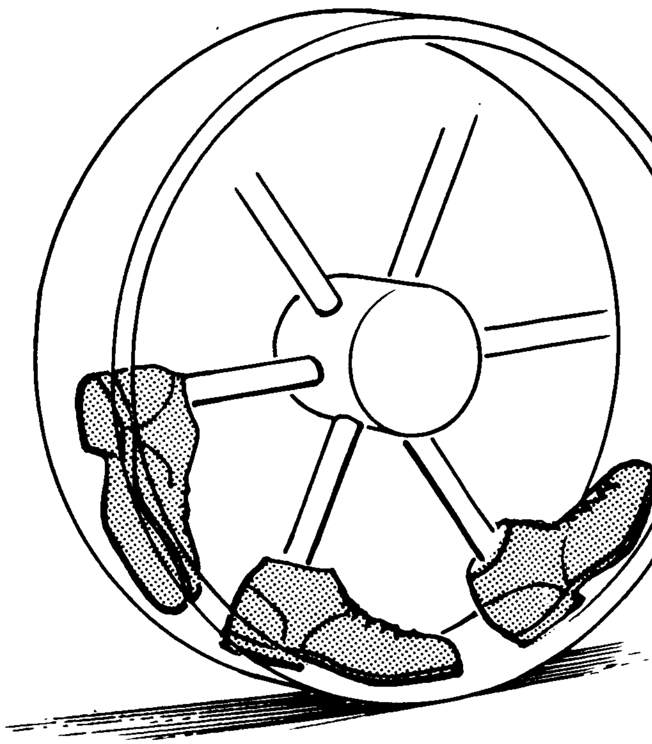

AFTER PROFESSOR J. GRAY

Fig. III.1-11. The Wheel – An Idealized Walking Machine

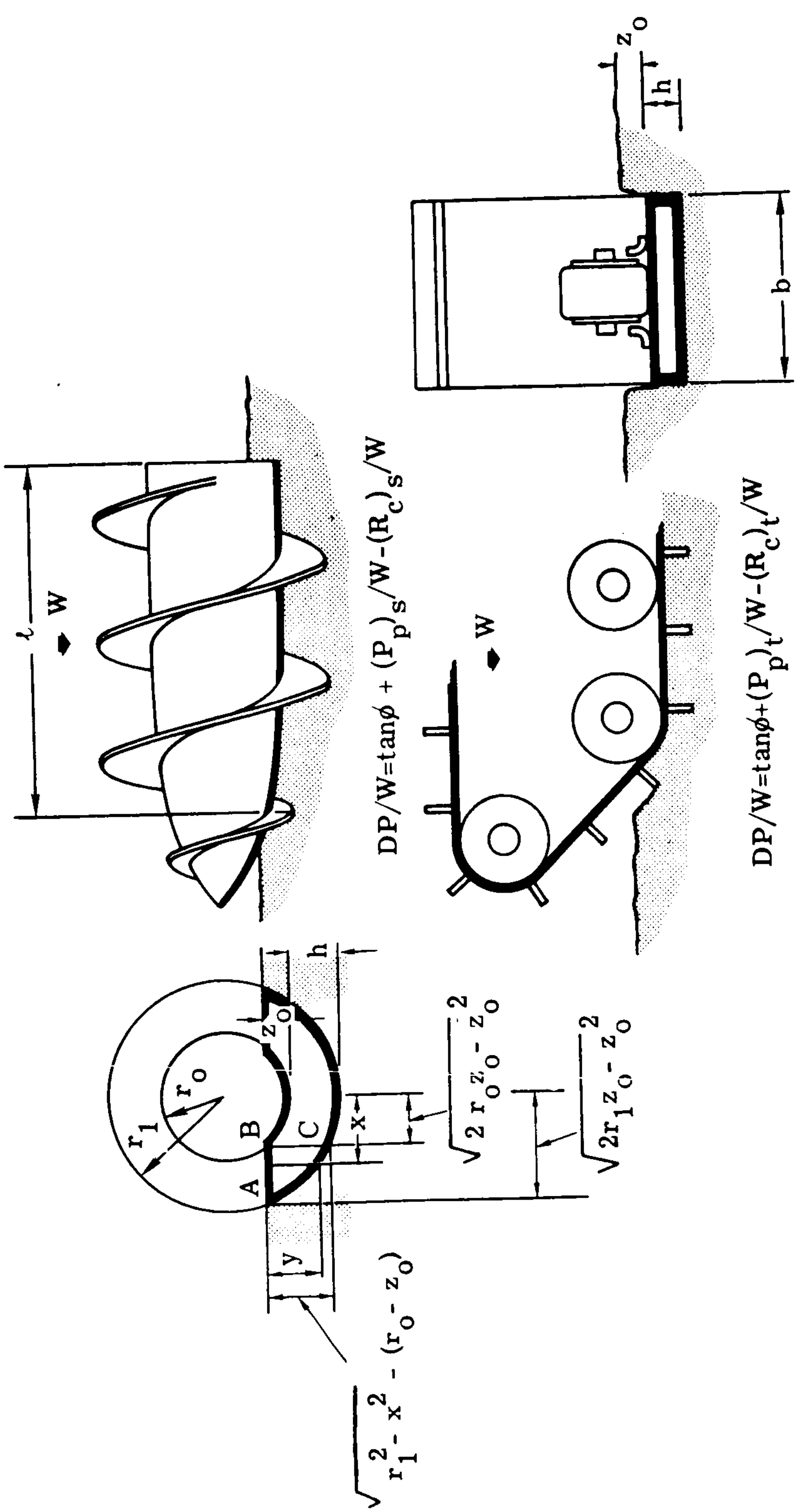

Fig. III.1-12. Similarity Between a Screw and a Track drawbar pull (DP) of both mechanisms can be calculated by means of the same equation.[3,4] (soil cohesion c is assumed to be zero):

$$DP = W \tan_{\Phi} + P_p - R_c \qquad \text{(III. 1-28)}$$

where P_p is the additional thrust produced by the circular (screw) or rectangular (track) spud. Bulldozing resistance was neglected for the sake of simplicity in this presentation. From this simple equation, the relatively complex ground contact surfaces and load distribution of the screw produce other equations which cannot be solved explicitly and which require much computation, as follows:

Using the same methodology as when dealing with tracks as shown in References 3 and 4, we may construct the following from Fig. III.1-12 for cohesionless soil with $n = 1.0$:

Load-Ground Pressure:

$$W = 2\ell k_{\Phi} \int_0^b \left[z_o - r_o + \sqrt{r_o^2 - x^2} \right] dx \qquad \text{(III. 1-29)}$$

The solution yields:

$$W = \ell k_{\Phi} \left[-(r_o - z_o) b + r_o^2 \sin^{-1} \left(\frac{b_1}{r_o} \right) \right] \qquad \text{(III. 1-30)}$$

from which sinkage z_o may be determined for known W.

Screw Thrust

Additional thrust P_p due to screw blades extending beyond the vehicle body (see Fig. III.1-12 - heavily outlined area):

$$P_p = 2N_3 \gamma N_{\Phi} \int_{b_1}^{a_1} \int_0^{y_o} y \, dy \, dx \qquad \text{(III. 1-31)}$$

where $N_\Phi = \tan^2 (45^o + \Phi/2)$ and N_3 is the number of screw blades sunk in the ground.

The solution of this equation produces:

$$P_p = N_3 \gamma N_\Phi \left\{ r_1^2 (a_1 - b_1) - \frac{1}{3}(a_1^3 - b_1^3) + (r_o - z_o)^2 (a_1 - b_1) - \right.$$

$$\left. (r_o - z_o) \left[\left(a(r_1 - z_o) + r_1^2 \sin^{-1} \left(\frac{a_1}{r_1}\right) \right) - \left(b\sqrt{r_1^2 - b_1^2} + r_1^2 \sin^{-1} \left(\frac{b_1}{r_1}\right) \right) \right] \right\} \quad \text{(III.1-32)}$$

where

$$a_1 = \sqrt{2r_1 z_o - z_o^2} \quad \text{(III.1-33)}$$

$$b_1 = \sqrt{2r_o z_o - z_o^2} \quad \text{(III.1-34)}$$

Compaction Resistance of the Cylindrical Screw Body:

Motion resistance due to compaction can be obtained by double integration

$$R_c = 2k_\Phi \int_0^b \int_0^{z_o} z \, dz \, dx \quad \text{(III.1-35)}$$

Solution yields:

$$R_c = k_\Phi \left\{ r_o^2 b_1 - \frac{1}{3} b_1^3 + (r_o - z_o)^2 b_1 - (r_o - z_o) \left[b_1 (r_o z_o) + r_o^2 \sin^{-1} \left(\frac{b_1}{r_o}\right) \right] \right\} \quad \text{(III.1-36)}$$

Drawbar Pull

The drawbar pull can be expressed as in the case of the tracked vehicle:

$$DP = W \tan\Phi + P_p - R_c \quad \text{(III.1-37)}$$

The meaning of symbols and the geometry of load distribution and ground contact configuration are shown in Figure III.1-12.

Trial computations of this type have disclosed that there is not much difference in DP/W ratio between dimensionally comparable tracks and screws. Thus, it was deduced that a screw used for propulsion is no more advantageous than the track (See comparison in Fig. III. 1-13). The notoriously low mechanical efficiency of the screw drive is another hindrance to accepting this type of propulsion.

To sum up, one may conclude that a "crawling" vehicle of the screw type does not represent, at this time, an attractive solution for lunar locomotion.

COMPARISON BETWEEN TRACKS AND WHEELS

The problem of track versus wheel must be viewed from many angles. The most important aspects of this question were reviewed elsewhere[3, 4, 16] and it was concluded that both wheels and tracks have their merits. Under certain terrain conditions a track must replace a wheel, while under other conditions the wheel, particularly one equipped with an elastic tire, should replace the track; and, under still other conditions, both wheels and tracks behave alike from the viewpoint of soil-vehicle relationship.

In the case of a lunar roving vehicle, however, new problems enter the picture. One of these problems is what might be designated the fitting of the maximum amount of vehicle mobility into a given spaceship envelope.

As has already been mentioned, both soft ground and obstacle-crossing ability are ultimately determined by the weight and linear dimensions of the vehicle, which, in turn, are limited by the dimensions and the payload of the spaceship. To investigate these limitations in more detail, for both wheels and tracks, compare in general terms their soft-ground performance. This may be done if the drawbar-pull/weight ratio is used as a base of comparison. Such a comparison is quite general, since this ratio is equivalent to the most general index of mobility in air and water, namely the drag/lift ratio.

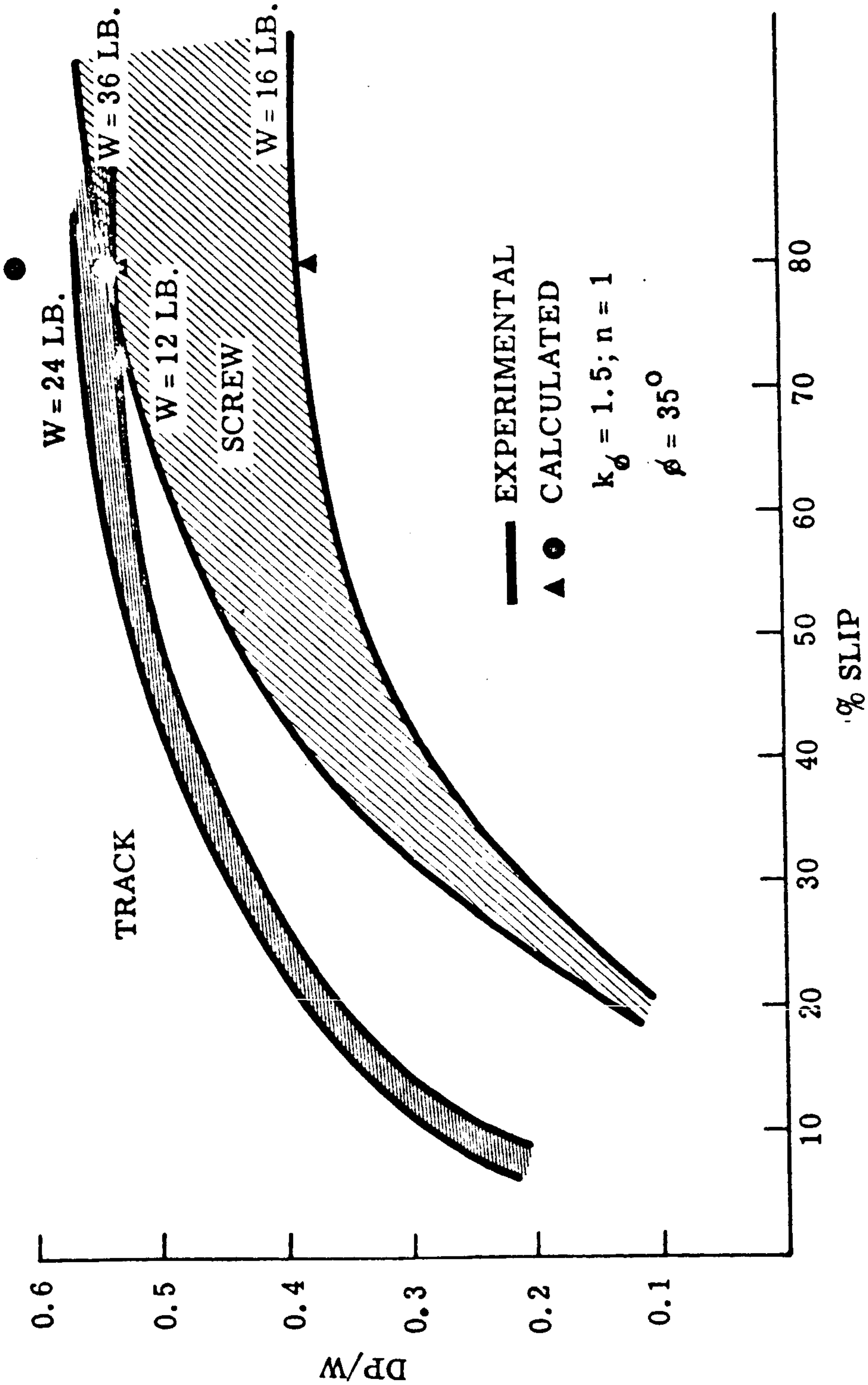

Fig. III.1-13. Relation Between Comparable Track and Screw Propelled Vehicles at Various Gross Weights

To this end, Equations (III.1-17 and 1-18) may be applied. Group in each member of these equations all the values which do not pertain to vehicle weight W and to its linear dimensions D, b, and ℓ, and denote all the linear dimensions by L. Then, for n = 1, $k_c = 0$ and c = 0:

$$\left(\frac{DP}{W}\right)_{track} = A - B\left(\frac{W}{L^3}\right) \qquad (III.1-38)$$

$$\left(\frac{DP}{W}\right)_{wheel} = A - C\sqrt[3]{\frac{W}{L^3}} \qquad (III.1-39)$$

where $A = \tan\Phi$; $B = 1/2\, k_\Phi$ and $C = (3/2)^{4/3}/2k_\Phi{}^{1/3}$

Gross vehicle weight W and its linear dimensions L can be identified with spaceship payload and with the linear dimensions of the cargo space of the booster. Equations (III.1-38 and 1-39) thus quantitatively define the previously expressed truism and indicate to what extent the soft-ground mobility of the lunar roving vehicle depends on the size of the ship which transports it to the lunar surface.

This illustrates that the real problem faced by the designer of a lunar roving vehicle is to squeeze into a limited space as much DP/W ratio as possible. This can only be done by designing a vehicle with minimum weight W and maximum linear dimensions L, a formidable task. Equations (III.1-38 and 1-39) provide general information as to what can be done, and how.

Direct comparison between the discussed formula suggests that for a given DP/W ratio, the mobility of a wheeled vehicle is less sensitive to change or adjustment of the vehicle's gross weight, since W enters Equation (III.1-39) under a cubed root. Also any change in linear dimensions of wheels has the same effect, since L enters the wheel formula for the first power while in the track equation it is cubed.

Conversely, one may say that an increase of linear dimensions of the track will have a more powerful effect upon performance increase than a similar increase in the dimensions of a wheel. But the addition of weight to the track will deteriorate its performance to a larger extent than a similar addition of weight to a wheeled vehicle. Furthermore, it is well known that the rolling resistance of a tracked vehicle due to internal friction is several times that of a wheeled vehicle.

It is evident that a simultaneous change of weight and linear dimensions in wheels and tracks will cause changes in performance depending on the direction and preponderance of the induced variations in the W-and L-values. This suggests that a morphological analysis of the described type becomes useful as an integral part of preliminary-concept evaluation, and helps to determine the most fruitful area of approach.

Equations (III.1-38 and 1-39) pertain, in a strict sense, to the load applied to a given contact area as well as to the linear dimensions of that area, and not to vehicle weight and size. Therefore, they illustrate the trend rather than specific values.

To evaluate a specific track vs a specific wheel in a more rigorous way, Equations (III.1-17 and 1-18) have to be used as shown in subsequent examples.

EFFECT OF TYPE, NUMBER, AND SIZE OF WHEELS

These problems have been considered in detail in References 3 and 4. It may be worthwhile to repeat some of the considerations involved, as they bear directly upon a solution for lunar surface locomotion.

In order to compare the performance of rigid and elastic wheels in soft soil, Equations (III.1-15 and 1-16) can be used, where it is assumed that the form of the ground-contact area of a highly elastic wheel approaches a flat surface. Comparing two wheels of identical overall dimensions, it can be seen from Figure III.1-14 that the elastic wheel is clearly superior from the point of view of motion resistance over a wide range of soil consistencies. Although not clear from the graph, the soil would have to be very hard (high k_ϕ values) before the performances of the two types of wheels approached each other.

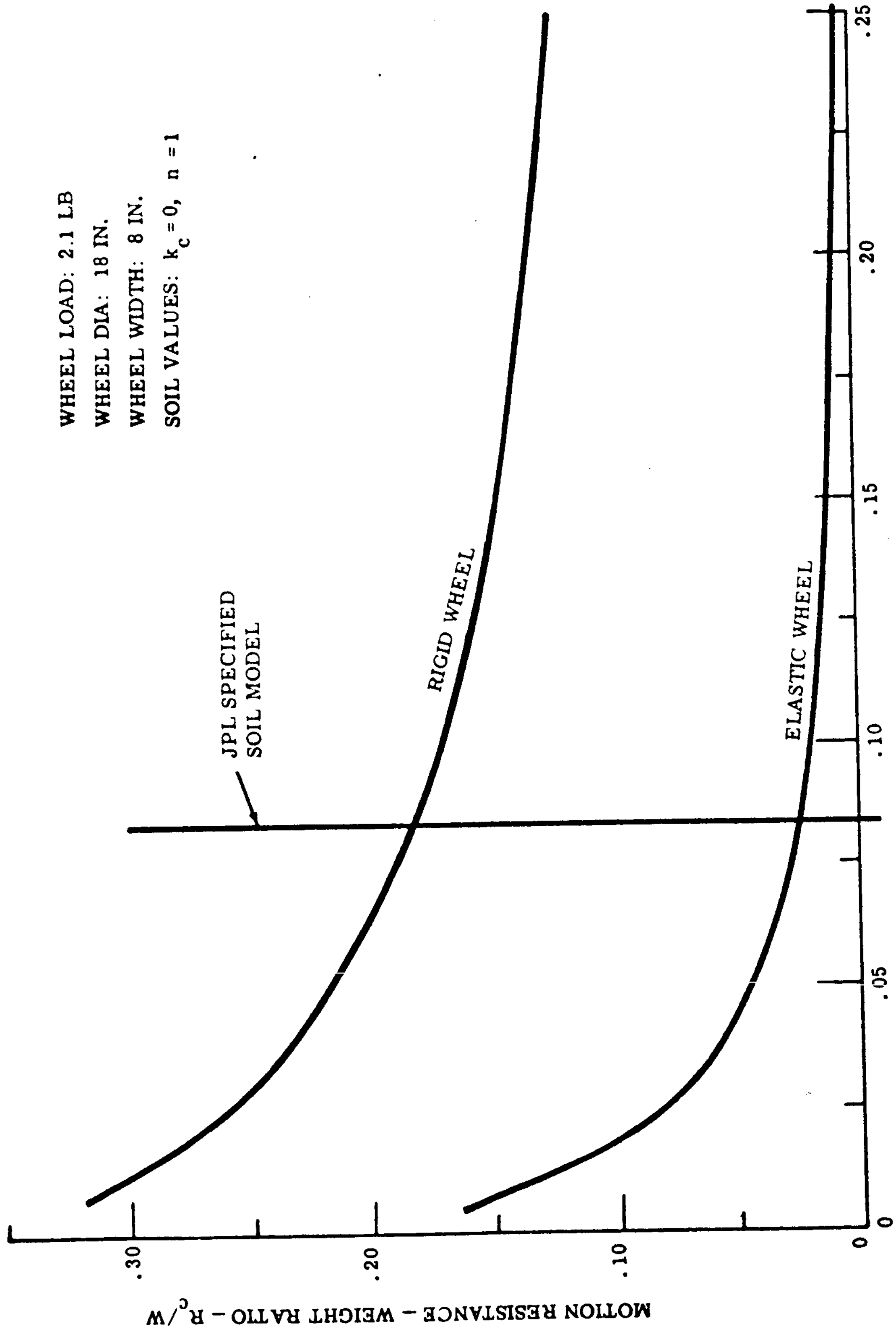

Fig. III. 1-14. Comparison of Motion Resistances for Rigid and Elastic Wheels of Equal Size

The effect of wheel number is summarized in Fig. III. 1-15. A group of vehicles, each weighing W = 12.5 lb, was evaluated from the R_c/W ratio viewpoint while assuming that the vehicles were equipped with 2, 4, 6, and 8 wheels and tracks. The computations were performed for the wheel and track dimensions specified in Figure III. 1-15.

The significance of these computations lies in the effect of soil type upon performance of the various wheeled and tracked configurations.

It can be seen from the graph that the effect of wheel number is very significant at low soil strength. However, the increase in the number of wheels beyond six does not result in significant motion-resistance reduction. The performance of a tracked vehicle is only slightly superior to that of the six-and eight-wheel vehicle configuration.

The effect of wheel diameter in soft soil can be investigated for elastic wheels by using Equation (III.1-15), and plotting the motion resistance weight ratio (R_c/W) as a function of wheel diameter, for various soil consistencies. A typical result is shown in Fig. (III.1-16). It indicates that there is an asymptotic value of wheel diameter beyond which it does not pay to go for the assumed soil-value range. In the considered case of a 12.5 lb, 6-wheel vehicle, it is not worthwhile to use wheels larger than 18 inches in diameter, even for the soft lunar surface model specified by JPL (k_Φ = .083) in the subject RFP.

OBSTACLE CROSSING

As has been stated previously, the mobility of vehicles depends not only on their soft-ground-crossing ability but also on their ability to overcome obstacles and respond to ground-surface unevenness with minimum shock and vibration.

In this discussion, only obstacle crossing will be considered in view of our lack of knowledge of the microroughness of the lunar surface.

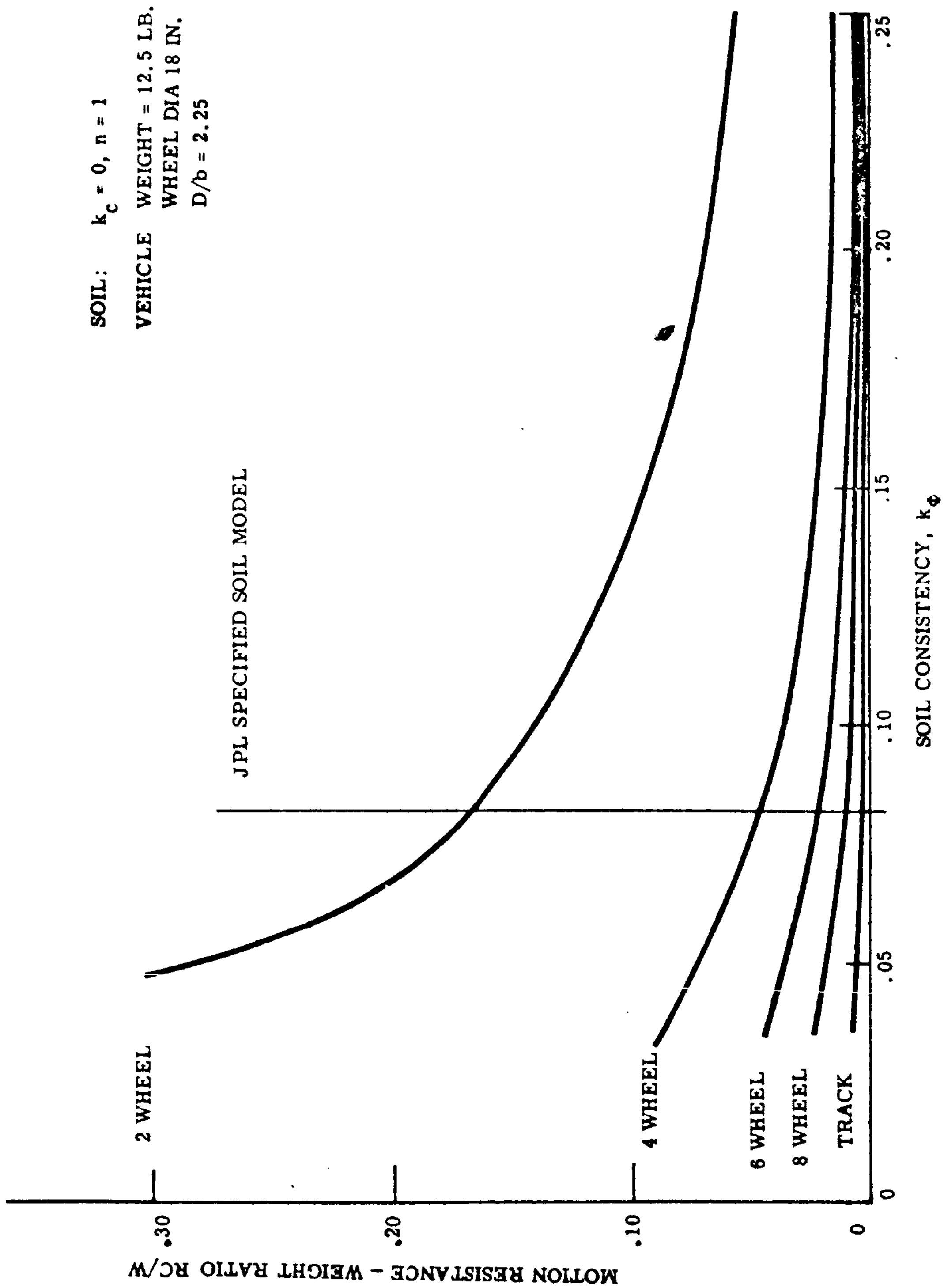

Fig. III.1-15. Motion Resistance of Various Vehicle Configurations

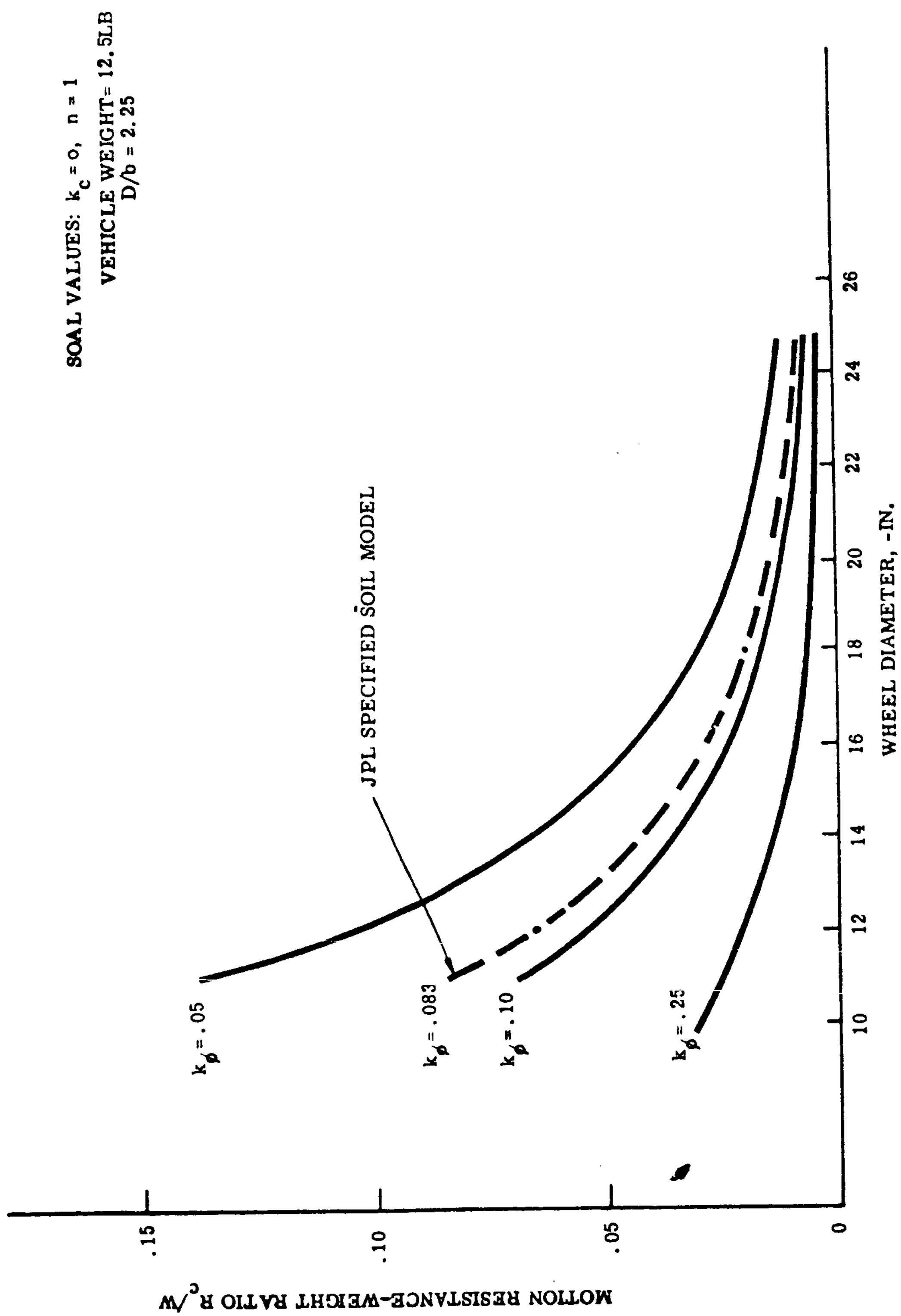

Fig. III.1-16. Motion Resistance of a 6 x 6 Wheeled Vehicle with Various Wheel Sizes

As in the evaluation of soft-ground performance, analytical methods can be utilized to compare and evaluate the obstacle performance of various types of vehicle configurations.

For example, the obstacle-climbing ability on a hard surface of a rigid frame wheeled vehicle with all wheels driven can be expressed(9) by the following equation:

$$\left[\frac{1}{\mu} - \frac{1+\mu^2}{2\mu} - \frac{r}{L'}\right]\cos\theta - \left[1 - \mu\frac{r}{L'}\right]\sin\theta = \mu\frac{r}{L'} \qquad \text{(III.1-40)}$$

where μ = coefficient of friction between wheels and surface

r = wheel radius (in.)

L' = distance between first and last axles (in.)

$\sin\theta = (1 - h/r)$

h = height of vertical obstacle (in.)

The obstacle climbing ability of an articulated elastic frame wheeled vehicle * with three or more axles can be expressed by:

$$h = \frac{(N-3)W_O\mu + (2W_O - K'r)\mu - (W_O - K'r)}{K'(1-\mu^2)} \qquad \text{(III.1-41)}$$

for condition $r < h < (L + r)$, and

L = wheel base (axle-to-axle distance, in.)

N = number of axles

K' = elastic frame spring constant (lb/in.)

W_o = load per axle (lb)

For $r > h$, the climbing ability of the elastic frame vehicle is given by:

$$\frac{\sin\theta + \mu\cos\theta}{\cos\theta - \mu\sin\theta} = \frac{1}{(N-1)\mu} \qquad \text{(III.1-42)}$$

where again $\sin\theta = (1 - h/r)$

---

*Patent Applied For, M.G. Bekker, GM Defense Research Laboratories, Serial No. 224,754.

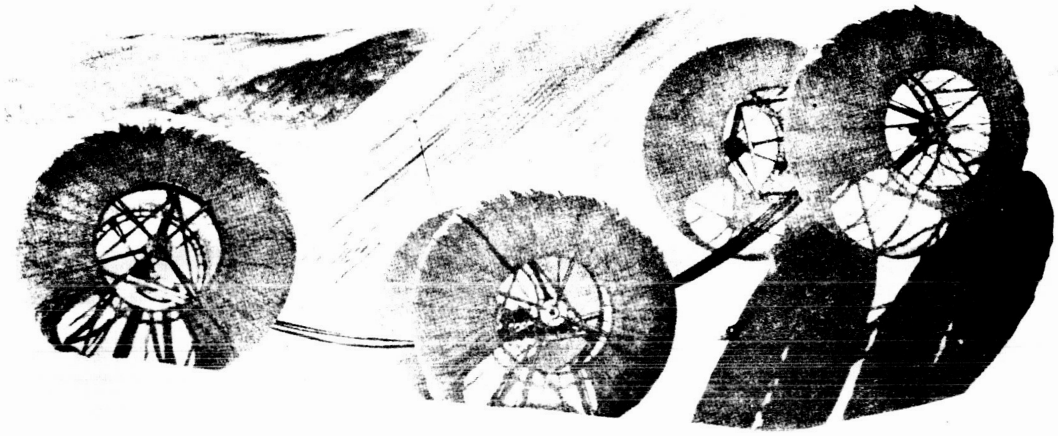

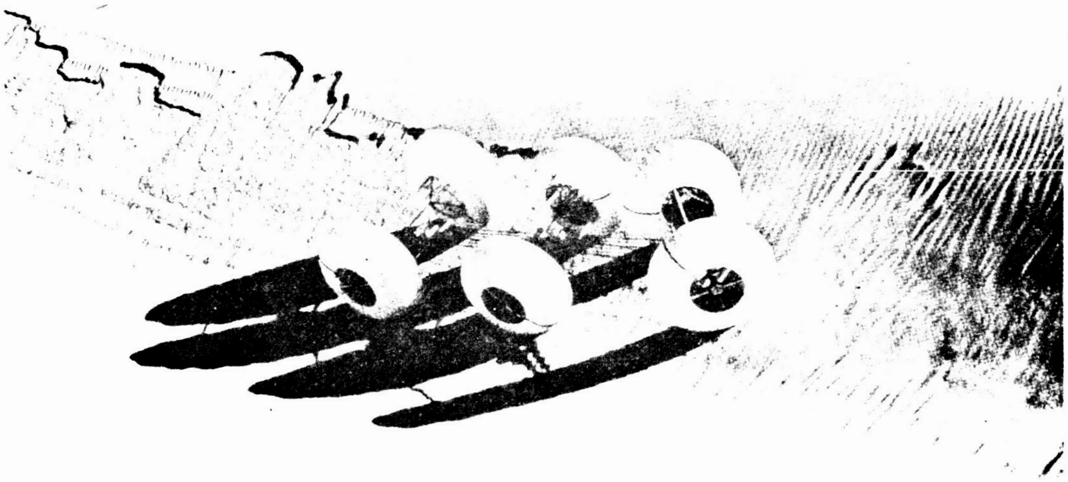

Fig. III. 1-17. Elastic Frame Wheeled Lunar Vehicle with
3-Foot Diameter Wheels Operating in Sand Dunes

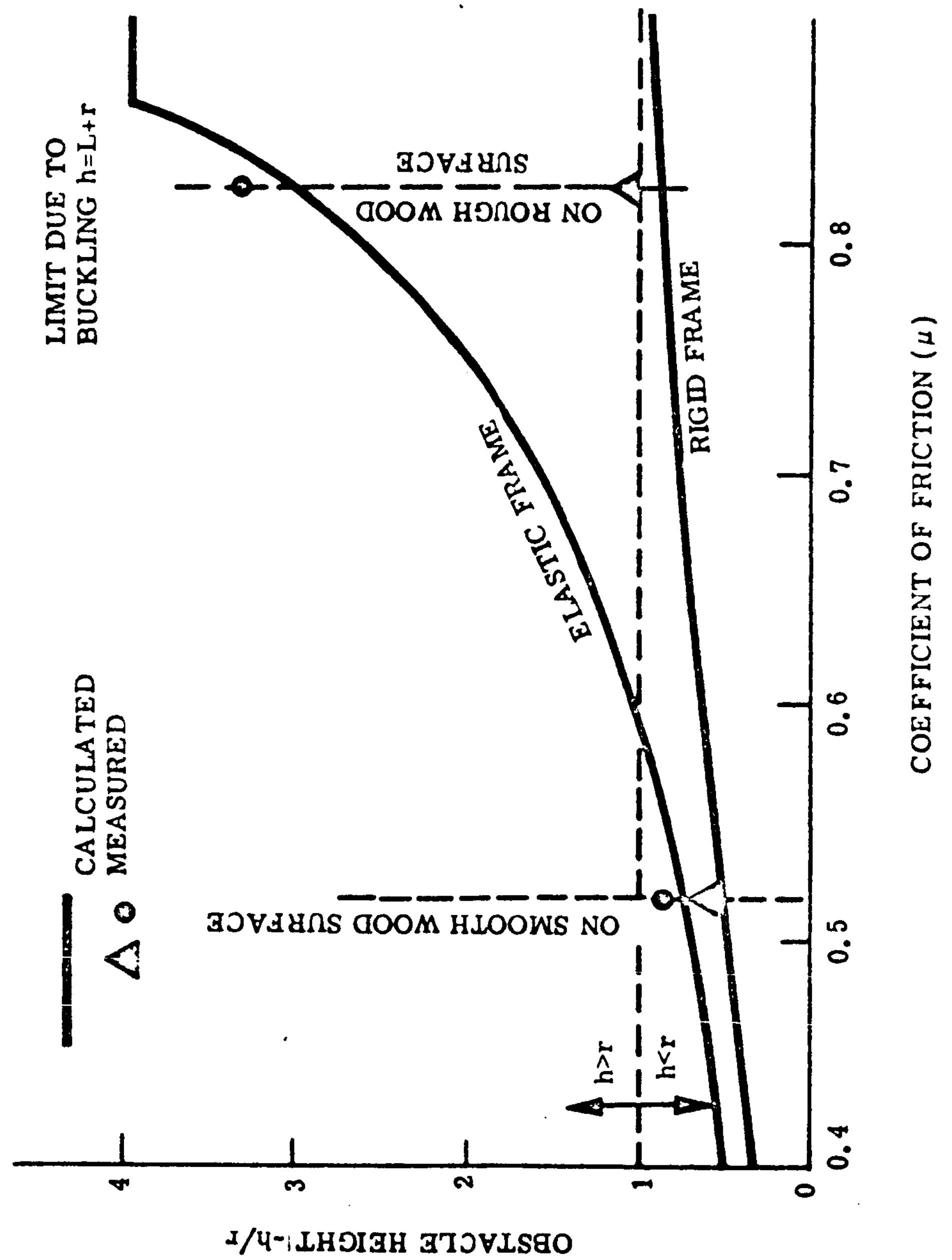

Fig. III. 1-18. Comparison of Abilities of Elastic and Rigid Frame Vehicles in Negotiating Vertical Obstacles

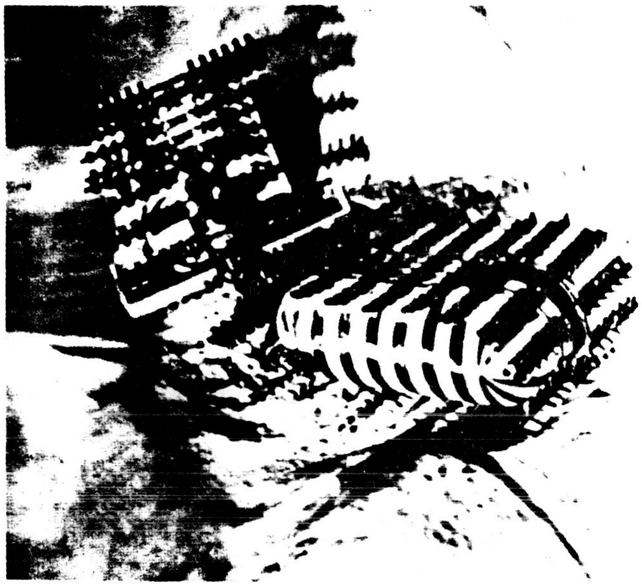

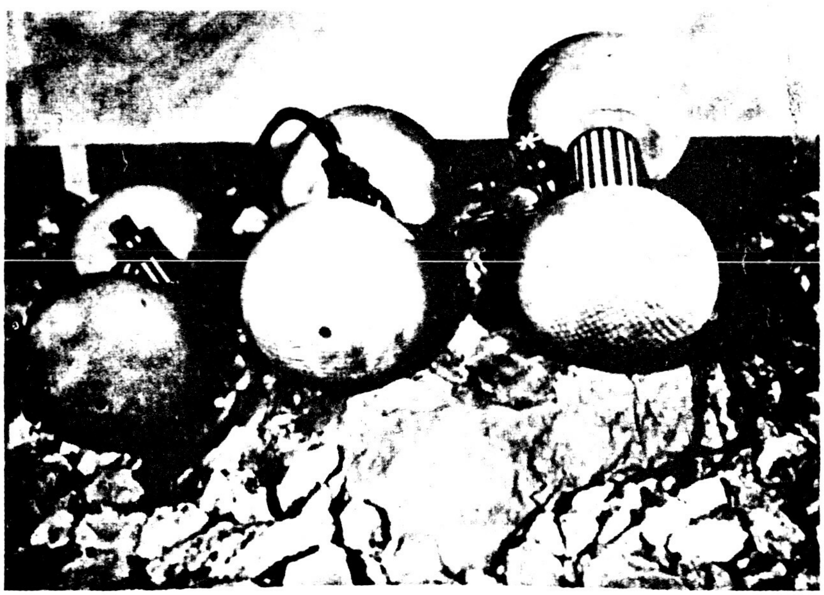

Fig. III. 1-19. Three Types of Lunar Roving Vehicles

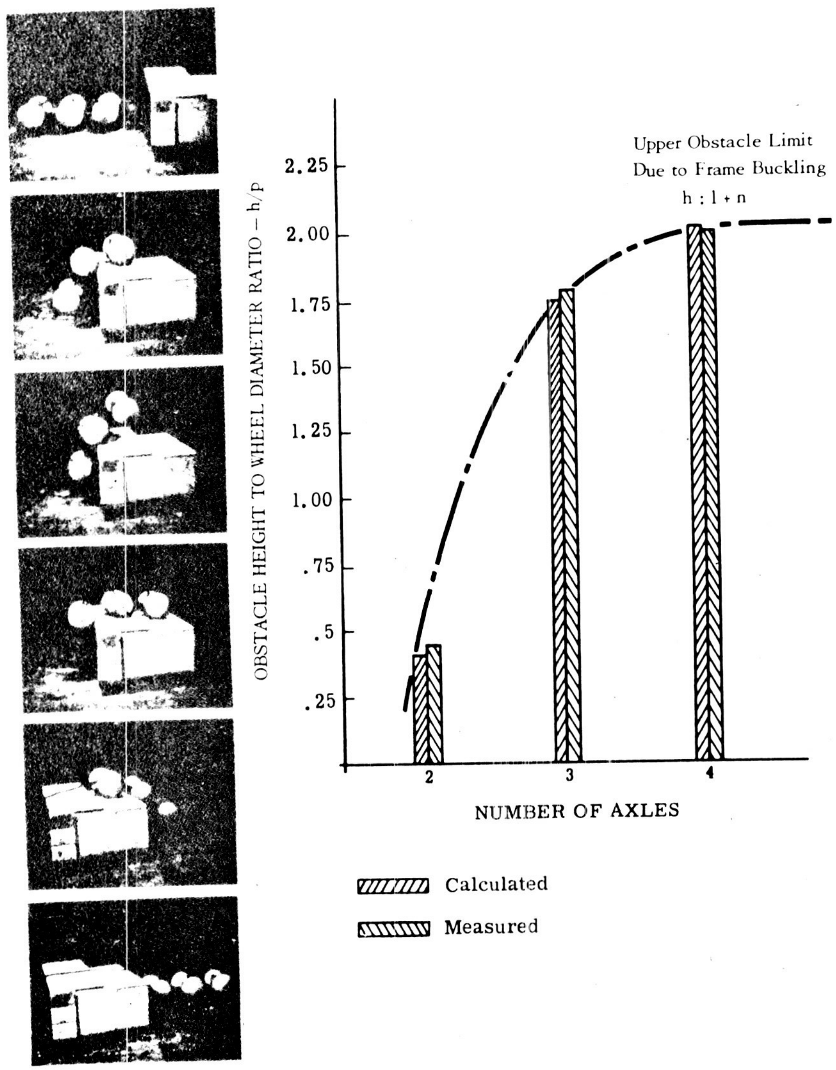

Fig. III. 1-20. Obstacle Crossing Performance of Elastic Frame Articulated Lunar Roving Vehicle Model

Using the foregoing equations, the comparative performances of rigid and elastic-frame vehicles, and effect of the number of axles, can be evaluated.

The ability to negotiate a vertical obstacle of the elastic-frame, wheeled lunar vehicle shown in Fig. III.1-17 is compared in Fig. III. 1-18 to that of the same vehicle equipped with a rigid frame. Note that the superiority of the elastic-frame version increases markedly as the coefficient of friction between the wheels and surface increases. Further note that although the rigid frame version can only negotiate an obstacle approximately equal to its wheel radius, the elastic-frame vehicle can climb an obstacle several times higher than its wheel radius.

Three types of lunar roving vehicles are shown in Fig. III.1-19. Fig. III. 1-20 shows the effect on obstacle performance of the number of axles for the elastic-frame, wheeled lunar vehicle model at the bottom of Fig. III. 1-19. This demonstrates that up to the point where the frame buckles, increasing the number of axles will increase the maximum negotiable obstacle height.

ACCURACY OF PREDICTIONS

Questions often arise as to the accuracy of the analytical methods utilized herein. Extensive field and laboratory tests by GM DRL and such organizations as the Land Locomotion Laboratory of the Army Tank-Automotive Command have demonstrated a high degree of correlation between calculated and experimental results.

This can be illustrated by means of several examples.

Fig. III.1-13 has compared calculated drawbar-pull values for the screw and tracked models shown in Fig. III.1-19 each at two weights, with results of tests conducted in the laboratory in dry pumice.

Fig. III.1-21 shows predicted versus measured drawbar-pull values for the six-wheeled (7.5-inch-diameter tires) lunar vehicle model shown in Fig. III. 1-19. Tests again were conducted in dry pumice under laboratory conditions.

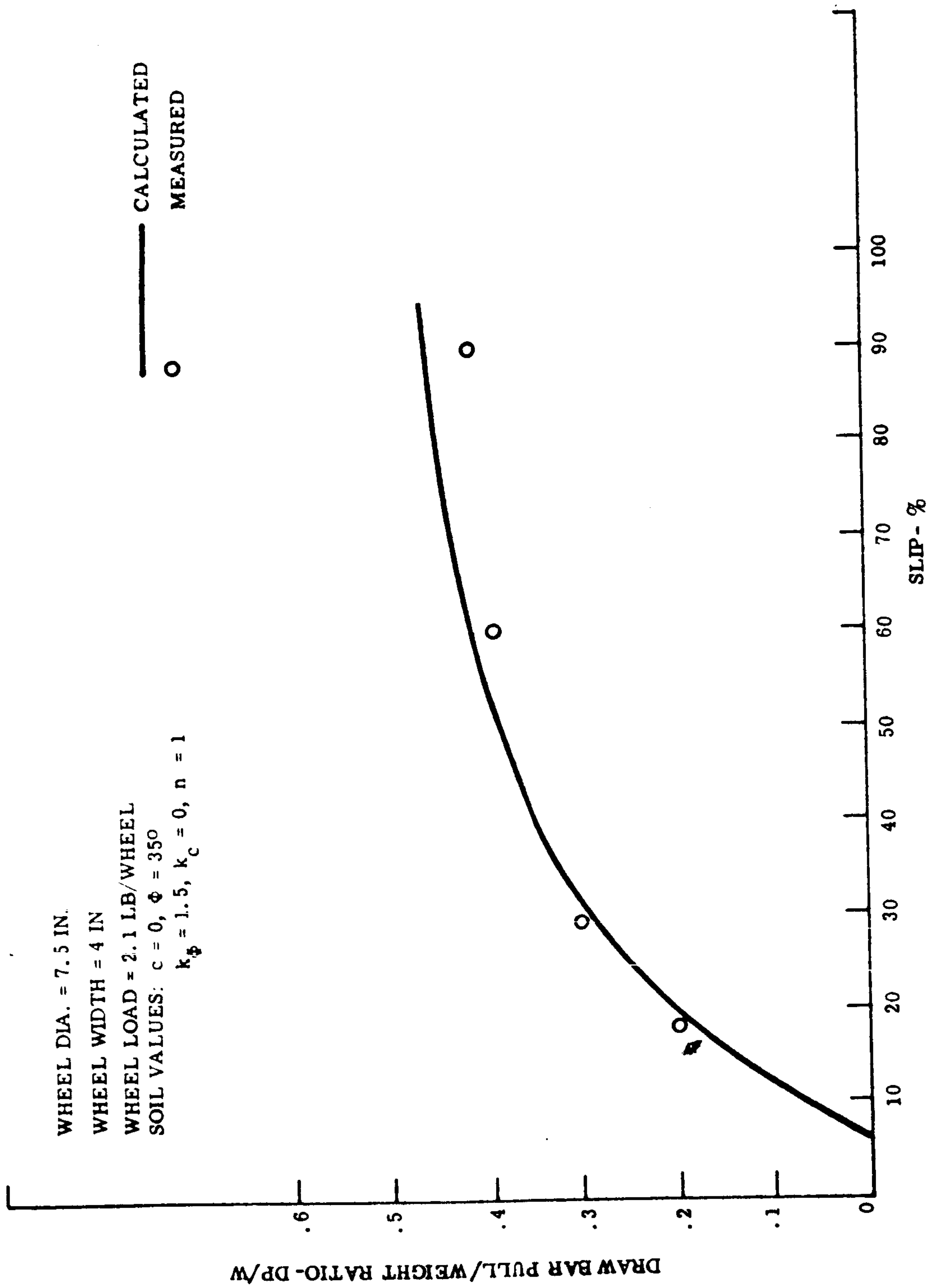

Fig. III. 1-21. Comparison of Calculated Drawbar Pull/Weight Ratio with Results of Laboratory Tests

Fig.III.1-22 compares calculated values of Drawbar Pull/Weight ratio with results of tests conducted under field conditions with the six-wheeled lunar vehicle shown in Fig.III.1-17. The wheel diameter for this vehicle is 3 feet, and test weight was 67 pounds.

Figs.III.1-23 and 1-24 show comparisons of predicted and measured drawbar pull as a function of slip for full-size tracked and wheeled tractors, as well as their 1/4-scale models. These tests were conducted in the laboratory under controlled soil conditions. The calculated values are shown by solid lines. Since the processing of the sandy loam for the number of tests required could not possibly result in reproducing the original soil state at all times, the measured spread of soil values resulted in the prediction of drawbar pulls within the hatched band as determined by two standard deviations, or by approximately 90% of the soil values measured. In dry sand, which is very easy to handle and does not appreciably change its state, only one set of soil values, hence one line, was produced. The experimental results are marked by solid and open dots.

The agreement between theory and experiment may be described as quite good for both the full-size and scaled-down tracked and wheeled vehicles. It is most interesting that the accuracy illustrated in Figs.III.1-23 and 1-24 may be obtained by means of the same equations, irrespective of whether one is concerned with a 50-inch-diameter wheel or its replica of 12.5-inch diameter; or if the evaluation is performed for a 15,000-pound tractor or a 200-pound model.

It has also been demonstrated that good agreement can be obtained between predicted and experimental obstacle performance.(9) Figs.III.1-18 and 1-20 demonstrate this for the case of the wheeled lunar vehicle models shown in Figures III.1-17 & 1-19 respectively. In each case, the data points measured in the laboratory show excellent agreement with the calculated results.

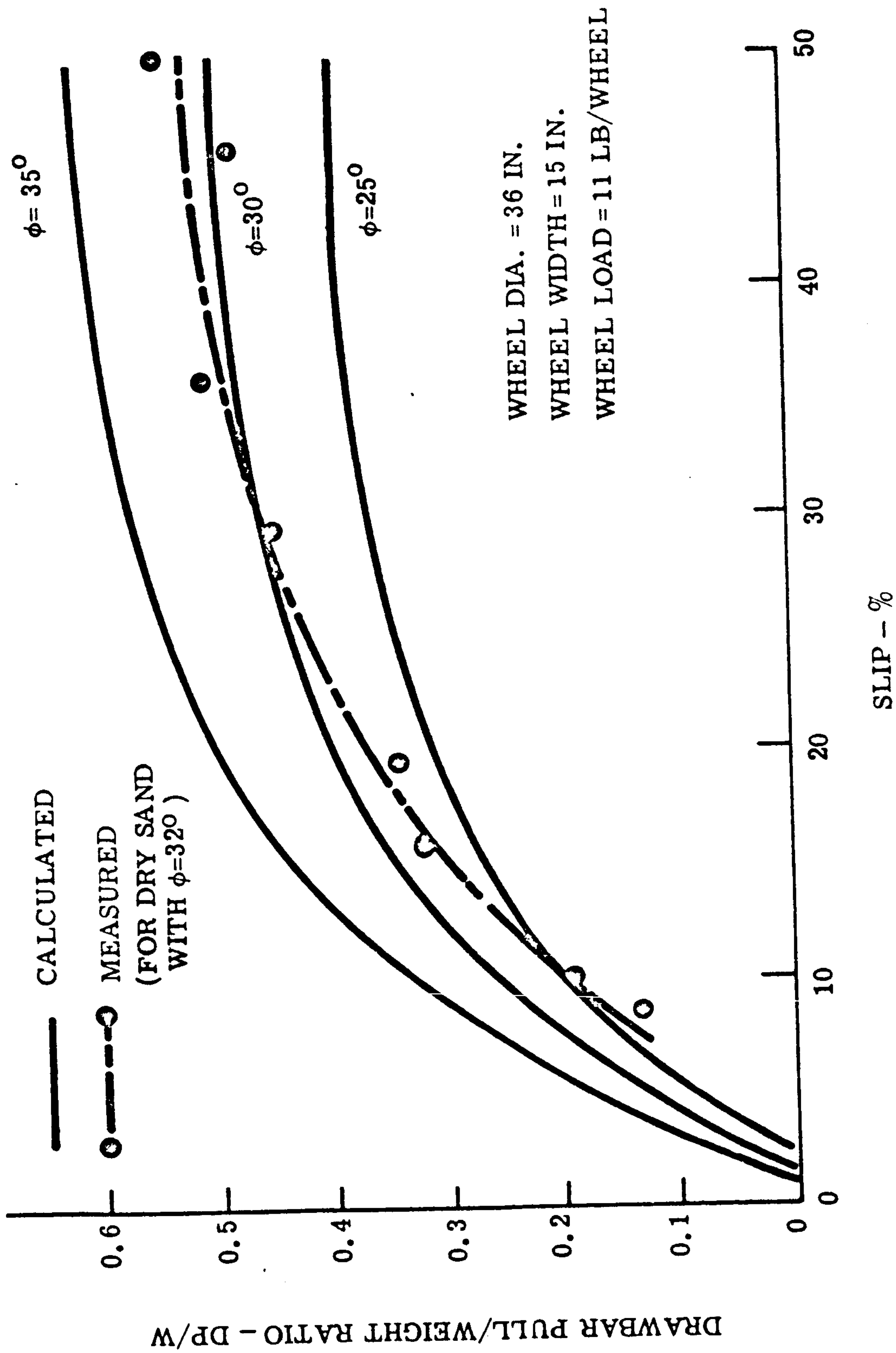

Fig. III.1-22. Comparison of Calculated Drawbar Pull/Weight Ratio with Results of Field Tests

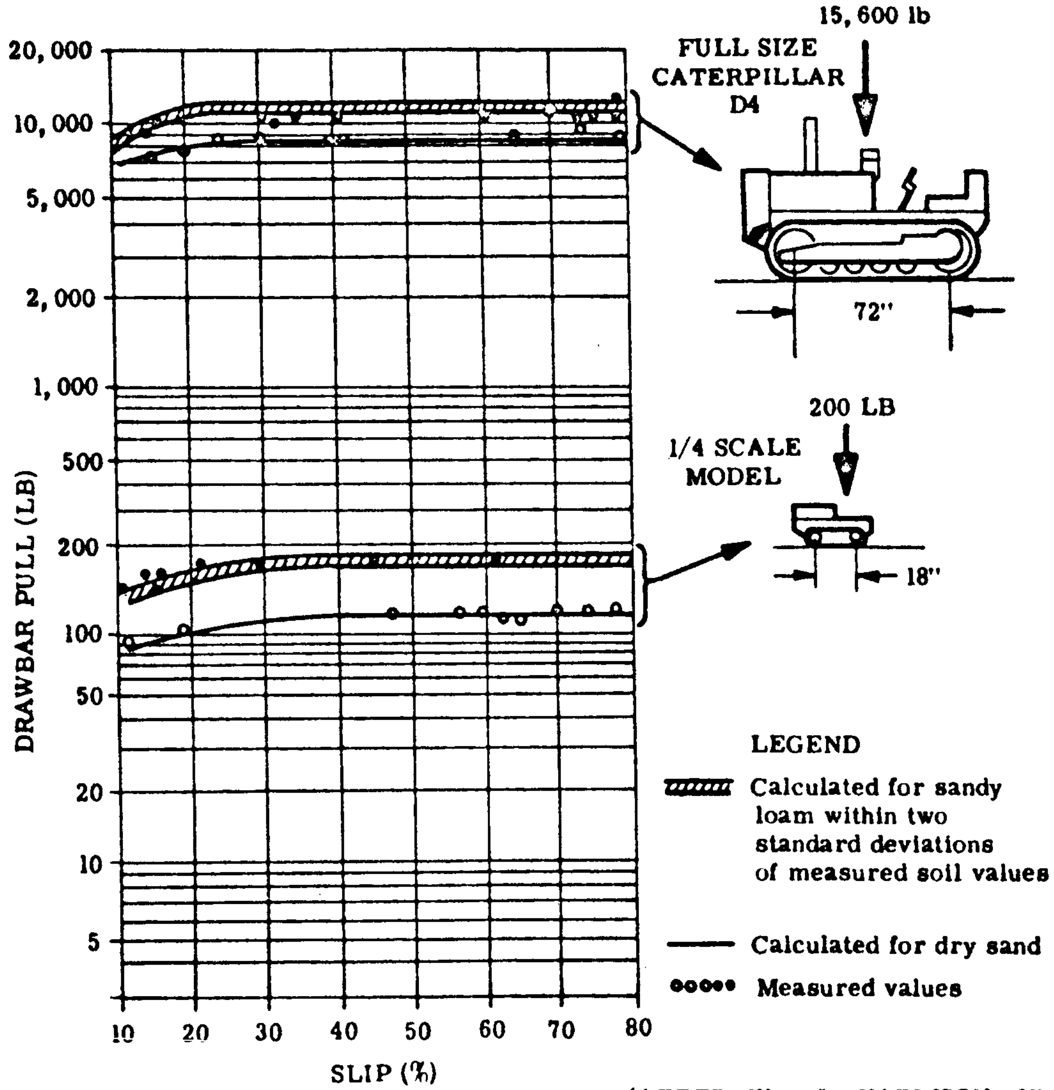

(AFTER Wm. L. HARRISON, JR. AND Z. JANOSI)

SAND: $k_c = 0.05$; $k_\Phi = 3.58$; $n = 1.18$

$c = 0.1$; $\Phi = 28°$; $K = 0.31$

SANDY LOAM: $k_c = 8.6 - 11.1$; $k_\Phi = 4.85 - 6.46$

$n = 0.68 - 0.78$; $c = 0.25 - 0.34$

$\Phi = 35.5° - 37°$; $K = 0.1$

Fig. III. 1-23. Predicted and Measured Drawbar Pull Versus Slip; Full-Size Tractor and Its 1/4 Scale Model

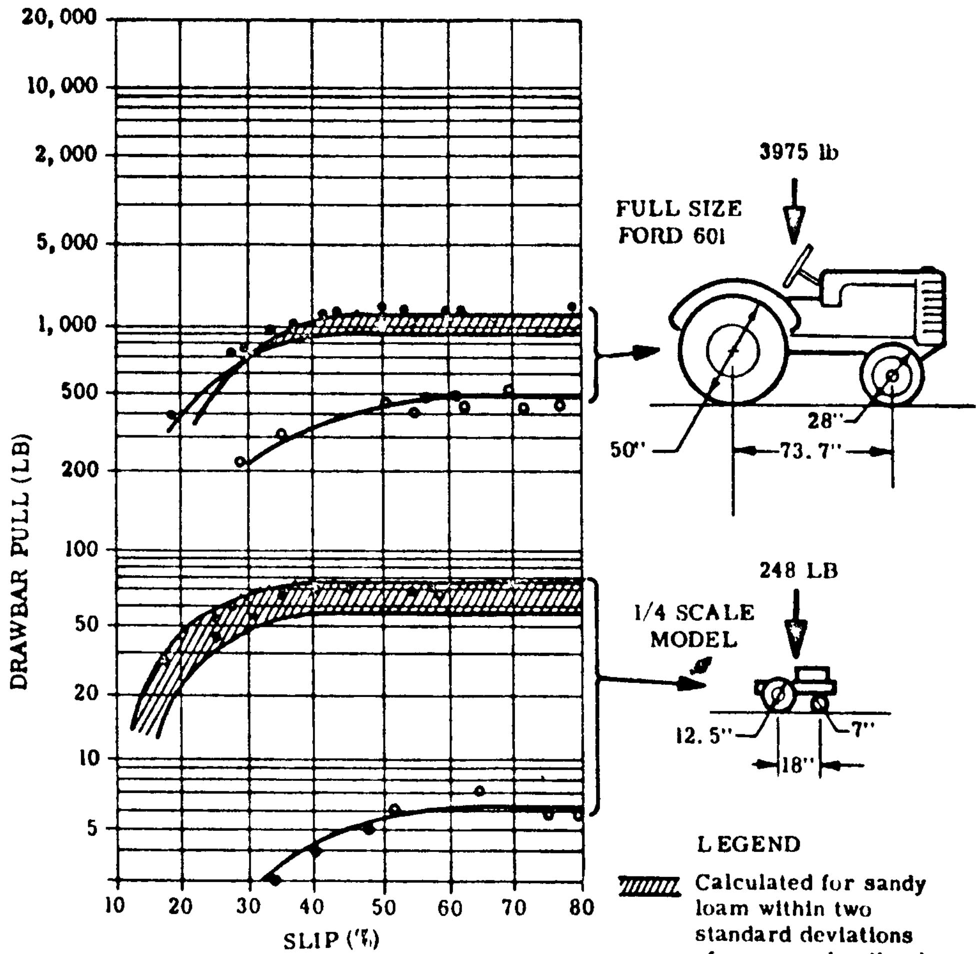

SAND: $k_c = 0.05$; $k_\Phi = 3.58$; $n = 1.18$
$c = 0.1$; $\Phi = 28$; $K = 0.31$

SANDY LOAM: $k_c = 8.6 - 11.1$; $k_\Phi = 4.85 - 6.46$
$n = 0.68 - 0.78$; $c = 0.25 - 0.34$
$\Phi = 35.5 - 37$; $K = 0.1$

LEGEND

Calculated for sandy loam within two standard deviations of measured soil values

Calculated for dry sand

Measured values

(AFTER Wm. L. HARRISON, JR. AND Z. JANOSI)

Fig. III. 1-24. Predicted and Measured Drawbar Pull Versus Slip; Full-Size Tractor and Its 1/4 Scale Model

3. Payload Envelope Limitations

The study of both soft-ground crossing and obstacle crossing inevitably has led to the conclusion that the larger the vehicle, the more mobile it is. Perhaps this was not a new discovery. Nevertheless, the quantitative relationships involved are new enough to dramatize the problem. The problem of designing the most mobile lunar roving vehicle now can be simply stated: fit into a given space envelope the largest possible vehicle.

The usual space limitations, together with the requirements from the mobility-performance point of view for a vehicle of relatively large physical size, make this a most difficult problem.

To help resolve the problem, various studies of a general nature were made of folding and collapsible configurations and mechanisms.

Fig. III.1-25 shows a wheel whose diameter can be changed for stowage purposes. In the top photographs of Fig. III.1-26, a lunar vehicle model is shown stowed in a cylindrical container in two different ways.

Various methods of vehicle stowage have also been studied to satisfy the payload envelope limitations and center of gravity constraints given in Hughes Aircraft Co. Specification No. 239503.* These requirements are shown in the sketches of Fig. III. 1-27. To aid in these studies, full-size mock-ups were constructed of the Surveyor spaceframe and payload envelope (Fig. III. 1-28).

From the previous discussions of lunar terrain characteristics and mobility performance an elastic frame vehicle of large dimensions was chosen to be packaged in this envelope. With elastic or deformable wheels, the vehicle

*"Surveyor Basic Bus (2100 lb) Payload Interface Requirements and Spacecraft System Description."

UNFOLDED FOR NORMAL OPERATION

COLLAPSED FOR STORAGE

Fig. III. 1-25. Collapsible Wire Frame Wheel

(CYLINDRICAL CONTAINER)

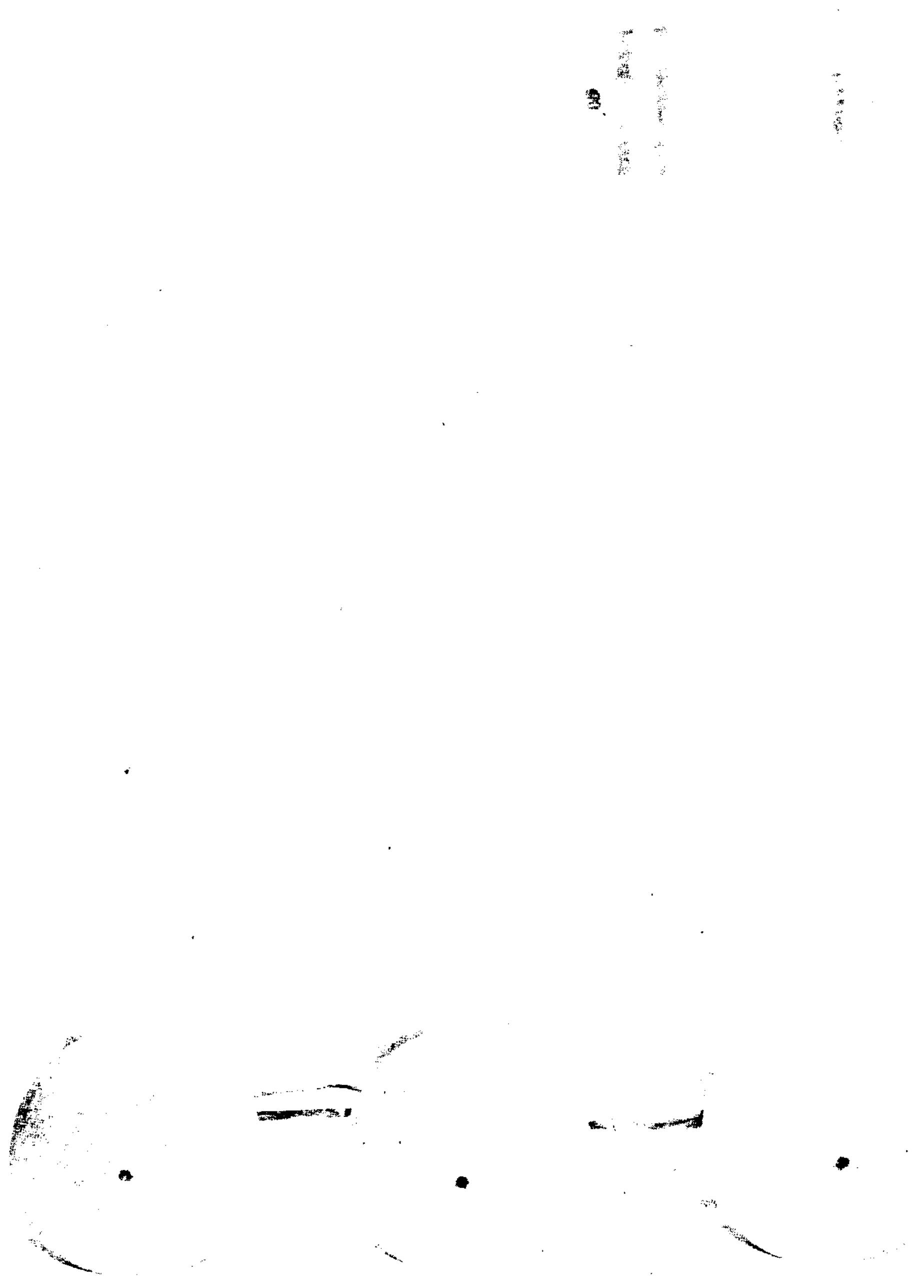

Fig. III. 1-26. Wheeled Lunar Vehicle Model in Various Storage Configurations

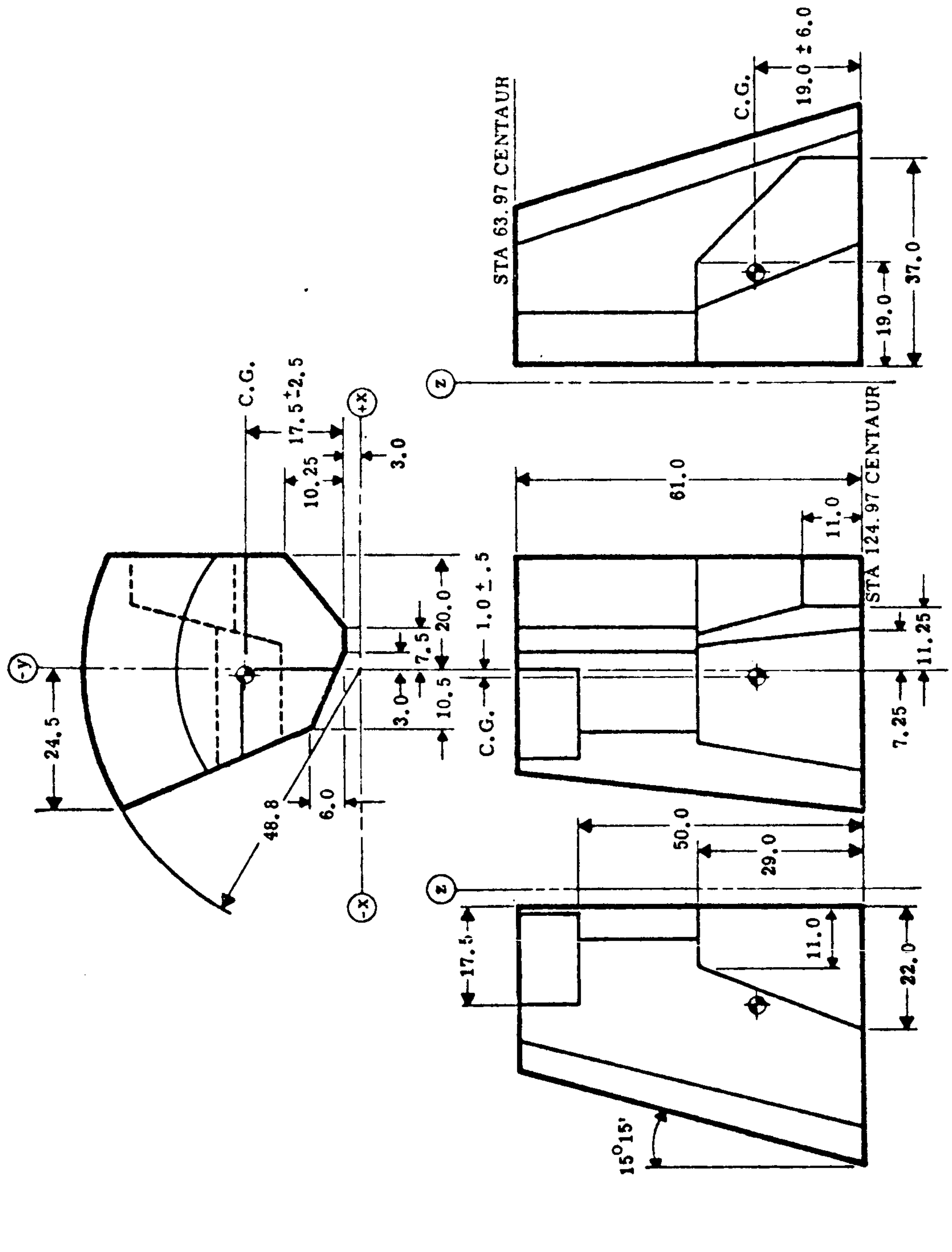

Fig. III.1-27. Specified Payload Envelope Limitations and Center of Gravity Constraints

Fig. III.1-28. Mock-up of Maximum Space Envelope Mounted On Surveyor Frame can be efficiently packaged as shown in Fig.III.1-29. The vehicle is folded into a triangular shape, with the wheels deflected to fit the envelope contour.

Surveyor flight-control requirements make it necessary to maintain the CG of the entire spacecraft within a cylindrical volume 1.8 inches in diameter by 1.5 inches long, centered around the vertical axis approximately 18.5 inches above the plane of the lower frame. Therefore, compliance with the CG tolerances specified is to be considered carefully.

To fit this package on the Surveyor spaceframe, within the specified space, two methods of stowage were considered; these are shown in Fig.III.1-30.

Although configuration (b) is more readily adaptable to the shape of the envelope, it was decided that configuration (a) was superior due to preferred center of gravity location and ease of vehicle deployment and unfolding. The mechanisms of this configuration are discussed in considerable detail in a later section.

64-406

VOL. I APP.
SEC. III

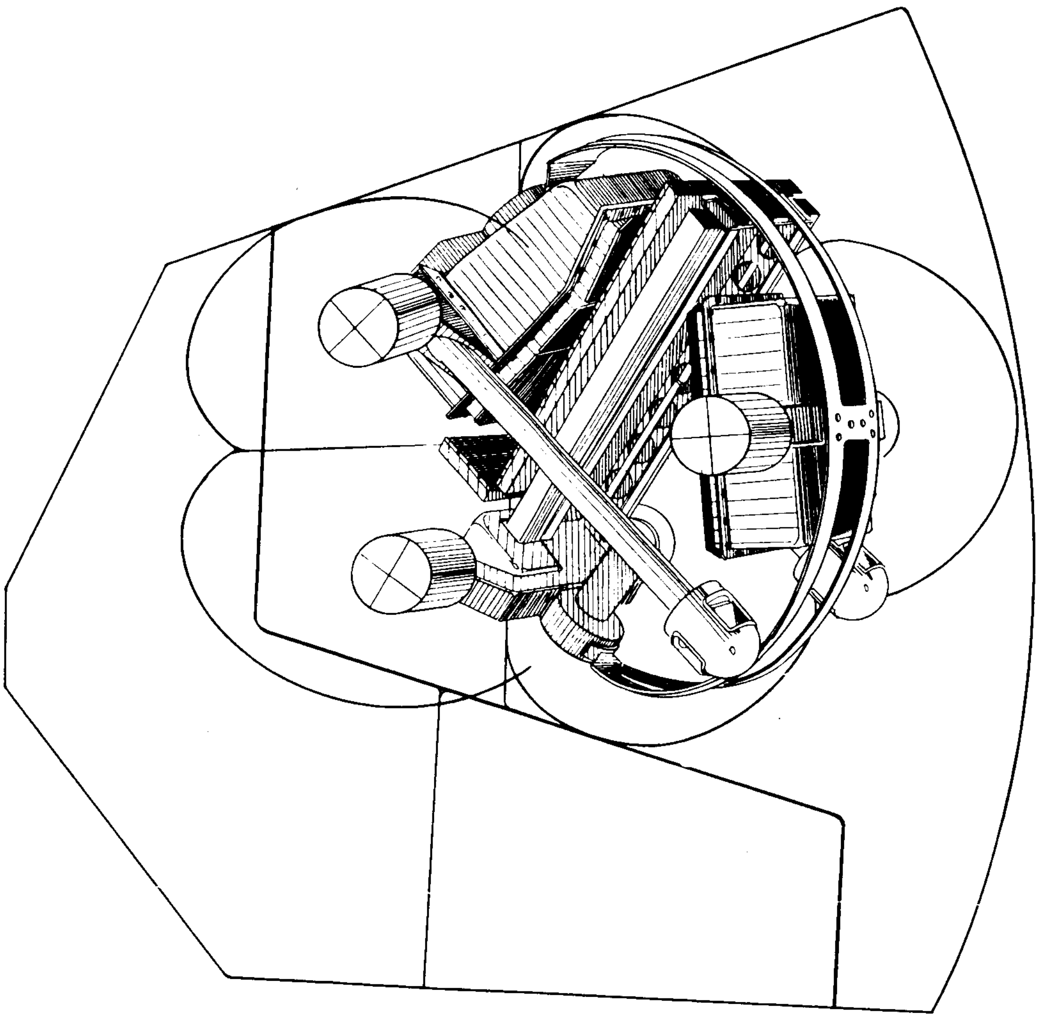

Fig. III. 1-29. Stowed Configuration in Allowable Space Envelope, Top View

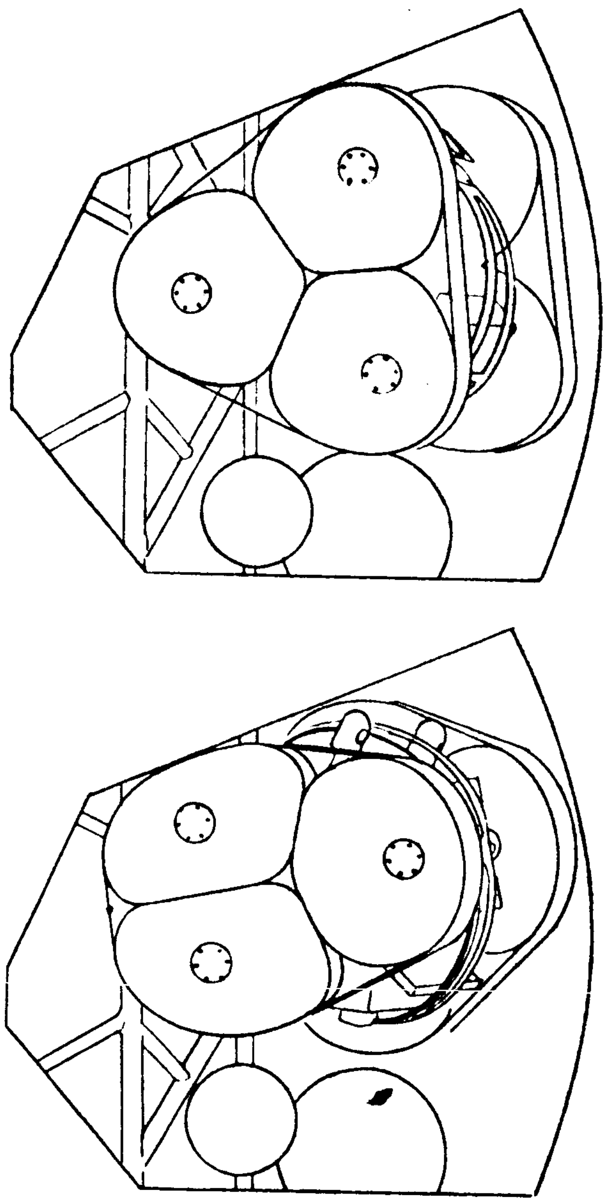

(a) (b)

Fig. III.1-30. Considered Stowage Configurations Mounted On Surveyor Frame

4. Proposed Configuration

SUMMARY OF CONCLUSIONS

Based on the foregoing considerations regarding mobility performance, lunar terrain characteristics, and payload envelope limitations, it was determined that the proposed SLRV should have the following general characteristics:

(1) Capability of being stowed on the current Surveyor in a space approximately 3 ft x 2. 5 ft x 2 ft, within the envelope and center of gravity location constraints given in HAC Specification No. 239503

(2) Maximum gross vehicle weight of 75 Earth pounds (12. 5 lb lunar), including payloads such as soil-properties-measuring instrument, stadia rod for topographical survey, communication equipment, etc.

(3) Simplicity of design for reliable operation

(4) Ability to cross the weakest specified soil with minimum motion resistance

(5) Ability to negotiate obstacles large in comparison to vehicle size

(6) Ability to keep all vehicle tractive elements in contact with the ground even in the case of severe surface undulations

(7) High degree of maneuverability

(8) Identical operational characteristics in forward and reverse

(9) Reliability and ease of deployment from Surveyor frame to the lunar surface

To fulfill the foregoing requirements, it was decided that the preferred configuration should be a three-element articulated wheeled vehicle with as large and as highly elastic wheels as practicable. Furthermore, it was determined that articulation should be accomplished by providing the vehicle with a flexible frame that would permit large amounts of roll and pitch.

This type of construction, together with the elastic characteristics of the wheels, would permit a vehicle of relatively large physical size to be folded within the given space envelope without the necessity of providing mechanisms to collapse the wheels or fold the frame. In addition, the freedom in pitch and roll between axles would greatly improve overall mobility by permitting individual wheel loadings to remain essentially equal over a wide range of surface unevenness; this also results in excellent obstacle-crossing ability.

As a result of these considerations, the vehicle configuration shown in Fig. III. 1-31 was chosen for further development. Specifications and characteristics for the proposed vehicle are summarized in Table III. 1-1. (Unless otherwise stated, all values following are in terms of lunar equivalents.)

DESCRIPTION

The vehicle is a six-wheeler in three units coupled together with a pair of thin flexible bars. It is symmetrical fore and aft about the center unit in order to obtain identical performance and operational characteristics in forward and reverse. Nominal maximum vehicle speed is approximately 0.75 ft/sec.

Overall length and width are 72 inches and 36 inches respectively. Distance between axles is 27 inches and the tread is 28 inches.

Angles of approach and departure are a minimum of 120°, and the outline of the payload compartments on the front and rear axles are a minimum of 3 inches inside the wheel circumference outline, at and below the axle centerline.

The bottoms of the compartments are provided with skids or runners for protection when running over obstacles.

Minimum ground clearance under the payload compartments is 6 inches when the wheels are deflected in the static condition.

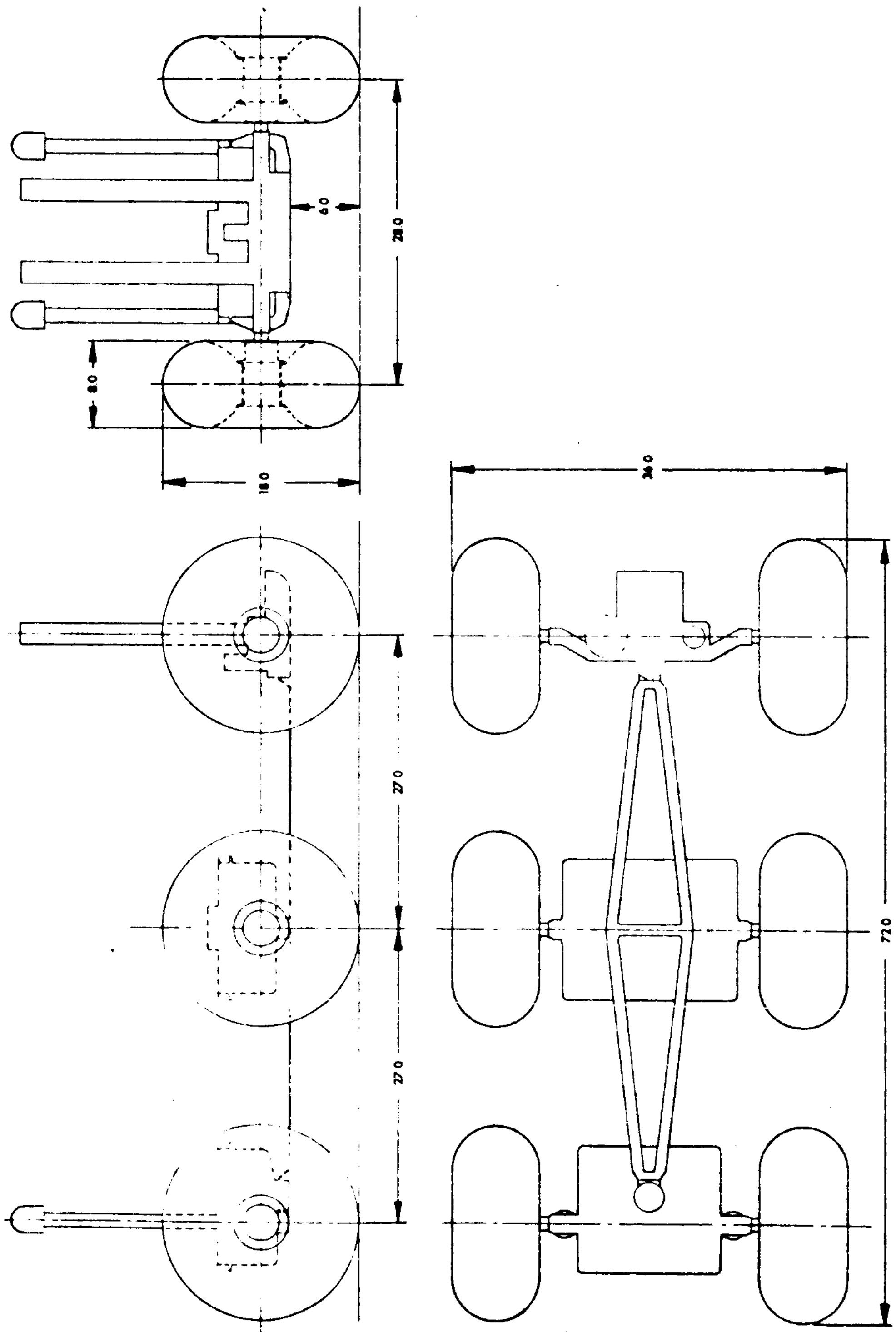

Fig. III. 1-31. Outline of Proposed Vehicle Configuration

TABLE III. 1-1

SURVEYOR LUNAR ROVING VEHICLE CHARACTERISTICS AND SPECIFICATIONS

General	
Gross Weight	12. 5 lb(lunar)
Length, Overall	72 in.
Width, Overall	36 in.
Wheel Base	27 in.
Tread	28 in.
Wheel Diameter	18 in.
Wheel Width	8 in.
Ground Contact Area, Per Wheel	31. 5 sq in.
Ground Contact Pressure	0. 065 psi
Ground Clearance	6 in. (min)
Hang-up Radius	5. 6 in.
Angle of Approach	120°(min)
Angle of Departure	120°(min)
Center of Gravity (above axle centerline)	3 in. (max)
Performance	
Lateral Stability, Static	45°(min)
Gradeability ($\mu > 0.7$)	45°
Steering Radius, Wall-to-Wall (30° steering angle)	71. 5 in.
Tracking Encroachment (30° steering angle)	6 in. (max)
Speed, Nominal	0. 75 fps (max)
Obstacle Crossing Ability (for $\mu = 0.8$)	
Vertical Step	30 in.
Crevice, Spanning	20 in.
Wheel Drive Requirements	
Nominal Torque, Per Wheel (at 10 rpm)	6 in. -lb
Torque, Per Wheel (at 2 rpm)	50 in. -lb
Stall Torque, Per Wheel	60 in. -lb
Steering Driving Characteristics	
Nominal Torque, Per Axle (at 2 rpm)	33 in. -lb
Stall Torque, Per Wheel	100 in. -lb

Gross vehicle weight is 75 Earth pounds or 12.5 lunar pounds, and is distributed fairly equally over the six wheels.

The vertical centers of gravity of the individual units are a maximum of 3 inches above the axle centerlines.

Wheel Characteristics

Wheel diameter and width are 18 inches and 8 inches respectively. Hub diameter is a maximum of 5 inches. Under static conditions, wheel deflection is on the order of 0.5 inch, resulting in a ground contact-area (per wheel) of 31.5 sq in. and an average ground pressure of 0.065 psi. This is achieved with a wheel effective-spring-rate of 4 lb/in.

As shown in Fig. III. 1-32 this extremely low ground loading results in minimal vehicle motion resistance, even for extremely weak soils. At the specified soil condition (k_c=o, n=1, ϕ=20^o, c=o, k_ϕ=0.083) the motion resistance is only approximately 8% of vehicle weight, while the drawbar pull is over 25% of vehicle weight. This signifies the ability of the vehicle to climb slopes of approximately 25% even if composed of soft, loose soil. Furthermore, the wheel is able to be deflected 4 inches for stowage purposes without overstressing the wheel spring wires.

Wheel Drive Characteristics

It is assumed that the nominal maximum vehicle speed will be 0.75 ft/sec. This requires a wheel speed of 10 rpm at zero slip. For an assumed Resistance/Weight ratio of 0.3, each wheel requires a nominal torque input of 6 in.-lb.

Stall torque at the wheel is on the order of 60 in.-lb., and 50 in.-lb. is available at a wheel speed of 2 rpm.

Each wheel drive is provided with a device that permits the wheel to become free-wheeling in case of motor or drive-line failure.

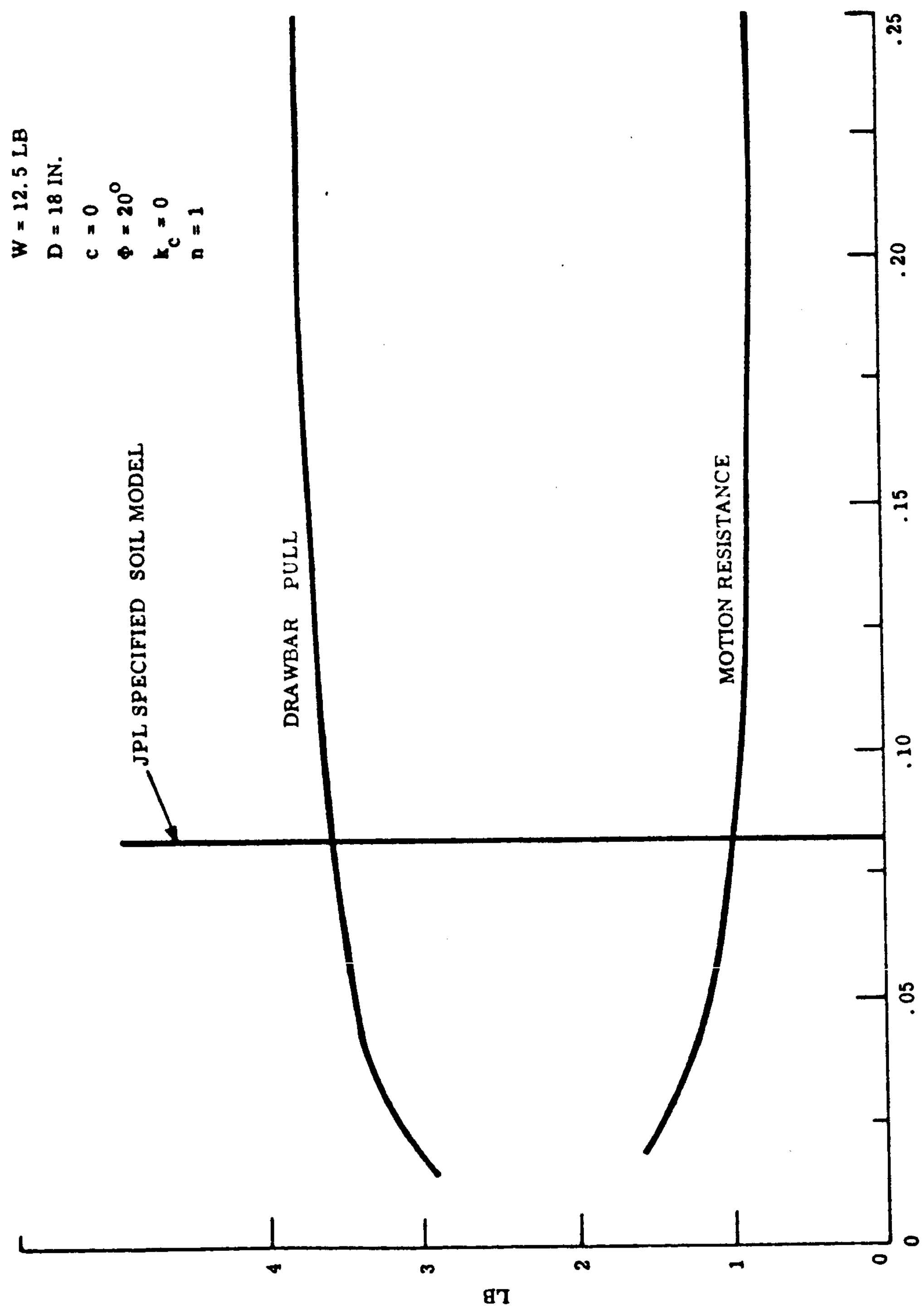

Fig. III. 1-32. Soft Ground Performance of Proposed Surveyor Lunar Roving Vehicle

Steering Characteristics

Both front and rear axles will be steered simultaneously. Synchronization is provided at the straight-ahead position, and at each 7.5^{o} increment up to the maximum steering angle. The steering pivots are located about 2.5 inches from the axle centerline (aft of front axle and in front of rear axle.) The maximum steering angle is at least 30^{o}. These conditions result in a wall-to-wall turning radius of 71.5 inches and a maximum tracking encroachment of the center wheels of 6 inches.

Steering Drive Characteristics

Nominal steering torque required is based on an assumed coefficient of friction of 0.5 when the vehicle is in motion. For equal wheel loading, this results in a torque requirement per axle of 33 in.-lb. Under these conditions speed of steering should be about 2 rpm.

For steering when the vehicle is stationary, and keeping in mind that no differential action exists between wheels, the torque requirement is on the order of 100 in.-lb.

In case of failure of a steering motor, a device rotates the axle back to its zero position and locks it there. Steering is then accomplished by the remaining motor.

A system is also provided whereby some or all of the wheels on one side of the vehicle can be disengaged, stopped, or reversed, resulting in a differential torque between the sides of the vehicle. This would enable skid steering to be used in case of total failure of the primary steering system.

Elastic Frame Characteristics

In order to obtain an optimum compromise between the requirements for payload compartment volume and mobility performance, the bottom of the elastic frame is 6 inches above the ground when the wheels are in their deflected condition.

Free length of the elastic frame between axles is approximately 24 inches, and the effective spring rate of the frame is on the order of 0.25 lb/in. This gives the vehicle the ability to climb vertical-step obstacles 30 inches high and to cross crevices 20 inches wide with vertical faces and a hard surface.

Furthermore, the frame stiffness in roll permits a minimum axle rotation of $\pm 45^{o}$; payload compartments are shaped in such a manner as to permit the necessary amounts of roll and pitch.

FULL-SIZE MOBILITY MODEL

In order to further evaluate the obstacle and mobility performance of the proposed vehicle, as well as to study stowage and deployment problems, a full-size powered model with simulated equipment compartments of maximum volume was constructed using lunar-wheel and elastic-frame spring stiffnesses. Sequence photos of the model automatically deploying from the Spacecraft and unfolding are shown in Figure III.1-33, and photographs of the model, showing pitch and roll characteristics are given in Figure III.1-34.

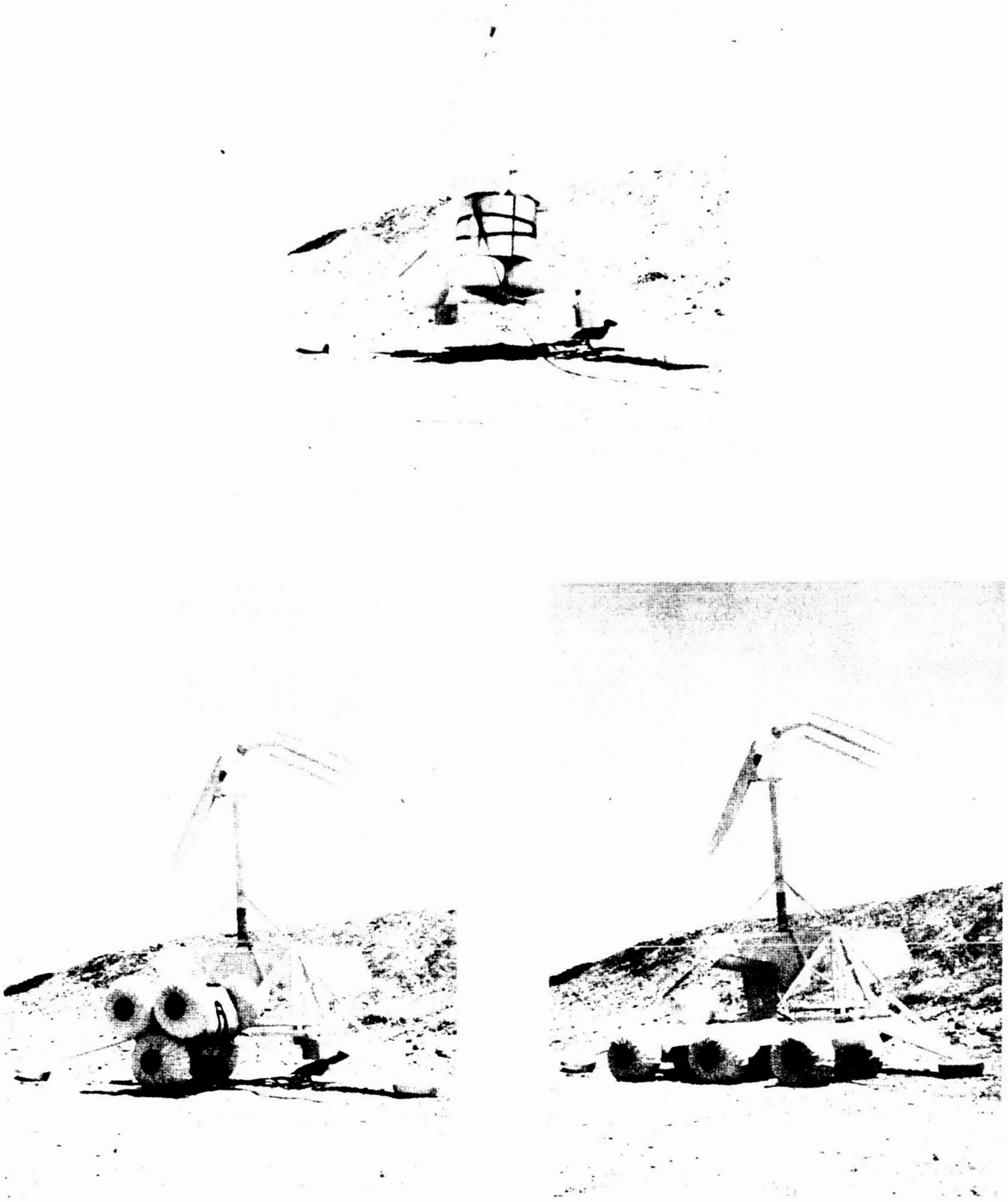

Fig. III. 1-33. Deployment Sequence of Surveyor Lunar Roving Vehicle

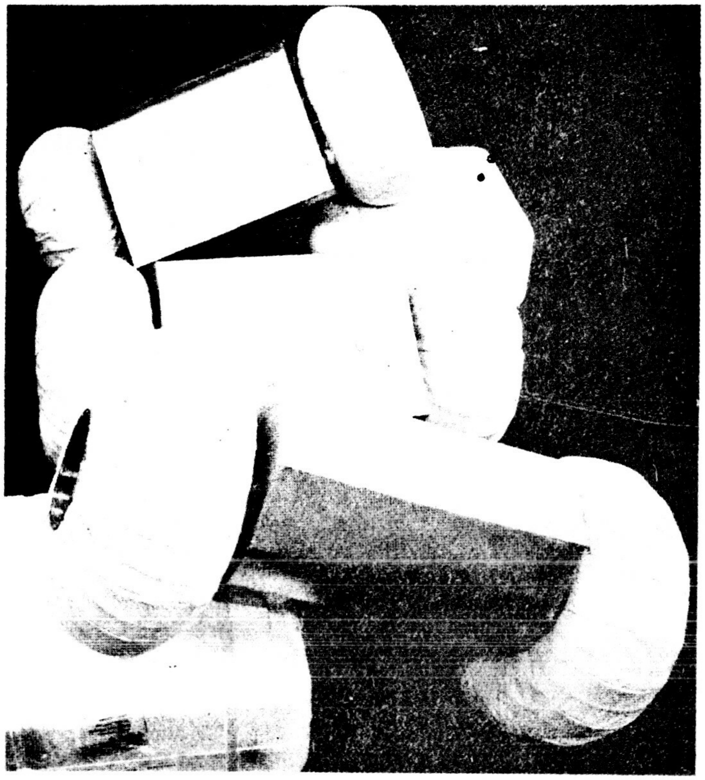

(a)

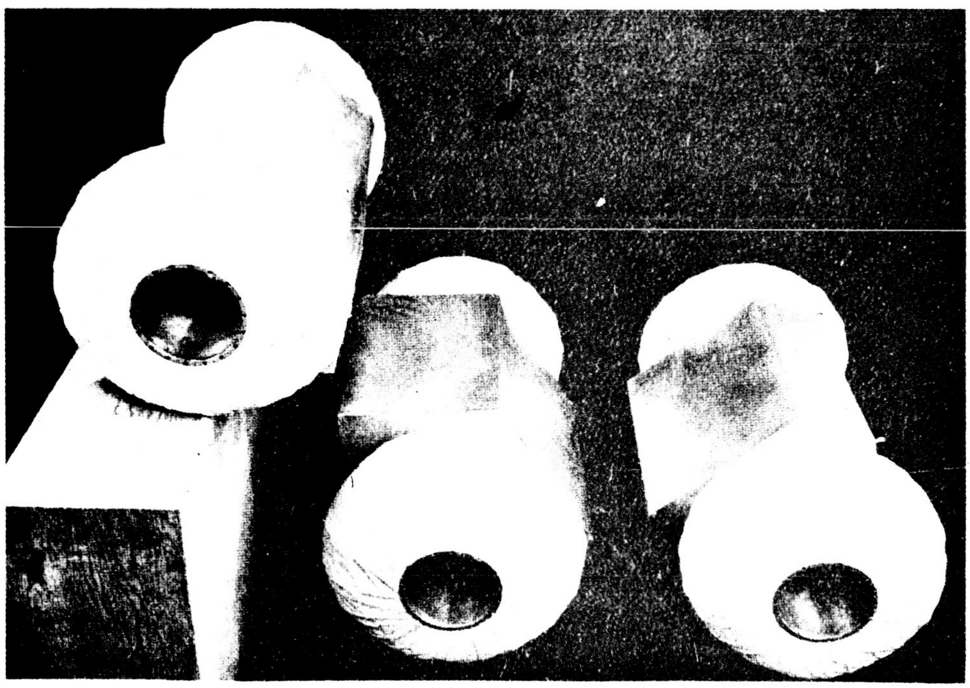

(b)

Fig. III. 1-34. Pitch and Roll Characteristics of Surveyor Lunar Roving Vehicle

References

(1) M. G. Bekker,"A System of Physical and Geometrical Soil Values for the Determination of Soil Trafficability and Vehicle Performance," Vehicle Mobility Symposium, Office of Ordinance Research and Stevens Institute of Technology. Published by Land Locomotion Research Laboratory, Army Tank-Automotive Command, Detroit, Michigan, 1955.

(2) "A Soil Value System for Land Locomotion Mechanics," Land Locomotion Research Laboratory, Army Tank-Automotive Command, Research Report No. 5, Detroit, Michigan, 1958.

(3) M. G. Bekker, Off-the-Road Locomotion - Research and Development in Terramechanics, The University of Michigan Press, Ann Arbor, Michigan, 1960.

(4) M. G. Bekker, Theory of Land Locomotion - The Mechanics of Vehicle Mobility, The University of Michigan Press, Ann Arbor, Michigan, 1957.

(5) Z. Janosi, and B. Hanamoto, "The Analytical Determination of Drawbar Pull as a Function of Slip for Tracked Vehicles in Deformable Soils," Proceedings of the 1st International Conference on the Mechanics of Soil-Vehicle Systems, Edizioni Minerva Tecnica, Torino, Italy, June, 1961.

(6) J. L. Bogdanoff, and F. Kozin, "On the Statistical Analysis of Linear Vehicle Dynamics," Proceedings of the 1st International Conference on the Mechanics of Soil-Vehicle Systems, Edizioni Minerva Tecnica, Torino, Italy, June 1961.

(7) I. J. Sattinger, and S. Sternick, "An Instrumentation System for the Measurement of Terrain Geometry," Proceedings of the 1st International Conference on the Mechanics of Soil-Vehicle Systems, Edizioni Minerva Tecnica, Torino, Italy, June, 1961.

(8) V. P. Head, "A Lunar Surface Model for Engineering Purposes," American Rocket Society Paper No. 2475-62 (Presented at Semi-Annual Meeting on Lunar Missions, Cleveland, Ohio, 17–19 July, 1962).

(9) G. P. Rettig, and M. G. Bekker, "Obstacle Performance of Wheeled Vehicles," Land Locomotion Laboratory, Army Tank-Automotive Command, Research Report No. 29, Detroit, Michigan, March 1958.

(10) M. G. Bekker, "Mechanics of Off-the-Road Locomotion," the James Clayton Lecture (paper presented at the Institution of Mechanical Engineers, London, England, 13 November 1962).

(11) M. G. Bekker, "Land Locomotion on the Surface of Planets," Am. Rocket Soc. J., Vol. 32, No. 11, Nov 1962, pp. 1651-1659.

(12) M. G. Bekker, "The Evolution of Locomotion," (paper delivered at the Annual Meeting of American Society of Mechanical Engineers, Nov. 1961)

(13) J. D. McKenney, "Investigation for a Walking Device for High Efficiency Lunar Exploration," (presented at American Rocket Society Annual Meeting, New York, New York, 9–15 Oct. 1961)

(14) M. G. Bekker, "Is The Wheel The Last Word in Land Locomotion?" New Scientist, Vol. II, No. 248, London, August 1961

(15) J. Gray, How Animals Move, Cambridge University Press, Cambridge, 1959

(16) M. G. Bekker, "Methods of Evaluation of Off-the-Road Locomotion," Operations Res. Office, Johns Hopkins University, TM-217, Washington, D. C., 1953

B. SLRV OBSTACLE-PERFORMANCE ANALYSIS

INTRODUCTION

An analytical and experimental study was undertaken by GM DRL's Mobility Research Laboratory to investigate the obstacle and crevice-crossing capabilities of the 6 x 6 flexible frame vehicle concept proposed for SLRV. The investigation consisted of a theoretical analysis of the elastic frame-obstacle characteristics and a laboratory test program using the SLRV Mobility Investigation Model.

Theoretical Analysis

A simplified analysis was made for expressing the maximum step obstacle height a vehicle provided with an elastic frame may negotiate. The equations of obstacle crossing were obtained by applying the conditions of static equilibrium only, neglecting dynamic effects in the interest of simplicity. Since vehicles are usually operating at low speeds when crossing high obstacles, this assumption does not appear to be objectionable.

As a result of this analysis the following relations were obtained for the limiting obstacle height of a 6 x 6 flexible frame vehicle:

(a) condition $h < r$

$$\frac{h}{r} = 1 - \frac{1 - 2\mu^2}{\sqrt{1 + 5\mu^2 + 4\mu^2}}$$

(b) condition $h > r$

$$\frac{h}{r} = 1 + \frac{C}{1 + \mu^2}\left(2\mu^2 + \frac{15}{4}\frac{r}{L}\mu^2 - 1\right)$$

where $C = \frac{2}{3}\frac{WL^3}{EIr}$

EXPERIMENTAL INVESTIGATION

A test program was conducted using the full-scale mobility model of the SLRV to further investigate the obstacle and crevice-crossing capability of the vehicle as affected by various factors and to provide a basis for trade-off studies in the design program of the SLRV.

The self-propelled, full-scale mobility model was designed so that the vehicle configuration could easily be changed.

Adjustable height, solid, vertical obstacles were used in the test program. The maximum negotiable obstacle height and crevice width was determined on the basis of "go" and "no go" experiments with an accuracy of one (1) inch.

The factors which can effect the obstacle and crevice performance are as follows:

(a) Surface friction coefficient
(b) Flexible frame stiffness
(c) Gross vehicle weight
(d) Axle load distribution
(e) Wheelbase
(f) Location of C.G.

(a) The effect of the surface friction coefficient is shown in Fig.III.1-35. Experimental results of obstacle performance for flexible frame vehicle, semi-flexible frame vehicle, and rigid frame vehicle of the same size and weight are shown on the graph.

(b) The effect of the stiffness of the flexible frame was investigated by changing the thickness of the leaf springs connecting the three axles. A wide range of frame stiffness – from the completely rigid (C = 0) to a highly flexible (C = 6) condition was covered in the test program. The test results are plotted in Fig.III.1-36. The sudden drop in obstacle performance beyond C = 4 is due to the buckling of the spring frame. The opposite effect of frame stiffness on obstacle and crevice performance can be clearly seen.

(c) The effect of gross weight (at equal axle load distribution) was investigated by changing the vehicle weight from 24 to 54 lbs. with all other parameters kept constant. It is evident from the results (Fig.III.1-37 that both obstacle and crevice performance are independent of vehicle weight. The same conclusion was arrived at in the theoretical analysis.

(d) The effect of axle load distribution was investigated by overloading one of the three axles at a time keeping the other two axle loads constant. The test results are presented in Fig.III.1-38. It can be seen from the graph that the overloading of the center unit results in the least amount of drop in obstacle performance. Overloading the rear unit is the most detrimental and therefore it should be avoided.

When the overload of the center unit was transferred to the front and rear units by means of prestressing the flexible spring frame, no detrimental effect on obstacle performance was found (see dotted line in Fig.III.1-38.

(e) The effect of wheelbase on obstacle and crevice performance is shown in Fig.III.1-39. The drop in obstacle performance beyond L = 27 inches is due to the hang-up on the frame between the axles.

(f) The location of C.G. in the vertical direction also effects obstacle performance as shown in Fig.III.1-40.

In addition to the test program conducted to determine the effects of various factors on obstacle performance as described in (a) to (f) above, a series of experiments were performed, to help to determine wheel drive torque requirements in obstacle crossing. The vehicle model was instrumented for this purpose to be able to measure wheel torque and wheel slip on all three axles independently. Obstacle crossing tests were then conducted for obstacle heights ranging from 4 to 32 inches and the torque on all three axles were recorded as a function of elapsed time. Typical torque curves for obstacle crossing are shown in Figs.III.1-41 and III.1-42 for 18 and 32 inches high obstacles respectively.

For energy calculation purposes the average obstacle crossing resistance was determined then from these test results and plotted as a function of obstacle height in Fig.III.1-43.

The average slip i obstacle climbing as a function of obstacle height is presented in Fig.III.1-44.

CONCLUSIONS

1. The gross vehicle weight does not effect obstacle performance.
2. At surface friction coefficients higher than 0.6, the obstacle capability of the vehicle is 32 inches.
3. The optimum flexible frame stiffness is between 2.5 and 3.5.
4. If equal axle load distribution is not possible then consideration should be given to design the center unit heavier, rather than the front or rear units.
5. The optimum wheelbase was found to be L = 27 inches.
6. The location of C.G. should be less than 3 inches above the wheel axis.

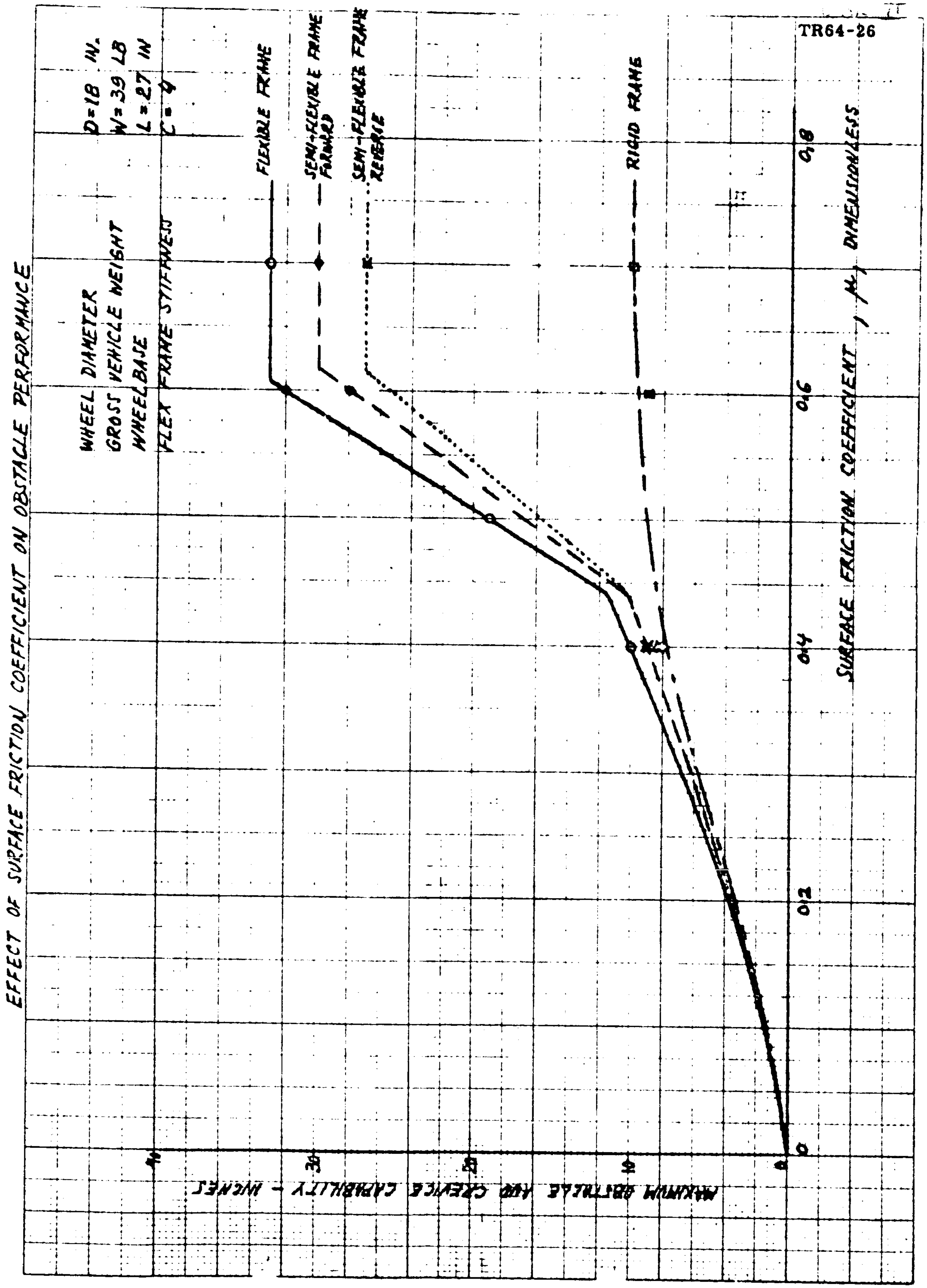

Figure III.1-35

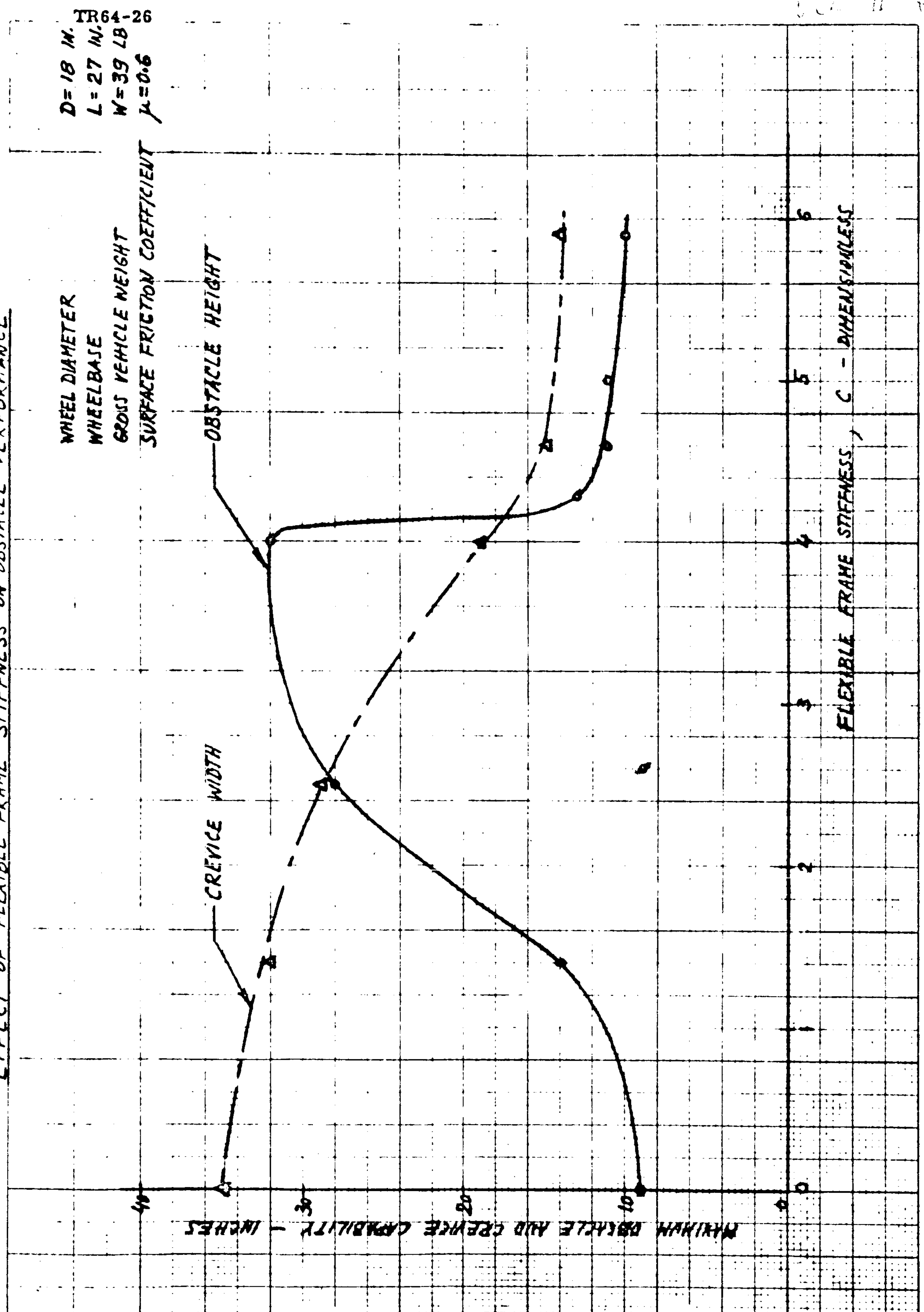

Figure III.1-36

77

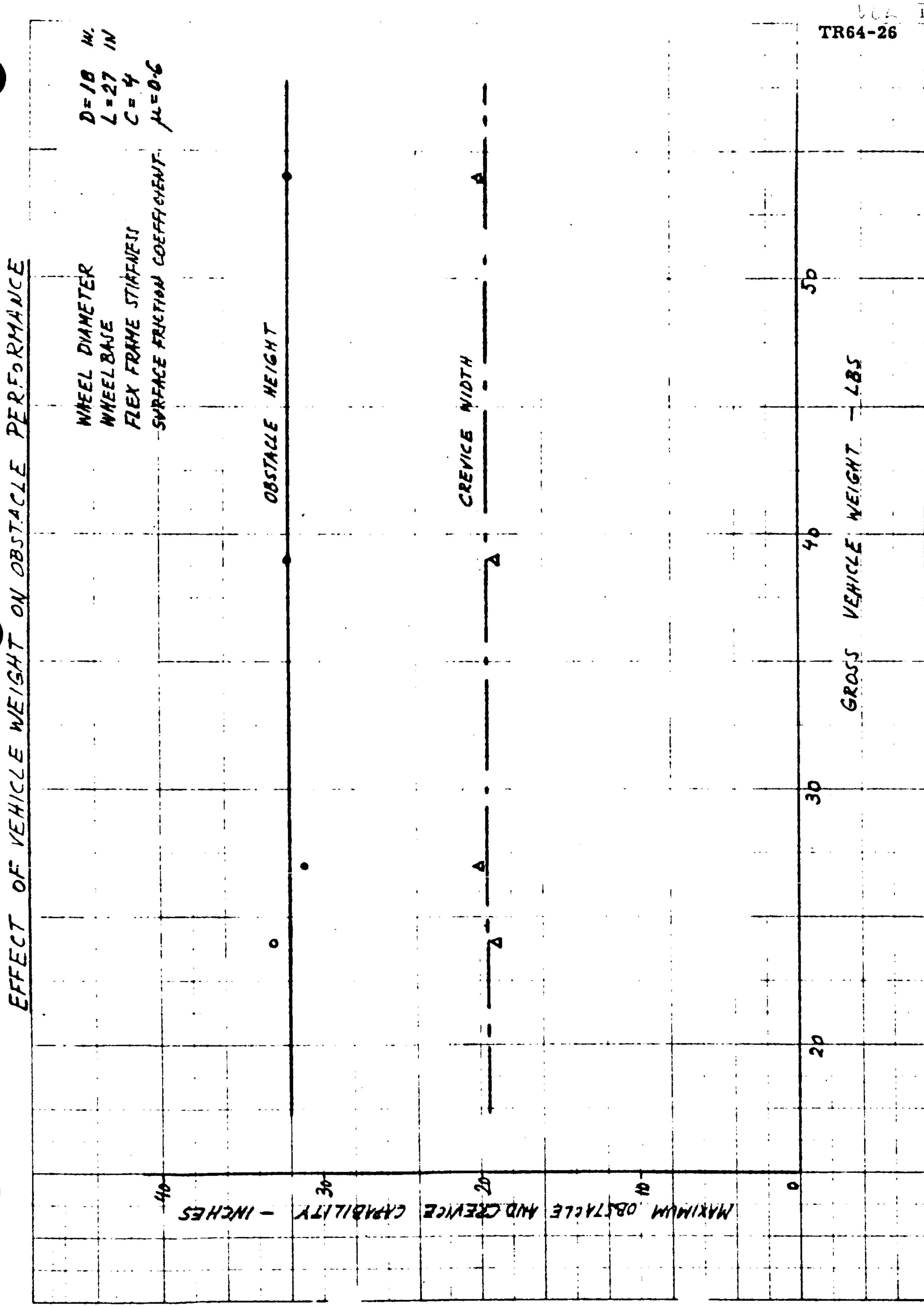

Figure III. 1-37

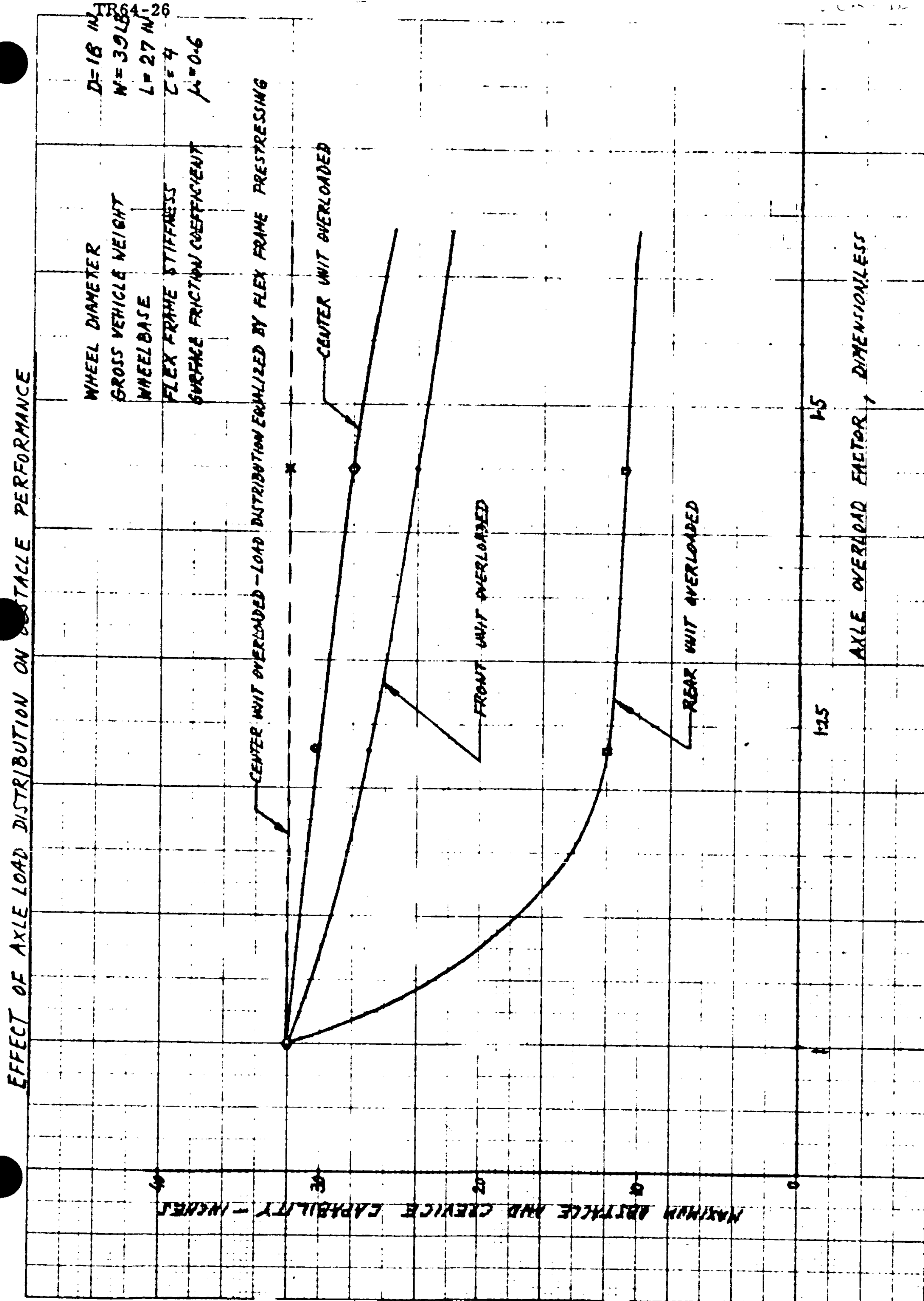

Figure III.1-38

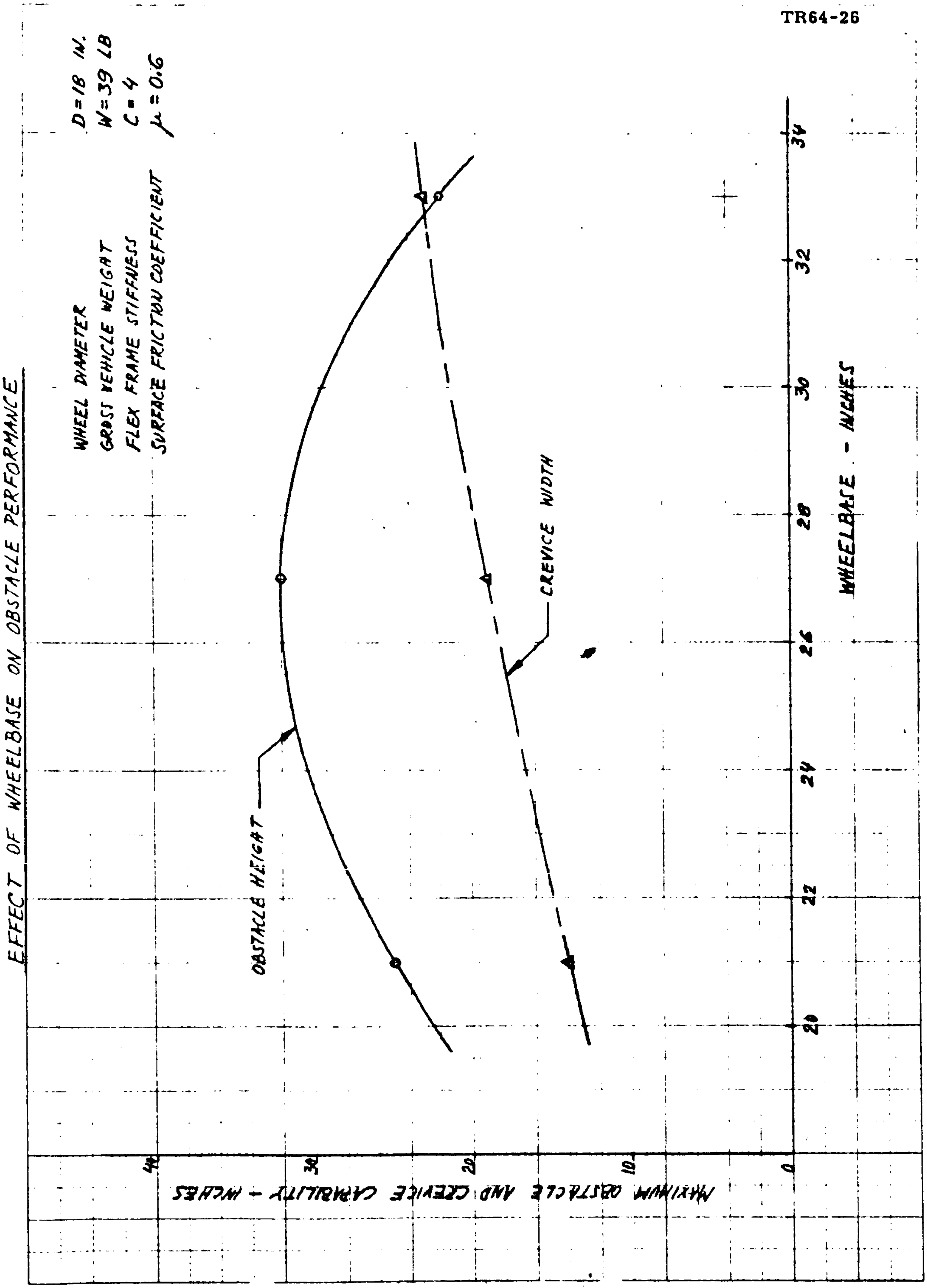

Figure III. 1-39

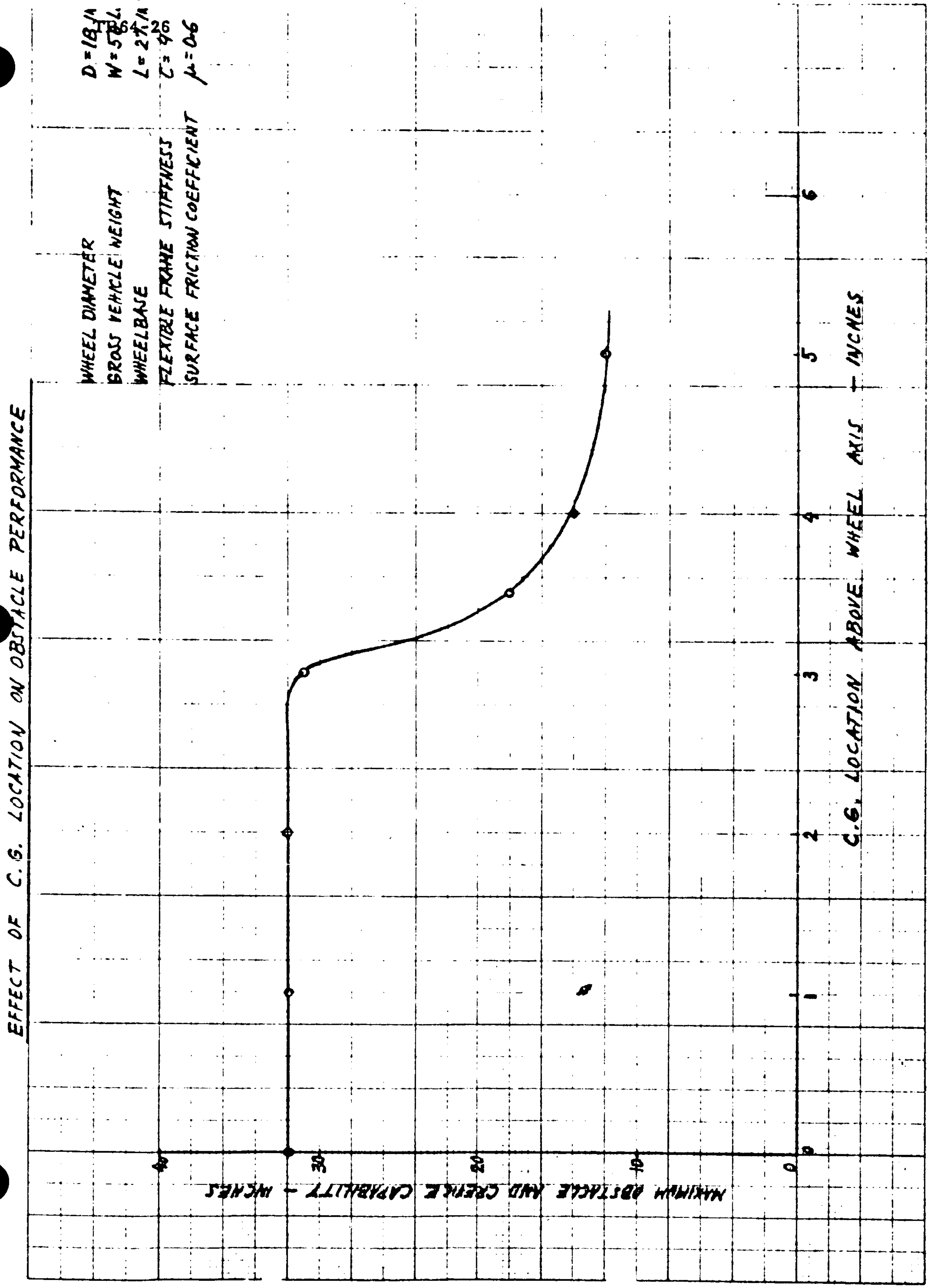

TR64-26
EFFECT OF C.G. LOCATION ON OBSTACLE PERFORMANCE
WHEEL DIAMETER D=18 IN
GROSS VEHICLE WEIGHT
WHEELBASE
FLEXIBLE FRAME STIFFNESS
SURFACE FRICTION COEFFICIENT μ=0.6
C.G. LOCATION ABOVE WHEEL AXIS — INCHES
0
1
2
3
4
5
6
MAXIMUM OBSTACLE AND CREVICE CAPABILITY — INCHES
0
10
20
30
40

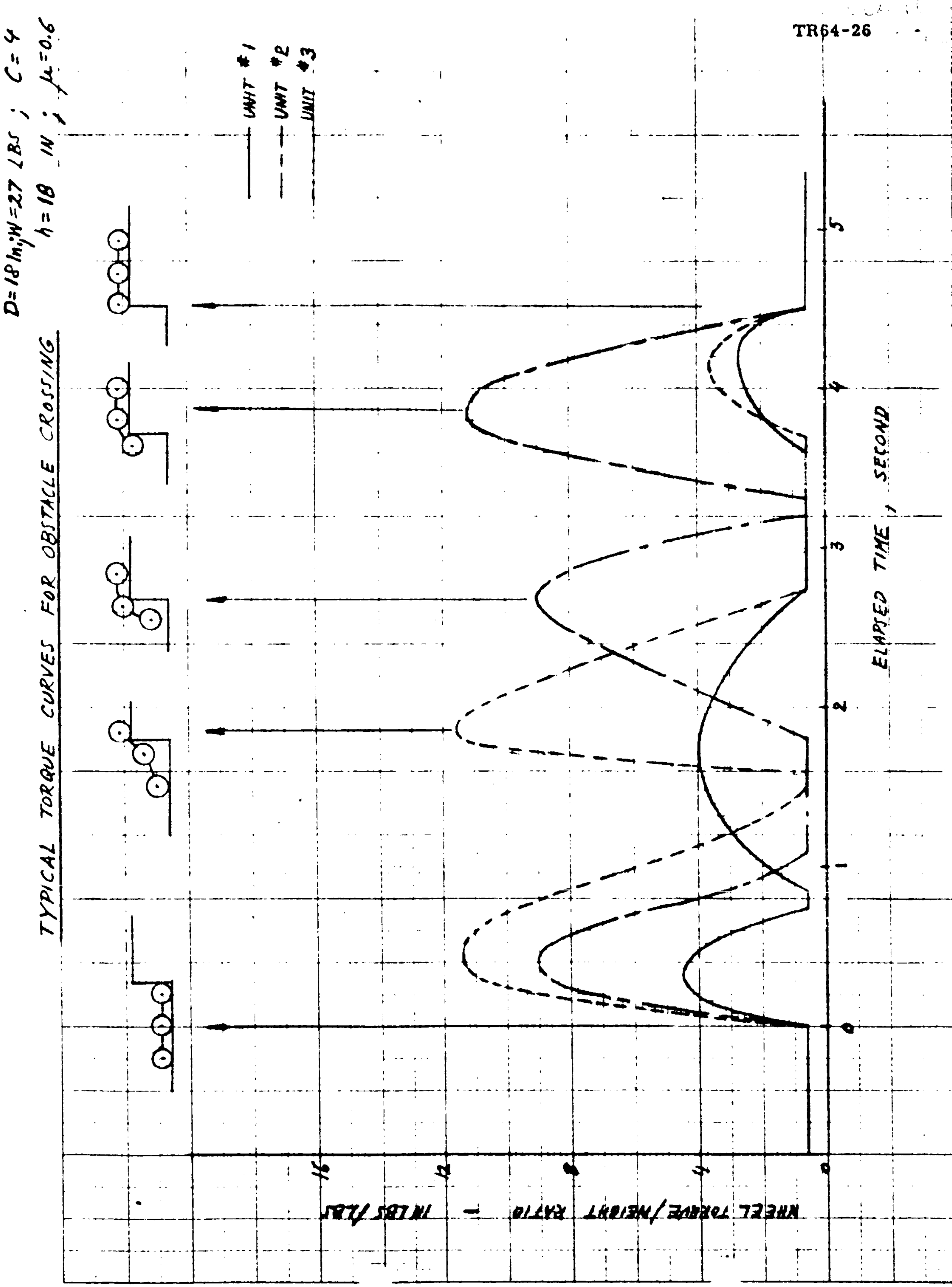

Figure III. 1-41

TR64-26

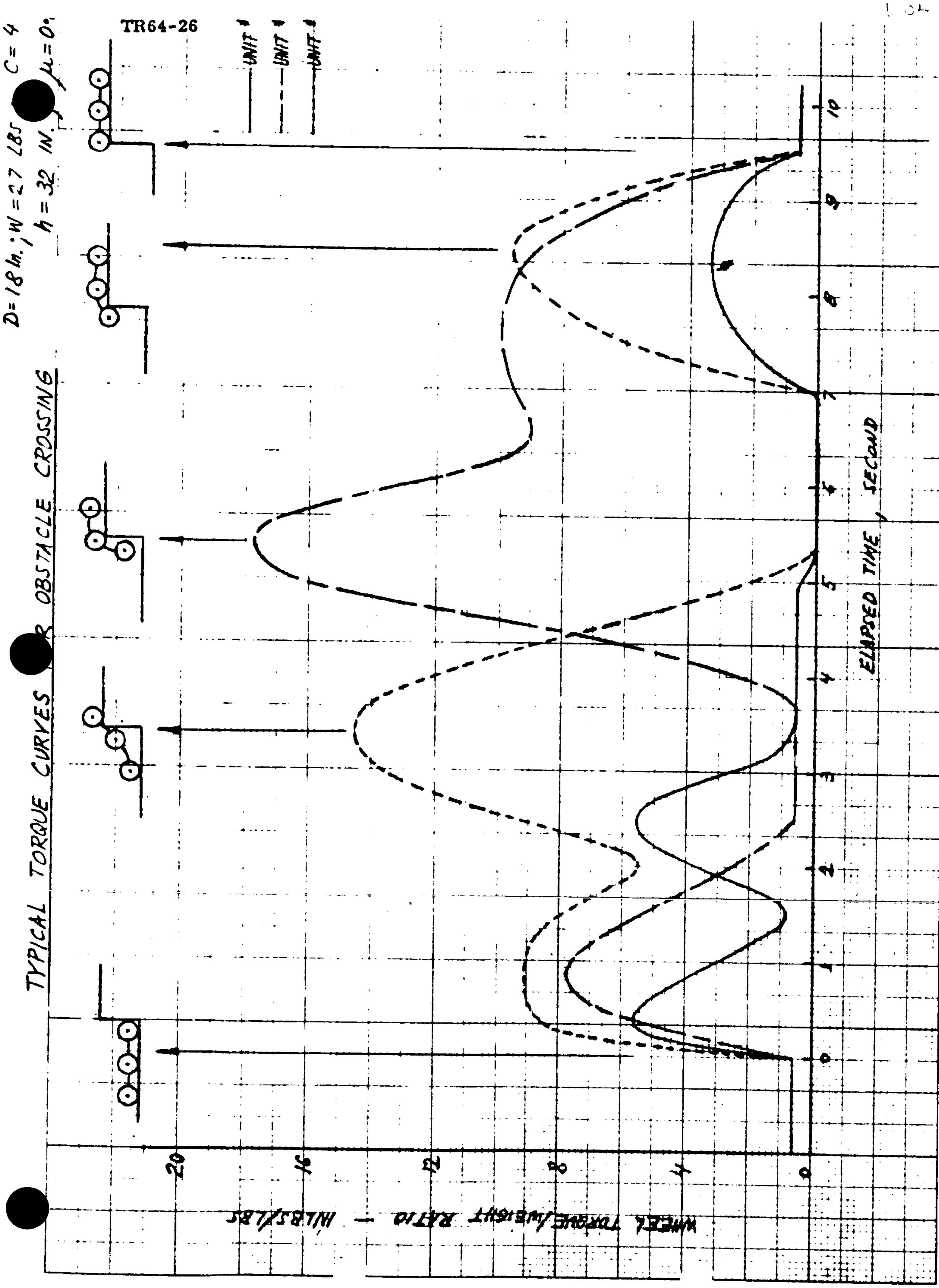
TYPICAL TORQUE CURVES FOR OBSTACLE CROSSING
D = 18 in.; W = 27 LBS; C = 4
h = 32 IN.; μ = 0
UNIT
UNIT
UNIT
ELAPSED TIME, SECOND
0
1
2
3
4
5
6
7
8
9
10
WHEEL TORQUE/WEIGHT RATIO – IN.LBS/LBS
0
4
8
12
16
20

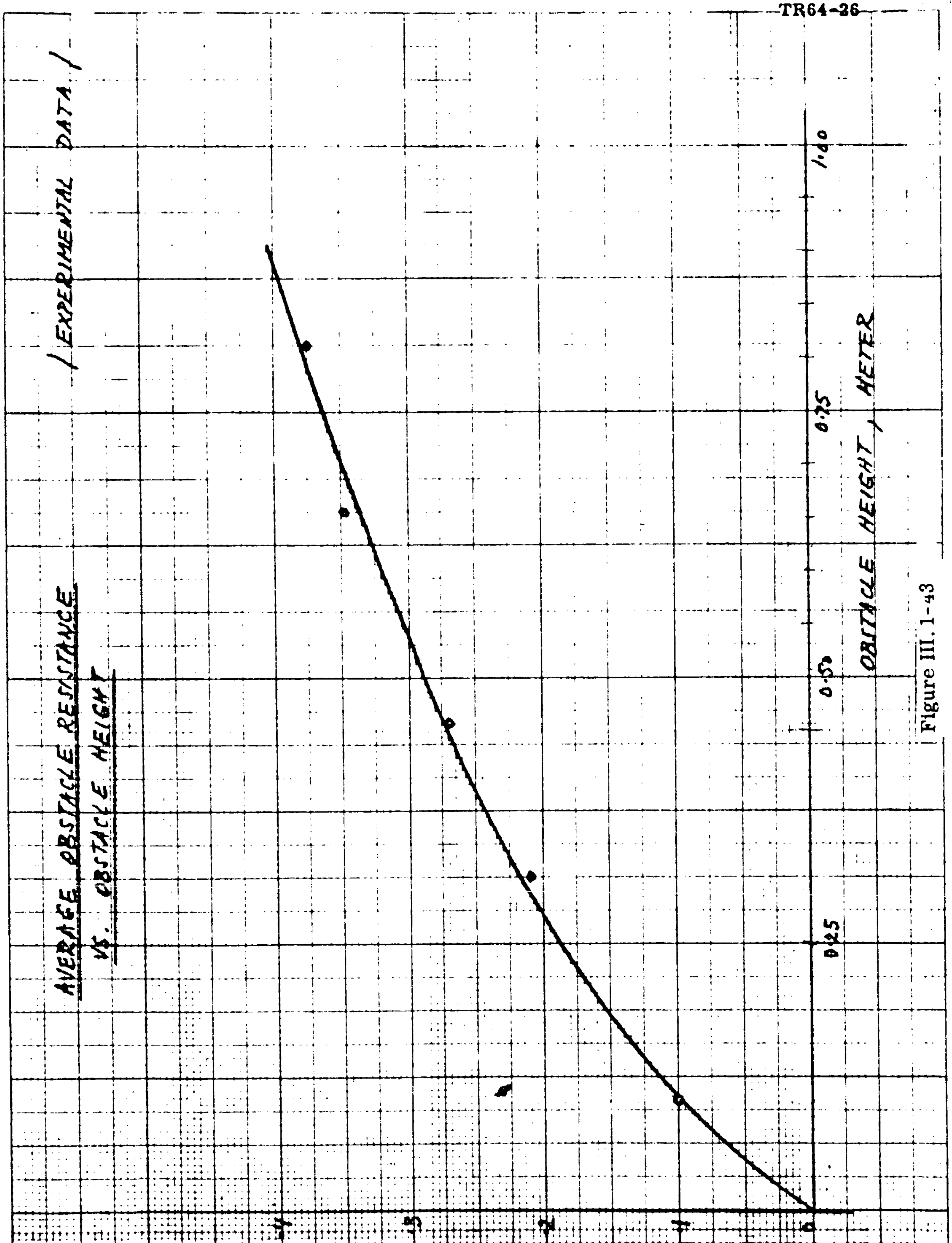

Figure III. 1-43

20 x 20 PER INCH

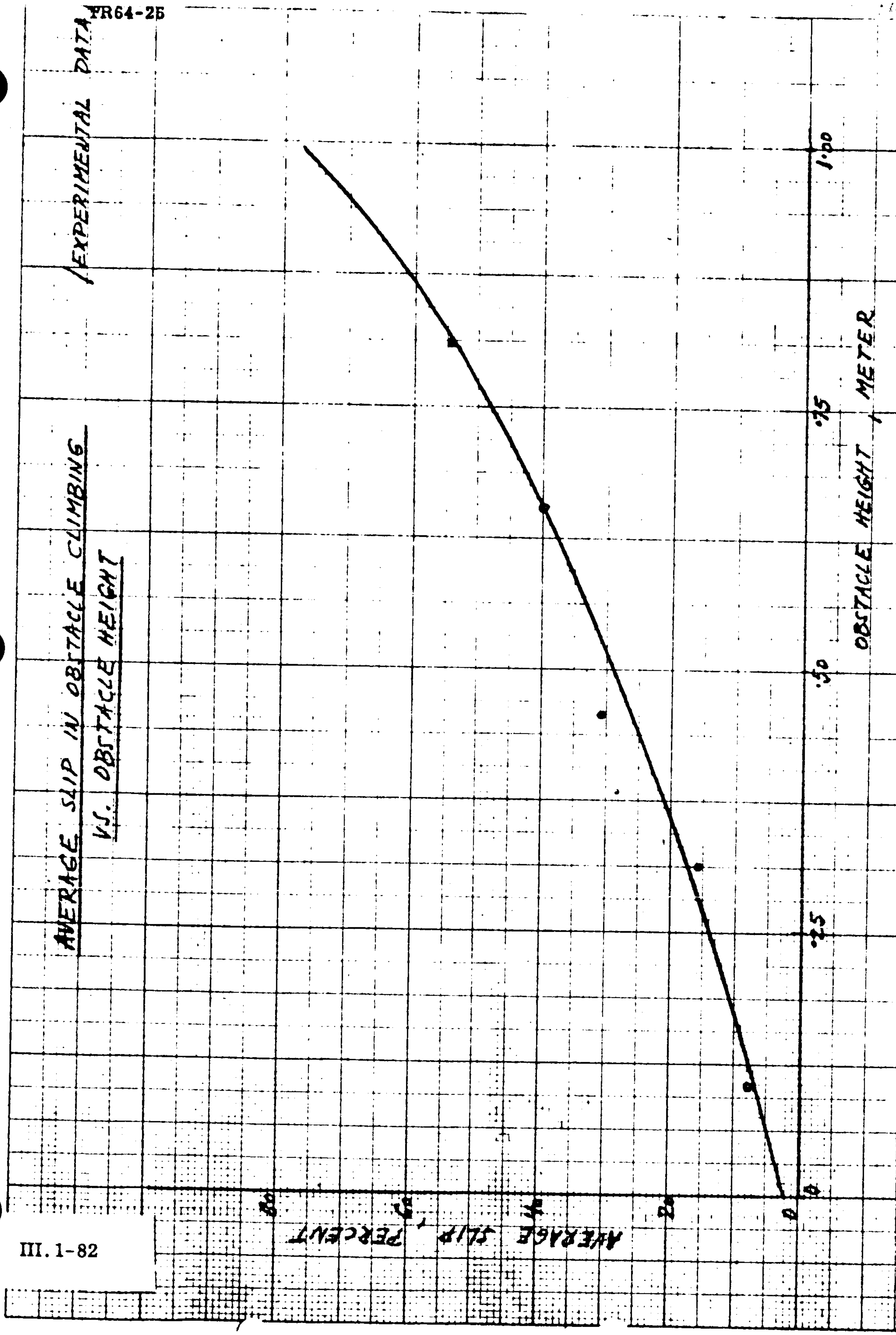

Figure III.1-44

A simplified analysis is presented here for predicting the obstacle height which a vehicle provided with an elastic frame may negotiate.

The equations of obstacle performance are obtained by applying the conditions of static equilibrium only. Various dynamic effects which are present in actual vehicles are neglected in the interest of simplicity. This assumption does not appear to be objectionable for the purposes of this analysis, since the vehicles are usually operating at low forward speeds when crossing high vertical obstacles.

For this study the EFV is considered to consist of three equally loaded axle assemblies connected by a massless elastic frame. The wheels of the vehicle are assumed to be rigid, i. e., the deformations of the pneumatic tires are neglected for reasons of simplification. All six wheels of the vehicle are supposed to be driven, and the stiffness of the elastic frame is the same along the entire frame. It is also assumed that the vehicle is operating on a hard, friction-type surface of a known coefficient of friction.

In considering the obstacle performance of the EFV it is found that two cases exist depending on the height h of the obstacle and the radius r of the wheel. These two conditions are as follows:

Condition $h < r$

A vehicle climbing a vertical obstacle is shown schematically in Figure III. 1-45. Let W be the total load carried by each axle assembly, and ℓ be the distance between two consecutive axles. The effective coefficient of friction between the tire and ground is denoted by μ. Other symbols are as indicated in the figure.

For the condition of equilibrium of the horizontal forces we have

$$\mu(F_3 + F_2) = N\cos\alpha - \mu N\sin\alpha \qquad \text{(III. 1-43)}$$

and the equilibrium of vertical forces yields:

$$3W = F_3 + F_2 + N\sin\alpha + \mu N\cos\alpha \qquad \text{(III. 1-44)}$$

At the onset of obstacle crossing, the vertical force reactions F_2 and F_3 can be assumed to be substantially the same and equal to the axle load. On this basis we obtain

$$F_2 = F_3 = W$$

and solving Equations (III. 1-43) and (III. 1-44) simultaneously gives

$$\frac{\sin\alpha + \mu\cos\alpha}{\cos\alpha - \mu\sin\alpha} = \frac{1}{2\mu}$$

After some obvious manipulation, the angle α is obtained as

$$\tan\alpha = \frac{1-2\mu^2}{3\mu} = \frac{1}{3\mu} - \frac{2}{3}\mu \qquad \text{(III. 1-45)}$$

From the geometry of the system, the obstacle height is given by

$$h = r(1 - \sin\alpha) \qquad \text{(III. 1-46)}$$

Making use of Equation (III. 1-45) and the trigonometric relation

$$\sin x = \frac{\tan x}{\sqrt{1 + \tan^2 x}}$$

the limiting obstacle height is found to be

$$\frac{h}{r} = 1 - \frac{1 - 2\mu^2}{\sqrt{1 + 5\mu^2 + 4\mu^4}} \qquad \text{for} \quad \mu^2 \leq \frac{1}{2} \qquad \text{(III. 1-47)}$$

It is interesting to note that below values of $\mu = \sqrt{1/2}$, the obstacle performance of the EFV depends only upon the friction coefficient μ, and there is no difference in the performance of the EFV regardless of the stiffness parameters involved.

Condition $h > r$

Now a vehicle is considered when the obstacle height h is higher than the wheel radius r. In Fig. III. 1-46 a schematic sketch of such a condition is presented with the front wheel of the vehicle climbing the rigid vertical obstacle.

When the conditions of equilibrium are applied to the whole vehicle, we have for the horizontal forces

$$\mu (F_3 + F_2) = N \qquad \text{(III. 1-48)}$$

and for the vertical forces

$$3W = F_3 + F_2 + \mu N \qquad \text{(III. 1-49)}$$

In this case the performance equations cannot be obtained from the principles of statics alone, and it is thus necessary to consider the stiffness of the elastic frame as a parameter. As illustrated in Figure III. 1-47, the elastic frame may be regarded as a simple beam with a concentrated load and a moment at a distance l from the support. For small deflections of the beam, the longitudinal force is not significant. After introducing the beam reactions at the wheel centers, it is evident that each axle assembly can be considered separately. The free bodies of the individual wheels are drawn schematically in Figure III. 1-48.

The equilibrium of the first wheel yields:

$$P = \mu N - W \qquad \text{(III. 1-50)}$$

$$M = \mu N r \qquad \text{(III. 1-51)}$$

For the condition of equilibrium of the vertical forces at the second wheel we get

$$F_2 = W - 2P - M/\ell$$

and making use of Equations (III. 1-50) and (III. 1-51), we obtain

$$F_2 = 3W - \mu N \left(2 + \frac{r}{\ell}\right) \qquad \text{(III. 1-52)}$$

In a similar manner, the equilibrium of the vertical forces at the last wheel is:

$$F_3 = W + P + M/\ell$$

and with Equations (III. 1-50) and (III. 1-51), we obtain

$$F_3 = \mu N \left(1 + \frac{r}{\ell}\right) \qquad \text{(III. 1-53)}$$

Substituting these relations, Equations (III. 1-52) and (III. 1-53), in Equation (III. 1-48) give the value for N as

$$N = \frac{3\mu}{1 + \mu^2} W \qquad \text{(III. 1-54)}$$

By the principle of linear superposition, the elastic deformation of the elastic frame at the first wheel is given by

$$h - r = K_1 P + K_2 M \qquad \text{(III. 1-55)}$$

with $K_1 = \frac{2}{3} \frac{\ell^3}{EI}$ and $K_2 = \frac{5}{6} \frac{\ell^2}{EI}$

where E is the modulus of elasticity of the elastic frame and I its area moment of inertia.

Inserting the values for P and M from Equations (III. 1-50), (III. 1-51) and (III. 1-54) yields

$$h - r = K_1 \frac{2\mu^2 - 1}{1 + \mu^2} W + K_2 \frac{3\mu^2}{1+\mu^2} W r$$

After making the expression dimensionless, the following relation is obtained for the limiting obstacle height of the EFV:

$$\frac{h}{r} = 1 + \frac{C}{1+\mu^2} \left[2\mu^2 + \frac{15}{4} \frac{r}{\ell} \mu^2 - 1 \right] \qquad \text{(III. 1-56)}$$

with

$$C = \frac{2}{3} \frac{W \ell^3}{E I r}$$

It can be seen that for $h > r$ the obstacle performance of the EFV depends on the friction coefficient μ as well as on the geometry of the vehicle as expressed by the dimensionless value C and the ratio r/ℓ.

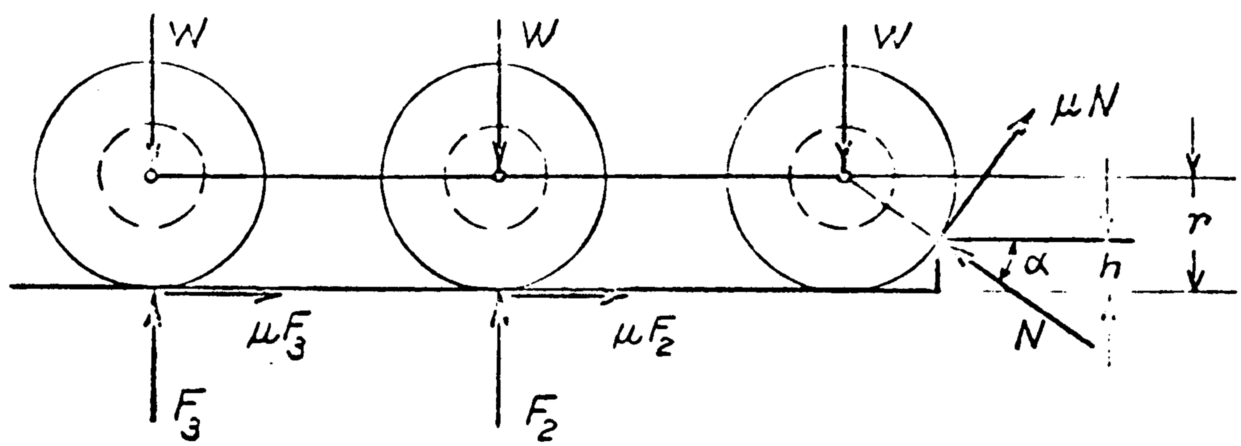

Figure III. 1-45 Obstacle Climbing of EFV. Condition $h < r$

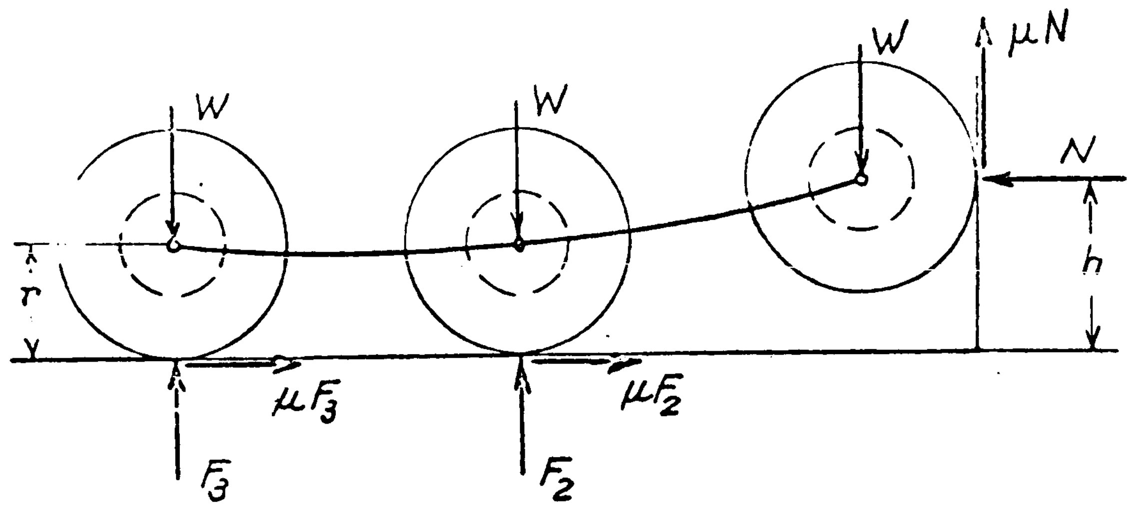

Figure III. 1-46 Obstacle Climbing of EFV. Condition $h > r$

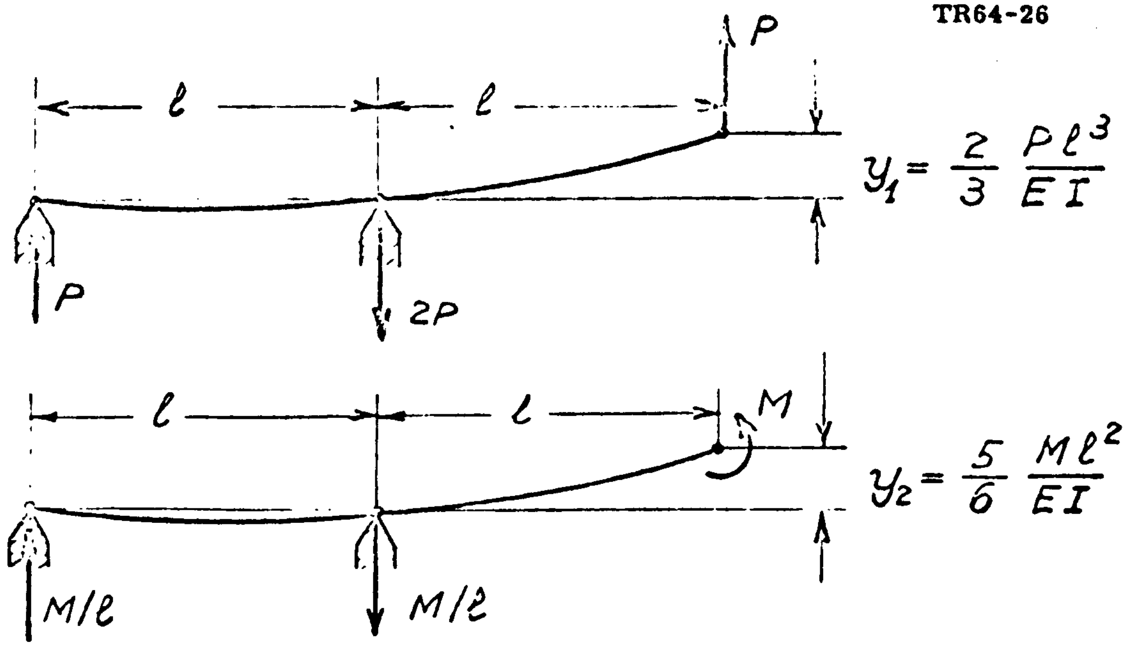

Figure III. 1-47   Elastic Deformation of a Simple Beam

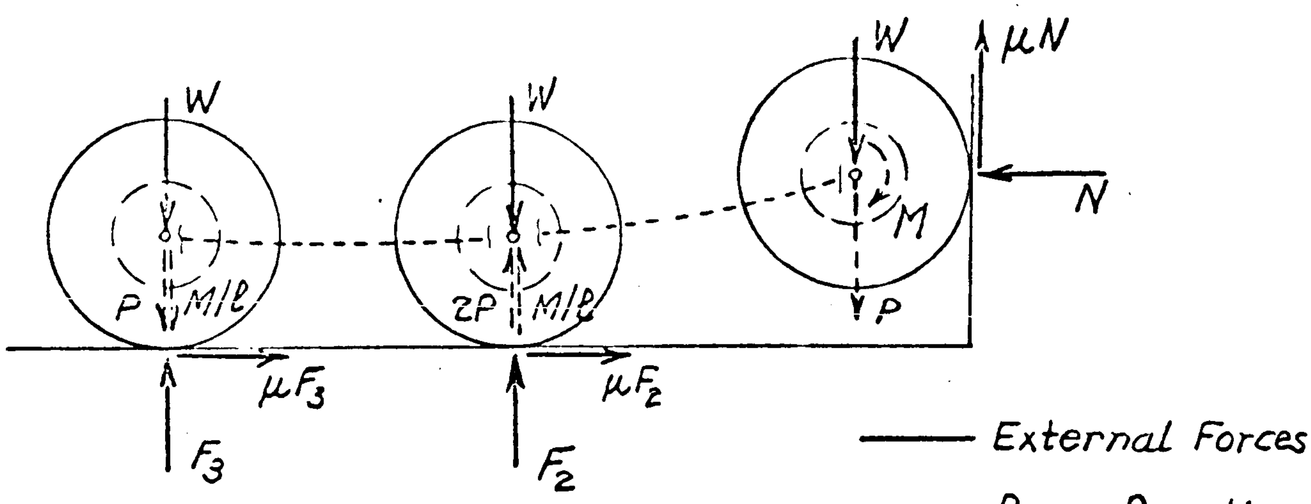

Figure III. 1-48   Free Bodies of EFV

TERRAIN VALUES

Based on the description of lunar sites given by JPL in EPD 98, four lunar surface models were postulated for our mobility analysis.

The first two types of surface configurations correspond to a soft surface composed of fine dust. The second two surface configurations relate to the rough, hard irregular model of the lunar surface.

The description of these four postulated lunar surface models is given in Table III.1-2.

The surface roughness distribution for the hard lunar surface models was determined as follows:

Surface Roughness Distribution

For our mobility analysis we assume the distribution of negotiable obstacles only in the path of the vehicle between 1 meter and 5 cm in size, since larger than 1 meter obstacles will have to be avoided. Obstacles less than 5 cm in size do not considerably affect mobility.

It was assumed furthermore that the surface roughness consists of protuberances conforming to the size distribution equation

$$N_s = \left(\frac{Xmax}{X} \right)^n \quad \text{(See Figure III.1-49)}$$

where N_s is the number of protuberances larger than X over a surface area, Xmax is the largest considered particle size (1 meter) and n is a constant which experimentally was found to be n = 2.3 for impact cratering formation processes (Shoemaker, V. Head).

Assuming that the spacing of protuberances equals twice of their size (gap between obstacles is equal to the obstacle size) as the worst condition (Lunar model No. 4) the number of protuberances in the path of the vehicles can be computed. The results of these computations are presented in Table III.1-3.

VEHICLE VALUES

The vehicle selected for SLRV is a six wheeled, articulated vehicle composed of three units coupled together with flexible frame that permits large amounts of pitch and roll. The general characteristics of the vehicle are given in Table III. 1-4. Since the weight and weight distribution of the vehicle is continuously changing as the design study progresses therefore the weight of the vehicle in our mobility analysis was considered as a parameter covering a range of 1.5 to 3.0 lunar lbs. per wheel (corresponding to a total vehicle earth weight of 54 to 108 lbs.)

MOBILITY PERFORMANCE EVALUATION

The mobility performance of the SLRV was evaluated according to the methods used in off-the-road mobility research. This method is based on an analytical approach, where mathematical models expressing the physico-geometric relationship between vehicle and terrain are used to evaluate vehicle performance characteristics. Laboratory and field tests are also utilized in this approach, either to confirm calculated predictions or to help to solve mobility problems that are not readily amenable to analytical treatment.

Mobility Performance over Soft Lunar Surface
(Lunar surface model 1 and 2)

The procedure followed in this evaluation consisted of the following steps:

(a) The length of the ground contact area was computed as follows:

$$\lambda = 2\sqrt{d(D-d)} \quad \text{(in)}$$

(b) The width of the ground contact area was calculated as

$$b = 2\sqrt{d(B-d)} \quad \text{(in)}$$

(c) The ground contact area was determined assuming an elliptical shape:

$$A = \frac{\lambda b \pi}{4} \quad \text{(sq. in/sheel)}$$

(d) The average ground pressure was computed by:

$$p = \frac{Wo}{A} \quad \text{(psi)}$$

(e) The wheel sinkage was obtained by means of the following equation:

$$Z = \left[\frac{p}{k\phi} \right]^{\frac{1}{n}} \qquad \text{(in)}$$

(f) The gross tractive effort as a function of wheel slip was computed by:

$$H = Wo \tan \phi \; (1 - e^{\frac{-i_o \lambda}{K}}) \qquad \text{(lb/wheel)}$$

(g) The motion resistance due to soil compaction was determined by:

$$R_c = \left[\frac{b\ k\phi}{n + 1} \right] Z^{n+1} \qquad \text{(lb/wheel)}$$

(h) The motion resistance dur to soil bulldozing was computed by:

$$R_b = \left(b\,\gamma\, z^2/_2 \right) \left[\cot\beta + \frac{(\cot\beta)^2}{\cot\beta} \right] \tan(\beta + \phi)$$

(lb/wheel)

(i) The rolling resistance was estimated at 7 percent of the wheel load:

$$R_r = 0.07\ Wo \qquad \text{(lb/wheel)}$$

(j) The slope resistance was calculated by:

$$R_s = Wo \sin \alpha \qquad \text{(lb/wheel)}$$

(k) The drawer-pull/weight ratio was determined by:

$$DP/W = \frac{H - (R_e + R_b + R_r + R_s)}{W} \qquad \text{(dimensionless)}$$

(l) Energy requirement for locomotion was computed by:

$$E = \frac{1.23\ (R_c + R_b + R_r + R_s)}{(1 - i_o)} \qquad \text{(Watt hrs per KM)}$$

The numerical results of the computations are collected in Table III.1-5.

The locomotion energy requirements for the soft lunar surface models (case I and II) are summarized in Table III.1-6.

The gross tractive effort as a function of wheel slip for various wheel loads is plotted in Figure III.1-50.

The motion resistance as a function of wheel load is presented in Figure III.1-51.

The motion resistance at various slopes is plotted as a function of wheel load in Figure III.1-52.

The drawbar - pull/weight ratio as a function of slip for various wheel loads is given in Figure III.1-53.

The locomotion energy requirement is plotted as a function of wheel load for the two soft lunar surface models in Figure III.1-54.

Mobility Performance over Hard Lunar Surface (Lunar surface models 3 and 4)

The mobility performance of the vehicle over hard ground was calculated by means of the following procedures:

(a) The gross tractive effort as a function of wheel slip was computed by:

$$H = Wo\ \mu\ (1-e^{\frac{-i_o \lambda}{K}}) \qquad \text{(lb/wheel)}$$

(b) The rolling resistance was estimated at 7 percent of the wheel load:

$$R_r = 0.07\ Wo \qquad \text{(lb/wheel)}$$

(c) The clope resistance was calculated by:

$$R_s = Wo \sin \alpha \qquad \text{(lb/wheel)}$$

(d) The obstacle resistance and energy required for obstacle climbing was determined experimentally using a full size mobility model of the SLRV. The results of these tests are given in Figures III.1-43 and III.1-44.

(e) Energy requirement for locomotion was computed as a sum of energy required to overcome

(1) rolling and slope resistance
(2) obstacle resistance

The energy requirement was computed by means of the following equation:

$$E = \frac{1.23\ R}{1-i_o} \qquad \text{(Watt hrs per KM)}$$

The gross tractive effort as a function of wheel slip for various wheel loads is plotted in Figure III. 1-55.

The motion resistance at various slopes is plotted as a function of wheel load in Figure III. 1-56.

The energy requirement for locomation is computed in Tables III. 1-7 and III. 1-8 for lunar-surface models 3 and 4 respectively.

The locomotion energy requirement is plotted as a function of wheel load for the two hard lunar surface models in Figure III. 1-57.

TABLE III. 1-2

	Surface Model	Model Description	SLOPE Degree	SLOPE Distribution %	Physical Properties
SOFT SURFACE	CASE I	Soft flat surface except for 1/4 area covered by protuberances, such as cones and ridges	0 +5 -5 +10 -10 +15 -15	75 7 7 3.5 3.5 2 2	Bearing strength values: $k_\phi = 0.083$, $k_c = 0$, $n = 1$ (1 psi per ft, linear with depth) Shear strength values: $\phi = 20^o - 40^o$ $c = 0 - 0.5$
	CASE II	Soft continuously undulating surface; slopes 15^o; distance between high points at least six meters	0 +5 -5 +10 -10 +15 -15	25 14 14 13 13 10.5 10.5	Bearing strength values: $k_\phi = 0.083$, $k_c = 0$, $n = 1$ (1 psi per ft, linear with depth) Shear strength values: $\phi = 20^o - 40^o$ $c = 0 - 0.5$
HARD SURFACE	CASE III	Hard irregular surface on meter scale. Surface covered by blocks, spines, flow structures and ejecta except for isolated areas up to 100 meters diameter	0 +10 -10 +20 -20 +30 -30 +40 -40	30 12 12 9 9 7.5 7.5 6.5 6.5	Bearing strength: Infinitely hard Surface friction coefficient $\mu = 0.75$
	CASE IV	Hard, continuously irregular surface	0 +10 -10 +20 -20 +30 -30 +40 -40	30 12 12 9 9 7.5 7.5 6.5 6.5	Bearing strength: Infinitely hard Surface friction coefficient $\mu = 0.75$

TABLE III. 1-3

SURFACE ROUGHNESS DISTRIBUTION

Obstacle Size Range Meter	Obstacle Size (Mean Dia) Meter (d)	Space Between Obstacles Meter (b)	Number Distribution over surface (N_s)	Number Distribution over Linear Path		Length of Path with 100 Obstacles Meter	Length of Path with Obstacles Meter/KM Model No. 4	Number of Obstacles per Kilometer		Length of Path with Obstacles Meter/KM Model No.
				Number	Percent			Lunar Model No. 4	Lunar Model No. 3	
1-0.7	0.85	0.85	2.3	1.51	2.8	4.76	140.9	82.8	62.1	105.6
0.7-0.5	0.60	0.60	2.7	1.64	3.1	3.72	110.1	91.7	68.8	82.6
0.5-0.3	0.40	0.40	11.5	3.39	6.4	5.12	151.5	189.3	141.9	113.6
0.3-0.2	0.25	0.25	25.5	5.05	9.5	4.75	140.0	280.2	210.2	105.0
0.2-0.1	0.15	0.15	168.0	12.96	24.7	7.41	219.0	730.0	547.5	164.2
0.1-0.05	0.075	0.075	790.0	28.10	53.5	8.02	238.5	1590.0	1192.5	179.0
				52.65	100.0	33.78	1000	2964.0	2223.0	750.0

TABLE III. 1-4

GENERAL CHARACTERISTICS OF
SURVEYOR LUNAR ROVING VEHICLE

Gross Vehicle Weight	9 to 18	lb. (lunar)
Length, overall	72	in.
Width, overall	36	in.
Wheelbase	27	in.
Thread	28	in.
Wheel diameter	18	in.
Wheel width	8	in.
Wheel deflection under nominal wheel load	0.9	in.
Ground Clearance	6	in.
Angle of approach	120	degrees
Angle of departure	120	degrees
Center of gravity location	3	in. (max)

TABLE III. 1-5

SUMMARY OF COMPUTATIONS

Wheel Load (Lunar lbs)		1.5	2.0	2.5	3.0
Wheel Deflection (ins)		.90	.90	.90	.90
Length of Contact Area (ins)		7.86	7.86	7.86	7.86
Width of Contact Area (ins)		5.06	5.06	5.06	5.06
Contact Area (in^2)		31.2	31.2	31.2	31.2
Average Ground Pressure (psi)		.048	.064	.080	.096
Wheel Sinkage (ins)		.578	.771	.964	1.16
Compaction Resistance (lbs)		.070	.125	.195	.282
Rolling Resistance (lbs)		.105	.140	.175	.210
Slope Resistance (lbs)	$\alpha = 5^\circ$	.131	.174	.218	.261
	$\alpha = 10^\circ$	.260	.347	.434	.521
	$\alpha = 15^\circ$	.388	.518	.647	.776
	$\alpha = 20^\circ$	.513	.684	.855	1.03
Bulldozing Resistance	$\phi = 20^\circ$	.026	.047	.073	.105
(lbs)	$\phi = 30^\circ$	.045	.090	.141	.204
Total Resistance (lbs)					
$\alpha = 0^\circ$	$\phi = 20^\circ$	.201	.312	.443	.597
	$\phi = 30^\circ$	.220	.355	.511	.696
$\alpha = 5^\circ$	$\phi = 20^\circ$	.332	.486	.661	.858
	$\phi = 30^\circ$	.351	.529	.729	.957
$\alpha = 10^\circ$	$\phi = 20^\circ$	.461	.659	.877	1.12
	$\phi = 30^\circ$	.480	.702	.945	1.22
$\alpha = 15^\circ$	$\phi = 20^\circ$	.589	.830	1.09	1.37
	$\phi = 30^\circ$	.608	.873	1.16	1.47

TABLE III. 1-6

ENERGY REQUIREMENT FOR LOCOMOTION

Lunar Model I

Slope Degrees	Motion Resistance, LBS/ Wheel Weight per wheel, LBS				Percent Occurence	Energy per wheel, Watt hrs per KM Weight per wheel, LBS			
	1.5	2.0	2.5	3.0		1.5	2.0	2.5	3.0
0	0.220	0.355	0.511	0.696	75	0.211	0.344	0.543	0.690
+5	0.351	0.529	0.729	0.957	7	0.032	0.049	0.069	0.092
-5	0.089	0.181	0.293	0.435	7	0.008	0.016	0.026	0.039
+10	0.480	0.702	0.945	1.220	3.5	0.023	0.034	0.051	0.062
-10	0	0.008	0.077	0.175	3.5	0	0.001	0.004	0.008
+15	0.608	0.873	1.160	1.470	2	0.017	0.026	0.036	0.048
-15	0	0	0	0	2	0	0	0	0
Total					100	0.291	0.470	0.729	0.939

Lunar Model II

Slope Degrees	Motion Resistance, LBS/ Wheel Weight per wheel, LBS				Percent Occurrence	Energy per wheel, Watt hrs per KM Weight per wheel, LBS			
	1.5	2.0	2.5	3.0		1.5	2.0	2.5	3.0
0	.220	0.355	0.511	0.696	25	0.070	0.116	0.167	0.231
+5	0.351	0.529	0.729	0.957	14	0.064	0.099	0.138	0.184
-5	0.089	0.181	0.293	0.435	14	0.016	0.033	0.052	0.078
+10	0.480	0.702	0.945	1.220	13	0.086	0.128	0.189	0.230
-10	0	0.008	0.077	0.175	13	0	0.001	0.012	0.027
+15	0.608	0.873	1.160	1.470	10.5	0.092	0.137	0.189	0.252
-15	0	0	0	0	10.5	0	0	0	0
Total					100	0.328	0.514	0.747	1.002

TABLE III. 1-7

ENERGY REQUIREMENT FOR LOCOMOTION

Lunar Model III

	Slope Degree	Motion Resistance, LBS/Wheel — Weight per wheel, LBS 1.5	2.0	2.5	3.0	Percent Occurence	Energy per wheel, Watt hrs per — Weight per wheel, LBS 1.5	2.0	2.5	3.
Slope Climbing	0	0.105	0.140	0.175	0.210	30	0.039	0.052	0.065	0.
	+10	0.365	0.487	0.609	0.731	12	0.055	0.074	0.092	0.
	-10	0	0	0	0	12	0	0	0	
	+20	0.618	0.824	1.030	1.240	9	0.074	0.097	0.120	0.
	-20	0	0	0	0	9	0	0	0	
	+30	0.855	1.140	1.420	1.710	7.5	0.085	0.116	0.143	0.
	-30	0	0	0	0	7.5	0	0	0	
	+40	1.070	1.420	1.780	2.140	6.5	0.098	0.134	0.168	0.
	-40	0	0	0	0	6.5	0	0	0	
	Total energy for slope climbing						0.351	0.473	0.588	0.

	Obstacle Height, Meter	Motion Resistance, LBS/Wheel — Weight per wheel, LBS 1.5	2.0	2.5	3.0	Length of Path with Obstacles Meter per KM	Energy per wheel, Watt hrs per — Weight per wheel, LBS 1.5	2.0	2.5	
Obstacle Climbing	0.85	0.570	0.760	0.950	1.140	105.6	0.176	0.235	0.294	0.
	0.60	0.480	0.640	0.800	0.960	82.6	0.076	0.101	0.126	0.
	0.40	0.172	0.230	0.287	0.345	113.6	0.026	0.035	0.043	0.
	0.25	0.063	0.084	0.105	0.126	105.0	0.009	0.011	0.014	0.
	0.15	0.026	0.034	0.042	0.051	164.2	0.006	0.008	0.009	0.
	0.075	0.007	0.010	0.012	0.015	179.0	0.002	0.002	0.003	0.
	Total energy for obstacle climbing					750	0.295	0.392	0.489	0.5
	Total locomotion energy						0.646	0.865	1.077	1.2

TABLE III. 1-8

ENERGY REQUIREMENT FOR LOCOMOTION

Lunar Model IV

Slope, Degrees		Motion Resistance, LBS/Wheel Weight per wheel, LBS				Percent Occurence	Energy per Wheel, Watt hrs per KM Weight per wheel, LBS			
		1.5	2.0	2.5	3.0		1.5	2.0	2.5	3.0
Slope Climbing	0	0.105	0.140	0.175	0.210	30	0.039	0.052	0.065	0.078
	+10	0.365	0.487	0.609	0.731	12	0.055	0.074	0.092	0.110
	-10	0	0	0	0	12	0	0	0	0
	+20	0.618	0.824	1.030	1.240	9	0.074	0.097	0.120	0.143
	-20	0	0	0	0	9	0	0	0	0
	+30	0.855	1.140	1.420	1.710	7.5	0.085	0.116	0.143	0.170
	-30	0	0	0	0	7.5	0	0	0	0
	+40	1.070	1.420	1.780	2.140	6.5	0.098	0.134	0.168	0.199
	-40	0	0	0	0	6.5	0	0	0	0
	Total energy for slope climbing						0.351	0.473	0.588	0.700
Obstacle Height, Meter		Motion Resistance, LBS/Wheel Weight per wheel, LBS				Length of Path with Obstacles Meter/KM	Energy per Wheel, Watt hrs per KM Weight per wheel, LBS			
		1.5	2.0	2.5	3.0		1.5	2.0	2.5	3.0
Obstacle Climbing	0.85	0.570	0.760	0.950	1.140	140.9	0.235	0.313	0.391	0.469
	0.60	0.480	0.640	0.800	0.960	110.1	0.101	0.135	0.169	0.202
	0.40	0.172	0.230	0.287	0.345	151.5	0.035	0.047	0.058	0.070
	0.25	0.063	0.084	0.105	0.126	140.0	0.012	0.015	0.019	0.023
	0.15	0.026	0.034	0.042	0.051	219.0	0.007	0.009	0.012	0.014
	0.075	0.007	0.010	0.012	0.015	238.5	0.002	0.003	0.004	0.005
	Total energy for obstacle climbing						0.392	0.522	0.653	0.783
	Total locomotion energy						0.743	0.995	1.241	1.483

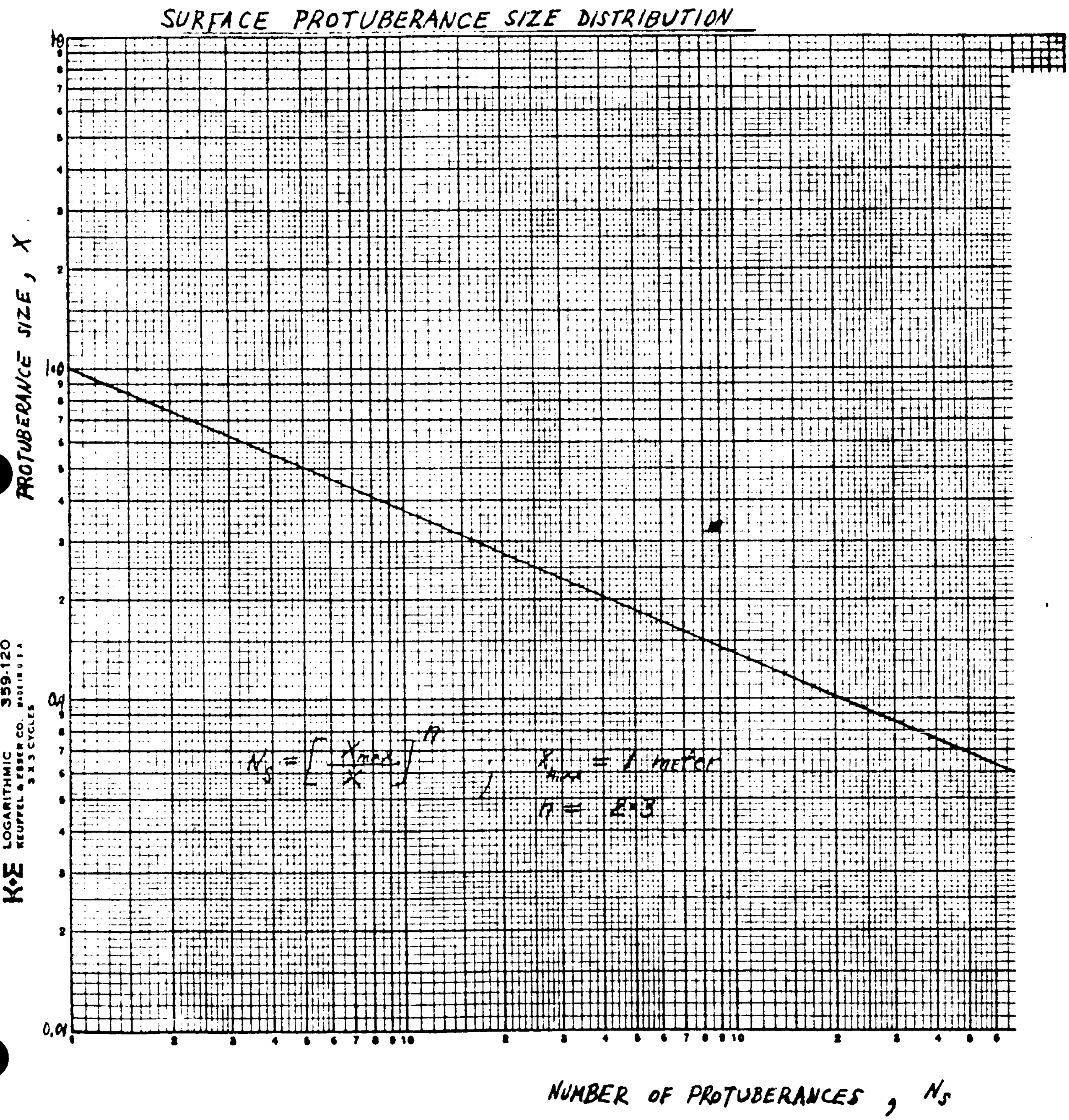

Figure III. 1-49

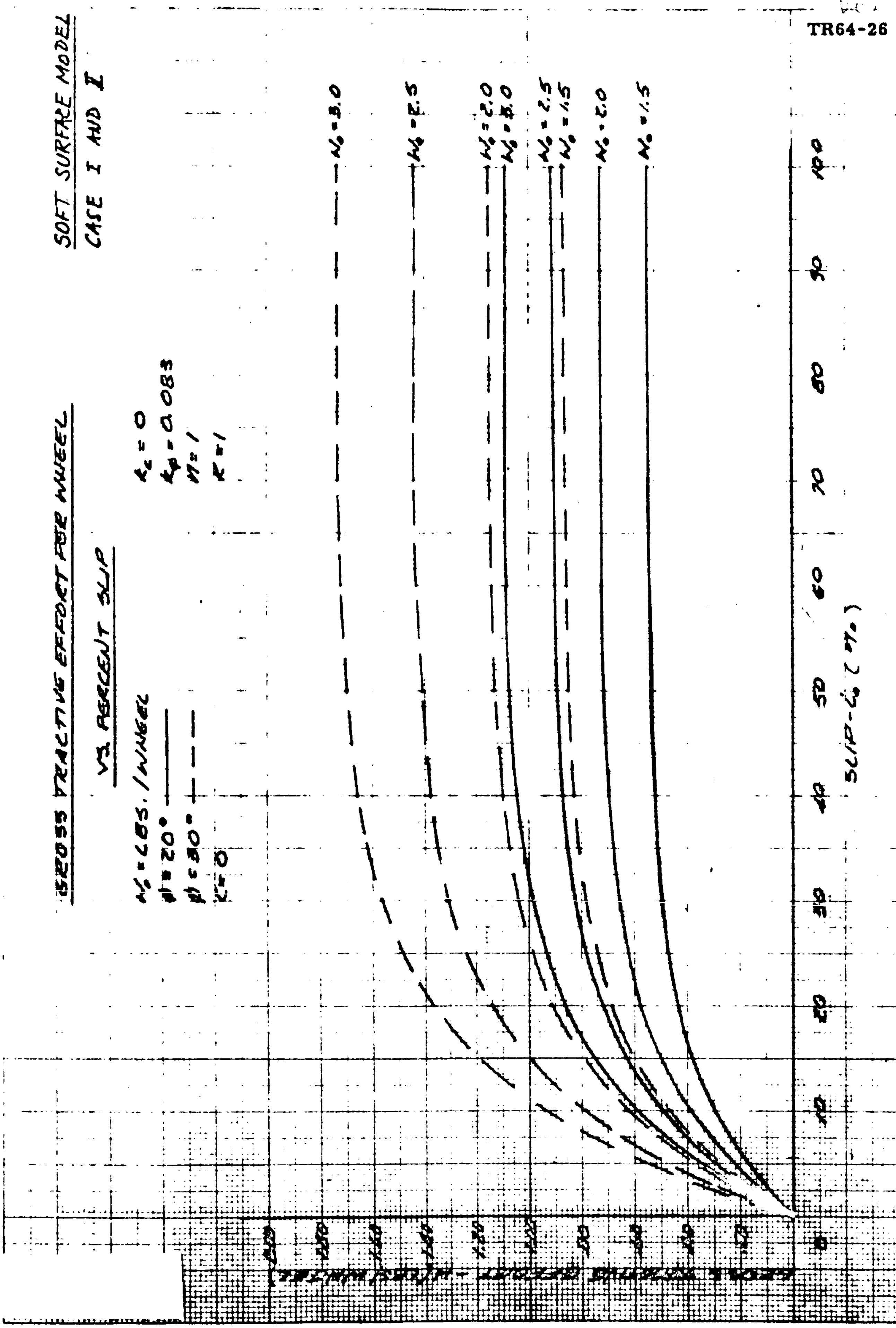

Figure III.1-50

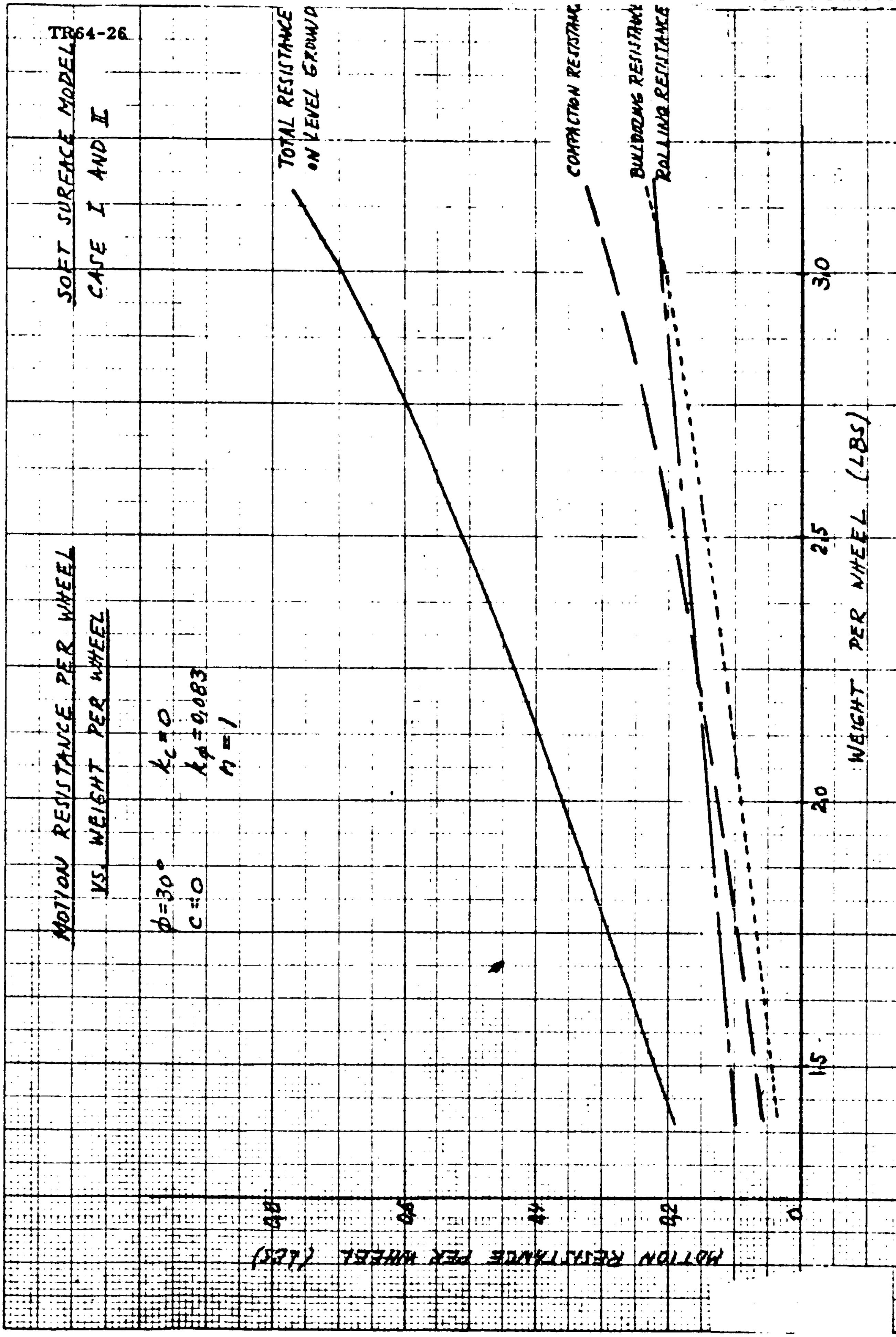

Figure III.1-51

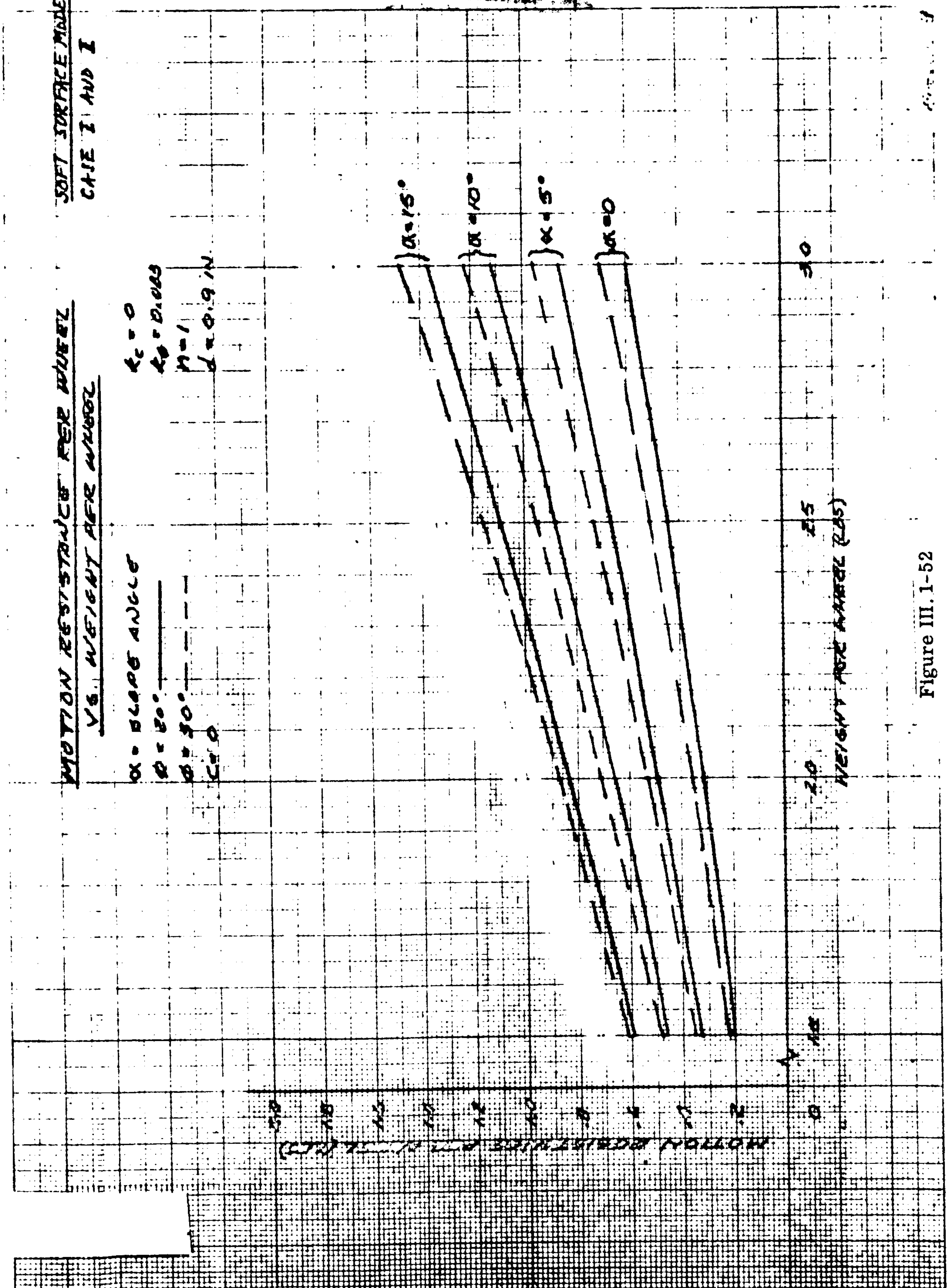

Figure III. 1-52

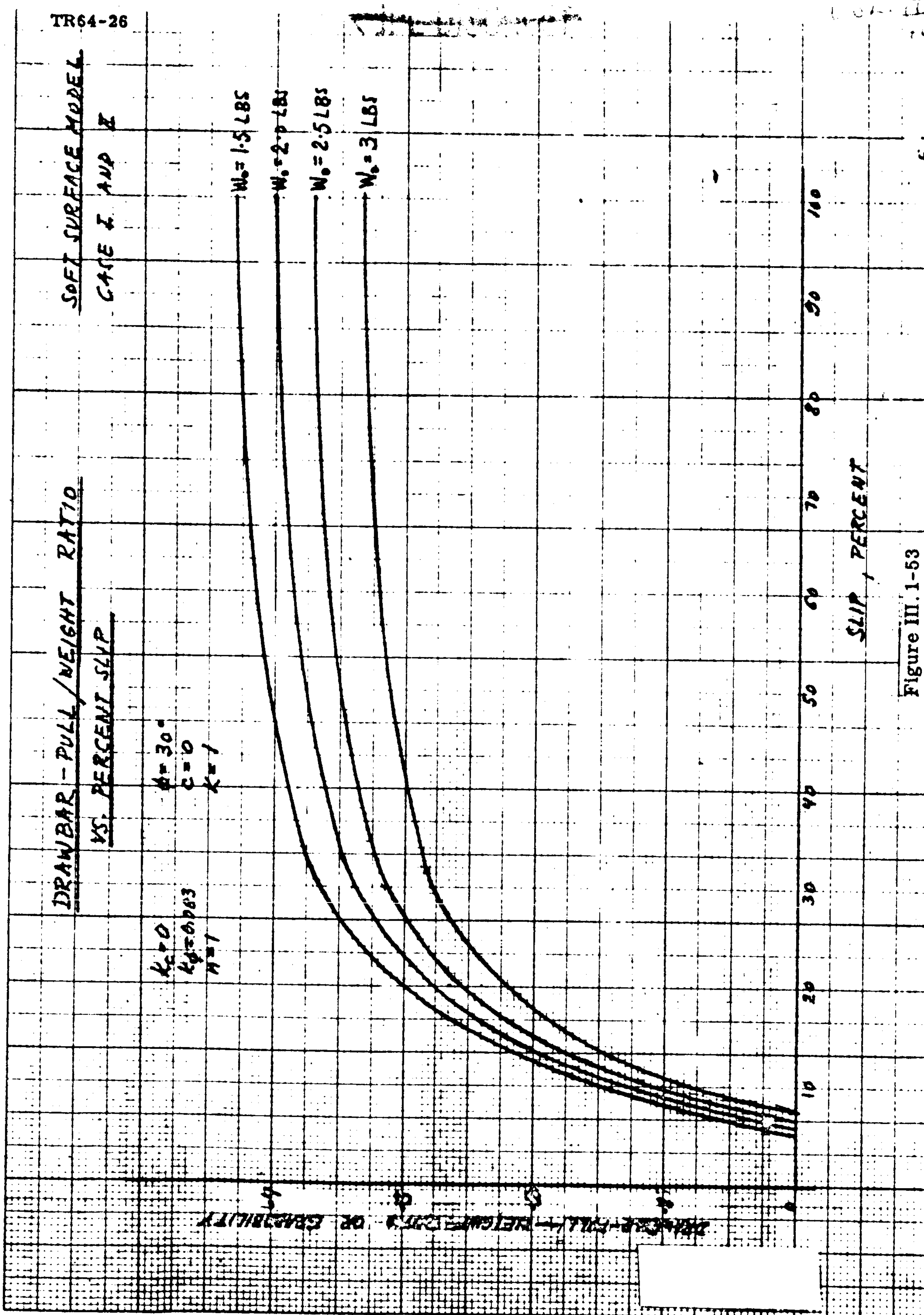

Figure III.1-53

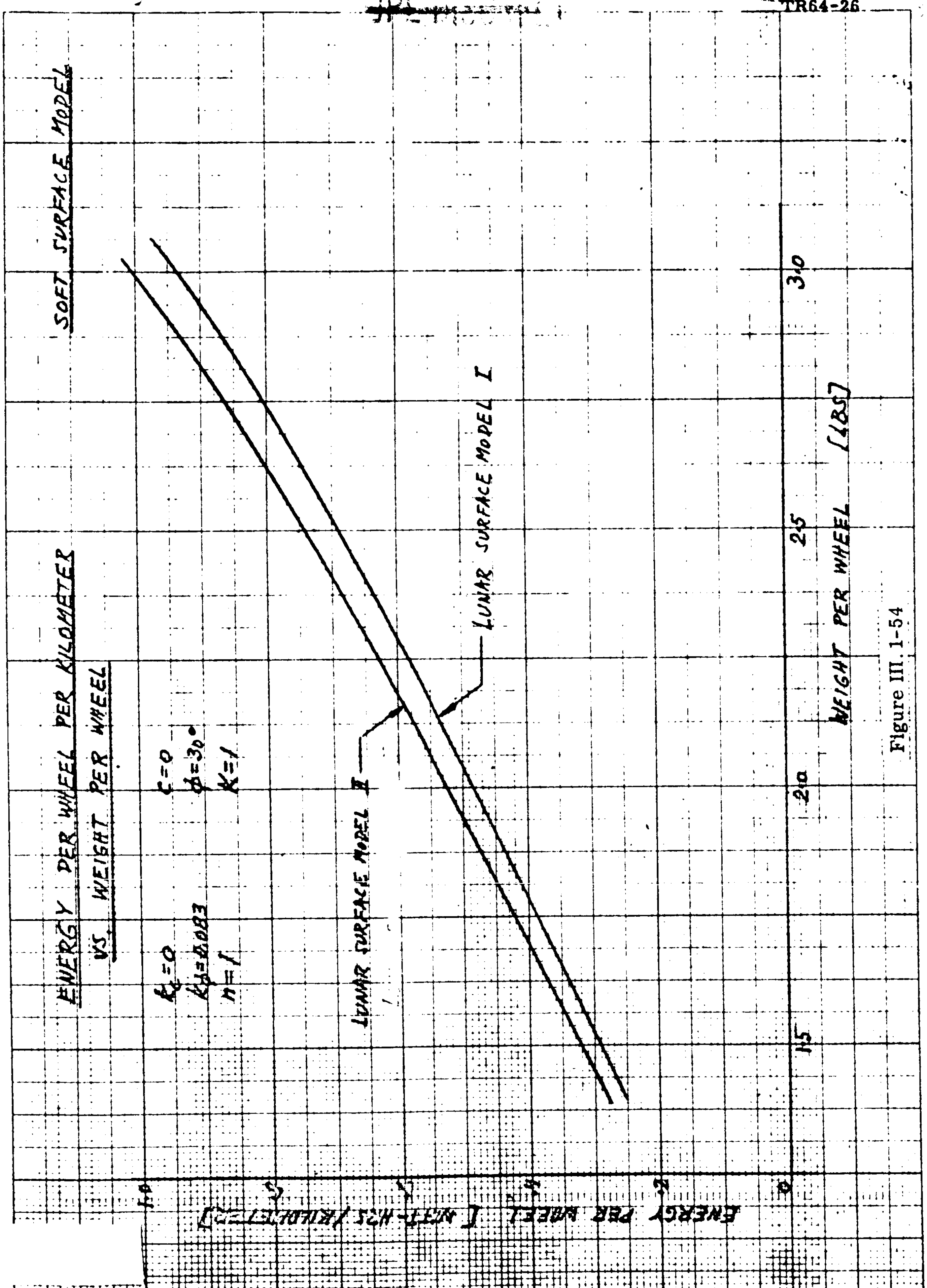

Figure III.1-54

TR64-26

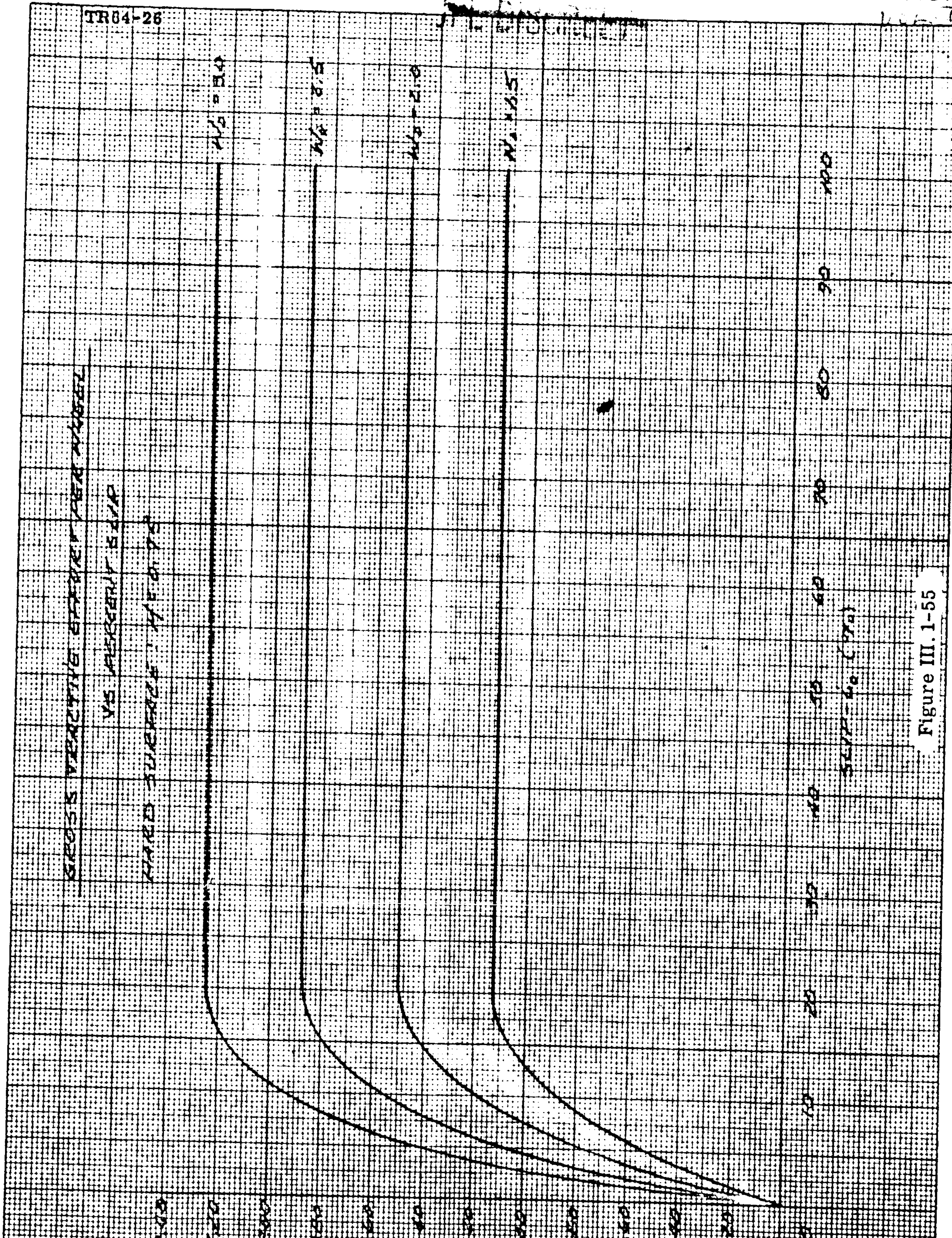

Figure III.1-55

111

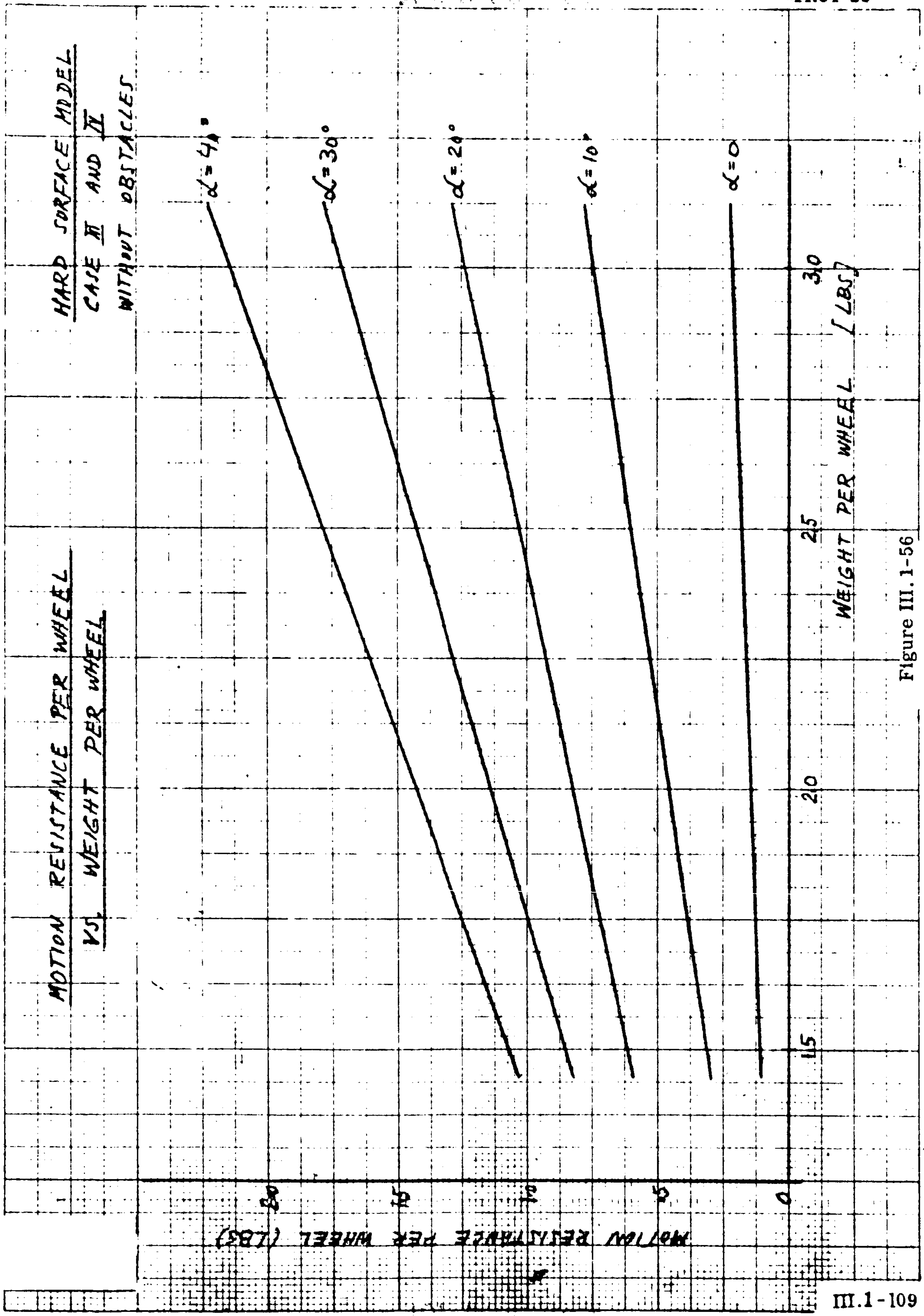

Figure III.1-56

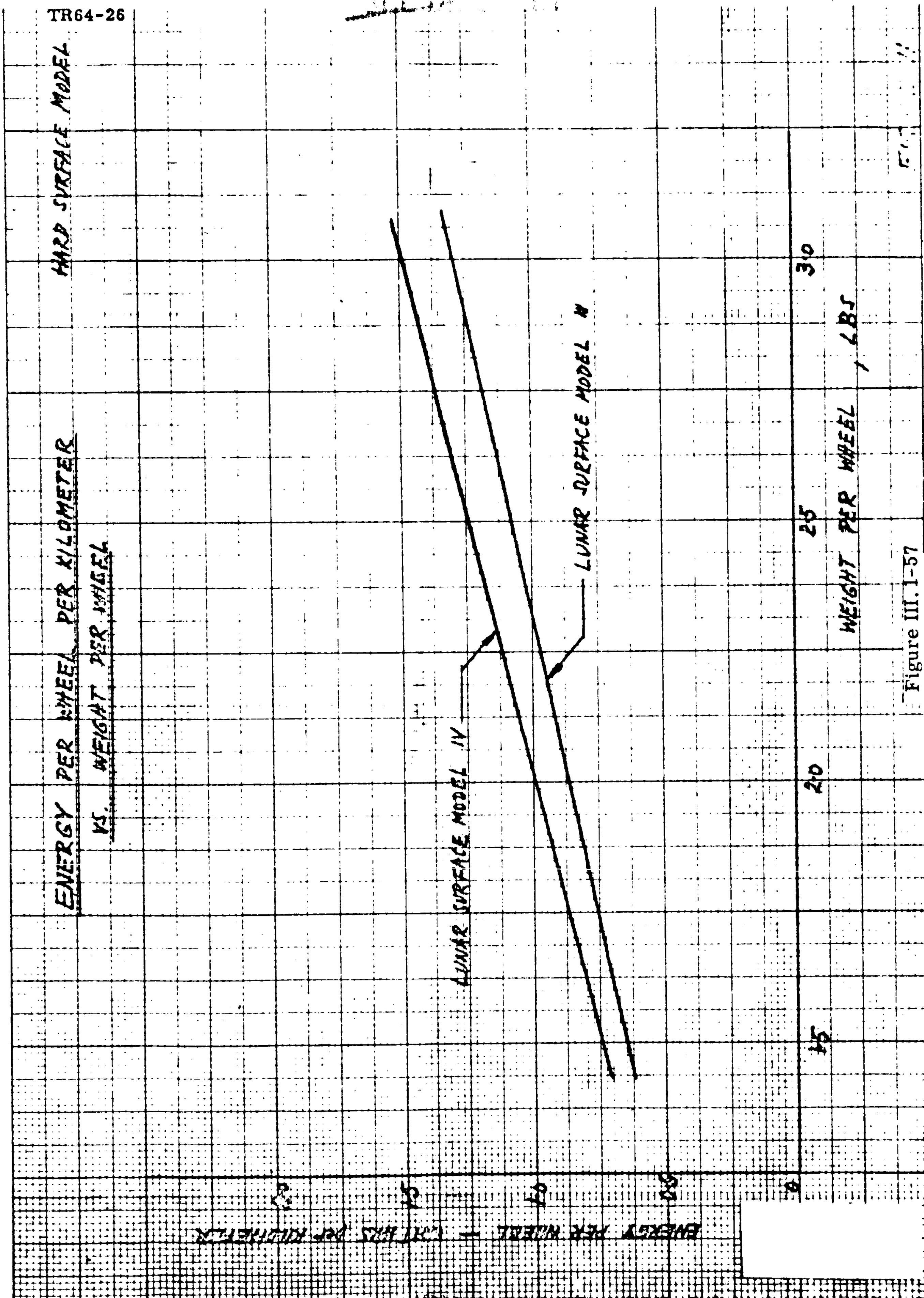

Figure III.1-57

D. WHEEL DESIGN

REQUIREMENTS

The wheel design has to satisfy requirements for:

(a) Mobility over both soft, and hard rough surfaces

(b) Environmental conditions of high vacuum, high and low temperatures, radiation, micrometeorite bombardment, etc

(c) Durability

(d) Vehicle stowage.

APPROACH

To satisfy the mobility requirements over soft surfaces the wheel has to have high traction and low motion resistance characteristics. For rough, hard surface conditions the primary requirement is related to the dynamic performance of the vehicle. Both of these requirements are satisfied with the selection of a non-pneumatic flexible elastic wheel with deflection characteristics similar to those of a low pressure pneumatic tire. The use of pneumatic tires was rejected because of environmental and reliability considerations. With a highly flexible elastic wheel, large ground contact areas can be produced, thus providing excellent traction and flotation characteristics. From the dynamic point of view the flexible wheel has the effect of lessening gross chassis motions, maintaining wheel contact with the surface and reducing dynamic loads to the wheel and chassis.

The flexible wheel design can also satisfy the environmental and durability requirements. For example, mobility performance will be affected little if at all by punctures. The elastic characteristics also offer the advantage of permitting the vehicle to be stowed in a minimum payload volume by predeflecting the wheels.

DERIVED DESIGNS AND TEST RESULTS

During a development under the GM DRL Basic Lunar Program a number of elastic wheels of different construction were built and tested in cooperation with Goodyear Tire and Rubber Company. Three basic designs are shown in Fig.III.1-58. They are:

(a) Radial wire frame type, fabric covered

(b) Angular wire frame type, fabric covered

(c) Angular wire frame type, with pads.

The results of mobility tests performed with these three types of wheels in GM DRL's Mobility Research Laboratory are displayed in Fig.III.1-59.

These results indicate that when comparing the mobility performance of the covered type wheels (a, b) with the open pad type wheel (c) they both have about the same drawbar pull-weight ratio, $\frac{DP}{W}$, but the efficiency of mobility or traction efficiency, (defined as the drawbar pull-thrust ratio, $\frac{DP}{H}$), is superior for the covered type wheels. This is due to the "digging in" action of the open wheel which results in higher sinkage and therefore higher motion resistance.

Comparing the angular and radial wire frame wheels, both covered, the latter has slightly higher drawbar pull-weight ratio, but the stability and durability of the angular wire type has proven to be superior.

The elastic wheel design selected for further development, based on the above preliminary investigation, is shown in Fig.III.1-60. The elastic wire frame is constructed in an angular pattern. The wires are joined together at each intersection. These joints are free to pivot in order to allow pantographing movement of the wire frame when the wheel deflects. The joints are encapsulated in neothane to increase life. The ends of the wires are attached to the wheel hub in a manner to allow free pivoting. The wire frame is covered with a flexible fabric material. Stainless steel mesh is considered for this purpose, unless plastic type materials such as mylar can be developed for the specific environmental conditions. The elastic wire frame is designed to be able to permit a maximum of four inches deflection without overstressing the wires. A stiff inner-spring frame structure is incorporated in the design to prevent deflections larger than four inches.

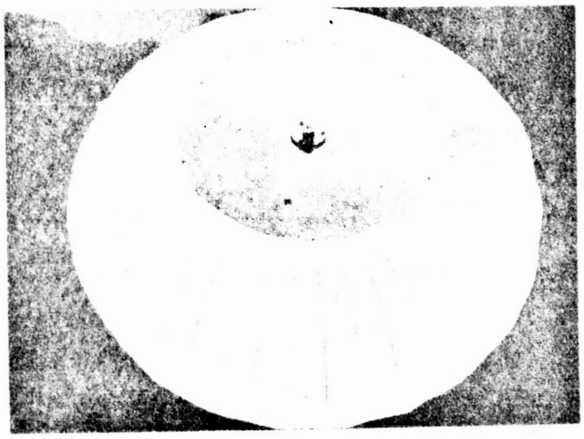

(a) Radial wire frame

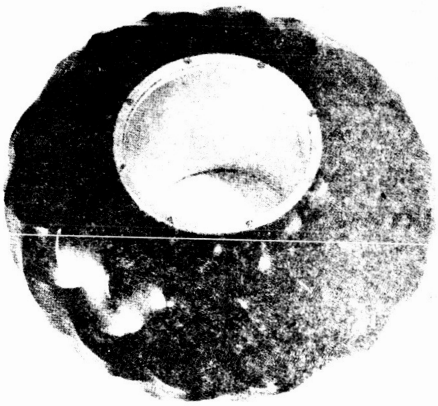

(b) Angular wire frame, fabric-covered

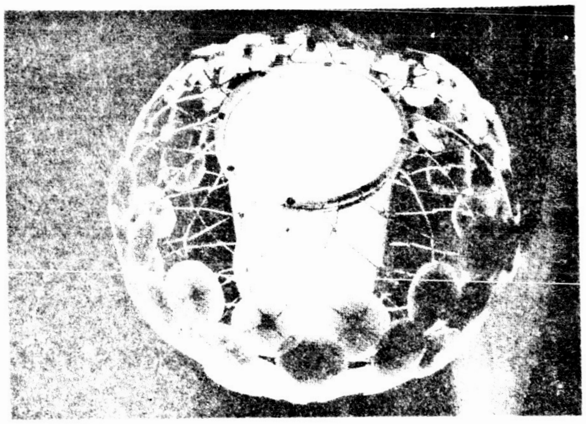

(c) Angular wire frame, with pads

Fig. III. 1-59. Basic Wheel Designs

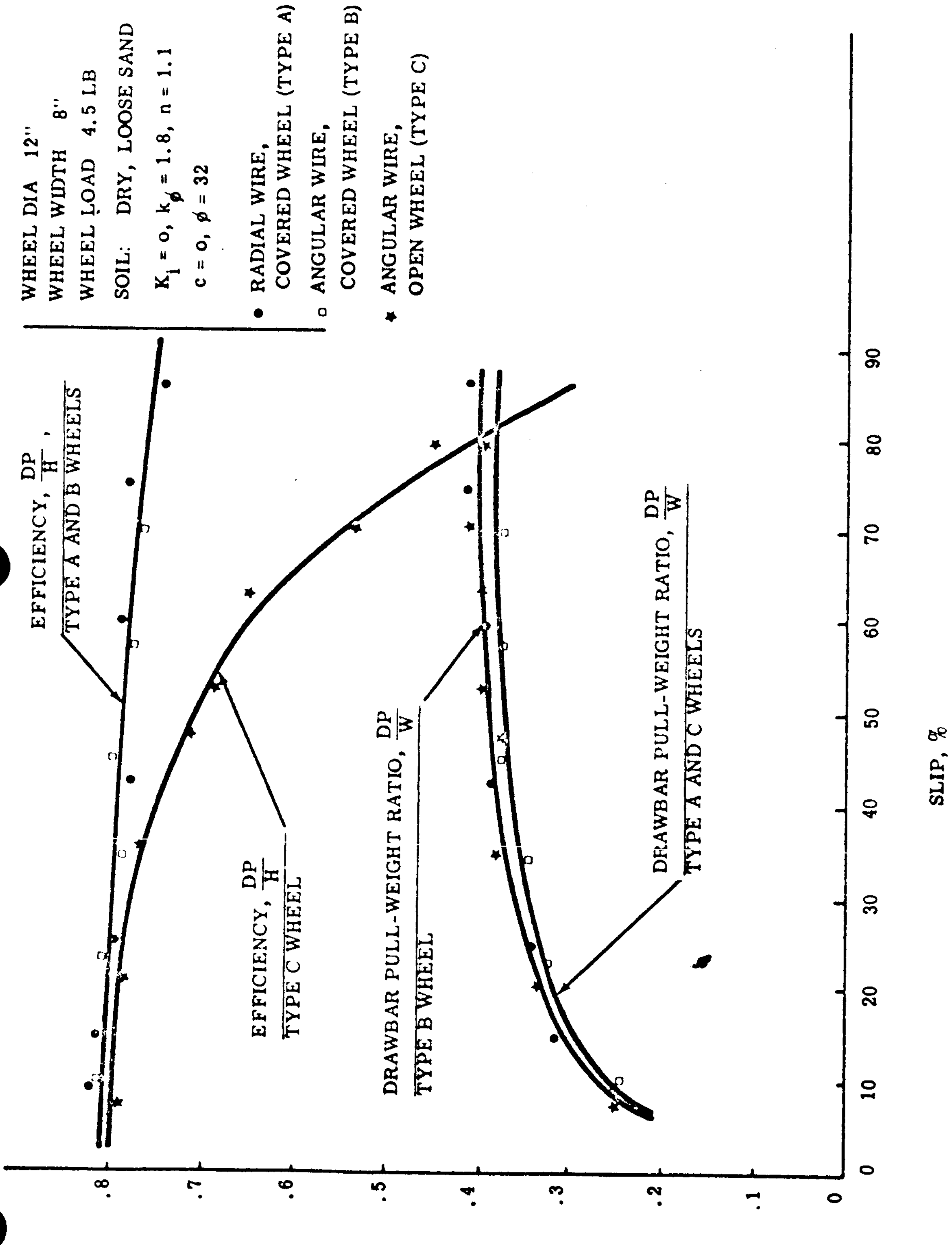

Fig. III. 1-59. Mobility Test Results, Basic Wheel Designs

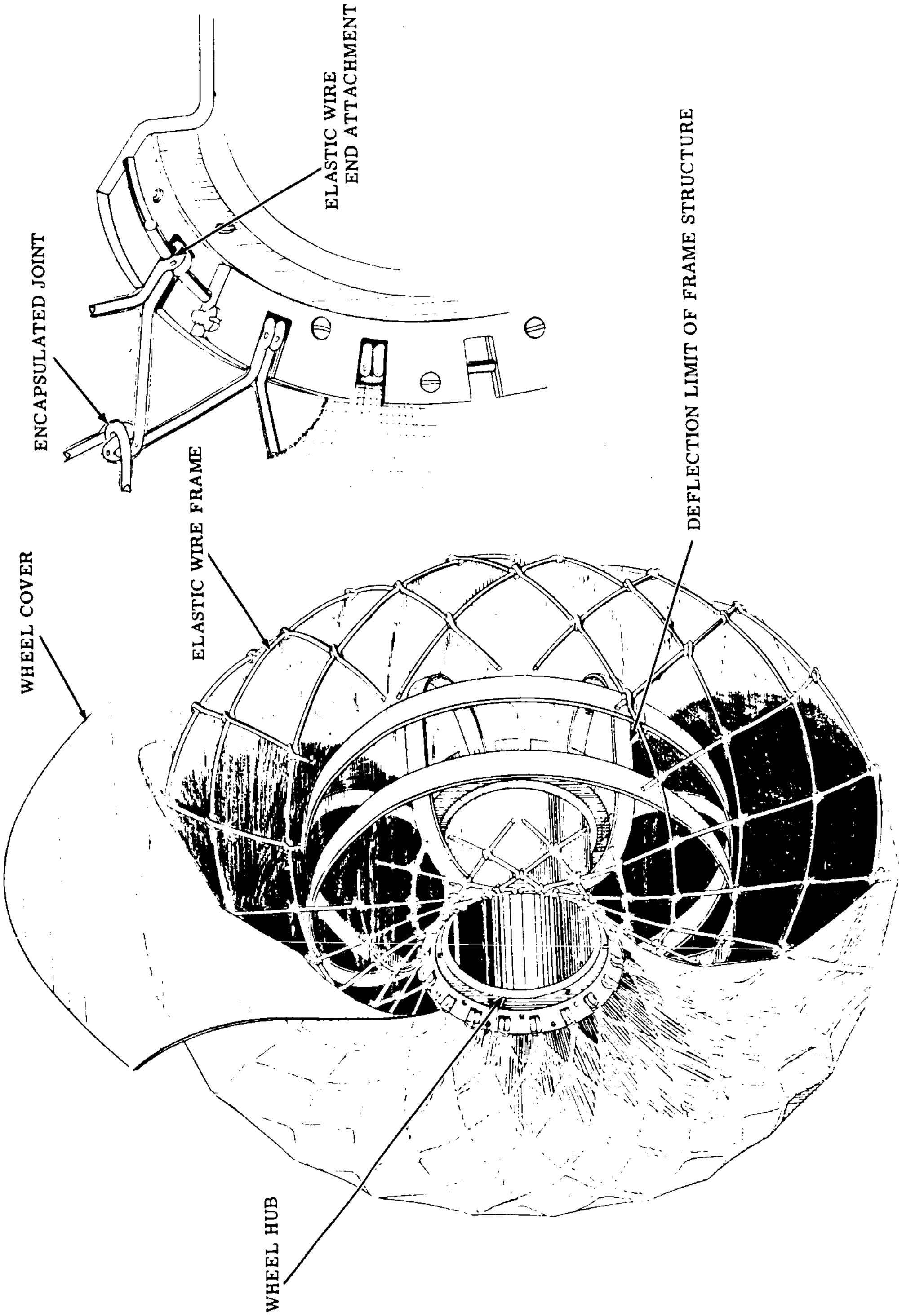

Fig. III.1-60. Elastic Wheel, Preferred Design

The specifications of the proposed wheel design are as follows:

Wheel diameter	18 inches
Wheel width	8 inches
Maximum wheel deflection	4 inches
Nominal static wheel load	2.08 lb
Nominal wheel torque	6 in.-lb
Maximum static wheel load	6.25 lb
Maximum static side load	4.40 lb
Maximum wheel torque	60 in.-lb
Maximum dynamic wheel load	40 lb
Spring rate	4 lb/in.
Nominal ground pressure	.065 psi

APPENDIX II
STRUCTURES

APPENDIX II
STRUCTURES

A. THERMAL

1. Thermal Control

APPROACH

System thermal design must provide a suitable thermal environment for components and subsystems in stowed condition (launch phase, in-flight and after lunar landing) as well as when the vehicle is functioning on the lunar surface. The variety of environmental conditions and systems activities which characterize the thermal problem during operating periods of the lunar day and during hibernation through the lunar night, however, largely determine the approach to thermal design. Vehicle thermal design for the stowed configuration will be made as adjustments to the basic thermal design for lunar operation and as a part of the attachment and deployment system design.

Thermal compartments can be designed for the equipment which is permanently mounted on the Surveyor; however, the possibility of mounting this equipment in compartment "B" will be investigated.

Thermal control requirements are based on a three-month system life. Thermal conditions on the lunar surface are significantly different than those experienced on an orbiting spacecraft. The lunar landing spacecraft must survive under exposure to wide temperature fluctuations of long duration. Equipment on the lunar surface will be exposed to two major external heat sources:

1) direct solar energy with the intensity of 1.39 kw/m^2
2) infrared radiation from the lunar surface at approximately 120^oC.

Direct solar radiation on the lunar surface will last for 336 hours (14 earth days). During the lunar night, the surface will cool to approximately -157°C. This condition will last for 336 hours.

The storage and operating temperature ranges of critical components and duration of the lunar night require special provision for night-time heating of the thermal payload compartments of the vehicle, if the vehicle electrical power is derived exclusively from solar cells. For R. T. E. power options it is likely that sufficient electric heating power will be available.

With solar primary power, it is expected that night-time heat would be provided by a small radioisotope pellet connected to each of two vehicle payload compartments. Preliminary analysis indicates that approximately three watts heating power is required for each compartment. The Oak Ridge National Laboratory has estimated that a heating unit using Curium 242 as the radioactive source could have the characteristics given in Table I.

TABLE III. 2-1

Representative Heat Source Characteristics

Thermal Output	5. watts
Weight	40. grams
Size	.75 inch diam.
Impact Tolerance	500. ft/sec
Temperature Tolerance	>1000. degrees F
Radiation	<2.4 mrem/hr/3 ft.
Isotope	Cm^{242}

The night-time heat sources may be left in the payload compartment throughout the mission, if adequate primary radiation surface is available. If not, they may be transferred from the interior of the payload compartments to a side or the bottoms of the compartments during the lunar day. Design studies will be performed to decide. A third alternative of connecting the heat source to an external side or bottom of the compartment and making or breaking a conductive connection between it and the payload is not considered desirable, because it is most sensitive to covering of exposed surfaces by lunar material.

It can be seen that five of the six sides of the middle equipment compartments of the SLRV will be exposed to the lunar surface. Because of the high temperature of the surface during the lunar day period, these sides must be isolated from the equipment. The top of the compartment is the only side which does not have a view of the lunar surface and therefore represents the only thermal control surface available. To accomplish this control, the electronic component must be coupled to the top surface. However, during the lunar night the external inputs are extremely small and it is desirable to decouple the components. This condition obviously requires a thermal controller.

The controller planned for use is the passive thermal switch developed by Hughes Aircraft Company for the Surveyor payload compartments. Arrangements allowing for the use of this component were made with HAC prior to the current procurement. Use of this thermal switch reduces the development effort for thermal control of the vehicle compartments.

THERMAL SWITCH REQUIREMENTS

A preliminary analysis of the middle compartment of the current vehicle design indicates the requirements for thermal switches:

The radiator surfaces are assumed to be Vycor glass with the following properties: $\alpha = .12$, $\epsilon = .85$.

In addition it is assumed that the wheels and the soil properties instrument are at 120 degrees C and that the mast is at 60 degrees C. These represent conservative estimates of the temperatures which will exist on these components.

Using the above values, the radiator temperature versus dissipation was determined. The results are shown in Figure III.2-1.

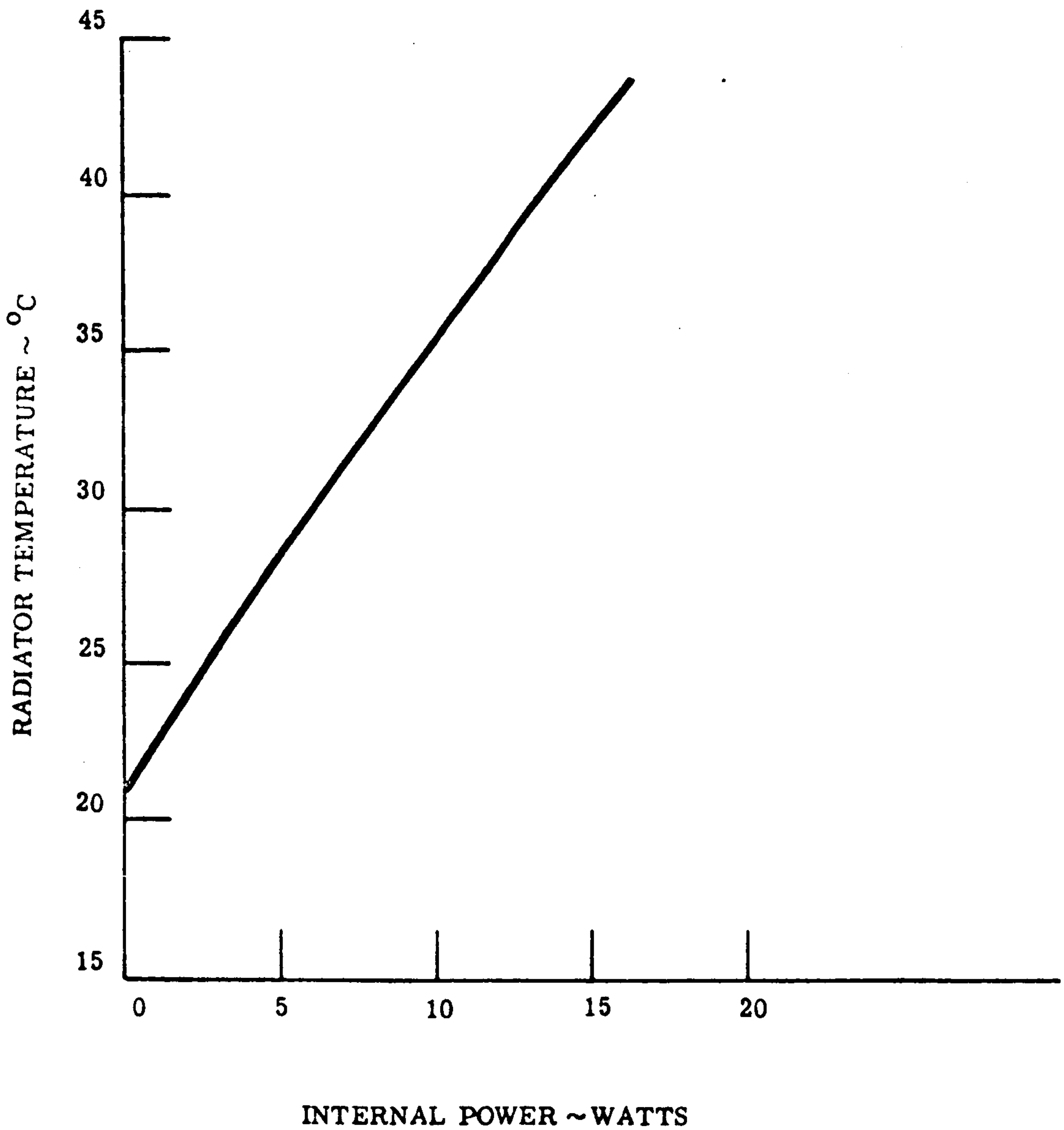

Fig. III.2-1. Radiator Temperature vs. Internal Power

The conductance per switch used was .24 watts/C degree (switch closed).

The heat flow across the switch is given by the following equation:

$$Q_d = Kn\,(T_{HS} - T_R)$$

where

T_{HS} = temperature at mounting surface of components

T_R = temperature of radiator

K = switch conductance

n = number of switches

Using the above equation and Fig. III.2-1, the number of switches for various values of Q_d and T_{HS} were determined. The results are shown in Fig. III. 2-2. Examining Fig. III.2-2 it can be seen that 5 to 6 switches are adequate. The exact component temperature level will depend upon the internal power dissipation. The component temperatures shown on Fig. III.2-2 were picked as being representative of space electronic equipment acceptable operating levels.

Other features of the design approach for thermal control that have been employed in current design studies for the Surveyor Lunar Roving Vehicle are evident in the following discussion of compartment design.

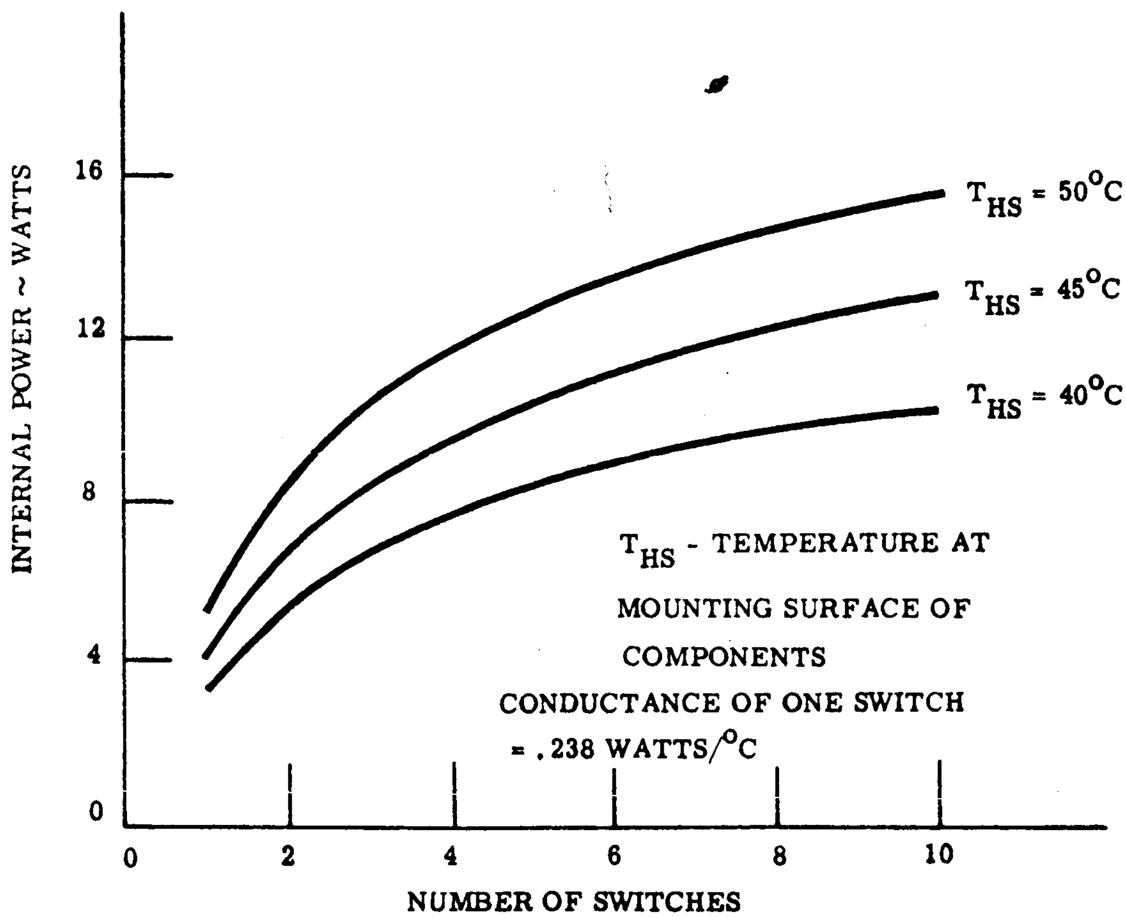

Fig. III.2-2. Internal Power vs. Number of Switches

COMPARTMENT STRUCTURE

Requirements

The first and second axle compartments of the Surveyor Lunar Roving Vehicle carry batteries and the electronic payload. As a consequence the design of these two compartments requires thorough integration of the thermal and structural considerations. Thermal requirements are set by the operating temperature limits of the electronic payloads. Structural requirements are established by general vehicle mobility criteria, deployment and stowage limitations, and environmental loads imposed during launch, transit, and landing.

Using the proposed configuration, the compartments would be designed for the following payload requirements:

	Internal Temp. ^{o}F	Volume in^{3}	Weight lbs.
Axle #1	-75 to 170	275	11.0
Axle #2	0 to 125	500	17.3

On the basis of the above, a feasible approach to compartment design can be discussed which will serve as a basis for study.

A preliminary analysis of the middle compartment of the Rover Vehicle has been carried out. This analysis considered three aspects of the vehicle thermal control:

1) Radiator temperatures (top surface) as a function of internal power
2) Thermal controller requirements as a function of component temperature limit and internal power
3) Insulation effectiveness and lunar night power requirements.

Because of the extended duration of the lunar night, careful attention was given to payload insulation. One hundred layers of aluminized mylar are employed as insulation. With a layer emissivity of .1, the effective emissivity (Eff) is 5.32×10^{-4}. In the thermal analysis, this value of emissivity was increased by a factor of ten to compensate for conduction losses and heat leaks.

As discussed previously, the present approach is to supply this power from a radioactive pellet. This offers a considerable weight saving over a battery source. The pellet could be moved in and out of the compartment by a transfer switch, supplying power when needed. This approach maintains the minimum component temperature at $+10^{O}C$, thus improving the system reliability by reducing the stress on the electronic components.

Typical Compartment Structure

Both forward and center compartment structures are similar in construction. A compartment structure, typical of the type of construction proposed, is illustrated in Fig. III.2-3 and is described in detail below for the center compartment.

The compartment consists of a recessed rectangular box with a continuous-lip flange to which an upper mounting cover panel is attached by screws and thermal insulator stand offs.

The box serves both as a structure to provide a load path between the compartment payload and the wheel axle, and as protection against environmental damage to the internal electronic packages. The material used is 2014 aluminum alloy, Alclad. A hat-shaped channel is spot-welded to the bottom of the box, which is made of .020 sheet. Vertical, hat-shaped beams are spot-welded to the sides of the compartment and to the lower channel. These side members also include a thin-walled cylindrical fitting to which the wheel assembly is attached. The side members, lower channel, and upper flange of the compartment comprise an integral body-axle assembly, and serve as the load path for transferring the body loads to the wheels.

The upper panel consists of a honeycomb sandwich panel integrally fabricated with an outer epoxy-resin fiberglass mounting frame, bonded together in a thermal vacuum. The honeycomb sandwich panel is fabricated of two (.030) 2014 aluminum alloy, Alclad face sheets, and a 1/8-5052-.001 P perforated aluminum alloy foil core (4.5 lbs/ft^{-3} density) 3/16-inch thick; six (1/8-inch wall x 3-inch O.D.) aluminum alloy short cylindrical spacers are located

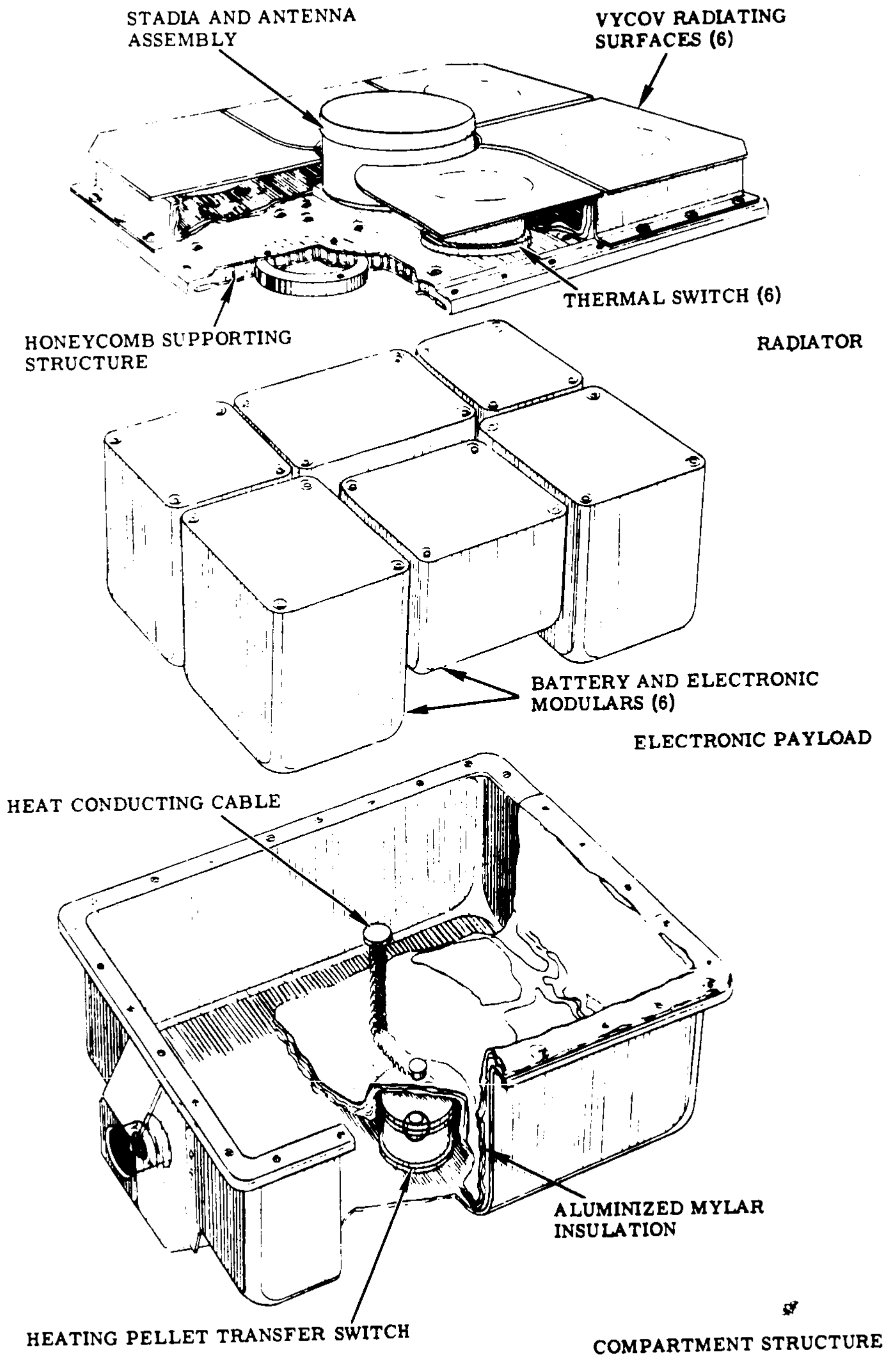

Fig. III.2-3. Typical Compartment Construction under six thermal switches, providing an additional thermal conduction path between the lower and upper face sheets. The electronic packages are attached to the lower surface of the panel. A pure aluminum, heavy-foil gasket is sandwiched between the lower face sheet of the panel and the electronics box to provide for more effective thermal conductivity between the box and the face sheet. Grommet type, thru-bolt, sandwich panel fasteners are used for attaching the electronics packages to the panel.

Attached to the upper face sheet of the panel are the six thermal switches mentioned above. Also attached to the upper surface is a thin-walled 2014 aluminum alloy cylinder, welded to the face sheet, for housing the stadia inflatable structure. Located in the bottom of the compartment is a transfer switch for housing a radioactive pellet.

A thermal insulation of 100 layers of aluminized mylar, sandwiched with thin-sheet insulation material, lines the inside of the compartment to serve as a radiation insulator. To conduct heat from the isotope heat source to the heat sink and compartments, braided aluminum alloy straps, which penetrate the mylar insulation, are provided. The entire compartment assembly is attached to the elastic frame with screws and nut plates.

The compartment associated with the first axle, while of similar construction, becomes more complex structurally. The attachment of the steering mechanism and its heat sink and the viewing periscopes present additional thermal and structural difficulties requiring careful layout. However, the proposed structure is readily adaptable to overcome these design difficulties.

The compartment design study will be closely integrated with the overall multi-body analysis in which all vehicle components are coupled together. However, there will be effort peculiar to the compartment. These efforts can be tabulated as follows:

1) Establish compartment detail thermal design requirements.

2) Review comparative performance and capabilities of various thermal controllers.

3) Study structural materials used in the compartment to establish the heat conductance paths.

4) Design a low weight compartment adequate for all loading conditions.

5) Study structural materials from a thermal standpoint to establish a basis for compromise between structural and thermal considerations.

6) Analyze structure to assure that design requirements will result in a high natural frequency for the compartments and a high strength-to-weight ratio.

7) Study the effect of the temperature – vacuum environment on the structural integrity of the compartment.

ANALYTICAL RESULTS

The methods used and representative results obtained in analyzing the thermal characteristics of Surveyor roving vehicles are described below. Two methods have been considered for primary thermal study of the vehicle: transient and equilibrium analyses. Work performed to date has been of the equilibrium type. It is intended that transient analysis be performed also at an appropriate point in the program to investigate design details.

The equilibrium method of analysis used was to subdivide the vehicle configuration into discrete constant temperature elements called "nodes". Each of the nodes is connected to all other nodes through a conduction matrix and a grey-body-radiation-view factor matrix. Each node also may receive solar heat directly or by reflection from other nodes and may have an arbitrary heat source attached to it. These heat sources represent the various electronic packages and motors in the vehicle. This method of analysis is valid provided that the temperature differences between nodes is small. This may be accomplished by selecting small enough nodes in regions where temperature gradients are large.

Basic Equations *

Using the above analysis, a digital machine program was written to find the equilibrium temperatures of a system of nodes. The equations this program solves result from the application of the First Law of Thermodynamics to each node, i.e., the sum of the heat entering a node must equal the sum of the heat leaving the node. The various heat fluxes entering or leaving a node are as follows.

1) Solar Heat Flux

$$QSOL_j = \alpha_j q_s A_j \cos \psi_j + q_s \sum_{n=1}^{NN} \left[\left(\frac{1 - \alpha_n}{\alpha_n} \right) A_n \mathcal{F}^{s}_{n,j} \cos \psi_n \right] \qquad \text{(III.2-1)}$$

2) Re-radiation Heat Flux

$$QRAD_j = \sigma A_j \sum_{n=1}^{NN} \left[\mathcal{F}^{G}_{n,j} (T_j^4 - T_n^4) \right] \qquad \text{(III.2-2)}$$

3) Conductive Heat Flux

$$QCON_j = C_{NN-1,j}(T_{NN-1} - T_j) + \sum_{n=1}^{NC} \left[C_{n,j}(T_n - T_j) \right] \qquad \text{(III.2-3)}$$

4) Source Heat Flux

$$QSOR_j = \text{Constant} \qquad \text{(III.2-4)}$$

---

* Symbols used in the equations in the analyses are described on page III.2-39.

Combining Equations III.2-1, 2-2, 2-3, and 2-4 according to the First Law gives the equilibrium equation for a given node, j.

$$\alpha_j q_s A_j \cos\psi_j + q_s \sum_{n=1}^{NN} \left[\left(\frac{1-\alpha_n}{\alpha n} \right) A_n \mathcal{F}^{s}_{n,\,j} \cos\psi_n \right] + C_{NN-1,\,j}(T_{NN-1} - T_j)$$

$$+ \sum_{n=1}^{NC} \left[C_{n,\,j}(T_n - T_j) \right] + C\,R_j - \sigma A_j \sum_{n=1}^{NN} \left[\mathcal{F}^{G}_{i} (T_j^4 - T_n^4) \right] = 0 \quad \text{(III.2-5)}$$

or

$$F_j(T_1,\ T_2,\ \ldots\ldots\ldots\ldots\ T_{NN-2}) = 0 \quad \text{(III.2-6)}$$

Method of Solution

Since the set of equations (see Eq. III.2-6) are non-linear in the variables T_j, an iterative method of solution must be used. The method chosen was the Newton-Raphson approximation. This method requires an initial starting point, which was taken as

$$T_j = \text{Constant} \quad \text{(III.2-7)}$$

Then the following set of linear equations are solved for the correction ΔT_j, to be applied to the starting guess;

$$\sum_{n=1}^{NN-2} \left[\frac{\partial F_j}{\partial T_n} (\Delta T_n) \right] = -F_j \quad \text{(III.2-8)}$$

$$T^1_j = T_j + \Delta T_j \quad \text{(III.2-9)}$$

The above method is repeated until

$$\left| \Delta T_j \right| < e = 0.1 \quad \text{(III.2-10)}$$

The node index, j, takes on the values $1 \leq j \leq NN-2$, where NN is the total number of nodes in the system plus the lunar surface node and outer space node as two other nodes whose temperatures are specified constants.

Thermal Models

The technique of Thermal Models is well known and can be applied to any particular design. The particular models of the SLRV to be discussed are illustrated in Figs.III.2-4, 2-5 and 2-6. The first two units of the three unit vehicle have been analyzed for these configurations. The first unit contains the TV electronics and the camera, while the second unit contains the batteries, receiver, transmitter, and control electronics. For analytically evaluating view factors, the wheels are considered to be cylinders rather than a torus, and each flat body surface will be a node. An additional node is used inside the body to represent the payload. Certain general conclusions can be drawn from proposed model changes.

a) An increase in radiator area will reduce the payload temperature or conversely permit an increase in payload heat dissipation for the same temperature.

b) An increase in the thermal conductance between the payload and the radiator will have a similar effect as in a) above but much less pronounced.

c) An increase in α or a reduction in ϵ of the radiator will increase the payload temperature or reduce the heat dissipated.

Other significant model changes usually are linked strongly with the whole node system so that specific calculations must be made before any conclusions can be drawn.

Fig. III.2-4, represents the maximum compartment size consistent with the vehicle configuration and stowage constraints on the Surveyor spacecraft. Solar panels in this configuration are mounted on the first and third carriages.

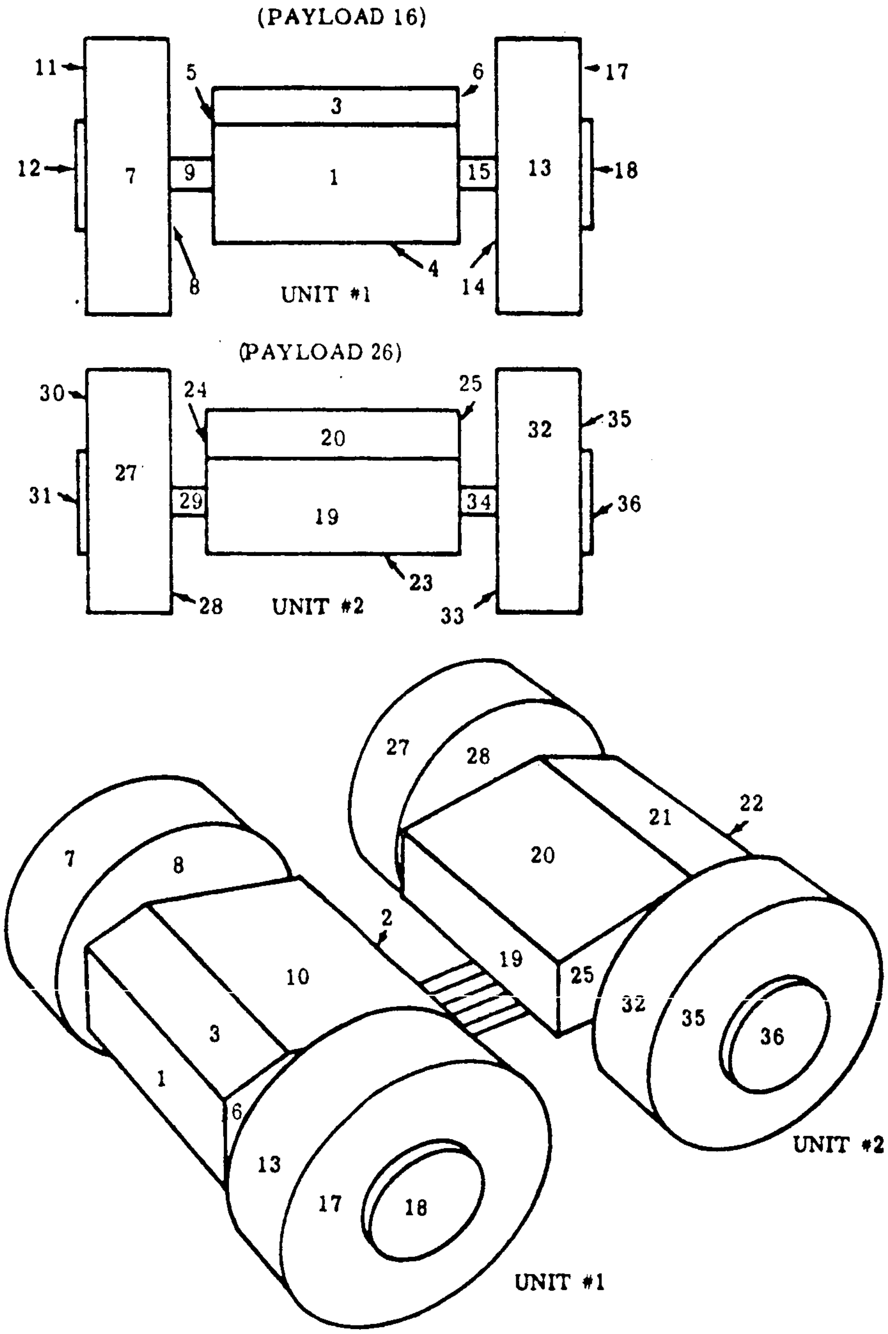

Fig.III.2-4. Thermal Models for Maximum Configuration

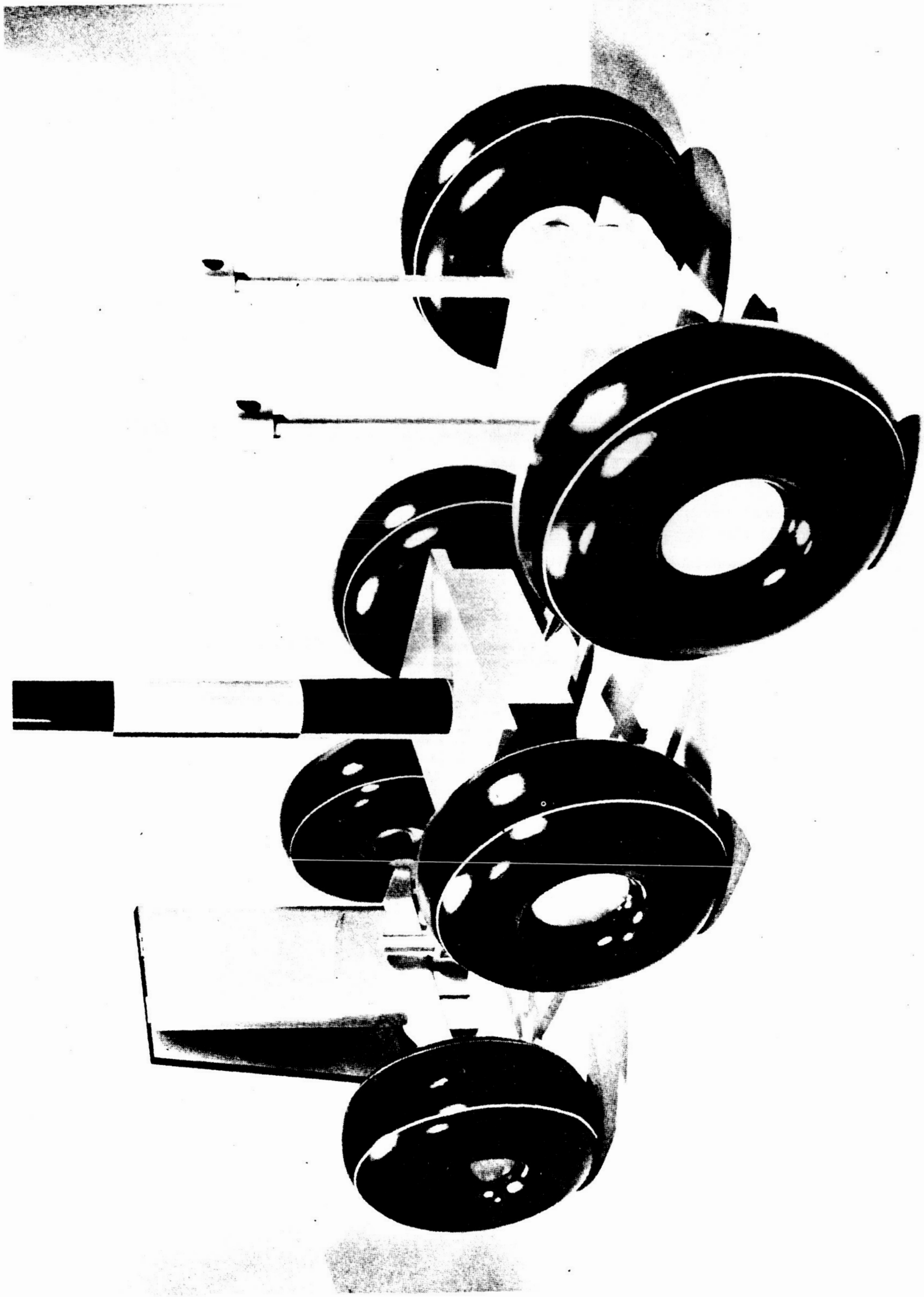

Fig. III.2-5. Thermal Model of the Current Vehicle Configuration Using Solar Power

64-406
VOL. II APP.
SEC. III

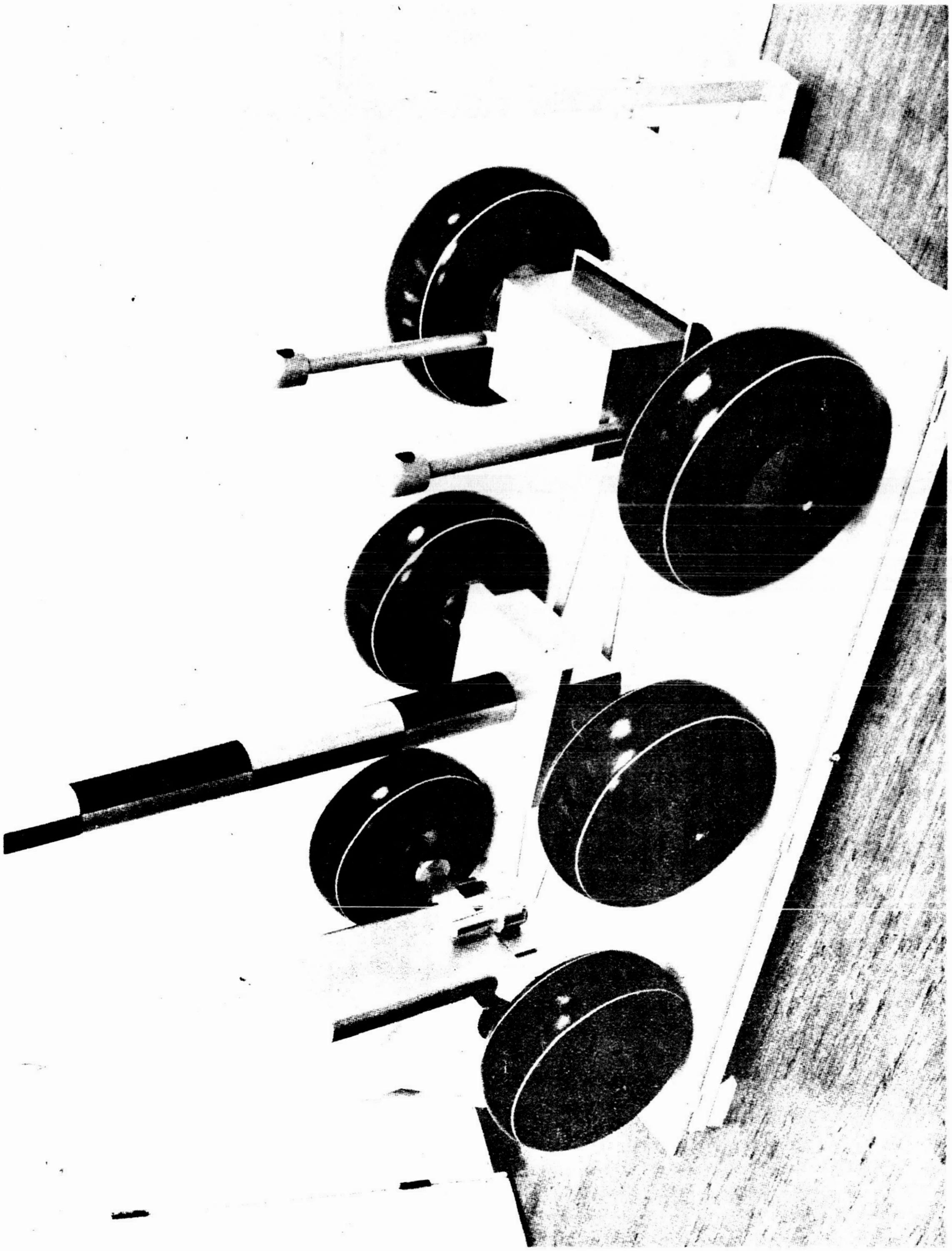

Fig. III.2-6. Thermal Model of the Current Vehicle Configuration Using R. T. E. Power.

Fig. III.2-5 is the thermal model of the current vehicle configuration using solar power. The solar panel in this design is mounted at the rear of the soil properties instrument as described in Subsections G and D, Power and Vehicle Configurations.

Fig. III.2-6 is the thermal model of the current vehicle configuration using power. This design concept mounts the R. T. E. on the third vehicle carriage.

A geometric view factor is defined as the fraction of heat emitted from a black surface which is intercepted by another black surface, or mathematically

$$F_{1,2} = \frac{1}{\pi A_1} \int\limits_{A_2}\int\limits_{A_1} \frac{\cos \phi_1 \cos \phi_2}{r^2} \, dA_2 dA_1 \qquad \text{(III.2-11)}$$

For some simple geometric shapes, it is possible to obtain a solution to Eq. III. 2-11 in closed form but in general it is impossible to carry out the integrations. Solutions to many geometric shapes have been published in the literature. One of the most useful is Reference 1*. This reference has been used to obtain many of the view factors used in this analysis directly or by Flux Geometry, see also Reference 1. Another analytical method which simplifies Eq. III. 2-11 by the application of Stoke's Theorem is covered in Reference 2. This method will be programmed for future use but was not used in this analysis.

An experimental method of obtaining view factors by use of a button mirror is covered in Reference 3. This method will handle any geometric shape and is used in future work for those complex surfaces which are not plane figures. The button method has previously been used to measure the view factors for thermal models, including those shown in Figures III. 2-5 and 2-6.

Basic Thermal Data

Certain of the basic data inputs are given in Table II on page J-19 for the maximum configuration calculations. The three matrices $C_{n,j}$, $\mathcal{F}^{S}_{n,j}$, and $\mathcal{F}^{G}_{n,j}$ are not tabulated because of their size and the fact that they are wholly dependent

* References are listed on page III. 2-41.

upon the specific design considered. In general, the conductances were taken to be similar to those of Reference 4 or computed where the specific geometry and materials were known at this time. The conductance from the payload to the radiator is varied by a thermal switch as in Reference 4. To determine the temperature limits of the system the switches are considered in the closed position (maximum value of conductance) for this analysis except when determining the required night survival heat source. The dependency of the conduction path to the lunar surface upon the thermal characteristics of the lunar surface has been eliminated because, in general, the vehicle is moving and therefore encountering a fresh surface layer at a constant temperature at all times. For those cases where the vehicle is stationary, the lunar surface is still considered to be at a constant temperature. This is not correct in the near vicinity of the vehicle but the assumption is considered valid until it can be checked by transient conduction methods at a later date. The grey body view factors were computed from

$$[R_{i,j}] \times [\mathcal{F}_{i,j}] = [Q_{i,j}] \tag{III.2-12}$$

where

$$R_{i,j} = \left[\sum_{j=1}^{NN} F_{i,j}(1-\epsilon_j)/\epsilon_j\right]_{i \neq j} + \left[F_{i,j}(1-\epsilon_j)/\epsilon_j - \frac{1}{\epsilon_j}\right]_{i=j} \tag{III.2-13}$$

and $Q_{i,j} = -F_{i,j}\,\epsilon_j$ for $\mathcal{F}_{i,j}^{G}$. To obtain $\mathcal{F}_{i,j}^{S}$ use α_j in place of ϵ_j. The above method is from Chapter 4 of Reference 5.

TABLE III.2-2. Basic Thermal Data

Surface	α	ϵ	
Lunar	.875	.875	Lunar Surface Temperature as a function of sun position was taken from Reference 6.
Solar Cell	.70	.84	
Radiator	.122	.85	The solar flux of 1.394 kw/m^2 was taken from JPL EPD-98.

RF-ORDER No. 64-466
LCK II APP.

The SLRV has a variable power dissipation requirement which depends upon the particular mission requirement. The particular thermally important missions which were analyzed are:

- Night hibernation
- Day step mode
- Day hibernation
- Day stall mode

The power dissipated at various nodes for these missions is given in Table III.2-3 below.

TABLE III.2-3. Nodal Heat Loads, Watts

Node No.	Night	Day			Remarks
	Hibernation	Step Mode	Hibernation	Stall Mode	
16	2.7	2.3 to 5.8	0	2.3	Payload Unit 1
1	---	2.7	2.7	2.7	Day storage of night survival source
9	---	1.7	---	24.0	Wheel motor
15	---	1.7	---	24.0	Wheel motor
4	---	2.3	---	10.9	Steering motor
26	3.6	2.2 to 2.6	0.25	2.2	Payload Unit 2
19	---	3.6	3.6	3.6	Day storage of night survival source
31	---	1.7	---	24.0	Wheel motor
36	---	1.7	---	24.0	Wheel motor

During the day step mode, the power level will vary according to the rate at which TV pictures are taken and the frequency of use of the transmitter. The payload figures given above are considered to be the minimum. The effect of variable payload power is shown on Fig. III.2-7, later in this discussion.

Results of Analysis of Maximum Configuration

A preliminary analysis has been made of the two units shown in Fig. III.2-4. The results are discussed below:

PAYLOAD NIGHT TIME HEATING REQUIREMENTS The payloads of units 1 and 2 must be kept warm during the lunar night to permit the use of standard electronic components and to prevent damage to the batteries. The effect of heat source strength on payload temperature during the coldest portion of the lunar night, just prior to lunar dawn, is shown on Fig. III.2-7. The temperature limits for the two units differ because unit 1 has no batteries which require a minimum temperature of $-18^{\circ}C$. As shown, the minimum required heat sources are 2.7 watts and 3.6 watts for units 1 and 2, respectively. Since these heat sources would add to the daytime heat load, it is intended to switch them to an outside surface when the payload reaches operating temperature. Nodal surfaces 1 and 19 were chosen for this purpose. In general, any increase in body external area will require an increase in these night time heat sources.

PAYLOAD TEMPERATURE PROFILES. The variation of payload equilibrium temperature with sun position for various power schedules is shown on Fig. III.2-8, (a and b). These profiles are for the case where the thermal switches to the radiators are closed, giving the minimum temperatures possible. Depending upon the payload temperature limits imposed, it can be seen that under certain combinations of power schedule and sun position, there will be certain portions of the lunar day during which operation of the vehicle is not possible. The periods during which it is possible to operate the vehicle are called the operating windows; these are shown in Fig. III.2-9 for hypothetical values for equipment tolerance. Note that the windows of the two units are different; thus, it is possible to reduce the radiator area of unit 2 because the window of unit 1 is the controlling factor for the vehicle. The most desirable design would be one for which the window was wide open. It may be possible to achieve this if unit 1 uses a radiator for node 10 rather than a solar panel. The concentration of all solar cells in a folding array on unit 3 will be discussed below:

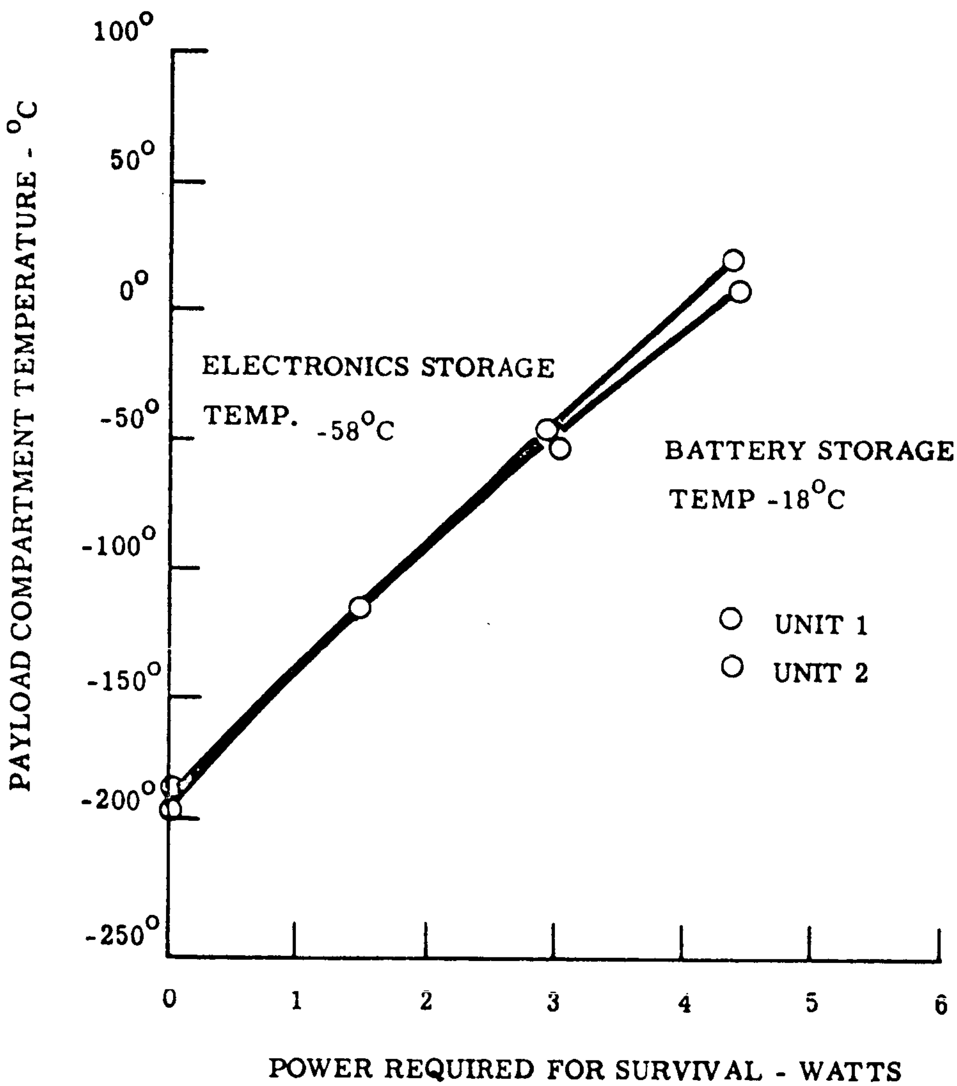

Fig. III. 2-7. Payload Compartment Temperature Vs. Night Heat Source Strength (Maximum Configuration) Lunar Surface Temperature = -185°C

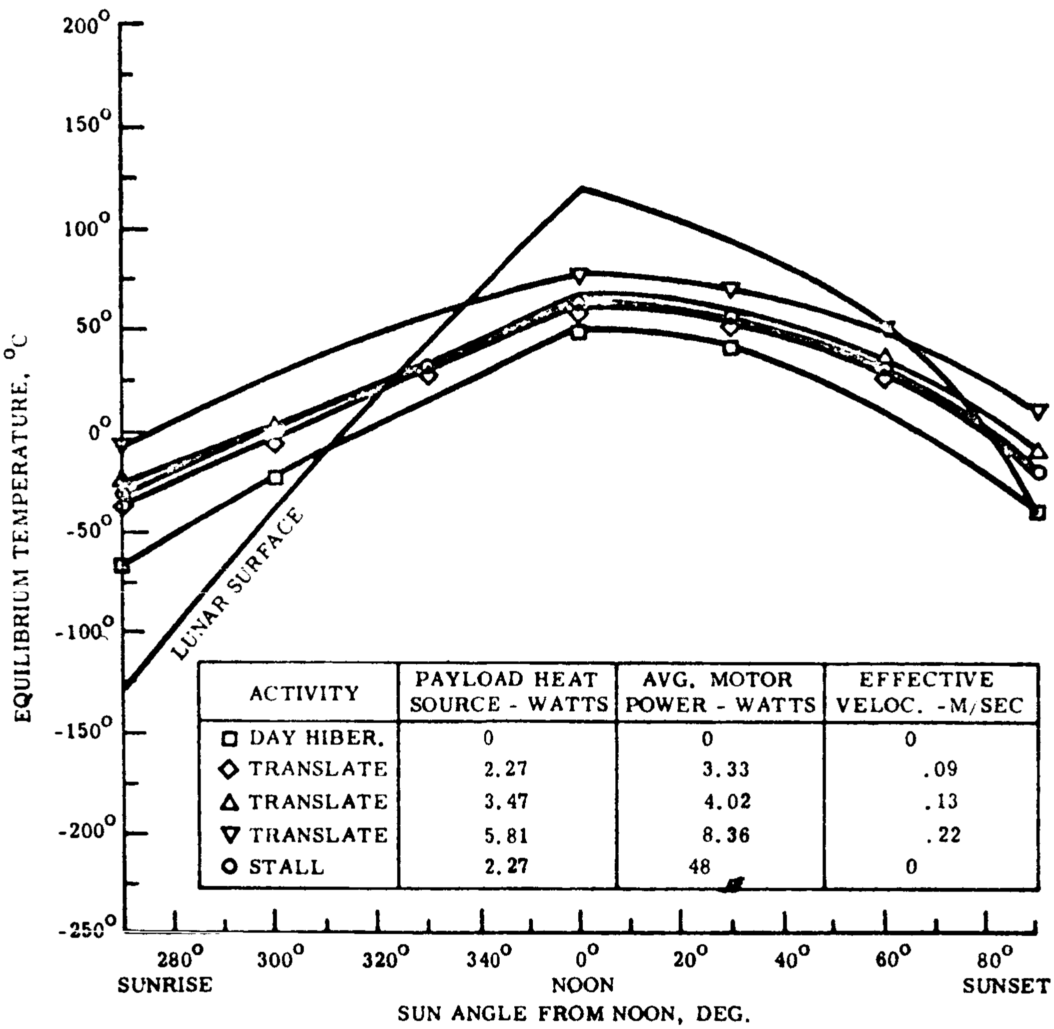

ACTIVITY	PAYLOAD HEAT SOURCE - WATTS	AVG. MOTOR POWER - WATTS	EFFECTIVE VELOC. -M/SEC
◻ DAY HIBER.	0	0	0
◇ TRANSLATE	2.27	3.33	.09
△ TRANSLATE	3.47	4.02	.13
▽ TRANSLATE	5.81	8.36	.22
○ STALL	2.27	48	0

Fig.III.2-8a, Unit 1. Maximum Configurations. Night Heat Source on Node 1. All Thermal Switches Closed.

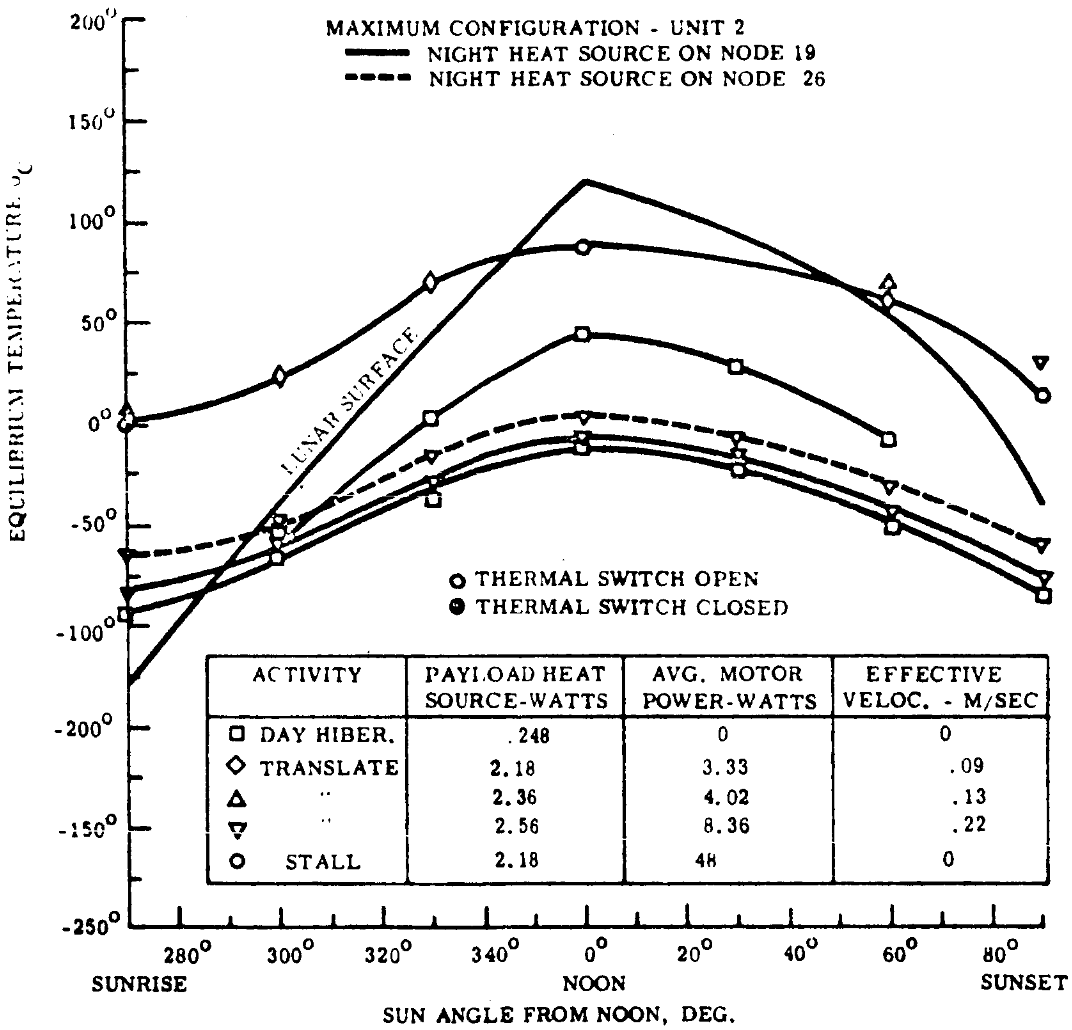

ACTIVITY	PAYLOAD HEAT SOURCE-WATTS	AVG. MOTOR POWER-WATTS	EFFECTIVE VELOC. - M/SEC
□ DAY HIBER.	.248	0	0
◇ TRANSLATE	2.18	3.33	.09
△ "	2.36	4.02	.13
▽ "	2.56	8.36	.22
○ STALL	2.18	48	0

Fig. III.2-8. Payload Compartment Temperature vs. Sun Position

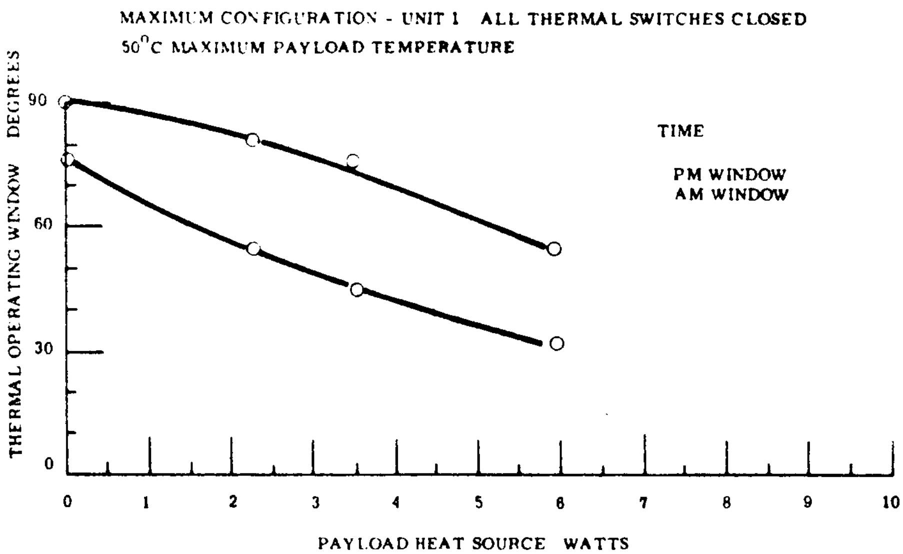

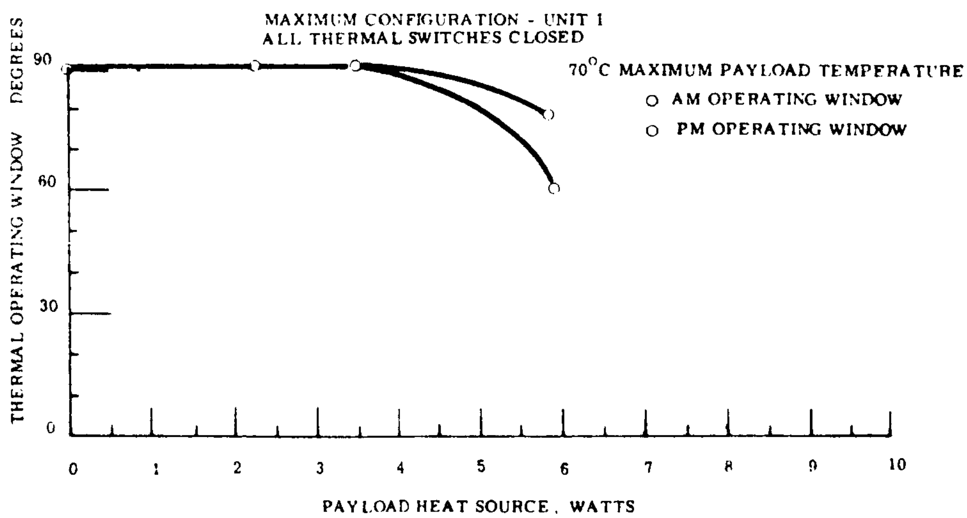

Fig. III.2-9a & b. Thermal Operating Window vs. Payload Heat Source Strength

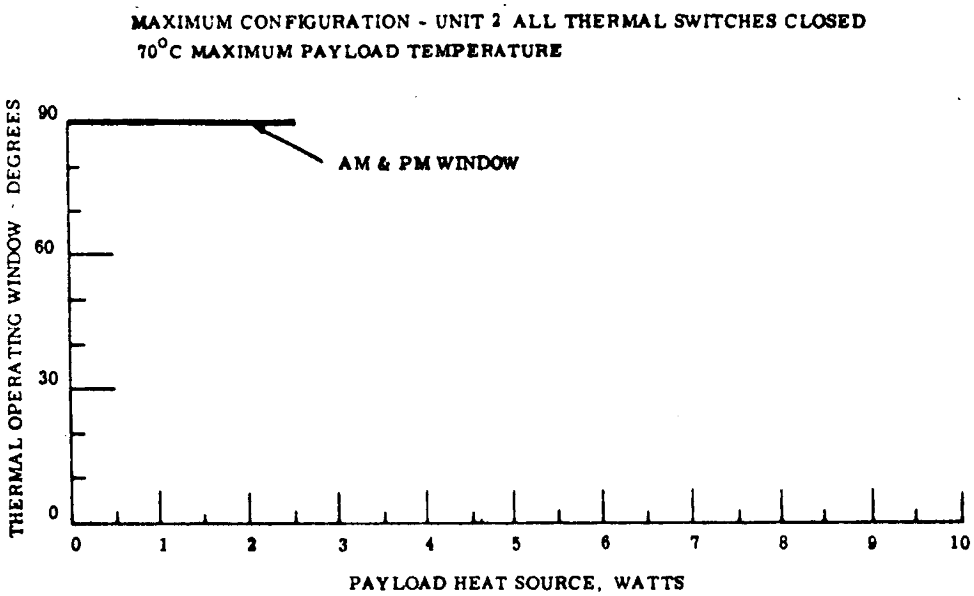

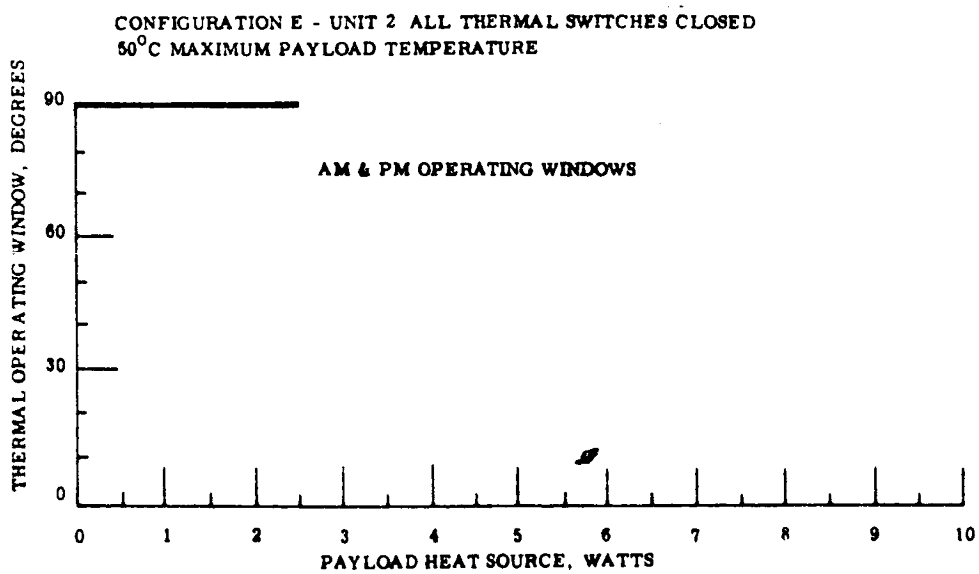

Fig. III. 2-9c & d. Thermal Operating Window vs. Payload Heat Source Strength

THERMAL OPERATING WINDOWS. The periods during a lunar day during which it is possible to operate the vehicle without exceeding any of the temperature limits imposed by the equipment characteristics are called thermal operating windows. During the portion of the lunar day when these temperature limits restrict the operation of the vehicle, it will hibernate, dissipating a minimum amount of power. The operating windows for unit 1 and 2 are shown in Fig.III.2-9 as a function of payload power dissipated for assumed values of equipment tolerance. Note that the windows of the two units are different; thus it is possible to reduce the radiator area of unit 2. An optimum design will be arrived at when both operating windows are identical, and the best thermal design when a completely open window is obtained for all power schedules. It may be possible to achieve this "best" design if unit 1 does not contain any solar cells so that node 10 may be used as a radiator as well as node 3.

Representative estimates of equipment tolerances are given in Table III.2-4.

TABLE III.2-4

Electronic Equipment Tolerances

Unit	Operating	Storage
Transceiver	-55^{0} to 100^{0}C	-70^{0}C to 150^{0}C
Telemetry and Logic	-55^{0}C to 75^{0}C	-70^{0}C to 125^{0}C
Television Circuits	-55^{0}C to 100^{0}C	-70^{0}C to 125^{0}C
Vidicon	25^{0}C to 35^{0}C	-15^{0}C to 60^{0}C
Battery	-18^{0}C to 50^{0}C	$-18^{0}$to 50^{0}C

MOTOR RADIATOR TEMPERATURE PROFILES. The wheel motors are conductively connected primarily to the external wheel hub radiators, nodes 12, 18, 31, and 36. The temperature profiles for these nodes are shown in Figs.III.2-10a and b.

The radiator temperature ranges from 77^{0} to 413^{0}K. About a 14 to 28^{0}C rise can be expected from the radiator to the motor itself.

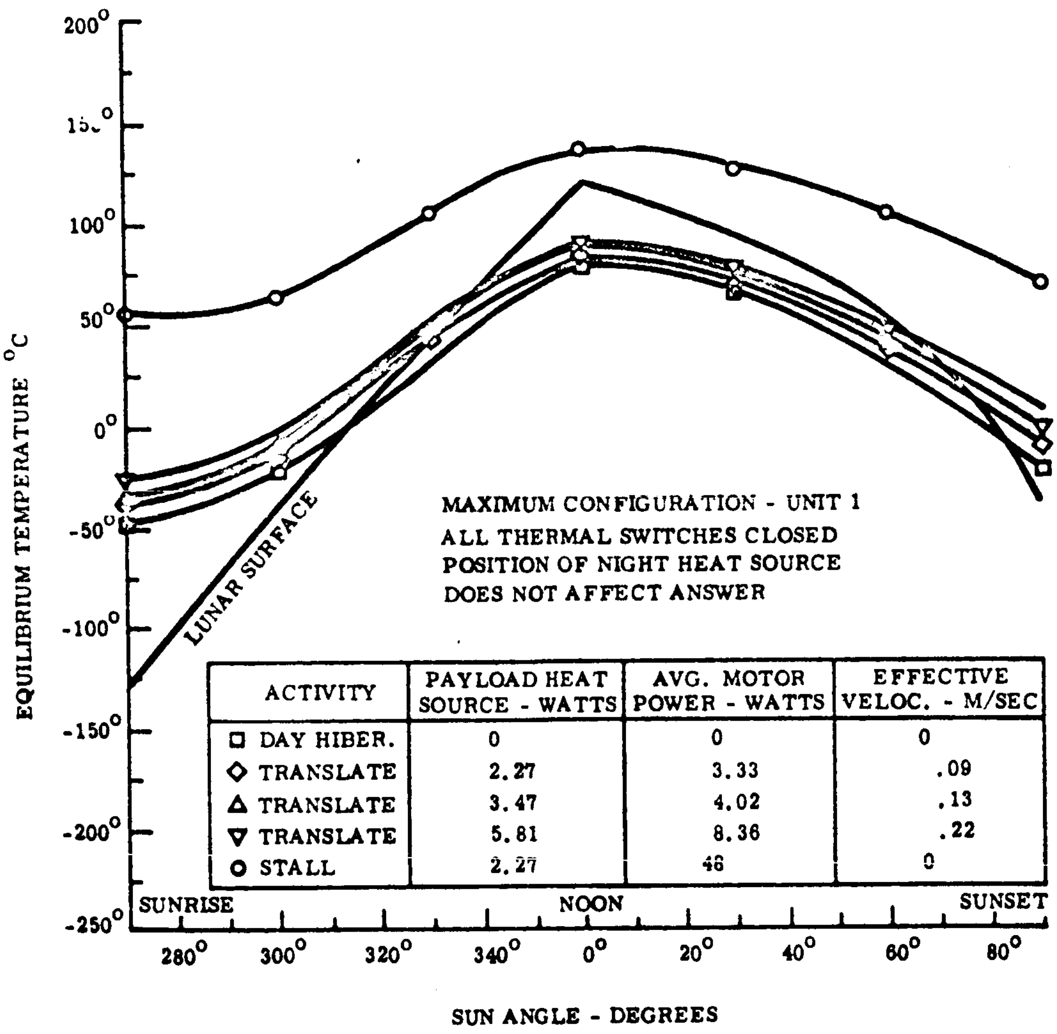

ACTIVITY	PAYLOAD HEAT SOURCE - WATTS	AVG. MOTOR POWER - WATTS	EFFECTIVE VELOC. - M/SEC
□ DAY HIBER.	0	0	0
◇ TRANSLATE	2.27	3.33	.09
△ TRANSLATE	3.47	4.02	.13
▽ TRANSLATE	5.81	8.36	.22
○ STALL	2.27	46	0

Fig. III.2-10a. Drive Motor Radiator Temperature vs. Sun Angle

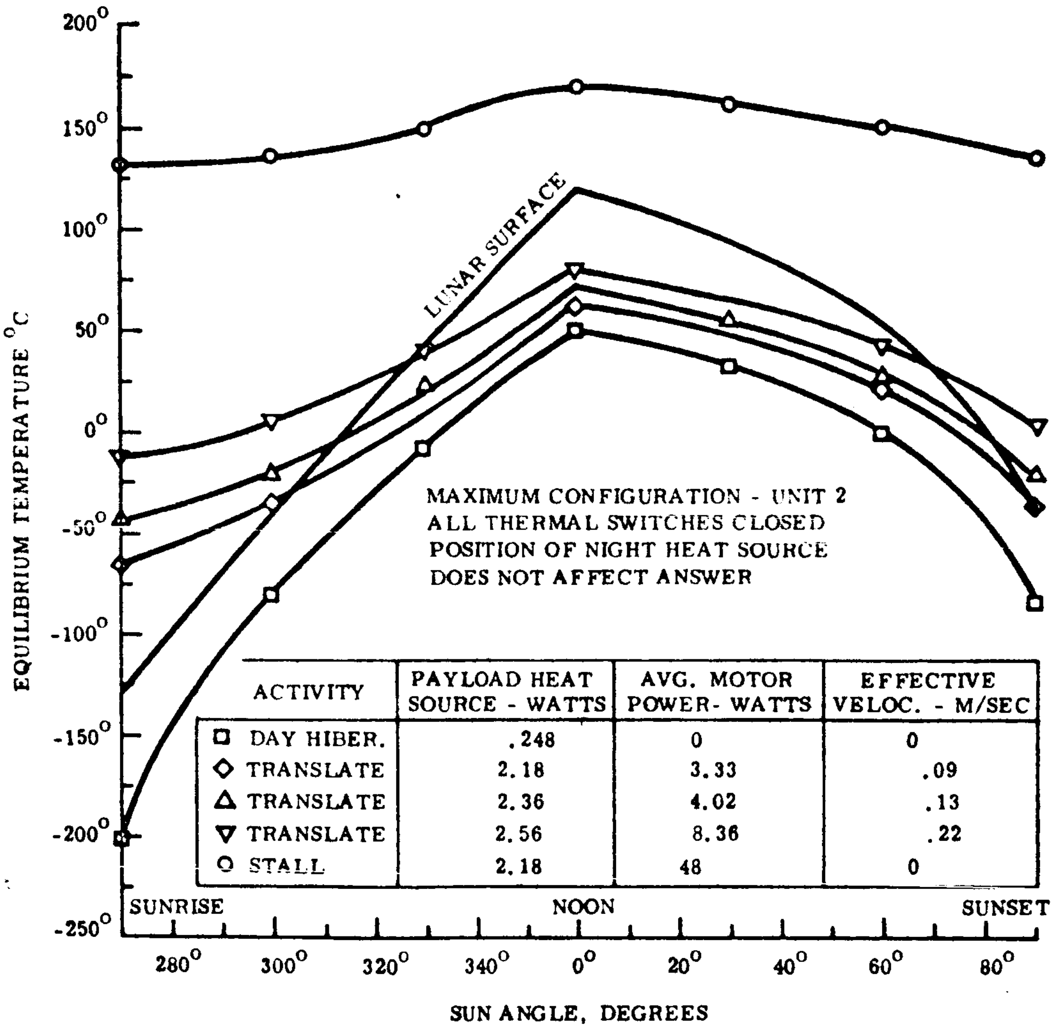

ACTIVITY	PAYLOAD HEAT SOURCE - WATTS	AVG. MOTOR POWER- WATTS	EFFECTIVE VELOC. - M/SEC
□ DAY HIBER.	.248	0	0
◇ TRANSLATE	2.18	3.33	.09
△ TRANSLATE	2.36	4.02	.13
▽ TRANSLATE	2.56	8.36	.22
○ STALL	2.18	48	0

Fig. III.2-10b. Drive Motor Radiator Temperature vs. Sun Angle

VIDICON TEMPERATURE. The temperature limits on the vidicon tube are very restrictive and for this reason it was decided that a separate radiator will be supplied along with an electrical heating and control system. By this means, the temperature of the vidicon faceplate may be controlled separately from that of the remaining electronics.

Results of Analysis of Configuration E

To improve the thermal operating windows and reduce the solar panel temperatures, configuration E shown on Fig. III.2-5 was studied. For this configuration all the solar cells are concentrated in a folding array on unit 3. It is thus possible to increase materially the radiator area of unit 1. The results of this analysis are shown on Figs. III. 2-11 through III. 2-14.

Analysis of Stowed Configuration

At this point in the study the stowed configuration has not been analyzed, so that data is not available. The general method previously discussed will be used in determining these temperatures when this point in the study is reached. The main problems to be resolved in the stowed configuration are placement of the night heating sources and whether these sources will require special radiators in this configuration. At present these sources are switched out of the payload to nodes 1 and 19 when the payload temperature comes up to operating temperatures. This choice of nodes is quite arbitrary and a study of the stowed configuration may dictate another location. In particular, the bottom surfaces 4 and 23 would be best for the stowed configuration.

FUTURE STUDIES

The thermal analysis of the Surveyor Lunar Roving Vehicle will include the procedure discussed above plus an extensive transient study in local areas – such as the wheel motors steering motors, solar panels, electronics, etc. At this point in the study a transient analysis is not practical because the configuration is not well enough defined. It is expected that local transients will cause minor design modifications in the final vehicle. Major phases of the Future Studies are as follows:

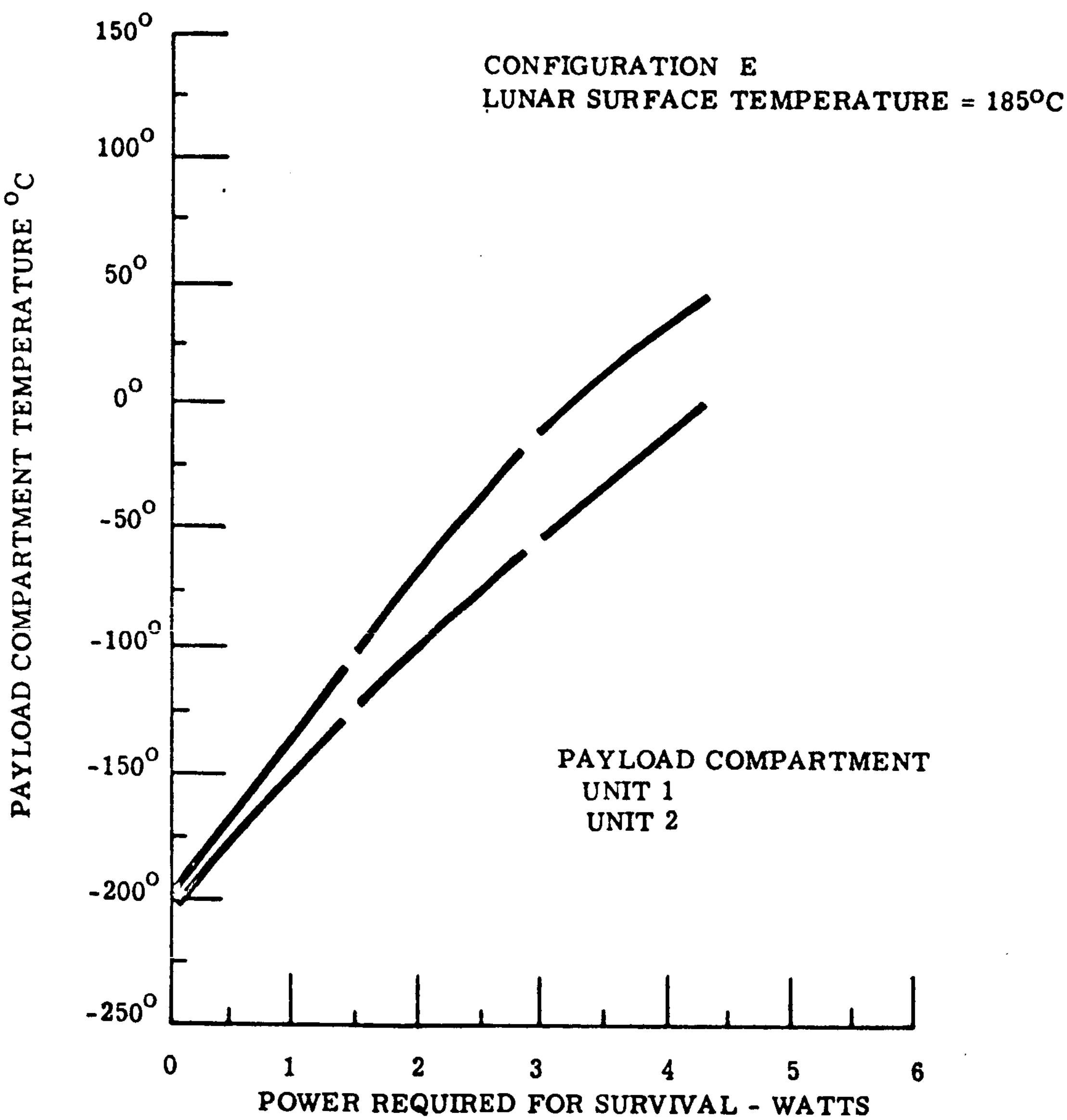

Fig. III.2-11. Payload Compartment Temperature vs. Night Heat Source Strength

64-406

Vol. II App.

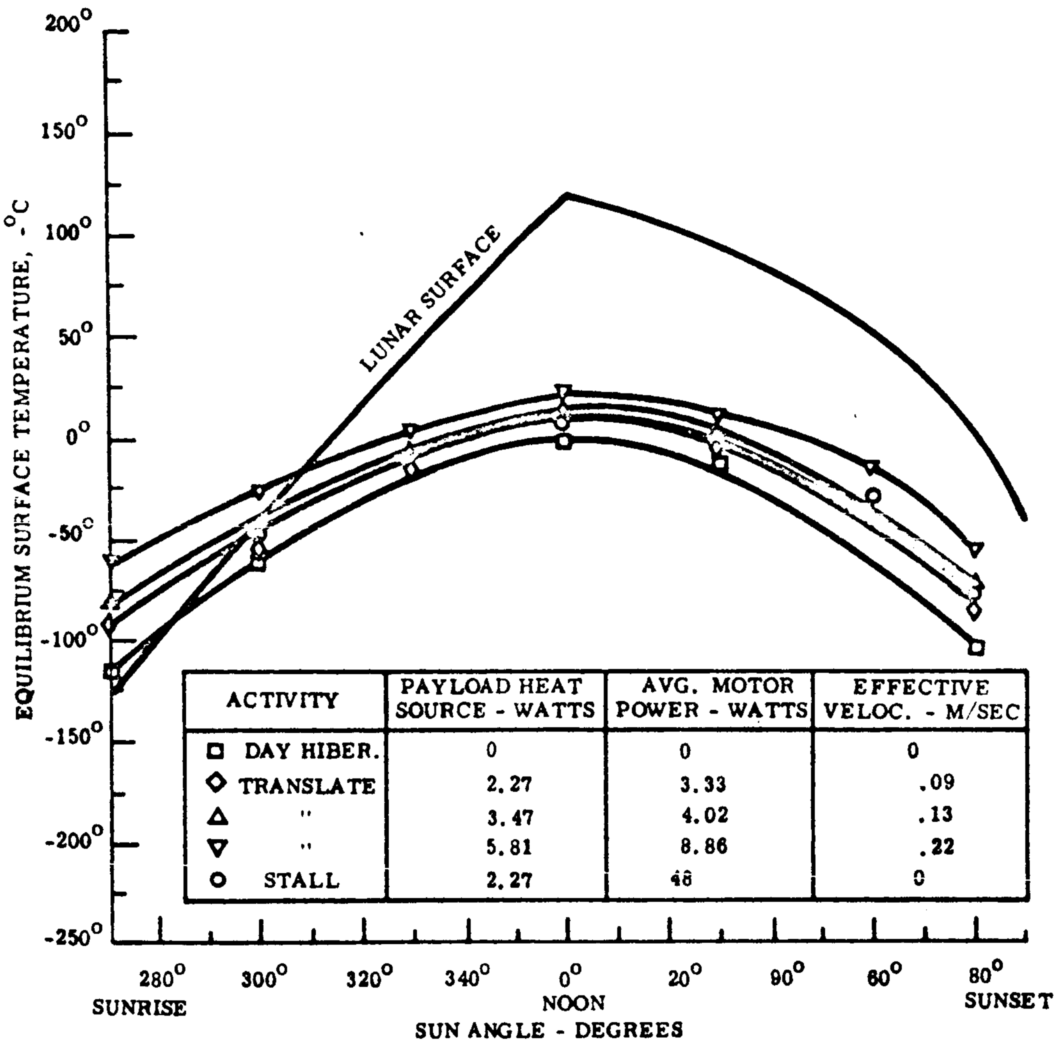

ACTIVITY	PAYLOAD HEAT SOURCE - WATTS	AVG. MOTOR POWER - WATTS	EFFECTIVE VELOC. - M/SEC
□ DAY HIBER.	0	0	0
◇ TRANSLATE	2.27	3.33	.09
△ "	3.47	4.02	.13
▽ "	5.81	8.86	.22
○ STALL	2.27	48	0

Fig. III.2-12a. Payload Compartment Temperature vs. Sun Angle

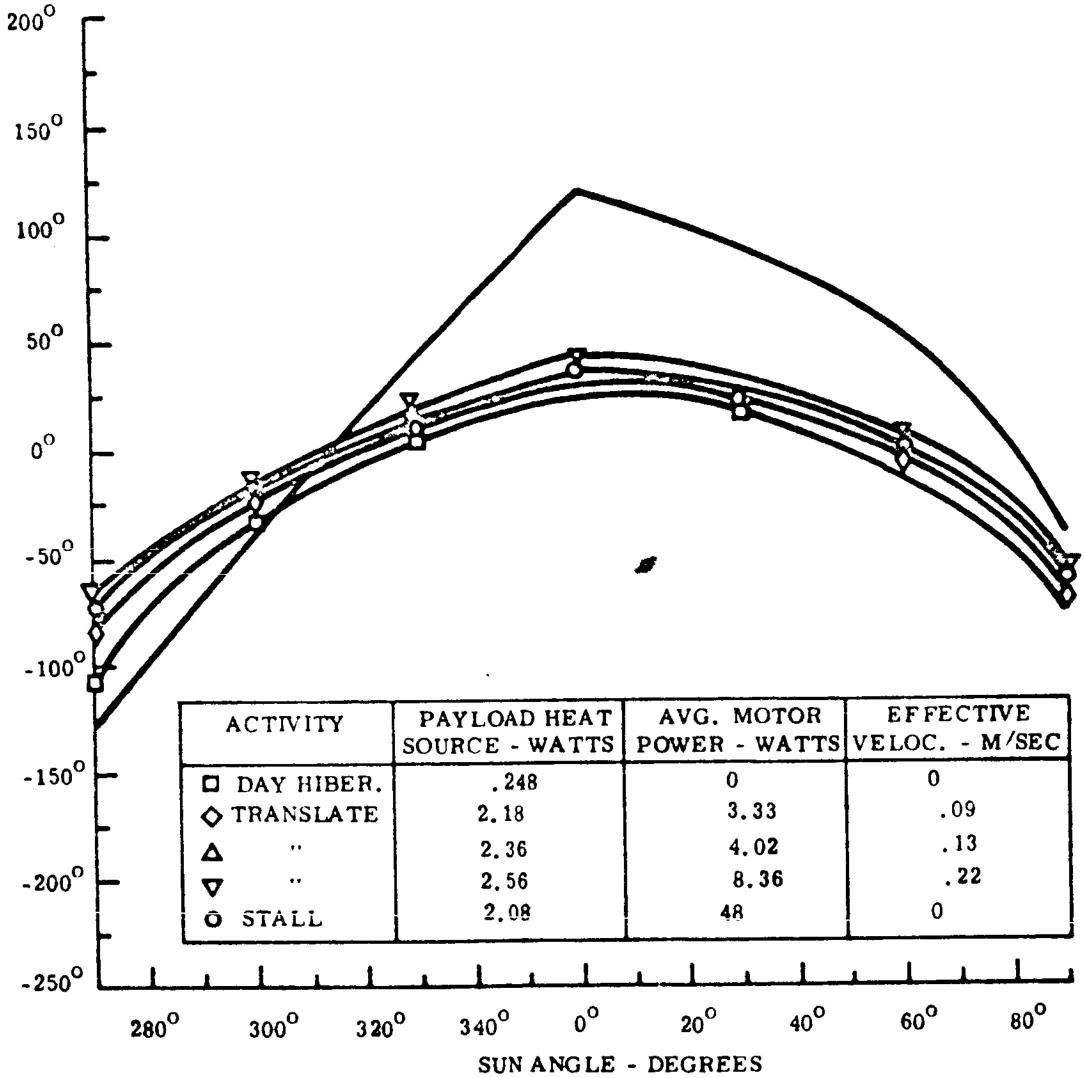

ACTIVITY	PAYLOAD HEAT SOURCE - WATTS	AVG. MOTOR POWER - WATTS	EFFECTIVE VELOC. - M/SEC
□ DAY HIBER.	.248	0	0
◇ TRANSLATE	2.18	3.33	.09
△ "	2.36	4.02	.13
▽ "	2.56	8.36	.22
○ STALL	2.08	48	0

Fig. III.2-12b. Payload Compartment Temperature vs. Sun Angle

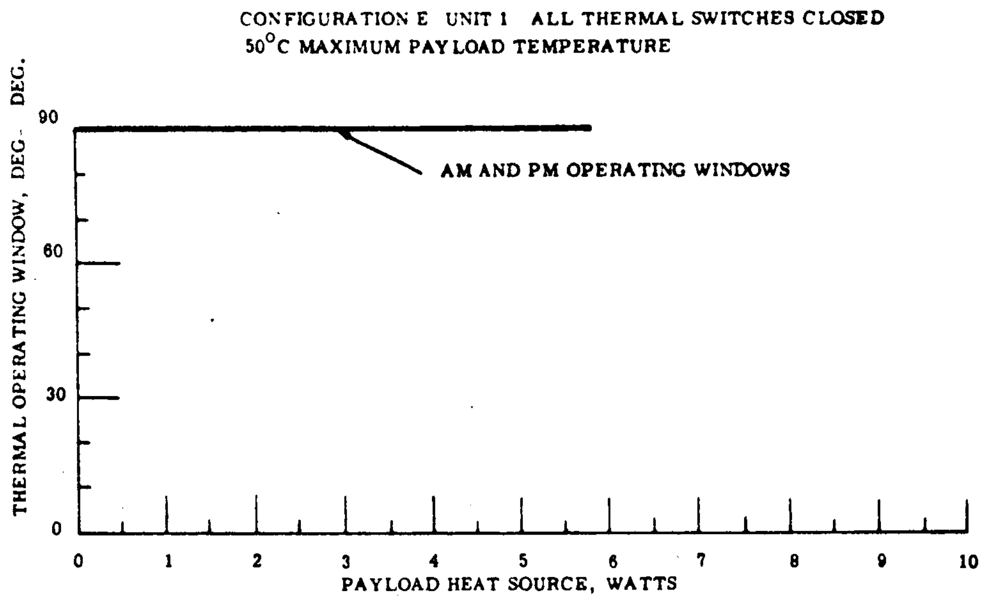

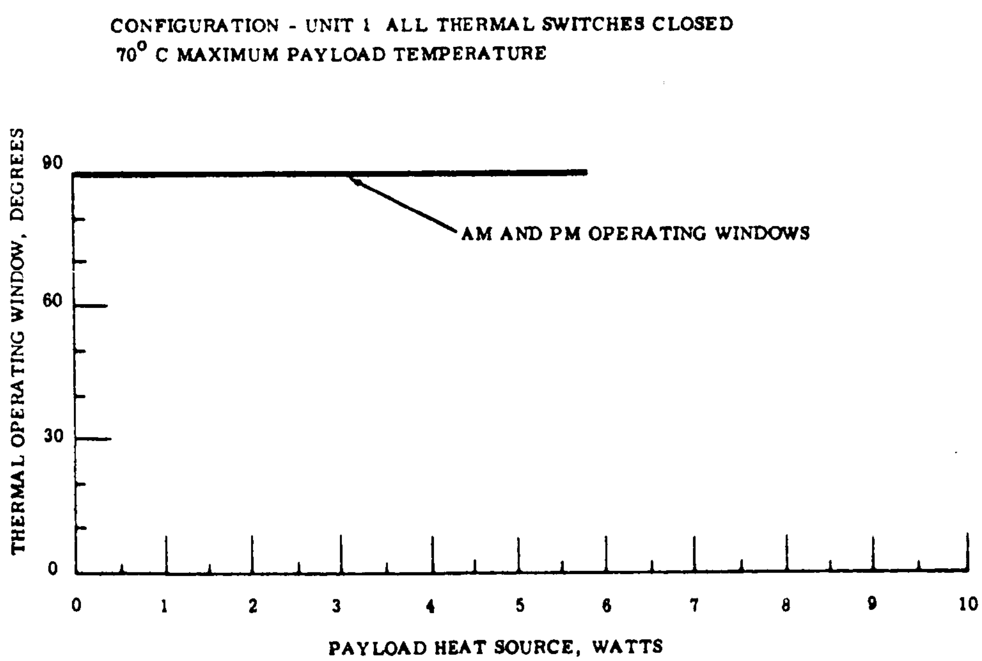

Fig. III.2-13a & b. Thermal Operating Window vs. Payload Heat Source Strength

MAXIMUM CONFIGURATION - UNIT 2
ALL THERMAL SWITCHES CLOSED
$50^{\circ}C$ MAXIMUM PAYLOAD TEMPERATURE

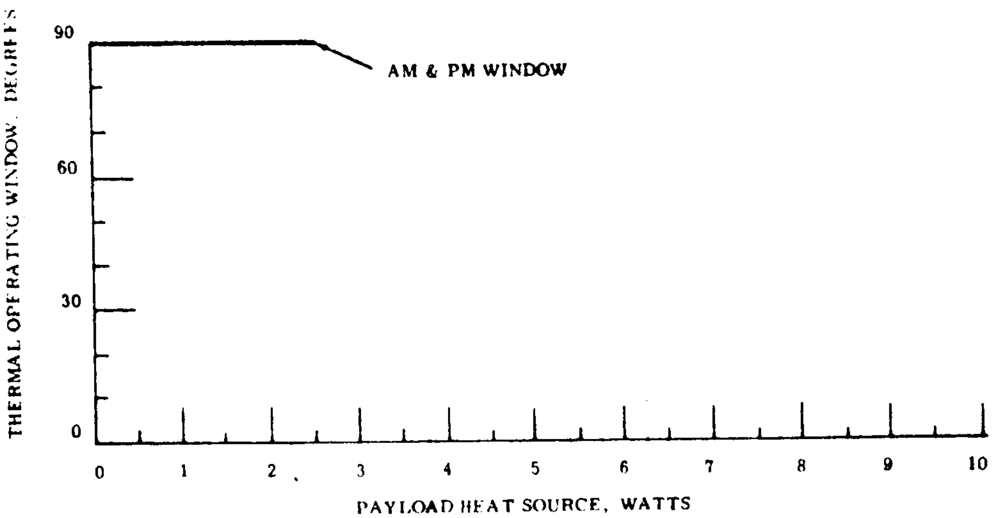

CONFIGURATION E - UNIT 2 ALL THERMAL SWITCHES CLOSED
$70^{\circ}C$ MAXIMUM PAYLOAD TEMPERATURE

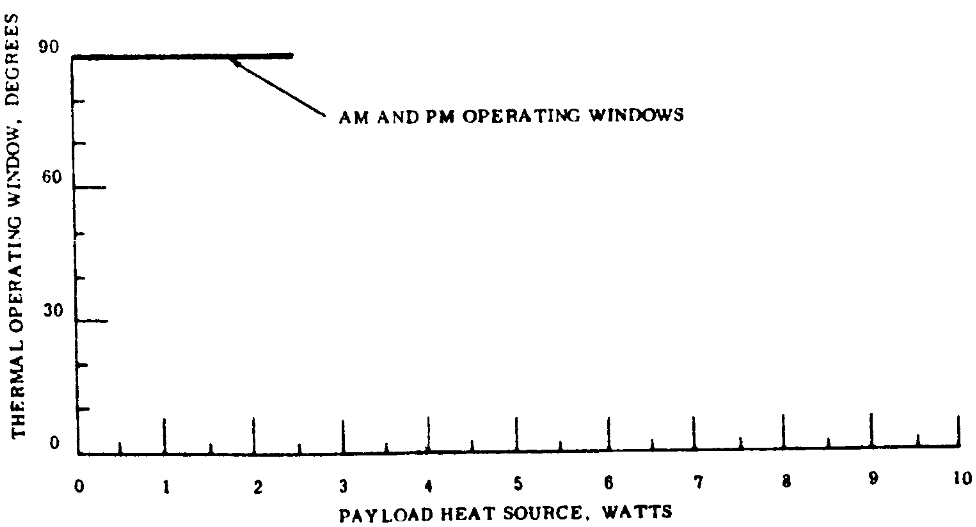

Fig. III.2-13c & d. Thermal Operating Window vs. Payload Heat Source Strength

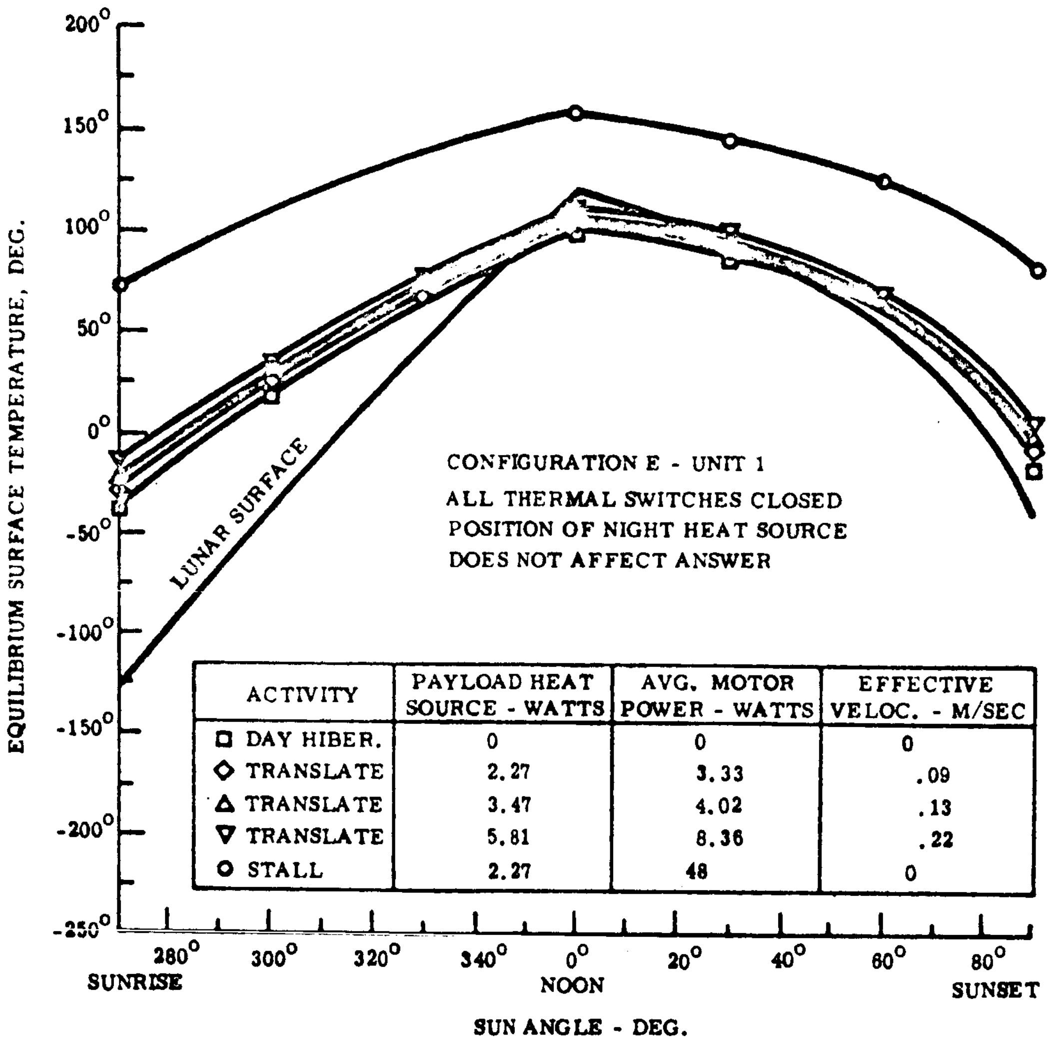

ACTIVITY	PAYLOAD HEAT SOURCE - WATTS	AVG. MOTOR POWER - WATTS	EFFECTIVE VELOC. - M/SEC
□ DAY HIBER.	0	0	0
◇ TRANSLATE	2.27	3.33	.09
△ TRANSLATE	3.47	4.02	.13
▽ TRANSLATE	5.81	8.36	.22
○ STALL	2.27	48	0

Fig. III.2-14a. Drive Motor Radiator Temperature vs. Sun Angle

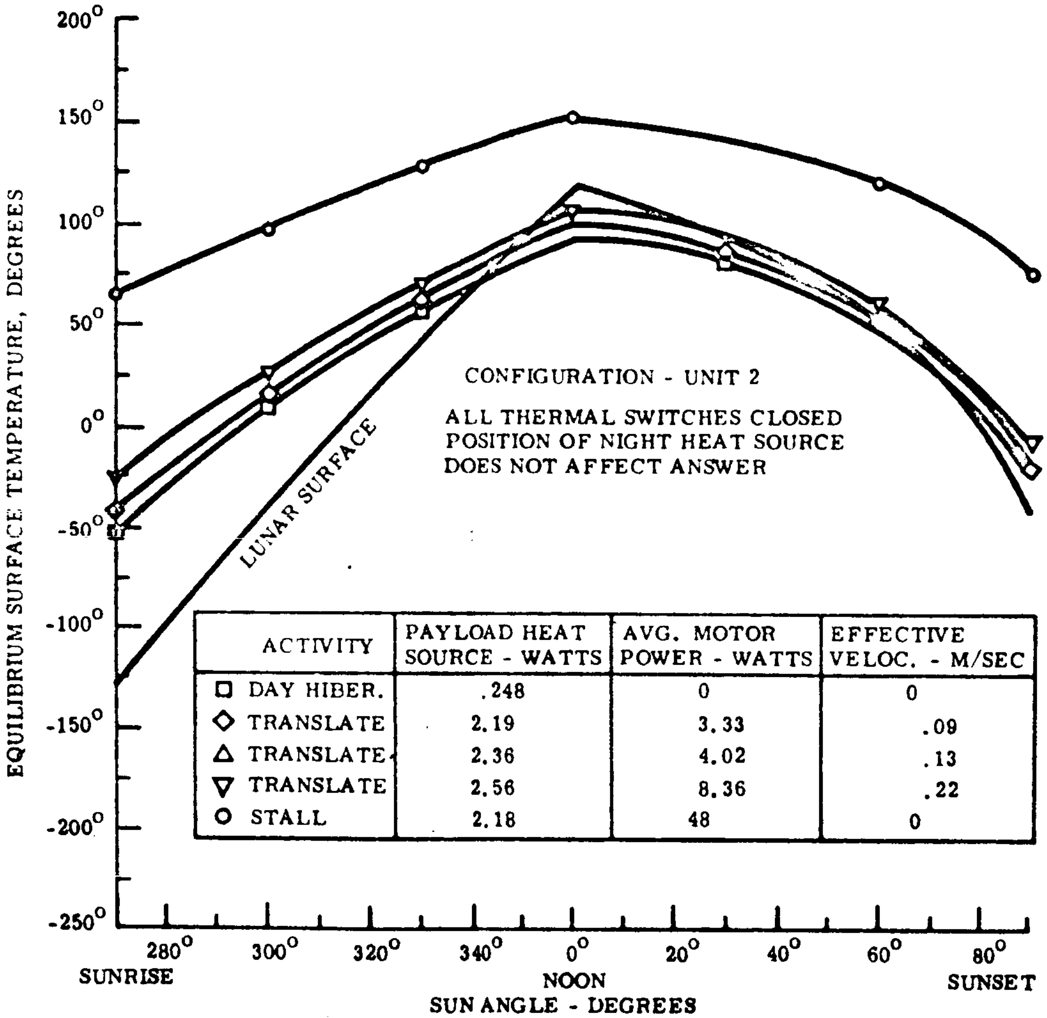

ACTIVITY	PAYLOAD HEAT SOURCE - WATTS	AVG. MOTOR POWER - WATTS	EFFECTIVE VELOC. - M/SEC
□ DAY HIBER.	.248	0	0
◇ TRANSLATE	2.19	3.33	.09
△ TRANSLATE	2.36	4.02	.13
▽ TRANSLATE	2.56	8.36	.22
O STALL	2.18	48	0

Fig. III.2-14b. Drive Motor Radiator Temperature vs. Sun Angle

- Thermal studies to maximize the operating window and/or to equalize the operating windows of each unit of the vehicle
- Determination of all material temperature ranges to permit proper selection and specification of materials
- Studies to check the stowed configuration to determine that no temperature limits are exceeded
- Transient analysis of the vehicle to check that none of the temperature limits are locally exceeded and that an equilibrium analysis is indeed an adequate method of analysis. A transient analysis will also permit a close simulation of the vehicle's mission.
- Augmentation of the analytical program by an experimental program to supply basic data and check the results of the analytical studies. This will be done by thermal models.

LIST OF SYMBOLS

Symbol	Description	Units
a	Angle between the sun's rays and the lunar surface	Degrees
A_j	Surface area of node j	ft^2
$C_{n,j}$	Thermal conductance from node n to node j	BTU/hr-^oR
e	Iteration error limit for the Newton-Raphson method, 0.1	^oR
F_j	Sum of the heat fluxes entering or leaving of leaving node j	BTU/hr
$F_{i,j}$	Geometric view factor from node i	None
$\mathfrak{J}^G_{i,j}$	Grey-body view factor from node i to node j	None
$\mathfrak{J}^S_{i,j}$	Solar-reflectance view factor from node i to node j	None
NC	Number of nodes connected by conduction	None
NN	Total number of nodes	None
Q	Total integrated heat flux received by a solar panel from the sun	BTU
q_s	Solar constant, 439 BTU/hr-ft^2	BTU/hr-ft^2
$Q_{i,j}$	Radiation view factor product matrix	None
$QSOL_j$	Heat flux received from the sun by node j	BTU/hr
$QRAD_j$	Heat flux re-radiated from node j	BTU/hr
$QSOR_j$	Heat source located on node j	BTU/hr
$QCON_j$	Heat flux received from all other nodes by conduction on node j	BTU/hr
r	Distance between two surfaces, A_1 and A_2	ft
$R_{i,j}$	Radiation view factor coefficient matrix	None
α_j	Solar absorbtivity of node j	None
ϵ_j	Thermal emissivity of node j	None
ϕ_1	Angle between the normal to surface 1 and the line of sight between 1 and 2	Degrees

Symbol	Description	Units
ϕ_2	Angle between the normal to surface 2 and the line of sight	Degrees
ψ_j	Angle between the normal to surface j and the sun's rays	Degrees
δ	The Stephen-Boltzman constant, 0.1713×10^{-8}	$BTU/hr\text{-}ft^2\text{-}(^\circ R)^4$

Subscripts

i, j, n	Node number
L, NN-1	Lunar surface
NN	Outer space

REFERENCES

1. "Radiant-Interchange Configuration Factors", by D. C. Hamilton and W. R. Morgan, NACA TN 2836, December 1952

2. "A New and Simpler Formulation for Radiative Angle Factors", by E. M. Sparrow, ASME J. HEAT TRANSFER, Vol. 85, No. 2, Series C, May 1963

3. "The Measurement of Radiation Configuration Factors with Parabolic Mirrors", by R. S. Hickman, THERMOSPACE Co

4. "Space Programs Summary No. 37-10, Vol. II", JPL CIT, No. 37-10, S546-C-61, August 1, 1961; also No. 37-11, -12, -13, -14, -15, -16, -17, -18, -19, and -20

5. HEAT TRANSMISSION, McAdams, Third Edition, McGraw-Hill Book Company, Inc., New York and London

6. "A Hypothetical Model of the Lunar Surface for Use in Lunar Logistics Systems Studies", NASA, Working Paper LLS-SSG-1001, August 7, 1962

2. Compartment Structural and Heat Transfer Considerations

An examination has been made of advantages gained through substitution of beryllium for 7075 T6 aluminum alloy in the payload compartments. Compartment No. 2 was used as the example. The payload mounting panel was taken as being a titanium honeycomb core, faced with sheets of .015-inch beryllium, in a brazed assembly.

Lowest Mode – Mounting Panel

From the expression for the lowest mode

$$f_1 = \frac{\pi}{2}\left(\frac{1}{a^2} + \frac{1}{b^2}\right)\left(\frac{gD}{\gamma H}\right)^{1/2} \qquad \text{(III. 2-14)}$$

where a, b = panel length and width
γ = payload weight per unit panel volume
H = total panel thickness
D = panel flexural rigidity

a direct comparison is possible between aluminum and beryllium. This is shown in the table below:

	Aluminum	Beryllium
Core density – lb/ft^3	5.	5.
Facing Sheet thickness–inch	0.020	0.015
Panel depth – inch	0.218	0.375
Weight – lb	0.484	0.342
Lowest mode – cps	93.	122.

In each case the panel dimension was about 12 inches to 16 inches.

Compartment Structure

Some thought has been given to fabrication techniques if a beryllium structure is chosen. Because of its low ductility, brake-forming of components would give way to machining and chem-milling. Figures III.2-15 through 2-17 are sketches of what a beryllium compartment might look like. Because of its high Young's Modulus a box made from Be would be about 1/2 the weight of a 7075 T6 box of the same strength.

A plan view of the box, indicating thoughts in payload arrangement, is shown on Figure III. 2-18.

<u>Heat Transfer – Mounting Panel</u>

Expressions have been derived for the variation in specific heat, C_p, and thermal conductivity, k, for beryllium These are:

$$C_p \simeq \frac{T^{0.215}}{6.40} \qquad \text{(III. 2-15)}$$

$$k \simeq 0.0313e^{-0.00067T} \qquad \text{(III. 2-16)}$$

where T is expressed in degrees F.

Four sheets showing computation of a typical steady-state heat conduction are attached hereto. In summary, a brazed Be/Ti panel exhibits an effective thermal conductivity nearly three times as great as that of an aluminum hexcell bonded panel:

$$k_{alum} \simeq 0.069 \text{ Btu ft}^{-1}\text{hr}^{-1}\ {}^{o}\text{F}^{-1}$$

$$K_{Be/Ti} \simeq 0.180 \text{ Btu ft}^{-1}\text{hr}^{-1}\ {}^{o}\text{F}^{-1}$$

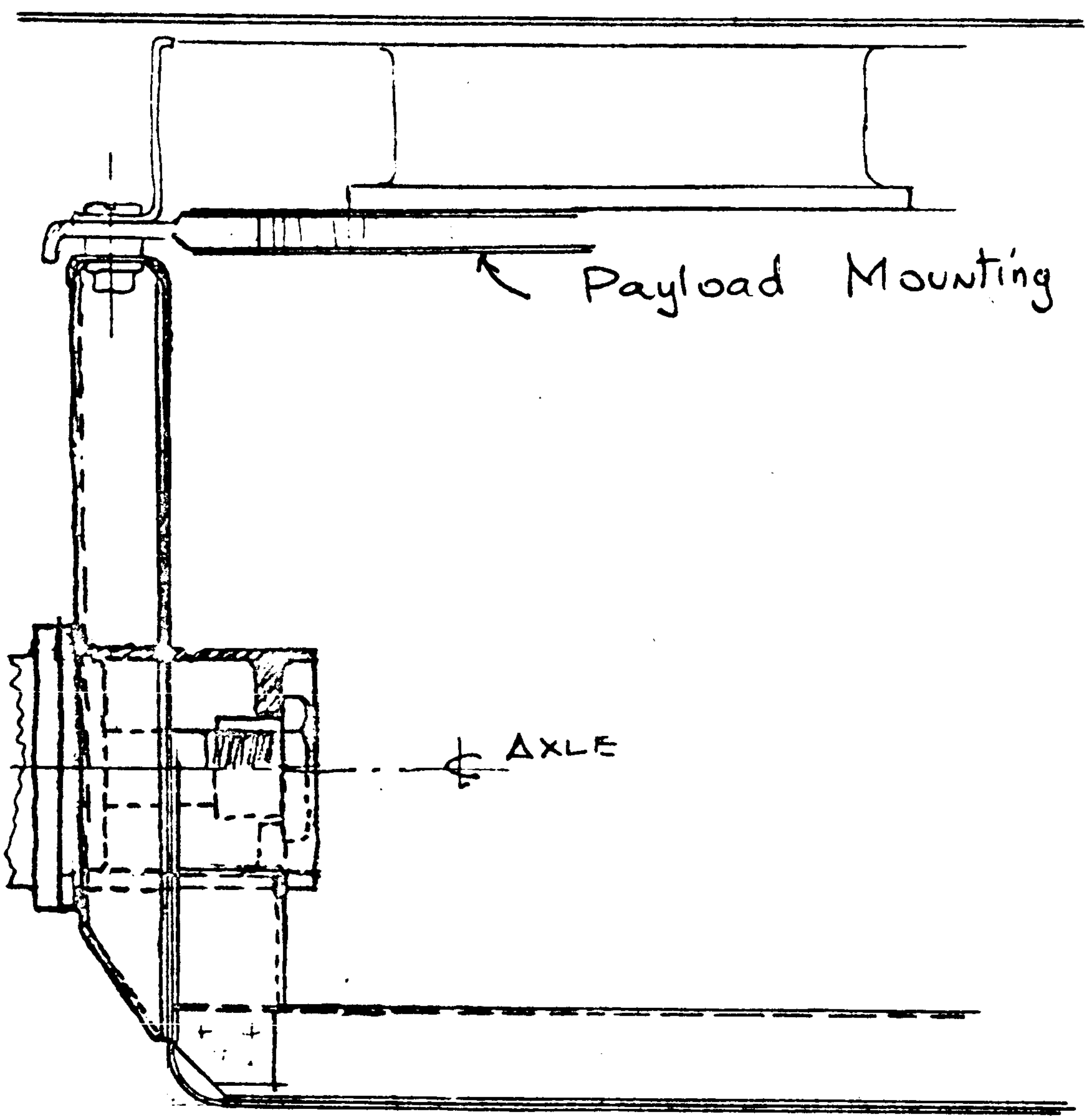

Figure III. 2-15

G M Defense Research Laboratories General Motors Corporation	REPORT NO.	PAGE	JOB NO.	TR64-26	PAGE
TITLE Integral Compt-Axle L.R.V.		PREPARED		11 Nov 63	DATE
		CHECKED			
		APPROVED			

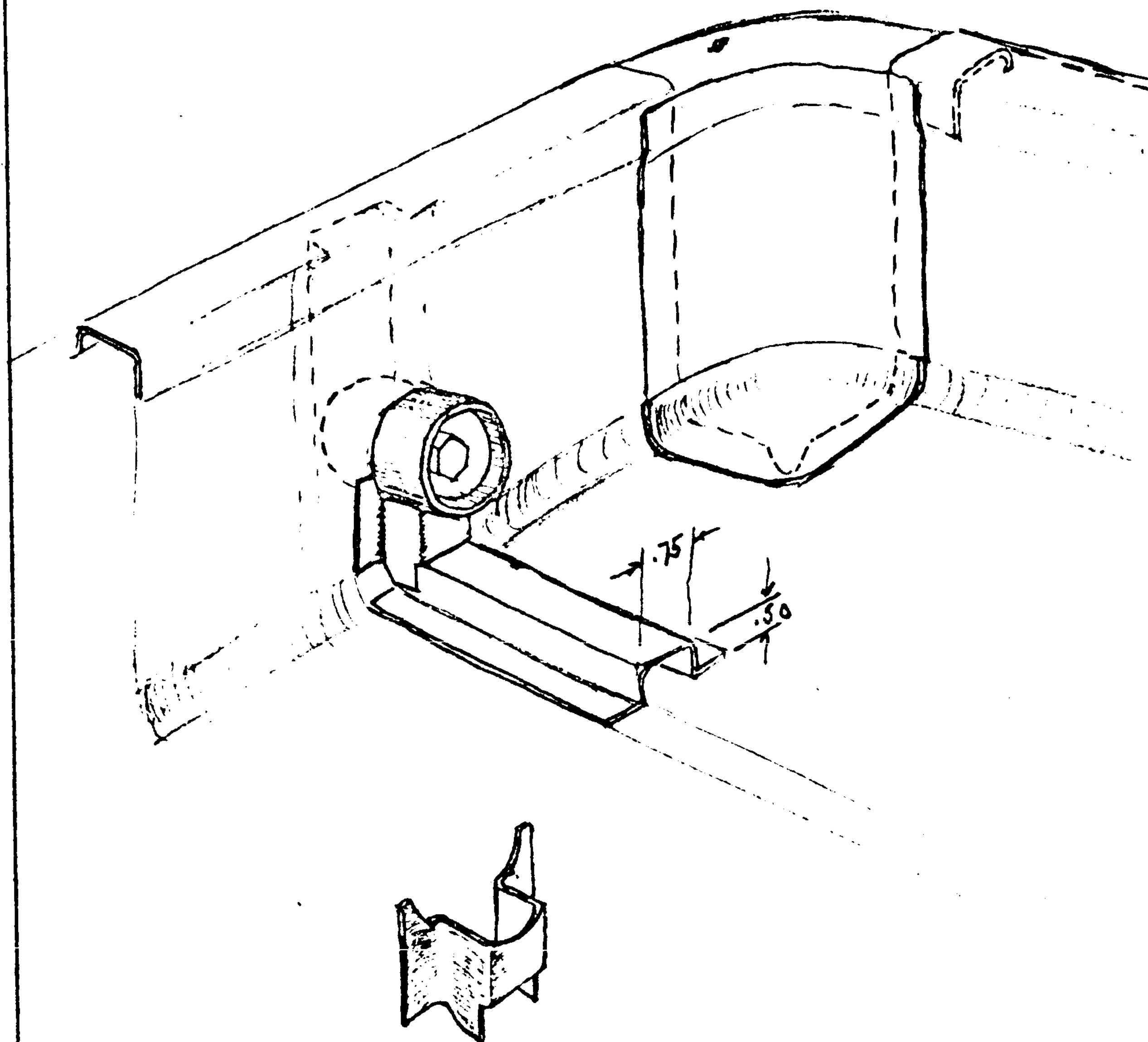

No Scale

Figure III. 2-16

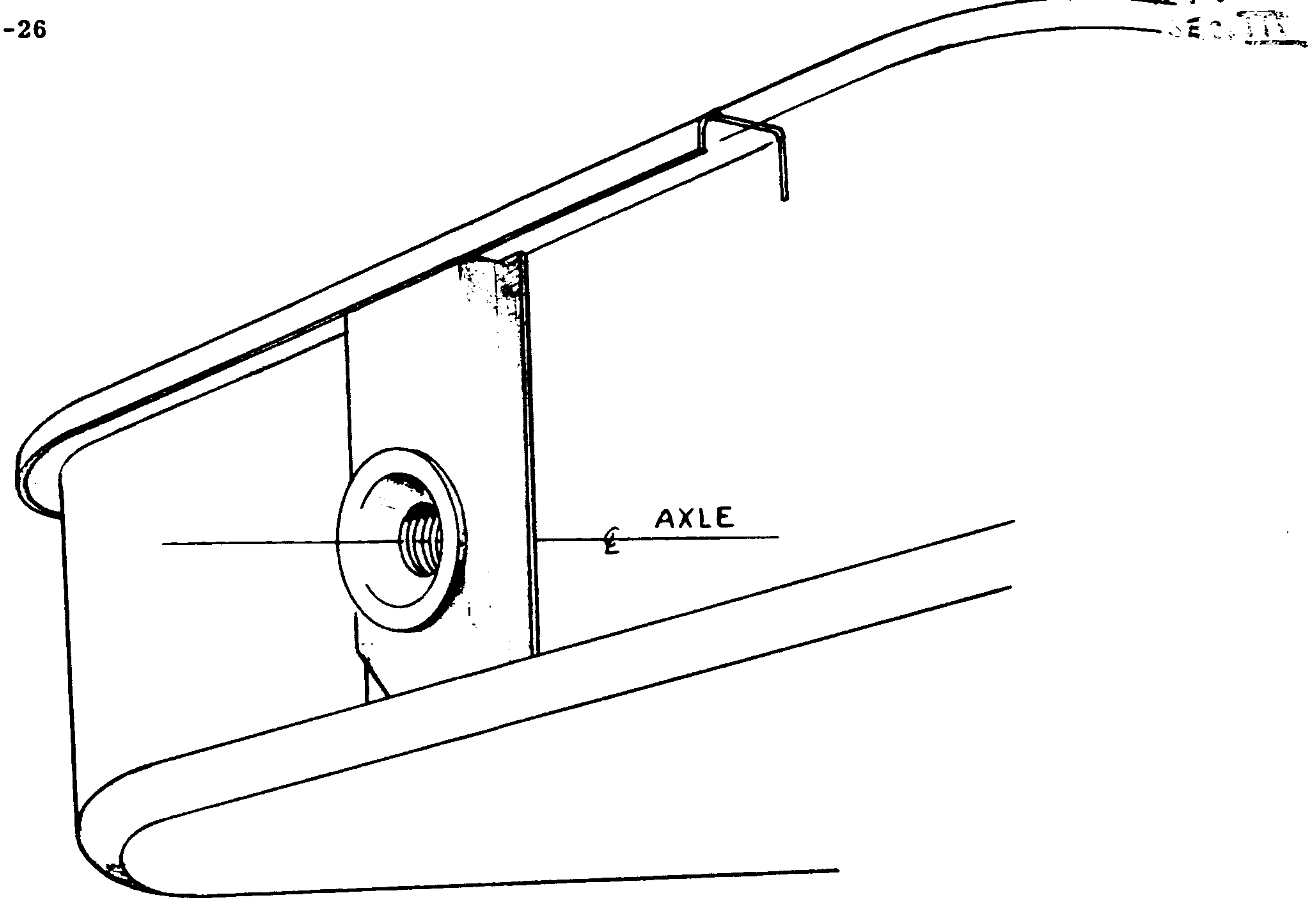

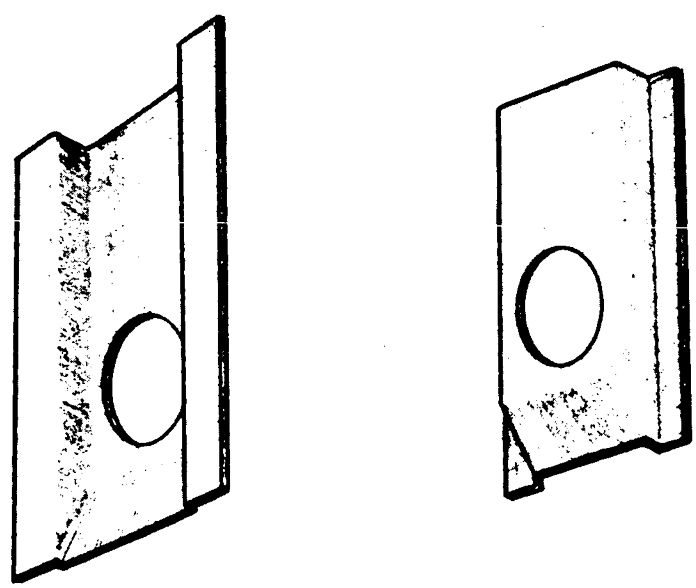

No Scale

Figure III. 2-17

G M Defense Research Laboratories General Motors Corporation	REPORT NO.	PAGE	JOB NO. TR64-28	PAGE
TITLE Fig. III.2-18 SLRV - Space Considerations Plan - 1/2 Scale	PREPARED ⊖		DATE 8 Nov. 1963	
	CHECKED			
	APPROVED			

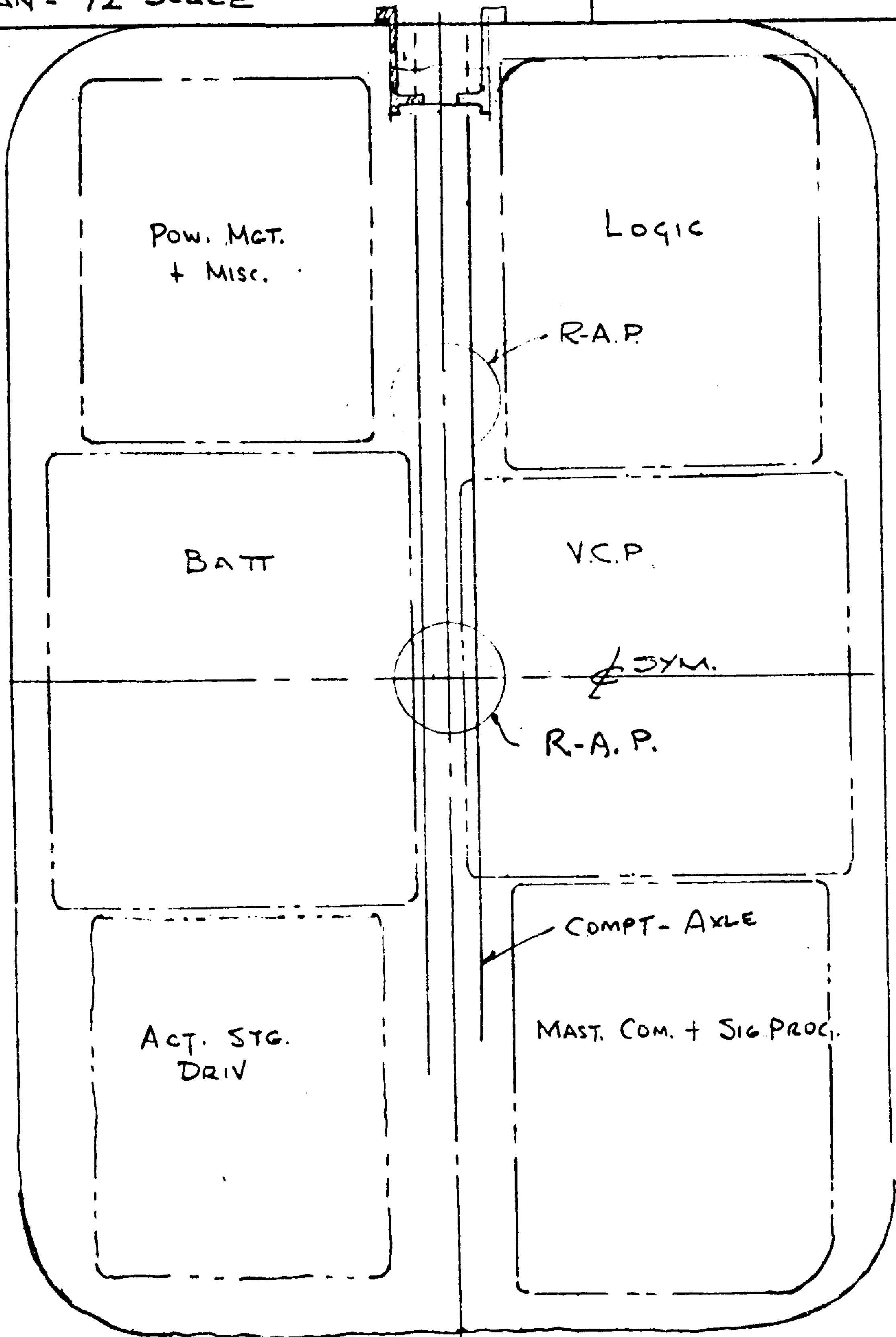

G M Defense Research Laboratories General Motors Corporation	REPORT NO.	PAGE	JOB NO.	PAGE 1
TITLE SLRV PAYLOAD MOUNTING PANEL HEAT TRANSFER	PREPARED OAKES	DATE 12 Nov. 63	CHECKED	APPROVED

T.1 Useful Expressions

T.1.1 C_p vs T

Data from Brush Beryllium Co. was plotted on 2-cyc. ln paper and a straight line approximation drawn. Now C_p will vary with temperature by an expression of the type:

$$C_p = A T^B \qquad (T.1.1)$$

similarly $\ln C_p = \ln A + B \ln T \qquad$ (T.1.2)

ln A and B are obtained from two points on the straight line approximation, fig T.1

Thus $C_p \doteq \frac{T^{0.215}}{6.40} \qquad$ (T.1.3)

where T given in °F.

T.1.2 Thermal Conductivity vs T

The thermal resistivity, or reciprocal conductivity 1/K was plotted on 2-cyc. semi-ln paper. 1/K will then vary w.r.t. temperature by an expression of the type:

$$R = \frac{1}{K} = A e^{BT} \qquad (T.1.4)$$

$$\text{or } \ln R = \ln\left(\frac{1}{K}\right) = \ln A + BT \qquad (T.1.5)$$

By an operation similar to that used in T.1.1 and the straight line approx on Fig. T.2

$$R = \frac{1}{K} = 32 e^{0.00067 T}$$

$$\text{or } K = 0.0313 e^{-0.00067 T} \qquad (T.1.6)$$

T in °F, K - BTU $FT^{-1} SEC^{-1} °F^{-1}$

G M Defense Research ⊗ Laboratories General Motors Corporation	REPORT NO.	PAGE	JOB NO.	PAGE 2
TITLE SLRV PAYLOAD MTG. PANEL HEAT TRANSFER		PREPARED		DATE 12 Nov 63
		CHECKED		
		APPROVED		

T.2 Conduction

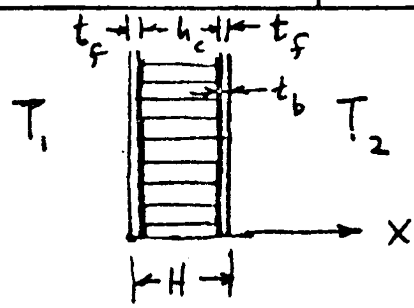

T.2.1 Steady-State Condition

The rate of heat flow per hour, per unit area of panel surface is given by:

$$\frac{dQ}{dA} = \frac{T_1 - T_2}{\sum R_x} \qquad (T.2.1)$$

$$\sum R_x = \frac{2t_f}{k_f} + \frac{h_c}{k_c} + \frac{2t_b}{k_b} \qquad (T.2.3)$$

where t_f = facing sheet thick – in
t_b = thickness of braze layer – in
h_c = core depth – in
k_f = conductivity, beryllium face sheet
k_c = " titanium core
k_b = " , braze alloy

T.2.2 Effective conductivity – Overall Sandwich

$$K_{eff} = \frac{H}{\sum R_x}$$

If, now, we assume
$k_f = 0.028$ BTU ft^{-1} sec^{-1} $^\circ F^{-1}$
$k_c = 0.00117$ " " " "
$k_b = 0.067$ " " " "

$t_f = 0.015$ in (0.00125 ft)
$h_c = 0.300$ in (0.025 ft)
$t_b = 0.001$ in (0.000083 ft)

G M Defense Research Laboratories General Motors Corporation	REPORT NO.	PAGE	JOB NO. TR64-26	PAGE 3
TITLE SLRV PAYLOAD MTG. PANEL HEAT TRANSFER		PREPARED		DATE 12 NOV 63
		CHECKED		
		APPROVED		

T.2.2 Eff. Conductivity (Cont.)

T.2.2.1 Cell Size

Assume core density $\rho_c = 5\ \text{lb}/\text{ft}^3$

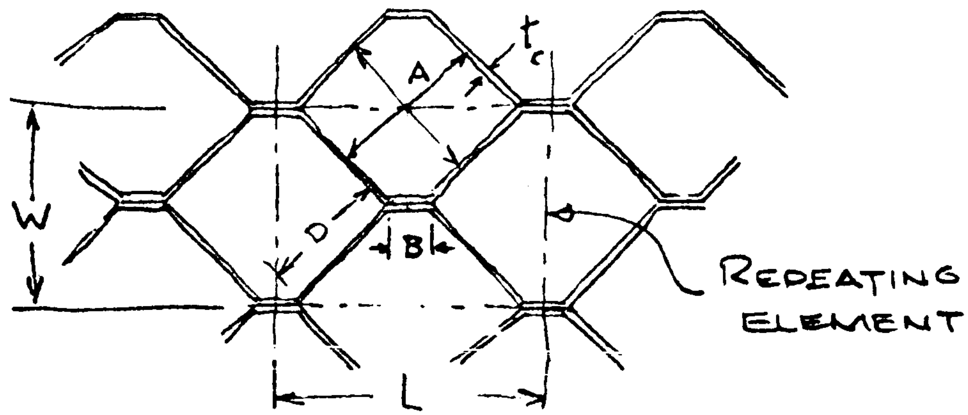

$$L \doteq A\sqrt{2} + 2B$$
$$W \doteq A\sqrt{2} - B$$
$$LW = 2(A^2 - B^2) + AB\sqrt{2}$$ ← Area of repeating section

$$C = 2t_c(2B + 2D)$$
$$D = A - \frac{\sqrt{2}}{2}B$$
$$\therefore C = t_c(4B + 2A - \sqrt{2}B)$$ ← Cell cross-sec'n area.

Solidity index.

$$S = \frac{C}{LW} = \frac{t_c\left[2A + B(4-\sqrt{2})\right]}{2(A^2-B^2) + AB\sqrt{2}}$$

For Ti $\rho \doteq .276\ \#/\text{ft}^3$

$$\therefore S = 0.0182$$

TR64-26

G M Defense Research Laboratories General Motors Corporation	REPORT NO.	PAGE	JOB NO.	PAGE 4
TITLE SLRV PAYLOAD MTG. PANEL		PREPARED	13 Nov 63	DATE
		CHECKED		
		APPROVED		

T.2.2.1 Cell Size (cont.)

Take $B = \frac{A}{4}$

$t_c = 0.010$ IN $\therefore \begin{cases} A = 0.655 \text{ IN} \\ B = 0.164 \text{ IN} \end{cases}$

$$\sum R_x = \frac{2t_f}{k_f} + \frac{h_c}{Sk_c} + \frac{2t_b}{Sk_b}$$

$$\sum R_x = \frac{0.00250}{0.028} + \frac{0.025}{(0.0182)(0.00117)} + \frac{0.000166}{(0.0182)(0.067)}$$

$$\sum R_x = 0.0893 + 1174 + 0.138 \doteq 1174 \ ft^2 sec\,°F\,(BTU)^{-1}$$

$$K_{eff} = \frac{(0.332)(3600)}{(1174)(12)}$$

$$K_{eff} = 0.085 \ BTU\ FT^{-1}\ hr^{-1}\ °F^{-1}$$

T.2.2.2 Effect of braze in node and fillet

From Norair Report NOR 59-381 p 13

$$\frac{1}{K} = 1.2 \ \frac{ft^2\ sec\ °F}{in\text{-}BTU} \quad @ \ 75\ °F$$

$$\text{or } K = \left.\begin{array}{l} 250 \ BTU\ FT^{-1}\ hr^{-1}\ °F^{-1} \\ = 0.0695 \ BTU\ FT^{-1}\ sec^{-1}\ °F^{-1} \end{array}\right\} \text{Litho braze}$$

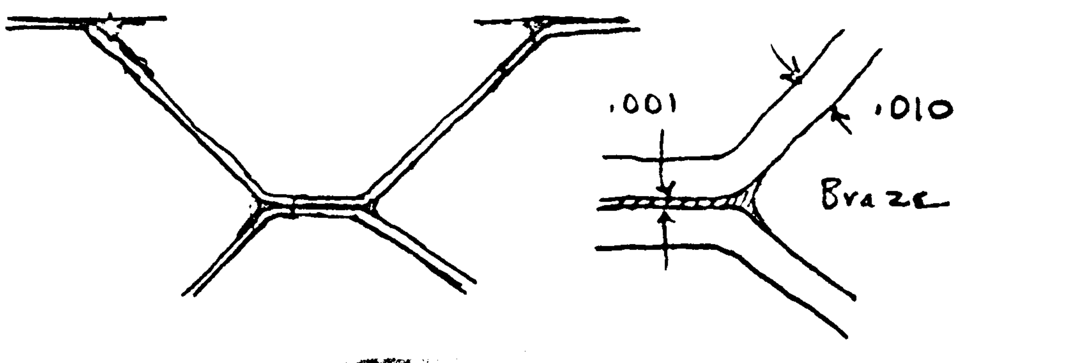

170

TITLE SLRV
Payload Mtg. Panel
Effective Conductivity

PREPARED 13 Nov. 63
CHECKED
APPROVED

Assume braze area per node $a_N = 0.001\ B$
2 NODES / REPEATING ELEMENT

$$\therefore a_{bc} = 2a_N$$
$$= (2)(0.001)(0.164)$$
$$a_{bc} = 0.000328\ \text{IN}^2$$

$$a_{rE} = 2.2285\ A^2$$
$$= 2.2285(0.655)^2 =$$

$$\delta_{bc} = \frac{a_{bc}}{a_{rE}} = \frac{0.000328}{0.953} = 0.000344$$

$$\sum R_x = \underset{2t_s/k_f}{0.0893} + \underset{2t_b/3k_b}{0.138} + \frac{0.025}{(0.0182)(0.00117) + (0.000344)(0.0195)}$$

$$= 0.2273 + \frac{0.025}{0.0000213 + 0.0000239}$$

$$\sum R_x \doteq 553$$

$$K_{eff} = \frac{(0.332)(300)}{553}$$

$K_{eff} = 0.18\ \text{BTU FT}^{-1}\ \text{HR}^{-1}\ {}^\circ\text{F}^{-1}$ *

or $K_{eff} \doteq 0.0079\ \text{watt in}^{-1}\ {}^\circ\text{C}^{-1}$

$$\frac{dQ}{dA} = \frac{\Delta T \cdot K_{eff}}{H}$$

Now, If $dA = 200\ \text{in}^2$
$H = 0.35\ \text{in}$

$$\frac{dQ}{\Delta T} = 4.5\ \text{watt}\ {}^\circ\text{C}^{-1}$$

* for Hexcel panel $k_{eff} = 0.069\ \text{BTU FT}^{-1}\ \text{HR}^{-1}\ {}^\circ\text{F}^{-1}$

G M Defense Research Laboratories General Motors Corporation	REPORT NO.	PAGE	JOB NO. TR64-20 1 of 2
TITLE SLRV PAYLOAD MOUNTING PANEL -THERMAL ISOLATION		PREPARED C. GOOHS DATE 10/15/63	
		CHECKED	
		APPROVED	

CONDUCTION FROM LOWER PAN TO TOP PANEL

C = CONDUCTION FACTOR $= \frac{A}{x} = \frac{\text{CROSS-SECTIONAL AREA (FT}^2)}{\text{DISTANCE (FT)}}$

FOR THERMAL STANDOFFS

ASSUME 30 BUTTONS 5/16" DIA x 1/8" THICK

$$C_{T.S.O.} = \frac{30 \times .156^2 \pi \times 12}{144 \times .125}$$

$$= 1.526$$

FOR TOP PANEL FIBERGLASS FLANGE

$$C_{F.F.} = \frac{.3125 \times \overset{54}{(12+12+15+15)} \times 12}{144 \times .75}$$

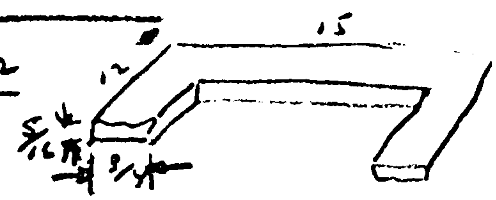

$$= 1.88$$

COMBINED CONDUCTION FACTOR

$$C_{COMB} = \frac{1}{\frac{1}{1.53} + \frac{1}{1.88}} = \frac{1}{1.185} = .845$$

CONDUCTION HEAT INPUT TO TOP PANEL DURING DAYTIME OPERATION

$$q = .17 \times .845 \times 144$$

$$= 20.7 \text{ BTU/HR}$$

$$= \underline{6.1 \text{ WATTS}} \text{ (DAYTIME)}$$

$K = .17$ BTU/HR/□/1°F

$\Delta t = 120°C - 40°C$

$= 80°C = 144°F$

ASSUMING PERFECT CONDUCTANCE AT JOINTS.

G M Defense Research ⊗ Laboratories General Motors Corporation	REPORT NO.	PAGE	JOB NO.	PAGE 2 OF 2
TITLE SLRV PAYLOAD MOUNTING PANEL — THERMAL ISOLATION	PREPARED C. GOOHS			DATE 10/15/63
	CHECKED			
	APPROVED			

TR64-26

NIGHT LOSSES

$\Delta t = 157° - 0°$

$= 157°C = 283°F$

$q = .17 \times .845 \times 283$

$= 40.8$ BTU/HR

$= 11.9$ WATTS (ASSUMING PERFECT CONDUCTANCE AT JOINTS.)

IF ASSUMPTION IS MADE THAT JOINTS ARE ONLY 50% EFFICIENT, CONDUCTION LOSSES WILL BE:

DAYTIME $= \frac{1}{2}(20.7$ BTU/HR$) = 10.4$ BTU/HR

$=$ 3 WATTS

NIGHT LOSS $= \frac{1}{2}(40.8) = 20.4$ BTU/HR

$= 5.9$ WATTS.

RECOMMEND — THAT THERMAL STANDOFFS BE MADE OF MULTIPLE LAYERS OF INSULATING MATERIAL TO SUBSTANTIALLY REDUCE THE JOINT CONDUCTIVITY EFFICIENCY.

173

General Motors Corporation

TR64-26

TITLE SLRV
RADIATOR TEMPERATURE
VS. RADIATOR AREA VS. LOAD

PREPARED C. GOODS 11/7/63
CHECKED
APPROVED

REFER TO PAGE f OF PRELIMINARY THERMAL ANALYSIS BY S. HELMUS DATED 7/25/63.

ASSUMING SIMILAR CONDITIONS EXIST TO THAT SHOWN, THEN

$$\frac{q}{A_R} + .22 = 29.8 \times 10^{-12} T_R$$

WHEN

q = ELECTRONIC INTERNAL LOAD-WATTS

A_R = RADIATOR AREA, SQ. IN.

T_R = RADIATOR TEMPERATURE - °K.

A PLOT OF T_R VS. q FOR FOUR VALUES OF A_R IS SHOWN ON THE PRECEDING PAGE.

General Motors Corporation
TR64-36

TITLE RTG POWER SOURCE RADIATOR TEMPERATURE SLRV	PREPARED C. GOOHS DATE 4/15/63
	CHECKED
	APPROVED

RADIATOR TEMPERATURE RESULTING FROM RTG POWER SOURCE

IF 70 WATTS OF POWER ARE REQUIRED, THERE WILL BE 706 WATTS OF HEAT TO BE RADIATED (BASED ON 9% EFF.).

ASSUMING THE TOP OF THE COMPARTMENT IS ISOLATED FROM THE BOTTOM AND ALL OF THIS HEAT (706 W) MUST BE RADIATED FROM THE BOTTOM (ONLY) TO THE LUNAR SURFACE.

$A = 12 \times 15 = 180^{in^2}$

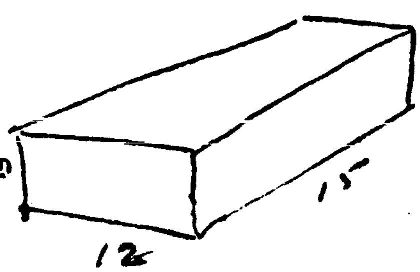

$F = 1$ (assumed)

T_L = LUNAR SURFACE T $= 120°C = 393°K$

$\varepsilon_1 = .875 = \varepsilon_2$ (est)

$$\underbrace{q_{RTG} + \Sigma Q_{REFLECTED} + \Sigma Q_{LUNAR}} = Q_{RADIATOR}$$

$$706 + \varepsilon_1 F A \sigma T_L^4 = \varepsilon_2 F A \sigma T_R^4$$

$$706 + .875(1)180 \times 36.85 \times 10^{-12} \times \overline{393°K}^4 = .875 \times 1 \times 180 \times 36.85 \times 10^{-12} T_R^4$$

$$706 + \overset{845}{139} = 5800 \times 10^{-12} T_R^4$$

$$T_R = 618°K$$

$$= 345°C$$

$$= 653°F$$

HOT!!

TOO HOT FOR ALUMINUM STRUCTURAL MEMBERS.

TITLE SLRV STUDY OF RADIATOR TEMPERATURE VS. RADIATOR AREA VS LOAD	PREPARED C. GOOHS 11/7/63 TR64-26 CHECKED APPROVED

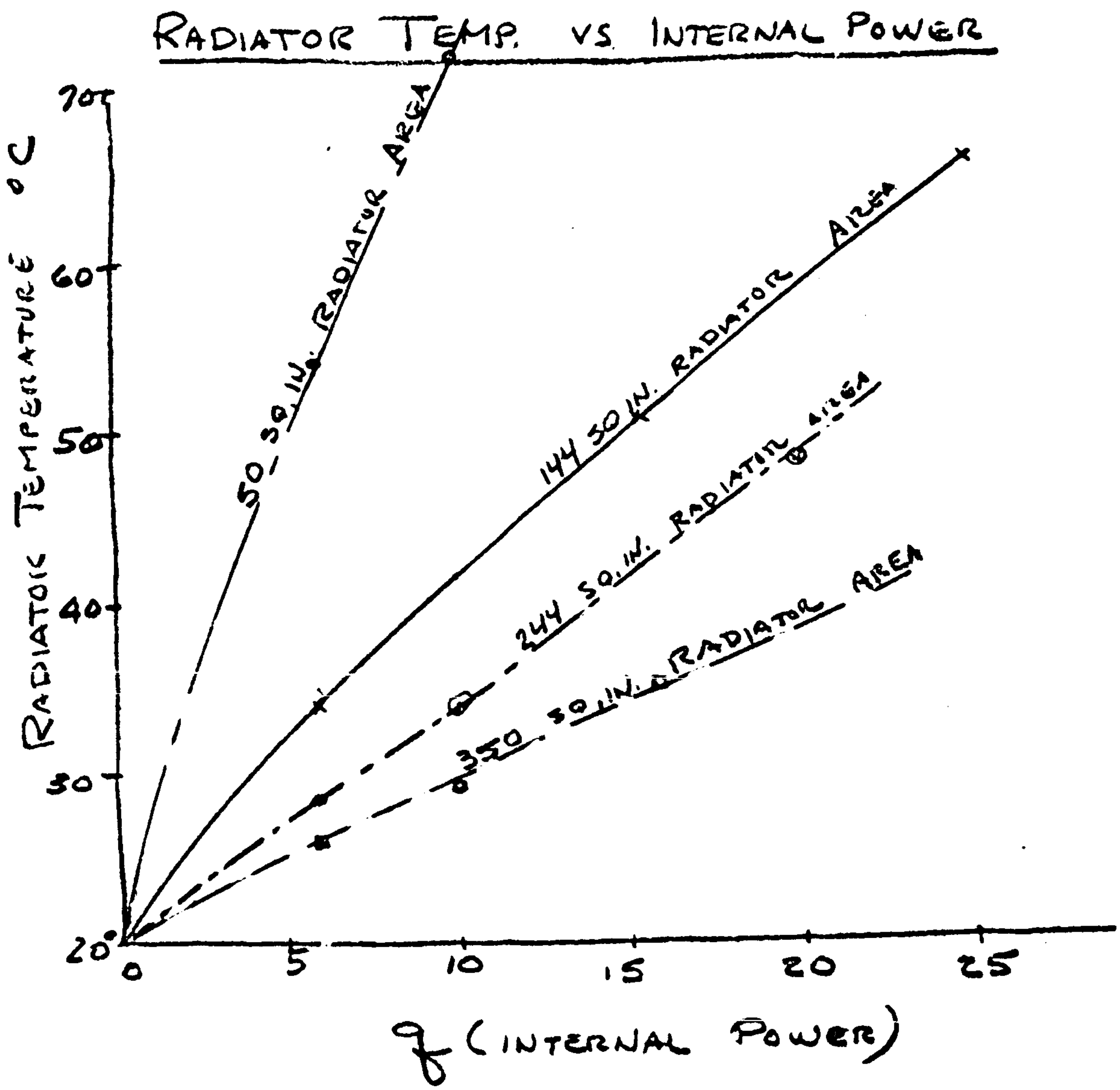

B. STRUCTURE

1. Structural Design Analysis

COMPARTMENT STRUCTURE

Requirements

The first and second axle compartments of the Surveyor Lunar Roving Vehicle carry batteries and the electronic payload. As a consequence the design of these two compartments requires thorough integration of the thermal and structural considerations. Thermal requirements are set by the operating temperature limits of the electronic payloads. Structural requirements are established by general vehicle mobility criteria, deployment and stowage limitations, and environmental loads imposed during launch, transit, and landing.

Using the proposed configuration, the compartments would be designed for the following payload requirements:

	Internal Temp. ^{o}F	Volume in.^{3}	Weight lbs
Axle No. 1	-75 to 170	275	11.0
Axle No. 2	0 to 125	500	17.3

On the basis of the above, a feasible approach to compartment design can be discussed which will serve as a basis for study.

A preliminary analysis of the middle compartment of the Surveyor Lunar Roving Vehicle has been carried out. This analysis considered three aspects of the vehicle thermal control:

1) Radiator temperatures (top surface) as a function of internal power
2) Thermal controller requirements as a function of component temperature limit and internal power
3) Insulation effectiveness and lunar night power requirements.

Because of the extended duration of the lunar night, careful attention was given to payload insulation. One hundred layers of aluminized mylar are employed as insulation. With a layer emissivity of .1, the effective emissivity (Eff) is 5.32×10^{-4}. In the thermal analysis, this value of emissivity was increased by a factor of ten to compensate for conduction losses and heat leaks.

The present approach is to supply this power from a radioactive pellet. This offers a considerable weight saving over a battery source. The pellet could be moved in and out of the compartment by a transfer switch, supplying power when needed. This approach maintains the minimum component temperature at $+10^{\circ}C$, thus improving the system reliability by reducing the stress on the electronic components.

Typical Compartment Structure

Both forward and center compartment structures are similar in construction. A compartment structure, typical of the type of construction proposed, is illustrated in Figs. III.2-19 & 2-20 and is described in detail below for the center compartment.

The compartment consists of a recessed rectangular box with a continuous-lip flange to which an upper mounting cover panel is attached by screws and thermal insulator stand-offs.

The box serves both as a structure to provide a load path between the compartment payload and the wheel axle, and as protection against environmental damage to the internal electronic packages. The material used is 2014 aluminum alloy, Alclad. A hat-shaped channel is spot-welded to the bottom of the box, which is made of .020 sheet. Vertical, hat-shaped beams are spot-welded to the sides of the compartment and to the lower channel. These side members also include a thin-walled cylindrical fitting to which the wheel assembly is attached. The side members, lower channel, and upper flange of the compartment comprise an integral body-axle assembly, and serve as the load path for transferring the body loads to the wheels.

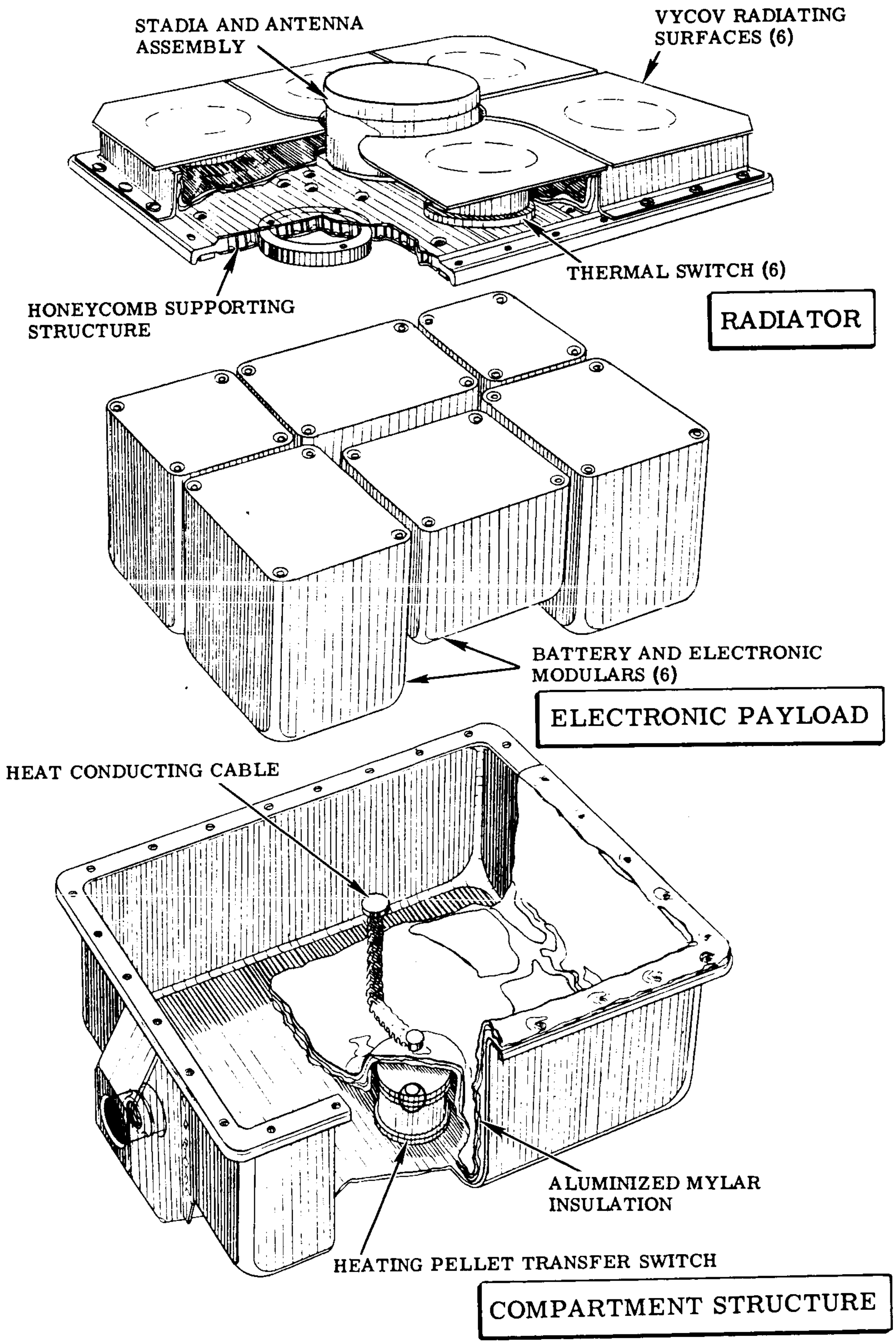

Fig. III. 2-19. Typical Compartment Structure

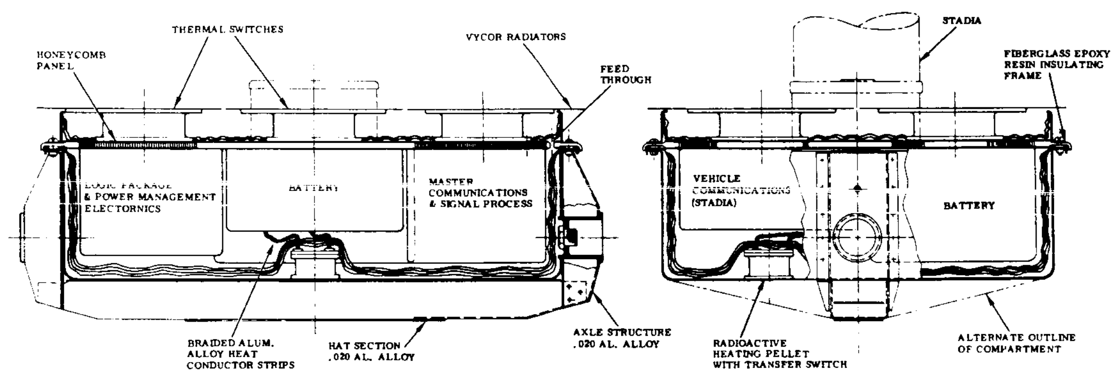

Fig. III.2-20. Compartment No. 2 Details

The upper panel consists of a honeycomb sandwich panel integrally fabricated with an outer epoxy-resin fiberglass mounting frame, bonded together in a thermal vacuum. The honeycomb sandwich panel is fabricated of two (.030) 2014 aluminum alloy, Alclad face sheets, and a 1/8-5052-.001 P perforated aluminum alloy foil core (4.5 lbs/ft^{-3} density) 3/16-inch thick; six (1/8-inch wall x 3-inch O.D.) aluminum alloy short cylindrical spacers are located under six thermal switches, providing an additional thermal conduction path between the lower and upper face sheets. The electronic packages are attached to the lower surface of the panel. A pure aluminum, heavy-foil gasket is sandwiched between the lower face sheet of the panel and the electronics box to provide for more effective thermal conductivity between the box and the face sheet. Grommet-type, thru-bolt, sandwich panel fasteners are used for attaching the electronics packages to the panel.

Attached to the upper face sheet of the panel are the six thermal switches mentioned above. Also attached to the upper surface is a thin-walled 2014 aluminum alloy cylinder, welded to the face sheet, for housing the stadia inflatable structure. Located in the bottom of the compartment is a transfer switch for housing a radioactive pellet.

A thermal insulation of 100 layers of aluminized mylar sandwiched with thin-sheet insulation material, lines the inside of the compartment to serve as a radiation insulator. To conduct heat from the isotope heat source to the heat sink and compartments, braided aluminum alloy straps, which penetrate the mylar insulation, are provided. The entire compartment assembly is attached to the elastic frame with screws and nut plates.

The compartment associated with the first axle, while of similar construction, becomes more complex structurally. The attachment of the steering mechanism and its heat sink and the viewing periscopes present additional thermal and structural difficulties requiring careful layout. However, the proposed structure is readily adaptable to overcome these design difficulties.

The compartment design study will be closely integrated with the overall multi-body analysis in which all vehicle components are coupled together. However, there will be effort peculiar to the compartment. These efforts can be tabulated as follows:

1) Establish compartment detail thermal design requirements.
2) Review comparative performance and capabilities of various thermal controllers.
3) Study structural materials used in the compartment to establish the heat conductance paths.
4) Design a low-weight compartment adequate for all loading conditions.
5) Study structural materials from a thermal standpoint to establish a basis for compromise between structural and thermal considerations.
6) Analyze structure to assure that design requirements will result in a high natural frequency for the compartments and a high strength-to-weight ratio.
7) Study the effect of the temperature-vacuum environment on the structural integrity of the compartment.

SLRV STRUCTURAL ANALYSIS

The following discussion contains the preliminary calculations used for sizing of the integral compartment-axle and the elastic frame structures.

The upper mounting panel, to which the electronics thermal switches and stadia payloads are attached, is assumed to be a uniformly loaded panel, simply supported at its edges. This assumption is not wholly accurate, however, but for purposes of first-cut sizing it is a reasonable one. The load factor used in this analysis (± 35g) is obtained from Reference (1)* In the stowed position, the Surveyor Lunar Roving Vehicle (SLRV) is inclined at an angle of 20 degrees from the vertical; however, for this analysis the ± 35g load factor is assumed

*References are listed on page III.2-66

to be acting coincident with the wheel axle centerline. The equations used for designing the honeycomb sandwich panel are obtained from Reference (2) and (3). These calculations are presented on pages III. 2-67 through III. 2-70.

Natural frequency (first mode) estimates were calculated taking two different approaches, hereinafter referred to as methods 1 and 2. Method 1 assumes the panel to be a uniformly loaded and simply supported honeycomb sandwich panel, where the fiberglass edge frame is not considered. The equation used to calculate the natural frequency is taken from Reference (5). These calculations are present on pages III.2-71 & 2-72. Method 2 assumes the plate to be made up of a series of beams attached to each other where the maximum deflection of the panel is taken as 1/2 that of a beam of unit width. This is a close approximation for the deflection of a plate. This method of solution permits consideration of the fiberglass outer frame in computing the deflection, as shown by the calculation on pages III. 2-73 & 2-74. (The equation used for estimating the first mode natural frequency by this method is that described in Reference (6).)

The plate loading is based on a preliminary weight estimate of 18.0 pounds (one "g" load) for the upper plate assembly, uniformily distributed over the entire area of the plate. This weight includes all electronics, thermal switches, stadia structure, etc. (which attach to the mounting plate), along with the weight of the plate.

The compartment axle structure is analyzed in a conventional manner where the side members beam the axial axle loading in to the upper lip flange and the lower hat-shaped compartment reinforcement member. The allowable member crippling and bending stresses are obtained from crippling stress versus b/t ratio test data curves for 2014 aluminum alloy formed sheet-metal stiffeners. The portion of the axle loading beamed to the upper lip flange of the compartment is assumed to be reacted into the upper mounting panel by the nearest pair of attach screws bracketing the upper member (screws spaced approximately four inches on center) where the lip flange serves as a partially fixed-ended beam to transfer the member loading to the screws as shown in the analysis on pages III. 2-75 through III. 2-77.

The elastic frame analysis is sized, based on the stowage and lunar roving requirements. The stowage requirements design the frame in bending using the fundamental equation $\left[EI \left(\frac{d^2 y}{dx^2} \right) = M \right]$, where $\left(\frac{d^2 y}{dx^2} \right)$ is the reciprocal of the frame bend radius. The lunar roving requirements, presented in subsection D, "Vehicle System" of this proposal design the frame in torsion and bending. For this analysis the frame is assumed to be two flat-strip springs with the equations for torsion of a flat spring taken from Reference (7). The elastic frame structural analysis is presented on pages III.2-78 through III.2-84.

The natural frequencies (first mode) obtained from methods 1 and 2 were 46 and 41 cps, respectively. In neither of the cases was the additional stiffness provided by the attachment of the electronics boxes which would probably be fabricated of deep-drawn cans of aluminum alloy sheet metal with a minimum of four attachments per box (one at each corner), to the mounting panel, or the additional, though small, stiffness offered by the sandwich core material considered. Both methods of calculating the natural frequency of the mounting plate appear to be in good agreement with each other, with the latter method indicating a slight reduction in value due to the consideration of the fiberglass mounting frame which was neglected in method 1. These results however are only preliminary estimates of the natural frequency of the mounting plate.

During the continuing study, a multibody type of analysis in which all of the compartment components are coupled together will be conducted, along with verification of the calculations by model testing in order that the compartment package can be appropriately designed thermally and structurally for an excellent strength-to-weight ratio,with a natural frequency of sufficient magnitude to reduce the transmissibility between the SLRV payload and the Surveyor spacecraft.

The use of materials such as beryllium and titanium should be investigated and employed in improving the structure, wherever feasible to do so.

References

1. JPL Request for proposal 3146 entitled "Surveyor Lunar Roving Vehicle," dated 22 June 1963

2. Hexcel Products brochure "E" entitled "Honeycomb Sandwich Design "

3. Hexcel Products brochure "D" entitled "Honeycomb Sandwich "

4. R.J. Roark, "Formulas for Stress and Strain," McGraw-Hill Book Company, Third Edition

5. S. Timoshenko - "Vibration Problems in Engineering," McGraw-Hill Book Company, Second Edition

6. W.T. Thomson - "Mechanical Vibrations," Prentice-Hall Book Company, Second Edition

7. D.J. Perry - "Aircraft Structures," McGraw-Hill Book Company, 1950 Edition

G M Defense Research ⊗ Laboratories General Motors Corporation	REPORT NO	PAGE 1	JOB NO 80-22001-400	PAGE
TITLE SURVEYOR LUNAR ROVING VEHICLE STRUCTURAL ANALYSIS		PREPARED Pascaloff / Jui... DATE 7/29/63	CHECKED CJP 8/9/63	APPROVED

LRV COMPARTMENT STRESS ANALYSIS

PAYLOAD MOUNTING PANEL CHECK

a. HONEYCOMB SANDWICH PANEL

MATERIAL: 2014-T62 ALUM ALLOY FACE SHEETS
1/8 - 5052 - .001 P ALUM ALLOY CORE

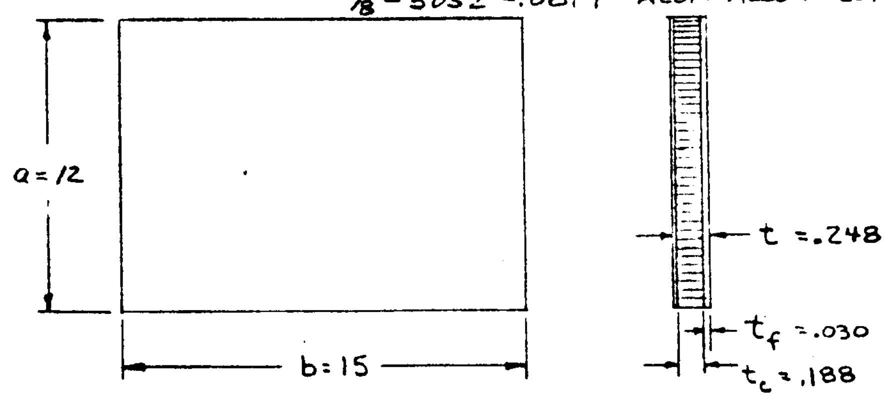

WEIGHT SUPPORTED BY PANEL = 18# (FROM PRELIM DESIGN WEIGHT ESTIMATE)

UNIFORM LOAD q, @ 35 g's REF. 1

$$q = \frac{WN}{ab} = \frac{18 \times 35}{12 \times 15} = 3.5 \ \#/\text{IN}^2$$ (N = LOAD FACTOR)

MAXIMUM BENDING MOMENT (M) ... (REF. 2, PG. 10)

$$M = \beta q a^2 = .066 \times 3.5 \times 12^2 = 33.3 \ \text{IN.}\#$$

MAX. FACING STRESS (σ_f) ... (REF. 2 PG. 10)

$$\sigma_f = \frac{M}{t_c t_f} = \frac{33.3}{.188 \times .030} = 5900 \ \#/\text{IN}^2$$

ALLOWABLE FACING STRESS = 55,000 psi

MAX. CORE SHEAR STRESS (τ_c) ... (REF. 2 PG. 10)

$$\tau_c = \frac{2\gamma q a}{t + t_c} = \frac{2 \times .46 \times 3.5 \times 12}{.248 + .188} = 88.5 \ \#/\text{IN}^2$$

ALLOWABLE CORE SHEAR STRESS = 210 psi ... (REF. 3 PG. 14)

DRL-255

G M Defense Research ⊗ Laboratories General Motors Corporation	REPORT NO	PAGE 2	JOB NO.	PAGE
TITLE SURVEYOR LUNAR ROVING VEHICLE STRUCTURAL ANALYSIS		PREPARED Pascaloff/Juntunen		DATE 7/29/63
		CHECKED CLP		8/9/63
		APPROVED		

LRV COMPARTMENT STRESS ANALYSIS

PAYLOAD MOUNTING PANEL CHECK

a. HONEYCOMB SANDWICH PANEL ---(CONT'D.)

MAX. PANEL DEFLECTION (W)
(NEGLECTING FIBERGLASS EDGE) ---(REF. 2 PG.10)

$$W = \alpha_1 \frac{q a^4}{D} + \alpha_1 \alpha_2 \frac{q a^2 \pi^2}{t_c G_c}$$

WHERE: D = BENDING STIFFNESS OF PLATE WHICH IS APPROXIMATED BY THE EQUATION BELOW

$$D \approx \frac{E_f t_f t_c t}{2\lambda_f}$$ ---(REF. 2 PG.7)

$$D \approx \frac{10^7 \times .03 \times .188 \times .248}{2(1-.3^2)} = 7680$$

CORE DENSITY = $4.5 \ \#/FT^3$ (AL $\frac{1}{8}$ - 5052 .001 P)

$G_c = 32{,}000 \ \#/IN^2$ ---(REF. 3 PG.14)

$\frac{a}{b} = .80 \qquad \alpha_1 = .006 \qquad \alpha_2 = 1.48$

$$W = .006 \times \frac{3.5 \times 12^4}{7680} + .006 \times 1.48 \times \frac{3.5 \times 12^2 \times \pi^2}{.188 \times 32000}$$

$$W = .0567 + .0073 = .064 \text{ IN.}$$

DRL-255

G M Defense Research ⊗ Laboratories General Motors Corporation	REPORT NO	PAGE 3	JOB NO	PAGE
TITLE SURVEYOR LUNAR ROVING VEHICLE STRUCTURAL ANALYSIS	PREPARED PASCALOFF/JUNTUNEN	DATE 7/29/63		
	CHECKED CJP	8/9/63		
	APPROVED			

LRV COMPARTMENT STRESS ANALYSIS

PAYLOAD MOUNTING PANEL CHECK --(CONT'D.)

b. BENDING STRESS IN FIBERGLASS (EPOXY RESIN) MOUNTING FRAME:

CONSIDER A 1-INCH WIDE STRIP OF PANEL AS A UNIFORMLY LOADED AND SIMPLY SUPPORTED BEAM AS SHOWN BELOW:

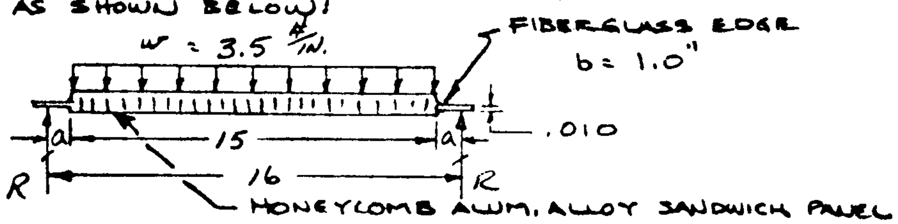

$$R = \frac{wL}{2} = \frac{3.5 \times 15}{2} = 26.3^{\#}$$

$$M = Rx = 26.3(.5) = 13.2 \text{ IN.}^{\#}$$

$$\frac{I}{c} = \frac{t^2}{6} = \frac{.10}{6} = .0167 \text{ IN}^3$$

$$\sigma = \frac{M}{I/c} = \frac{13.2}{.0167} = 790 \ \#/\text{IN}^2$$

SHEAR STRESS IN FIBERGLASS

$$f_s = \frac{3}{2}\frac{V}{A} = \frac{3}{2} \times \frac{26.3}{1 \times .10} = 395 \ \#/\text{IN}^2$$

ALLOWABLE SHEAR STRESS (F_s)

$$F_s = 6{,}500 \ \#/\text{IN}^2$$

DRL-255

G M Defense Research Laboratories General Motors Corporation	REPORT NO	PAGE 4	JOB NO.	PAGE
TITLE SURVEYOR LUNAR ROVING VEHICLE STRUCTURAL ANALYSIS	PREPARED PASCALOFF/JUUTUNEN DATE 7/29/63			
	CHECKED CJP 8/9/63			
	APPROVED			

LRV COMPARTMENT STRESS ANALYSIS

PAYLOAD MOUNTING PANEL

b. BENDING STRESS IN FIBERGLASS (EPOXY RESIN) MOUNTING FRAME: ---(CONT'D.)

$$I_{F.G.} = \frac{bt^3}{12} = \frac{1 \times .1}{12} = 83.3 \times 10^{-6} \text{ IN.}^4$$

$$I_{PANEL} = 2bt_f\left(\frac{t_c+t_f}{2}\right)^2 = 2 \times 1 \times .03 \times .09^2$$

$$= .00178 \text{ IN.}^4$$

FIBERGLASS DEFLECTION @ 35 g's

$$P = \frac{wL}{2} = \frac{3.5 \times 15}{2} = 26.2^{\#}$$

$$a = .5 \text{ IN.}$$

$$\delta_{F.G.} = \frac{Pa^3}{3EI} = \frac{26.2 \times .5^3}{3 \times 5 \times 10^5 \times 83.3 \times 10^{-6}} = .0262 \text{ IN.}$$

HONEYCOMB SANDWICH PANEL DEFLECTION (δ_p):

$$\delta_p = \frac{5wL^4}{384EI} = \frac{5 \times 3.5 \times 15^4}{384 \times 10^7 \times 178 \times 10^{-5}} = .130 \text{ IN.}$$

PANEL SLOPE (θ_p), ½-INCH AWAY FROM EDGE:

$$\theta_p = \frac{wL^3}{24EI} = \frac{3.5 \times 15^3}{24 \times 10^7 \times 178 \times 10^{-5}} = .00274 \text{ RAD.}$$

MAXIMUM PANEL DEFLECTION (δ):

$$\delta = \frac{1}{2}\left(\delta_p + \theta_p a + \delta_{FG}\right)$$

$$= \frac{1}{2}\left(.130 + .00274 \times .5 + .0262\right) = \underline{.079 \text{ IN.}}$$

(@ 35 g's)

G M Defense Research Laboratories General Motors Corporation	REPORT NO	PAGE 5	JOB NO	PAGE
TITLE SURVEYOR LUNAR ROVING VEHICLE STRUCTURAL ANALYSIS		PREPARED Pascaloff/Juumilev 7/29/63		
		CHECKED CJP 8/9/63		
		APPROVED		

LRV COMPARTMENT STRESS ANALYSIS

PAYLOAD MOUNTING PANEL CHECK ... (CONT'D)

c. NATURAL FREQUENCY CALCULATION:

METHOD I – (ASSUMING PLATE TO BE A UNIFORM SANDWICH PANEL)

$$\lambda_k = \pi^4 D\left(\frac{m^2}{a^2}+\frac{n^2}{b^2}\right)^2 \quad \cdots (\text{REF. } 5,\ \text{PG. } 335)$$

$$\lambda = p_n^2 \mu$$

$$p_n = \pi^2\sqrt{\frac{D}{\mu}}\left(\frac{m^2}{a^2}+\frac{n^2}{b^2}\right) \quad \cdots\ \text{RADS/SEC.}$$

$$f_n = \frac{p}{2\pi} = \frac{\pi}{2}\sqrt{\frac{D}{\mu}}\left(\frac{m^2}{a^2}+\frac{n^2}{b^2}\right) \cdots \text{cps}$$

NATURAL FREQUENCY OF PLATE

μ = MASS OF PLATE / UNIT AREA $= \frac{w}{g}$

FOR A HONEYCOMB SANDWICH PLATE

$$D = \frac{EI}{1-\nu^2} \quad \ldots \text{ FLEXURAL STIFFNESS OF PLATE}$$

$$I = \frac{t_f(t_f+h)^2}{2}$$

$$D = \frac{E\,t_f(t_f+h)^2}{2(1-\nu^2)} \qquad t_f = .030,\ h = .188$$

FOR FIRST MODE NATURAL FREQUENCY

$m = 1,\ n = 1$

FOR ALUM ALLOY

$E = 10.5 \times 10^6\ \#/in^2,\ \nu = .3 \qquad a = 16'',\ b = 12.5''$

DRL-255

G M Defense Research ⊗ Laboratories General Motors Corporation	REPORT NO	PAGE 6	JOB NO	PAGE
TITLE SURVEYOR LUNAR ROVING VEHICLE STRUCTURAL ANALYSIS	PREPARED PASCALOFF / JUNTUNEN	DATE 7/29/63		
	CHECKED CJP	8/9/63		
	APPROVED			

LRV COMPARTMENT STRESS ANALYSIS

PAYLOAD MOUNTING PANEL CHECK

c. NATURAL FREQUENCY CALCULATION:

METHOD 1 --- (CONT'D.)

$$D = \frac{10.5 \times 10^6 \times .03 \times (.218)^2}{2(.91)} = 8225$$

$$w = \frac{W}{VOL} \approx \frac{18.0}{12 \times 15.5 \times .248} = .390 \ \#/IN^3$$

$$g \approx 386.4 \ \frac{IN}{SEC^2}$$

$$f_n = \frac{\pi}{2}\sqrt{\frac{8225 \times 386.4}{.390}}\left(\frac{1}{256} + \frac{1}{156.25}\right)$$

f_n = 46.2 CPS --- (FIRST MODE APPROXIMATION BY METHOD 1.)

G M Defense Research ⊗ Laboratories General Motors Corporation	REPORT NO	PAGE 7	JOB NO	PAGE
TITLE SURVEYOR LUNAR ROVING VEHICLE STRUCTURAL ANALYSIS	PREPARED Pascaloff / [illegible] DATE 7/24/63			
	CHECKED CJP 8/9/63			
	APPROVED			

LRU COMPARTMENT STRESS ANALYSIS

PAYLOAD MOUNTING PANEL CHECK

c. NATURAL FREQUENCY CALCULATION ---(CONT'D.)

METHOD 2 ----(ASSUMING PLATE TO CONSIST OF NUMEROUS BEAMS ATTACHED TOGETHER)

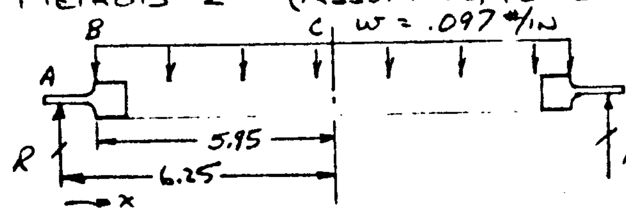

$$w = \frac{W}{ab} = \frac{18}{12 \times 15.5} = .097 \frac{\#}{IN.}$$

$$R = \frac{wL}{2} = .097 \times \frac{11.9}{2} = .576^{\#}$$

A - B:

$$M = Rx \;;\; m = x \qquad I = \frac{1 \times .10^3}{12} = .0000833 \text{ IN}^4$$

$$EI = 250 \qquad E = 3 \times 10^6 \ \#/\text{IN}^2$$

B - C:

$$M = Rx - w\frac{(x-.3)^2}{2} \;;\; m = x$$

$$I = \frac{1 \times .03 \times .218^2}{2} = .0007128 \text{ IN}^4 \;,\; E = 10.5 \times 10^6$$

$$EI = 7485 \;;\; \delta_A = \int \frac{Mm\,ds}{EI}$$

$$\delta_A = \frac{2R}{250}\int_0^{0.3} x^2\,dx + \frac{2R}{7485}\int_{0.3}^{6.25} x^2\,dx - \frac{w}{7485}\int_{0.3}^{6.25}(x^2 - .6x + .09)x$$

$$\delta_A = \frac{2R}{250}\left[\frac{x^3}{3}\right]_0^{.3} + \frac{2R}{7485}\left[\frac{x^3}{3}\right]_{.3}^{6.25} - \frac{w}{7485}\left[\frac{x^3}{3} - .3x^2 + .09x\right]_{.3}^{6.25}$$

$$= 2R\left[\frac{.009}{250} + \frac{81.37}{7485}\right] - w\left[\frac{81.37 - 11.69 + .54}{7485}\right]$$

DRL-255

G M Defense Research⊗Laboratories General Motors Corporation	REPORT NO	PAGE 8	JOB NO.	PAGE
TITLE SURVEYOR LUNAR ROVING VEHICLE STRUCTURAL ANALYSIS		PREPARED Pascaloff/Juntunen DATE 7/4/63		
		CHECKED CVP 8/9/63		
		APPROVED		

LRV COMPARTMENT STRESS ANALYSIS

PAYLOAD MOUNTING PANEL CHECK

C. NATURAL FREQUENCY CALCULATION;
METHOD 2 - - CONT'D.

$$\delta_A = .0125 - .0009 = .0116 \text{ IN.}$$

FOR A PLATE, A CLOSE APPROX. OF $\delta_p = \frac{\delta_A}{2}$, OR

$$\delta_p = .0058 \text{ INCH}$$

FROM REFERENCE 6, FIRST MODE NATURAL FREQUENCY (f_n)

$$f_n = \frac{1}{2\pi}\sqrt{\frac{g}{\delta}} = \frac{1}{2\pi}\sqrt{\frac{386.4}{.0058}} = \underline{41.0 \text{ cps}}$$

(FIRST MODE APPROXIMATION BY METHOD 2)

DRL-255

G M Defense Research Laboratories, General Motors Corporation	REPORT NO	PAGE 9	JOB NO	PAGE
TITLE: SURVEYOR LUNAR ROVING VEHICLE STRUCTURAL ANALYSIS		PREPARED: PASCALOFF / JUNTUNEN		DATE: 7/29/63
		CHECKED: CWP		8/9/63
		APPROVED:		

LRV COMPARTMENT STRESS ANALYSIS

INTEGRAL COMPARTMENT-AXLE CHECK:

a. LOWER HAT-SHAPED CHANNEL CHECK

MATERIAL: 2014-T62 ALUM ALLOY CLAD SHEET ($t = .020$)

LOADING

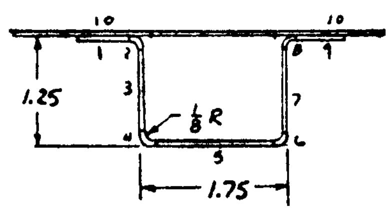

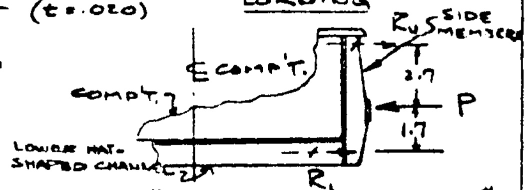

$P = 1008^{\#}$; $R_L = 619^{\#}$; $R_U = 389^{\#}$

ITEM	b or R	$\frac{b}{t}$ or $\frac{R}{t}$	A	F_{cc}	AF_{cc}
1	.293	14.6	.00586	16,500	
2	.135	6.75	.00424	35600	
3	.980	49.0	.01960	19000	
4	.135	6.75	.00424	35600	
5	1.460	73.0	.02920	13500	$\Sigma = 1936^{\#}$
6	.135	6.75	.00424	35600	
7	.980	49.0	.01960	19000	
8	.135	6.75	.00424	35600	
9	.293	14.6	.00586	16500	
10	1.20	—	.0240	19940	$478^{\#}$

ΣA (LESS ITEM 10) $= .09708$ IN.^{2}

$$F_{cc} = \frac{\Sigma A F_{cc}}{\Sigma A} = \frac{1936}{.09708} = 19{,}940\ ^{\#}/_{IN^2}$$

$$P_{ALLOW.} = 1936 + 478 = 2414^{\#}$$

$$R_L = 619^{\#}$$

$$M.S. = \frac{2414}{619} - 1 = +2.90$$

DRL-255

G M Defense Research ⊗ Laboratories General Motors Corporation	REPORT NO	PAGE 10	JOB NO.	PAGE
TITLE SURVEYOR LUNAR ROVING VEHICLE STRUCTURAL ANALYSIS		PREPARED Pascaloff/Juntunen 7/29/63	CHECKED CJP 8/9/63	APPROVED

LRV COMPARTMENT STRESS ANALYSIS

INTEGRAL COMPARTMENT-AXLE CHECK --(CONT'D.)

b. SIDE MEMBER CHECK:

MAT'L.: 2014-T62 ALUM ALLOY CLAD SHEET (t=.020)

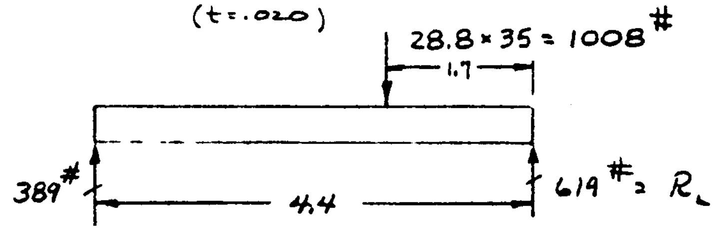

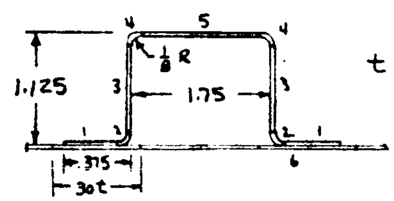

t = .020

SECTION 3/4" AWAY FROM AXLE ℄

ITEM	b or R	A	Y	AY^2	I_o	F_{cc}	AF_{cc}
1	.460	.0092	.030	.000008	—		
2	.135	.00848	.079	.000053	.00002		
3	1.670	.03340	.582	.011313	.00097		
4	.135	.00846	1.086	.010001	.00002	35600	302
5	1.500	.0300	1.135	.038647	—	13500	405
6	1.200	.0240	.010	.000002	—		
Σ		.11356		.060024	.00101		707#

$\bar{Y}$ = .5816 IN., ΣAY = .06604, c = .5534 IN.

$I = \Sigma AY^2 + \Sigma I_o - \Sigma AY(\bar{Y}) = .0610 - .06604 \times .5816 = .0226\ \text{IN.}^4$

$\frac{I}{c} = .0409\ \text{IN.}^3$

$M = R_L x = 619 \times 1 = 619\ \text{IN.}\#$

$f_c = \frac{M}{I/c} = \frac{619}{.0409} = 15{,}100\ \#/\text{IN.}^2$

$F_{cc} = \frac{\Sigma AF_{cc}}{\Sigma A} = \frac{707}{.0385} = 18370\ \#/\text{IN.}^2$

$M.S. = \frac{18370}{15100} - 1 = +.22$

G M Defense Research ⊗ Laboratories General Motors Corporation	REPORT NO	PAGE 11	JOB NO	PAGE
TITLE SURVEYOR LUNAR ROVING VEHICLE STRUCTURAL ANALYSIS		PREPARED PASCALOFF/JUUNTUNEN 7/29/63	CHECKED CJP 8/9/63	APPROVED

LRV COMPARTMENT STRESS ANALYSIS

INTEGRAL COMPARTMENT - AXLE CHECK -- (CONT'D.)

C. COMPARTMENT UPPER FLANGE CHECK IN VICINITY OF SIDE MEMBER

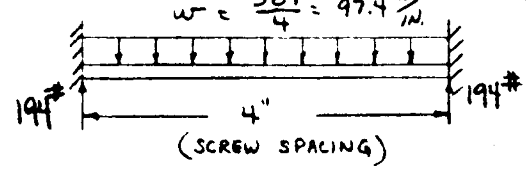

[4-INCHES OF FLANGE IS ASSUMED EFFECTIVE IN DISTRIBUTING LOAD INTO COVER PLATE AS SHOWN IN SKETCH.

SINCE FULL FIXITY DOES NOT EXIST AT ENDS, M_{MAX} IS BETWEEN $\frac{wL^2}{12}$ AND $\frac{wL^2}{24}$, ASSUME $M_{MAX} = \frac{wL^2}{18}$

$$M_{MAX} = \frac{wL^2}{18} = \frac{97.4 \times 16}{18} = 86.6 \ in.\#$$

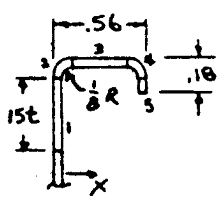

ITEM	b or R	A	X	Ax^2	I_o
1	.300	.006	.010	—	—
2	.135	.00848	.059	.00003	.00001
3	.270	.00540	.280	.000423	.000033
4	.135	.00848	.501	.002128	.00001
5	.035	.0007	.550	.000212	—
Σ		.02906		.00279	.000053

$\Sigma Ax = .0067$, $\bar{x} = .2308$ in. , $c = .3192$ in.

$$I = \Sigma Ax^2 + \Sigma I_o - \Sigma Ax(\bar{x})$$

$$I = .002846 - .2308 \times .0067 = .001298 \ in.^4$$

$$I/c = .004067 \ in.^3$$

$$f_b = \frac{Mc}{I} = \frac{86.6}{.004067} = 21{,}290 \ \#/in.^2$$

ALLOWABLE STRESS FOR OUTER LIP

$R_e = R_4 + b_5 = .170$

$\frac{R_e}{t} = \frac{.170}{.02} = 8.5$, $F_{cc} = 28{,}500 \ \#/in.^2$

$$M.S. = \frac{28{,}500}{21290} - 1 = +.34$$

DRL-255

G M Defense Research ⊗ Laboratories General Motors Corporation	REPORT NO	PAGE 12	JOB NO.	PAGE
TITLE: SURVEYOR LUNAR ROVING VEHICLE STRUCTURAL ANALYSIS		PREPARED C. PASCALOFF	DATE 8/6/63	
		CHECKED		
		APPROVED		

ELASTIC FRAME ANALYSIS

GEOMETRY:

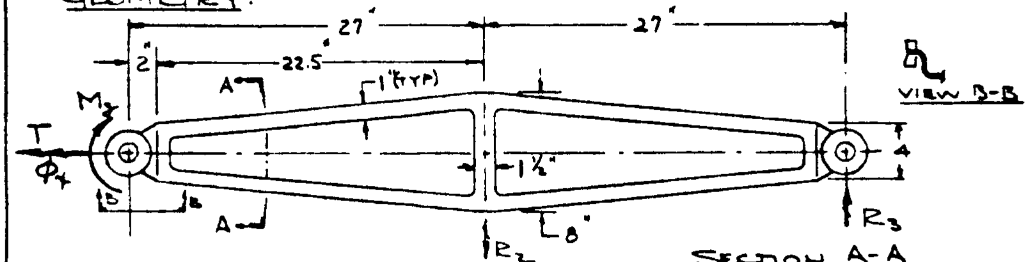

SECTION A-A

MATERIAL: SPRING STEEL (ELASTIC LIMIT > 80 KSI; E = 29 × 10⁶ PSI)

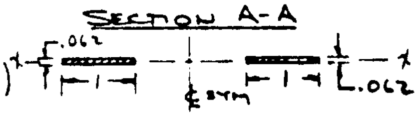

DESIGN REQUIREMENTS: REF.: SUBSECTION D - VEHICLE SYSTEM - (THIS PROPOSAL)

1) BENDING SPRING RATE ≥ 0.23 LBS/INCH
2) TORSION SPRING RATE ≥ 75 IN-LBS/RADIAN
3) SLRV ROLL ANGLE (ϕ_x) ≥ ±45 DEGREES BETWEEN AXLES.
4) STEERING MOMENT (M_z) ≥ 100 IN-LBS.

BENDING STRESS CHECK:

$$\frac{d^2y}{dx^2} = \frac{1}{R} = \frac{M}{EI}$$

... WHERE: E = YOUNG'S MOD. = 29×10^6; R = RADIUS OF CURVATURE; M = BENDING MOMENT

$$I_{xx} = 2 \times \frac{bt^3}{12} = 2 \times \frac{1 \times .062^3}{12}$$

$$I_{xx} = 0.00003971 \text{ IN}^4$$

$$\left(\frac{I}{c}\right)_{xx} = 2\frac{bt^2}{6} = 2 \times \frac{1 \times .062^2}{6}$$

$$\left(\frac{I}{c}\right)_{xx} = 0.001281 \text{ IN}^3$$

BENDING STRESS $(\sigma_m) = \dfrac{M}{(I/c)_{xx}}$

FOR AN ALLOWABLE WORKING STRESS OF 80,000 PSI

$M = 80000 \times (I/c)_{xx} = 80000 \times .001281 = 102.48$ IN-LBS (MAX. ALLOW. BENDING MOMENT.)

$$R_{CRIT} = \frac{EI}{M} = \frac{29 \times 10^6 \times 39.71 \times 10^{-6}}{102.48} = 11.23 \text{ INCHES}$$

MINIMUM BEND RADII EXPECTED IN STOWED POSITION IS APPROXIMATELY 12 INCHES

$$M.S. = \frac{12}{11.23} - 1 = +0.07$$

DRL-255

G M Defense Research ⊗ Laboratories General Motors Corporation	REPORT NO	PAGE 13	JOB NO	PAGE
TITLE SURVEYOR LUNAR ROVING VEHICLE STRUCTURAL ANALYSIS		PREPARED C. PASCALOFF		DATE 8/6/63
		CHECKED		
		APPROVED		

ELASTIC FRAME ANALYSIS ... (CONT'D.)

BENDING SPRING RATE:

FOR THIS CALCULATION THE FRAME IS ASSUMED TO BE CANTILEVERED AT ITS MID POINT AS SHOWN SCHEMATICALLY BELOW.

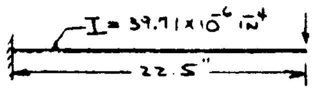

FOR A CANTILEVER BEAM DEFLECTION AT LOAD POINT P IS GIVEN AS $\delta = \frac{PL^3}{3EI}$ .. REF. (4)

BENDING SPRING RATE $(k_M) = \frac{P}{\delta} = \frac{3EI}{L^3}$ ... WHERE $L = 22.5''$

$$k_M = \frac{3 \times 29 \times 10^6 \times 39.71 \times 10^{-6}}{22.5^3} = 0.303 \text{ LB/INCH} > 0.23 \text{ LB/INCH}$$

∴ SPRING RATE MEETS DESIGN REQUIREMENTS.

TORSION SPRING RATE:

FOR A RECTANGULAR CROSS SECTION MEMBER IN TORSION THE EQUATIONS FOR MAXIMUM SHEAR STRESS (τ_s), AND ANGLE OF TWIST (ϕ) ARE GIVEN AS

$$\tau_s = \frac{T}{\alpha b t^2} \quad ; \quad \phi = \frac{TL}{\beta b t^3 G} \quad \cdots \text{ REF. (7), PG. 331}$$

WHERE:

α & β ARE GEOMETRICAL COEFFICIENTS WHICH ARE FUNCTIONS OF (b/t).

b = CROSS SECTION WIDTH -- INCHES

t = CROSS SECTION THICKNESS --- INCHES

T = TORQUE ON CROSS SECTION -- IN-LBS

L = LENGTH OF MEMBER -- INCHES

G = SHEAR MODULUS --- PSI

$b/t = \frac{1}{.062} = 16 > 10$. ∴ $\alpha = \beta = 1/3$ - REF (7), PG 331

$$\text{TORSION SPRING RATE } (k_T) = \frac{T}{\phi} = 2\beta \frac{bt^3G}{L} = \frac{2bt^3G}{3L}$$

FOR STEEL $G = 11 \times 10^6$ PSI

$$k_T = \frac{2 \times 1.0 \times .062^3 \times 11 \times 10^6}{3 \times 22.5} = 77.6 \text{ IN-LB/RADIAN} > 75 \frac{\text{IN-LB}}{\text{RAD.}}$$

∴ SPRING RATE MEETS DESIGN REQUIREMENTS

DRL-255

G M Defense Research ⊗ Laboratories General Motors Corporation	REPORT NO	PAGE 14	JOB NO.	PAGE
TITLE Surveyor Lunar Roving Vehicle Structural Analysis	PREPARED C. Pascaloff	DATE 9/6/63	CHECKED	APPROVED

ELASTIC FRAME ANALYSIS ...(CONT'D.)

TORSION STRESS CHECK:

ALLOWABLE TORSIONAL STRESS $(\tau_s)_{ALLOW.}$ FOR SPRING STEEL $\approx \frac{1}{2}$ ALLOWABLE BENDING STRESS $= 40{,}000$ PSI

MAXIMUM ALLOWABLE TWIST ANGLE FOR ELASTIC FRAME $(\phi_{MAX}) = \frac{T_{MAX} L}{\beta b t^3 G} = \frac{\alpha b t^2 (\tau_s)_{ALLOW.} L}{\beta b t^3 G} = \frac{L (\tau_s)_{ALLOW.}}{t G}$

$$\phi_{MAX} = \frac{22.5 \times 40000}{.062 \times 11 \times 10^6} = 1.320 \text{ RADIANS } (75.7 \text{ DEGREES})$$

$\therefore$ ROLL ANGLE DESIGN REQ'MT. SATISFIED

AT $\pm 45°$ ROLL ANGLE, THE SPRING TORSION STRESS (τ_s) IS

$$\tau_s = \frac{3T}{bt^2} = \frac{3 k_{T} \phi}{b t^2} = \frac{3 \times 77.6 \times 45\pi}{2 \times 1.0 \times .062^2 \times 180} = 23{,}800 \text{ PSI}$$

$$M.S. = \frac{40000}{23800} - 1 = +0.68$$

SLRV CRITICAL ROLL ANGLE:

THE CRITICAL ROLL ANGLE (ϕ_{CRIT}) OF THE SLRV IS HEREIN DEFINED AS THE ANGLE AT WHICH THE FRONT COMPARTMENT CAN TWIST WITH RESPECT TO THE CENTRE COMPARTMENT SUCH THAT CENTER COMPARTMENT WHEEL LIFT-OFF WILL OCCUR (ON THE LUNAR SURFACE).

FOR $T = 0$, $R_L = R_R = \frac{W}{2}$

FOR WHEEL LIFT-OFF $T = 14\,W$

FROM PRELIMINARY WEIGHT STUDIES $W \approx 32.8$ LBS

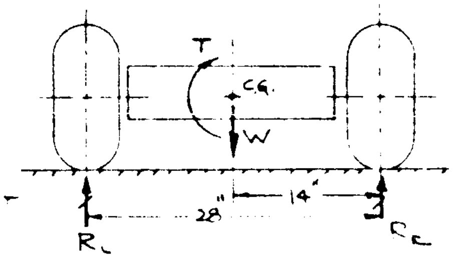

ON THE LUNAR SURFACE $T = 14\frac{W}{6} = \frac{14 \times 32.8}{6} = 76.5''^{\#}$

$$\phi_{CRIT} = \frac{T}{k_T} = \frac{76.5}{77.6} = 0.986 \text{ RADIAN } (56.5 \text{ DEGREES})$$

DRL-255

Revised 4/9/63

G M Defense Research ⊗ Laboratories General Motors Corporation	REPORT NO	PAGE 15	JOB NO	PAGE
TITLE SURVEYOR LUNAR ROVING VEHICLE STRUCTURAL ANALYSIS		PREPARED C. PASCALOFF	DATE 8/7/63	
		CHECKED		
		APPROVED		

ELASTIC FRAME ANALYSIS ... (CONT'D.)

STEERING MOMENT STRESS CHECK

THE STEERING MOMENT (M_γ) IS REACTED BY FORCES R_2 & R_3 AS SHOWN IN THE FIGURE ON PG. H-26.

THE FRAME WILL BE ANALYZED AS TWO SEPARATE TRAPEZOIDAL BENTS WHICH ARE ASSUMED TO BE FIXED AT THE MID SECTION PARALLEL TO THE CENTER AXLE. CENTERLINE FRAME GEOMETRY IS USED IN CALCULATING THE FRAME STRESSES BY EMPLOYING THE MOMENT DISTRIBUTION (HARDY-CROSS) METHOD OF SOLUTION.

$M_\gamma = 100$ IN-LBS (REF PG. H-26)

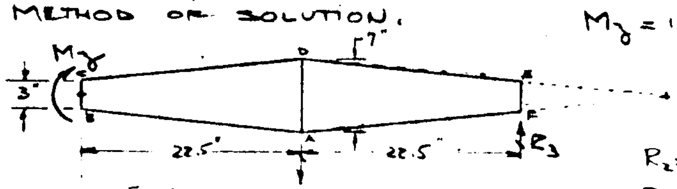

FIG. (13)

$R_2 = R_3 = \frac{M_\gamma}{22.5} = \frac{100}{22.5}$

$R_2 = R_3 = 4.44$ LBS

$I_{BC} = I_{EF}$ IS ASSUMED TO BE 10 TIMES GREATER THAN I_{CD}

$I_{CD} = I_{AB} = I_{AF} = I_{DE} = 39.71 \times 10^{-6}$ IN^4 ... (REF. PG. H-30)

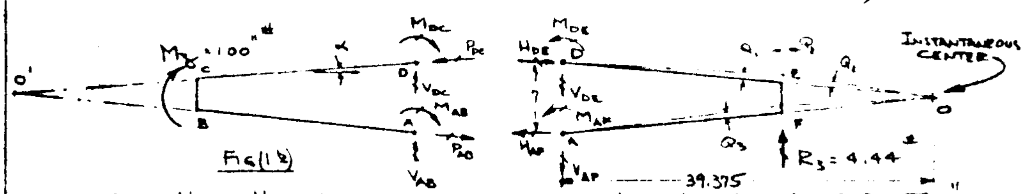

FIG. (14) FIG. (15)

$H_{AB} = H_{AF}$; $H_{DC} = H_{DE}$

$V_{AB} + V_{AF} + V_{DC} + V_{DE} = R_2 = 4.44$#

$L_{AB} = L_{AF} = L_{CD} = L_{ED} = 22.589$"

$L_{DA} = L_{DE} = 16.941$"; $L_{EF} = L_{BC} = 3$"

$K = \frac{I}{L}$

$K_{CD} = K_{BA} = K_{FA} = K_{ED} = \frac{39.71 \times 10^{-6}}{22.589} = 1.758 \times 10^{-6}$

$K_{BC} = K_{CB} = K_{FE} = K_{EF} = \frac{39.71 \times 10^{-5}}{3} = 132.367 \times 10^{-6}$

RELATIVE VALUES OF K:

$K'_{CD} = K'_{BA} = K'_{FA} = K'_{ED} = 1$

$K'_{BC} = K'_{CB} = K'_{FE} = K'_{EF} = 75.3$

$\alpha = 5° - 4.778'$
$\sin\alpha = .088541$
$\cos\alpha = .996073$
$\tan\alpha = .088889$

MOMENT DISTRIBUTION FACTORS:

$(DF)_{BA} = (DF)_{CD} = (DF)_{ED} = (DF)_{FA} = \frac{1}{75.3+1} = 0.0131$

$(DF)_{BC} = (DF)_{CB} = (DF)_{FE} = (DF)_{EF} = \frac{75.3}{76.3} = 0.9869$

FIXED-END MOMENT DUE TO M_γ:

$(M_F)_{BC} = (M_F)_{CB} = (M_F)_{EF} = (M_F)_{FE} = \frac{M_\gamma}{4} = 25$ IN-LBS

DRL-255

REVISED 8/9/63

G M Defense Research⊗Laboratories General Motors Corporation	REPORT NO	PAGE 16	JOB NO.	PAGE
TITLE SURVEYOR LUNAR ROVING VEHICLE STRUCTURAL ANALYSIS	PREPARED C. PASCALOFF			DATE 8/7/63
	CHECKED			
	APPROVED			

ELASTIC FRAME ANALYSIS

STEERING MOMENT STRESS CHECK --- (CONT'D.)

FIXED-END MOMENT DUE TO R_3:

$\frac{Q_1}{22.589} = \frac{-Q_2}{16.941}$; $Q_2 = -0.750\,Q_1$; $Q_3 = Q_1$

$(M_F)_{FA} = (M_F)_{AF} = +6EK'_1Q_1 = +6E(1)Q_1 = +6EQ_1$

$(M_F)_{FE} = (M_F)_{EF} = +6EK'_2Q_2 = +6E(75.3)Q_2 = -6E(75.3)(.750)Q_1 = -338.85EQ_1$

$(M_F)_{ED} = (M_F)_{DE} = +6EK'_3Q_3 = +6E(1)Q_3 = +6EQ_1$

FROM FIGURE (1B) ON PREVIOUS PAGE:

$\Sigma V = 0$: $V_{DC} = P_{DC}\sin\alpha$; $V_{AB} = P_{AB}\sin\alpha$

DUE TO SYMMETRY ABOUT THE x- & y-AXES,

$V_{AB} = V_{DC}$; $P_{AB} = P_{DC}$; $M_{AB} = M_{DC}$

$\therefore \boxed{V_{AB} = 0.08854\,P_{AB}}$ --- (1)

$\Sigma M_{O'} = 0$:

$M_3 + 2M_{AB} = 7P_{AB}\cos\alpha = 7 \times 0.996073\,P_{AB}$; OR,

$\boxed{6.972511\,P_{AB} - 2M_{AB} = 100}$ --- (2)

$H_{AB} = P_{AB}\cos\alpha$; $\boxed{H_{AB} = 0.996073\,P_{AB}}$ --- (3)

MOMENT DISTRIBUTION DUE TO R_3:

(TABLE 1)

	A	F		E		D
JOINT	AF	FA	FE	EF	ED	DE
D.F.	0	0.0131	0.9869	0.9869	0.0131	0
F.E.M	0	+6EQ₁	−338.85EQ₁	−338.85EQ₁	+6EQ₁	0
C.O.	0	+4.36	+328.49	+328.49	+4.36	0
BAL.	+2.18	0	+164.24	+164.24	0	+2.18
C.O.	0	−2.15	−162.09	−162.09	−2.15	0
BAL.	−1.07	0	−81.04	−81.04	0	−1.07
C.O.	0	+1.06	+79.98	+79.98	+1.06	0
BAL.	+0.53	0	+39.99	+39.99	0	+0.53
C.O.	0	−0.52	−39.47	−39.47	−0.52	0
BAL	−0.26	0	−19.74	−19.74	0	−0.26
C.O.	0	+0.26	+19.48	+19.48	+0.26	0
BAL	+0.13	0	+9.74	+9.74	0	+0.13
C.O.	0	−0.12	−9.61	−9.61	−0.13	0
BAL.	−0.07	0	−4.80	−4.80	0	−0.07
C.O.	0	+0.06	+4.74	+4.74	+0.06	0
BAL	+0.03	0	+2.37	+2.37	0	+0.03
C.O.	0	−0.03	−2.34	−2.34	−0.03	0
BAL	−0.01	0	−1.17	−1.17	0	−0.01
C.O.	0	+0.02	+1.15	+1.15	+0.02	0
BAL.	+0.01	0	+0.58	+0.58	0	+0.01
C.O.	0	−0.01	−0.57	−0.57	−0.01	0
BAL	0	0	−0.29	−0.29	0	0
C.O.	0	0	+0.29	+0.29	0	0
Σ	+1.47EQ₁	+8.92EQ₁	−8.92EQ₁	−8.92EQ₁	+8.92EQ₁	+1.97EQ₁

$M_{AF} = M_{DE} = +1.47EQ_1$

$M_{FA} = M_{ED} = +8.92EQ_1$

$M_{FE} = M_{EF} = -8.92EQ_1$

DRL-255

REVISED 8/7/63

G M Defense Research ⊗ Laboratories General Motors Corporation	REPORT NO	PAGE 17	JOB NO	PAGE
TITLE SURVEYOR LUNAR ROVING VEHICLE STRUCTURAL ANALYSIS		PREPARED C. PASCALOFF		DATE 8/7/63
		CHECKED		
		APPROVED		

ELASTIC FRAME ANALYSIS

STEERING MOMENT STRESS CHECK --- (CONT'D.)

MOMENT DISTRIBUTION DUE TO M_γ:

(TABLE 2)

	A	B		C		D
JOINT	AB	BA	BC	CB	CD	DC
D.F.	0	0.0131	0.9869	0.9869	0.0131	0
FEM.	0	0	+25.00	+25.00	0	0
C.O.	0	−0.33	−24.67	−24.67	−0.33	0
BAL.	−0.16	0	−12.33	−12.33	0	−0.16
C.O.	0	+0.16	+12.17	+12.17	+0.16	0
BAL.	+0.08	0	+6.08	+6.08	0	+0.08
C.O.	0	−0.08	−6.00	−6.00	−0.08	0
BAL.	−0.04	0	−3.00	−3.00	0	−0.04
C.O.	0	+0.04	+2.96	+2.96	+0.04	0
BAL.	+0.02	0	+1.48	+1.48	0	+0.02
C.O.	0	−0.02	−1.46	−1.46	−0.02	0
BAL.	−0.01	0	−0.73	−0.73	0	−0.01
C.O.	0	+0.01	+0.72	+0.72	+0.01	0
BAL.	0	0	+0.36	+0.36	0	0
C.O.	0	0	−0.36	−0.36	0	0
Σ	−0.11	−0.22	+0.22	+0.22	−0.22	−0.11

$M_{AB} = M_{DC} = -0.11$ IN-LBS

$M_{BA} = M_{CD} = -0.22$ IN-LBS

$M_{BC} = M_{CB} = +0.22$ IN-LBS

AT CENTER SECTION OF FRAME:

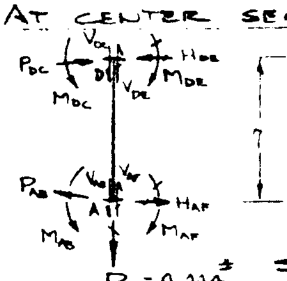

FIG(1d)

$H_{AB} = 0.996073\, P_{AB}$ ... REF. EQ (3)

ALSO BECAUSE OF SYMMETRY OF FRAME ABOUT BOTH THE X- & Y-AXES

$H_{DE} = H_{AF}$; $M_{DE} = M_{AF}$; $V_{DE} = V_{AF}$

$\Sigma M_A = 0$:

$7H_{DE} - 2M_{DE} = 7H_{AB} - 2M_{AB}$

SUBSTITUTING $M_{AB} = -0.11$ IN-LBS & $M_{DE} = +1.47\, EQ_1$ IN-LBS INTO ABOVE EQUATION GIVES

$\boxed{7H_{DE} - 2.94\, EQ_1 = 7H_{AB} + 0.22}$ --- (4)

TAKING $\Sigma V = 0$: $2V_{AF} = 4.444 + 2P_{AB} \times .033541 - 2V_{AB}$. NOW, FROM EQ (1) WHERE $V_{AB} = 0.033541\, P_{AB}$, THE EQUATION FOR V_{AF} BECOMES:

$\boxed{V_{AF} = 2.222 \text{ LBS}}$ ---(5)

FROM FIGURE (1e) ON PAGE H-24 TAKING MOMENTS ABOUT THE INSTANEOUS CENTER AT POINT "O" GIVES

$16.875 \times 4.444 + 7H_{DE} = 2 \times 37.375\, V_{AF} - 2M_{AF} = 175 + 2M_{AF}$.

SUBSTITUTING $M_{AF} = +1.47\, EQ_1$ ... (REF. TABLE 1)

$\boxed{7H_{DE} - 2.94\, EQ_1 = 100}$ ---(6)

DRL-255

REVISED 8/9/63

G M Defense Research ⊗ Laboratories General Motors Corporation	REPORT NO	PAGE 18	JOB NO	PAGE
TITLE SURVEYOR LUNAR ROVING VEHICLE STRUCTURAL ANALYSIS		PREPARED C PASCALOFF		DATE 8/7/63
		CHECKED		
		APPROVED		

ELASTIC FRAME ANALYSIS

STEERING MOMENT STRESS CHECK ---(CONT'D.)

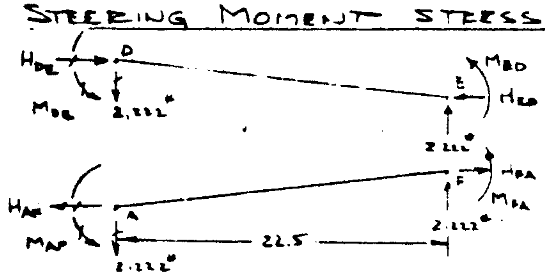

FROM TABLE 1

$M_{AF} = M_{DE} = +1.47 EQ_1$

$M_{FA} = M_{ED} = +8.92 EQ_1$

$\Sigma M_F = 0$: (MEMBER AF)

$2 H_{AF} = M_{AF} + M_{FA} + 2.222 \times 22.5$

$\boxed{H_{DE} = 5.195 EQ_1 + 25}$ ---(7)

SUBSTITUTING EQ. (7) INTO EQ (6) GIVES FOR EQ_1

$36.365 EQ_1 + 175 - 2.94 EQ_1 = 100$

$\underline{EQ_1 = -2.24333}$

$\underline{M_{AF} = M_{DE} = +1.47 EQ_1 = -3.2934}$ "#; $\underline{M_{FA} = M_{ED} = +8.92 EQ_1 = -20.0150}$ "#

SUBSTITUTING INTO EQ (2) FOR VALUE OF M_{AB} GIVEN IN TABLE 2

$6.97251 P_{AB} = 100 - 0.22$; $\underline{P_{AB} = P_{DC} = 14.3105 \text{ LBS}}$

$\underline{H_{AB} = H_{DC} = 14.2543 \text{ LBS}}$; $\underline{V_{AB} = V_{DC} = 1.2671 \text{ LBS}}$

RETURNING TO FIGURE (12), ON PAGE #31, A MOMENT CHECK SHOWS THAT

$3.2984 \times 2 + 7 \times 13.4344 = 0.22 + 7 \times 14.2543$

$100 = 100$ ... CHECKS!

MAXIMUM COMPRESSIVE LOAD IN SPRING LEAF $(P_s)_{MAX}$:

$$(P_s)_{max} = P_{DC} = \underline{14.3105 \text{ LBS}}$$

$$\text{MAXIMUM COLUMN STRESS} = \frac{14.3105}{1.0 \times .062} = 231 \text{ psi}$$

RADIUS OF GYRATION FOR SECTION (2) $= \sqrt{\frac{I}{A}} = \sqrt{\frac{bt^3}{12bt}} = \frac{t}{2}\sqrt{\frac{1}{3}}$

$\rho = 0.2887 t = .2887 \times .062 = 0.01790$ INCH

$L/\rho = \frac{22.589}{.01790} = 1262$

USING EULER'S EQUATION TO DETERMINE THE ALLOWABLE COLUMN STRESS (σ_{COL})

$\sigma_{COL} = \frac{C \pi^2 E}{(L/\rho)^2}$ --- WHERE C IS COLUMN FIXITY FACTOR REF. 4, PG. 235

ASSUMING A COLUMN FIXITY FACTOR OF 1.5

$\sigma_{COL} = \frac{1.5 \times \pi^2 \times 29 \times 10^6}{(1262)^2} = 270$ psi

$M.S. = \frac{270}{231} - 1 = \underline{+0.17}$

STEERING MOMENT OF 100 IN-LBS DOES NOT BUCKLE SPRING LEAF.

DRL-255

REVISED 8/9/63

G M Defense Research ⊗ Laboratories General Motors Corporation	REPORT NO	PAGE 19	JOB NO.	PAGE
TITLE SURVEYOR LUNAR ROVING VEHICLE STRUCTURAL ANALYSIS		PREPARED C. PASCALOFF 8/7/63 CHECKED APPROVED		

ELASTIC FRAME ANALYSIS -- (CONT'D.)

IMPACT BUCKLING OF ELASTIC FRAME:

FOR THIS INVESTIGATION, THE FRAME IS ASSUMED TO BE PIN-ENDED AT THE FRONT AND REAR AXLE PIVOTS WITH THE CENTER AXLE SERVING AS A HINGE SUPPORT AS SHOWN IN THE SKETCH BELOW.

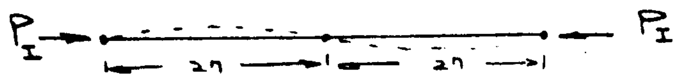

USING THE ALLOWABLE BUCKLING STRESS OF 231 PSI / LEAF FROM THE PREVIOUS CALCULATIONS, THE BUCKLING LOAD / LEAF IS EQUAL TO $270 \times .062 = 16.71$ LBS

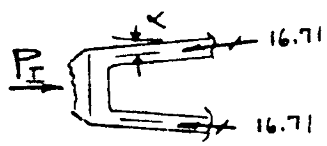

$\cos\alpha = 0.996073$ .. (PG H-29)

$$P_I = 2(16.71 \times 0.996073) = \underline{33.30 \text{ LBS}}$$

THIS CALCULATION ASSUMES THAT THE ELASTIC FRAME NEUTRAL AXIS IS COINCIDENT WITH THAT OF THE LOAD (P_I). ANY ECCENTRICITIES DUE TO BENDING OF THE FRAME WILL DRASTICALLY REDUCE THE VALUE CALCULATED ABOVE.

TITLE	PREPARED / DATE
SURVEYOR LUNAR ROVING VEHICLE EARTH MODEL	Noel. 11-14-63
	CHECKED
	APPROVED

2. ELASTIC FRAME ANALYSIS

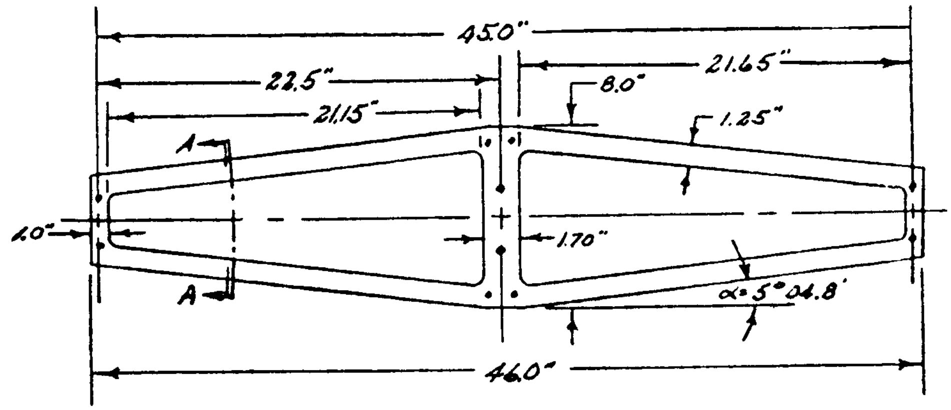

MATERIAL: 7075 T6 AL ALLOY.
F_{SU} = 46,000 PSI
F_{TY} = 66,000 PSI

SECTION A-A

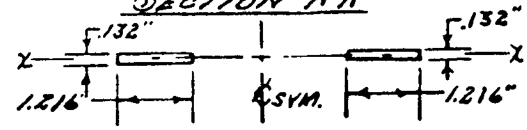

DESIGN REQUIREMENTS:

1. BENDING SPRING RATE ----- 1.38 TO 1.40 LBS/INCH.
2. TORSION SPRING RATE --- ≤ 450 TO 475 IN.-LBS/RADIAN
3. S.L.R.V. ROLL ANGLE (θ) --- ≥ 45° DEGREES

TORSION STRESS CHECK:

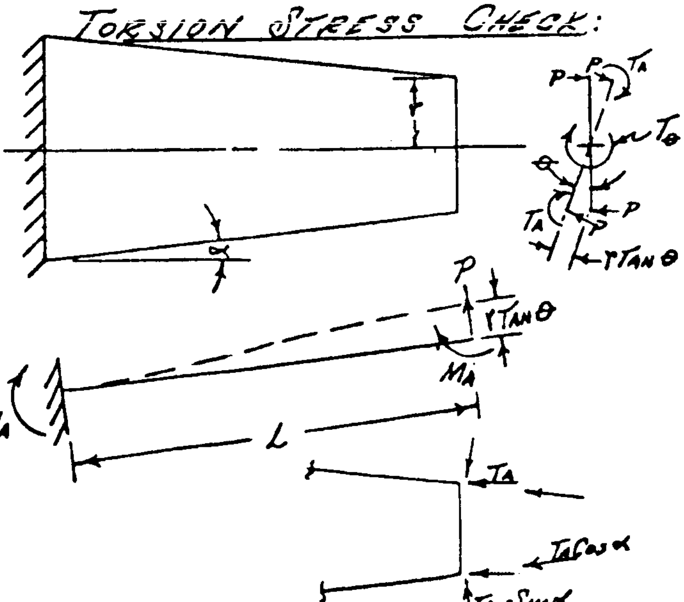

GIVEN:

$b = 1.216"$ $\quad b/t = 9.212$

$t = 0.132"$ $\quad t^3 = .0023$

$L = 21.1"$ $\quad \alpha = \beta = .311$

$E = 10^7$ $\quad 2B = .622$

$G = 3.9 \times 10^6$

$\tan\alpha = .088541$

$\sin\alpha = .088541$

$\cos\alpha = .996073$

$r = 1.44"$ $\quad r^2 = 2.074$

ELASTIC FRAME ANALYSIS

TORSION STRESS CHECK (CONT.)

$$T_\theta = 2T_A + 2P_r \qquad P = \frac{12EI(r\,\text{TAN}\,\theta)}{L^3}$$

$$2Pr = \frac{24EI(r^2\,\text{TAN}\,\theta)}{L^3}$$

① $$T_\theta = \left(\frac{2\beta b t^3 G}{L\,\text{Cos}\,\alpha}\right)\theta + \frac{24EI}{L^3}(r^2\,\text{TAN}\,\theta)$$

$$M_A = \frac{6EI(r\,\text{TAN}\,\theta)}{L^2}$$

② $$M_A = \frac{6EI(r\,\text{TAN}\,\theta)}{L^2}$$

$$T_A \text{Cos}\,\alpha = K_T\theta = \left(\frac{\beta b t^3 G}{L}\right)\theta$$

$$2T_A = \left(\frac{2\beta b t^3 G}{L\,\text{Cos}\,\alpha}\right)\theta$$

③ $$(\sigma_b)_{MAX} = \frac{M_A C}{I} = \frac{6M_A}{bt^2} \qquad C = t/2 \quad I = \frac{bt^3}{12}$$

$$\tau_s = \frac{T_A\,\text{Cos}\,\alpha}{\alpha b t^2} = \frac{\beta b t^3 G}{\alpha b t^2 l}\times\theta$$

④ $$\tau_s = \frac{Gt}{L}\theta$$

⑤ $$M_c = \left[\frac{6EI\,r\,\text{TAN}\,\theta}{L^2} - \frac{\beta b t^3 G\,\text{Sin}\,\alpha}{L\,\text{Cos}\,\alpha}\right]\theta$$

⑥ $$\sigma_{MAX} = \left[\frac{\sigma_b}{2} + \sqrt{\left(\frac{\sigma_b}{2}\right)^2 + \tau_s^2}\right.$$

⑦ $$\tau_{MAX} = \sqrt{\left(\frac{\sigma_b}{2}\right)^2 + \tau_s^2}$$

ELASTIC FRAME ANALYSIS

TORSION STRESS CHECK (CONT.)

SUB. IN EQ (1)

$$T_\theta = \left(\frac{.622 \times 1.216 \times .0023 \times 3.9 \times 10^6}{21.1 \times .996073}\right)\theta + \left(\frac{24 \times 10^7 \times 1.216 \times .0023 \times 2.074}{12 \times 9393931}\right) \tan\theta$$

$$T_\theta = 322.807\,\theta + 12.35 \tan\theta$$

SUB. IN EQ (2)

$$M_A = \left(\frac{6 \times 10^7 \times 1.216 \times .0023 \times 1.44}{12 \times 4.452}\right) \tan\theta$$

$$M_A = 452.31 \tan\theta$$

SUB. IN EQ (3)

$$(\sigma_b)_{max} = \frac{6 \times 45.231}{1.216 \times .01742} \tan\theta$$

$$(\sigma_b)_{max} = 8,656.64 \tan\theta$$

SUB. IN EQ (4)

$$T_s = \left(\frac{3.9 \times 10^6 \times .132}{21.1}\right)\theta$$

$$T_s = 24,398.1\,\theta$$

G M Defense Research Laboratories General Motors Corporation	REPORT NO	PAGE 4	JOB NO. TR64-26	PAGE 4

TITLE: SURVEYOR LUNAR ROVING VEHICLE EARTH MODEL

PREPARED: Noel — DATE: 11-14-63
CHECKED:
APPROVED:

ELASTIC FRAME ANALYSIS

TORSION STRESS CHECK (CON'T)

θ	θ	TAN θ	T_θ	M_A	σ_b	τ_s	τ_{max}	σ_{max}
DEG	RADIANS		IN-LB'S	IN-LB'S	PSI.	PSI.	PSI.	PSI.
0	0	0	0	0	0	0	0	0
5	.087266	.087489	28.3	39.6	757	2,129	2,162	2,541
10	.174533	.176327	58.5	79.8	1,526	4,258	4,326	5,089
15	.261799	.267949	87.8	121.2	2,320	6,387	6,491	7,651
20	.349066	.363970	117.2	164.6	3,151	8,517	8,661	10,237
25	.436332	.466308	146.6	210.9	4,037	10,646	10,836	12,855
30	.523599	.577350	176.2	261.1	4,998	12,775	13,017	15,516
35	.610865	.700208	205.8	316.7	6,061	14,904	15,209	18,240
40	.698132	.839100	235.7	379.5	7,264	17,033	17,416	21,048
45	.785398	1.000000	265.9	452.3	8,657	19,162	19,645	23,974
57.296	1.000000	1.557408	342.0	704.4	13,482	24,398	25,312	32,053

TORSION SPRING RATE

$$(@45°)\ K_T = \frac{T_\theta}{\theta} = \frac{265.9}{.785398} = 338.6 \text{ IN-LB'S/RADIAN} < 450 \text{ (R1)}$$

TITLE	5	5
SURVEYOR LUNAR ROVING VEHICLE EARTH MODEL	PREPARED Noel	DATE 11-14-63
	CHECKED	
	APPROVED	

ELASTIC FRAME ANALYSIS

BENDING STRESS CHECK

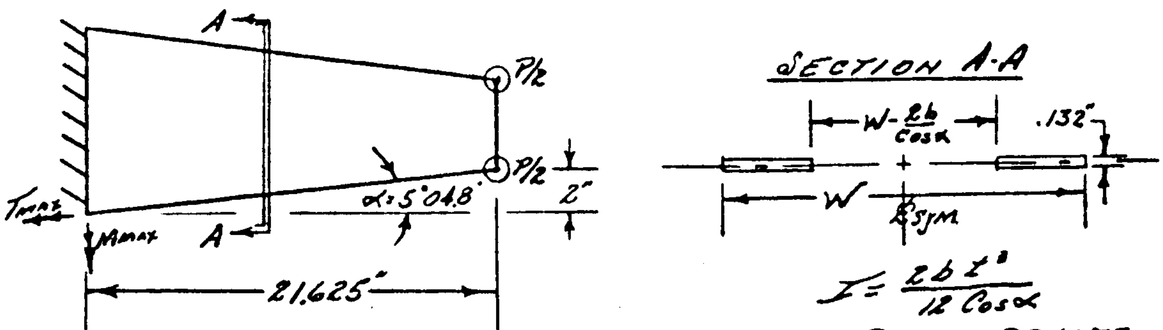

$$I = \frac{2bt^3}{12\cos\alpha}$$

$\cos\alpha = .996073$

$C = t/2$

$$\delta = \frac{PL^3}{3EI} = \left(\frac{\overline{21.625}^3 \times 12 \times .996073}{3 \times 10^7 \times 2 \times 1.216 \times .0023}\right)P$$

① $\delta = 0.72038\,P \rightarrow$ or $P/\delta = 1.388$ Lbs/INCH.

$$(\sigma_b)_{MAX} = \frac{MC}{I} = \frac{21.625 \times P \times \frac{.132}{2} \times 12 \times .996073}{2 \times 1.216 \times \overline{.132}^3}$$

$$(\sigma_b)_{MAX} = \left(\frac{21.625 \times 3 \times .996072}{1.216 \times .0174}\right)P$$

② $(\sigma_b)_{MAX} = 3,049.868\,P$ PSI

$$T_{MAX} = P/2 \times 2 = P\ ;\ \tau_s = \frac{T}{\alpha b t^2}$$

$$\tau_s = \frac{P}{\alpha b t^2} = \frac{P}{.311 \times 1.216 \times .0174}$$

③ $\tau_s = 151.97\,P$ PSI.

④ $\tau_{MAX} = \sqrt{\left(\frac{\sigma_b}{2}\right)^2 + (\tau_s)^2}$

⑤ $\sigma_{MAX} = \frac{\sigma}{2} + \sqrt{\left(\frac{\sigma_b}{2}\right)^2 + (\tau_s)^2}$

209

ELASTIC FRAME ANALYSIS

BENDING STRESS CHECK (CONT.)

P (LB's)	δ (IN)	σ_b PSI	τ_s PSI	τ_{MAX} PSI	σ_{MAX} PSI
0	0	0	0	0	0
5	3.60	15,249	760	7,662	15,287
10	7.20	30,499	1,520	15,358	30,608
15	10.81	45,748	2,280	22,987	45,861
20	14.41	60,997	3,039	30,650	61,149
25	18.01	76,247	3,799	38,312	76,436
30	21.61	91,496	4,559	45,975	91,723
35	25.21	106,745	5,319	53,637	107,010
40	28.82	121,995	6,079	61,300	122,298
45	32.42	137,244	6,839	68,962	137,584
50	36.02	152,493	7,599	76,624	152,871
55	39.62	167,743	8,358	84,287	168,159
60	43.22	182,992	9,118	91,949	183,445

BENDING SPRING RATE:

$P/\delta = 1.388$ LB's/INCH ≤ 1.40 & ≥ 1.38

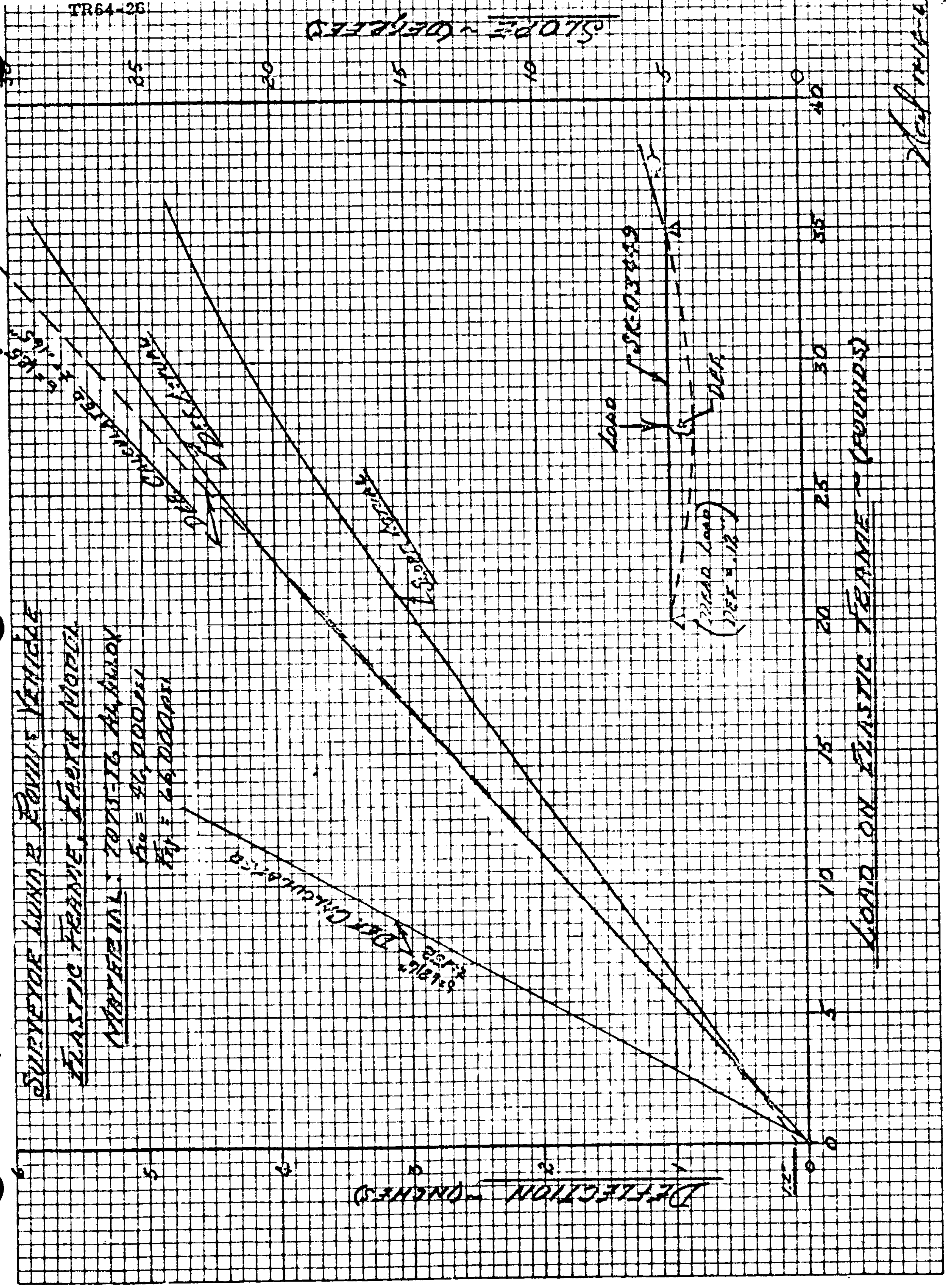
SLOPE ~ DEGREES
DEFLECTION ~ (INCHES)
LOAD ON ELASTIC FRAME ~ (POUNDS)

TR64-26

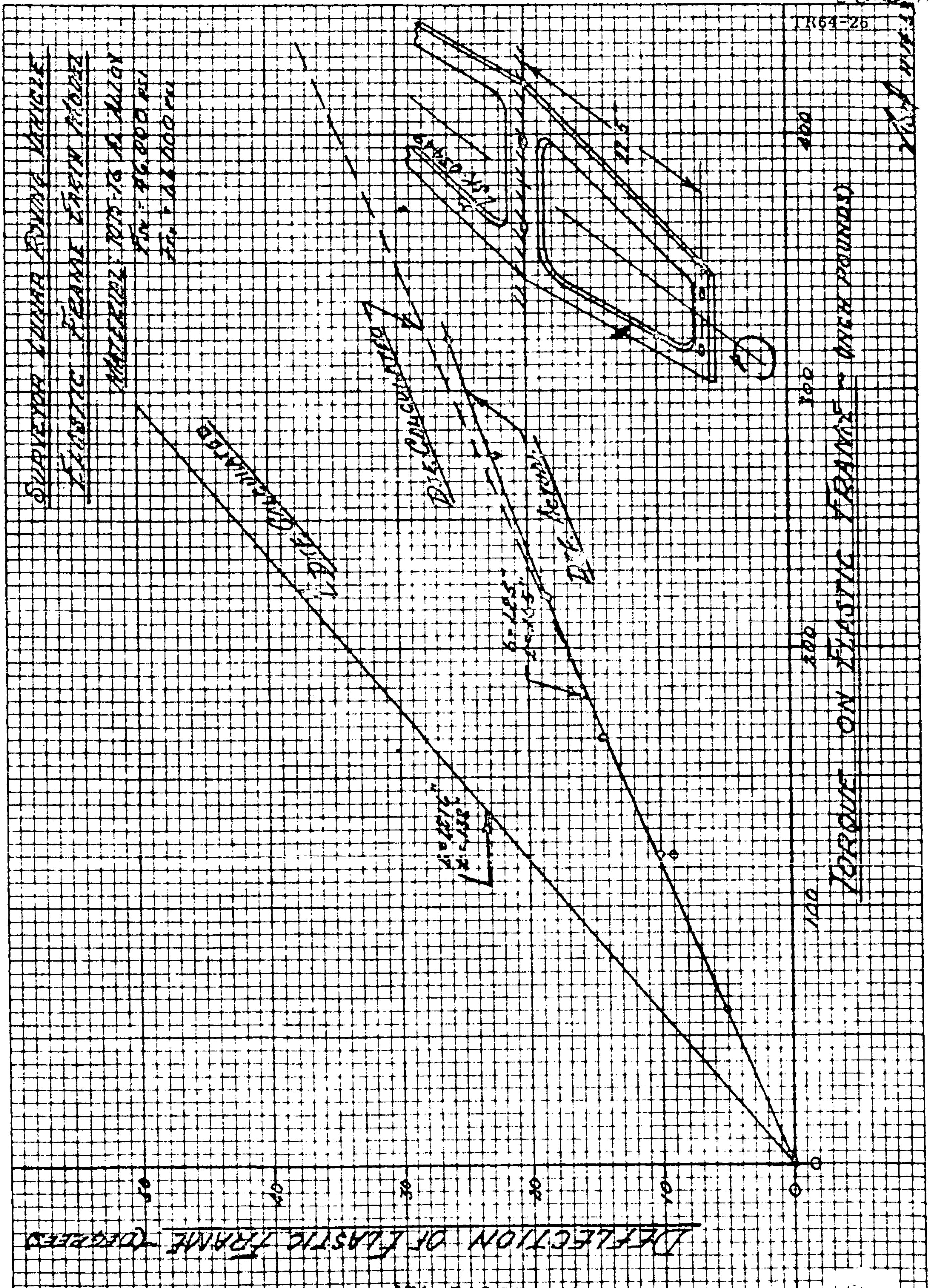

JPL DISCREET

TR64-26

TEST REPORT

DEFENSE RESEARCH LABORATORIES GENERAL MOTORS CORPORATION

Report No.	ETR-24
Test Req. No.	
Date	11-11-63
Page	of

TITLE: LRV ELASTIC FRAME TEST

Prepared by: RHL Approved by and Date:

Bending Test

t = .165

b=1.25

Load (lbs)	Center Deflection (inches)	End Deflection Front (deg)	End Deflection Rear (deg)
0	1/8	3/4	3/4
5	.088	4	4
10	1.80	7-3/4	7-3/4
15	2.80	11-1/2	11-1/2
20	3.60	14-3/4	14-3/4
0	0	1	1
5	0.87	4	4+
10	1.82	7-3/4	8-
15	2.77	11-1/2	11-1/2
20	3.61	14-3/4	14-3/4
25	4.40	18	18
30	5.10	20-3/4	20-3/4
35	5.77	23-1/2	23-1/2
0	0	1-	1

213

64-4706

TR64-26

TEST REPORT

DEFENSE RESEARCH LABORATORIES GENERAL MOTORS CORPORATION

Report No. ETR-24
Test Reg. No.
Date 11-8-63
Page ___ of ___

TITLE:

Prepared by: Approved by and Date:

Torque Test	Load (lbs)	Torque (in-lbs) (11" lever)	Angle (degrees)	t = .165 b = 1.25
	5	55	5	
	10	110	9-1/2	
	15	165	14-1/2	
	20	220	18-1/2	
	0	0	0	
	5	55	5+	
	10	110	10	
	15	165	14-1/2	
	20	220	18-1/2	
	25	275	22-1/2	
	30	330	26	
	0	0	0	

G M Defense Research Laboratories General Motors Corporation	REPORT NO.	PAGE /	JOB NO.	PAGE /
TITLE: SURVEYOR LUNAR ROVING VEHICLE		PREPARED		DATE 11-20-63
		CHECKED		
		APPROVED		

ELASTIC FRAME ANALYSIS

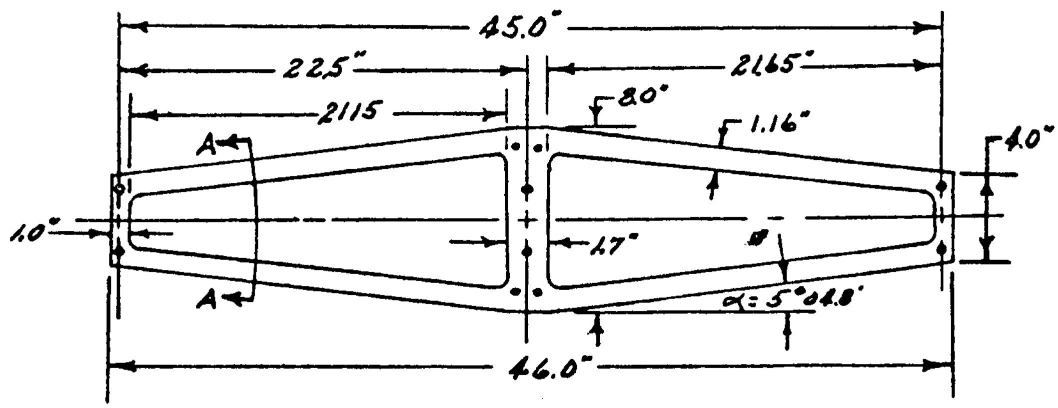

MATERIAL:

BERYLLIUM HPS-20 (CROSS-ROLLED SHEET)

$\sigma_u = 78{,}000$ psi

$\sigma_y = 53{,}000$ psi

$E = 44 \times 10^6$

$G = 21.5 \times 10^6$

SECTION A-A

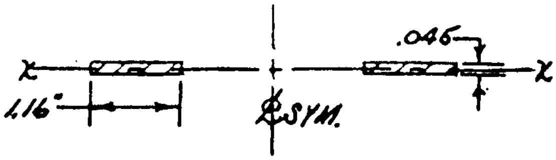

DESIGN REQUIREMENTS

1. BENDING SPRING RATE $\geq$ 0.23 LBS/INCH.
2. TORSION SPRING RATE $\geq$ 75 IN-LBS/RADIAN.
3. S.L.R.V. ROLL ANGLE θ $\geq$ ±45°
4. STEERING MOMENT M_z $\geq$ 100 IN-LBS.

G M Defense Research ⊗ Laboratories General Motors Corporation	REPORT NO	PAGE 2	JOB NO.
TITLE SURVEYOR LUNAR ROVING VEHICLE	PREPARED Neal	DATE 11-20-63	
	CHECKED		
	APPROVED		

ELASTIC FRAME ANALYSIS Con't

BENDING STRESS CHECK

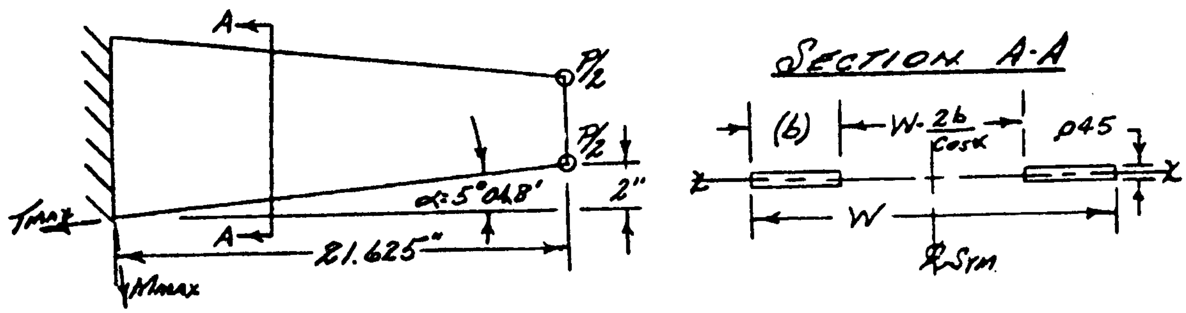

GIVEN:

$L = 21.625 \quad t = .045 \quad b = 1.16$

$L^3 = 10{,}113 \quad bt^3 = 10.57 \times 10^{-8}$

$\cos\alpha = .996073 \quad \sin\alpha = .088541 = \tan\alpha$

$I = \frac{bt^3}{12\cos\alpha} \times 2$

$I = 17.69 \times 10^{-6}$

$C = t/2$

$I/c = 7.862 \times 10^{-4} = S$

$\alpha \text{ } 8B = .333$

$$\delta = \frac{PL^3}{3EI} = \frac{P\,10{,}113}{3 \times 44 \times 10^6 \times 17.69 \times 10^{-6}}$$

① $\delta = 4.33\,P \quad \therefore \quad P/\delta = .23$ Lbs/INCH

$$(\sigma_b)_{MAX} = \frac{Mc}{I} = \frac{M}{S} = \frac{21.625\,P}{7.862 \times 10^{-4}}$$

② $(\sigma_b)_{MAX} = 27{,}506\,P$ PSI.

$T_{MAX} = P/2 \times 2 = P \; ; \; \tau_s = \frac{T}{\alpha b t^2}$

$$\tau_s = \frac{P}{.333 \times 1.16 \times 20.25 \times 10^{-4}}$$

③ $\tau_s = 1{,}278\,P$ PSI

④ $\tau_{MAX} = \sqrt{\left(\frac{\sigma_b}{2}\right)^2 + \tau_s^2}$

⑤ $\sigma_{MAX} = \frac{\sigma}{2} + \tau_{MAX}$

ELASTIC FRAME ANALYSIS CONT.

BENDING STRESS CHECK CONT.

P (lbs)	δ (IN)	σ_b PSI	τ_s PSI	τ_{MAX} PSI	σ_{MAX} PSI
0	0	0	0	0	0
1	4.33	27,506	1,278	13,812	27,565
2	8.66	55,012	2,556	27,625	55,131
3	12.99	82,518	3,834		
4	17.32	110,024	5,112		
5	21.65	137,530	6,390		
6	25.98	165,036	7,668		
7	30.31	192,542	8,946		
8	34.64	220,048	10,224		
9	38.97	247,554	11,502		
10	43.30	275,060	12,780		

BENDING SPRING RATE:

$P/\delta = 0.23$ lbs/INCH $= 0.23$ lbs/INCH REQ'D.

MINIMUM BEND RADII EXPECTED IN STOWED POSITION IS APPROX. 12 INCHES.

$M = \sigma_{ALLOW} \times S = 53{,}000 \times 7.862 \times 10^{-4}$

$M = 41.67$ IN-lbs.

$$R_{CRIT.} = \frac{EI}{M} = \frac{44 \times 10^6 \times 17.69 \times 10^{-6}}{41.67}$$

$R_{CRIT.} = 18.68'' > 12.0''$ EXPECTED

MAX $P = 1.93$ lbs. MAX $\delta = 8.36''$ @ $\sigma_{Y\,ALLOW} = 53{,}000$ psi

G M Defense Research ⊗ Laboratories General Motors Corporation TR64-26	REPORT NO	PAGE 4	JOB NO.	PAGE 4
TITLE SURVEYOR LUNAR ROVING VEHICLE		PREPARED Noel		DATE 11-20-63
		CHECKED		
		APPROVED		

ELASTIC FRAME ANALYSIS Cont.

TORSION STRESS CHECK.

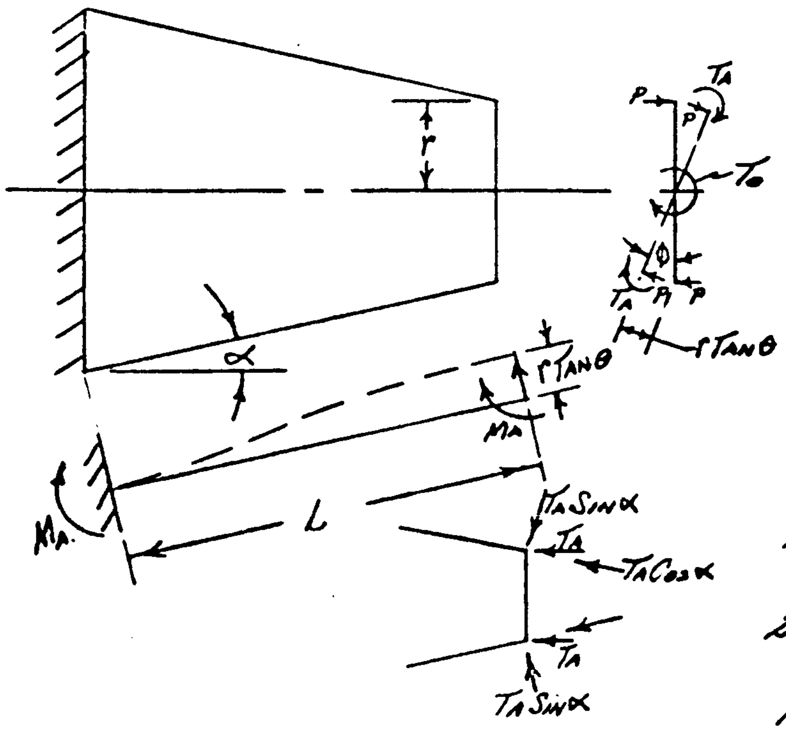

GIVEN:

$b = 1.16 \qquad b/t = 25.8$

$t = .045 \qquad bt^3 = 10.57\times10^{-5}$

$L = 21.1 \qquad \alpha = \beta = .333$

$r = 1.42 \qquad 2\beta = .666$

$\cos\alpha = .996073$

$I = \frac{bt^3}{12} = 8.81\times10^{-6}$

$C = t/2 = .020$

$$P = \frac{12EI(r\,\mathrm{Tan}\,\theta)}{L^3}$$

$$2Pr = \frac{24\,EI\,r^2\,\mathrm{Tan}\,\theta}{L^3}$$

$$M_A = \frac{6EI(r\,\mathrm{Tan}\,\theta)}{L^2}$$

$$T_A\cos\alpha = K_T\theta = \left(\frac{\beta b t^3 G}{L}\right)\theta$$

$$2T_A = \left(\frac{2\beta b t^3 G}{L\cos\alpha}\right)\theta$$

$$T_\theta = 2T_A + 2Pr$$

$$T_\theta = \left(\frac{2\beta b t^3 G}{L\cos\alpha}\right)\theta + \left(\frac{24EI\,r^2}{L^3}\right)\mathrm{Tan}\,\theta$$

$$T_\theta = \left(\frac{.666\times10.57\times10^{-5}\times21.5\times10^6}{21.1\times.996073}\right)\theta + \left(\frac{24\times44\times10^6\times8.81\times10^{-6}\times2.02}{9{,}393.931}\right)\mathrm{Tan}\,\theta$$

① $\underline{T_\theta = 72.01\,\theta + 2.0\,\mathrm{Tan}\,\theta}$

$$M_A = \frac{6EIr}{L^2}\mathrm{Tan}\,\theta = \left(\frac{6\times44\times10^6\times8.81\times10^{-6}\times1.42}{445.21}\right)\mathrm{Tan}\,\theta$$

② $\underline{M_A = 7.42\,\mathrm{Tan}\,\theta}$

$$\tau_s = \frac{T_A\cos\alpha}{\alpha b t^2} = \left(\frac{\beta b t^3 G}{\alpha b t^2 L}\right)\theta = \left(\frac{Gt}{L}\right)\theta = \frac{21.5\times10^6\times.045}{21.1}\theta$$

③ $\underline{\tau_s = 45{,}853\,\theta}$

TR64-26 GM Defense Research ⊗ Laboratories General Motors Corporation	REPORT NO	PAGE 5	JOB NO.	PAGE 5
TITLE: SURVEYOR LUNAR ROVING VEHICLE		PREPARED Nad. DATE 11-20-63		
		CHECKED		
		APPROVED		

ELASTIC FRAME ANALYSIS CONT.

TORSION STRESS CHECK CONT.

ALLOWABLE STRESS & SPRING RATE AT $\theta = 45°$

$T_\theta = 72.01 \times .785398 + 2 \times 1$

$T_\theta = 58.56$ IN-LBS.

$\frac{T_\theta}{\theta} = \frac{58.56}{.785398} = 74.5$ IN-LBS/RADIAN $\cong$ 75 REQD.

$M_A = 7.42 \times 1 = 7.42$ IN-LBS.

$\tau_s = 45{,}853 \times .785398$

$\tau_s = 36{,}013$ P.S.I.

④ $(\sigma_b)_{MAX.} = \frac{6 M_A}{b t^2} = 2{,}553\, M_A$

$(\sigma_b)_{MAX} = 2{,}553 \times 7.42$

$(\sigma_b)_{MAX} = 18{,}943$ PSI

⑤ $MAX\ \tau = \sqrt{\left(\frac{\sigma_b}{2}\right)^2 + \tau_s^2}$

$= 37{,}238$ PSI

⑥. $MAX\ \sigma = \left(MAX\ \tau + \frac{\sigma_b}{2}\right)$

$= 46{,}709$ PSI $< \sigma_y\ 53{,}000$ PSI

$M.S. = \frac{53{,}000}{46{,}709} - 1 = +13.6\%$

G M Defense Research ⊗ Laboratories General Motors Corporation	REPORT NO	PAGE 1	JOB NO. TR64-26	PAGE 6
TITLE SURVEYOR LUNAR ROVING VEHICLE		PREPARED [signature]		DATE 11-22-63
		CHECKED		
		APPROVED		

ELASTIC FRAME ANALYSIS

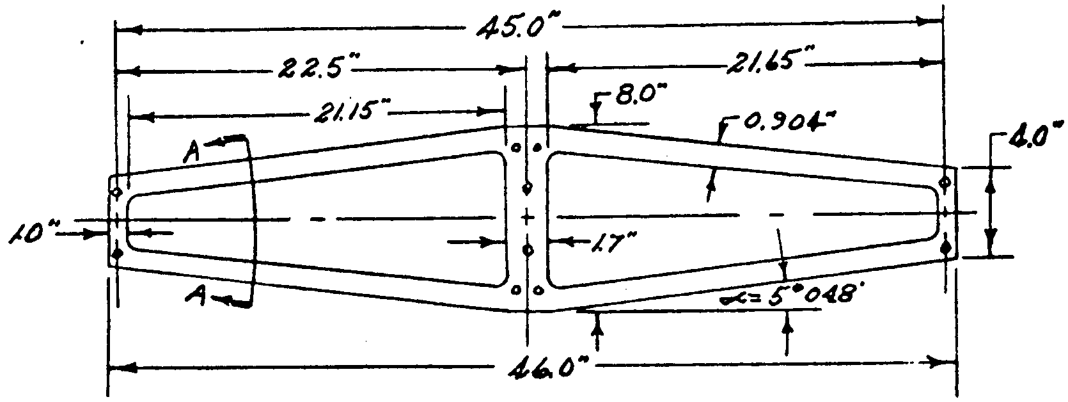

MATERIAL:

7075 T6 AL. ALLOY

$\sigma_{su} = 46,000$ PSI.

$\sigma_{TY} = 66,000$ PSI.

$E = 10^7$

$G = 3.9 \times 10^6$

SECTION A-A

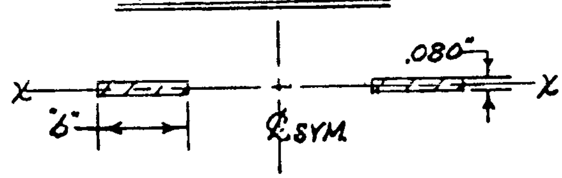

DESIGN REQUIREMENTS:

1. BENDING SPRING RATE $\geq$ 0.23 LBS/INCH.
2. TORSION SPRING RATE $\geq$ 75 IN-LBS/RADIAN
3. S.L.R.V. ROLL ANGLE θ $\geq$ ± 45 DEGREES
4. STEERING MOMENT M_z $\geq$ 100 IN-LBS.

G M Defense Research ⊗ Laboratories General Motors Corporation	REPORT NO	PAGE 2	JOB NO.	PAGE 7
TITLE SURVEYOR LUNAR ROVING VEHICLE		PREPARED Noel	DATE 11-22-63	
		CHECKED		
		APPROVED		

ELASTIC FRAME ANALYSIS CONT.

CASE I: BENDING STIFFNESS PREDOMINATE OVER TORSIONAL REQM'T.

BENDING STRESS CHECK

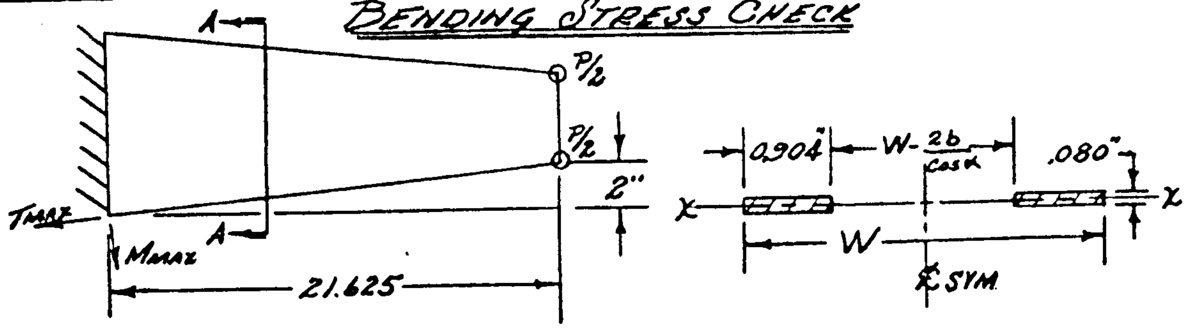

GIVEN:

$L = 21.625''$ $b = 0.904$ $t = .080$

$L^3 = 10,113$ $bt^3 = 4.63 \times 10^{-4}$

$\cos\alpha = .996073$ $\sin\alpha = \tan\alpha = .088541$

$I = \frac{bt^3}{12\cos\alpha} \times 2$

$I = 77.48 \times 10^{-6}$

$I/c = S = 19.38 \times 10^{-4}$

$\alpha \, \& \, \beta = .333$

$$\delta = \frac{PL^3}{3EI} = \frac{10,113\,P}{3 \times 10^7 \times 77.48 \times 10^{-6}}$$

① $\delta = 4.35P$ ∴ $P/\delta = .23$ Lb's/INCH $= .23$ REQ'D.

$$(\sigma_b)_{MAX} = \frac{Mc}{I} = \frac{M}{S} = \frac{21.625\,P}{19.38 \times 10^{-4}}$$

② $(\sigma_b)_{MAX} = 11,158P$

$T_{MAX} = P/2 \times 2 = P$ ∴ $\tau_s = \frac{T}{\alpha b t^2}$

$$\tau_s = \frac{P}{.333 \times .904 \times 6.4 \times 10^{-3}}$$

③ $\tau_s = 519P$

④ $\tau_{MAX} = \sqrt{\left(\frac{\sigma_b}{2}\right)^2 + \tau_s^2}$

⑤ $\sigma_{MAX} = \frac{\sigma_b}{2} + \tau_{MAX}$

G M Defense Research ⊗ Laboratories General Motors Corporation	REPORT NO	PAGE 3	JOB NO.	PAGE 8
TITLE SURVEYOR LUNAR ROVING VEHICLE		PREPARED Noel		DATE 11-22-63
		CHECKED		
		APPROVED		

ELASTIC FRAME ANALYSIS CONT.

BENDING STRESS CHECK CONT.

MAX. STRESS AND SPRING RATE IN STOWED POSITION.

MINIMUN BEND RADII EXPECTED IN THE STOWED POSITION IS APPROX. 12 INCHES.

$M = \sigma_{ALLOW} \times S = 66{,}000 \times 19.38 \times 10^{-4}$

$M = 128$ IN-LBS. $\therefore P = 5.92^{\#}$

$R_{CRIT.} = \frac{EI}{M} = \frac{10^7 \times 77.48 \times 10^{-6}}{128}$

$R_{CRIT.} = 5.31'' <$ THAN $12''$ MIN. EXPECTED

$(\sigma_b)_{MAX} = 11{,}158 \times 5.91$

$(\sigma_b)_{MAX} = 65{,}944$ PSI.

$\tau_s = 519 \times 5.91$

$\tau_s = 3{,}067$ P.S.I.

$\tau_{MAX} = \sqrt{32{,}972^2 + 3{,}067^2}$

$\tau_{MAX} = 33{,}114$ PSI

$\sigma_{MAX} = 32{,}972 + 33{,}114$

$\sigma_{MAX} = 66{,}086$ PSI. $\simeq \sigma_{ALLOW}$

MAX STRESS AT 12" BEND RADII.

$M = \frac{10^7 \times 77.48 \times 10^{-6}}{12}$

$M = 64.5$ IN-LBS. $\therefore P = 2.98^{\#}$

$\sigma_{MAX} = 33{,}322$ PSI $\sigma_{ALLOW} = 53{,}000$

$M.S. = \frac{53{,}000}{33{,}322} - 1 = +59\%$ @ $12''R.$

G M Defense Research ⊗ Laboratories General Motors Corporation TR64-26	REPORT NO.	PAGE 4	JOB NO.	PAGE 9
TITLE: SURVEYOR LUNAR ROVING VEHICLE		PREPARED Noel		DATE 11-22-63
		CHECKED		
		APPROVED		

ELASTIC FRAME ANALYSIS CON'T

TORSION STRESS CHECK

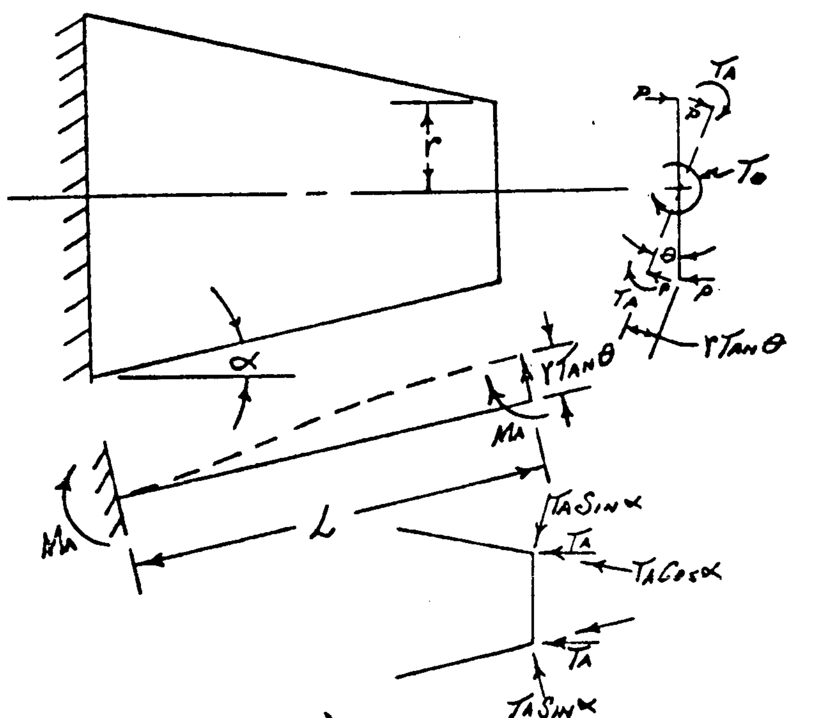

GIVEN:

$b = 0.904''$ $\quad b/t = 11.3$

$t = .080$ $\quad bt^3 = 4.63\times10^{-4}$

$L = 21.1$ $\quad \therefore \beta = .316$

$r = 1.50$ $\quad 2\beta = .632$

$\cos\alpha = .996073$

$I = \frac{bt^3}{12} = 3.86\times10^{-5}$

$S = I/c = 9.65\times10^{-4}$

$$P = \frac{12EI(r\tan\theta)}{L^3} \qquad 2Pr = \frac{24EI(r^2\tan\theta)}{L^3}$$

$$M_A = \frac{6EI(r\tan\theta)}{L^2}$$

$$T_A\cos\alpha = K_T\theta = \left(\frac{\beta bt^3G}{L}\right)\theta$$

$$2T_A = \left(\frac{2\beta bt^3G}{L\cos\alpha}\right)\theta$$

$$T_\theta = 2T_A + 2Pr$$

$$T_\theta = \left(\frac{2\beta bt^3G}{L\cos\alpha}\right)\theta + \left(\frac{24EIr^2}{L^3}\right)\tan\theta$$

$$T_\theta = \frac{.632\times4.63\times10^{-4}\times3.9\times10^6}{21.1\times.996073}\theta + \left(\frac{24\times10^7\times3.86\times10^{-5}\times2.25}{9{,}393.931}\right)\tan\theta$$

(1) $\underline{T_\theta = 54.3\,\theta + 2.2\tan\theta}$

G M Defense Research ⊗ Laboratories General Motors Corporation	REPORT NO	PAGE 5	JOB NO. TR64-26	PAGE 10
TITLE: SURVEYOR LUNAR ROVING VEHICLE		PREPARED Noel		DATE 11-22-63
		CHECKED		
		APPROVED		

ELASTIC FRAME ANALYSIS CONT.

TORSION STRESS CHECK CONT.

$$M_A = \frac{6EI\Gamma}{L^2}\tan\theta = \frac{6\times10^7\times3.86\times10^{-5}}{445.21}\tan\theta$$

(2) $M_A = 5.2\tan\theta$

$$\tau_s = \frac{T_A\cos\alpha}{\alpha b t^2} = \left(\frac{\beta b t^3 G}{\alpha b t^2 L}\right)\theta$$

$$\tau_s = \left(\frac{Gt}{L}\right)\theta = \frac{3.9\times10^6\times.080}{21.1}\theta$$

(3) $\tau_s = 14{,}787\,\theta$

$$(\sigma_b)_{max} = \frac{6M_A}{bt^2} = \frac{6\times5.2}{57.86\times10^{-4}}\tan\theta$$

(4) $(\sigma_b)_{max} = 5{,}392\tan\theta$

(5) $\tau_{max} = \sqrt{\left(\frac{\sigma_b}{2}\right)^2 + \tau_s}$

(6) $\sigma_{max} = \frac{\sigma_b}{2} + \tau_{max}$

MAX STRESS AND SPRING RATE AT 45°

$T_0 = 54.3\times.785398 + 2.2\times1$

$T_0 = 46.9$ IN-LBS.

$\frac{T_0}{\theta} = \frac{46.9}{.785398} = 59.7$ IN-LBS/RADIAN < 75 IN-LBS/RADIAN REQ'D.

$\tau_s = 14{,}787\times.785398$

$\tau_s = 11{,}614$ PSI

$(\sigma_b)_{max} = 5{,}392\times1$

$(\sigma_b)_{max} = 5{,}392$ P.S.I.

~~JPL DISCREET~~

GM DEFENSE RESEARCH LABORATORIES ⊗ GENERAL MOTORS CORPORATION

~~TR64-26~~

G M Defense Research ⊗ Laboratories General Motors Corporation	REPORT NO.	PAGE 6	JOB NO.	PAGE 11
TITLE: SURVEYOR LUNAR ROVING VEHICLE	PREPARED			DATE 11-22-63
	CHECKED			
	APPROVED			

ELASTIC FRAME ANALYSIS CON'T

TORSION STRESS CHECK CONT.

$$\tau_{MAX} = \sqrt{2{,}696^2 + 11{,}614^2}$$

$$\tau_{MAX} = 11{,}923 \text{ psi}$$

$$\sigma_{MAX} = 2{,}696 + 11{,}923$$

$$\sigma_{MAX} = 14{,}619 \text{ psi} < \sigma_{ALLOW}$$

~~JPL DISCREET~~

III 2-106

G M Defense Research ⊗ Laboratories General Motors Corporation	REPORT NO	PAGE 7	JOB NO.	PAGE 12

TITLE	
SURVEYOR LUNAR ROVING VEHICLE	PREPARED Noel. DATE 11-25-63 CHECKED APPROVED

ELASTIC FRAME ANALYSIS CONT.

CASE II: TORSIONAL STIFFNESS PREDOMINATE OVER BENDING REQMT.

BENDING STRESS CHECK

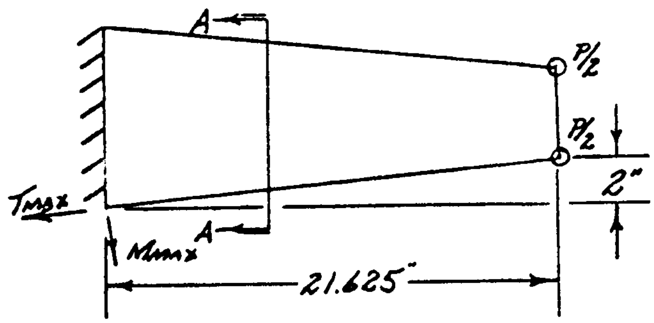

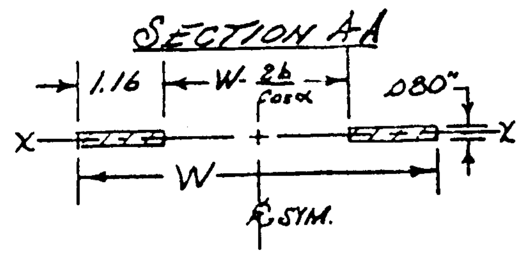

GIVEN:

$L = 21.625"$ $\quad b = 1.16$ $\quad t = .080$

$L^3 = 10{,}113$ $\quad bt^3 = 5.96 \times 10^{-4}$

$\cos\alpha = .996073$ $\quad \sin\alpha \approx \tan\alpha = .088541$

$I = \dfrac{bt^3}{12\cos\alpha} \times 2$

$I = 99.38 \times 10^{-6}$

$I/c = S = 24.85 \times 10^{-4}$

$\alpha = B = .32$

(1)
$$\delta = \frac{PL^3}{3EI} = \frac{10.13P}{3\times10^7 \times 99.38\times10^{-6}}$$
$$\underline{\delta = 3.39P} \quad \therefore \quad \underline{P/\delta = .295 \text{ lbs/inch} > .23 \text{ REQ'D}}$$

(2)
$$(\sigma_b)_{max} = \frac{M}{S} = \frac{21.625P}{24.85\times10^{-4}}$$
$$\underline{(\sigma_b)_{max} = 8{,}702\,P}$$

(3)
$$\tau_s = \frac{P}{B\,b\,t^2} = \frac{P}{.32 \times 1.16 \times .0064}$$
$$\underline{\tau_s = 421\,P}$$

(4)
$$\underline{\tau_{max}} = \sqrt{\left(\frac{\sigma_b}{2}\right)^2 + \tau_s^2}$$

(5)
$$\underline{\sigma_{max} = \frac{\sigma_b}{2} + \tau_{max}}$$

GM Defense Research ⊗ Laboratories General Motors Corporation TR64-26	REPORT NO	PAGE 8	JOB NO.	PAGE 13
TITLE SURVEYOR LUNAR ROVING VEHICLE		PREPARED		DATE 11-25-63
		CHECKED		
		APPROVED		

ELASTIC FRAME ANALYSIS CONT.

BENDING STRESS CHECK CON'T.

MAX STRESS AND SPRING RATE IN STOWED POSITION

MINIMUN BEND RADII EXPECTED IN THE STOWED POSITION IS APPROX. 12 INCHES

$M = \sigma_{ALLOW} \times S = 66{,}000 \times 24.85 \times 10^{-4}$

$M = 164$ IN-LBS. $\therefore P = 7.58^{\#}$

$R_{CRIT} = \frac{EI}{M} = \frac{10^{7} \times 99.38 \times 10^{-6}}{164}$

$R_{CRIT} = 6.06''$ < THAN 12" MIN EXPECTED

$(\sigma_b)_{MAX} = 8{,}702 \times 7.58$

$(\sigma_b)_{MAX} = 65{,}961$ PSI

$\tau_s = 421 \times 7.58$

$\tau_s = 3{,}191$ PSI

$\tau_{MAX} = \sqrt{32{,}985^2 + 3{,}191^2}$

$\tau_{MAX} = 33{,}139$ PSI

$\sigma_{MAX} = 32{,}985 + 33{,}139$

$\sigma_{MAX} = 66{,}124$ PSI $\cong \sigma_{ALLOW}$

MAX STRESS AT 12" BEND RADII.

$M = \frac{10^{7} \times 99.38 \times 10^{6}}{12}$

$M = 83$ IN-LBS. $\therefore P = 3.84^{\#}$

$\sigma_{MAX} = 33{,}461$ PSI $< \sigma_{ALLOW}$ 66,000

$M.S. \ \frac{66{,}000}{33{,}461} - 1 = +97\%$ @ 12" R

G M Defense Research ⊗ Laboratories General Motors Corporation	REPORT NO	PAGE 9	JOB NO.	TR64-20 14

TITLE	
Surveyor Lunar Roving Vehicle	PREPARED Nael DATE 11-26-63
	CHECKED
	APPROVED

Elastic Frame Analysis Con't.

Torsion Stress Check.

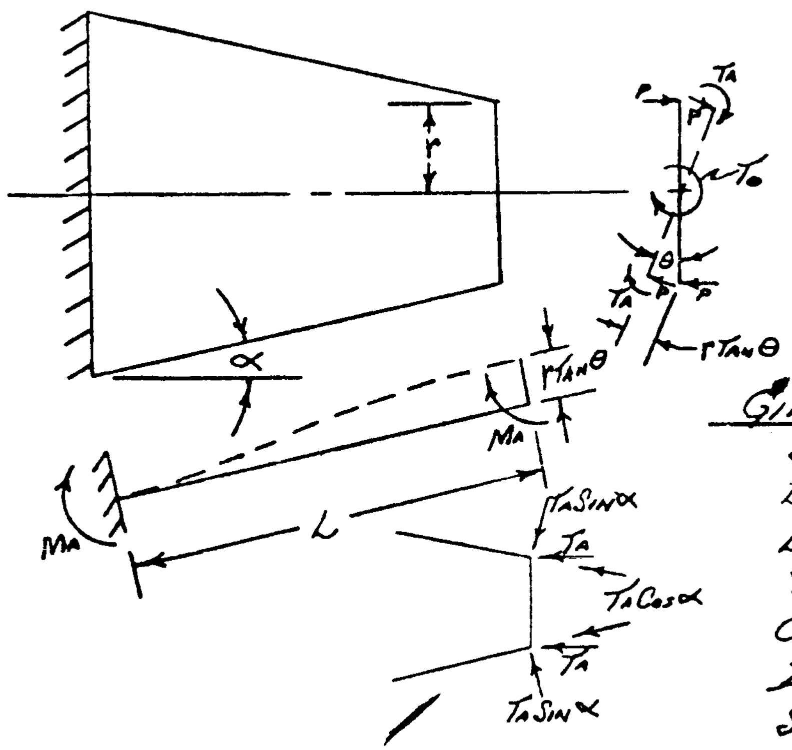

Given:

$b = 1.16$ $\quad b/t = 14.5$

$t = .080$ $\quad bt^3 = 5.96\times10^{-4}$

$L = 21.1$ $\quad \alpha = \beta = .32$

$r = 1.42$ $\quad 2\beta = .64$

$\cos\alpha = .996073$

$I = \frac{bt^3}{12} = 4.97\times10^{-5}$

$S = I/c = 12.43\times10^{-4}$

$$T_0 = \left(\frac{2\beta b t^3 G}{L\cos\alpha}\right)\theta + \left(\frac{24EIr^2}{L^3}\right)\tan\theta$$

$$T_0 = \left(\frac{.64\times5.96\times10^{-4}\times3.9\times10^{6}}{21.1\times.996073}\right)\theta + \left(\frac{24\times10^{7}\times4.97\times10^{-5}\times2.02}{9393.931}\right)\tan\theta$$

① $T_0 = 70.78\,\theta + 2.56\tan\theta$

$$M_A = \frac{6EIr}{L^2}\tan\theta = \frac{6\times10^{7}\times4.97\times10^{-5}\times1.42}{445.21}$$

② $M_A = 9.51\tan\theta$

$$T_s = \left(\frac{Gt}{L}\right)\theta = \frac{3.9\times10^{6}\times.080}{21.1}$$

③ $T_s = 14{,}787\,\theta$

$$(\sigma_b)_{max} = \frac{6M_A}{bt^2} = \frac{6\times9.51}{74.24\times10^{-4}}\tan\theta$$

④ $(\sigma_b)_{max} = 7{,}686\tan\theta$

TR64-26 GM Defense Research ⊗ Laboratories General Motors Corporation	REPORT NO	PAGE 10	JOB NO	PAGE 15
TITLE SURVEYOR LUNAR ROVING VEHICLE	PREPARED Noel 11-25-63			
	CHECKED			
	APPROVED			

ELASTIC FRAME ANALYSIS CONT.

TORSION STRESS CHECK CONT.

(5) $\tau_{MAX} = \sqrt{\left(\frac{\sigma_b}{2}\right)^2 + \tau_s^2}$

(6) $\sigma_{MAX} = \frac{\sigma_b}{2} + \tau_{MAX}$

MAX. STRESS AND SPRING RATE AT 45°

$T_\theta = 70.78 \times 785398 + 2.56 \times 1$

$T_\theta = 58.15$ IN-LBS.

$T_\theta/\theta = \frac{58.15}{.785398} = 74.0$ IN-LBS/RADIAN ≈ 75 IN-LBS/RAD. REQD.

$\tau_s = 14,787 \times .785398$

$\tau_s = 11,614$ PSI

$(\sigma_b)_{MAX} = 7,686 \times 1$

$(\sigma_b)_{MAX} = 7,686$ PSI

$\tau_{MAX} = \sqrt{3,843^2 + 11,614^2}$

$\tau_{MAX} = 12,233$ PSI

$\sigma_{MAX} = 3,843 + 12,233$

$\sigma_{MAX} = 16,076$ PSI $< \sigma_{ALLOW}$ 66,000 PSI

229

G M Defense Research Laboratories General Motors Corporation	REPORT NO.	PAGE 11	JOB NO. TR64-20	PAGE 16
TITLE: SURVEYOR LUNAR ROVING VEHICLE		PREPARED Hall		DATE 11-25-63
		CHECKED		
		APPROVED		

ELASTIC FRAME ANALYSIS. CONT.

STEERING MOMENT STRESS CHECK

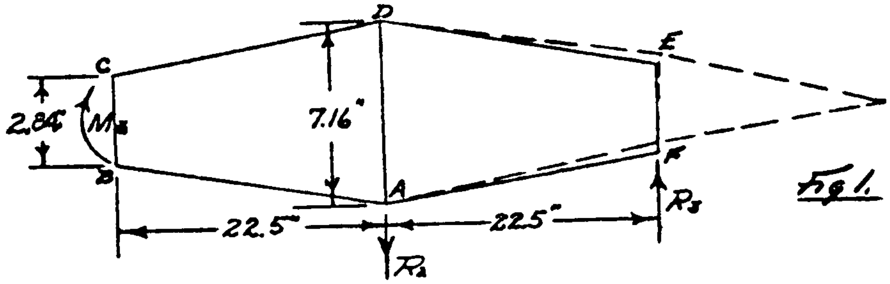

Fig 1.

$$R_2 = R_3 = \frac{M_z}{22.5} = \frac{100}{22.5} = 4.44 \text{ IN-LBS.}$$

$I_{BC} = I_{FE}$ ASSUMED TO BE 10 TIMES GREATER THAN $I_{BA} = 49.7 \times 10^{-5}$

$I_{AB} = I_{CD} = I_{DE} = I_{FA} = 49.7 \times 10^{-6}$ (REF. Fig 9)

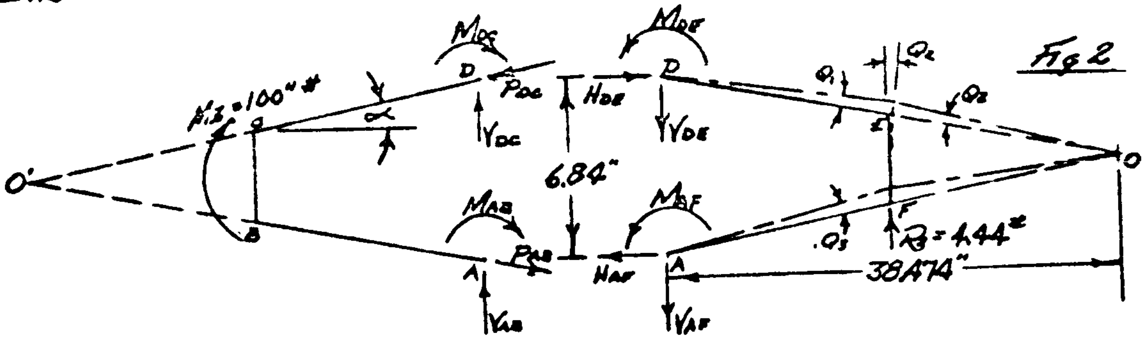

Fig 2

$H_{AB} = H_{AF}$; $H_{CD} = H_{DE}$

$V_{AB} + V_{DC} + V_{AF} + V_{DE} = R_2 = 4.44\#$

$L_{AB} = L_{CD} = L_{DE} = L_{FA} = 22.589"$

$L_{OE} = L_{OF} = 16.037"$; $L_{FE} = L_{BC} = 2.84"$

$K = I/L$

$$K_{BA} = K_{CD} = K_{ED} = K_{FA} = \frac{49.7 \times 10^{-6}}{22.589} = 2.20 \times 10^{-6}$$

$$K_{BC} = K_{CB} = K_{EF} = K_{FE} = \frac{49.7 \times 10^{-5}}{2.84} = 175.0 \times 10^{-6}$$

RELATIVE VALUES OF K:

$K'_{BA} = K'_{CD} = K'_{ED} = K'_{FA} = 1$

$K'_{BC} = K'_{CB} = K'_{EF} = K'_{FE} = 79.5$

230

TITLE
SURVEYOR LUNAR ROVING VEHICLE

PREPARED Noel DATE 11-25-63
CHECKED
APPROVED

ELASTIC FRAME ANALYSIS CONT.

TORSION STRESS CHECK CONT.

(5) $\tau_{MAX} = \sqrt{\left(\frac{\sigma_b}{2}\right)^2 + \tau_s^2}$

(6) $\sigma_{MAX} = \frac{\sigma_b}{2} + \tau_{MAX}$

MAX. STRESS AND SPRING RATE AT 45°

$T_\theta = 70.78 \times 785398 + 2.56 \times 1$
$T_\theta = 58.15$ IN-LBS.

$T_\theta/\theta = \frac{58.15}{.785398} = 74.0$ IN-LBS/RADIAN ≈ 75 IN-LBS/RAD. REQD.

$\tau_s = 14{,}787 \times .785398$
$\tau_s = 11{,}614$ PSI

$(\sigma_b)_{MAX} = 7{,}686 \times 1$
$(\sigma_b)_{MAX} = 7{,}686$ PSI

$\tau_{MAX} = \sqrt{3{,}843^2 + 11{,}614^2}$
$\tau_{MAX} = 12{,}233$ PSI

$\sigma_{MAX} = 3{,}843 + 12{,}233$
$\sigma_{MAX} = 16{,}076$ PSI $< \sigma_{ALLOW}$ 66,000 PSI

ELASTIC FRAME ANALYSIS. CONT.

STEERING MOMENT STRESS CHECK

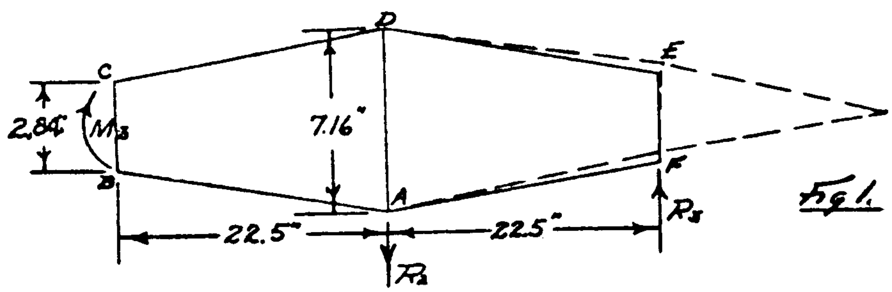

Fig 1.

$R_2 = R_3 = \frac{M_z}{22.5} = \frac{100}{22.5} = 4.44$ IN-LBS.

$I_{BC} = I_{FE}$ ASSUMED TO BE 10 TIMES GREATER THAN $I_{BA} = 49.7 \times 10^{-5}$

$I_{AB} = I_{CD} = I_{DE} = I_{FA} = 49.7 \times 10^{-6}$ (REF. Pg 9)

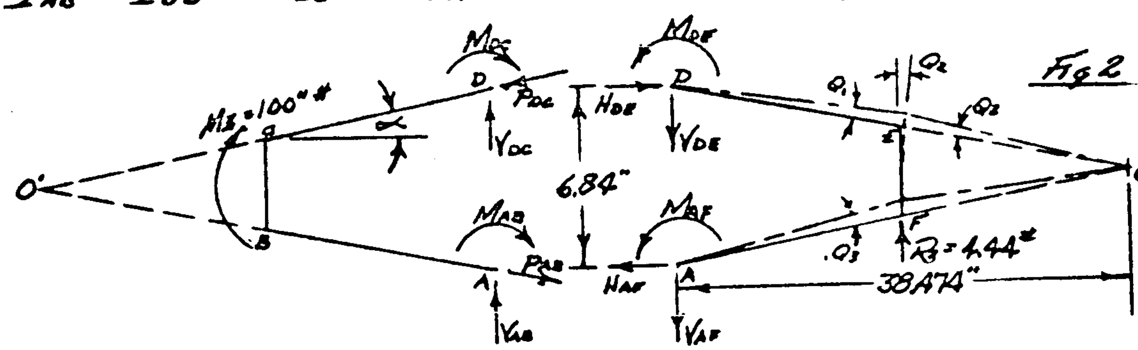

Fig 2

$H_{AB} = H_{AF}$; $H_{CD} = H_{DE}$

$V_{AB} + V_{DC} + V_{AF} + V_{DE} = R_2 = 4.44\#$

$L_{AB} = L_{CD} = L_{DE} = L_{FA} = 22.589"$

$L_{OE} = L_{OF} = 16.037"$; $L_{FE} = L_{BC} = 2.84"$

$K = I/L$

$K_{BA} = K_{CD} = K_{ED} = K_{FA} = \frac{49.7 \times 10^{-6}}{22.589} = 2.20 \times 10^{-6}$

$K_{BC} = K_{CB} = K_{EF} = K_{FE} = \frac{497 \times 10^{-6}}{2.84} = 175.0 \times 10^{-6}$

RELATIVE VALUES OF K:

$K'_{BA} = K'_{CD} = K'_{ED} = K'_{FA} = 1$

$K'_{BC} = K'_{CB} = K'_{EF} = K'_{FE} = 79.5$

TITLE

SURVEYOR LUNAR ROVING VEHICLE

ELASTIC FRAME ANALYSIS CONT.

STEERING MOMENT STRESS CHECK CONT.

MOMENT DISTRIBUTION FACTORS.

$$(DF)_{BA} = (DF)_{CD} = (DF)_{ED} = (DF)_{FA} = \frac{1}{79.5+1} = .0124$$

$$(DF)_{BC} = (DF)_{CB} = (DF)_{EF} = (DF)_{FE} = \frac{79.5}{79.5+1} = .9876$$

FIXED-END MOMENT DUE TO M_Z:

$$(M_F)_{BC} = (M_F)_{CB} = (M_F)_{EF} = (M_F)_{FE} = \frac{M_Z}{4} = 25 \text{ IN-LBS.}$$

FIXED-END MOMENT DUE TO R_Z:

$$\frac{Q_1}{22.589} = \frac{-Q_2}{16.037} \; ; \; Q_2 = -0.71 Q_1 \; ; \; Q_3 = Q_1$$

$$(M_F)_{FA} = (M_F)_{AF} = +6EK_1 Q_1 = +6E(1)Q_1 = +6EQ_1$$

$$(M_F)_{FE} = (M_F)_{EF} = +6EK_2 Q_2 = +6E(79.5)(-.71)Q_1 = -338.67EQ$$

$$(M_F)_{ED} = (M_F)_{DE} = +6EK_3 Q_3 = +6E(1)Q_3 = +6EQ_1$$

$\Sigma V = 0$ (REF FIG 2 PG 11)

$V_{DC} = P_{DC} \sin\alpha$: $V_{AB} = P_{AB} \sin\alpha$

DUE TO SYMMETRY

$V_{DC} = V_{AB}$ ∴ $P_{DC} = P_{AB}$; $M_{AB} = M_{DC}$

$\boxed{V_{AB} = 0.088541 P_{AB}}$ ---------- (1)

$\Sigma M_O = 0$

$M_Z + 2M_{AB} = 6.84 P_{AB} \cos\alpha = 6.813139 P_{AB}$

$\boxed{6.813139 P_{AB} - 2M_{AB} = 100}$ ---------- (2)

$H_{AB} = P_{AB} \cos\alpha$: $\boxed{H_{AB} = .996073 P_{AB}}$ ---------- (3)

233

G M Defense Research ⊗ Laboratories General Motors Corporation	REPORT NO	PAGE 13	JOB NO.	TR64-20 18
TITLE SURVEYOR LUNAR ROVING VEHICLE		PREPARED Noel		DATE 11-26-63
		CHECKED		
		APPROVED		

ELASTIC FRAME ANALYSIS

STEERING MOMENT STRESS CHECK CONT.

MOMENT DISTRIBUTION DUE TO R_z:

TABLE I

	A	F		E		D
JOINT	AF	FA	FE	EF	ED	DE
D.F.	0	0.0124	0.9876	0.9876	0.0124	0
F.E.M.	0	+6EQ.	-33867EQ	-33847EQ	+6EQ.	0
CO	0	+4.13	+328.54	+328.54	+4.13	0
F.E.M.	+2.06	0	+164.27	+164.27	0	+2.06
CO	0	-2.04	-162.22	-162.22	-2.04	0
FEM.	-1.02	0	-81.11	-81.11	0	-1.02
CO	0	+1.01	+80.10	+80.10	+1.01	0
FEM	+0.51	0	+40.05	+40.05	0	+0.51
CO	0	-0.50	-39.56	-39.55	-0.50	0
FEM	-0.25	0	-19.78	-19.78	0	-0.25
CO	0	+0.25	+19.53	+19.53	+0.25	0
FEM	+0.13	0	+9.76	+9.76	0	+0.13
CO	0	-0.12	-9.64	-9.64	-0.12	0
FEM	-0.06	0	-4.82	-4.82	0	-0.06
CO	0	+0.06	+4.76	+4.76	+0.06	0
FEM	+0.03	0	+2.38	+2.38	0	+0.03
CO	0	-0.03	-2.35	-2.35	-0.03	0
FEM	-0.02	0	-1.18	-1.18	0	-0.02
CO	0	+0.02	+1.17	+1.17	+0.02	0
FEM	+0.01	0	+0.58	+0.58	0	+0.01
CO	0	-0.01	-0.57	-0.57	-0.01	0
FEM	-0.00	0	-0.29	-0.29	0	-0.00
CO	0	0	+0.28	+0.28	0	0
Σ	+1.39EQ	+8.77EQ.	-8.77EQ.	-8.77EQ.	+8.77EQ.	+1.39EQ.

$M_{AF} = M_{DE} = +1.39EQ$

$M_{FA} = M_{ED} = +8.77EQ.$

$M_{FE} = M_{EF} = -8.77EQ.$

MOMENT DISTRIBUTION DUE TO M_z

TABLE II

	A	B		C		D
JOINT	AB	BA	BC	CB	CD	DC
D.F.	0	0.0124	0.9876	0.9876	0.0124	0
F.E.M.	0	0	+25.00	+25.00	0	0
C.O.	0	-0.31	-24.69	-24.69	-0.31	0
BAL.	-0.15	0	-12.34	-12.34	0	-0.15
CO.	0	+0.15	+12.19	+12.19	+0.15	0
BAL	+0.07	0	+6.09	+6.09	0	+0.07
CO.	0	-0.08	-6.01	-6.01	-0.08	0
BAL.	-0.04	0	-3.00	-3.00	0	-0.04
CO.	0	+0.04	+2.96	+2.96	+0.04	0
BAL.	+0.02	0	+1.48	+1.48	0	+0.02
CO.	0	-0.02	-1.46	-1.46	-0.02	0
BAL.	-0.01	0	-0.73	-0.73	0	-0.01
CO.	0	+0.01	+0.72	+0.72	+0.01	0
BAL.	+0.00	0	+0.36	+0.36	0	+0.00
CO.	0	0	-0.36	-0.36	0	0
Σ	-0.11	-0.21	+0.21	+0.21	-0.21	-0.11

$M_{AB} = M_{DC} = -0.11$ in·lbs.

$M_{BA} = M_{CD} = -0.21$ in·lbs.

$M_{BC} = M_{CB} = +0.21$ in·lbs.

~~TR64-26~~ G M Defense Research ⊗ Laboratories General Motors Corporation	REPORT NO	PAGE 14	JOB NO.	PAGE 19
TITLE	PREPARED Noel			DATE 11-26-63
SURVEYOR LUNAR ROVING VEHICLE	CHECKED			
	APPROVED			

ELASTIC FRAME ANALYSIS CONT.

STEERING MOMENT STRESS CHECK CONT.

AT CENTER SECTION OF FRAME

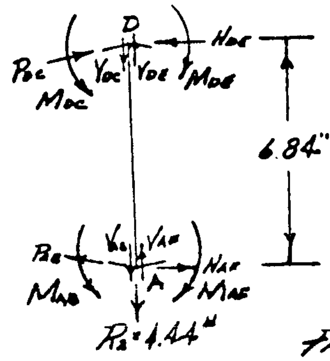

$\Sigma M_A = 0$

$6.84\,H_{DE} - 2\,M_{DE} = 6.84\,H_{AB} - 2\,M_{AB}$

$M_{DE} = +1.39\,EQ.\ ;\ M_{AB} = -0.11$ IN-LBS.

$\boxed{6.84\,H_{DE} - 2.78\,EQ. = 6.84\,H_{AB} + 0.22}$ — (4)

$\Sigma V = 0$

$2\,V_{AF} = 4.44 + 2\,P_{AB} \times .088541 - 2\,V_{AB}$

FROM EQ(1) $V_{AB} = .088541\,P_{AB}$ $\therefore$ $\boxed{V_{AF} = 2.22}$ — (5)

$\Sigma M_O = 0$

$16.037 \times 4.44 + 6.84 \times H_{DE} = 2 \times 38.474\,V_{AF} + 2\,M_{AF} = 171 + 2\,M_{AF}$

$6.84\,H_{DE} - 2\,M_{AF} = 100\ ;\ M_{AF} = 1.39\,EQ.$

$\boxed{6.84\,H_{DE} - 2.78\,EQ = 100}$ — — — — — — — — — — (6)

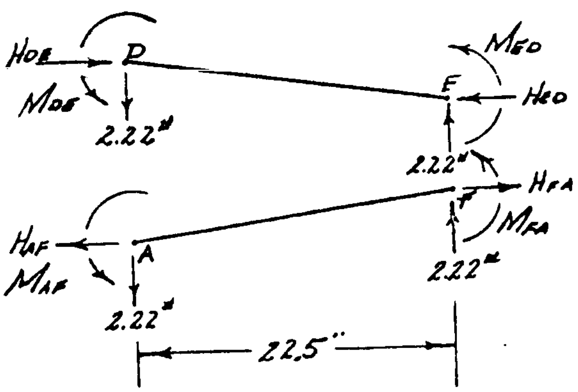

$\Sigma M_F = 0$ (MEMBER AF)

$2.0\,H_{AF} = M_{AF} + M_{FA} + 2.22 \times 22.5$

$M_{AF} = +1.39\,EQ.\ ;\ M_{FA} = +8.77\,EQ.$

$\boxed{H_{AF} = 5.08\,EQ. + 25}$ — — — — 7

$H_{AF} = H_{DE}$ $\therefore$ SUB. (7) INTO (6)

$34.75\,EQ + 171 - 2.78\,EQ = 100$

$31.97\,EQ. = -71$

$EQ. = -2.2208$

$\therefore\ M_{AF} = M_{DE} = -3.0869$ & $M_{FA} = M_{ED} = -19.4764$

G M Defense Research Laboratories General Motors Corporation	REPORT NO.	PAGE 15	JOB NO.	PAGE 20
TITLE: SURVEYOR LUNAR ROVING VEHICLE		PREPARED Heel		DATE 11-26-63
		CHECKED		
		APPROVED		

ELASTIC FRAME ANALYSIS CONT.

STEERING MOMENT STRESS CHECK CONT.

SUB. IN EQ. ② WITH $M_{AB} = -.11$ IN-LBS.

$P_{AB} = \frac{100-.22}{6.813139} = 14.646$ LBS $= P_{DC} = P_{AB}$

SUB. IN EQ. ③

$H_{AB} = .996073 \times 14.646 = 14.588$ LBS. $= H_{AB} = H_{DC}$

SUB. IN EQ ①

$V_{AB} = .088541 \times 14.646 = 1.2971$ LBS $= V_{AB} = V_{DC}$

MOMENT CHECK

$2 M_{AF} + 6.84 H_{DE} = 2 M_{AB} + 6.84 \times H_{AB}$

$2 \times 3.0869 + 6.84 \times 13.719 = 2 \times .11 + 6.84 \times 14.588$

$6.17 + 93.83 = .22 + 99.78$

$100 = 100$ CHECK.

CHECK FOR MAX COLUMN STRESS.

MAX COMPRESSIVE LOAD $= (P_3)_{MAX} = P_{DC} = 14.646$ #/LEAF

MAX COLUMN STRESS $P/A = \frac{14.646}{1.16 \times .08} = 158$ PSI

$I = \frac{bt^3}{12} = 4.97 \times 10^{-5}$ $\rho = \sqrt{I/A} = \sqrt{\frac{4.97 \times 10^{-5}}{.0928}}$

$\rho = \sqrt{.000536} = .0232$

$L/\rho = \frac{22.589}{.0232} = 974$

$\sigma_{COL.} = \frac{C \pi^2 E}{(L/\rho)^2} = \frac{1.5 \times 9.87 \times 10^7}{948,676} = 156$ PSI

$M.S. = \frac{158}{156} - 1 = -1.3\%$

∴ ALLOW. STEERING MOMENT = 98.7 IN-LB ≈ 100 IN-LB

VOL II APP

C. WEIGHT ESTIMATE

TR64-26

1. SLRV Weight Estimate (RTE Power)

(Revised 15 Dec 63)

	Direct Line E-V				Indirect Line E-S-V			
	Allocation	Last Est.	Latest Est.	Dev. ±	Allocation	Last Est.	Latest Est.	Dev. ±
I VEHICLE SYSTEM			34.1				34.1	
A. Element #1			12.3				12.3	
1. Wheel Assembly			5.8				5.8	
2. Steering Assembly			1.0				1.0	
3. Structural Frame			0.4				0.4	
4. Thermal Compartment			5.1				5.1	
B. Element #2			11.8				11.8	
1. Wheel Assembly			5.8				5.8	
2. Structural Frame			0.5				0.5	
3. Thermal Compartment			5.5				5.5	
C. Element #3			10.0				10.0	
1. Wheel Assembly			5.8				5.8	
2. Steering Assembly			1.0				1.0	
3. Structural Frame			0.4				0.4	
4. Axle and Attachments			2.6				2.6	
5. Bumper			0.2				0.2	
II SURVEY INSTRUMENTATION			22.7				22.7	
A. Television			13.5				13.5	
1. Electronics			5.5				5.5	
2. Optics			8.0				8.0	
B. Soil Bearing Strength			8.8				8.0	
C. Clinometer			1.2				1.2	
III SUPPORTING SUBSYSTEM-ELECTRONICS			29.2				21.5	
A. Communications			19.0					
1. Vehicle Based T-R etc.			19.0				5.0	
2. Surveyor Based (Incl. Ant.)							5.0	
B. Command and Control (Vehicle)			5.2				5.2	
C. Telemetry			2.5				2.5	
D. Cabling			2.5				2.5	
IV SUPPORTING SUBSYSTEM-POWER			16.0				16.0	
A. RTE (incl. HSG & radiators)			9.0				9.0	
B. Batteries			5.0				5.0	
C. Electronics			2.0				2.0	
V SUPPORTING SUBSYSTEM-MECHANISMS			8.9				8.9	
A. Fenders			0.9				0.9	
B. Antenna Stadia Masts (Vehicle)			*				*	
C. Deployment Systems			8.0				8.0	
VI SURVEYOR T.V.								
TOTALS			110.0				101.9	

* Included in Communications

2. Stowed Condition Center of Gravity

As noted in the Monthly Progress Report No. 2 for the SLRV Phase I Program, the stowed SLRV c. g. estimate exceeded the allowable c. g. limits by -1.8, -3.9, and 4.0 inches with respect to the x, y, and z reference axes. As a result of this estimate, a study was initiated to investigate methods to relocate the SLRV stowed condition c. g. within specified limits.

These methods included:

a. Increasing weight of associated equipment mounted in Compartment B.

b. Moving stowed vehicle toward center of spacecraft by allowing local protrusions into specified interference envelope.

c. Moving stowed vehicle toward center of spacecraft by eliminating interference areas by means of cutting off compartment corners, etc.

d. Redesigning vehicle to allow the use of another stowage technique. Possible redesign areas are reduction in wheel cross sectional diameter, reduction in vehicle tread, reduction in vehicle wheel base, etc., or combinations of these.

e. Use present configuration but shift weight from compartment #2 to #3 (or possibly #1).

All calculations were based on a total system weight of 100 pounds.

Stowage Configurations

Configurations A through K concern a basic vehicle stowage configuration as shown in Fig. III. 2-21. In this method, the vehicle is folded into a triangular shape with the wheels deflected to fit the specified space envelope.

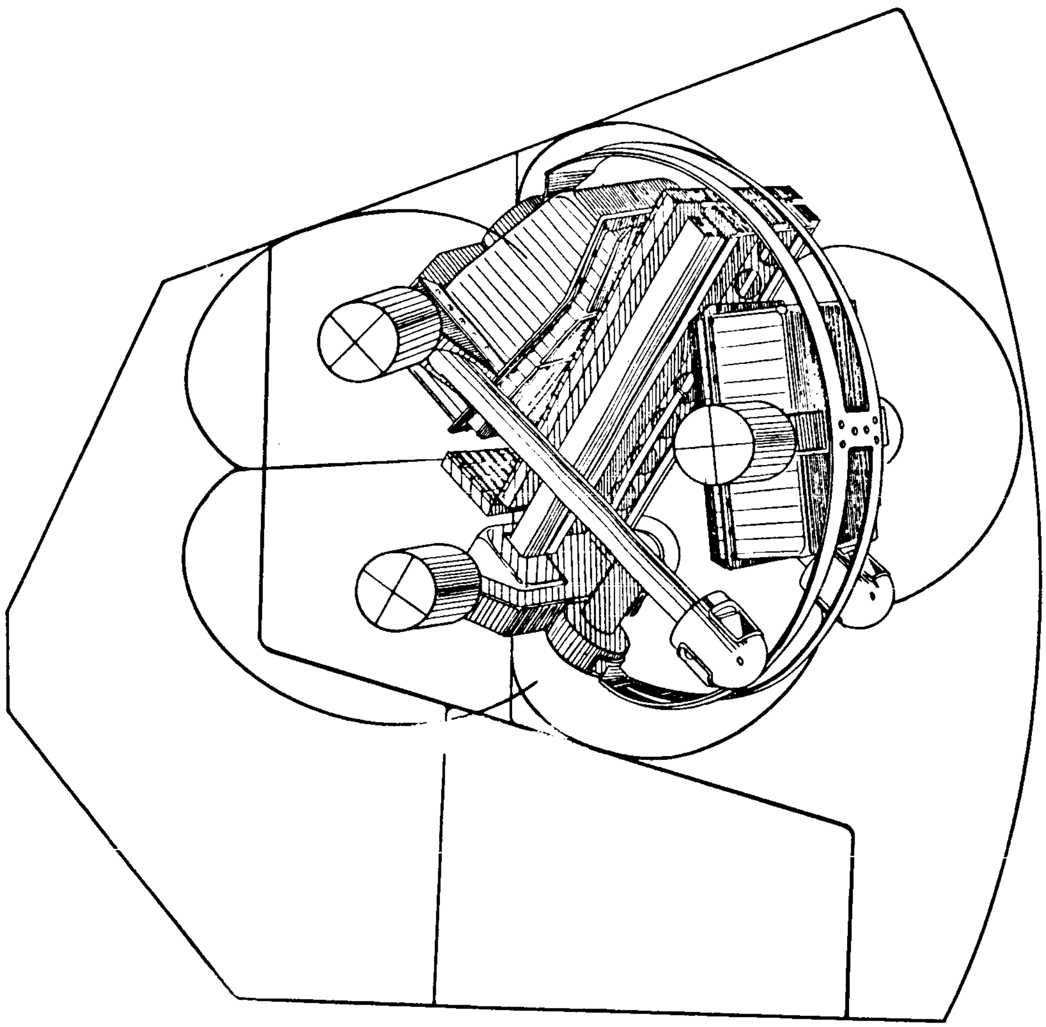

Fig. III. 2-21 Stowed Configuration in Allowable Space Envelope, Top View

Table III. 2-5 lists the pertinent data for configurations A through K and has accompanying Fig. III. 2-22, III. 2-23 which show the location of the c. g. with respect of the specified limits and changes associated with shifting the vehicle. It should be noted that Fig. III. 2-22 shows only the gross changes associated with shifting the space envelope in y-z plane. The minor changes associated with shifting the c. g. in the x-y plane are not shown.

Configuration L considers a vehicle stowage and deployment change from the previous configurations A through K . Fig. III. 2-24 shows the revised stowage scheme. In addition, the overall width of the vehicle has been reduced from 36 inches to 30 inches in order to adapt the configuration to the space envelope. The resultant c. g. falls within the allowable limits on the X-X and Z-Z axes, but is outboard of the Y-Y limit by 1. 3 inches. See data table for Configuration L.

Further modifications were made to provide a configuration M. This configuration has identical stowage to configuration L but the payload c. g. 's are adjusted to more favorable positions and take into account an extended television mast. The new c. g. remains within the Z-Z axis limit by 0. 01 inches. As the adjustments made were moderate, further trim can put the c. g. within the allowable limits. See data tables for Configuration M.

64-406

Conf.	Coordinates of C.G. X	Y	Z	Vehicle Weight Frame	Axle 1	Axle 2	Axle 3	Total	Deploy-ment Weight	Surveyor Commun Weight	Total Weight	Explanation
A	-2.8	-25.8	+23.9	1.3	28.8	31.5	24.7	86.3	8.0	5.7@	100.0	See Note "1"
B	-2.8	-22.7	+24.8	1.3	28.8	31.5	24.7	86.3	8.0	5.7@	100.0	See Note "2"
C	-2.2	-24.5	+23.2	1.3	39.2	20.1	24.7	86.3	8.0	5.7@	100.0	See Note "3"
D	-2.2	-21.6	+23.8	1.3	39.2	20.1	24.7	86.3	8.0	5.7@	100.0	See Note "4"
E	-1.9	-24.8	+23.2	1.3	28.8	31.5	24.7	86.3	8.0	5.7@	100.0	See Note "5"
F	-1.9	-21.8	+23.8	1.3	28.8	31.5	24.7	86.3	8.0	5.7@	100.0	See Note "6"
G	-1.0	-20.8	+25.8	1.3	28.8	31.5	24.7	64.3	8.0	27.7@	100.0	See Note "7"
H	-.65	-22.5	+23.6	1.3	28.8	31.5	24.7	81.1	8.0	10.9@	100.0	See Note "8"
J	-1.52	-24.2	+23.2	1.3	32.5	23.7	28.8	86.3	8.0	5.7@	100.0	See Note "9"
K	-1.52	-21.3	+23.8	1.3	32.5	23.7	28.8	86.3	8.0	5.7@	100.0	See Note "10"

TABLE III. 2-5 LIST - STOWED CONFIGURATIONS A THROUGH K

241

NOTES FOR TABLE III. 2-5

Note 1: This configuration is the conventional vehicle with electronics and structures distributed in a logical manner compatible with mission requirement as shown in table.

Note 2: In order to shift the vehicle c. g. within the limits, the vehicle has been moved as shown in Fig. III. 2-22. The resultant c. g. shifts are shown in Fig. III. 2-23. Rear axle bumper and front compartment interference is encountered at the Surveyor interference envelope.

Note 3: This configuration has a vehicle position of configuration A, but also has a weight redistribution of 10.4 lbs. from axle 2 to axle 1. Refer to Fig. III. 2-23 for c. g. locations.

Note 4: Configuration D has a vehicle position as shown in "B" and has a weight redistribution of 10.4 lbs from axle 2 to axle 1. Refer to Fig. III. 2-23 for c. g. locations. Interferences are the same as Note 2.

Note 5: This configuration has a vehicle position as noted in configuration A with 5.7 lbs. shifted from Surveyor compartment A to B.

Note 6: This configuration has a vehicle position as noted in configuration B with 5.7 lbs. shifted from Surveyor compartment to B. Interferences are as in note 2.

Note 7: This configuration has a vehicle position as noted in configuration A with 27.7 lbs. concentrated at Surveyor compartment

Note 8: This configuration has a vehicle position as noted in configuration A with 10.9 lbs. concentrated at Surveyor compartment B.

Note 9: This configuration has a vehicle position as noted in configuration A with compartments interchanged as follows:

a) axle 1 shifted to previous axle 3 position

b) axle 3 shifted to previous axle 2 position

c) axle 2 shifted to previous axle 1 position

Note 10: This configuration is identical to note 9 except vehicle position is as noted in configuration B. Interferences occur as in note "2".

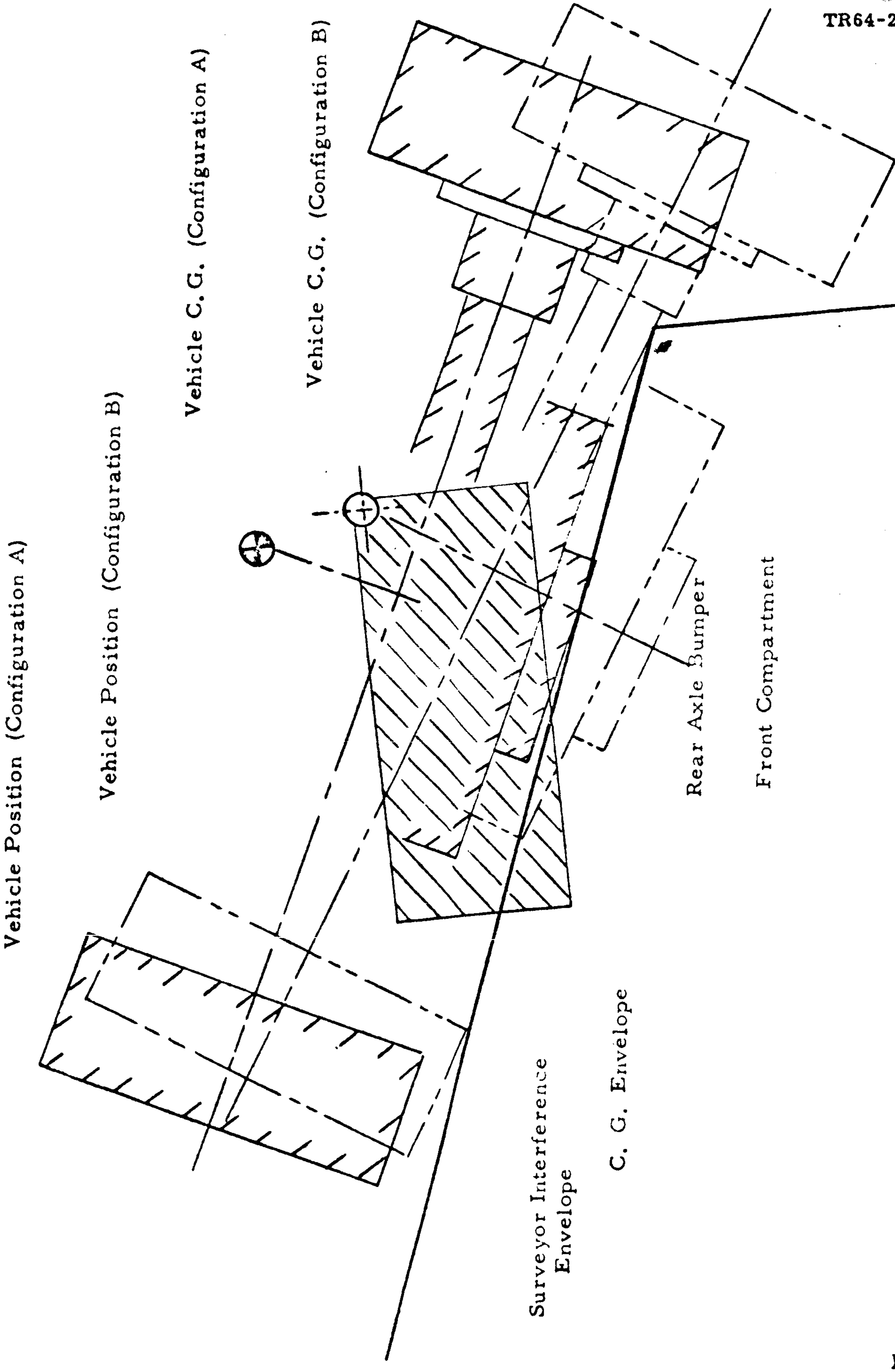

Fig. III. 2-22 Vehicle Position Change Showing Shift of c.g. and Interferences

64-406

TR64-26

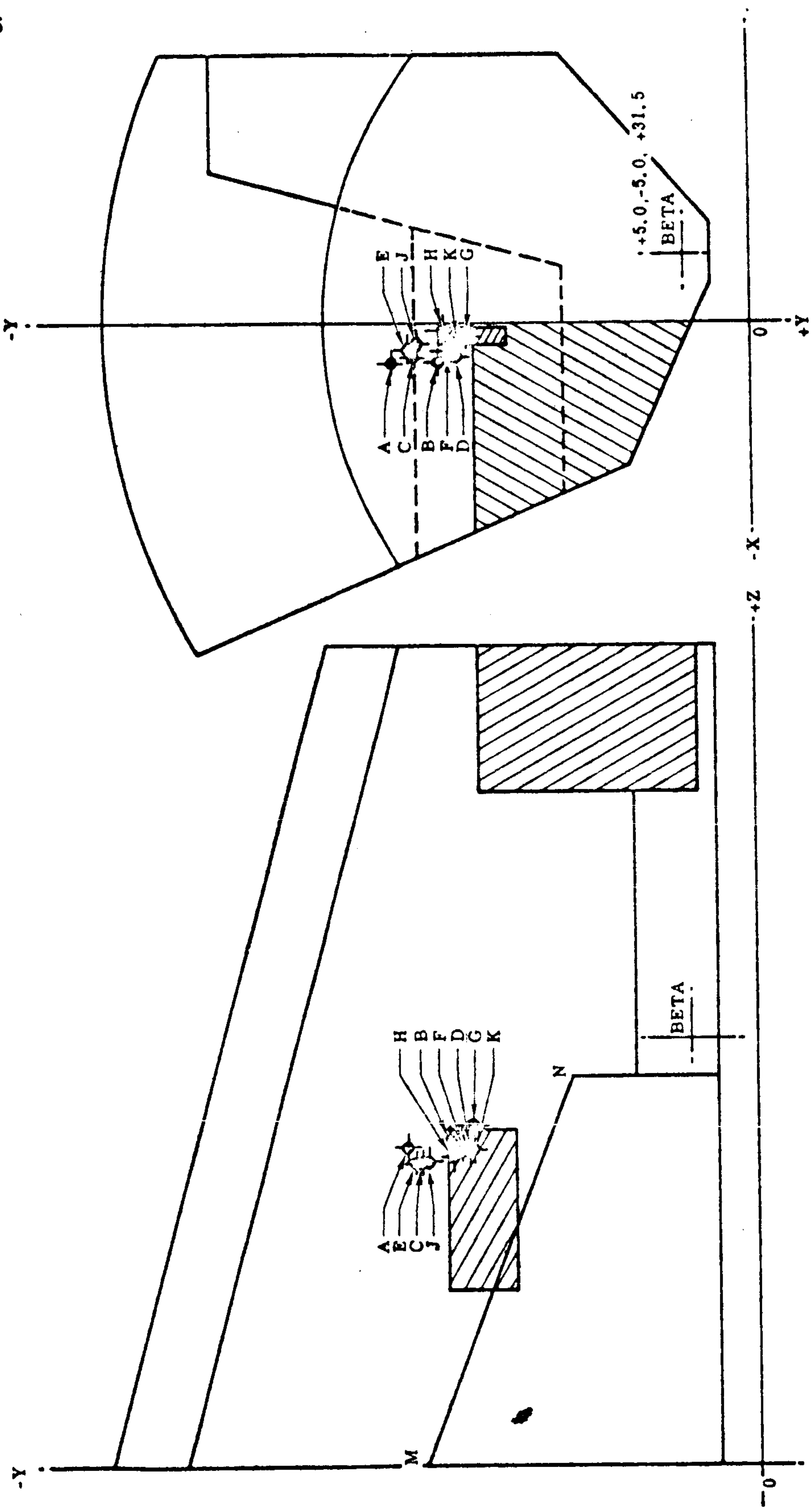

Fig. III. 2-23 C-G Locations for Configurations A through K

245.

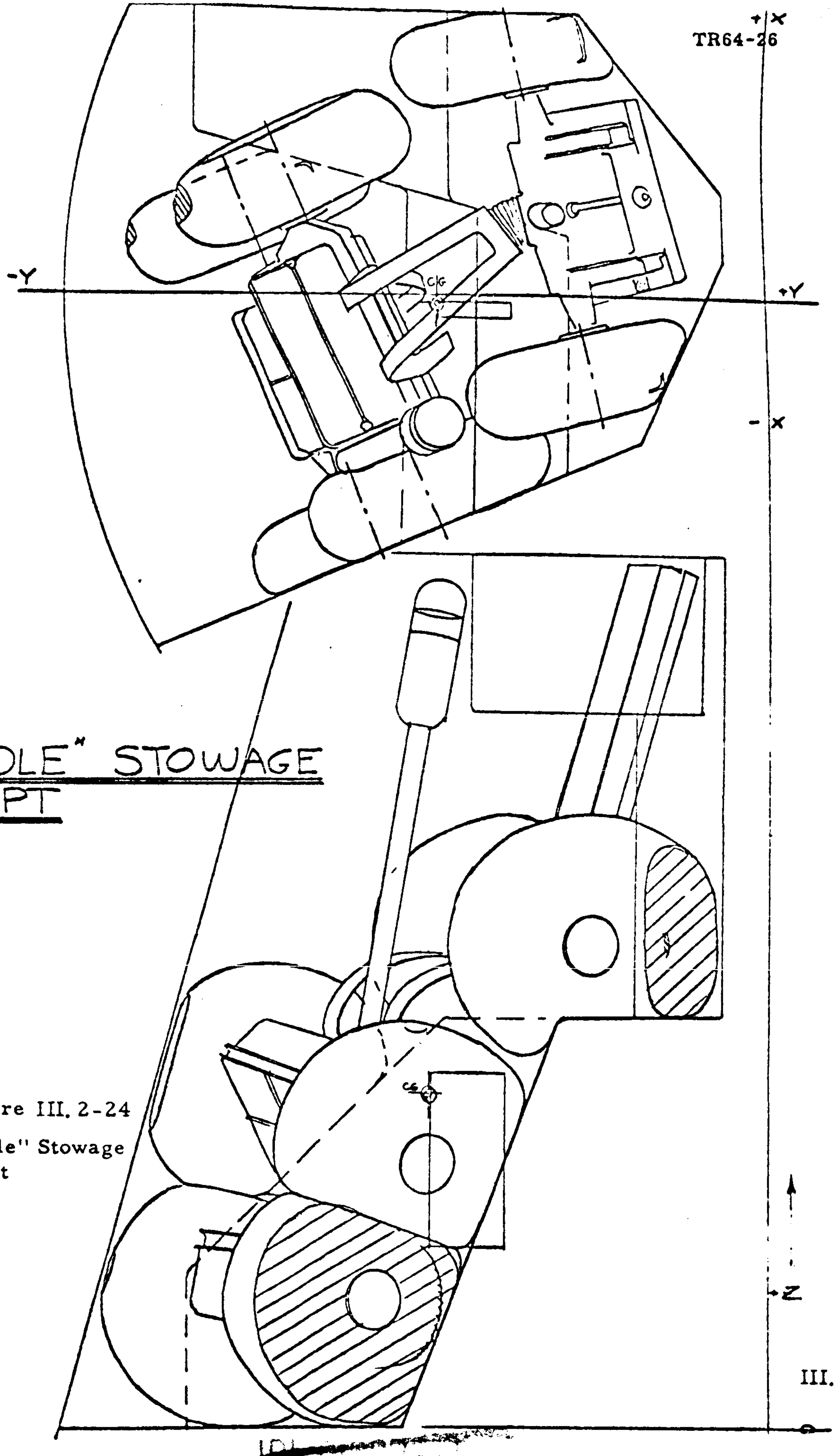

Figure III. 2-24
"Straddle" Stowage Concept

ESTIMATED SLRV C.G.'s
STOWED CONDITION
IN CENTAUR UPPER STAGE

Configuration L

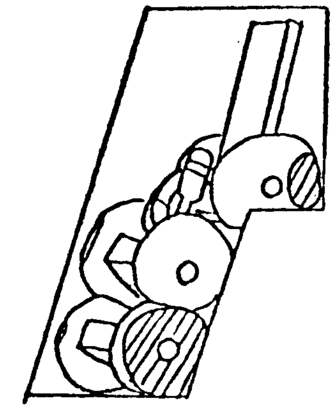

Balance Table

CG No	ITEM	WT~#	X-Dist"	X-Mom"#	Y-Dist"	Y-Mom"#	Z-Dist"	Z-Mom"#
1	ELEMENT #1	28.8	-5.2	-149.8	-31.7	-913.0	+10.8	311.0
2	ELEMENT #2	31.5	-2.9	-91.4	-29.3	-923.0	+20.8	655.2
3	ELEMENT #3	24.7	+6.2	+153.1	-14.1	-348.3	+37.2	918.8
4	SLRV FRAME -- #4	1.3	-2.0	-2.6	-27.2	-35.4	+23.0	29.9
5	SLRV DEPLOYMENT -- #5	8.0	0	0	-22.3	-178.4	+20.5	+164.0
6	TOTAL ~ ITEMS 1-5 INC	94.3	-0.96	-90.7	-25.4	-2398.1	+22.0	2078.9
7	SURVEYOR BASED COMM'S.	5.7	+5.0	+28.5	-5.0	-28.5	+31.5	+179.6
8	TOTAL - ITEMS 6 & 7	100.0	-.62	-62.2	-24.3	-2426.6	+22.6	2258.5

NOTE : C.G.'s on plane of symmetry
ITEM 7 located at pt B

OVERALL WIDTH OF VEHICLE IS REDUCED TO 30" BUT WEIGHTS ARE ASSUM[ED] THE SAM[E]

DEPLOYMENT IS CHANGED TO ROLL VEHICLE DIRECTLY OFF AND UPRIGHT.

ESTIMATED SLRV C.G!s STOWED CONDITION IN CENTAUR UPPER STAGE

Configuration M

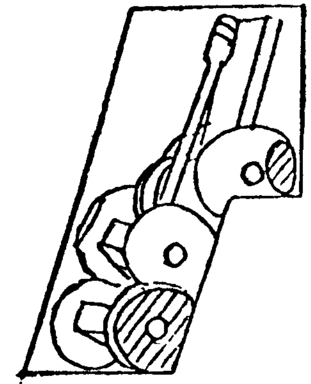

Balance Table

CG No.	ITEM	WT~#	X-Dist"	X-Mom"#	Y-DIST"	Y-Mom"#	Z-Dist"	Z-Mom"#
1	ELEMENT #1	28.8	-4.4	-126.7	-29.7	-855.4	+16.6	478.1
2	ELEMENT #2	31.5	-3.3	+103.9	-27.9	-878.9	+19.7	620.6
3	ELEMENT #3	24.7	+6.3	+155.6	-13.3	-328.5	+36.8	909.0
4	SLRV FRAME -- #4	1.3	-2.0	-2.6	-27.2	-35.4	+23.0	29.9
5	SLRV DEPLOYMENT--#5	8.0	0	0	-22.3	-178.4	+20.5	164.0
6	TOTAL~ ITEMS 1-5 inc	94.3	-.82	-77.60	-24.14	-2276.6	+23.34	2201.6
7	SURVEYOR BASED COMM'S.	5.7	+5.0	+28.5	-5.0	-28.5	+31.5	179.6
8	TOTAL - ITEMS 6 & 7	100.0	-.49	-49.10	-23.05	-2305.1	+23.81	2381.2

NOTE: DEPLOYMENT IS THE SAME AS IN CONFIGURATION L, IE STRADDLING SIDE OF SURVEYOR MAXIMUM VEHICLE WIDTH IS 30". THE TOTAL WEIGHTS OF THE COMPONENTS ARE ASSUMED TO REMAIN UNCHANGED BUT THEIR CENTER OF GRAVITIES ARE ADJUSTED INTO MORE REALISTIC OR MORE DESIREABLE POSITIONS ITEM 7 IS at pt

	H-ARM	V-ARM	LATERAL
ELEMENT #1	10.0	16.0	℄
ELEMENT #2	34.75	10.2	1.0 LEFT
ELEMENT #3	64.0	12.2	℄
ELEMENT #4	36.0	6.5	℄

ESTIMATED SLRV CG's
TRANSLATING CONDITION

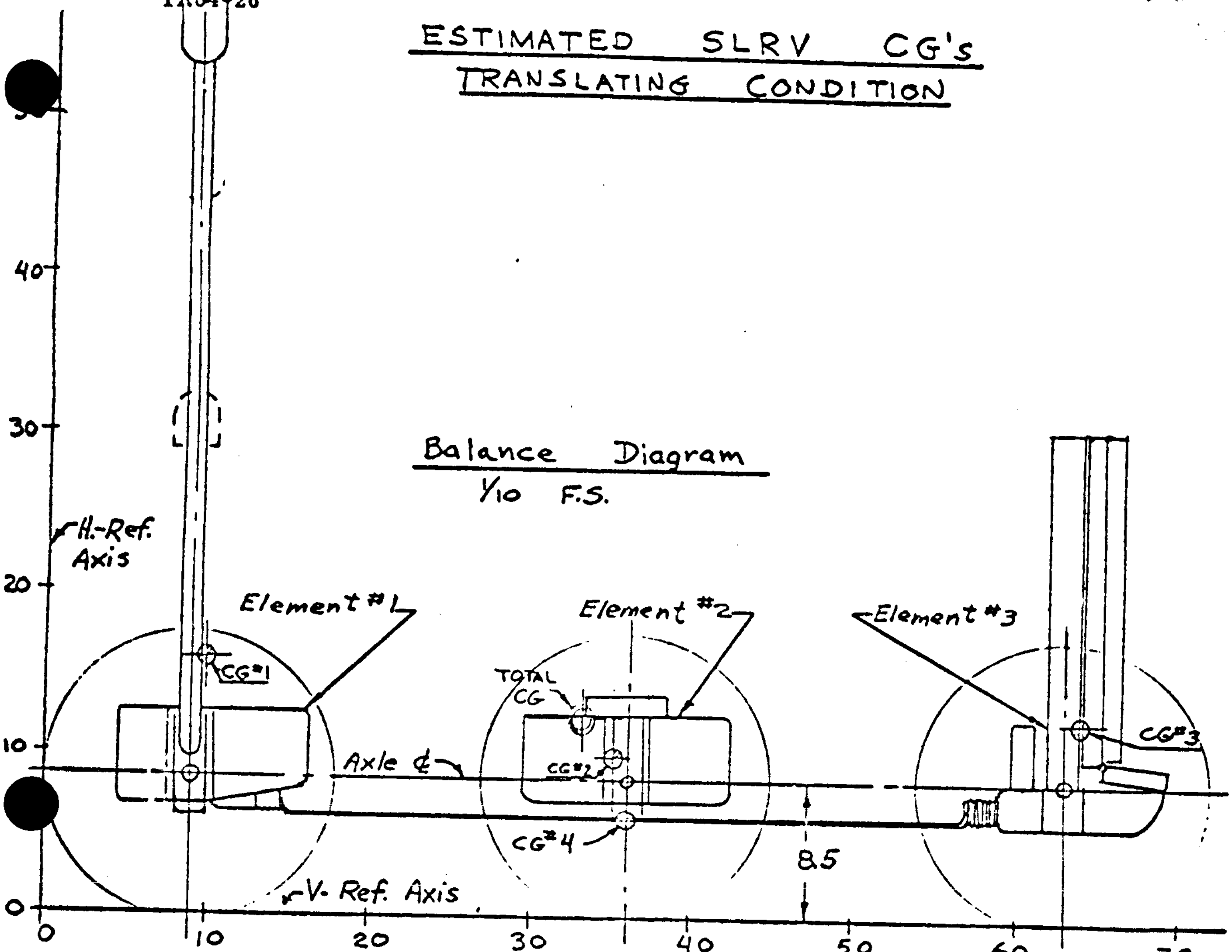

Balance Table

ITEM	WT. #	H-ARM"	H-MOM."#	V-ARM"	V-MOM"#	L-DIST"	L-MOM"#
ELEMENT #1	28.8	10.0	288.0	16.0	460.8	0	0
ELEMENT #2	31.5	34.75	946.2	10.2	321.3	+1.0	+31.5
ELEMENT #3	24.7	64.0	1580.8	12.2	301.3	0	0
FRAME ---#4	1.3	36.0	46.8	6.5	8.5	0	0
TOT. VEHICLE	86.3	33.16	2861.8	12.65	1091.9	0.365	31.5

CONFIGURATION M WITH IMPROVED T.V. LOCATION

NOTE. THIS CONFIGURATION HAS REDUCED VEHICLE WIDTH OF 30" OVERALL

D. SOLAR PANEL INVESTIGATION

INTRODUCTION

The solar panel investigation was performed to determine a means to increase the effective area of the SLRV solar array, so that the vehicle operation time could be maximized during one lunar day. The operation time can be maximized by providing sufficient effective areas during vehicle operation and charging modes that the following conditions are met:

(1) The solar array has the capability of continuous charging during vehicle operation. This provides for increases in power-source efficiency, as partial power can be transferred directly to the load, thus eliminating the conversion losses in the battery system.

(2) A minimum number of "parking" charge cycles is required.

(3) A decrease in the minimum time per "parking" charge cycle is achieved.

REQUIREMENTS

The preliminary requirement for accomplishing (1) above has been set at a minimum average of 1.5 square feet of effective solar array area. The preliminary requirement for the "parking" mode has been set at a minimum average effective area of 4.0 square feet.

CONFIGURATIONS

Fig. III.2-25 shows four configurations studied in an effort to achieve the requirements. Included in this appendix is the analysis performed on a configuration similar to configuration D. Configuration D varies slightly from the analysis configuration in an attempt to eliminate shadowing from the SMI; however, the results are not changed appreciably.

64-406
Vol. II APP.
SEC. III

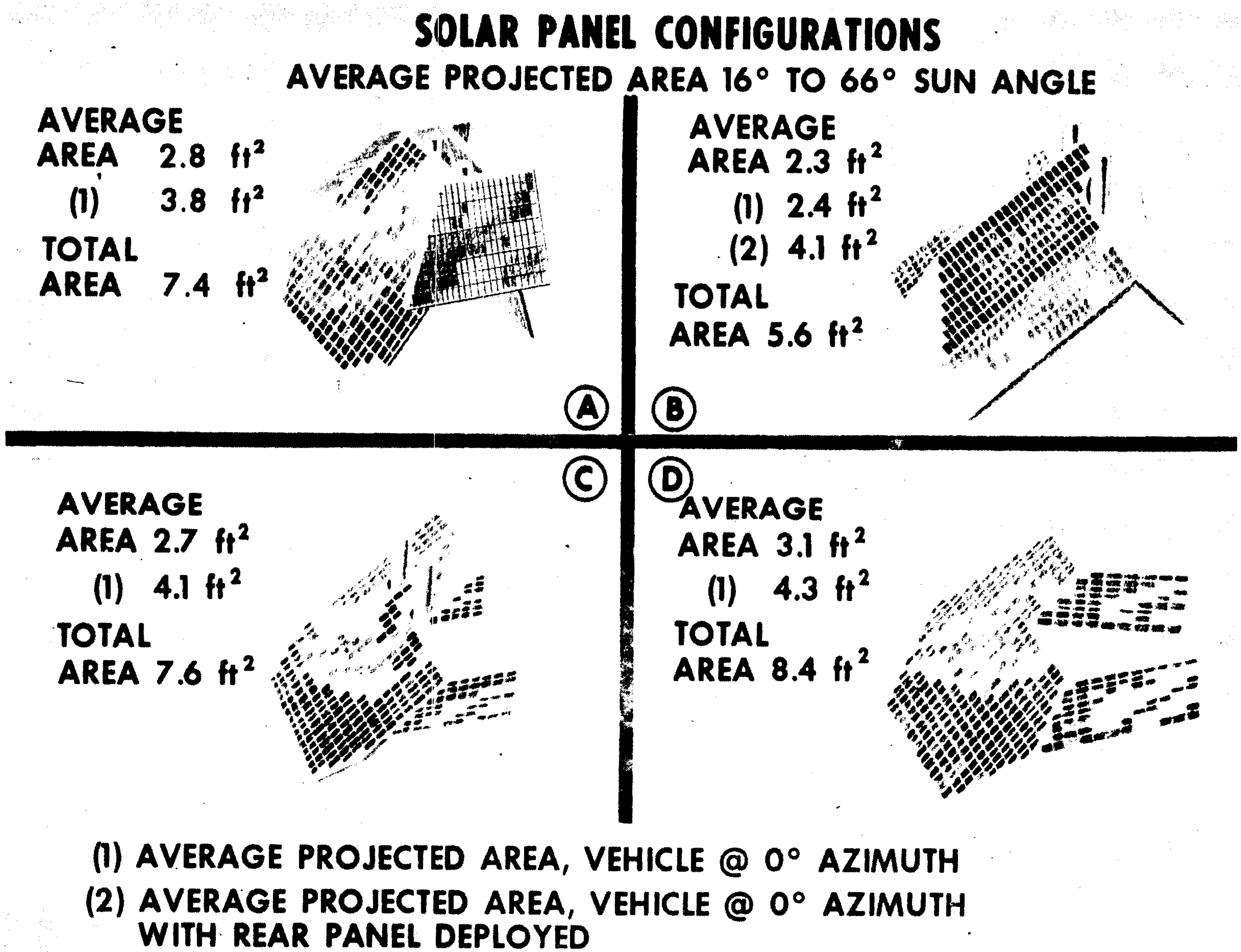

Fig. III.2-25 Configurations for Solar-Panel Investigation

CONCLUSIONS

Configuration D approaches an optimum in projected area. This configuration provides 3.0 square feet average at sun angles from 16° to 66° over the range of headings, and also provides 4.3 square feet average at 0° heading over the same sun angles.

In addition, an envelope diagram (see Fig. III.2-26 has been generated which depicts the preliminary allowable envelope for a solar array of the type shown in Fig. III.2.25, D, without affecting the mobility characteristics of the vehicle.

DISCUSSION

This investigation was a first-approximation effort to obtain a feel for what can be achieved with various configurations. The ability to utilize the projected area for generation of power (effective area) was not considered; this of course, is a significant factor. This aspect of the investigation was undertaken by RCA.

The results of the GM DRL investigation are summarized in Fig. III.2-27 and III.2-28.

Fig. III.2-27 shows the solar array projected areas as a function of vehicle azimuth heading for 0, 15, 30, 45, 60, and 90-degree sun angles.

Fig. III.2-28 shows the average projected area as a function of the range of sun angles for 0° azimuth heading and the average of all azimuth headings.

Nomograms 1 through 12 were used to calculate the solar array projected area. These nomograms are essentially a plane projection of a hemisphere with appropriate coordinates. At the center of the hemisphere, a plane at a given angle has its normal projected on the spherical surface. Extending radially from this point are the multiplying factors for any view of the plane other than normal. Accuracy in the use of the nomograms varies from better than 5% near the normal point or maximum value to very poor at the extreme angles. However, it is felt that overall accuracy would tend to be fairly good, thus permitting a simple, direct technique for reviewing a variety of configurations. Calculations performed on the configuration as shown in Fig.III.2-27 are presented in Table III.2-6.

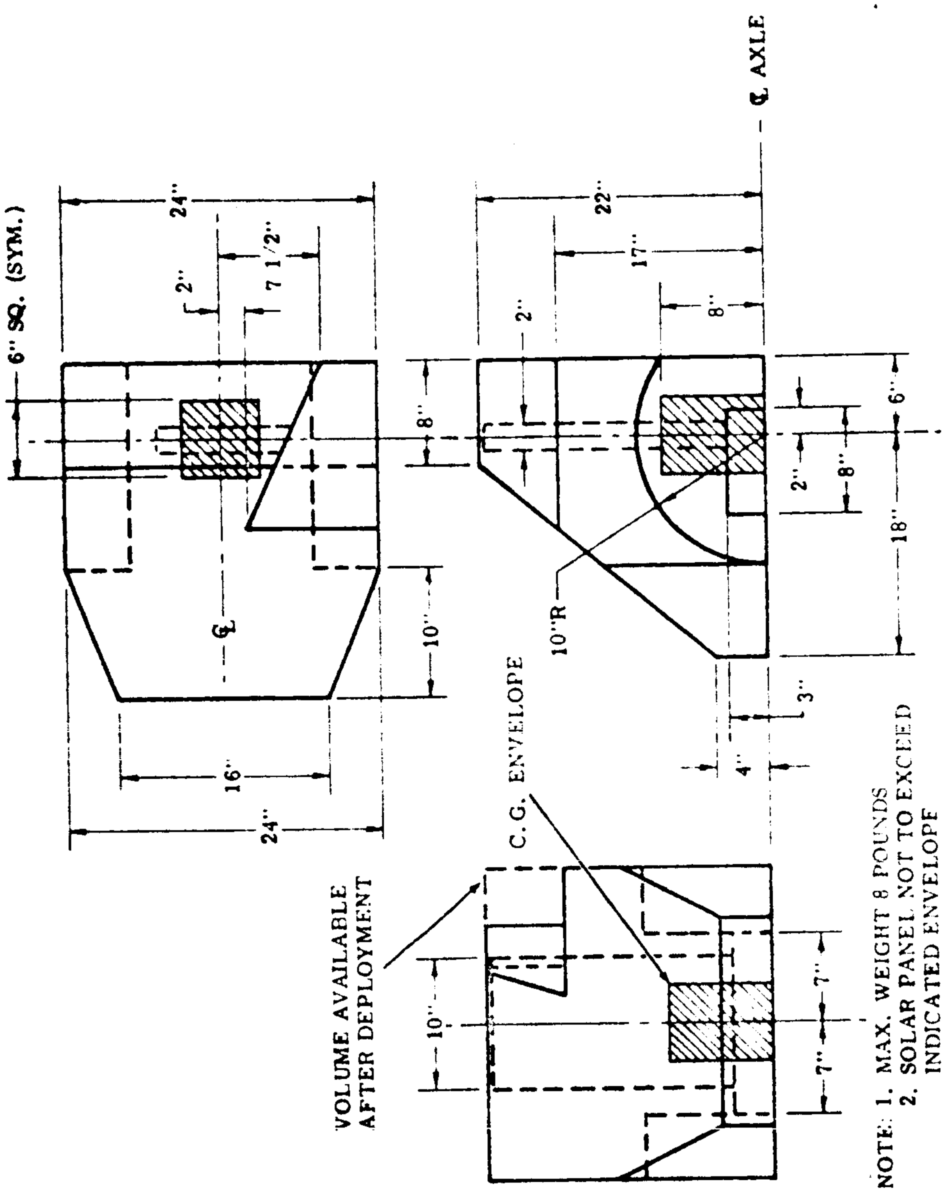

Fig. III.2-26 Solar Panel Envelope Diagram

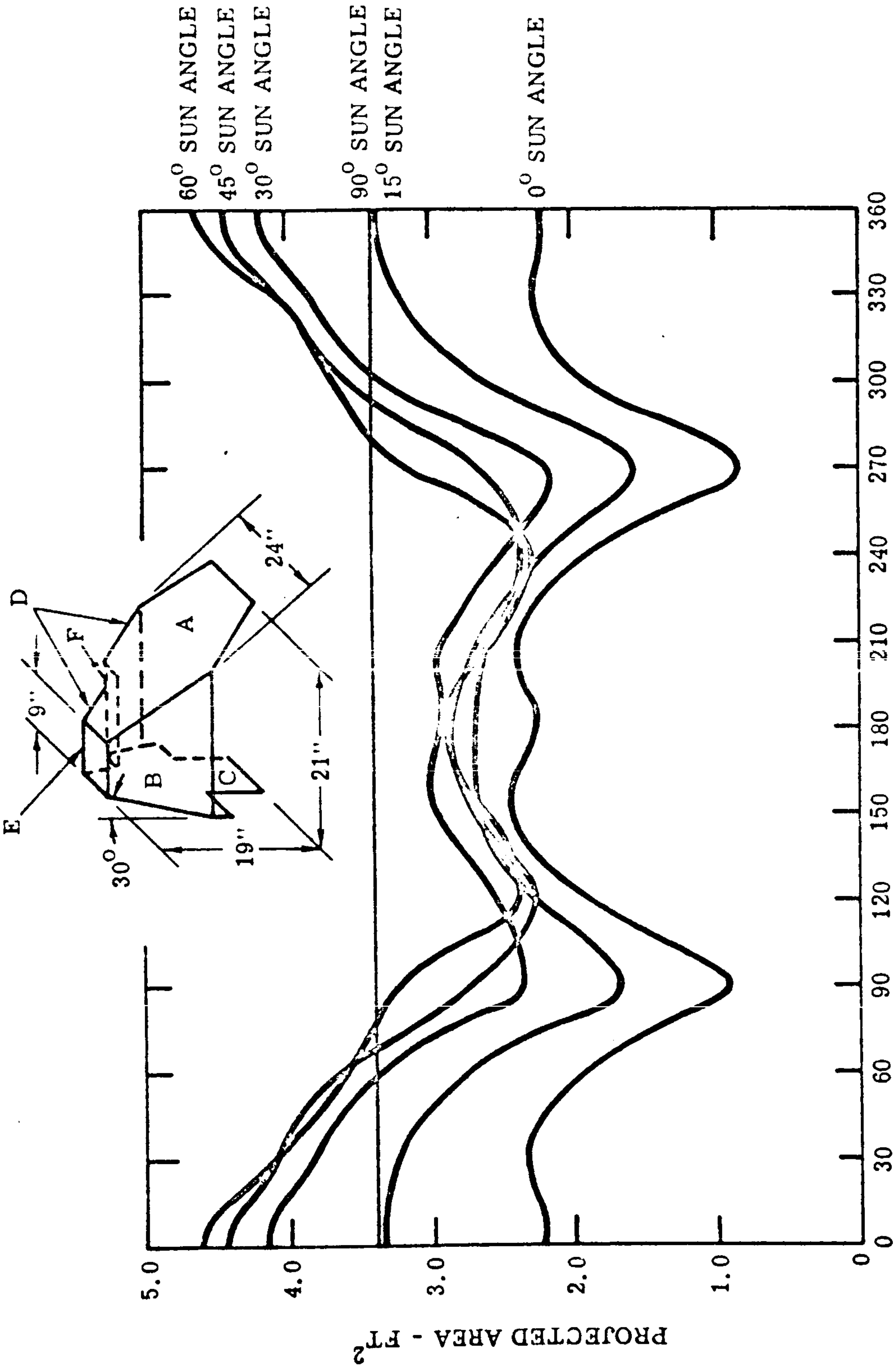

Fig. III.2-27 Solar Panel Projected Area vs Azimuth Orientation

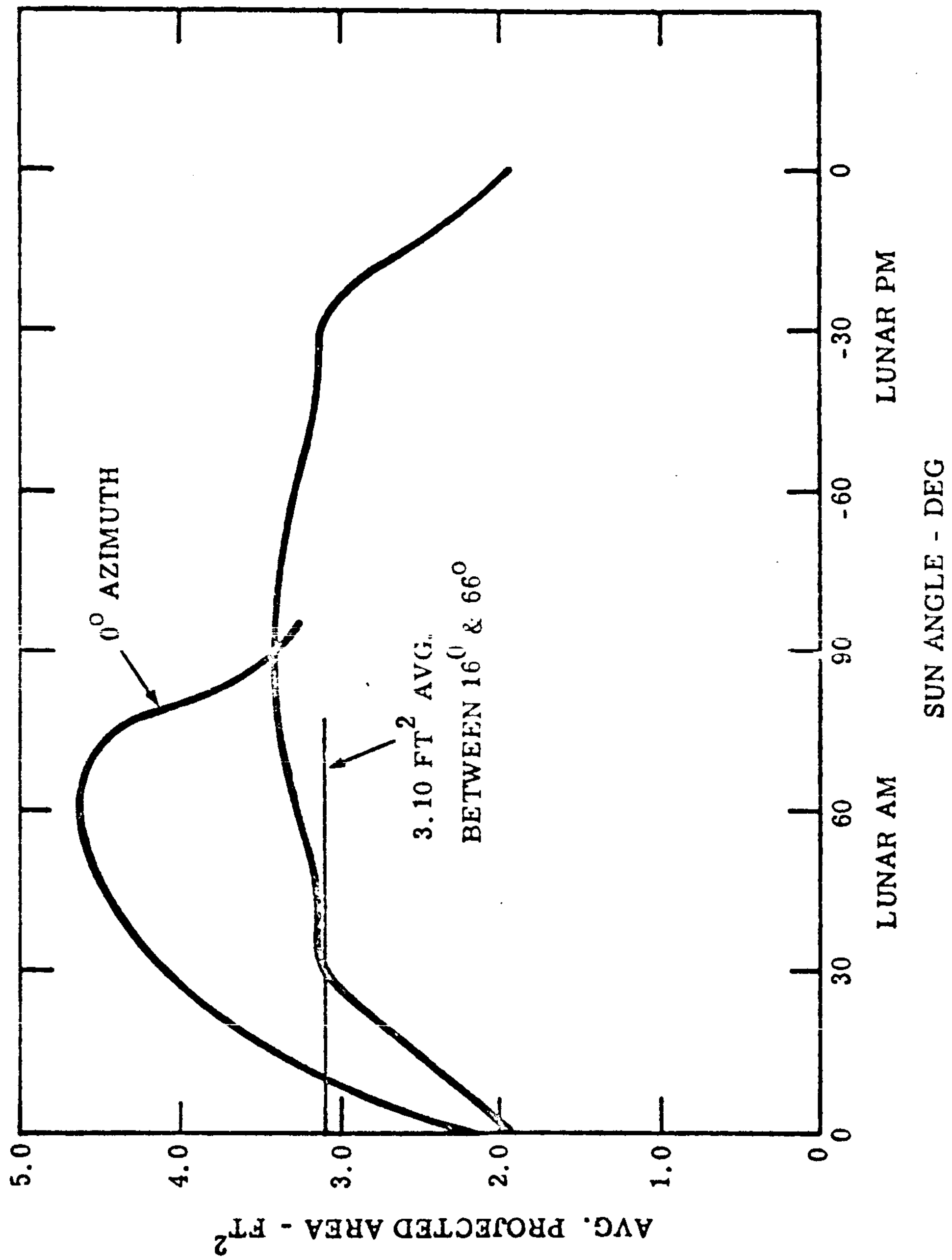

Fig. III.2-28 Average Solar Panel Projected Area vs Sun Angle

64-406

Vol. II APP

APPENDIX III
MECHANISMS

APPENDIX III
MECHANISMS

A. WHEEL DRIVES - GENERAL

1. Wheel Drives

APPROACH TO DESIGN

In order to obtain high mobility from the six-wheeled vehicle proposed, it is very desirable to drive each wheel with its own individual mechanical power source. Since the wheel motion is inherently rotary it is logical to utilize a source of rotary mechanical power to drive the wheels. Many types of rotary mechanical power sources are available; they include reciprocating and turbine internal and external combustion engines; pneumatic and hydraulic motors; and electric motors of various types. Internal and external combustion machines would obviously not be suited to this application. Pneumatic and hydraulic motors have some attractions and were considered, but reliability, weight, and efficiency problems associated with having to convert electrical energy into pneumatic or hydraulic energy and pipe it to each wheel made them unattractive. This leaves a-c and d-c motors to be considered.

Since the vehicle prime power source is direct current rather than alternating current it would seem desirable to use direct current motors to power the wheels. However, it is well known that brush-commutator operation in high vacuum presents serious problems. When water vapor is outgassed from carbon brushes they become abrasive and severe arcing and short life result. New brush compounds, special brush coatings, new commutator alloys, etc., have been tried in an effort to alleviate this problem but it is felt that reliable, long life operation of brush-type motors at the present time or in the near future requires pressurization to levels considerably above lunar pressure. While "brushless" d-c motors exist, most of them are simply a-c motors with a built-in d-c to a-c electronic converter. Other types of "brushless" d-c motors have been built, but a fairly thorough market survey revealed that none was available in the size and characteristics needed for the wheel drives.

Generally speaking, a-c motors are larger and heavier than permanent-magnet type d-c motors. In addition, electronics to convert the d-c battery power to a-c would have to be provided. In order to obtain the type of torque-speed curve desired, an inefficient servo-type motor would have to be used. In summary, initial investigations reveal that d-c motors are more desirable than a-c motors for this application. Investigation will continue, however, and should studies show that a-c motors are more appropriate, they will be used.

The tentative decision to use d-c motors to drive the wheels requires that another decision must be made as to what type to use and how to pressurize the brushes and commutator for reliable operation at lunar pressure. Several types of brusn type d-c motors exist. The wheel torque-speed curve desired can be supplied by a shunt-wound motor or its equivalent, a permanent-magnet field type. The permanent-magnet type is lighter, smaller and more efficient than the wound field type.

Three types of permanent-magnet field motors exist: 1) the power variety characterized by few commutator segments, straight armature poles, relatively high speed and low torque; 2) the servo type, similar to the power type but with a greater number of commutator segments and skewed armature poles; and, 3) the torque type with a large number of commutator segments, skewed armature poles, lower speed and higher torque.

Three motors, each representative of the type previously mentioned. were investigated in terms of general characteristics as illustrated in Table III.3-1. Motor characteristics were tabulated for each motor at 1/4, 1/2 and 3/4 stall torque as well as the peak efficiency point. Parameters tabulated included developed torque, input and output power, efficiency, weight/unit input power (@peak efficiency), and weight/unit output power (@maximum power output).

In general, for the SLRV application, the motors manufactured by Inland Motor Corporation of Virginia (representative of the torque type motor) appeared to have greater advantages than the other two considered.

As discussed previously, it is necessary to pressurize the brushes and commutator of a brush-type d-c motor to obtain reliable operation on the lunar surface.

TABLE III. 3-1

Tabulation of General D-C Motor Characteristics *

	% of Stall Torque %	Torque (oz-in)	Input Power (watts)	Output Power (watts)	Eff. % (%)	Weight/Unit Input Power (oz/watt)	Weight/Unit Output Power (oz/watt)
Inland-T-0701B @ 28 volts	25	1.75	11.2	4.25	38		
	50	3.5	22.2	10.3	46		.272
	75	5.25	3.5	8.5	27		
	(Peak eff. @ 33%)	2.3	14.0	9.5	68	.20	
Globe SS @ 27 volts	25	.585	7.17	3.8	53		
	50	1.17	12.5	5.5	44		.364
	75	1.76	17.8	4.1	23		
	(Peak eff. @ 21%)	.5	6.36	3.5	55	.315	
CPPC @ 28 volts	25	.25	5.5	3.27	59.5		
	50	.5	11.4	5.07	44.5		.277
	75	.75	16.5	4.05	24.5		
	(Peak eff. @ 25%)	.25	5.5	3.27	59.5	.254	

* All calculations based upon manufacturer's published catalog data.

Also, to obtain the high efficiencies resulting from the use of fluid as opposed to dry-type lubricants, it is desirable to pressurize not only the motor brushes and commutator but the motor bearings and all associated gears and bearings. Three pressurization methods were given preliminary consideration and will be given further study. The three methods are:

1. Seal the system as well as possible by limiting leaks thru bearing-shaft clearances or ball bearing seal clearances and maintaining internal pressure by means of a subliming solid or evaporating liquid. A material must be chosen with a vapor pressure high enough to provide reliable motor operation and low enough to maintain pressure by incorporating a limited amount of material for the desired operating period.

2. A capillary film-type fluid seal suggested by RCA, Hughes and others. Here, the sealed volume is maintained at a pressure of approximately 30 millimeters of mercury by sealing it with a circumferential oil film between the inner and outer ball bearing rings. The oil film is replenished from a sintered plastic reservoir through a number of radial capillary tubes leading to the sealed surfaces. The oil film evaporates down to its vapor pressure into a space between the oil film and the lunar atmosphere. From here it leaks very slowly out to the lunar atmosphere through a long-path-length gap between the fixed and rotating members. Although this leakage gap is quite widely spaced (up to .100 inch), the "impedance" is very high due to the low vapor pressure of the oil and the resultant leakage rate is very low.

3. A bellows sealed rotary coupling which provides a true hermetic seal.

While all three methods will continue to be studied, it is felt that of the three, the bellows-type coupling will provide the most reliable operation. GM DRL studies and vendor evaluations of Kearfott, Div. General Precision, Inc., Hoffman Electronics Corp. and Mechmetals Corp. Subsidary of Mechmetals-

Tronics, Inc. have indicated that the state-of-the-art of this field has advanced considerably in the last few years and that this approach is a sound one. Processes have been developed which result in bellows of high mechanical strength and high quality; one such process is a chemical deposition which yields an extremely high quality bellows of almost unlimited shape variation and an ultimate strength of 240,000 psi. Such a bellows coupled with good mechanical design, to reduce bellows stress to a low level, will result in a true hermetically sealed mechanical rotary coupling of high reliability and long life. Couplings similar in design were used in the GM DRL Surveyor Soil Mechanics Instrument Program and are being proposed for use in other applications on the Surveyor Lunar Roving Vehicle, including the DIBSI deployment system.

The simplest way to drive the wheel from a d-c permanent magnet field motor would be to use a motor whose speed-torque characteristics were identical to those desired at the wheel. Attempts to obtain such a motor will be made but, to date, motors with these characteristics are too large, too heavy and are inefficient.* In lieu of this, a motor can be coupled to the wheel through a speed reducer of some type. Three types will be considered: spur gear, planetary and "hunting tooth" gearboxes such as harmonic drives, Ferguson Paradox, etc. Preliminary studies indicate that the planetary gearbox is the most attractive from the standpoint of reliability, weight, and volume. In addition, the planetary gearbox provides a convenient means of uncoupling the drive from the wheel when desired.

Preliminary calculations show the additional weight due to the un-clutching re-clutching feature is only .16 pounds per wheel or less than 1 pound for the entire vehicle.

Although several revolution counting techniques were considered,among these the simplest, most reliable technique appeared to be closing a hermetically sealed magnetic reed switch with a small permanent magnet rotating with the wheel.

*The method used in determining d-c motor characteristics for the SLRV wheel requirements is described in some detail a few pages later under the heading "Method of Determining d-c Motor Characteristics . . . etc.".

PREFERRED DESIGN

A preferred wheel drive design is depicted in Fig. III.3-1 A small permanent magnet-field, brush type d-c, torque motor drives the wheel hub through a 400-to-1 planetary gearbox coupled to a bellows-sealed crank mechanism. The crank mechanism allows the entire assembly, except the two low speed wheel bearings and one crank bearing, to be hermetically sealed and to operate in an environment known to be suitable for the motor brush-commutator assembly. The coupling torque is not transmitted through the bellows itself in this design. The frictional torque of only one small diameter ball bearing is actually transmitted through the bellows.

A solenoid-operated slider enables the planetary gearbox output ring gear to be disconnected from the housing, thereby effecting free wheeling upon electrical command. Over-center springs retain the slider in either position so that no power is required to hold the drive in either the clutched or unclutched position. A magnetically operated reed switch to signal each wheel revolution completes the assembly.

The d-c motor characteristics for each of the three motors, CPPC, Globe, and Inland, were calculated for the specific application in the wheel drive assembly. Calculated characteristics included the gearbox ratio, operation and stall torques, no-load and operation speeds, operation and stall input powers, and the overall system efficiency. (Refer to Table III.3-2 for details.)

For the specific application the torque-type motor was again superior to the other two types with the overall system efficiency 46 percent better than the power-type motor and 60 percent better than the servo-type motor. The efficiency plus the low motor speed and low gearbox ratio(which increase reliability) make this motor favorable for use in the wheel drive assembly.

Contaminants will be kept from entering the three bearings operating in the lunar atmosphere by sealing the inside wheel bearing with a single labyrinth or rubbing type seal. The remaining two bearings, sealed in the space between the

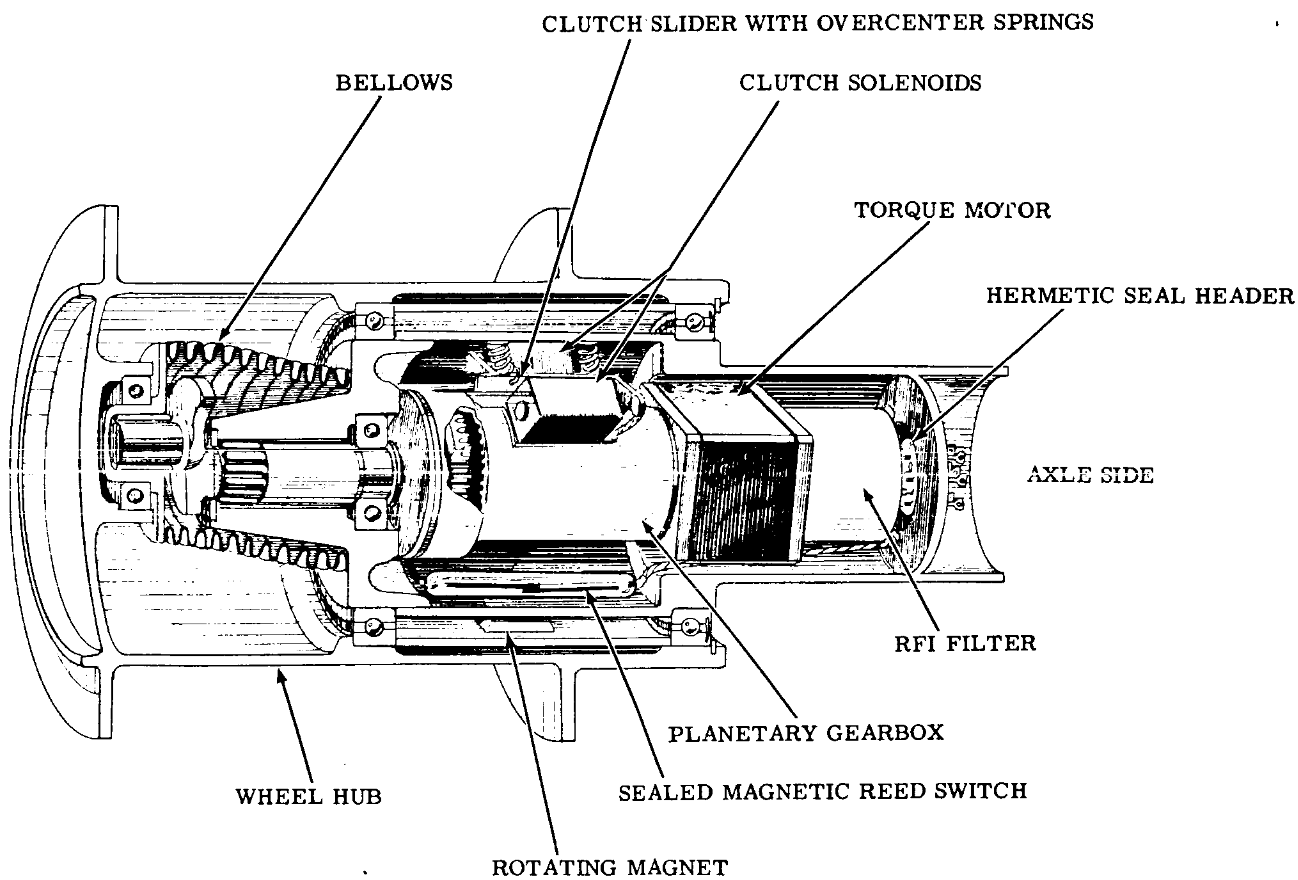

Fig. III. 3-1. Wheel Drive Configuration, Preferred Design

TABLE III.3-2

Tabulation of Wheel Drive Calculated D-C Motor Characteristics*

Torque Requirements $T = 96$ oz-in @ 10 RPM @ Wheel
$T_{stall} = 960$ oz-in @ Wheel

MOTOR	Inland T-0701B	Globe SS	CPPC
Assumed Gearbox — Wheel Bearing Eff. (%)	60	60	60
Gearbox Ratio	405	848	1735
Motor Stall Torque (oz-in)	3.95	1.89	.925
Motor Torque for 96 oz-in @ Wheel (oz-in)	.395	.189	.092
Motor No Load Speed (RPM)	4660	9950	20,300
Motor Speed @ 10 RPM_w (RPM)	4050	8480	17,350
Input Motor Power @ Stall (Watts)	13.5	16.1	18.1
Input Motor Power @ 10 RPM_w (Watts)	1.65	3.07	4.14
Wheel Power @ 10 RPM (watts)	.71	.71	.71
OVERALL SYSTEM EFFICIENCY (%)	43	23.2	17.2

* All calculations are based upon manufacturer's data.

hermetic rotary coupling and the inner wheel bearing, do not require individual seals. They will be lubricated with dry lubricant impregnated plastic separators such as the "Bartemp" type or with a dry film lubricant such as "Micro Seal."

The proposed wheel design is an improvement of a design which was run successfully for many hours on all six wheels of the radio controlled pre-prototype GM DRL Lunar Roving Vehicle. A photo of a disassembled wheel from this vehicle appears in Fig. III.3-2. The design of this wheel drive is very similar to that proposed. A D. C. permanent-magnet field motor drives the wheel through a planetary gearbox and bellows-sealed angle-crank mechanism.

ALTERNATE DESIGNS

Alternate designs suggested by possible subcontractors are illustrated in Figures III.3-3 and III.3-4.

The design of Fig. III.3-4 features a single-wheel support bearing, utilizing an oil-film hermetic seal and a drive motor attached to and rotating with the wheel hub. This type of oil-film hermetic seal, discussed in detail previously, is presently under evaluation for possible use in a spacecraft radar antenna drive mechanism and shows great promise. Thermal conduction from the wheel hub to the wheel mount or axle is quite poor since the path includes the wheel bearing or bearings. Thermal studies will determine whether it is more desirable to connect the motor thermally to the wheel hub (and radiate from the hub cap) or to the axle. Since the motor rotates with the wheel, power is brought to it through slip rings. For simplification, no clutch mechanism, revolution counter, of RFI filter are shown – ample space is available, however, for these devices.

The wheel drive in Fig. III.3-3 incorporates a bellows-sealed drive similar to the preferred design. A planetary type "hunting tooth" gear reduction system provides a large gear reduction in what is essentially a single gear pass.

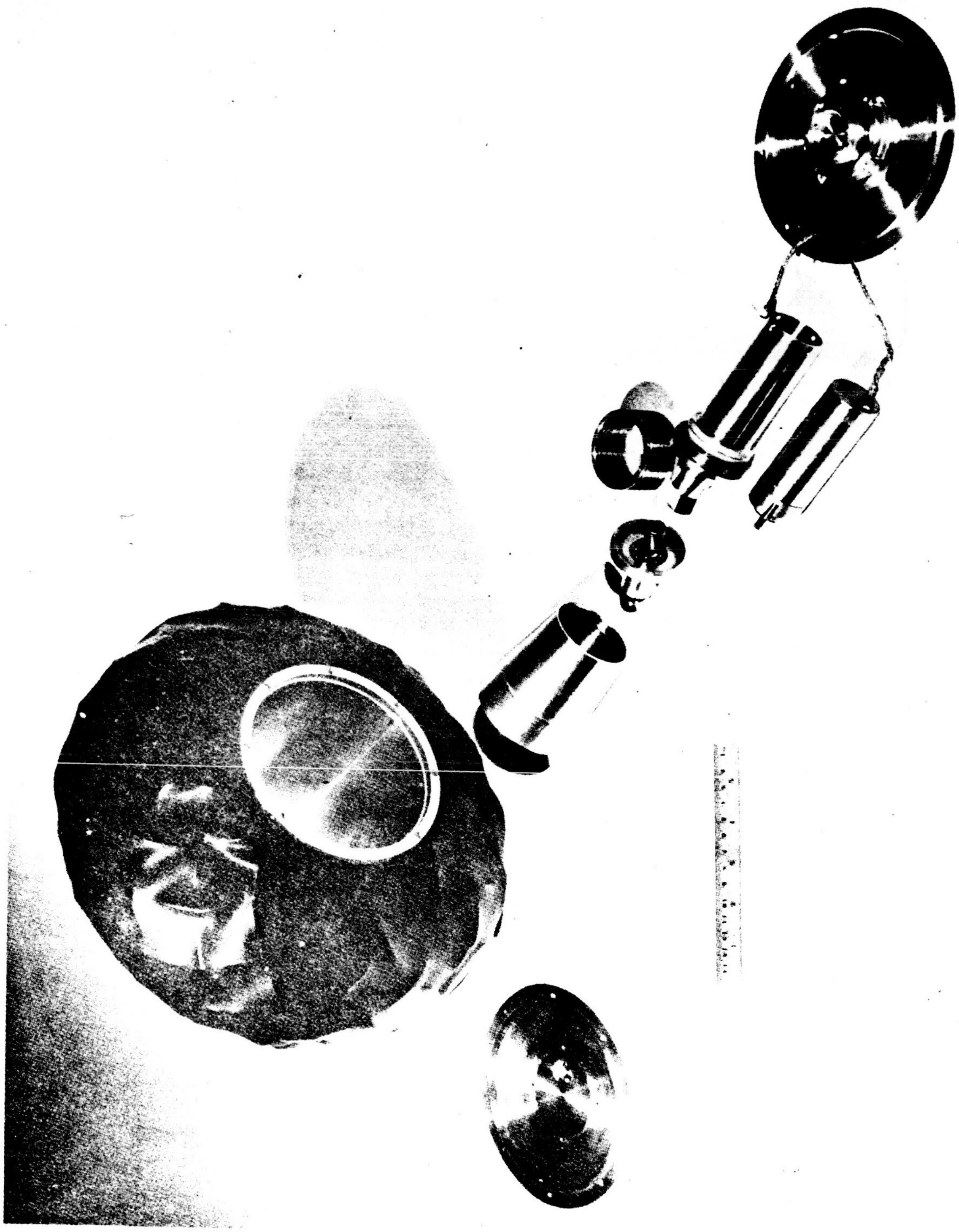

Figure III.3-2. Preprototype Wheel Drive, Disassembled

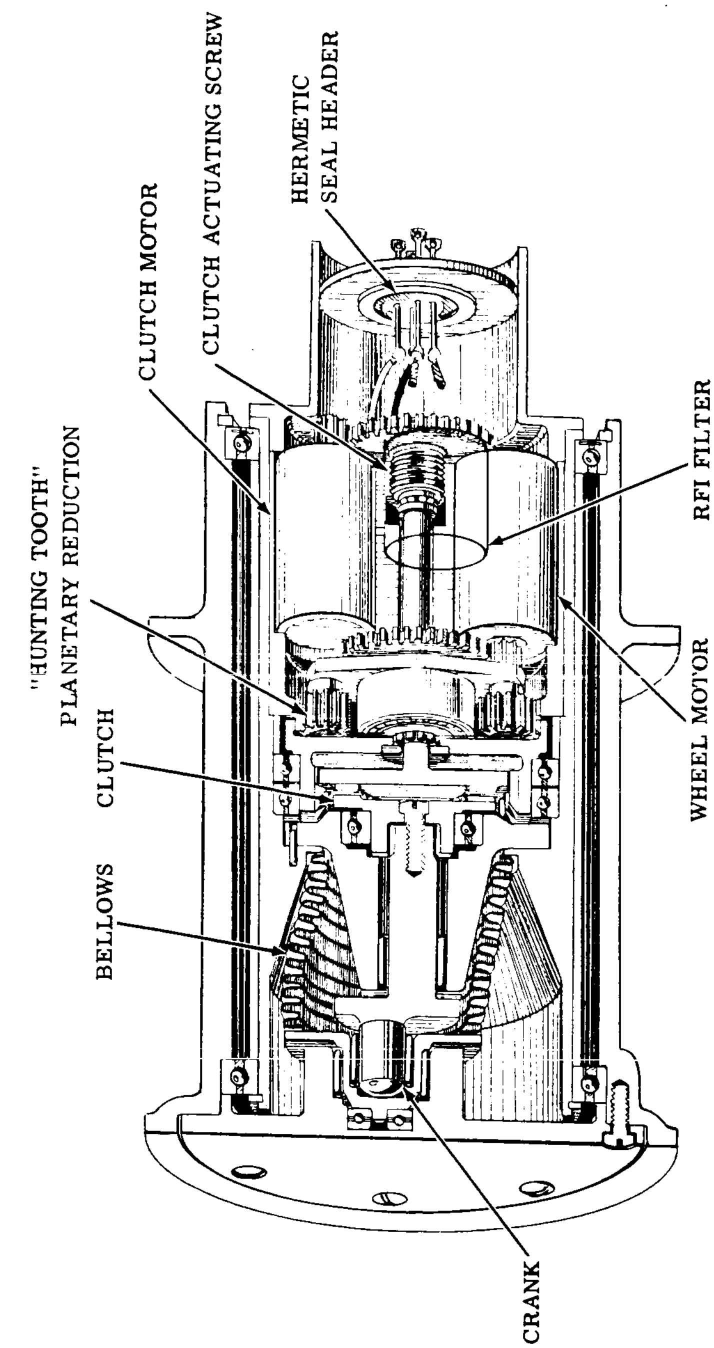

Figure III.3-3. Alternate Wheel Drive Configuration

64-406
VOL. II APP
SEC. III

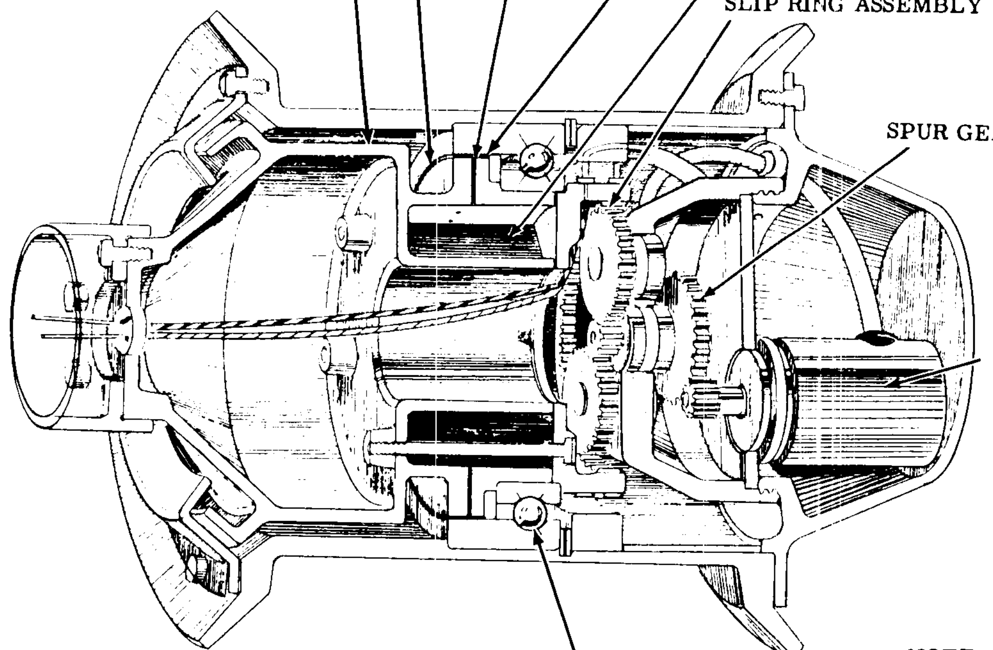

NOTE – FOR CLARITY, CLUTCH, RFI FILTER AND REVOLUTION COUNTER SWITCH ARE NOT SHOWN

Figure III.3-4. Alternate Wheel Drive Configuration

METHOD OF DETERMINING D-C MOTOR CHARACTERISTICS FOR SURVEYOR LUNAR ROVING VEHICLE WHEEL REQUIREMENTS

A method will be derived herein for determining the required d-c motor characteristics to meet the operating wheel requirements of the Surveyor Lunar Roving Vehicle.

Assumptions

In determining the d-c motor characteristics, the following assumptions have been made:

a) The d-c motor speed-torque and current-torque characteristics are straight line relationships and proportional according to

$$y = mx + b$$

b) The motor speed-torque curve is proportional to the applied voltage and thus describes a family of parallel lines for various applied voltages.

c) The stall current of the motor is a function of the brush resistance and the armature resistance according to $E = IR$.

d) The no-load current is a function of the losses in the motor – windage, brush contact, and mechanical losses.

e) The no-load speed of the motor is described as the speed at which the back emf generated is equal to the applied voltage; thus, the motor can accelerate no further.

f) The stall torque is a function of the stall current, the permanent-magnet field strength, and a d-c motor constant (different for each motor) according to:

$$T = K_t \Phi I_s .$$

Direct Wheel Drive

The requirements for a direct d-c motor wheel drive are dictated by the operation requirements for the Surveyor Lunar Roving Vehicle. Torque requirements

[redacted]

64-406

for the successful operation of a single vehicle wheel have been specified at 96 oz-in. at 10 RPM at the wheel and 960 oz-in. at stall. The d-c motor speed-torque characteristics for a direct drive motor can then be illustrated below:

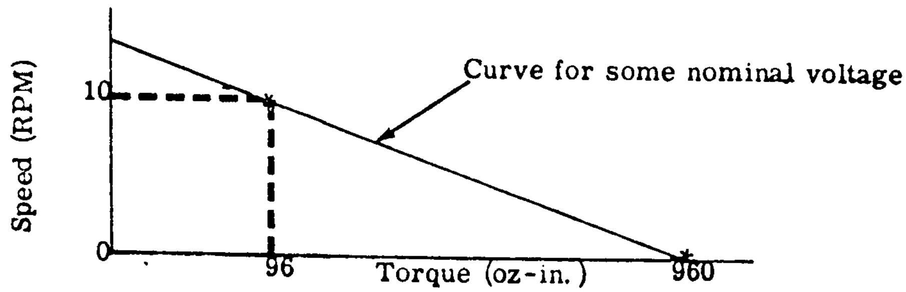

Using the above requirements, the characteristic equation for the required motor takes the form of

$$S_m = K' T + S_o$$

where S_m = motor speed

S_o = motor no-load speed

T = developed motor torque @ wheel

K' = slope of the speed-torque curve

Substituting for the numerical requirements yields

$$S_m \text{ (RPM)} = 11.6 - 1.16 \times 10^{-2} \text{ (oz-in.)}$$

Gear Reduction

However, if an intermediate gear train is used to transmit the torque to the wheel, the foregoing equation must be modified by $S'_m = S_m N$

where N = gear train ratio

S'_m = motor speed dictated by S_m and N

Thus, for an intermediate gear train,

$$S'_m = N (11.6 - 1.16 \times 10^{-2} T). \qquad \text{III.3-1}$$

D-C Motor Characteristics

A family of d-c motor speed-torque characteristic curves can be described by a characteristic equation of the form:

$$T_m = KS_m + K_1 E \qquad \text{III.3-2}$$

289

[redacted]

where

T_m = developed motor torque
S_m = motor speed
E = operating voltage
K = slope of speed-torque curve
K_1E = stall torque intercept

The motor constants, K and K_1, can be determined from data supplied with most d-c motors.

The current torque characteristic of a d-c motor is described by the equation:

$$T_m = K_2 i - T_o \qquad \text{III.3-3}$$

where

T_m = developed motor torque
i = motor current
T_o = torque intercept
K_2 = slope of the current-torque curve

In addition, the transmitted torque to the wheel (T) is a function of the motor torque, N, and the gear train efficiency (μ) according to:

$$T = \mu N T_m \text{ or}$$

$$T_m = \frac{T}{\mu N}$$

And substitution for T_m in Equation III.3-2 and combining equations III.3-1 and 3-2 yields:

$$T/\mu N = KN\,(11.6 - 1.16 \times 10^{-2}\,T) + K_1E \qquad \text{III.3-4}$$

which relates a d-c motor speed to the wheel torque and speed requirements as well as the gear train efficiency and reduction.

By substituting the two wheel operation requirements into Equation III.3-4 for T, the two equations generated can be solved simultaneously for N. The operating voltage can then be determined for $S_m = 0$ using the stall torque requirement.

By using Equations III.3-2, 3-3 & 3-4 the specific d-c motor characteristics of three motors where calculated and tabulated as shown in Table III. 3-2.

Note: The manufacturer's data was used to determine the characteristic equations for each motor. The gear train efficiency was assumed to be 60 percent.

TABULATION OF WHEEL DRIVE PERFORMANCE FOR VARIOUS DRIVE SYSTEMS*

Motor - Inland T-0701B

	6 wheel	4 wheel	2 wheel
Maximum Torque/wheel (oz-in)	960	960	960
Operating Torque @ 10 RPM @ wheel (oz-in)	96	143	288
Assumed Gearbox - Wheel Bearing Eff. (%)	60	60	60
Gearbox Ratio	365	355	322
Motor Stall Torque (oz-in)	4.4	4.5	4.97
Operating Motor Torque @ 10 RPM_{wheel} (oz-in)	.44	.67	1.49
Motor No Load Speed (RPM)	4060	4170	4600
Motor Speed @ 10 RPM_{wheel} (RPM)	3650	3550	3220
Wheel Speed for 6 wheel drive system (RPM)	10	10.6	13
Input Motor Power @ Stall (watts)	16.2	17	20.5
Input Motor Power @ 10 RPM_{wheel} (watts)	2.46	2.87	6.3
Wheel Power @ 10 RPM (watts)	.71	1.06	2.13
Overall SYSTEM EFFICIENCY (%)	29	37.3	33.8

* Performance per wheel

[redacted]

3. Wheel Declutching

A total of eight different methods of declutching the wheel from the wheel have been investigated. All eight methods can be incorporated into the basic wheel drive mechanism.

These methods are tabulated in the following table with comments on each concept as well as an attempt to evaluate the three factors, weight, reliability (as represented by complexity) and performance or mission value. The evaluation was performed by assigning numerical values to each factor for each concept. For example: Values of 2, 3, and 7 were assigned for weight, values of 1 through 8 for complexity and 1, 3, and 5 for performance. Fortunately the results tend to be in agreement with an intuitive evaluation.

As can be noted from the table the four concepts with best stores are:

- D. Multiple operation of a clutch by a single solenoid
- A. One shot declutching by an explosive device
- F. Over running sprag type clutch
- B. One shot declutching by an electrical solenoid

Of these four, number (F) must be ruled out since it has no reverse capability. Also, since (B) is basically a less desirable version of (A), we are left with only two concepts to consider.

Concept (D) meets the requirement for both free wheeling to improve odometer readings and of course, emergency decoupling. Its disadvantage of requiring continuous power in one position will need evaluation and further design study to determine if this disadvantage can be removed without placing this concept in the same class as device (E).

[redacted]

Wheel Declutching Study

Purpose: To provide emergency decoupling of a failed drive motor and/or free wheeling to improve odometer readings.

Concept	Advantages	Disadvantages	Wt. lbs	Weighted Value: Wt.	Weighted Value: Compl.	Weighted Value: Perf.	Total
A. One shot declutching by explosive device	1. Single engagement point on clutch 2. High reliability of actuator	1. Containment of explosive charge 2. Additional command	.10	2	1	5	8
B. One shot declutching by Electrical solenoid	1. Single engagement point on clutch 2. Simplicity	1. Additional command	.12	3	2	5	10
C. One shot declutching by means of a thermal wire actuator	1. Single engagement point on clutch	1. Additional command 2. Mechanical complexity	208	5	5	12	
D. Multiple actuation of a clutch by a single solenoid	1. Free wheeling to improve odometer reading possible	1. Solenoid power req'd in one position at all times 2. Additional command 3. Complexity 4. Multiple engagement points	.11	3	3	1	7
E. Multiple actuation of a clutch by a dual solenoid using over center spring	1. As for D above 2. Free wheeling to permit selective use of drive motors to improve efficiency	1. As for 2, 3, and 4 above in D.	.25	7	7	1	15
F. Over running sprag type clutch only	1. Free wheeling obtained whenever the motor is not driving 2. Simplicity 3. Automatic emergency mode in the forward direction	1. No reverse torque capability 2. No free wheeling capability in the reverse direction	.09	2	4	3	9
G. As for F with the addition of solenoid operated reverse pawl	1. Same as 1 and 3 for F 2. Can develop reverse torque 3. No separate command req'd	1. No emergency free wheeling in reverse 2. Complexity	.22	7	6	3	16
H. As for G with the addition of an emergency release of the sprag clutch	1. Same as 1, 2, and 3 for G 2. Emergency free wheeling in reverse direction	1. Complexity 2. Additional command circuit	.25	7	8	1	16

[redacted] 64-406

B. WHEEL DRIVE MOTORS

1. Method of Determining DC Motor Characteristics for SLRV Wheel Requirements

A method will be derived herein for determining the required dc motor characteristics to meet the operating wheel requirements of the Surveyor Lunar Roving Vehicle.

Assumptions

In determining the dc motor characteristics, the following assumptions have been made:

a) The dc motor speed-torque and current-torque characteristics are straight line relationships and proportional according to

$$y = mx + b$$

b) The motor speed-torque curve is proportional to the applied voltage and thus describes a family of parallel lines for various applied voltages.

c) The stall current of the motor is a function of the brush resistance according to $E = IR$.

d) The no-load current is a function of the losses in the motor -- windage, brush contact, and mechanical losses.

e) The no-load speed of the motor is described as the speed at which the back emf generated is equal to the applied voltage; thus, the motor can accelerate no further.

f) The stall torque is a function of the stall current, the permanent-magnet field strength, and a dc motor constant (different for each motor) according to:

$$T = K_t \Phi I_s \qquad \text{(III. 3-5)}$$

Direct Wheel Drive

The requirements for a direct dc motor wheel drive are dictated by the

[redacted]

295

operation requirements for the Surveyor Lunar Roving Vehicle. Torque requirements for the successful operation of a single vehicle wheel have been specified at 96 oz-in. at 10 RPM at the wheel and 960 oz-in. at stall. The dc motor speed-torque characteristics for a direct drive motor can then be illustrated below:

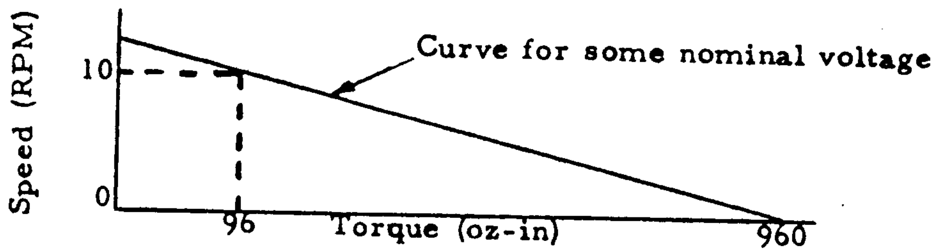

Using the above requirements, the characteristic equation for the required motor takes the form of

$$S_m = K'T + S_o$$

where S_m = motor speed

S_o = motor no-load speed

T = developed motor torque @ wheel

K' = slope of the speed-torque curve

Substituting for the numerical requirements yields

$$S_m \text{ (RPM)} = 11.12 - 1.16 \times 10^{-2} \text{(oz-in.)}$$

Gear Reduction

However, if an intermediate gear train is used to transmit the torque to the wheel, the foregoing equation must be modified by $S'_m = S_m N$

where N = gear train ratio

S'_m = motor speed dictated by S_m and N

Thus, for an intermediate gear train,

$$S'_m = N\ (11.12 - 1.16 \times 10^{-2}\ T).$$

DC Motor Characteristics

A family of dc motor speed-torque characteristic curves can be described by a characteristic equation of the form

$$T_m = KS_m + K_1E \qquad \text{(III. 3-6)}$$

where T_m = developed motor torque
S_m = motor speed
E = operating voltage
K = slope of speed-torque curve
K_1E = stall torque intercept

The motor constants, K and K_1, can be determined from data supplied with most dc motors.

The current torque characteristic of a dc motor is described by the equation:

$$T_m = K_2 i - T_o \qquad \text{(III. 3-7)}$$

where T_m = developed motor torque
i = motor current
T_o = torque intercept
K_2 = slope of the current-torque curve

In addition, the transmitted torque to the wheel (T) is a function of the motor torque, N, and the gear train efficiency (μ) according to:

$$T = \mu N T_m \quad \text{or}$$

$$T_m = \frac{T}{\mu N}$$

And substitution for T_m in Eq. (III. 3-6) and combining eq. (III. 3-5) and (3-6) yields:

$$T/\mu N = KN\ (11.12 - 1.16 \times 10^{-2}\ T) + K_1E \qquad \text{(III. 3-8)}$$

which relates a dc motor speed to the wheel torque and speed requirements as well as the gear train efficiency and reduction.

[redacted]

By substituting the two wheel operation requirements into Eq.(III. 3-8) for T, the two equations generated can be solved simultaneously for N. The operating voltage can then be determined for $S_m = 0$ using the stall torque requirement.

By using Equations (III. 3-6, 3-7,3-8) the specific dc motor characteristics can be calculated and checked for performance in the SLRV wheel drive.

[redacted]

2. SLRV Wheel Drive Motor Evaluations

To initially limit the scope of motor types considered for use in the SLRV, the following criteria were selected as primary design goals:

(1) Motor must be readily adaptable to the available power supplv

(2) Motor output power and speed must be consistent with the mission requirements.

(3) Available space envelope and motor weight are considered premium and must not exceed allocations.

By limiting the selection of motor type through the use of the above criteria, the final selection of a suitable SLRV motor or motors can be made with the following as design goals:

(1) Motor should provide maximum power output vs. weight.

(2) Motor should provide minimum power drain during SLRV operations.

(3) Motor should provide a minimum weight density (weight to volume ratio in ozs/in^3).

(4) Motor speed should be low to provide a minimum gear reducer ratio.

(5) Motor should provide operation in the specified temperature range.

(6) Motor selection must take into account necessity for hermetic sealing.

<u>Requirements</u>

Present specifications dictate a vehicle motor supply voltage of 28 vdc. Analysis of present weight allocations indicates that the wheel drive motor, gear reducer, filters, and associated equipment should not exceed 1.03 lbs. Envelope requirements are specified at a 3 inch diameter maximum with an overall length of 4.0 inches.

Note: This envelope includes provisions for hermetic sealing bellows and housing in addition to motor and associated equipment.

[redacted]

[redacted]

The torque requirements are 96 oz-in. at 10 rpm nominal operating mode and 960 oz-in. maximum.

AC Induction and Synchronous Motors

The prime reason for considering motors other than dc is the possibility of eliminating the problem of brushes in vacuum. The use of an ac motor could circumvent this problem and therefore warrant a discussion of their application to the SLRV.

Speed Torque Characteristics. The single phase ac induction (excluding the low inertia low torque servo motor) and the ac synchronous motors have typical speed-torque characteristics as follows:

Induction

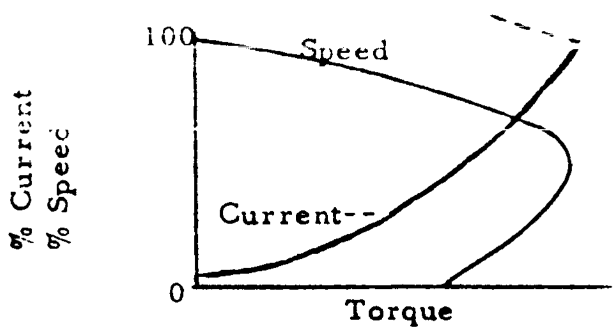

Synchronous

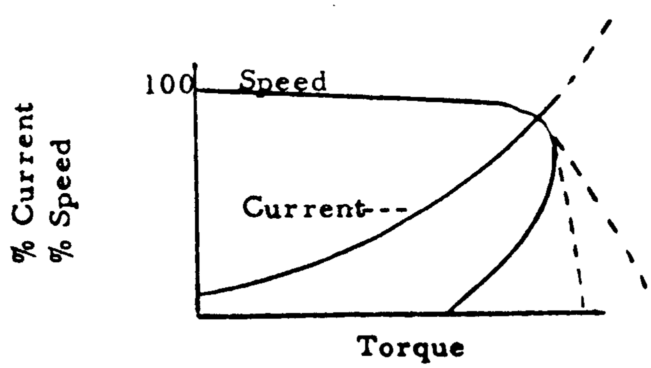

[redacted]

The application of either the induction or synchronous motors must consider the following speed-torque characteristics:

The speed-torque curve must have sufficient torque spread to accommodate both the nominal operating point and the maximum stall torque requirements. For the SLRV wheel drive this means that the spread must be greater than 1 order of magnitude or 1000% from the nominal operating torque to the maximum torque available. For example, a given induction or synchronous motor operating through a 2400:1, 60% efficient gear reducer will provide a nominal 96 oz-in. at 10 rpm at the wheel. The motor itself is loaded to .67 oz-in. This same motor then must provide 6.7 oz-in. maximum torque to meet the requirements of the vehicle.

The above considerations are for maximum torques only; the starting torques which can be somewhat less than the maximum are not considered. If necessary, starting torques can be adjusted to the maximum torques; further treatment will be given later in this section. The primary problem here is to find a motor with sufficient torque speed to accommodate the SLRV requirements.

Investigation of ac induction motors based upon the above indicate the following trends:

(1) In general, the lightweight single phase induction motors (less than one lb) operating 115 vac, 400 cps, are capable of providing the required torque in speed ranges varying from as low as 7000 RPM to as high as 22,000 RPM. See Table III.3-3.

(2) The lightweight polyphase induction motors operating on 200 vac and 400 cps are also capable of supplying the SLRV torque requirements. In this case speeds range from 8,000 RPM up to 22,000RPM. See Table III.3-4.

(3) A lightweight, 60 cps induction motor can be made to exhibit the SLRV torque requirements as illustrated in Table III.3-5. however, the bare motor alone weighs 0.01 lbs greater than the allocated weight of 1.03 lbs for the motor and associated equipment.

The maximum operating efficiency of the induction motor occurs near the maximum torque value. When the nominal operating point of the motor is far removed from the maximum efficiency point, as in the case of the SLRV requirements, the resultant operating efficiency occurs at the "low" for the system. In some cases, the SLRV torques require maximum operation below the maximum efficiency point. In each of these cases, there is a resultant loss of watt-hours and excessive motor and inverter heating. This in turn results in a needless battery or solar panel drain.

For a number of the motors maximum SLRV torque output will occur in the region of the "knee" of the speed-torque curve; i.e., the region between the starting torque and the maximum torques as illustrated below:

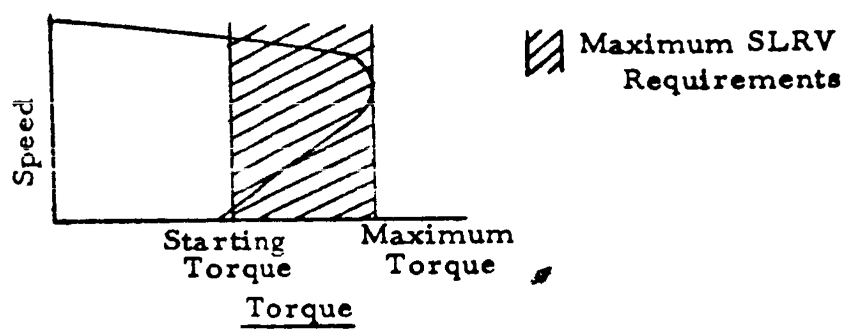

As indicated in the diagram, the motor would not function from "vehicle start" as the SLRV torque requirements exceed the motor starting torque. It would be desirable, then, to change the general motor characteristics to provide a compatible starting torque and operating torque.

By changing the rotor resistance sufficiently, the starting torque can be made to approach and/or equal the maximum motor torque as explained below:

From (1) the mathematical expression for the developed torque (T) as a function of the blocked rotor voltage (E_{rs}), slip (s), blocked rotor reactance (X_{rs}), and rotor resistance (R_{rs}) can be expressed as:

$$T = K \frac{sE_{rs}^2 R_{rs}}{R_r^2 + s^2 X_{rs}^2}$$

To maximize the torque as a function of the rotor resistance, take $\frac{dT}{dR_r} = 0$ with E_{rs} = constant. The solution becomes

$$R_r = \pm sX_{rs}$$

Therefore, the maximum torque occurs at the starting toroue when speed is zero and s is unity, thus making

$$R_r = X_{rs}$$

It should be noted that when the resistance is made eoual to the reactance, a compromise is made on motor performance. At nominal load conditions the rotor copper losses are high which reduces the power output and lowers the efficiency of the motor substantially.

In addition, from the above equality it can be seen that the maximum toroue developed by the motor:

$$T = K \frac{sE_{rs}^2 (\pm sX_{rs})}{(sX_{rs})^2 + s^2 X_{rs}^2} \qquad \text{or}$$

$$T = \pm K \frac{s^2 E_{rs}^2 X_{rs}}{2s^2 X_{rs}^2}$$

$$T_m = \pm K \frac{E_{rs}^2}{2X_{rs}}$$

Thus, to increase the maximum torque output when desirable, it is necessary to increase the applied voltage and/or decrease the inductive reactance of the rotor. It should be noted that for a given motor the X_{rs} is fixed. Decreasing the reactance initially is limited on small motors by miniaturization techniques in manufacturing of the parts.

Speed variations of up to 40% from no-load to full load are not significant for the selection of a motor provided the nominal operating speed of 10 RPM is maintained. Investigation of the ac synchronous motors has indicated the following trends:

(1) The synchronous motor operating on 115 v ac, 400 cps, single phase is, in general, not capable of supplying the maximum torque to the SLRV wheel and meet weight requirements. Refer to Table III. 3-6.

Although one motor can supply the required maximum, the maximum torque is over the starting torque; thus, changes would have to be made to bring the starting torque beyond the maximum. As with the induction motor, these changes would result in a low efficiency operation at maximum.

(2) The polyphase synchronous motor operating on 200 v ac and 400 cps is capable of supplying the required torques to the SLRV. The speed range is limited to 12,000 RPM. See Table III. 3-7.

(3) The single or polyphase synchronous motors operating on 115 or 200 v ac, and 60 cps are not capable of supplying the required torques. See Table III. 3-8.

Power Supply. The ac induction motor as well as the synchronous motor will require a dc to ac inverter to utilize the 28 v dc supply on the SLRV. A cursory inspection of the wheel drive power requirements indicates a motor power requirement in the range of 10 to 20 watts per wheel. Present information indicates that a suitable dc to ac inverter would have to be developed.

For example, Sorensen manufacturers a 25 watt dc to ac inverter which weighs 1.5 lbs. Temperature limitations are -30°C to 70°C or -22°F to +158°F. The inverter supplies 115 v ac at 400 cps up to a current capacity of .22 amps. Efficiency depending on the load ranges from 65 to 80%.

Factors to be considered here are temperature, current capacity, weight, and efficiency. By integrating the inverter into the compartment #2 electronics, the temperature problem can be minimized. It should be noted, however, that 6 units will be required to be placed in a compartment where space will become premium. Further development of an inverter might yield a model suitable for operation within the wheel drive temperature constraints.

Further development is also required to obtain a higher current capacity and a lower weight. In some cases at maximum load, the current drain may be as high as .8 amps depending upon the motor selection. The inverter weight to be compatible with the weight allocation should be reduced by one order of magnitude.

The inverter efficiency presents a problem for which no compromise can be made. The inverter with operating characteristics as previously mentioned would dissipate 20 to 35% of the input power as losses. For a motor requiring 15 watts at the maximum torque conditions, the losses could range from 4 to 8 watts per motor. For the total vehicle then the excessive drain from the battery or solar panels could be as high as 48 watts (sufficient power to drive 3 additional motors). Thus, development is required to obtain an inverter efficiency approaching unity.

Space Envelope and Weight. The envelope size is dictated by the size of the ac motor, RF filter, dc to ac inverter, and the gear reducer. A cursory inspection of the sizes of the lightweight ac motors indicates an envelope size of 1.25 in diameter with an overall length of 2.00 inches. Adequate room is available then to accommodate the gear reducer, filter, and bellows and crank. The inverter size may impose a problem if it cannot be integrated into the compartment electronics.

A few aspects of the weight problem have already been covered. The inverter poses the principal problem with the gear reducer following in importance. Weight reduction in the inverter might entail combining the inverter electronics with compartment electronics. As mentioned previously, a development program will be required in this area. A second area to be investigated is the gear reducer requirements. Reduction ratios for the ac motors can vary from 700 to 2200:1. In any case the higher reductions result in increased weights as stages of reduction are added. Selection of an ac motor would depend, then, on the weight to power ratios of the motors coupled with the lowest gear ratio.

<u>Summary</u>. (1) The ac induction motor can provide the torques required to drive the SLRV. (2) The synchronous motor torque outputs are marginal with respect to the maximum SLRV torque requirements. In addition, the synchronous motor supplies less torque than that of a similar size induction motor; thus, the synchronous motor shall be eliminated as a possible selection for the SLRV. (3) Selection of an ac motor can present a problem in the power supply. The necessary dc to ac inverter imposes weight, packaging, and efficiency problems which must be solved prior to definitization of ac motors for the SLRV. (4) The induction motor does not have brushes and therefore eliminates one of the reasons for hermetic sealing of the drive system.

DC Motors

The dc motor will in general have a linear speed variance from no load to full load torques. The dc motors then are particularly applicable to variable speed drives. In addition, the dc motor can readily be adapted to high torque applications.

Appendix B shows the methods used to establish the dc motor characteristics in conjunction with the SLRV wheel drive requirements.

This section will cover only the dc brush type motors, as brushless dc motors are considered in a separate section. In addition, only the permanent-magnet type dc motor is considered here since it is the lighter and smaller counterpart of the wound field type.

Speed Torque Characteristics. The dc motor must also provide sufficient torque spread to accommodate the nominal SLRV operating and maximum torque requirements. Since the dc motor has a general speed-torque characteristic described by $y = mx + b$, the maximum torque condition is at motor stall conditions. As previously mentioned the speed variance is of little significance provided the 10 RPM nominal operating speed is maintained. The dc motor lends itself well to mathematical determination of the required motor characteristics at optimum performance. The variable speed characteristics of the motor makes selection of suitable gear reducer ratios difficult except by mathematical determination.

Three types of permanent-magnet field motors exist: 1) the power variety characterized by few commutator segments, straight armature poles, relatively high speed and low torque; (2) the servo type, similar to the power type but with a greater number of commutator segments and skewed armature poles; and (3) the torque type with a large number of commutator segments, skewed armature poles, lower speed and higher torque.

Three motors, each representative of the type previously mentioned, were investigated for use in the SLRV wheel drive. It was determined that each motor could be utilized in the wheel drive. Moreover, each motor was substantially overpowered for this application and required a reduction of voltage to attain the given speed and torque (Refer to Table III. 3-9).

The efficiency of the dc permanent-magnet motor lends itself well to the SLRV application. The maximum efficiency of these motors occurs in a range of 20 to 40% of stall torque. Thus, the operating torque occurs near the maximum efficiency torque. Slight increases in operating torques during roving operations will result in even more efficient operation. The short term maximum torque condition, however, will occur at minimum efficiency.

Power Supply. The dc motor adapts itself to the available power supply with no accessory equipment. The selected dc rotor can be wound to accommodate 28 volts dc with no increase in weight and little or no change to the required performance characteristics.

Space Envelope and Weight. The space envelope required for dc motor operation is specified by the size of the motor, rf filter, and the gear reducer. Motor sizes vary with configurations as indicated by the sizes of the three motors in Table III. 3-9 as shown below:

	Length	Width	Height	Diameter
CPPC	1.38	--	--	.75
Globe	1.38	--	--	.875
Inland	1.0	1.0	1.0	--

All of the above motors readily meet the space envelope.

The weight of the permanent-magnet dc motor is inherently low in small sizes. The primary weight consideration in using the dc motor (other than its own weight) is the gear reducer weight. The reduction ratios for the dc power train vary from 365 to 1780 : 1. Again the higher reductions result in increased weight to do the same job as the lower reduction systems. Selections of the dc motors will depend on the weight to power ratios of the motors with gear reduction.

Summary. (1) The permanent-magnet dc motor can provide the torques required to drive the SLRV. (2) The dc motor inherently has speed-torque characteristics that readily match SLRV requirements. (3) The dc motor will operate directly off the available power supply.

Stepping Motors

The stepping motor is an incremental drive mechanism utilizing either ac or dc pulse activation. The motors are categorized into two distinct groups, mechanical and magnetic steppers. The mechanical steppers are essentially rotorary, solenoid actuated indexing devices while the magnetic stepper is an electric motor (usually modified ac design) operating either on an ac or dc supply. The mechanical stepper utilizes mechanical detents for torque holding and operate at relatively higher torques and low speeds. In general, the magnetic types secure the shaft by magnetic means and operate at somewhat lower torque levels and higher speeds than comparable mechanical types.

Performance Characteristics. The stepper motor speed is specified in terms of steps per second with the step equal to a specified angle of rotation. The stepper speed can be converted to nominal motor speed in rpm by the following manipulation:

$$\text{Motor Speed (RPM)} = S_s \times \frac{1}{R} \times 60 \quad \text{where}$$

S_s = Stepper speed in steps per second

R = Stepper rotation in steps per 1 revolution

In general, the stepper speed is a constant with the stepper rotation providing a wide selection of values. In addition, as the stepper rotation increases, the resultant speed decreases proportionally and likewise the required gear reducer ratio decreases in the same proporation. The stepper torque requirement, however, increases as the gear ratio is reduced. In some cases it may be necessary to decrease the stepper rotation to provide sufficient torque to perform on the SLRV. A limitation as to the extent of the decrease in stepper rotation is the resultant impacts or rough, hammering drive effect from the inherent acceleration and deceleration, through a large angle of rotation. Thus, it may be necessary to compromise between the smoothness of the drive and the operating speed.

The stepper output is analyzed with respect to two factors of the driven load to determine performance. These factors are the friction load of the driven mechanism (the required torques) and the inertia load of the driven body.

A critical limitation on the mechanical type stepper is its duty cycle while the magnetic type stepper has some critical weight problems associated with the motor and additional circuitry.

Data for the investigation on stepping motors was derived from Product Engineering, Volume 34, No. 3 and product catalogs.

Mechanical Stepping Motors. An investigation of the types of mechanical stepping motors has revealed the following (Refer to items (1) and (2) on pages III. 3-50 and III. 3-51.

Both the rotorary solenoid and ratchet and pawl type mechanical steppers are inadequate for use in SLRV. In both cases, the duty cycle is not continuous, and would result in cyclic operation of the wheel drive. In addition, the rotorary solenoid type does not have sufficient output to meet the torque requirements of the SLRV.

Magnetic Stepping Motors. The magnetic stepping motors are inherently continuous duty cycle devices. An investigation of the various types of magnetic steppers has revealed the following (refer to items (3) through (8) on pages III. 3-51 through III. 3-56:

Of the seven types of magnetic steppers investigated,

(1) Rotary transmitter and follower
(2) Sequential, permanent magnet rotor
(3) Cyclical, permanent-magnet rotor
(4) Permanent-magnet stator
(5) Variable reluctance
(6) DC synchronous stepper
(7) AC stepper

only two (items (4) and (5)) meet the specified torque, weight and envelope requirements of the SLRV. The permanent-magnet stator and the variable reluctance types of magnetic steppers are also capable of operation directly from the 28 vdc supply of the SLRV.

Summary. (1) The mechanical type stepping motors are not adequate for use in the SLRV. The fractional duty cycle of the mechanical stepper does not lend itself to the continuous operation required by SLRV. (2) The permanent-magnet stator and variable reluctance stepping motors (representative of magnetic steppers) provide the required SLRV torques within the weight and space envelope allocations and can be readily adapted to the dc power source of the SLRV.

Brushless DC Motors

Information on the dc brushless motor from Lamb Electric Division of Ametek, Inc., indicates that a brushless dc motor of weight and torque output that is required for SLRV is presently not feasible. Considerable development would have to be done to obtain a motor in the 3-4 oz. weight range with torques comparable to the miniature, permanent-magnet dc motors.

At the present time, Lamb has a brushless motor slightly less than one pound; however, it does not meet the speed-torque requirements of a direct drive for the SLRV and a gear reducer would add sufficient weight to cause the motor to exceed the drive mechanism weight allocation.

Motor Type Selection

Tables III. 3-10 and III. 3-11 show the tabulations of the power characteristics for the applicable ac induction, magnetic stepping, and dc permanent-magnet motors. As mentioned previously the selected motor should provide a maximum power to weight ratio. As indicated in Tables III. 3-10 and 3-11, five motors show favorable power to weight ratios. These motors are two highpower induction motors, the Kearfott AB-7-1 and the Westinghouse 78-480, and the three dc motors of Table III. 3-11. In each case, the motor has a high efficiency which ranges from 55 to 68%.

In terms of weight density the dc motors have values of 2.2, 2.3, and 2.8 oz/in^3 for the Globe CPPC, and Inland motors, respectively. The ac motors have weight densities of 1.63 and 3.09 oz/in^3 for the Westinghouse and Kearfott motors, respectively.

Although the ac motors have substantially better power to weight characteristics and comparable weight densities to the dc motors, two other important factors must be considered: (1) the amount of power drain including that of the inverter, and (2) the gear reducer required to operate the wheel drive to the requirements.

Tables III. 3-12 & 3-13 show the tabulations of SLRV wheel drive ac and dc motor characteristics. The overall operating efficiency shows that both the ac motors exhibit high losses at the nominal operating point such that the efficiency is 3 to 5 times lower than those obtained using the dc motors. In addition, the ac system efficiency is further degraded by the inverter efficiency such that the difference between ac and dc operation efficiency becomes as high as 4 to 6 times.

Each of the motors will require development to meet the temperature requirements of 0°F to 400°F operating range.

Although the dc motors will require hermetic sealing to protect the brushes, the weight increase for the hermetic sealing is more than compensated for through the difference in weights between the ac motors and the dc motors. For example, the Kearfott motor and the ideal inverter might attain a minimum of 10.2 ozs. with no hermetic sealing required. The heaviest dc motor presented herein is the Inland which is 2.8 ozs. The addition of hermetic sealing requires an inner housing and flange and bellows, the weights of which are listed below:

Inner housing and flanging estimate	.352 lbs. or 5.63 ozs.
Bellows estimate	.005 lbs. or .08 oz.

Thus, the total weight of the Inland motor with a hermetic seal would amount to approximately 8.41 ozs., the approximate weight of the ac motor without accessories.

Selection of the proper dc motor for use in the SLRV wheel drive will also result in the selection of a low gear reducer ratio which will increase reliability, efficiency, and decrease weight.

Summary

The selection of the dc permanent-magnet motor for use in the SLRV wheel drive is evident for the following reasons:

(1) The dc motor provides a higher overall system efficiency at the required SLRV operating torques than do the ac motors.

(2) The dc motor weight in conjunction with its associated hermetic sealing capabilities is less than the comparable ac motor and its accessory electronics. The inverter electronics can impose thermal control and compartment space problems for the dc motor adapts to the environment and the wheel mechanism space envelope.

(3) A dc motor selection of the "Inland class" will provide a low ratio gear reducer which increases reliability through the small number of stages and also decreases weight and increases efficiency.

TABLE III.3-3 - "Off-the Shelf", Small A-C Induction Motors

Voltage	115 v. ac
Frequency	400 cps
Phase	Single

Manufacturer	Model	Motor Speed	Gear Reduction Ratio to Maintain 10 RPM @ Wheel	Nominal Req'd Motor Torque	Maximum Req'd Torque	Available Torque	Weight	Suitability
A. Research	--	7,500	750	.214	2.14	2.0	.45	No
A. Research	--	7,000	700	.23	2.3	2.6	.45	Yes
A. Research	--	11,500	1,150	.139	1.39	1.45	.45	Yes
Air Marine	M2121-4	21,000	2,100	.075	.76	.8	.34	Yes
Air Marine	M2121-5	21,500	2,150	.075	.75	1.15	.50	Yes
Air Marine	M2141-5	11,000	1,100	.145	1.45	1.10	.50	No
Air Marine	M2161-2	7,100	710	.225	2.25	.90	.50	No
Air Marine	A2124-1	22,000	2,200	.073	.73	2.2	.70	Yes
Air Marine	A2141-1	10,000	1,000	.16	1.6	1.6	.66	Yes
American	4101	12,000	1,200	.133	1.33	1.6	--	Yes
American	5101	11,800	1,180	.135	1.35	3.5	--	Yes
Barber-Colman	Aylo 6766	10,500	1,050	.157	1.57	.36	.80	No
Barber Colman	Aylo 6876	10,500	1,050	.157	1.57	.35	.60	No
Calco	--	10,600	1,060	.156	1.56	2.2	.50	Yes
Control Data	5001	8,000	800	.20	2.0	.3	.25	No
Control Data	5000	12,000	1,200	.133	1.33	.35	.25	No
Kearfott	A-10-11	10,500	1,050	.157	1.57	.35	.22	No
Western Gear	KH36V1	11,800	1,180	.135	1.35	.6	.37	No
Chicago Pneumatic	V-1	10,200	1,020	.156	1.56	5.66	.80	Yes
Chicago Pneumatic	T-1	9,600	960	.167	1.67	3.96	.26	Yes

[redacted] 64-406 Vol II App

TABLE III.3-4 - "Off-the-Shelf", Small A-C Induction Motors

Voltage 200 v. ac
Frequency 400 cps
Phase 2 & 3

Manufacturer	Model	Motor Speed	Gear Reduction Ratio to Maintain 10 RPM @ Wheel	Nominal Req'd Motor Torque	Maximum Req'd Torque	Available Torque	Weight	Suitability
A. Research	--	10,000	1,000	.16	1.6	2.9	.45	Yes
Air Marine	M2143-4	10,000	1,000	.16	1.6	1.3	.34	No
Air Marine	M2183-1	5,200	520	.308	3.08	.65	.50	No
Air Marine	A2146-4	11,000	1,100	.145	1.45	1.4	.70	Yes
Air Marine	S2143	8,000	800	.2	2.0	2.0	.31	Yes
Chicago	R--	10,550	1,055	.152	1.52	5.35	.26	Yes
Westinghouse	78-480	11,800	1,180	.136	1.36	18	.5	Yes
Kearfott	AB-7-1	24,000	2,400	.067	.67	4	.5	Yes
Kearfott	B-5-1	5,400	540	.297	2.97	4	.5	Yes

[redacted]

TABLE III. 3-5 - "Off-the-Shelf", Small A-C Induction Motors

Voltage 115 v. & 200v. ac+
Frequency 60 cps
Phase 1 & 3+

Manufacturer	Model	Motor Speed	Gear Reduction Ratio to Maintain 10 RPM @ Wheel	Nominal Req'd Motor Torque	Maximum Req'd Torque	Available Torque	Weight	Suitability
Air Marine	A1121-26	3,100	310	.515	5.15	1.3	.60	No
Air Marine	A1121-26	3,100	310	.515	5.15	2.4	1.04	No
Air Marine	A1123-11+	3,100	310	.515	5.15	3.6	.66	No
Air Marine	A1123-7+	3,100	310	.515	5.15	7.5	1.04	Yes
Alliance	JS0300	3,300	330	.485	4.85	-	.75	No
Alliance	HS0300	2,500	250	.64	6.4	.3	.75	No

TABLE III.3-6 - "Off-the-Shelf", Small Synchronous Motors

Voltage	115 v. ac
Frequency	400 cps
Phase	Single

Manufacturer	Model	Motor Speed	Gear Reduction Ratio to Maintain 10 RPM @ Wheel	Nominal Req'd Motor Torque	Maximum Req'd Torque	Available Torque	Weight	Suitability
Air Marine	A2764-6	8,000	800	.20	2.0	.70	.70	No
Air Marine	A2744-1	12,000	1,200	.133	1.33	.80	1.08	No
Globe	18A 103	24,000	2,400	.067	.67	.78	.4	Yes
Globe	18A 114	12,000	1,200	.133	1.33	1.15	.4	No
Globe	18A 250	8,000	800	.20	2.0	.50	.4	No
Globe	C-53A-106-2	12,000	1,200	.133	1.33	.24	.15	No
SM/I	15HI-9	24,000	2,400	.067	.67	.2	.36	No
SM/I	15HI-9	12,000	1,200	.133	1.33	.2	.36	No
SM/I	11HI-17	8,000	800	.20	2.0	.1	.15	No
SM/I	11HI-22	12,000	1,200	.133	1.33	.17	.15	No

TABLE III. 3-7 - "Off-the-Shelf", Small Synchronous Motors

Voltage	200 v. ac, 115+v.ac
Frequency	400 cps
Phase	2 & 3

Manufacturer	Model	Motor Speed	Gear Reduction Ratio to Maintain 10 RPM @ Wheel	Nominal Req'd Motor Torque	Maximum Req'd Torque	Available Torque	Weight	Suitability
Air Marine	A2766-13	8,000	800	.20	2.0	1.0	.70	No
Air Marine	C2766-1	8,000	800	.20	2.0	1.8	1.08	No
Air Marine	A2746-1	12,000	1,200	.133	1.33	1.0	.70	No
Air Marine	A2746-2	12,000	1,200	.133	1.33	1.5	1.08	Yes
Globe +	75A-106-2	12,000	1,200	.133	1.33	1.5	.72	Yes
Globe +	75A-106-1	11,500	1,150	.139	1.39	4.5	.72	Yes
Globe +	18A 251	12,000	1,200	.133	1.33	1.4	.4	Yes
SM/I	11HI-61	12,000	1,200	.133	1.33	.15	.15	No
SM/I	11HI-67	6,000	600	.266	2.66	.1	.25	No

TABLE III.3-8 - "Off-the-Shelf", Small Synchronous Motors

Voltage 115 v & 200+ v.ac
Frequency 60 cps
Phase 1 and 3+

Manufacturer	Model	Motor Speed	Gear Reduction Ratio to Maintain 10 RPM @ Wheel	Nominal Req'd Motor Torque	Maximum Req'd Torque	Available Torque	Weight	Suitability
Air Marine	A1724-3	3,600	360	.445	4.45	1.0	.70	No
Air Marine	A1726-1+	3,600	360	.445	4.45	1.3	.70	No
Air Marine	A1726-3+	3,600	360	.445	4.45	1.8	.70	No
Globe	18A107	1,800	180	.89	8.9	1.05	.4	No
Globe	18A108	3,600	360	.445	4.45	.7	.4	No
Globe	144A100-4	1,700	170	.94	9.4	1.05	.45	No
Globe	144A100-2	3,600	360	.445	4.45	1.05	.45	No

TABLE III. 3-9 - D-C Motor Characteristics (power, servo, and torque types) for SLRV Wheel Drive

Manufacturer	Model	Operating Motor Speed	Gear Reduction Ratio to Maintain 10 RPM @ Wheel	Nominal Req'd Torque	Maximum Req'd Torque	Available Torque	Weight	Suitability
CPPC	#8	17,800	1,780	.09	.9	.9	.0875	Yes
Globe	SS	8,690	869	.184	1.84	1.34	.125	Yes
Inland	T-0701B	3,650	365	.44	4.4	4.4	.175	Yes

[redacted]

64-4706

TABLE III.3-10 - Power Characteristics, A-C and Stepper Motors

Manufacturer	Model	Speed (RPM)	Max. Eff. Torque (oz-in.)	Eff. (%)	Weight (oz)	P_{in} (watts)	P_{out} (max) (watts)	P_{out} / unit wt. @ max. output (watts/oz.)
AiResearch	--	7,000	2.2	20	7.2	33.9	6.8	.945
AiResearch	--	11,500	1.3	35	7.2	25	8.65	1.2
Air Marine	M2121-5	21,000	1.0	60	8.0	22.5	14.5	1.82
Air Marine	A2141-1	10,000	1.75	42.5	10.5	29	12.3	1.17
Air Marine	S2143	8,000	.75	31.4	4.95	15	5.17	1.04
American	4101	12,000	1.3	47	10.5	17.1	10.7	1.02
American	5101	11,800	2.8	65	12.0	28.4	22	1.83
Calco	--	10,600	2.3	--	8	--	8.48	1.06
Kearfott	B-5-1	5,400	2.25	25	8	17.5	10	1.25
Westinghouse	78-480	11,200	9.0	64	8	61.5	120	15.0
Kearfott	AB-7-1	22,000	2.25	55	8	38	59	7.39
Permanent-Magnet		3,000	--	--	14.5	--	8.9	.614
Stator		6,000	--	--	8.6	--	10.2	1.19
Variable Reluctance		1,250	--	--	13.6	--	8.52	.627

[redacted]

301

TABLE III.3-11 - Power Characteristics, D-C Motors

	% of Stall Torque	Torque (oz-in)	Input Power (watts)	Output Power (watts)	Eff. %	P_{out}/unit wt (watt/oz)
Inland-T-0701B @ 28 volts	25	1.75	11.2	4.25	38	
	50	3.5	22.2	10.3	46	3.68
	75	5.25	3.5	8.5	27	
	(peak eff. @ 33%)	2.3	14.0	9.5	68	
Globe SS @ 27 volts	25	.585	7.17	3.8	53	
	50	.17	12.5	5.5	44	2.75
	75	1.76	17.8	4.1	23	
	(peak eff. @ 21%)	.5	6.36	3.5	55	
CPPC @ 28 volts	25	.25	5.5	3.27	59.5	
	50	.5	11.4	5.07	44.5	3.61
	75	.75	16.5	4.05	24.5	
	(peak eff. @ 25%)	.25	5.5	3.27	59.5	

All calculations based upon manufacturer's data.

[redacted]

TABLE III.3-12 - Tabulation of Wheel Drive A-C Motor Characteristics

TORQUE REQUIREMENTS T = 96 oz-in @ 10 RPM @ Wheel
T_{stall} = 960 oz-in @ Wheel

MOTOR	Kearfott*	Westinghouse*
Assumed Gearbox-Wheel Bearing Eff. (%)	[illegible]	60
Gearbox Ratio	2,400	1,180
Maximum Torque (oz-in.)	.67	1.36
Motor Torque for 96 oz-in. @ Wheel (oz-in.)	.067	.136
Motor Maximum Torque Speed (RPM)	23,500	11,700
Motor Speed @ 10 RPM_w (RPM)	24,000	11,800
Impact Motor Power @ Maximum (watts) @ Motor	20	25.2
Input Motor Power @ 10 RPM_w (watts) @ Motor	15.6	15.0
Wheel Power @ 10 RPM_w (watts)	.71	.71
Overall System Eff. (%) (Motor to Wheel)	4.65	4.74
Input Motor Power @ 10 RPM_w (watts) (including inverter losses at 90%)	17.35	16.7
OVERALL SYSTEM EFF. (%) (including inverter losses)	4.1	4.25

* All calculations are based on manufacturer's data

[redacted]

TABLE III. 3-13 - Tabulation of Wheel Drive D-C Motor Characteristics

TORQUE REQUIREMENTS $T = 96$ oz-in. @ 10 RPM @ Wheel
$T_{stall} = 960$ oz-in. @ Wheel

MOTOR	Inland T-0701B	Globe SS*	CPPC*
Assumed Gearbox - Wheel Bearing Eff. (%)	60	60	60
Gearbox Ratio	365	869	1,780
Motor Stall Torque (oz-in.)	4.4	1.84	.9
Motor Torque for 96 oz-in. @ Wheel (oz-in.)	.44	.184	.09
Motor No Load Speed (RPM)	4060	9600	19,700
Motor Speed @ 10 RPM_w (RPM)	3650	8690	17,800
Input Motor Power @ Stall (Watts)	16.2	15.2	17.2
Input Motor Power @ 10 RPM_w (Watts)	2.46	2.95	3.89
Wheel Power @ 10 RPM (Watts)	.71	.71	.71
OVERALL SYSTEM EFFICIENCY (%)	29	24	18.3

* All calculations are based upon manufacturer's data.

GENERAL STEPPING MOTOR PERFORMANCE

(1) Ratchet & Pawl Type

Stepper speeds:

60 steps/sec. @ 10 to 64 steps/revolution

Comparable RPM ranges:

57 to 360 RPM

Gear reducer ratios* to maintain 10 RPM_{wheel}:

5.7 (min.) and 36 (max.)

Required torques:

@ 10 RPM, 3.14 oz-in. (min.) and 19.8 oz-in. (max.)

@ max. T, 31.4 oz-in (min.) and 198 oz-in. (max.)

Inertia load:

16.6 gm-cm^2 (min.) and 105 gm-cm^2 (max.)

Rated motor capacities:

torque = 47 oz-in.

inertia = 10^3 gm-cm^2

Comments

It is evident that the stepper will have to be operated near the maximum speed range to provide the required SLRV torques. Near the maximum speed, the inertia and torque values of this type stepper are adequate to meet the required values.

It should be noted that the duty cycle for this type mechanical stepper is only 60%. Since the SLRV will require a continuous duty cycle, this stepper is not adequate for SLRV usage.

* Note: Gear reducer efficiencies will be selected per the following table of values:

below 100 -----	85%
100 to 500 -----	80%
500 to 1000 ----	70%
1000 or more --	60%

(2) Rotary Solenoid Type

Stepper speeds:

4 to 15 steps/sec @ 8 to 24 steps/revolution

Comparable RPM ranges:

.4 to 114 RPM

Gear reducer ratios to maintain 10 RPM wheel:

1 (min.) and 11.4 (max.)

Required torques:

@ Max. T 9.8 oz-in (min.) and 96 oz-in. (max.)

Rated capacities:

torque = 1 oz-in.

inertia = 25 gm-cm^2

Comments

This type stepper cannot meet either the torque or inertia requirements imposed by the SLRV.

In addition, its maximum duty cycle is only 56%.

(3) Rotary Transmitter and Follower

Stepper speeds:

2.5 to 120 steps/sec @ 12, 24, and 120 steps/revolution

Comparable RPM ranges:

.125 to 600 RPM

Gear reducer ratios to maintain 10 RPM_{wheel}:

1 (min.) and 60 (max.)

Required torques:

@ 10 RPM, 1.89 oz-in. (min.) and 96 oz-in (max.)

@ max. T, 18.9 oz-in. (min.) and 960 oz-in (max.)

Inertia load:

9.5 gm-cm^2 (min.) and 597 gm-cm^2 (max.)

Rated capabilities:

torque = 55 oz-in. (max.)

Inertia = ?

Comments

The stepper motor torques range from 0.7 oz-in. up to 55 oz-in. and correspond to weight allocations from 2.5 oz. to 10 lb. Assuming a linear scaling factor, the comparable stepper weight to achieve the 18.9 oz-in. of torque would be 55.3 oz. or 3.46 lbs. In addition, extra weight must be added to accommodate the motor control circuitry. In any case the weight exceeds the allocated SLRV motor wheel drive requirements.

(4) Sequential, Permanent-Magnet Rotor Type

Stepper speeds:

145 to 400 steps/sec. @ 4 to 16 steps/revolution

Comparable RPM ranges:

544 to 6000 RPM

Gear reducer ratios to maintain 10 $\text{RPM}_{\text{wheel}}$:

54.4 (min.) and 600 (max.)

Required torques:

@ 10 RPM, .2 oz-in. (min.) and 2.08 oz-in (max.)

@ max T, 2 oz-in. (min.) and 20.8 oz-in. (max.)

Inertia load:

.95 gm-cm^2 (min.) and 11 gm-cm^2 (max.)

Rated capacities:

torque = .08 oz-in.

inertia = ?

Comments [redacted]

This type stepper provides proper weight characteristics, but the torque output is well below that required to drive the SLRV.

A possible trend in the magnetic stepper motors seems evident; when the torque is sufficient to maintain the SLRV, the weight will be in excess of the requirements and vice-versa.

(5) Cyclical, Permanent-Magnet Rotor Type

Stepper speeds:

80 steps/sec @ 24 steps/revolution

Comparable RPM:

192 RPM

Gear reducer ratio to maintain 10 RPM_{wheel}:

14.2

Required torques:

@ 10 RPM, 5.9 oz-in.

@ max. T, 59 oz-in.

Inertia load:

31 gm-cm^2

Rated capacities:

torque = 2 oz-in.

inertia = ?

Comments

This type stepper does not have sufficient power output to accommodate the SLRV requirements.

(6) Permanent-Magnet Stator Type

Stepper speeds:

1000+ steps/sec @ 10 or 20 steps/revolution

Comparable RPM:

3000 or 6000 RPM

Gear reducer ratios to maintain 10 RPM_{wheel}:

300 and 600

Required torques

@ 10 RPM, .23 oz-in. and .4 oz-in.

@ max. T, 2.3 oz-in. and 4 oz-in.

Inertia load

.95 gm-cm^2 and 1.99 gm-cm^2

Rated capacities:

torque = 5 oz-in.

inertia = ?

<u>Comments</u>

This type stepper is capable of meeting the SLRV torque requirements at either motor speed.

Stepper torque variance is 0.7 oz-in. to 5 oz-in. with a corresponding weight variance of 3 to 18 oz. For the required torques of 2.3 and 4 oz-in., the respective weights for linear scaling are 8.6 oz. and 14.5 oz. In addition, this stepper requires no special control circuitry and thus the motor weight is the total considerdd weight.

Although the maximum inertia load is not specified, it is likely that the load is within a range of acceleration compatible with SLRV.

It should be noted, however, that the envelope size of 2 x 3 x 1 indicates a possible problem in fitting the motor to the wheel mechanism envelope and still providing sufficent space for a gear reducer, filters, and hermetic sealing.

(7) <u>Variable Reluctance Type</u>

Stepper speeds:

500 and 1600 steps/sec @ 24 to 120 steps/revolution

Comparable RPM ranges:

@ 500 steps/sec, 250 to 1250 RPM

@ 1600 steps/sec, 800 to 4000 RPM

Required torques:

500 steps/sec

@ 10 RPM .96 oz-in (min.) and 4.53 oz-in. (max.)

@ max T, 9.6 oz-in. (min.) and 45.3 oz-in. (max.)

1600 steps/sec

@ 10 RPM, .3 oz-in (min.) and 1.5 oz-in (max.)

@ max. T, 3 oz-in (min.) and 15 oz-in (max.)

Inertia load:

@ 500 steps/sec, 4.77 gm-cm^2 (min.) and 23.8 gm-cm^2 (max.)

@ 1600 steps/sec, 1.49 gm-cm^2 (min.) and 7.45 gm-cm^2 (max.)

Rated capacities:

torque = 30 lb-in. @ 500 steps/sec

and 1 oz-in. @ 1600 steps/sec

Comments

The SLRV torque requirements can be satisfied by either the low speed or high speed reductions for the 500 step/sec design. The 1600 step/sec design is not adequate at eithr reduction.

For a torque variance of 1.0 oz-in. to 480 oz-in. (30 lb-in.) athere is a corresponding weight variance of .7 oz. to 720 oz. Thus, for the high speed reduction torque of 9.6 oz-in and the low speed reduction torque of 45.3 oz-in. the corresponding weights are 13.6 oz. and 67.2 oz.

The high speed reduction provides the necessary torques within the given weight allowance.

It should be noted that this motor requires a control circuit consisting of a logic unit and amplifier which could increase the weight beyond the designated limits.

(8) DC Synchronous Stepping and AC Stepping Types

Comments

The dc synchronous stepping motor exceeds both the weight and envelope limitations. Smallest of this type weighs approximately 4 lbs. with an envelope size of 4 x 4 x 6 inches.

The ac stepping motor also exceeds the weight limitation which is further increased by the control circuitry and the additional weight of the dc to ac inverter.

C. SOIL BEARING STRENGTH MEASUREMENTS

Introduction

Broadly speaking, there are two definitions for soil bearing strength: one is defined by Terzaghi[(1)*] as the critical load of incipient soil failure through plastic flow, and the other is defined by the relationship between load and sinkage after plastic deformation has taken place.[(2, 3)]

The first case can be expressed by the equation

$$p = cN_c + 2N_q + 1/2\ \gamma\, bN \tag{III.3-9}$$

where

p = bearing capacity in the broad sense (psi)

c = soil cohesion (psi)

q = surcharge (psi)

γ = soil density (lb/cu ft)

b = smaller dimension of loading area (in.)

and

N_c, N_q, N_γ = bearing capacity factors which are functions only of the soil angle of friction, θ (dimensionless).

The second case can be expressed by the equation

$$p = \left[\frac{k_c}{b} + k_\theta\right] z^n \tag{III.3-10}$$

which was previously given in the discussion on Vehicle Systems.

---

*Raised numbers in parentheses refer to references listed on page III.3-87.

[redacted]

In both cases the bearing capacity depends not only on the mechanical properties of the soil, but also on the size of the loading area.

There is no formal relationship between Eq. (III. 3-9 & 3-10), since Equation (9) describes a situation before appreciable sinkage takes place, while Equation(10) describes the load-sinkage process after plastic deformation of the soil has started. Furthermore, both equations are of an empirical nature. Since a rigorous general solution of the relationship between bearing capacity p and sinkage z does not exist and probably will not be forthcoming in the foreseeable future,[4, 5] Equation(10) has been accepted as a basis of prediction by a growing number of students of the problem, particularly with respect to the mechanics of off-road locomotion.[6, 7]

It may be pertinent to mention that Eq. (III.3-10) is nothing more than an empirical equation that fits families of experimental curves obtained from tests in a homogeneous semi-infinite media, within load and deformation limits that are normally of interest in land locomotion studies It is used in load-sinkage studies because it provides the minimum soil properties needed to quantitatively predict load-sinkage relationships of large loading areas. This information is provided by penetration tests performed by two plates of different dimensions. One advantage of using Equation(10) lies in its exponential form. Plotting values of p(z) on a log-log scale results in a simple method of solution for k_c, k_θ and n, as discussed under Vehicle Systems.

As mentioned above, to determine bearing capacity from Eq. (III. 3-10) penetration tests are required with two plates of different sizes, wherein z is obtained as a function of p. Plotting the p - z values on a log-log coordinate system results in two, essentially straight, parallel lines for the case of a homogeneous soil. Curvature does exist at relatively low sinkage, but at this condition plastic failure has not yet taken place and therefore Equation(10) does not apply. In this region Terzaghi's equation for bearing capacity (Eq. III. 3-9 should be used. Therefore, the soil parameters k_c, k_θ, and n are not affected by the curved portions and can be computed as described under Vehicle Systems.

[redacted]

Having determined these values, it is then possible to predict the load-sinkage relationship for any size plate in the same soil conditions.

EXAMPLE

Fig.III.3-5 shows experimental p-z curves obtained in snow with plates of 3, 6, 9 and 12-inch diameter. The p-z relationships for the 3, 6 and 9-inch plates are plotted in Fig.III.3-6. The values k_θ, k_c and n can then be obtained from any pair of the above plates, and the results used to predict the load-sinkage characteristics for the 12-inch plate.

Fig.III.3-7 shows measured-versus-predicted results for a 12-inch plate based on results obtained from the 3 and 6-inch combination, and from the 6 and 9-inch combination. As is to be expected, the calculated results obtained from the 6 and 9-inch pair correlate with the 12-inch plate's measured values with a higher degree of accuracy than do the results from the 3 and 6-inch combination. However, for most uses, both predictions can be considered satisfactory, especially at the higher pressures. Based on experience to date, it appears, depending on the soil type, that test plates of at least 2 or 3 inches in diameter are required to satisfactorily determine load-sinkage relationships for larger plates on the order of up to 12 inches

NON-HOMOGENEOUS SOILS

This method can also be extended to the case of non-homogeneous stratified media. For instance, Fig.III.3-8 is composed of a set of curved lines and shows a typical log-log plot for a stratified soil. Such a plot can be considered to consist of two sets of lines characterized by two sets of k and n values. The set to be used for prediction purposes will then depend on the pressure range of interest.

INSTRUMENTATION

To obtain experimental load-sinkage data, quasi-static tests are normally conducted using an instrument called a "Bevameter", shown and described under

[redacted]

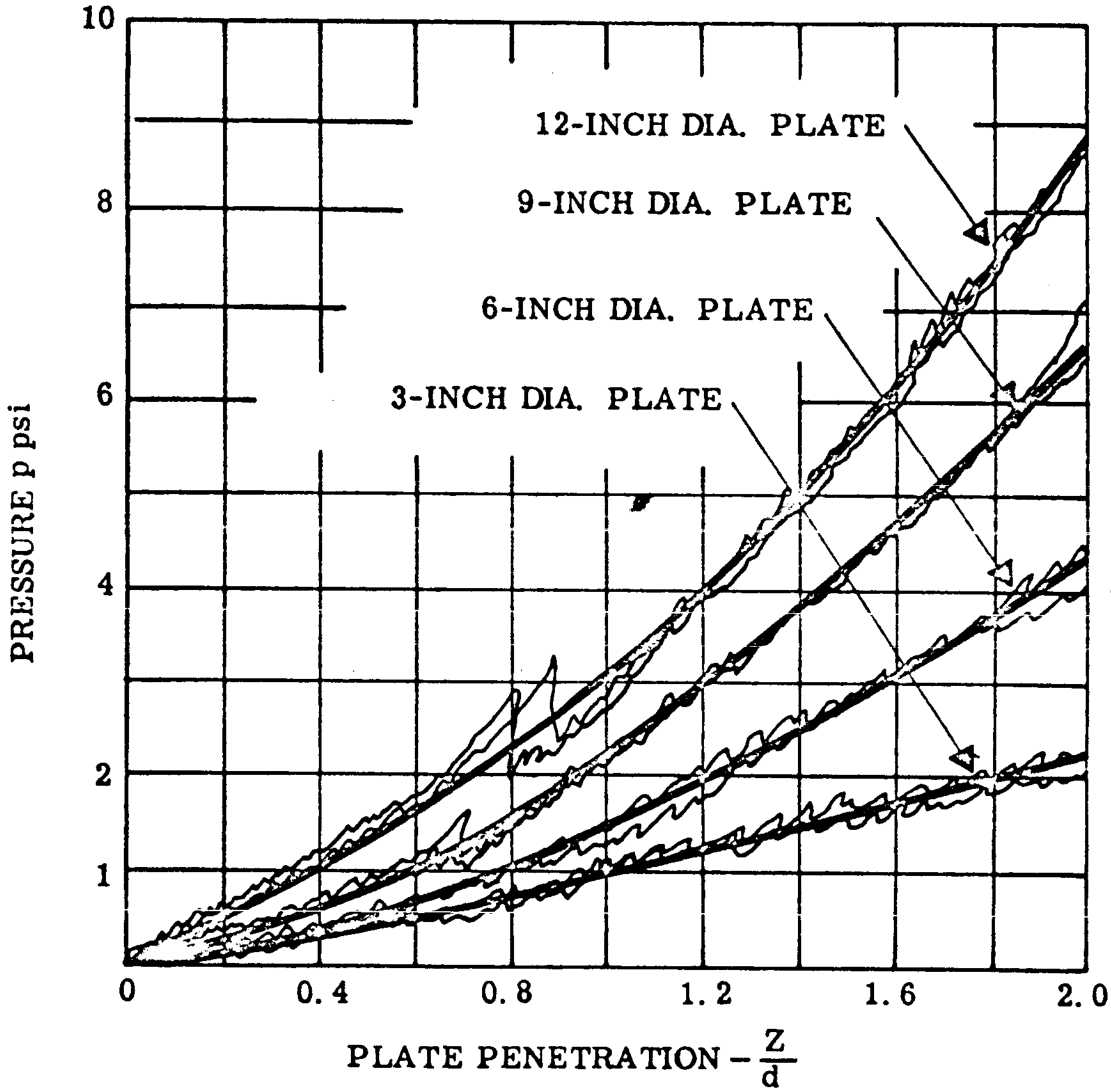

Fig. III. 3-5. Four Plate Sizes Tested in the Same Snow Pack

[redacted]

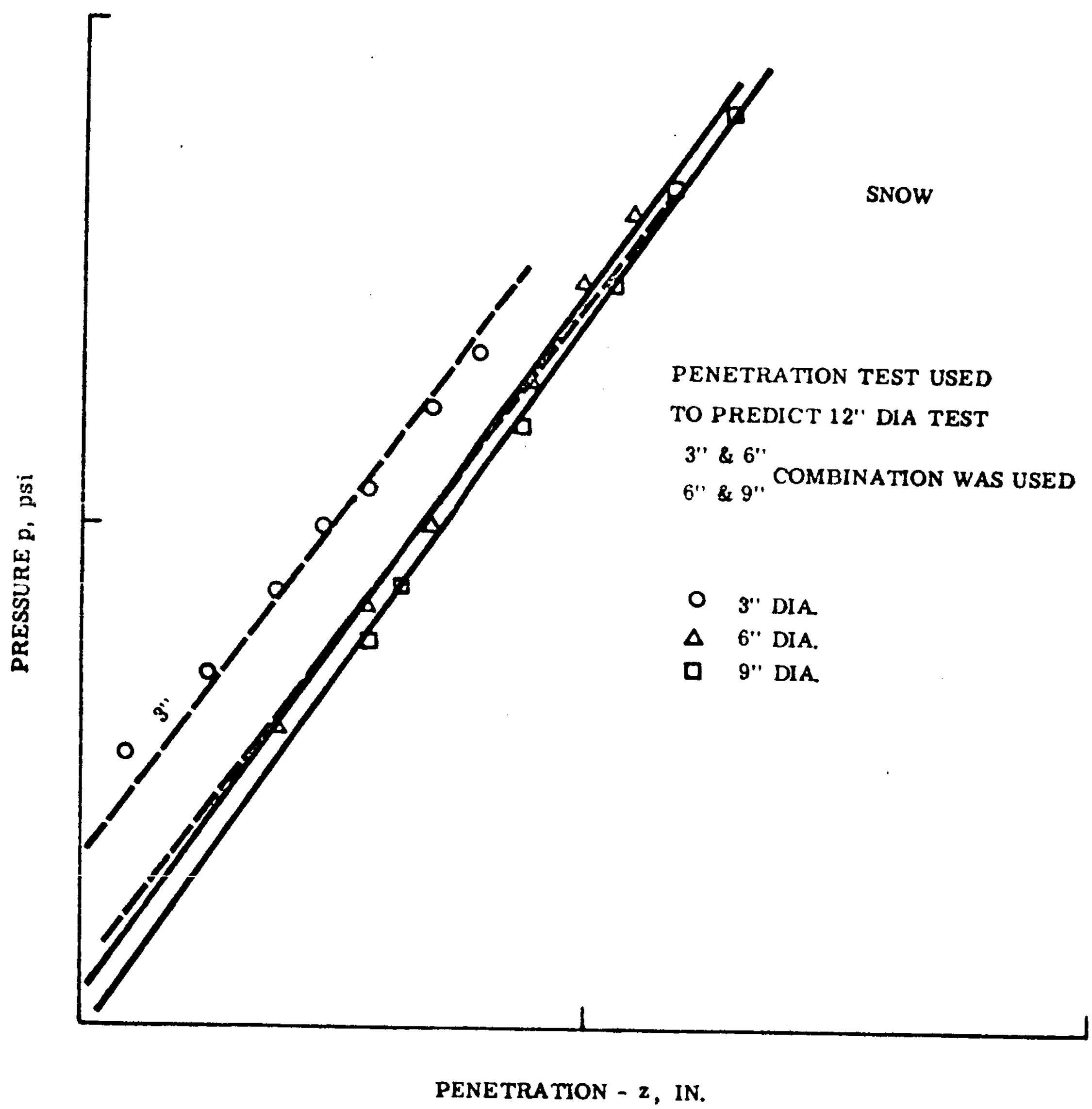

Fig. III.3-6. Load-Penetration Test on Snow with Test Plates of Various Diameters

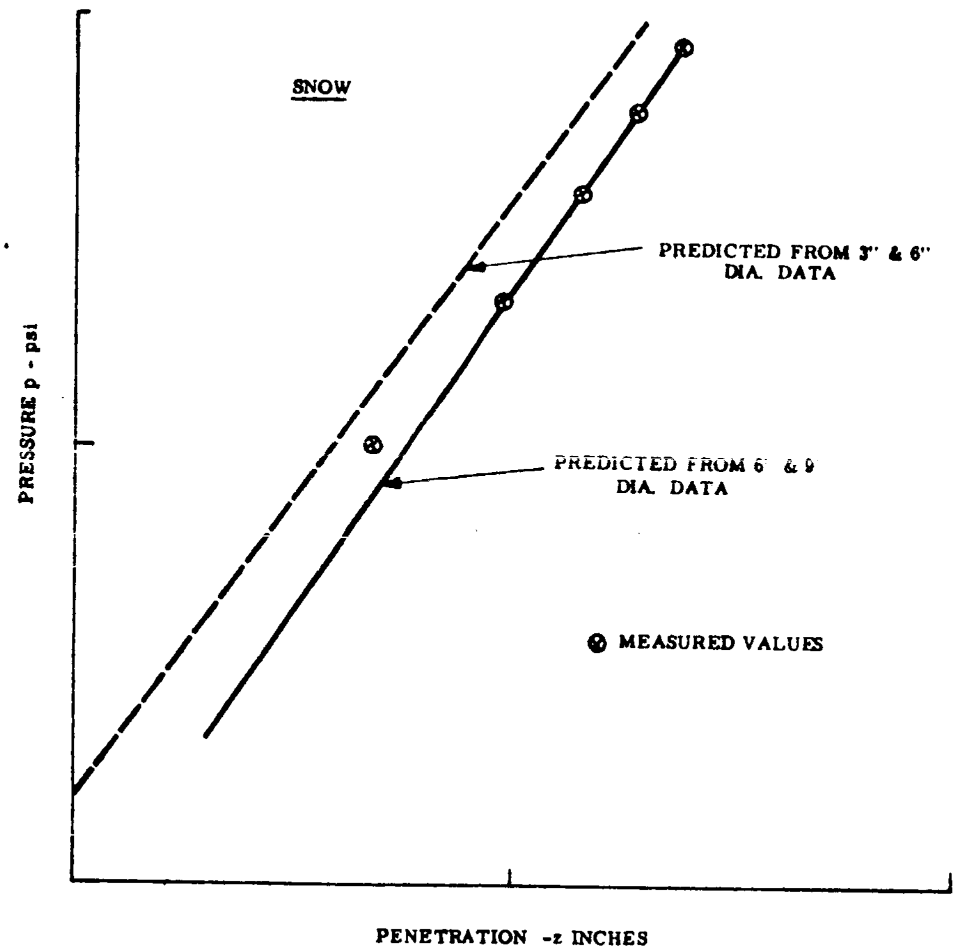

Fig. III. 3-7. Prediction vs Test Data of 12" Diameter Plate (Snow)

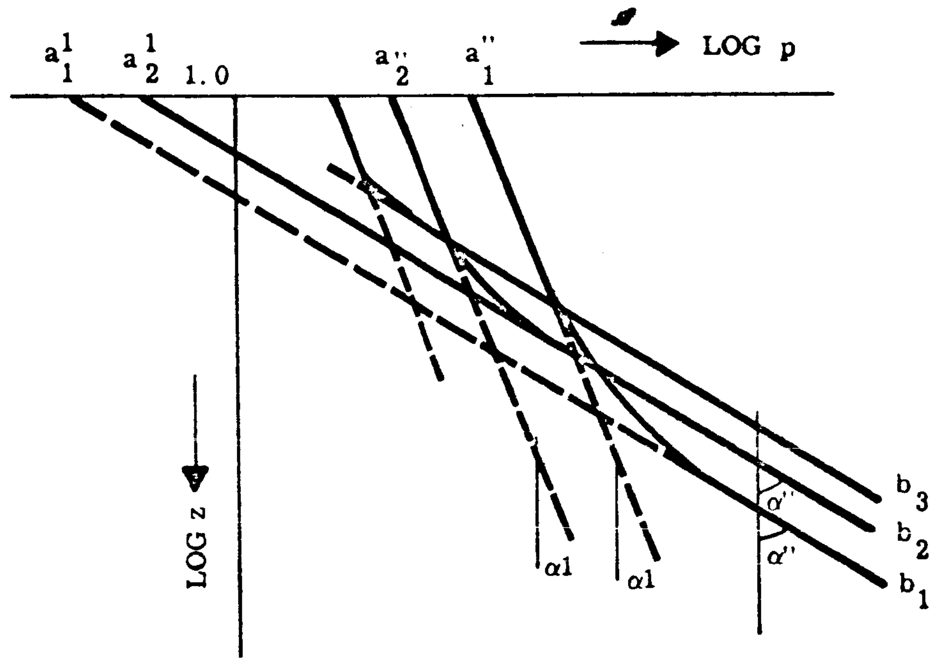

Fig. III. 3-8. Penetration in Non-Homogeneous Soils

"Vehicle Systems". With this instrument the test plates are forced into the soil at a slow, fairly uniform rate of penetration, and the load and sinkage are recorded simultaneously.

Sizeable pressures are necessary in the case of most soil types to obtain appreciable sinkage by means of static methods. In the case of the proposed SLRV the necessary static loads against which the test device would have to act are not attainable due to its light weight. For example, a lunar load of approximately only 5 to 7 pounds would be available for a static test measurement and to produce pressures of 15 psi the plate diameter would have to be on the order of 0.65 to 0.75 inch. This plate size is much too small to determine soil parameters necessary for bearing-capacity predictions. For this reason, a special instrument was built for incorporation on the SLRV to measure the bearing strength of the lunar surface. This instrument is called the Dynamic Iterative Bearing Strength Instrument, or DIBSI. A method was developed to obtain force amplification by kinetic loading in order to measure the surface-deformation characteristics with 2-inch and 4-inch diameter plates and unit loadings as high as 50 psi. The basic principle of the instrument involves vertical acceleration and deceleration of a mass at different rates. Because of its nature, this instrument is capable of measuring dynamic soil loading as well as correlating with static load tests.

REPETITIVE STATIC AND DYNAMIC LOADING

Before the dynamic tests were undertaken, repetitive static tests were made in order to obtain a quantitative "point of departure" into the new area. Fig. III.3-9 shows a typical curve of such static repetitive tests. The solid curves represent intermittent penetrations obtained in successive loading, unloading and reloading. The dashed-line envelope corresponds to the continuous penetration obtained in a single "static" test. It should be noted that in the case of reloading the penetration begins before the force reaches the envelope. This illustrates the well-known fact that the continuous-loading curve can be duplicated by repetitive loading only if the loads and reloads reach the threshold of a complete failure in plastic flow. Otherwise, different, misleading envelopes will be obtained, as shown by the last two loadings in Figure III. 3-9.

Soil force produced in repetitive dynamic loading can be considered as a sum of the static force, as previously defined, and of the additional forces due to the viscosity and acceleration of the soil mass. For this reason, the dynamic force is expected to be larger than the static threshold force, as shown in Fig. III. 3-10. It has been assumed that the velocity and the acceleration of soil are proportional to those of the plate.

Accordingly,

$$F_s = f_1(z) + f_2(z, \dot{z}) + f_3(z, \ddot{z}) \qquad \text{(III. 3-11)}$$

where

F_s = soil force acting on the plate

z = penetration of the plate

$\dot{z}$ = velocity of the plate

$\ddot{z}$ = acceleration of the plate

The first term in Eq. (III.3-11)represents the static force; the second, force due to lateral acceleration of soil particles and viscosity; and the third, the inertia force of vertically accelerated soil particles. With a low rate of penetration where $\dot{z}$ and $\ddot{z}$ are small, F_s becomes $f_1(z)$; this is the force of repetitive loading for a low penetration rate, discussed in the preceding paragraph. The relative size of f_2 and f_3 with respect to f_1 depends on the soil and the way the impact is applied to the plate. The softer the impact the smaller are f_2 and f_3.

[redacted]

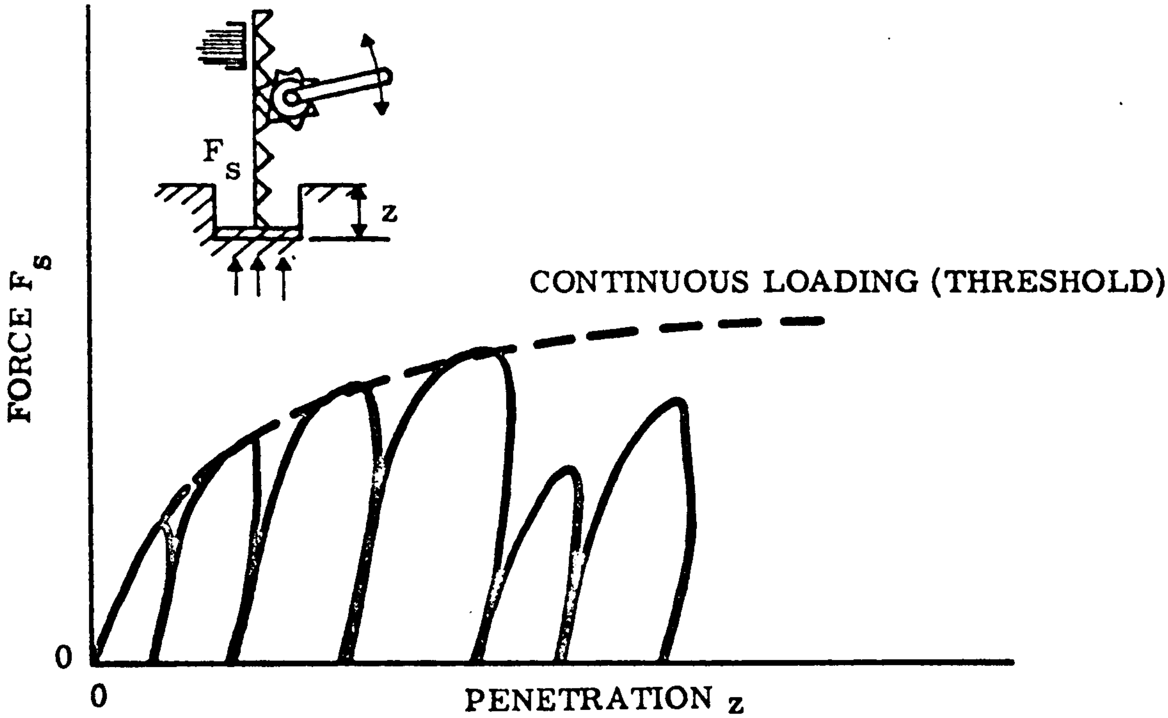

Fig. III. 3-9. Static Repetitive Loading of Soil

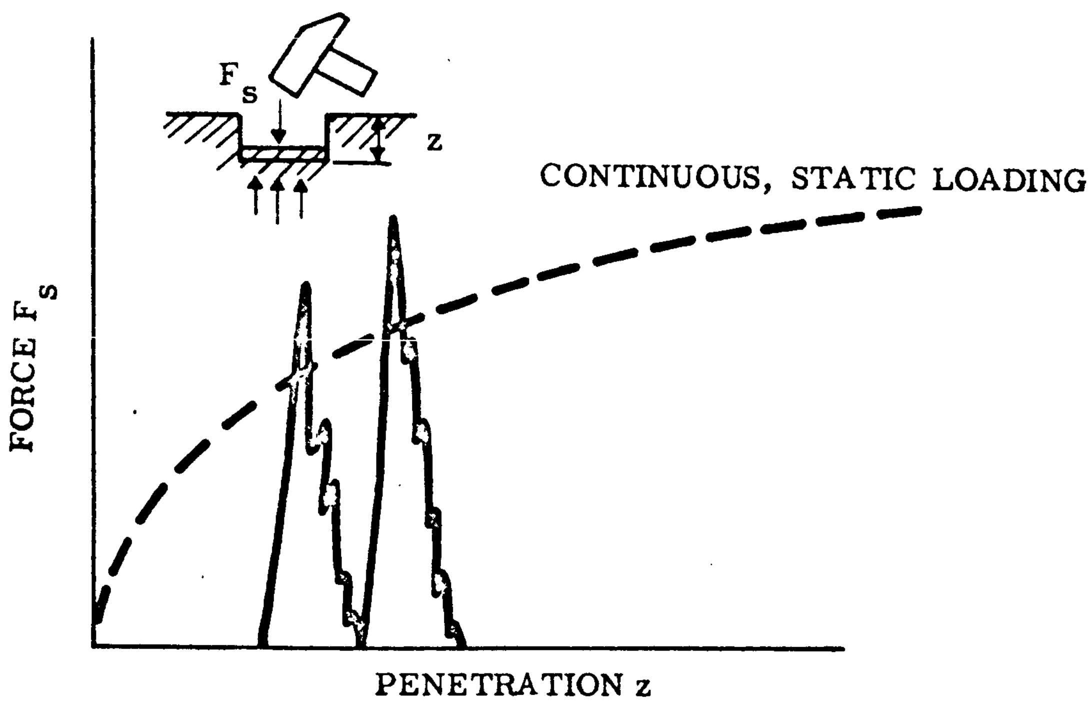

Fig. III. 3-10. Dynamic Repetitive Loading of Soil

[redacted]

321

PROBLEMS IN DYNAMIC REPETITIVE LOADING

The dynamic test method raises the questions:

1) How large should each particular impulse be in order to reach the threshold of the static curve?

2) Since the dynamic test produces much higher rates of penetration than the static tests, do high velocities of the displaced soil particles produce considerable viscous forces and inertial forces?

3) Is the degree of soil compaction unduly augmented by impact vibrations so that the dynamic method produces an intolerably high change in soil properties and, consequently, the results cannot compare with static test results?

4) The static method leads to a relatively simple apparatus, whereas the dynamic method requires a new and possibly more complicated arrangement of electric and mechanical devices. What configuration would give the desired optimum?

To answer some of these questions, instrumentation was developed to measure directly the soil force reacting on the plate during the impact, shown schematically in Fig. III.3-10. This method was based on the following considerations:

As indicated in Eq. (III.3-11) the dynamic force is composed of three major forces, i.e., static force f_1, the viscous force due to velocity of the plate f_2, and the force due to acceleration of the plate f_3. By measuring F_s, f_1, f_2, and f_3, it can be shown that

$$f_1 = F_s - f_2 - f_3 \tag{III.3-12}$$

The term $f_2\ (z, \dot{z})$ is dependent on velocity. By applying a spring located between the "hammer" and the plate (Fig. III.3-11) velocity $\dot{z}$ may be made small enough so that f_2 is negligible. (It has been well established that velocities up to 30 inches per second developed in static loading tests have very little effect on the force-penetration relationship). Acceleration $\ddot{z}$, on the other hand,

[redacted]

cannot be made negligibly small, even when using the cushioning effect of the spring. Note that f_3 is a function of $\ddot{z}$, and it is assumed to be zero when $\ddot{z} = 0$. F_s and $\ddot{z}$ can be recorded simultaneously, and the static force f_1 equals F_s at $\ddot{z} = 0$.

Referring again to Fig. III.3-11 the soil reaction, F_s, was determined in accordance with the following procedure: When impacting a plate, three forces acting on the plate can be distinguished. These are the impact force, the reaction force from the soil under the plate, and the force accelerating the plate mass. Therefore,

$$F_s = F_i - m\ddot{z} \qquad \text{(III.3-13)}$$

where

F_i = impact force

m = mass of the plate, transducer and accelerometer

$\ddot{z}$ = acceleration of the plate

The reaction force F_s of soil acting on the plate was obtained by measuring force F_i by means of a piezoelectric transducer; the acceleration of the plate $\ddot{z}$ was determined by an accelerometer (Figure III.3-11).

Fig. III.3-12 shows schematic records of F_i and $\ddot{z}$ vs time. As indicated by Eq. (III.3-13) $F_s = F_i$ when $\ddot{z} = 0$, hence at this particular moment

$$f_1 = F_s = F_i$$

It should be noted that, in this measurement, mass m is not critical as long as it behaves as a rigid body in the proper frequency range. Since the accuracy of the measurement depends on the relative phase shift of the recordings of F_i and $\ddot{z}$, the mechanical and electrical responses of both the

[redacted]

323

[redacted]

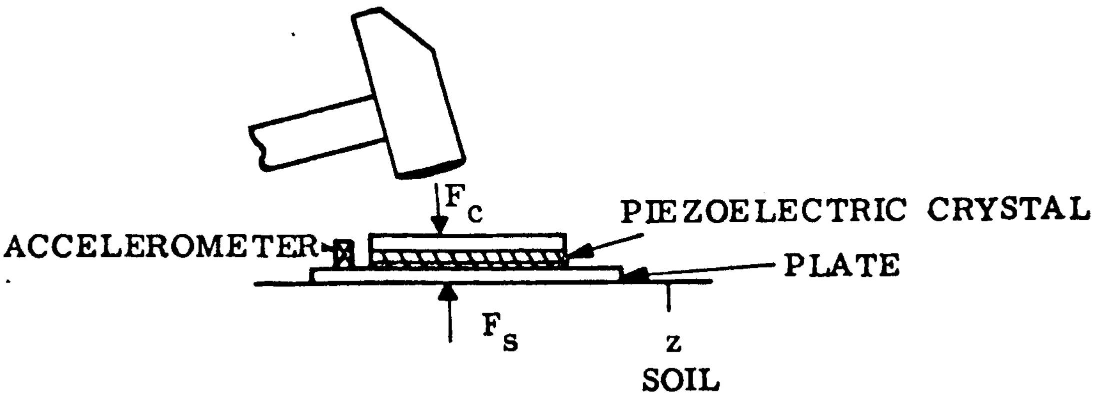

Fig. III. 3-11. Dynamic Testing Instrument

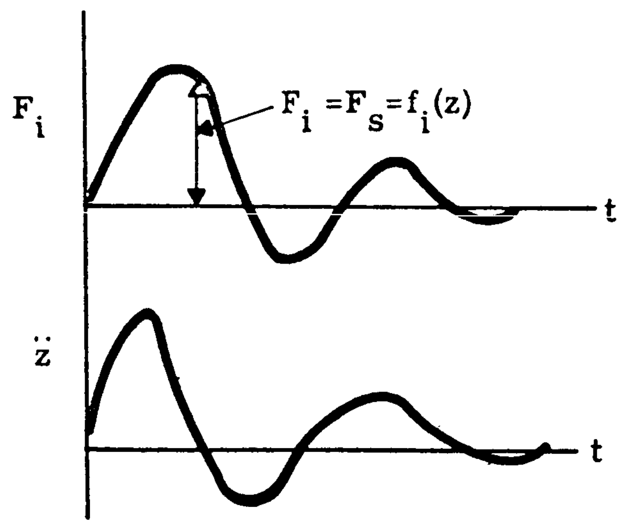

Fig. III.3-12. Impact Force F_i and Plate Acceleration $\ddot{z}$ vs Time transducer and accelerometer should cover the bandwidth, and the natural frequency of the plate should be kept high.

ENERGY LEVEL OF DROP WEIGHT

As mentioned in the preceding paragraphs, the threshold envelope of the continuous static loading should be reached by each dynamic loading, that is, $F_i(z)$ in Equation (2) should reach the threshold each time in order to retrace the continuous static loading characteristics. If, therefore, the instrument develops only one constant energy level, the dynamic measurement may end at the point where the energy of the drop weight is insufficient to reach the threshold, and the experimenter may not realize this. Generally speaking, the higher the energy level, the longer the dynamic experiment will follow the static curve. This is somewhat in conflict with the requirement to keep the energy small in order to minimize the velocity component of dynamic force (although this may be negligible), and to make the instrument compact and light.

To determine if the threshold is reached in dynamic repetitive measurements without prior knowledge of the static envelope, a minimum of two energy levels of impact have to be applied. As long as two consecutive readings obtained at those levels coincide, the measurements pertain to the threshold and are valid. If one of the readings starts to deviate from the other, the energy level is too small and no useful data can be obtained.

TEST RESULTS

Dynamic and static measurements were conducted in sand and clay. The dynamic results showed good agreement with static measurements, as illustrated in Figs. III. 3-13 & 3-14. Three energy levels were used in these tests. Note that the measurements with lowest energy level drop off the static curve much sooner than those with a higher energy level, as expected.

The measurements were performed with a light drop-weight at various energy levels, as specified on the drawings. Forces due to velocity and acceleration

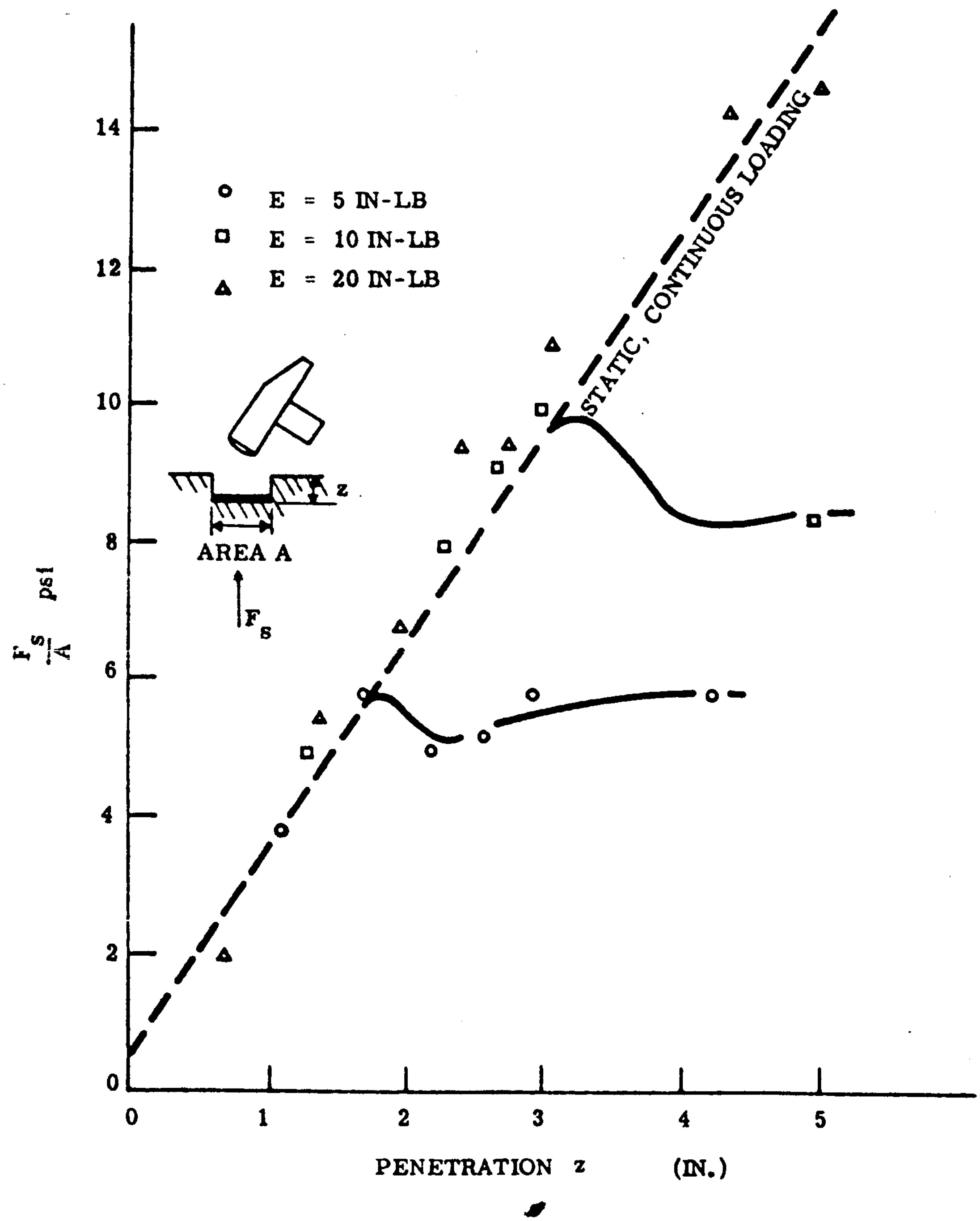

Fig. III. 3-13. Dynamic, Repetitive Loading vs Static, Continuous Loading. Soil: Sand

[redacted]

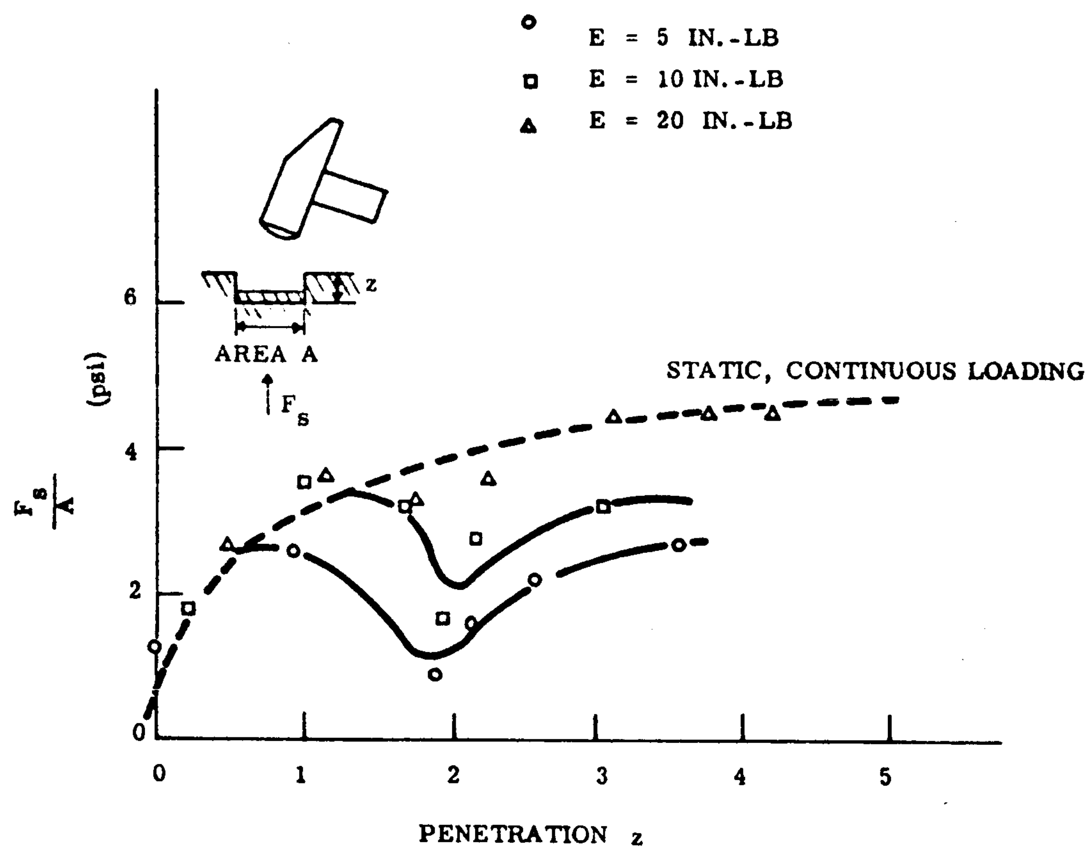

Fig. III. 3-14. Dynamic, Repetitive Loading vs Static, Continuous Loading. Soil: Clay

[redacted]

of soil were made negligible with respect to the static force by "softening" the impact. The soil reaction was determined at the points where plate acceleration was zero. Compaction of sand and clay seemed not to be different under static and dynamic repetitive loading, thus leading to agreement between the respective data.

A photograph of a typical oscilloscope record is shown in Figure III.3-15.

SOIL SHEAR STRENGTH

Although determination of the surface bearing strength is of higher priority this time for lunar landing purposes, knowledge of lunar soil shear strength will be essential in the near future for purposes of evaluating lunar-surface locomotion systems, construction of lunar bases, etc.

To this end, the soil cohesion c and soil angle of friction ϕ need to be determined. It is possible that gross estimates can be obtained with the presently proposed SLRV configuration.

For example, if the vehicle were stalled, say by leaving the DIBSI plates imbedded in the soil, then measuring the torque at the front wheels while the wheels were spinning would give an indication of soil shear strength.

Furthermore, ϕ can be estimated if the distance l of soil rupture from the DIBSI plates at incipient general failure can be observed by television (Figure III.3-15 The distance l depends on the angle of friction ϕ and the plate size. Thus, knowing l and b, ϕ can be calculated.[8] In the discussion of vehicle systems, the equation for shear strength is defined. Since $s = c + p \tan \phi$, and s, p, and ϕ are approximately known, c can then be calculated.

THE PROPOSED SLRV INSTRUMENT

The instrument proposed for obtaining soil bearing strength data from the SLRV is essentially a piledriver instrumented to obtain acceleration and force data at the time of impact. In its simplest form, it would be a device that

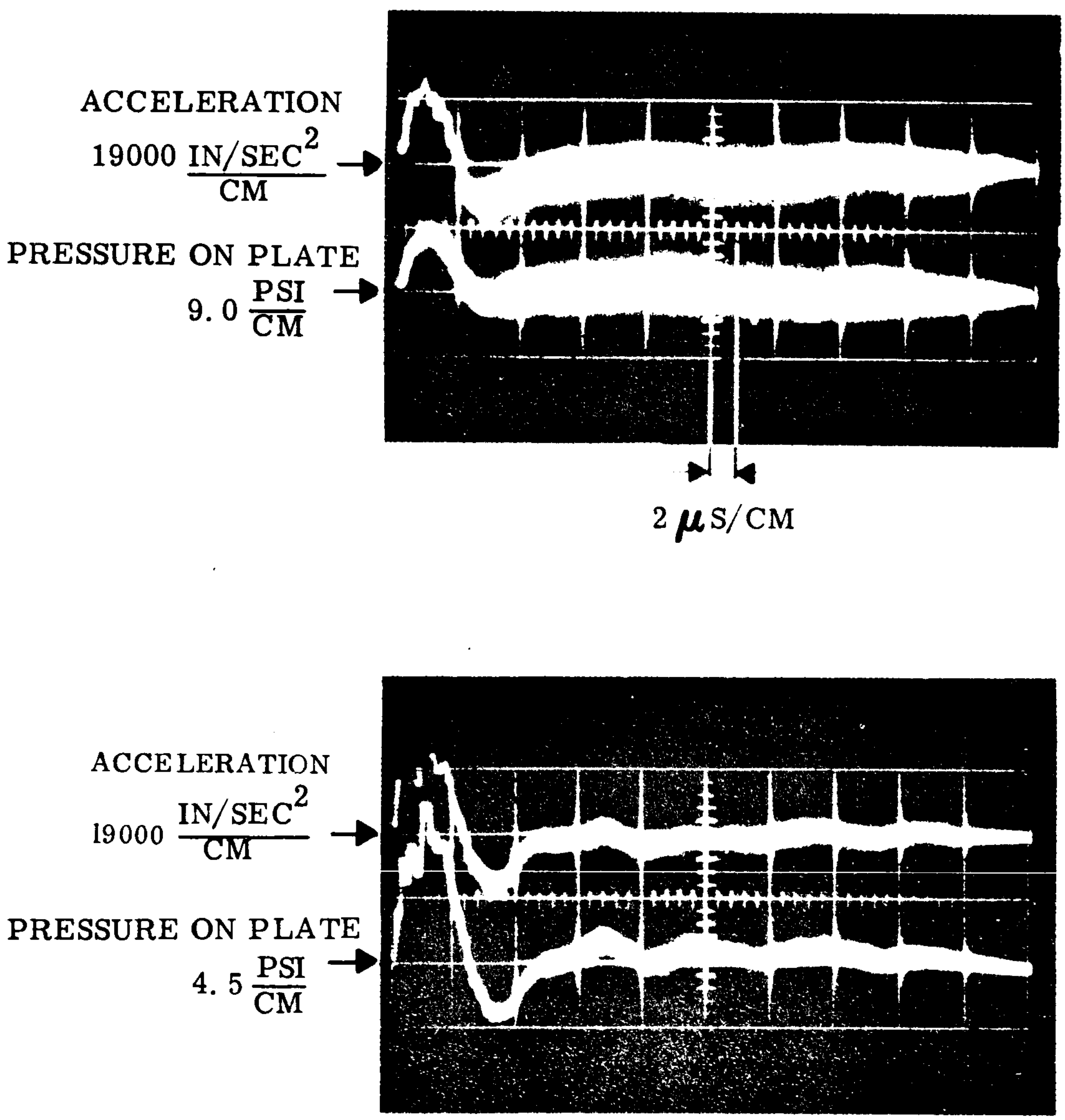

Fig. III.3-15. Typical Oscillograph Record would permit a weight to be dropped from varying heights to impact the bearing plates and force them into the soil. While this must remain the essential character of the instrument, the lunar-gravity and vehicle considerations will require modification of the concept. In addition, means of retracting the instrument from the soil and measuring its displacement relative to the vehicle must be provided; also, it is desirable to obtain a displacement measurement of the soil surface relative to the vehicle.

Requirements

The primary functions within the assembly are as follows:

1. Force Generator: A device that will impart kinetic energy into a mass or hammer that will in turn expend this energy by impacting the soil bearing plates.
2. Instrumentation Assembly: Transducers located near the bearing plate, or pad, that will measure the forces exerted against the soil and the acceleration of the pad.
3. Potentiometer Assembly: A displacement-measuring transducer.
4. Deployment Assembly: Mechanism to retract the pad from the soil and restore it to the stowed position.

Note: Items 1 and 2 constitute the soil mechanics instrument. Since it is required to extrapolate the data to bearing plates of a size much greater than can be carried on the SLRV, two assemblies will be required with bearing plates approximately two inches and four inches in diameter.

With pad sizes determined, the maximum penetration force required can be established, based on a model soil gradient of 8 psi/ft and a required travel of 50 cm. This value is 42 pounds for the small plate.

The energy at impact is not as readily established, and in fact, ideally should be a variable capability of the instrument. However, the value of 40 in. -lb is compatible with both data and vehicle requirements.

For the purpose of this discussion, the above requirements and certain additional requirements can be tabulated and used as a basis for design:

Hammer weight	1 to 2 lbs
Hammer travel	14 inches min
Kinetic energy	40 in. -lb
Maximum force	50 lbs
Maximum vehicle reaction force	3 lbs
Maximum cycling rate	10 cycles/minute

Force Generator

The force generator, illustrated in Fig.III.3-16 consists of a motor-driven screw that cycles a carriage up and down. The carriage in turn picks up the hammer at the bottom of its stroke and carries it to the top, where it is released. A constant-tension spring attached to the hammer accelerates it back to the bottom of the force generator. where it impacts the anvil. The anvil itself is spring loaded to clip the force at impact at approximately fifty pounds. The entire assembly is contained in the hermetically sealed body of the instrument.

The parameters for the design are the hammer mass, accelerating force, carriage cycling rate, and travel.

Variation of hammer weights over the range indicated have little effect on the required accelerating force but will change the velocity at impact, as indicated in Fig.III.3-17. Although a lower velocity appears more desirable from the standpoint of performance and reliability, the substantial weight savings possible with the small hammer cannot be neglected; this will have to be evaluated by further study and testing to establish an appropriate size.

The lead screw, aside from straightforward mechanical design considerations, can be constructed either as a continuously rotating screw with a reversing

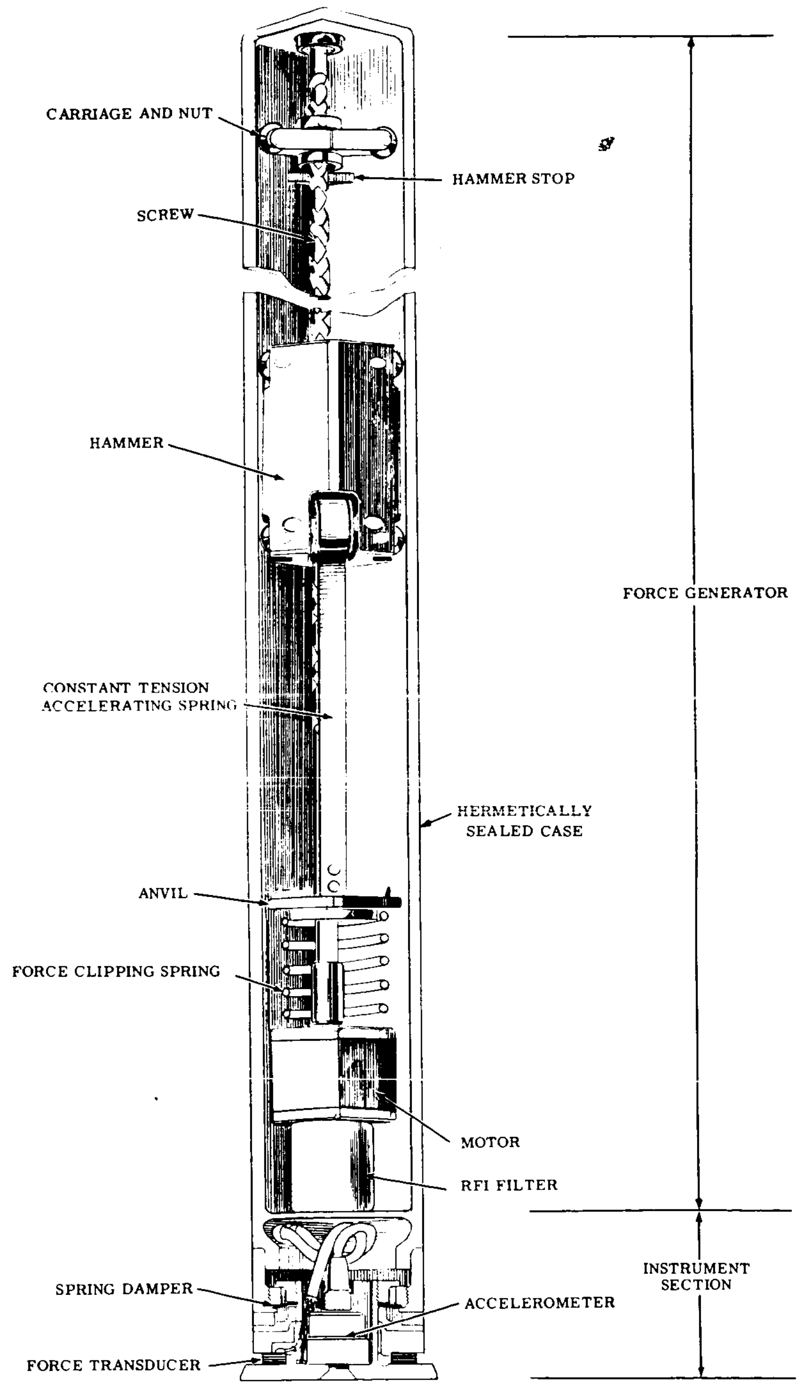

Fig. III. 3-16. DIBSI Assembly

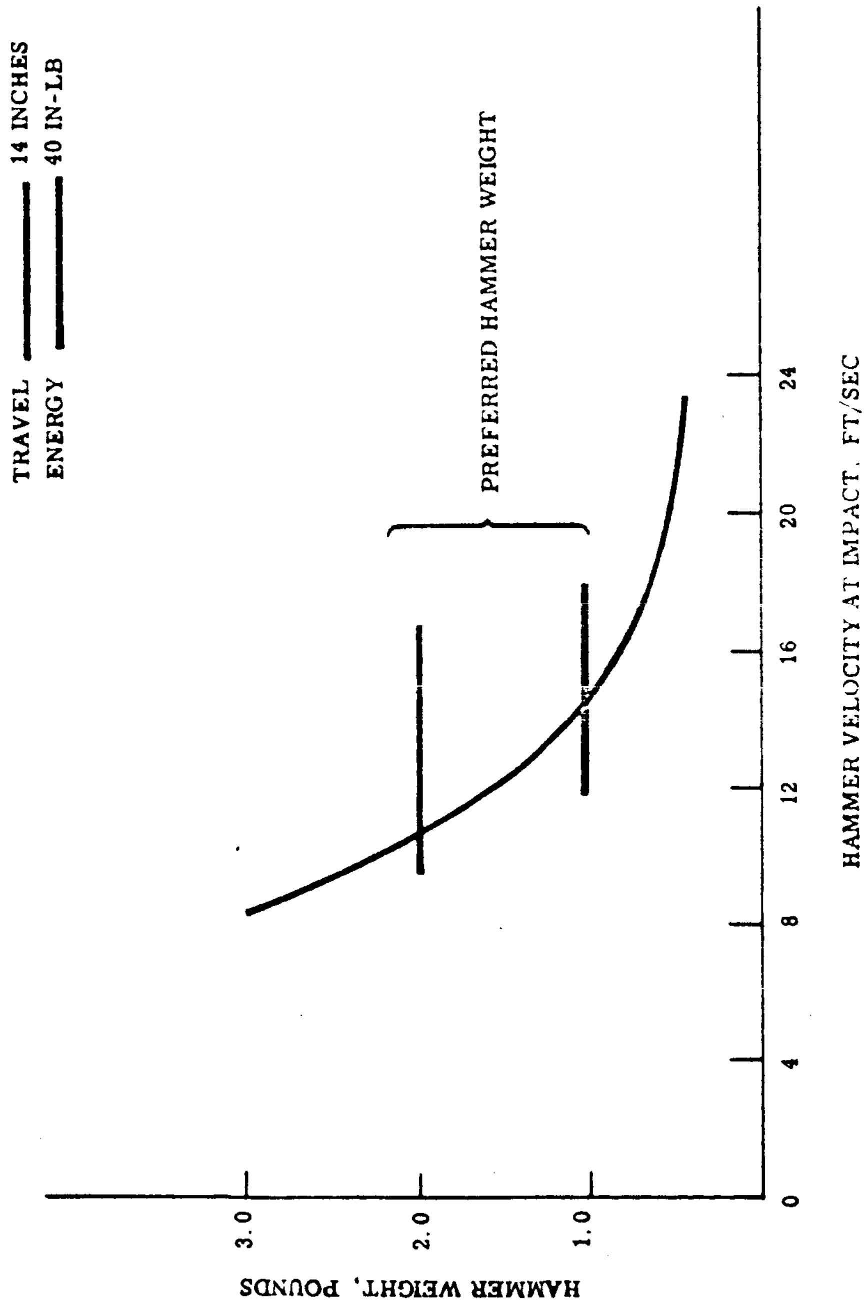

Fig. III.3-17. DIBSI Force Generator Hammer Velocity

[redacted]

lead to cycle the carriage, or can be reversed at the end of its stroke by signals from limit-switches. The latter entails additional circuitry, and therefore should be considered only as an alternate if mechanical reliability of a reversing lead cannot be achieved.

The carriage cycled by the screw can use mechanical, spring-loaded catches, that hook the hammer to the carriage at the bottom of the stroke and are automatically released when the carriage is at the top of its stroke. Similarly, a magnet mounted in the carriage can attach to the hammer at the bottom of the stroke; near the end of the upward stroke, a stop acting against the hammer can force separation and allow the hammer to drop.

The power drive, anvil design and other design details of the force generator as presently conceived present no peculiar problems. The proposed design is an improvement of a pre-prototype design fabricated and tested successfully at GM DRL. A photo of the disassembled pre-prototype instrument appears in Fig. III.3-18. In this design a weighted motor drives itself upward slowly along a track, stretching a negator spring. When the motor reaches the top of its travel, it is disengaged and is accelerated downward by the stretched spring and gravity. Reaching the bottom of its travel, it compresses a second prestressed spring which smoothly and rapidly decelerates the mass. The tension of the first cocking spring limits the upward force applied to the vehicle. The second prestressed spring shapes the downward test force that is applied to the instrument case.

Other concepts, including rotating inertial devices and the track arrangement of the original instrument have been compared and, in general, found less desirable for development than the screw-type actuator. Features such as reverse hammering to retract the mechanism and multi-energy steps have also been investigated and appear to unduly complicate the design. However, further study of these features will be made during the design study and will be incorporated if proven desirable.

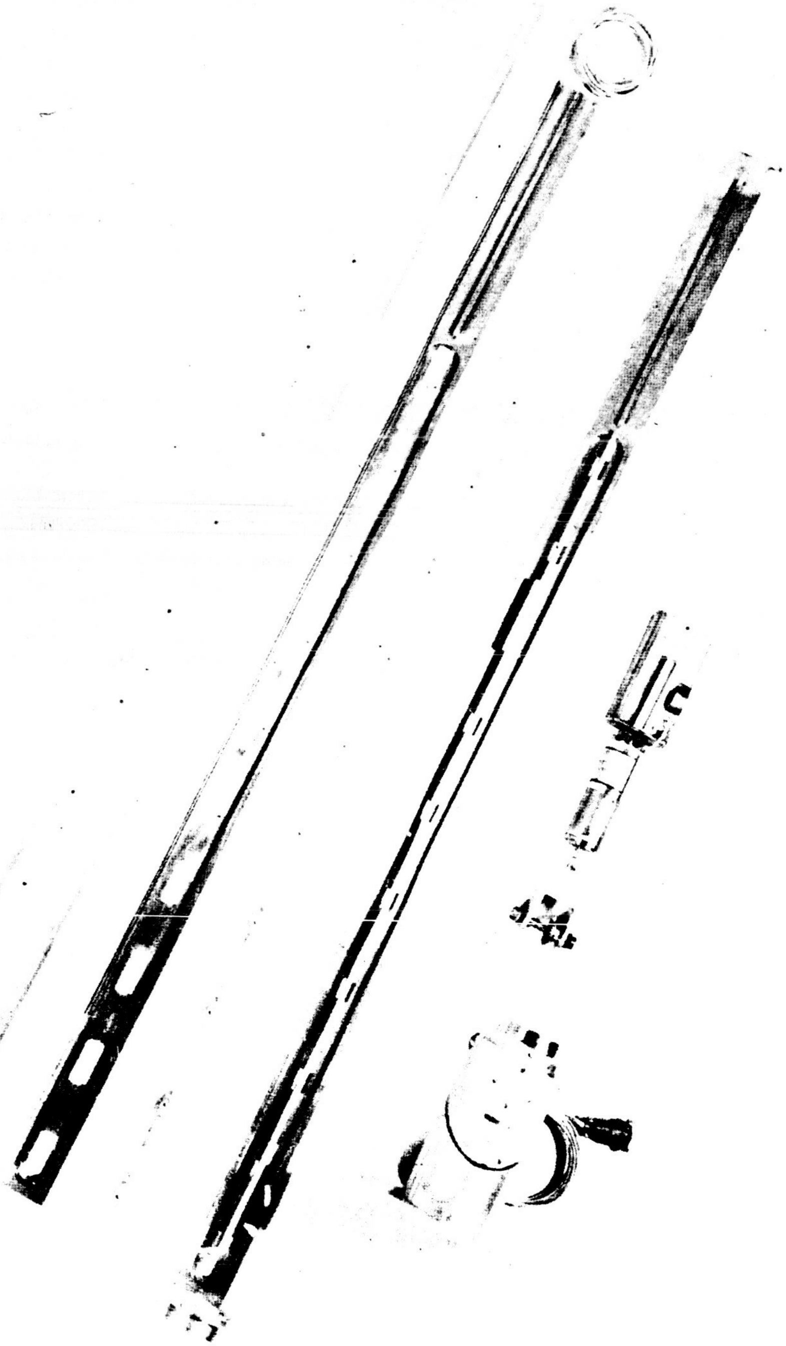

Fig. III. 3-18. Photo of Disassembled DIBSI

Instrument Section

The instrument (Fig. III. 3-16 consists of the soil measuring plate, force sensing piezoelectric crystal, accelerometer, dynamic vibration filter, and temperature measuring device.

Two plate diameters (2. 25 and 4. 0 inches) are being considered. The plate must be thick enough to act as a rigid body and have high damping characteristics so that undesirable high-frequency vibrations attenuate rapidly.

A preloaded piezoelectric crystal is used as a force sensing transducer. A lead-zirconate-titanate type, whose Curie point is higher than 300°C, will be used in the final instrument in order to withstand the estimated survival temperature of -250°F (-156°C) to 350°F (177°C).

A piezoelectric accelerometer will also be used. The spring and moving mass, which consists of the plate, accelerometer, and transducer, behaves as a dynamic vibration absorber for undesirable vibrations of higher frequencies caused by impacts generated by the hammer. The frequency response of the accelerometer must cover the frequency of this spring-mass vibration system.

A resistance thermometer is installed for the purpose of temperature-calibration of the transducer.

The reference point from which the penetration starts is to be measured by establishing the displacement of the instrument when the plate touches the soil surface. This can be accomplished by the same piezoelectric force transducer, except with higher amplification than for normal instrument operation. It appears that the transducer can be made sensitive enough to sense 0. 1 psi. This pressure is sufficiently low to be a reasonably accurate soil-level reference point.

Deployment Mechanism

The deployment mechanism has the functions of deploying the soil mechanics instrument to the soil surface, providing a reaction path to the vehicle to take advantage of the vehicle weight in applying an accelerating force to the hammer, and retracting the instrument to the stowed position. In addition, it will include the mechanism for measuring displacement.

The general arrangement of the mechanism to accomplish the above functions is illustrated in Fig. III.3-19. It consists of a hermetically sealed container that contains all the mechanism of the power train, a separate, sealed assembly for the displacement transducer, and the rollers for support. There are two such mechanisms, one for each instrument, mounted above the third axle. The linear actuator for positioning the Solar Panel is mounted between the two assemblies.

The power train drives a tape reel, the end of which is fastened to the bottom of the instrument. This reel is driven through a rotary hermetic seal by a DC gear-head motor, which also drives a rotary mechanical stop and limit-switch assembly.

A negator spring spool is also required. The end of the spring is fastened to the top of the instrument and this provides a constant downward force. The mechanism limits the upward reaction on the vehicle due to acceleration of the hammer, and tends to make the space relationships between the instrument and the vehicle independent of each other except for the spring force under dynamic conditions. The hub for the negator, in turn, is a nut that drives a screw to position a hermetically sealed linear potentiometer to provide a displacement signal.

The problems associated with the deployment mechanism are those pertaining to lubrication of the bearing surfaces in space, designing so that operation will not be impaired by dirt and contaminants carried up out of the lunar soil by the

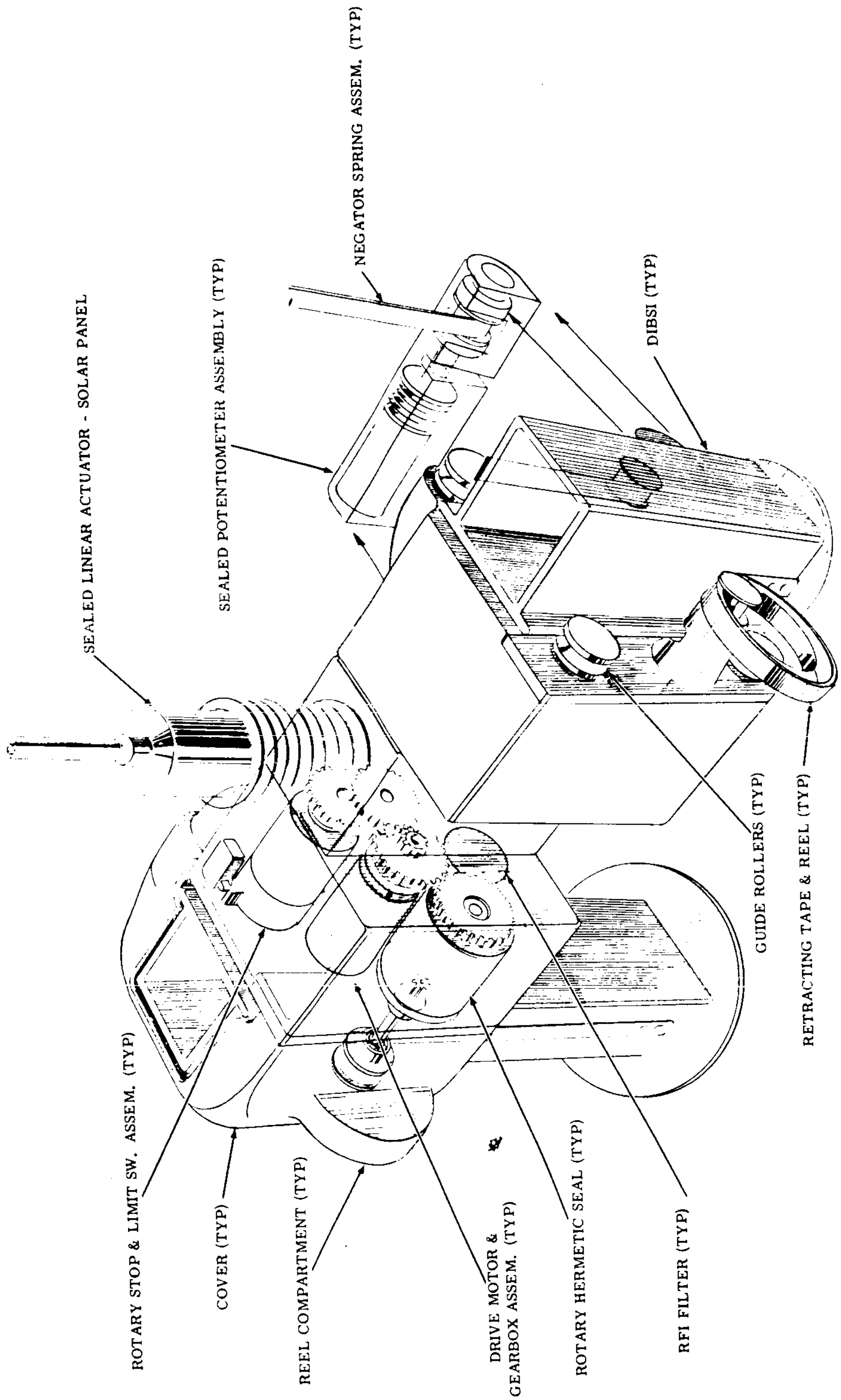

Fig. III. 3-19. DIBSI Deployment and Solar Panel Actuator Assembly instrument, and achieving a 50-cm-penetration capability without unduly complicating the instrument installation. The latter problem requires further discussion.

The geometry in the stowed position readily allows stowage of a 24-inch-long tube, and with the deployment mechanism illustrated a soil penetration of 14 to 15 inches can be achieved. The 20-inch depth-of-penetration requirement demands that the soil instrument be 29 inches long, or have some form of telescoping mechanism.

The ability to stow a 29-inch-long tube must be determined from detail layouts. The alternative of a telescoping extension adds additional complexity to the mechanism, which can be appreciated by a study of one possible means of attaining additional penetration illustrated in Figure III.3-20.

Associated with the soil mechanics instrument and the deployment mechanism on the third axle is the solar panel and its actuator. The solar panel is hinged at the top of a light-weight structure mounted on the top of the deployment assemblies. A short-stroke, sealed linear actuator provides the force for extending the solar panel to an angle of 45 degrees from the stowed position. This structure also provides channels for guiding and protecting the cable to the individual soil instrument assemblies.

Instrument Operation

The individual assemblies are maintained in the stowed position by the retracting tape. Upon command, the deployment motor is reversed, lowering one of the tubes. The tape continues to unwind from the reel even after contact with the ground, until enough slack loops are available in the reel compartment to allow unrestrained penetration of the instrument into the soil. (In soft soil, the force of the negator spring, along with the displacement measurement, will give an initial soil-bearing-pressure reading, independent of operation.) Once the signal from a limit-switch indicates that the retracting tape has been completely unreeled, the signal for starting the force generator can

[redacted]

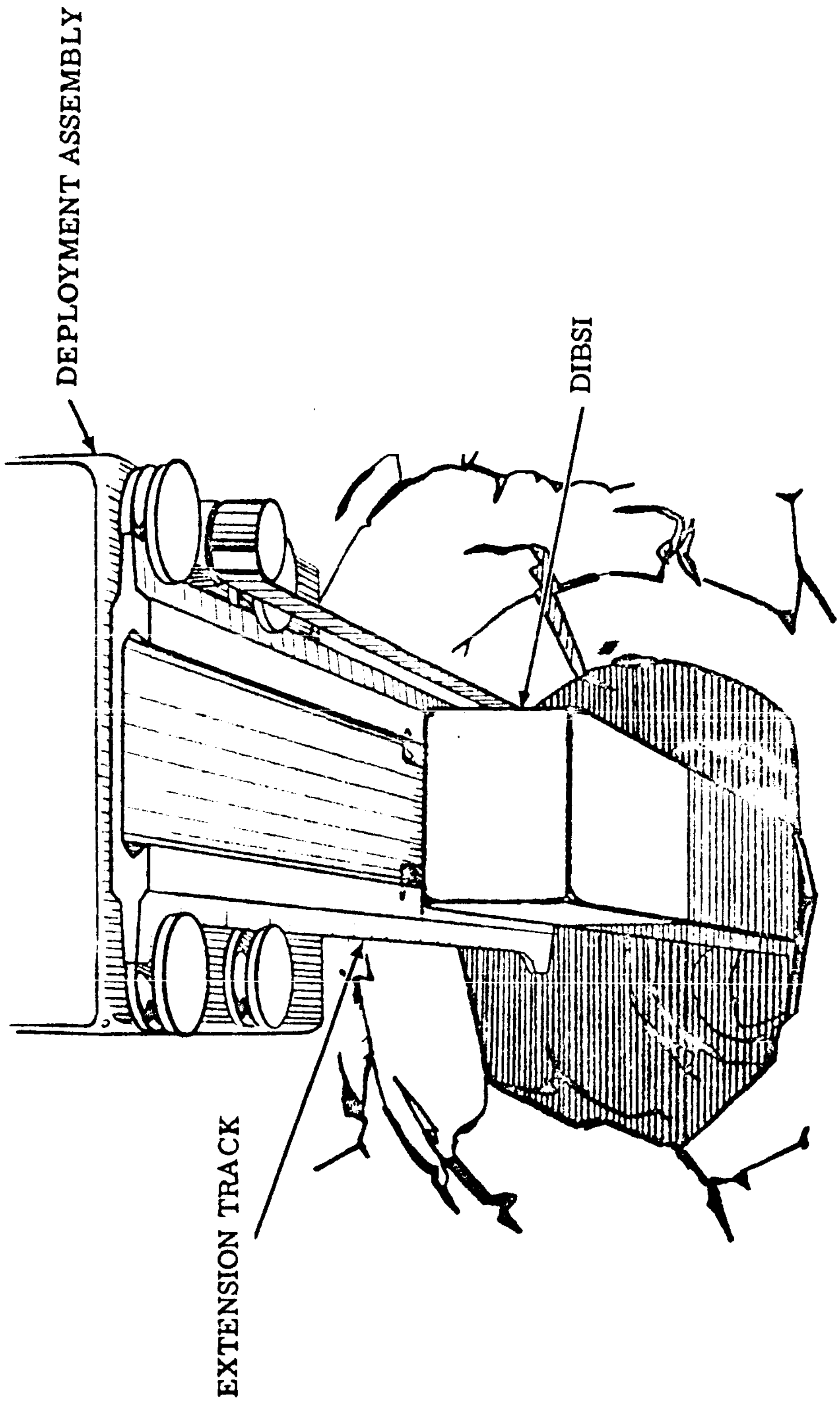

Fig. III. 3-20. Extension Mechanism

[redacted]

be given. This continues for the time period established by system considerations. A reverse-rotation signal to the deployment motor will retract the instrument with a pull of up to 75 pounds, or to the maximum that the vehicle design will permit.

REFERENCES (SOIL BEARING CAPACITY EXPERIMENT)

1. K. Terzaghi, Theoretical Soil Mechanics, John Wiley and Sons, New York, 1951.

2. D. Taylor, Fundamentals of Soil Mechanics, John Wiley and Sons, New York, 1948.

3. M. G. Bekker, Off-the-Road Locomotion, University of Michigan Press, Ann Arbor, Michigan, 1960.

4. D. C. Drucker, "On Stress-Strain Relations for Soils and Load Carrying Capacity," Proceedings of the 1st International Conference on the Mechanics of Soil-Vehicle Systems, Edizioni Minerva Tecnica, Torino, Italy, June, 1961.

5. R. M. Haythornthwaite, "Methods of Plasticity in Land Locomotion Studies," Proceedings of the 1st International Conference on the Mechanics of Soil-Vehicle Systems, Edizioni Minerva Tecnica, Torino, Italy, June, 1961.

6. Proceedings of the 1st International Conference on Soil-Vehicle Systems, Edizioni Minerva Tecnica, Torino, Italy, June, 1961.

7. "Environmental Factors Affecting Ground Mobility in Thailand", Technical Report No. 5-625, US Army Engineers Waterways Experiment Station, Vicksburg, Mississippi, May, 1963.

8. Verlag Von Wilhelm, Grundbau - Taschenbuch, Bund I, Ernst and Sohn, Berlin, 1955.

D. STEERING ACTUATOR

Requirements

The Surveyor Lunar Roving Vehicle is steered by turning wagon-type axles on either end. The torque and operating characteristics for steering are established by mobility requirements as follows:

1) Steering Characteristics – Both front and rear axles should be steered simultaneously to provide good tracking. Synchronization shall be provided at the straight-ahead position, and at increments no greater than 10 degrees up to the maximum steering angle. The maximum steering angle should be 30 degrees to provide a wall-to-wall turning radius of 71.5 inches and a maximum tracking encroachment of the center wheel of six inches.
2) Steering Drive – Nominal steering torque is based on an assumed coefficient of friction of 0.5 when the vehicle is in motion. For equal wheel loading, this results in a torque requirement per axle of 33 in.-lb., and a speed of 2 RPM.

For steering when the vehicle is stationary and wheels locked, the torque requirement is approximately 100 in.-lb.

Resisting torque required an be calculated from impact of one wheel at maximum speed into a wall and results in a torque of 350 in.-lb.

Additional consideration should be given to obtaining partial steering capability in case of steering actuator failure.

Design Approach

The proposed design is an improvement of a design successfully tested for many hours on the pre-prototype Surveyor Lunar Roving Vehicle.

A photo of a disassembled steering actuator from this vehicle appears in Fig.III.3-21. In this design the motor is mounted horizontally rather than vertically. The motor-planetary gearbox assembly is attached to the elastic vehicle frame and the bevel-sector gear, driven from a bevel pinion gear on the gearbox output shaft, is attached to and drives the front or rear axle. A micro switch assembly is used as an angle follow-up. The entire assembly is hermetically sealed with the metal can and large bellows shown in the photo. As a pre-prototype assembly of a lunar vehicle steering mechanism, it proved the feasibility of one design approach and provides available hardware for support of continuing development effort.

However, the extended mission requirement of the SLRV and the possible desirability of redundant steering modes requires additional design effort. The most difficult of these problems is that of centering the axle, in case of steering motor failure. It implies a requirement for de-clutching the steering motor and the release of a latch to lock the axle in the center position, as well as to center springs. The mechanical parts to accomplish this could add .3 pounds to an assembly. In addition, the thermal problems associated with an extended mission makes it desirable to change the design to a vertical assembly to simplify heat dissipation and isolation from heat sensitive areas.

Other steering possibilities have been considered. The use of wheel-drive motors operating differentially to position the axle in conjunction with a simple solenoid latch mechanism on the steering axle is attractive and requires further study. The additional controls in the wheel circuit and dependence on soil characteristics to develop steering torque vs. the positive control of a separate actuator are possible drawbacks. Cross coupling between axles would eliminate mechanisms or provide additional redundancy. Normally this could readily be accomplished. In this case, though, the extremely flexible chassis required for mobility and stowage makes it somewhat difficult to accomplish.

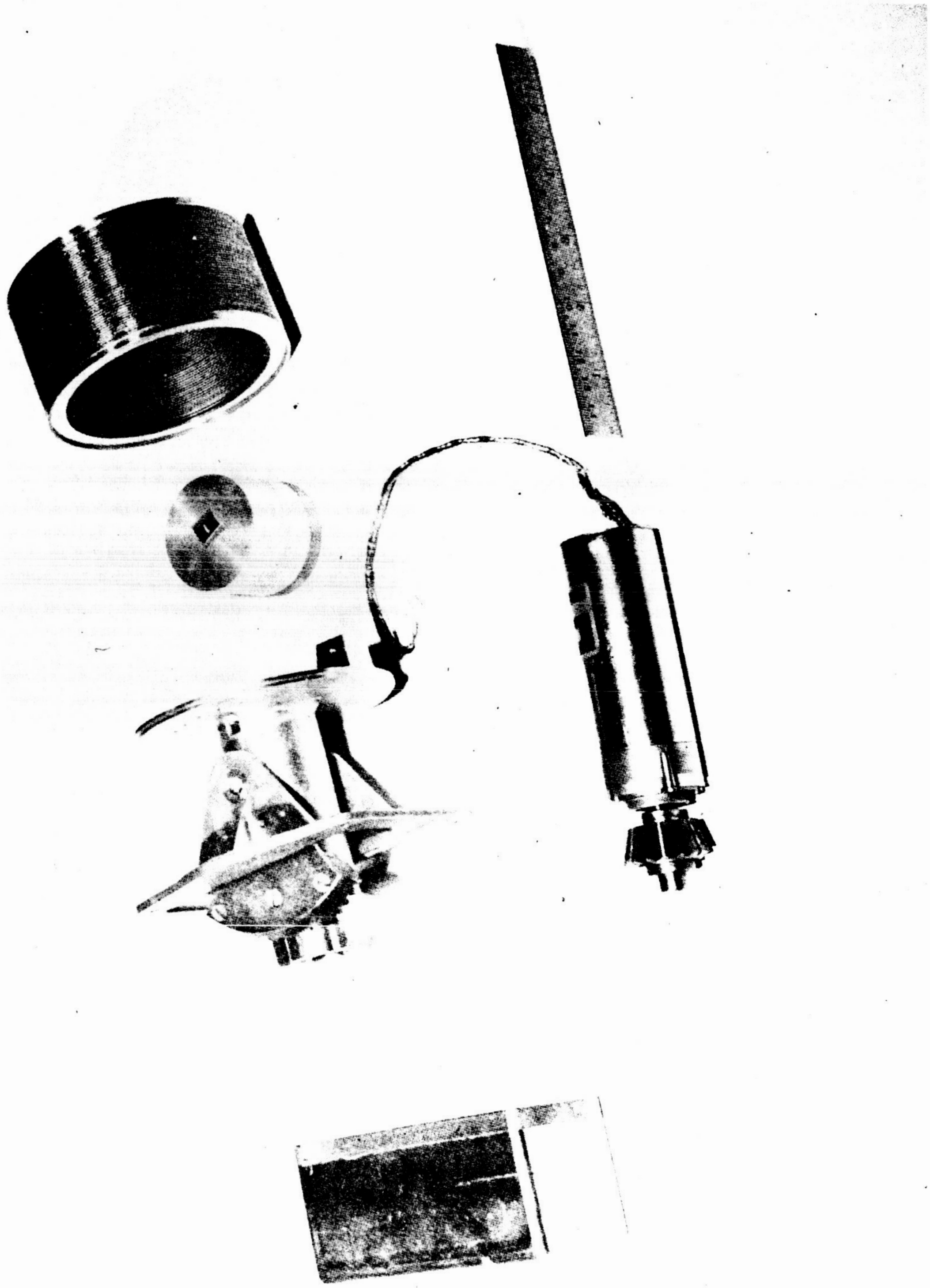

Fig. III. 3-21. Preprototype Steering Actuator, Disassembled

These design possibilities, along with the overall system requirements thermal, weight, and reliability tradeoffs-will have to be fully evaluated to derive an appropriate steering system for the vehicle. The GM DRL basic Lunar Program development effort to date indicates that a direct-drive steering actuator for each axle is the most desirable.

PROPOSED DESIGN

The proposed steering actuator design is shown in Fig.III.3-22. A small, low speed, high torque, permanent-magnet field, d-c brush-type motor drives a tongue attached to the vehicle frame through an 1100-to-1 reduction planetary gearbox. The steering actuator assembly is attached to the movable axle-compartment assembly while the frame tongue, connected to the vehicle center axle-compartment assembly, is attached directly to the gearbox output shaft. No additional support bearings are needed, since the gearbox output shaft is large in diameter and is mounted on two large ball bearings. To permit hermetic sealing of the actuator assembly the frame tongue is attached to the gearbox output shaft by means of a rugged ring-like structure. Two linear bellows permit rotation of this structure while maintaining the hermetic seal.

The 7.5 degree steering position switch and the plus and minus 30 degree steering limit switch are actuated by protrusions on the rear of the frame tongue-ring structure. A film type potentiometer coupled to the bottom of the gearbox shaft provides a true indication of axle angular position. A radio frequency interference filter mounts directly to the top of the motor and a thin-walled aluminum can, sealed to the bellows partition, completes the sealed assembly. Electrical leads are brought into the sealed space through a glass-to-metal seal header. All electrical components and all moving mechanical parts including bearings are located within the hermetically sealed, pressurized space.

64-406
VOL II APP. SEC. III

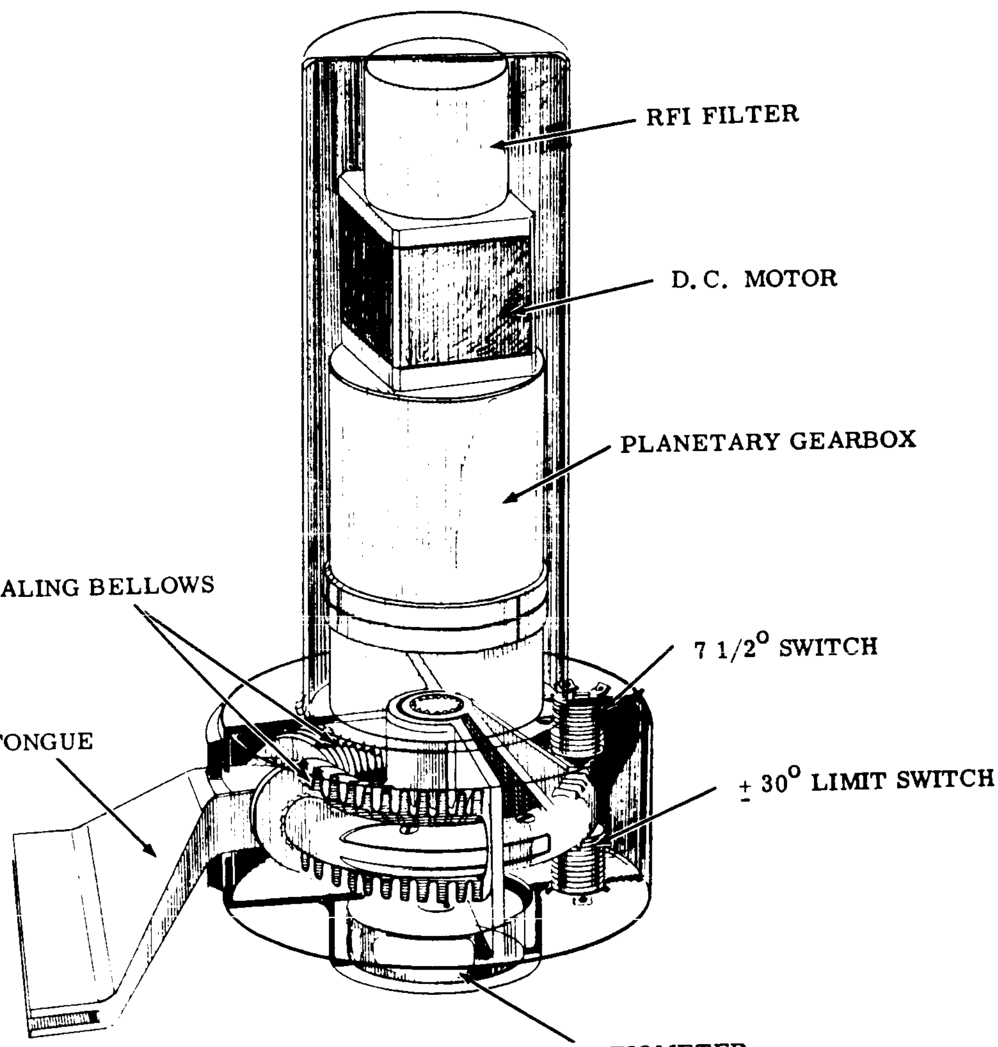

Fig. III. 3-22. Proposed Steering Actuator Configuration

3417

The same motor and RFI filter used in the wheel drives has been chosen for use in the steering actuators. The motor is mounted vertically to allow heat dissipation by means of a radiator mounted on top of the motor in the same plane and at the same level as the other radiators in Compartment No. 1. The use of a relatively low-speed torque motor instead of a high-speed motor was dictated by the higher efficiency of such motors and reduction in the number of passes needed in the gearbox. In this small size the weight penalty, because of motor size, is small and compensated by the smaller gearbox. The size of the power drive is determined by the stall torque requirements of 100 in. -lb and the running torque and speed requirement of 33 in. -lb and 2 RPM. With a mechanical efficiency of 60 percent, motor torque required is . 8 in. -oz. at 2200 RPM and 2. 7 in. -oz. at stall. Overall efficiency of the drive would be 48 percent at the design operating point. This compares with 30 percent, using a smaller high speed motor.

An alternate arrangement depicted in Fig. III.3-23 as suggested by Mechmetals, Inc. utilizes two wheels connected together by steel bands. Linear-type bellows seal the motor compartment as shown in the illustration.

The reasons for hermetically sealing the actuator components and using a d-c brush-type motor are discussed in detail under the "Wheel Drive" paragraph. The same philosophy applies here.

64-466
Vol II App Sec.

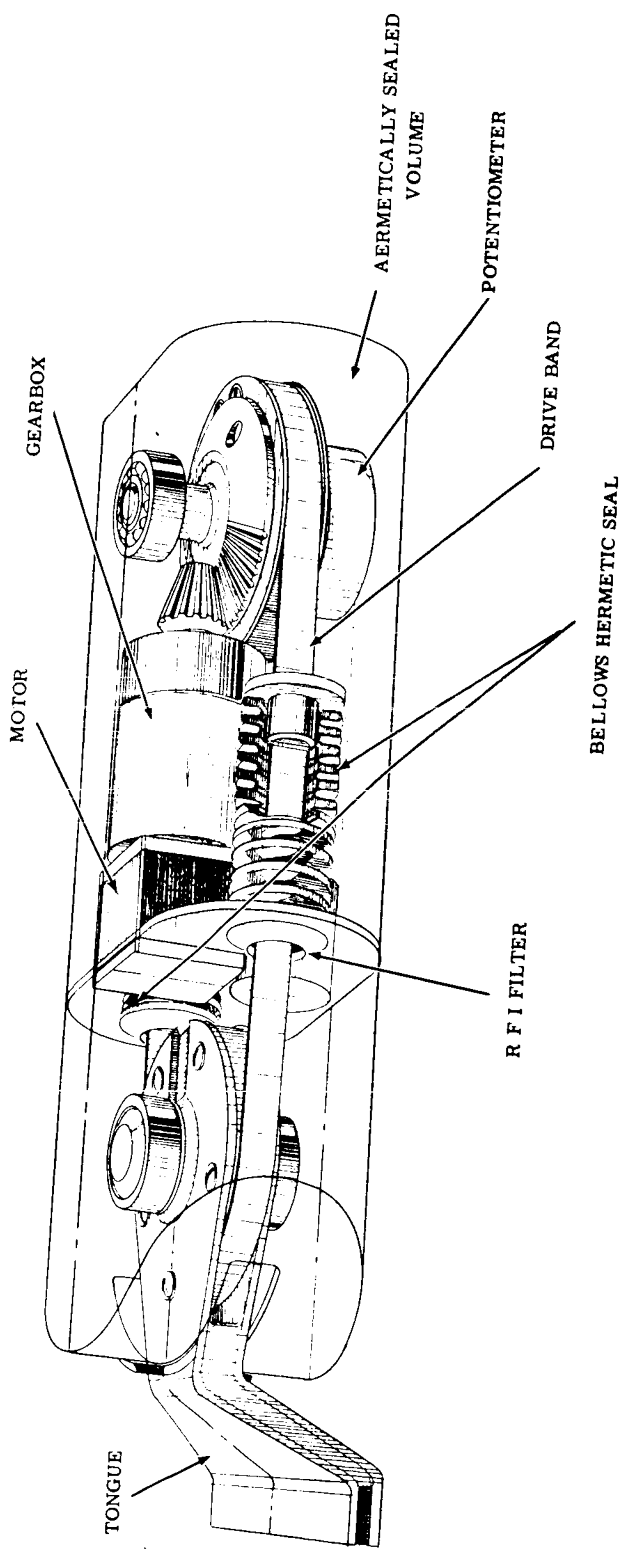

Fig. III. 3-23. Alternate Steering Actuator Configuration, Mechmetals Design

349

E. CLINOMETER

INTRODUCTION

Fulfillment of the SLRV mapping mission requires a knowledge of the orientation of the plane of the TV image, from which mapping measurements are to be taken, relative to a known reference. In order to establish such a reference, a two-axis clinometer is to be mounted in the vehicle compartment housing the television camera, such that the outputs of this instrument will indicate the tilt of the vehicle compartment along the roll and pitch axis with respect to the lunar gravitational field. Further, as a back-up in case of TV failure, with such an instrument aboard the surface topography may be obtained by integrating slope along the direction of travel as a function of distance traveled.

Preliminary estimates indicate that accuracies in the order of five minutes and thirty minutes may be needed, respectively, for TV photo-reference and topographic data. A maximum angular indication of plus and minus 45 degrees in both roll and pitch appears to be reasonable. To preclude inadvertent overturn of the roving vehicle, the clinometer incorporates sensors at the 45° limit in both directions.

DESIGN STUDY

General

To allow most efficient utilization of the roving vehicle, the clinometer measurements must be performed while the vehicle is in motion. This dictates that the natural frequency of the clinometer be considerably below the natural frequency of the vehicle. However, to permit identification of terrain irregularities, the response time must be sufficiently fast to follow external excitations in order to be able to identify topographical irregularities over the motion of the vehicle.

External Excitation

One of the requirements in topographical measurement is to identify a cone, the base of which is 700 centimeters (23.0 feet) in diameter which has a vertex half-angle of 82°. With an assumed vehicle speed of 1.0 fps, the time required to climb the cone is approximately

$$T = \frac{\ell/2}{V} = 12 \text{ sec}$$

where

ℓ = base diameter of the cone

V = vehicle velocity

T = climbing time

Thus the response of the clinometer must exceed this 12 second half-cycle time in order to properly follow such terrain irregularities.

Natural Frequencies of Vehicle

Many modes of vibrations exist in the vehicle assembly. These will be computed as follows:

(1) Longitudinal Vibrations

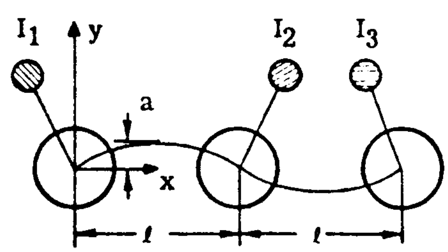

Let

x = distance from first axle

y = vertical displacement of elastic frame

$\theta = \frac{dy}{dx}$ = slope of deflected elastic frame

a = maximum vertical displacement of elastic frame

ℓ = length of elastic frame

b = width of the frame

h = thickness of the frame

ρ = density of the frame

I = moment of inertia of cross-sectional area of the frame

M = mass of the frame

E = modulus of elasticity of the frame material

I_1, I_2, I_3 = unbalanced mass moment of inertia on axles 1, 2, 3

M_1, M_2, M_3 = mass on axles 1, 2, 3

ω = natural frequency of the vibration of this mode and assume $y = a \sin \frac{\pi x}{\ell} \sin \omega t$.

Then the maximum kinetic energy of the system is the sum of the kinetic energy of unbalanced mass and rod, i. e.,

$$K = \frac{1}{2}(I_1 + I_2 + I_3)\,\dot{\theta}^2_{x=0\ max} + 2 \cdot \frac{1}{2}\rho b h \omega^2 a^2 \int_0^{2\ell} \operatorname{Sin}\frac{2\pi x}{\ell}\,dx$$

$$= \frac{1}{2}(I_1 + I_2 + I_3)\left(\frac{\omega a \pi}{\ell}\right)^2 + \rho b h \omega^2 a^2 \ell$$

On the other hand, the maximum potential energy is

$$P = 2\frac{EI}{2}\int_0^{2\ell}\left(\frac{d^2 y^2}{dx^2}\right)^2_{max} dx = EI a^2 \left(\frac{\pi}{\ell}\right)^4 \ell$$

By equating $P = K$, we have

$$\omega^2 = \frac{2\,EI\pi^2}{\ell\left[(I_1 + I_2 + I_3) + \frac{2M\ell^2}{\pi^2}\right]}$$

Substituting $E = 30 \times 10^6$ psi

$I = 1/12\ bh^3$

$b = 0.062$ inches

$h = 1.0$ inches

$$I = 19.85 \times 10^{-6} \text{ in.}^4$$

$$M = \frac{0.062 \times 1 \times 22}{386} = 3.53 \times 10^{-3} \ \frac{\text{lb sec}^2}{\text{in.}}$$

$$I_1 \approx 2.22 \text{ lb-in.-sec}^2$$

$$I_2 \approx 0.55 \text{ lb-in. -sec}^2$$

$$I_3 \approx 0.55 \text{ lb-in. -sec}^2$$

we have

$$\omega^2 = \frac{2 \times 30 \times 10^6 \times 19.85 \times 10^{-6} \times \pi^2}{22 \left[3.32 + \dfrac{2 \times 3.53 \times 10^{-3} \times 22^2}{\pi^2}\right]} = 147$$

$$\omega = 12.1 \text{ rad/sec}$$

$$f = 1.9/\text{sec}$$

(2) Vertical Vibration

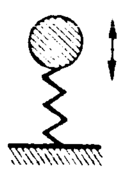

Mass on each axle and the spring action of the wheel form another mode of vibration, namely

$$\omega = \sqrt{\frac{2k}{M_i}}$$

where k = spring constant of one wheel and M_i = mass on the axle.

Substituting

$$k = 5.0 \text{ lb/in.}$$

$$M_i = \frac{30}{386} = 0.0777 \ \frac{\text{lb-sec}^2}{\text{in.}}$$

$$\omega = \sqrt{\frac{10.0}{0.078}} = \sqrt{128.6} = 13.5 \text{ rad/sec}$$

$$f = 1.8/\text{sec}$$

(3) Torsional Vibration

The torsional spring constant of the elastic frame is

$$\frac{b^3 h^3 G}{3.2\,(b^2 + h^2)} = 37.3 \text{ lb-in.}$$

where G = shear modulus of elasticity of the frame material = 11×10^6 psi.

The equivalent torsional spring constant due to the wheel is (tire spring constant) x $[1/2 \text{ (tread)}]^2$ = 980 lb-in.

Largest unbalanced mass moment of inertia on axle I_i is I_1 = 2.22 lb-in.-sec^2 and the total torsional spring constant is k_t = 2 x 37.3 + 980 = 1055 lb-in. Then

$$\omega = \sqrt{\frac{kt}{I}} = \sqrt{\frac{1055}{2.22}} = 475 = 21.8 \text{ rad/sec}$$

and f = 3.5/sec

It seems that the lowest natural frequency of the vehicle is approximately 1.5 cycles per second.

(4) Vibration Characteristics of Clinometer

The time required to climb the specified cone is about 12 seconds, as just discussed, and the information sampling rate is one per second. This means there will be 12 samplings to identify the specified cone. Since the natural frequency of the vehicle is not exactly known, it is difficult to compute the most preferable natural frequency and damping constant of the clinometer. However, the most desirable natural frequency would seem to be 1/2 to 1/3, that of the longitudinal mode of the vehicle, in order to reduce the probable error.

The general characteristics of the pendulum with external excitation can be expressed as

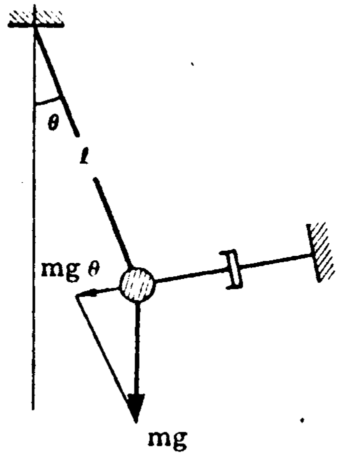

$$m\ddot{\theta} + c\dot{\theta} + k\theta = f(t)$$

where

m = mass of the pendulum

θ = small angle of swing

c = natural damping constant

k = spring constant

$f(t)$ = external excitation

g = gravitational constant

In case of free pendulum, k becomes $k = \frac{mg}{\ell}$.

The solution for this differential equation yields an undamped natural frequency equal to $\sqrt{k/m}$ and a damping constant of $c/2m$. The critical damping of the system is $C_c = 2\sqrt{mk}$.

If the natural frequency of the clinometer is taken in the order of 0.4 cycles/sec, i.e., $\sqrt{k/m} = 2.5$ radians/sec, and if the damping constant is determined so that 85 percent of the transient amplitude damps out in one second, which is the sampling time, i.e., $c/2m \times 1 = \ln 6.66$, or $c/m = 3.8$, then the ratio c/c_c will be approximately 1.3, or the system will be slightly underdamped.

PROPOSED DESIGN

Several clinometer designs have been investigated. However, one design suggested by Marshall Laboratories of Torrance, California, appears particularly attractive at this time. A block diagram of this system appears in Fig. III. 3-24.

This clinometer consists of a pendulous suspended mass, to which is fastened a plate which forms the center plate of a dual capacitive sensor. The center capacitor plate of the pendulum is located between two fixed plates. The configuration of the center plate is such that the capacitances formed by it with the outer plates are functions of the angular position of the pendulum with

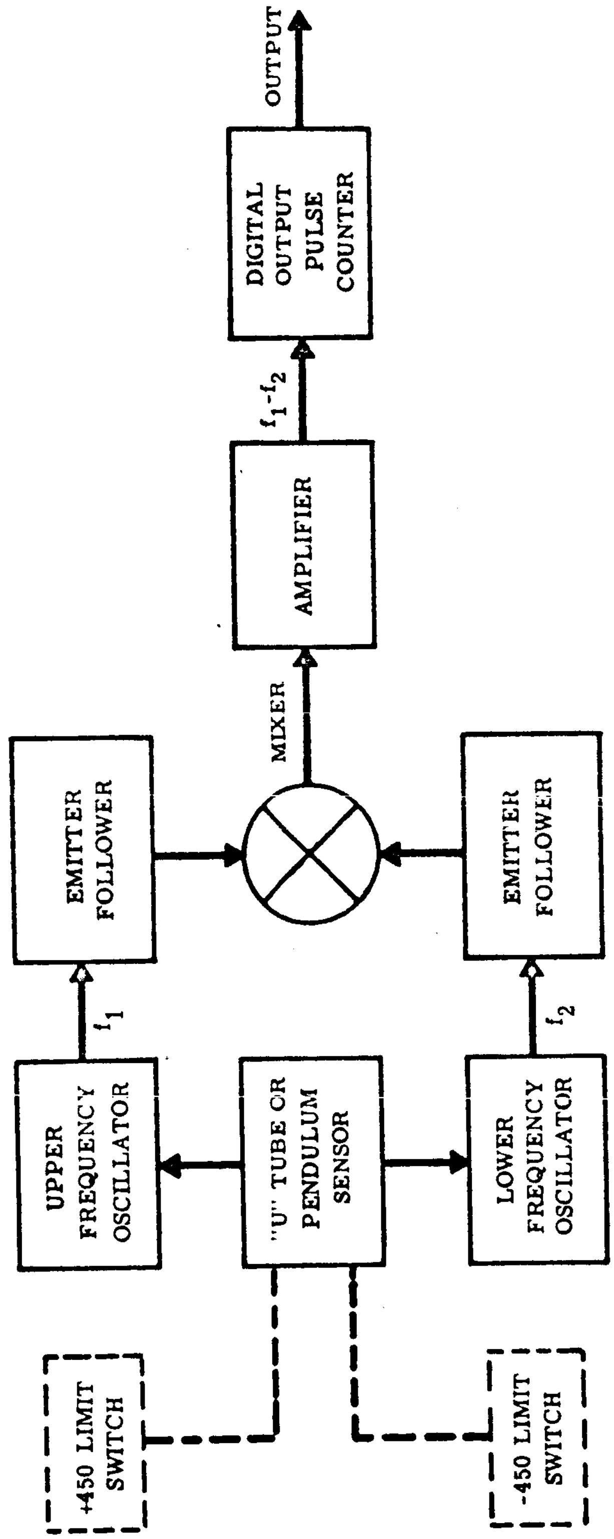

Fig. III. 3-24. Lunar Gravitational Clinometer Block Diagram respect to a vehicle reference plane. Since the pendulum will always assume an equilibrium position with the gravitational field, the capacitances of the plates will uniquely express the angular position of the pendulum with respect to the vehicle-borne reference plane.

The two capacitors are connected as frequency-determining components of two oscillators. The frequency of each oscillator as a function of the pendulum's angular position is shown in Figure III.3-25.

The outputs of the two oscillators are mixed and the frequency difference is applied to a bistable multivibrator counting chain in order to determine frequency, and thus the direction of the gravitational field with respect to the vehicle reference plane.

Two oscillators are used in order to compensate for rate of change of frequency with temperature.

The housing of the clinometer is hermetically sealed and filled with an inert gas. The proper level of viscous damping is achieved by controlling the space between the clinometer and its container.

ALTERNATE DESIGNS

An interesting alternate clinometer design has been conceived at GM DRL. In this design, a pair of concentric metal tubes forming capacitor plates are joined to either side of a "U"-shaped glass tube to form a structure resembling a U-tube manometer. The assembly is partially filled with a dielectric fluid such as silicone oil and mounted in a vertical position on the vehicle. Two such devices mounted along the pitch and roll axes of the vehicle will be used. When tilted along the proper axis the fluid will rise in one tube, increasing the capacitance of that side, and fall in the opposite tube, decreasing the capacitance. Proper damping is easily obtained by putting a restriction in the glass tube connecting the two sides. The two capacitors are connected in a circuit similar to that proposed by Marshall Laboratories. This system has the advantage of

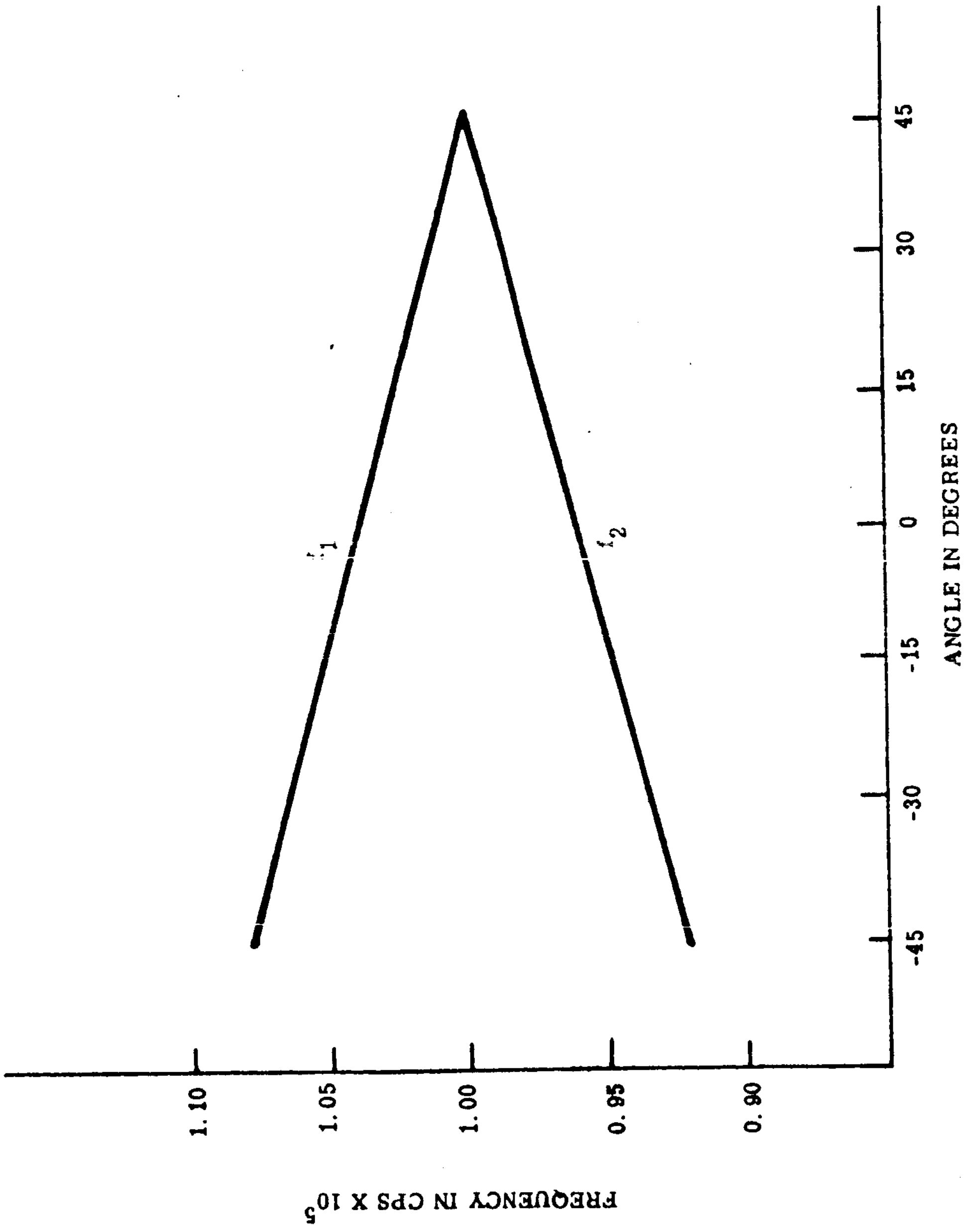

Fig. III. 3-25. Oscillator Frequency versus Gravitational Field Angle having no moving mechanical parts, being very rugged, and requiring no "caging" during lift-off, transit, lunar landing, etc.

Another clinometer scheme to be investigated utilizes two Bendix "Convectron" tubes, mounted at 90° with respect to each other and connected in a DC or AC bridge circuit. Each tube contains an electrically heated fine nickel wire under tension, surrounded by a gas. The angle of each tube with the true horizontal determines the amount of heat transfer from the wire by means of convection currents in the surrounding gas, thereby determining its resistance. Extremely small changes in roll and pitch angle can be detected in this manner, provided suitable electronics can be designed.

F. DEPLOYMENT SYSTEMS

REQUIREMENTS

Any system for the stowage and deployment of the Surveyor Lunar Roving Vehicle must meet the following requirements:

(1) Payload envelope limitations for stowage and deployment as specified in HAC Specifications No. 239503.

(2) Center of gravity constraints as given in above HAC specifications.

(3) Satisfy environmental requirements on Earth, in transit, and on the lunar surface.

(4) Satisfy thermal requirements of negligible heat flow through attachment points between deployment system and Surveyor frame.

(5) Structurally, the mounting and deployment frame has to withstand shock loads and vibrations as specified in HAC Spec. No. 239503.

(6) Design of stowage and deployment mechanism should be as independent of the Surveyor Basic Bus as practicable. Any major modification of the Surveyor spaceframe should be avoided.

(7) Simplicity of design and reliability of deployment.

APPROACH

A proposed method of mounting the packaged lunar roving vehicle on the Surveyor spaceframe, that meets the specified space and center of gravity limitations, is shown in Fig. III. 3-26. The approximate location of the vehicle within the payload envelope is shown in Figures III. 3-27 and III. 3-28.

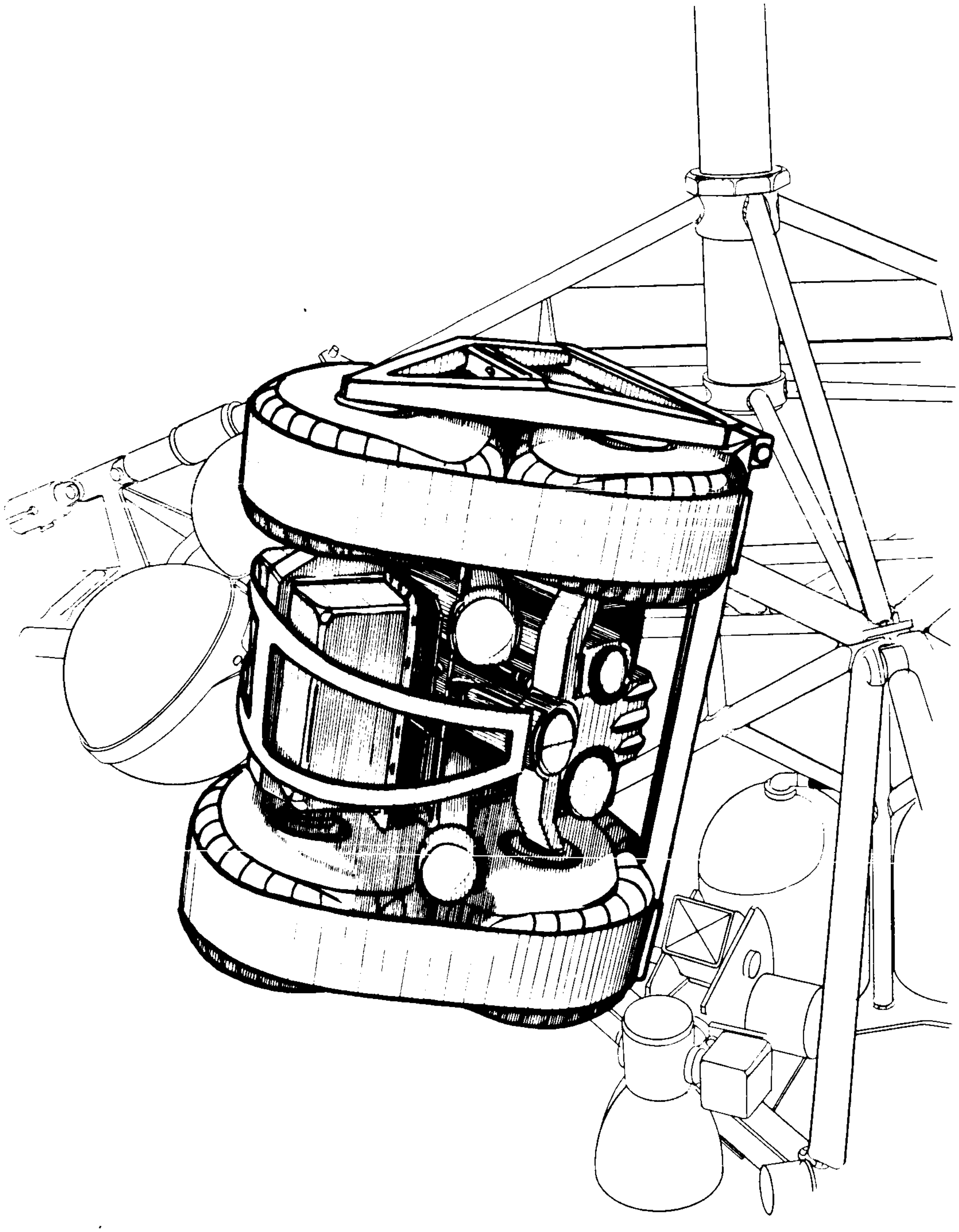

Fig. III. 3-26. Proposed Method of Mounting

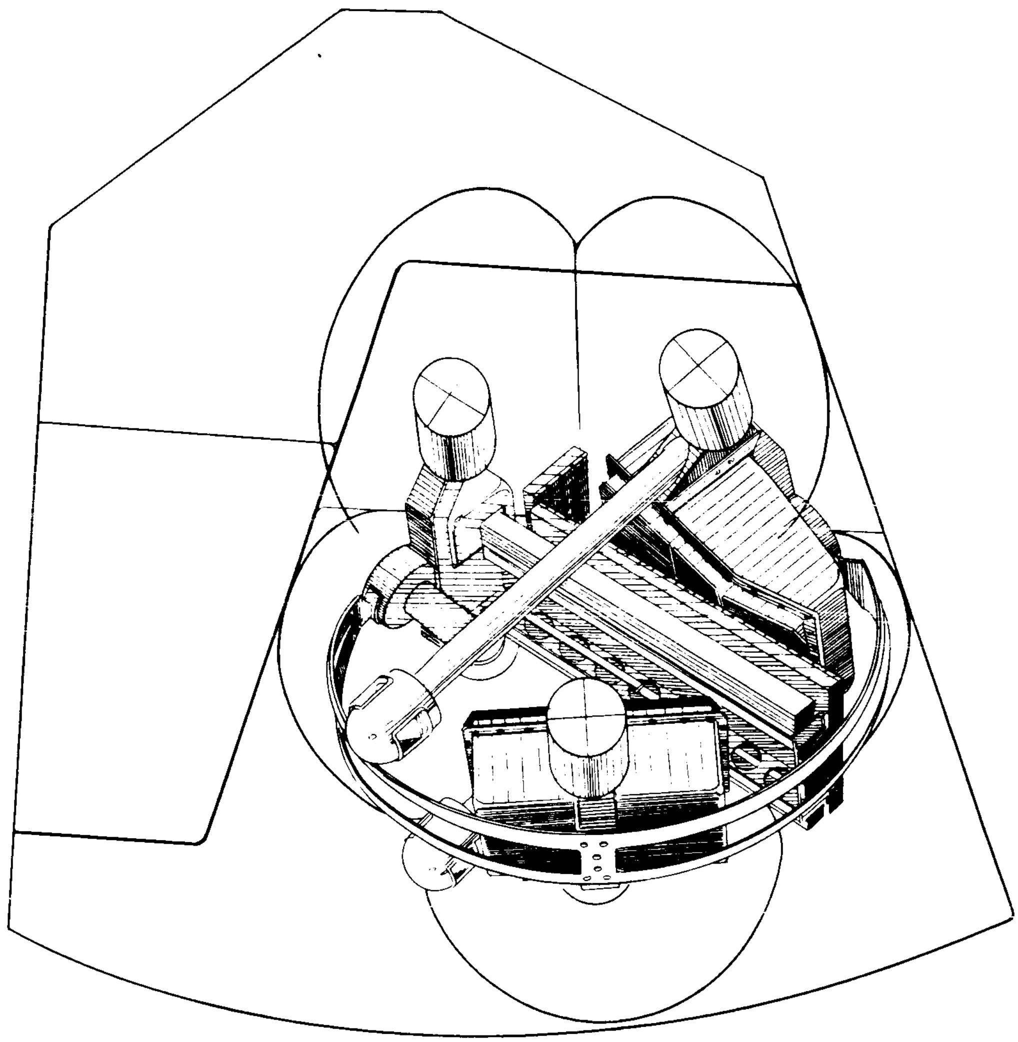

Fig. III.3-27. Stowed Configuration in Allowable Space Envelope, Top View

64-406

Vol. II App. Sec. III

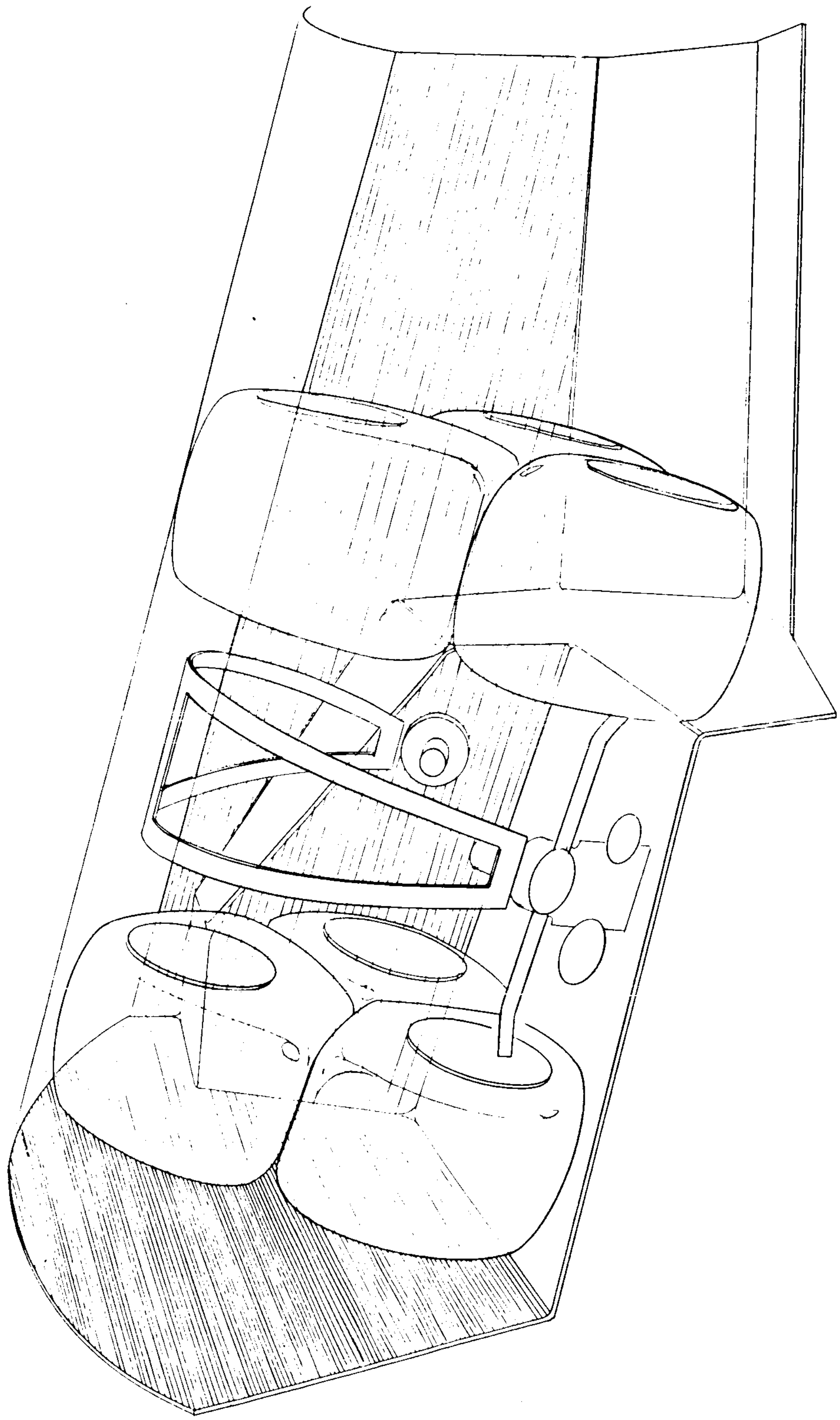

Fig. III. 3-28. Stowed Configuration in Allowable Space Envelope, Side View

363

To fit the envelope, the vehicle is folded into a triangular shape with the wheels deflected up to four inches on a side by means of bands which are attached to the frame of the mounting and deployment mechanism.

The mounting and deployment structure design permits clamping to the Surveyor tubular structure with no basic changes to the Surveyor frame. Furthermore, complicated actuating mechanisms are avoided. Deployment from Surveyor spaceframe to the ground and vehicle unfolding are accomplished by means of simple, preloaded spring mechanisms and explosive pins, leading to high reliability.

DERIVED DESIGN

The proposed mounting and deployment structure consists of an SLRV space flight support assembly which is attached to the upper and lower horizontal Surveyor spaceframe members by a vertical-to-horizontal shear pin deployment mechanism and a fixed cantilevered lower support frame assembly (Figure III. 3-29).

The SLRV space flight support assembly consists of an L-shaped space frame made up of two upright tubular sections that are gusseted and welded to the horizontal tubular members which, with a common transverse sheet metal angle welded to the uprights and the base members, form a triangular frame in the x-y plane. Near the upper end of the upright members, extruded channels with welded face sheets form the upper transverse beam which supports the shear pin mechanism and transmits the major portion of the 35g (amplification of 8 from 4.5g) payload loading into the Surveyor spacecraft structure. At the top of the upright members, another tubular triangular frame is attached by two coaxial hinge pins to allow placement of the SLRV package in the frame. Additional paired back-to-back channel beams are provided in the upper and lower horizontal triangular frames for beaming the tie-down cable loads and the lower hinge-fitting loads into the outer members.

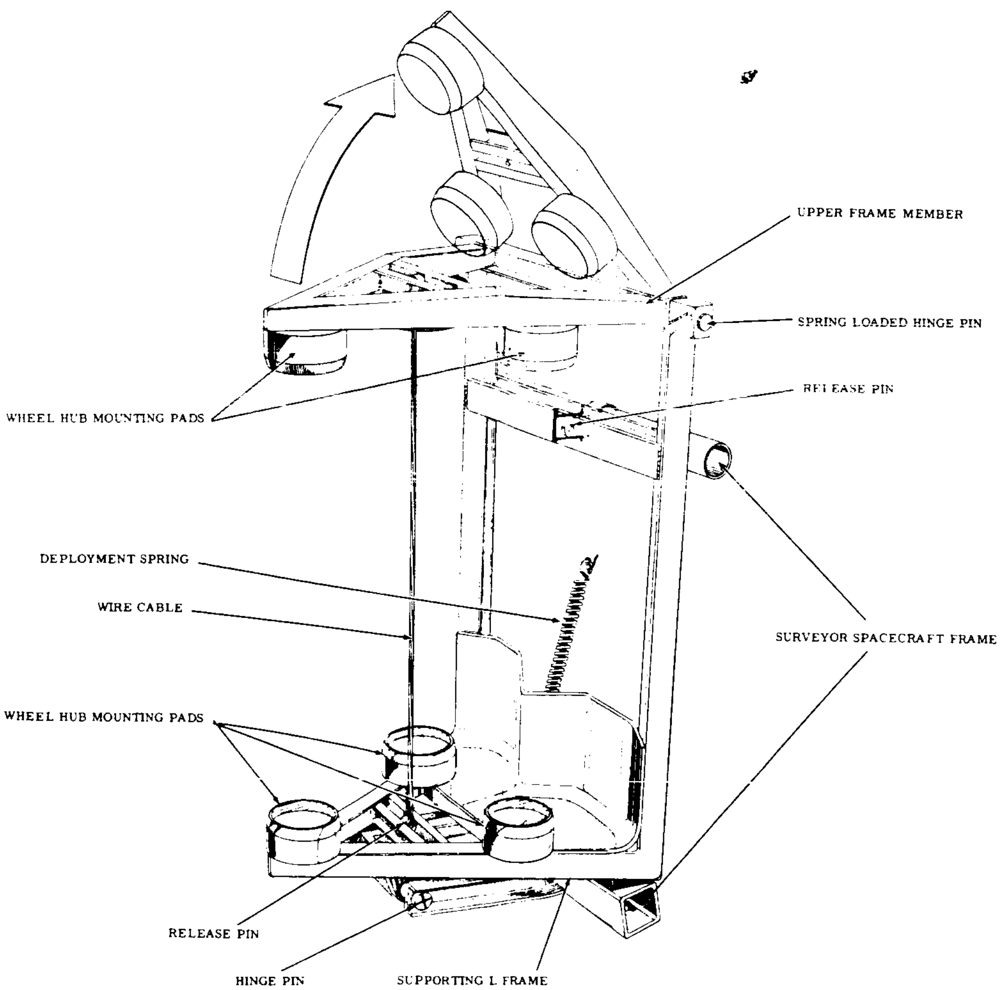

Fig. III. 3-29. Proposed Mounting and Deployment Structure

The lower support frame consists of two pairs of back-to-back channel extrusions welded to the lower horizontal member of the Surveyor spaceframe and transversely interconnected by a channel extrusion in the vicinity of the hinge pins. The male hinge fittings, located in the lower horizontal triangular frame of the L-shaped space frame, are sandwiched between each pair of channel extrusions through which each of the coaxial hinge pins pass. This lower support frame serves primarily as a support for the payload during deployment from the stowed condition, to the horizontal ready position while on the lunar surface; however, due to the elasticity of the mounting L-shaped space-frame structure and its mechanical tie to this member, additional loading is induced during the $\pm 35g$ Earth launch period. The design of this entire package is based on compatible deformations with L-shaped space frame at this hinge attachment, using elastic energy theory to establish loadings on the structure. For the +35 g condition, aluminum alloy bearing blocks are used to transmit the major portion of the load into the lower horizontal member of the Surveyor structure. The remaining portion of the load is transmitted through the lower support hinge into the same horizontal member; resulting torsion is due to the load transfer from the pin. Overturning moments are reacted as couple loads by the lower and upper hinge pins. For the -35g load condition, the load is transferred into the Surveyor spaceframe structure in a similar manner except that the upper hinge pin transfers the major portion of the payload, since the bearing blocks are ineffective in this load condition.

Thin cylindrical tubes with closed ends are provided in each of the horizontal triangular frames which mate into each of the SLRV wheel hubs during stowage for space flight. A 3/16 inch diameter 7 x 19 corrosion resistant steel cable, with one end connected to an explosive separation device and the other end to a retrieving reel mechanism, is provided to hold the SLRV package in place.

In order that deployment of the SLRV from the stowed to the horizontal position takes place after release of the upper hinge pins, a spring with a hinged link is provided. The spring, which is in tension with the package in the stowed position, provides a net force on the base of the space flight support assembly, causing it to rotate to the position where the CG of the SLRV is outboard of the lower hinge line. At this point, gravity on the lunar surface pulls the package through the remaining angle of travel to the horizontal position. During this operation, the hinged link, which is attached to the lower horizontal member of the Surveyor space craft structure and to the after-transverse member of the lower-horizontal triangular frame of the L-shaped space frame at its extremities, unfolds and becomes a straight tension link allowing the package to lock in the horizontal position. The spring, after having moved the package to the position where gravity takes over, now acts to retard rotation such that the shock force is minimized when the package reaches the horizontal position.

Polyurethane lightweight foam-molded blocks will probably be used to separate and restrain movement of the compartments while the payload is in stowed position as shown in Fig. III. 3-30, Springs will probably be used as needed, in the wheel hub areas and in the plastic blocks, to assure positive separation of the SLRV from the mounting and support structure.

All sheet metal and structural shapes used in this design are made of 2014 aluminum alloy. To optimize the strength-to-weight ratios, all tubular sections are made of paired 2014 aluminum alloy channel extrusions with legs machine tapered and welded end-to-end to form tapered rectangular hollow tubes. Hinge pins are made of 3140 steel, or equivalent. All areas which appear to have metal-to-metal contact and require movement of parts in space, will be coated with a suitable plasticizer, to prevent vacuum welding between moving surfaces.

The design presented herein is evolved from preliminary considerations based on assumed loadings and adequate kinematics of deployment. The load distribution on this type of structure is redundant and depends on the stiffness of the Surveyor spaceframe structure and the space-flight support assembly.

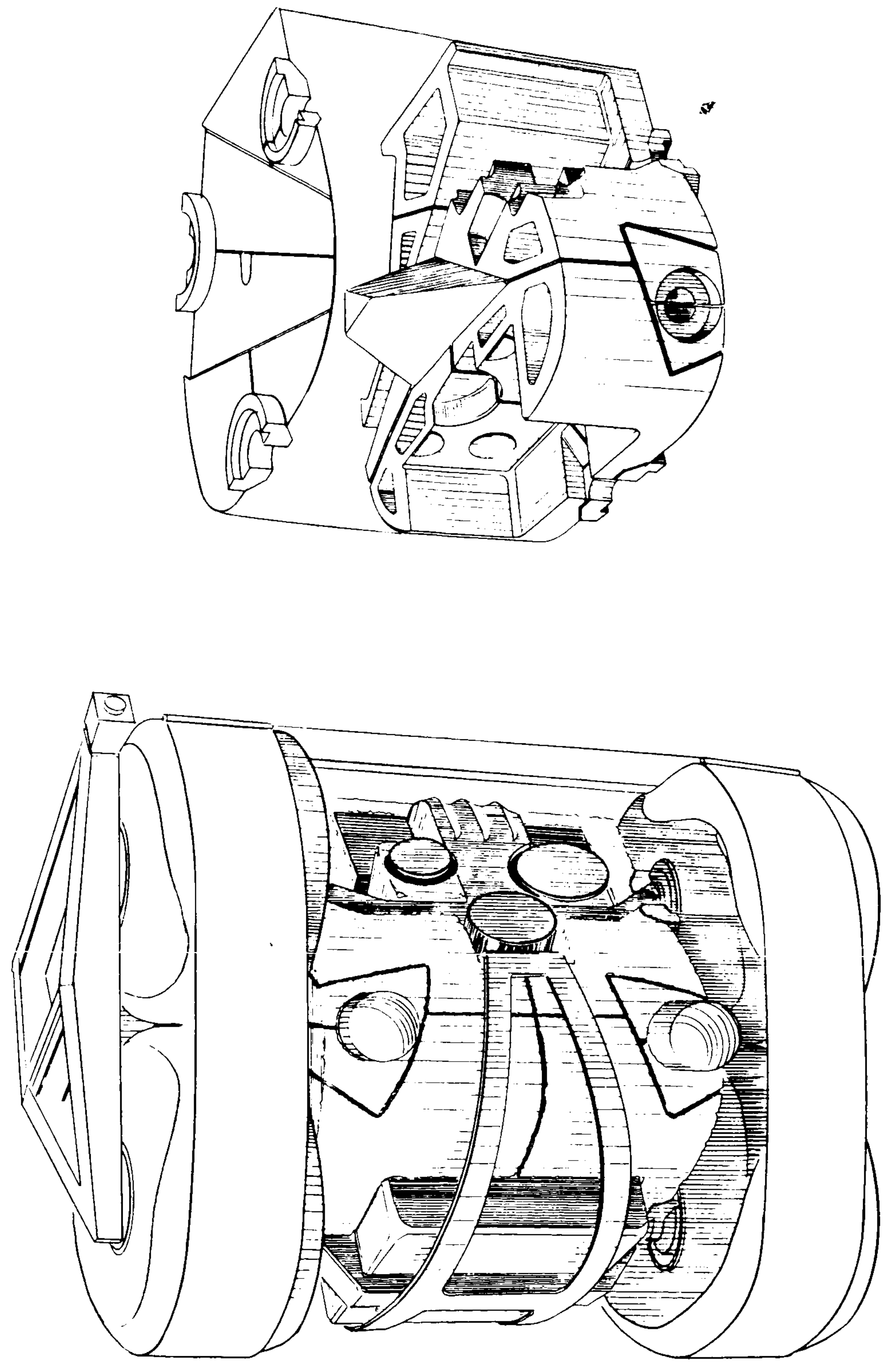

Fig. III. 3-30. Stowed Configuration Showing Polyurethane Foam Blocks

G. ANTENNA-STADIA MASTS

REQUIREMENTS

Communications requirements associated with extended vehicle travel from Surveyor emphasize interest in extensible masts. One important application is a turnstile antenna mast (approximately ten meters in length) for mounting on the Surveyor spacecraft. Another is the combination stadia-turnstile antenna mast (approximately three meters in length) for use on the roving vehicle. Both must be lightweight, stowed in a small volume prior to deployment, and extended upon electrical command; and both must be able to tolerate the lunar environment. The vehicle stadia-antenna mast must, in addition, withstand the dynamic forces imparted to it by motion of the vehicle.

Several schemes for implementing the above requirements have been considered. These include using coiled flat springs to raise a plastic structure, using a compressed helical spring for the same purpose, extending a plastic tubular structure by use of a foaming plastic, etc. The only principle found so far which meets all the requirements is that of inflating a thin plastic or plastic-metal foil laminated structure by gas pressurization. The resulting structure is rigidized by chemical or mechanical means to prevent collapse due to inherent long-term leakage or possible micrometeorite puncturing.

Such a scheme has been proposed by the G. T. Schjeldahl Co. of Northfield, Minnesota, a recognized widely experienced leader in this field. Proposed mast configurations are illustrated in Fig. III. 3-31. A photo of an experimental inflatable stadia-antenna mast appears as Figure III. 3-32.

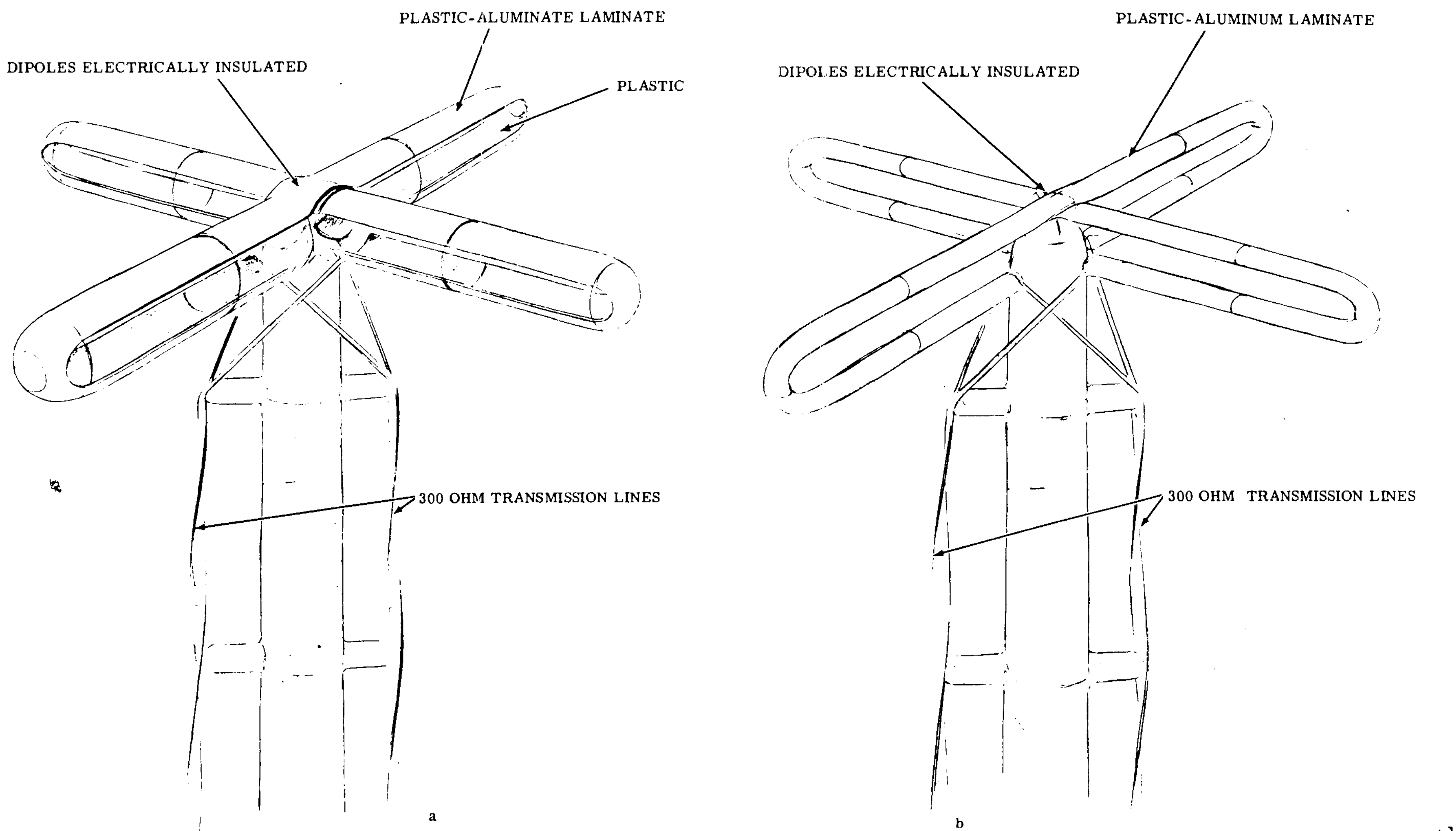

TOP OF LUNAR ROVING VEHICLE AND SURVEYOR MASTS
SHOWING ALTERNATE FOLDED DIPOLE TURNSTILE ANTENNA DESIGNS

Fig. III. 3-31. Proposed Mast and Antenna Configurations

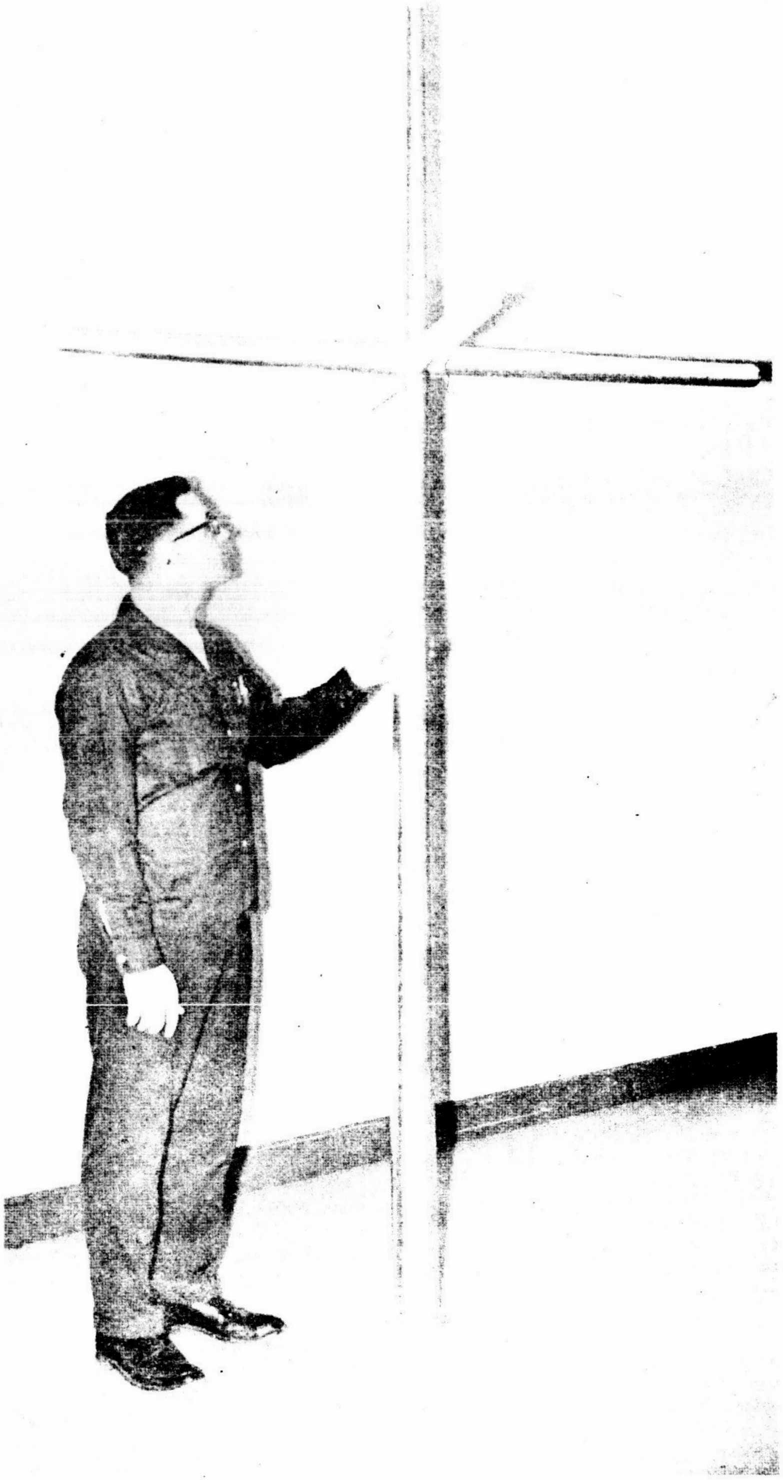

Fig. III. 3-32. Preprototype Stadia Mast

MATERIALS STUDY

Rigidity Requirements

The material required for the roving vehicle antenna and the Surveyor antenna must have a combination of properties that will permit:

- Compact folding and packing
- Sufficient rigidity to support the structural weight under the imposed dynamic and static loads
- Ability to withstand the effects of the lunar environment for 90 days.

The requirement for rigidity at high and low temperatures will necessitate that heat distortion properties of resin systems be upgraded to withstand the intense heat of the lunar day. The systems to be used, however, must be capable of cure in shadow so that a heat distribution mechanism and/or a low temperature cure system must be provided. It is also highly important that the resin systems do not pass through brittle phases when subjected to the deep cold of the lunar night. Heat transfer must be achieved by radiation, because the presence of metal for heat conduction would increase weight and possibly affect the properties of the antennae.

Materials which would be considered for the mast application are a composite of aluminum foil and Mylar, filler materials dispersed in a resin system, triallyl cyanurate used with an inert polymer or a copolymerizing polyester, resorcinols activated by water release, polystyrene used with a cross-linking agent and a fugitive plasticizer whose release from a plastic system will permit rigidization.

Metal Foil-Mylar

The foil-Mylar laminate proposed consists of a three-layer "sandwich" of aluminum-Mylar-aluminum and will be used for the vertical boom of the fixed and roving antennae. Such a three-layer material becomes rigidized by applying an excessive internal pressure which yields the aluminum and has a rigidizing effect on the system.

Polystyrene with Cross-Linking Agent

The crossarms, having a portion of their surface electrically transparent and thus precluding the use of metal foil in some areas, could be rigidized with a resin system such as a cross-linked polystyrene/organic solvent system. Possible cross-linking agents which could be used are divinyl benzene, ethylene dimethacrylate and triallyl cyanurate; each of these would have the effect of improving the temperature resistance of the rigidized structure. When the solvent is driven off, the polystrene is expanded to many times its original volume and forms a very hard and rigid foam.

The polystyrene system is a typical one-component system is which the components are already mixed. Such systems are normally activated by application of heat, UV radiation, vacuum or other external sources to initiate the reaction. In the lunar surface environment, the vacuum could be depended upon for volatilizing the solvent in the plastic system. Also, since inflation would take place during the lunar day, UV radiation and heat would contribute to rigidizing the plastic.

Filler Dispersed in Resin

If foam techniques are not feasible, Micro-balloon spheres (Union Carbide balloon spheres of cured phenolic resin) or hollow ceramic spheres available from Ferro Corporation could be used as fillers in several resin systems. Other promising fillers would include calcined clays, aluminum oxides, milled glass fibers and cellulose fibers. These materials would reduce shrinkage, improve strength and in some cases improve the temperature resistance.

Fugitive Plasticizers

Rigidizing systems can also be approached by use of a fugitive plasticizer whose release would cause a resin system to harden. Water in gelatin, or water glass, as well as organic solvents in various plastic systems are examples. One extension of this, which has been observed, is associated with exposure of Mylar to methylene chloride. It is possible that this might be used as a rigidizing system. Mylar used to form a honeycomb sandwich would have high rigidity.

Resorcinols

Phenolic systems, in general, are highly heat resistant but not generally applicable for low pressure use because of void formation. Their resorcinol cousins, however, are very responsive to acid catalysis and commercial materials curing with the addition of water. Such systems, with a plasticizer, could be activated and rigidized by release of water on arrival at the deployment site.

Triallyl Cyanurate

To achieve high temperature resistance, a system of potential promise would be based on triallyl cyanurate in combination with an inert polymer or a copolymerizing polyester. While such systems react somewhat slowly, much of the past experience has been directed toward high temperature, complete cure reactions. Vibrin No. 136 has shown excellent properties and a great deal of experience has been accumulated in its use. It is clear in appearance and has a 500° F temperature capability. While allyl polymerization systems are generally slow, redox polymerization systems may be expected to reduce the time or temperature required.

Column tests would be conducted on 1/4 or 1/5 scale model columns using the various materials selected for study. Column testing was done extensively on the Advanced Material Development Study conducted for NASA/Goddard using very thin laminates of plastic and aluminum and this experience can contribute appreciably to this program.

In addition, samples of rigidized materials would be tested to determine their stiffness by laying a strip between two supporting surfaces and measuring the load-deflection characteristics.

[redacted]

90-Day Useful Life

Useful life of the antenna material would be determined by conducting accelerated life tests in a 14 x 28 inch space chamber with a vacuum capability of 10^{-9} torr. A simulated solar source (carbon arc) which duplicates the sun's monochromatic wavelength distribution and has variable intensity from zero to two sun power; an Instron Integrator to determine changes in strength over a temperature range of -80 to + 300 C a Mettler Gram-atic balance to determine weight loss; and a spectrometer covering the UV, visible and IR Spectra to determine changes in optical and thermal properties, particularly solar absorptivity and reflectivity are also used.

Accelerated life tests can be run for a period of approximately three weeks at greater-than-normal sun power in the vacuum chamber. The samples would be removed and tested to determine any changes in physical, electrical, optical and thermal properties. Changes would then be incorporated as necessary to give assurance that the material complies with the specification requirements.

Feed Line Fabrication

The feed line will consist of a conductor-dielectric composite in strip form and will be laminated from two basic materials. Experience with Schjelclad Flexible Electrical Laminates shows that minor dimensional modification of an existing product will provide an item to meet the feed-line requirements. The conductor suggested for this application is copper; the dielectric is of Mylar or other materials found suitable from the accelerated life test. Sample strips of feed line will be tested electrically after the accelerated life test. Feed line impedance will be determined by standard methods, measuring both open-circuit and short-circuit impedance and calculating actual impedance.

DESIGN STUDY

The design study would in its initial stage, provide an analytical investigation of the various physical, electrical, optical and thermal properties of the antenna system components to provide backup data for the ensuing design effort and testing program.

Turnstile

The antenna turnstile would be designed generally in accordance with Fig. III. 3-31 previously shown. The turnstile would consist of two intersecting inflatable Mylar cylinders approximately two inches in diameter and 80 inches long. They would intersect at right angles, would be electrically insulated from each other at the juncture, and would have a metal foil conductor strip extending out ten inches on the top and bottom of each cylinder which is connected to form a closed circuit.

Rigidization of the turnstile or crossarms would be accomplished by use of the system which is determined to have the best all-around qualifications as a result of the material study.

Mast

The antenna masts for the roving and stationary systems would be rigidized after initial inflation using the best qualified technique developed during the material study.

Basic mast construction for the 104-inch high roving vehicle antenna could employ, as one possibility, a laminate of Mylar and Dacron cloth. The Mylar would serve as a gas barrier during inflation and the Dacron would contain the rigidizing chemicals. The 40-foot high fixed antenna mast would be fabricated of Mylar and helicallywound with a tape of aluminum Mylar or Dacron-Mylar laminate. The tape would provide a high degree of stiffness to prevent the tall mast from collapsing until the chemical rigidizing system cured.

Base and Canister

The base and canister would be designed as an integral unit. The base would have a rigid cylindrical section on its upper surface to permit attachment of the inflatable structure. Attachment of the mast to the base would be effected using GT-201 Polyester Thermosetting Adhesive which has been space-proven during the nearly three year orbital life of the Echo I Satellite. The base would be designed to provide the simplest mechanical and electrical attachment procedures consistent with design requirements and would be fabricated of metal (aluminum or similar lightweight metal) or a machined or molded plastic (phenolic or fiberglass).

The cannister material would be similar to the base material (either lightweight metal or rigid plastic) and would be fabricated of two or more basic elements which could be separated by electrical signal actuating a mechanical retraction or pyrotechnic device. The canister volume would be determined using the sum of the volumes of the inflation system and the inflatable structure. The inflatable structure packing volume would be determined, for preliminary design purposes, by taking the theoretical material volume and applying a packing factor of approximately six to eight, which is based on experience with similar shapes.

Inflation System

The lunar antennae inflation system must be capable of internally pressurizing the mast and crossarms during the temperature extremes encountered on the moon's surface. This would be accomplished using an inflatant powder or liquid. The inflatant would be chosen on the basis of extensive experience and documentation of test data, when more specific operating temperatures have been dictated and the material weight established. Once the material weight is established, the internal pressure required to support the static weight could be calculated and the inflatant with the required vapor pressure-temperature characteristics selected.

Acetamid, a sublimating powder, has proven very successful in space inflation of large passive communications satellites. Sublimating solids offer the advantage that they produce a given volume of gas with less packing space than a compress gas or contained liqued and have high reliability as inflatants.

Feed Line

The transmission line will be constructed of a composite of plastic-metal foil conductor. Information solicited from a manufacturer who has extensive experience in the manufacture of etched and laminated copper-plastic conductor strip material indicates that the 293 ohm line could be provided using a laminate of copper with H-film, polypropylene or Mylar. The dielectric material will be selected on the basis of its electrical insulation properties and ability to resist degradation effects of the lunar environment-micrometeorite impact, abrasion due to blowing and dust, and chemical decomposition due to radiation energy.

The initial cross-sectional dimensions of the transmission line can be determined using the following equation:

$$Z_o = \frac{276}{(E)^{1/2}} \log \frac{2D}{d}$$

where

- Z_o = characteristic impedance of line
- E = effective dielectric constant of medium surrounding conductors
- D = center-to-center distance between conductors
- d = effective diameter of each conductor

Existing samples of twin conductors embedded in plastic would be tested and the final dimensions of the feed line would depend on laboratory tests which prove out the 293 ohm characteristic impedance.

APPENDIX IV
MODELS

APPENDIX IV
MODELS

A. SCALE MODEL RULES FOR LUNAR VEHICLES

SYMBOLS

c = $\sqrt{E/\rho}$ velocity of sound; also cohesion

f = deflection of a beam

g = gravitational acceleration

ℓ = characteristic length

m = mass

m_r = reduced mass

ν = characteristic velocity

b = width

k_c = modulus of deformation

k_φ = modulus of deformation

p = pressure

z = penetration depth

η = viscosity

μ = Poisson's ratio

ρ = mass density

Δ = lunar vehicle on the moon

$\oplus$ = model on earth

τ = shear stress

φ = angle of internal friction

γ = specific weight

A = area

Ca = Cauchy number

E = Young's modulus

(E) = fictive Young's modulus

F = Force

F_e = elastic force

F_g = gravitation force

F_i = inertial force

Fr = Froude number

G = modulus of rigidity

P = power

Re = Reynolds number

W = weight

W_r = reduced weight

F_c = cohesion force

F_φ = friction force

$\left.\begin{array}{l} F_{kc} = \\ F_{k\varphi} = \end{array}\right\}$ force of vertical penetration

$\left.\begin{array}{l} N_q = \\ N_\gamma = \\ N_c = \end{array}\right\}$ pure numbers depending on φ

Q_D = bearing capacity

INTRODUCTION

If external forces act upon a vehicle moving on an elastic terrain, three forces chiefly determine the movements of the vehicle, regardless of whether it operates on the earth or on the moon:

Gravitation (weight) forces	F_g
Inertia (mass)forces	F_i
Elastic (spring)forces	F_e

If the terrain is not elastic, but soft like sand or clay, some extra forces are involved and the feasibility of scale model tests is questionable. Hence, we confine the following considerations to hard, elastic ground.

The performance of an earth vehicle is similar to that of a lunar vehicle, if the scale factors of forces are equal.

$$\frac{F_i^{\Delta}}{F_g^{\Delta}} = \frac{F_i^{\oplus}}{F_g^{\oplus}} \qquad \text{III. 4-1}$$

$$\frac{F_i^{\Delta}}{F_e^{\Delta}} = \frac{F_i^{\oplus}}{F_e^{\oplus}} \qquad \text{III. 4-2}$$

where

Δ denotes the lunar vehicle operating on the moon, and

$\oplus$ denotes the model of the lunar vehicle operating on the earth.

Further, the form of the two vehicles and the terrain surfaces (obstacles, unevenness) have to be similar, as shown in Fig. III. 4-1.

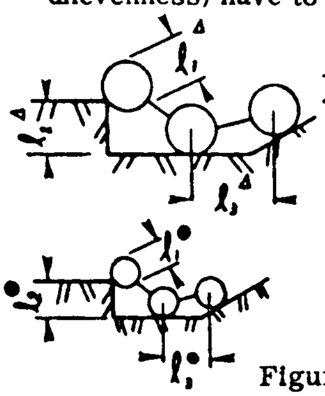

$$\frac{\ell_1^{\Delta}}{\ell_1^{\oplus}} = \frac{\ell_2^{\Delta}}{\ell_2^{\oplus}} = \frac{\ell_3^{\Delta}}{\ell_3^{\oplus}} = \text{constant} \qquad \text{III. 4-3}$$

or in general, $\frac{\ell^{\Delta}}{\ell^{\oplus}} = \text{constant}$

where ℓ^{Δ} is a characteristic length of the moon vehicle, and $\ell^{\oplus}$ is the pertinent characteristic length of the earth vehicle.

Figure III. 4-1

380

Equ. III. 4-1 leads to the Froude number:

$$\mathrm{Fr} = \frac{v}{\sqrt{\ell g}}$$

Hence $$\mathrm{Fr}^{\triangle} = \mathrm{Fr}^{\bullet}$$

or $$\frac{v^{\triangle 2}}{\ell^{\triangle} g^{\triangle}} = \frac{v^{\bullet 2}}{\ell^{\bullet} g^{\bullet}} \qquad \text{III. 4-4}$$

Equ. III.4-2 leads to the Cauchy number:

$$\mathrm{Ca} = \frac{v}{\sqrt{E/\rho}}$$

Hence $$\mathrm{Ca}^{\triangle} = \mathrm{Ca}^{\bullet}$$

or $$\frac{v^{\triangle 2}}{E^{\triangle}/\rho^{\triangle}} = \frac{v^{\bullet 2}}{E^{\bullet}/\rho^{\bullet}} \qquad \text{III. 4-5}$$

wherein v is a characteristic velocity, g is the gravitational acceleration, E is Young's modulus and ρ is the mass density.

By combining Equ.III.4-4 and -5, we obtain:

$$\frac{\ell^{\triangle} g^{\triangle}}{\ell^{\bullet} g^{\bullet}} = \frac{E^{\triangle}}{E^{\bullet}} \frac{\rho^{\bullet}}{\rho^{\triangle}}$$

The gravitational acceleration on the moon is 1/6 that of the earth.

$$g^{\bullet} = 6 \; g^{\triangle}$$

Therefore:

$$\frac{\ell^{\triangle}}{\ell^{\bullet}} = 6 \frac{E^{\triangle}}{E^{\bullet}} \frac{\rho^{\bullet}}{\rho^{\triangle}} \qquad \text{III. 4-6}$$

This equation demonstrates that the scale factor of length is a function of the physical properties of the vehicle materials.

PERFECT SIMILARITY BETWEEN THE MOON VEHICLE AND THE EARTH MODEL ON HARD GROUND

If the materials of the lunar vehicle and its model are the same, Equation III. 4-6 takes the form:

$$\frac{\ell^{\triangle}}{\ell^{\bullet}} = 6$$

Thus, the length of the model is 1/6 that of the lunar vehicle. The velocity of this vehicle is determined by Equation III. 4-5.

$$\frac{\nu^{\Delta}}{\nu^{\bullet}} = 1$$

The weight of a vehicle which is 1/6th the size is only $(1/6)^3$ of the weight of the full-scale vehicle (both on earth or moon). If, for instance, the weight of the lunar vehicle is 75 lbs on earth, the weight of the model would be only 0. 347 lbs. It might be difficult to build such a light, self-propelled vehicle. Therefore, one may look for another material which provides a higher scale factor of length. The formula for the velocity of sound = $c=\sqrt{E/\rho}$. Therefore, we obtain:

$$\frac{\ell^{\Delta}}{\ell^{\bullet}} = 6 \left(\frac{c^{\Delta}}{c^{\bullet}}\right)^2$$

Table III. 4-1 contains the values of c for several materials, and III. 4-2 contains the model values derived from Equ. III. 4-4 and -5. If the material of the moon vehicle is aluminum, the highest scale factor of length is seen to be beryllium. The model made of beryllium is nearly the same size as the moon vehicle; however, its velocity has to be 2. 6 times higher than the velocity of the moon vehicle, and its acceleration has to be divided by 6 and its force by 14. 8 to obtain the corresponding acceleration and power of the moon vehicle performing similar maneuvers. The frequencies of the model are 2. 3 times higher than the frequencies of the moon vehicle.

The disadvantage of beryllium is—besides the difficulties of machining—its low Poisson's ratio. This is $\mu_{ber} = 0.03$ compared with $\mu_{alum} = 0.3$. Since the coefficient of rigidity is:

$$G = \frac{E}{2(1+\mu)}$$

the elastic deformations of the model and of the moon vehicle are similar only in the case of $\mu^{\Delta} = \mu^{\bullet}$. Therefore, the deformation of the beryllium model caused by shear stresses is not similar to the shear deformation of the moon vehicle, which may complicate the evaluation of model tests.

Material	Velocity of Sound c (m/s)	$\frac{c}{c_{alu}} = \frac{c^{\oplus}}{c_{\Delta}}$	$\frac{\ell^{\oplus}}{\ell^{\Delta}} = \frac{1}{6}\left(\frac{c^{\oplus}}{c_{\Delta}}\right)^2$
Silver	2690	.53	1:21.3
Columbium	3470	.69	1:12.6
Copper	3570	.70	1:12.3
Vanadium	4750	.94	1:6.8
Aluminum	5060	1.00	1:6.0
Titanium	5060	1.00	1:6.0
Glass	5600	1.11	1:4.9
Molybdenum	5820	1.15	1:4.5
Chromium	5870	1.16	1:4.5
Silicon	6880	1.36	1:3.2
Beryllium	13100	2.59	1:0.95

TABLE III. 4-1. VELOCITY OF SOUND AND SCALE FACTOR OF LENGTH OF SEVERAL MATERIALS

(Material of the moon vehicle: aluminum)

		Model rule	Moon Vehicle Δ (on moon)			Model on earth $\oplus$			
Material			aluminum			alum.	steel	chromium	beryllium
Young's modulus E	$\frac{kg}{ms^2}$		$6.9 \cdot 10^{10}$			$6.9 \cdot 10^{10}$	$21 \cdot 10^{6}$	$24.8 \cdot 10^{10}$	$31.2 \cdot 10^{10}$
Mass density ρ	$\frac{kg}{m^3}$		$2.7 \cdot 10^{3}$			$2.7 \cdot 10^{3}$	$7.2 \cdot 10^{3}$	$7.2 \cdot 10^{3}$	$1.82 \cdot 10^{3}$
Velocity of sound c	$\frac{m}{s}$		5060			5060	5200	5870	13100
length		$\frac{\ell^\Delta}{\ell^\oplus} = 6\left(\frac{c^\Delta}{c^\oplus}\right)^2$	ℓ^Δ	1	$\frac{\ell^\oplus}{\ell^\Delta}$	1/6	1/5.7	1/4.5	1.12
time		$\frac{t^\Delta}{t^\oplus} = 6\,\frac{c^\Delta}{c^\oplus}$	t^Δ	1	$\frac{t^\oplus}{t^\Delta}$	1/6	1/5.8	1/5.2	.43
velocity		$\frac{\nu^\Delta}{\nu^\oplus} = \frac{c^\Delta}{c^\oplus}$	ν^Δ	1	$\frac{\nu^\oplus}{\nu^\Delta}$	1	1.03	1.16	2.6
acceleration		$\frac{a^\Delta}{a^\oplus} = \frac{1}{6}$	a^Δ	1	$\frac{a^\oplus}{a^\Delta}$	6	6	6	6
force (weight)		$\frac{F^\Delta}{F^\oplus} = 36\,\frac{\rho^\Delta}{\rho^\oplus}\left(\frac{c^\Delta}{c^\oplus}\right)^6$	F^Δ	1	$\frac{F^\oplus}{F^\Delta}$	1/36	1/10.5	1/5.5	5.7
power		$\frac{P^\Delta}{P^\oplus} = 36\,\frac{\rho^\Delta}{\rho^\oplus}\left(\frac{c^\Delta}{c^\oplus}\right)^7$	P^Δ	1	$\frac{P^\oplus}{P^\Delta}$	1/36	1/10.2	1/4.7	14.8

TABLE III.4-2, MODEL RULES OF PERFECT SIMILARITY

[redacted]

Other materials such as steel or chromium are not advantageous compared with aluminum, as Table III. 4-2 shows. Therefore, the concept of complete similarity is satisfied only if the scale factor of the length is about 1:6.

IMPERFECT SIMILARITY BETWEEN THE MOON VEHICLE AND THE EARTH MODEL ON HARD GROUND

The similarity is imperfect if one or more of the conditions (Equations III. 4-1, 2 or 3) are violated. The violation of the model rule is often connected with a geometrical distortion of the model. However, it is often useful to do this in order to obtain the answer to particular questions.

Distortion Due to a Fictive Weight of the Model

It is easy to deduct that

$$\frac{W^{\Delta}}{W^{\oplus}} = \frac{\rho^{\Delta}}{\rho^{\oplus}} \left(\frac{\ell^{\Delta}}{\ell^{\oplus}}\right)^2 \left(\frac{\nu^{\Delta}}{\nu^{\oplus}}\right)^2$$

is a special form of the Froude number, where W is the weight. By replacing the ratio $\frac{\nu^{\Delta}}{\nu^{\oplus}}$ by $\frac{E^{\Delta}/\rho^{\Delta}}{E^{\oplus}/\rho^{\oplus}}$ (Equation III. 4-5), one obtains:

$$\frac{W^{\Delta}}{W^{\oplus}} = \frac{E^{\Delta}}{E^{\oplus}} \left(\frac{\ell^{\Delta}}{\ell^{\oplus}}\right)^2 \qquad \text{III. 4-7}$$

If the materials of the two vehicles are the same, one can write:

$$\frac{W^{\Delta}}{W^{\oplus}} = \left(\frac{\ell^{\Delta}}{\ell^{\oplus}}\right)^2$$

In case of perfect similarity, we obtain:

$$\frac{W^{\Delta}}{W^{\oplus}} = \frac{1}{6} \left(\frac{\ell^{\Delta}}{\ell^{\oplus}}\right)^3 \qquad \text{III. 4-8}$$

Therefore, the term W in $\frac{W^{\Delta}}{W^{\oplus}} = \left(\frac{\ell^{\Delta}}{\ell^{\oplus}}\right)^2$ has to be a reduced weight W_r. Hence, the equation takes the form

$$\frac{W^{\Delta}}{W_r^{\oplus}} = \left(\frac{\ell^{\Delta}}{\ell^{\oplus}}\right)^2 \qquad \text{III. 4-9}$$

From Equ. III. 4-8 and -9 one obtains the reduced weight

$$W_r^{\oplus} = \frac{W^{\oplus}}{6} \frac{\ell^{\Delta}}{\ell^{\oplus}} \qquad \text{III. 4-10}$$

Fig. III.4-2 illustrates this formula. In the case of $\frac{\ell^{\Delta}}{\ell^{\oplus}} = 6$, no weight reducing is needed, as shown previously, and one obtains a free-roving model. The weight of the model can be changed greatly by suspending the model on quasi-elastic springs (Figure III. 4-3). The transmission of the levers is variable, such that the force of relief $W^{\oplus} - W_r^{\oplus}$ is independent of the vertical displacement of the model. The levers and the springs are practically without mass. Figure III. 4-4 shows how the velocity of the model depends on the scale factor of length (Equation III. 4-4).

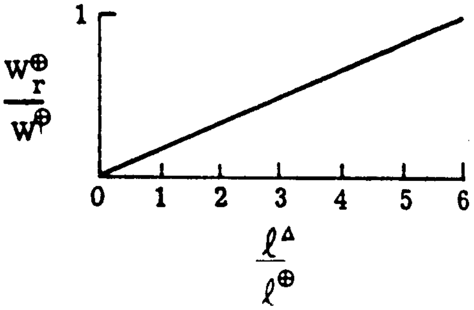

Figure III. 4-2

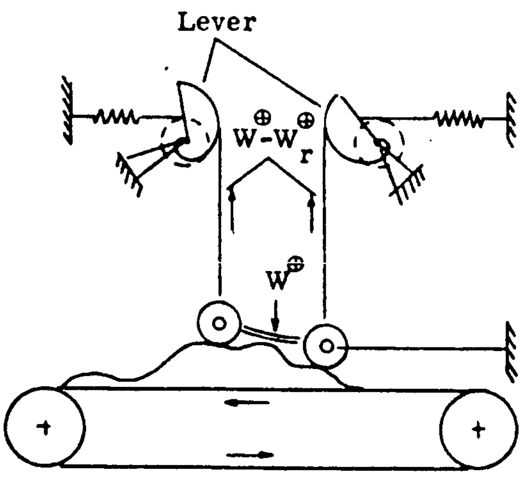

Figure III. 4-3

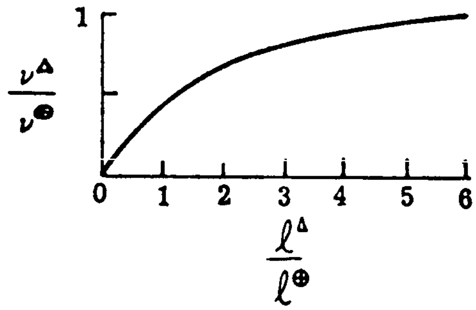

Figure III. 4-4

386

To conduct tests with a suspended vehicle is advantageous because the scale factor of length can be greater than 1/6. However, there are some other aspects of the problem.

- The vehicle cannot move horizontally, therefore the terrain has to be moved by means of a belt or similar device. Hence, it is difficult to simulate steering effects.
- Every mass of the vehicle has to be suspended in its center of gravity. This is very difficult if not impossible to achieve if the assembly is complicated (antenna, instruments, battery); in fact, the model can only be suspended in a few points.
- The experimental set-up becomes very large if a big model is investigated on a very rough terrain.
- Elastic forces and inertial forces have to be carefully avoided in the suspension.

Distortion Due to a Fictive Young's Modulus

Repeating Equ.III.4-6, the scale ratio of length depends on the physical properties of the material

$$\frac{\ell^{\Delta}}{\ell^{\oplus}} = 6\,\frac{E^{\Delta}}{E^{\oplus}}\,\frac{\rho^{\oplus}}{\rho^{\Delta}} \qquad \text{III. 4-10}$$

If the materials of the moon vehicle and the model are the same, one can distort the model to such a degree that a fictive Young's modulus ($\overset{\oplus}{E}$) can be calculated for every $\frac{\ell^{\Delta}}{\ell^{\oplus}}$:

$$\frac{\ell^{\Delta}}{\ell^{\oplus}} = 6\,\frac{E^{\Delta}}{(E^{\oplus})} \quad \text{where} \quad \rho^{\Delta} = \rho^{\oplus}$$

For example, it is assumed that a tube-shaped beam (elastic frame) would be replaced by another spring of the same material with the same cross-sectional area and the same length, but with a greater (fictive) Young's modulus. Fig. III.4-5 shows the cross sections of the beams. If the beams are bent by a Force F, their spring constants are

$$\frac{F_{o}}{f_{o}} \sim EI_{o} \quad \text{and} \quad \frac{F_{\diamond}}{f_{\diamond}} \sim E\,I_{\diamond}$$

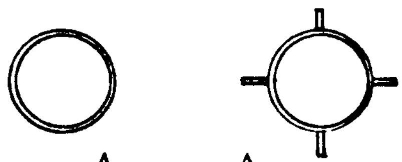

$A_{\circ} = A_{\diamond}$

Figure III. 4-5

where f is the deflection and I is the moment of inertia.

Suppose the second beam is a tube-shaped beam like the first, but is of another material with a different (fictive) Young's modulus (E). Then,

$$\frac{F_{\diamond}}{f_{\diamond}} \sim (E)\, I_o$$

Then, by combining the last equations, one obtains

$$(E) = E\,\frac{I_{\diamond}}{I_{\circ}}$$

If the material of the moon vehicle and the model are equal ($E^{\Delta} = E^{\bullet}$ and $\rho^{\Delta} = \rho^{\bullet}$) Equation III. 4-6 takes the form

$$\frac{\ell^{\Delta}}{\ell^{\oplus}} = 6\,\frac{E^{\Delta}}{E^{\Delta}\dfrac{I_{\diamond}}{I_o}} \quad \text{or} \quad \frac{\ell^{\Delta}}{\ell^{\oplus}} = 6\,\frac{I_o}{I_{\diamond}}$$

In order to guarantee the similarity of performance, the distortion of the elastic parts of the model is a matter of careful calculations, depending on the distribution of tensile and shearing stresses.

<u>Distortion Due to the Mass Distribution</u>

In terms of mechanics, the vehicle consists of springs and masses. The springs (elastic frame) have some mass and the masses have some elasticity. However, it might be possible to neglect the weight of the springs and the elasticity of masses. In this case Equation III. 4-6 takes the form:

$$\frac{\ell^{\Delta}}{\ell^{\oplus}} = \sqrt{\frac{1}{6}\;\frac{m^{\Delta}}{m^{\bullet}}\;\frac{E^{\oplus}}{E^{\blacktriangle}}} \qquad \text{III. 4-11}$$

Deduction: It is $\dfrac{F_e{}^{\Delta}}{F_g{}^{\Delta}} = \dfrac{F_e{}^{\bullet}}{F_g{}^{\bullet}}$

[redacted]

Further, $F_e \sim \ell^2 E$

$F_g \sim mg$, where m is the mass of the vehicle

Equ. III.4-11 was obtained by combining these formulas.

If $E^{\bullet} = E^{\Delta}$ one obtains:

$$\frac{m^{\Delta}}{m^{\bullet}} = 6 \left(\frac{\ell^{\Delta}}{\ell^{\oplus}}\right)^2 \qquad \text{III. 4-12}$$

In the case of perfect similarity one would obtain:

$$\frac{m^{\Delta}}{m^{\oplus}} = \left(\frac{\ell^{\Delta}}{\rho^{\oplus}}\right)^3 \text{ if } E^{\oplus} = E^{\Delta} \text{ and if } \rho^{\oplus} = \rho^{\Delta} \qquad \text{III. 4-13}$$

Therefore, the mass m in Equ. III.4-12 is not equal to the mass m in Equ. III.4-13. Hence, m in Equ. III.4-12 is a reduced mass m_r

$$\frac{m^{\Delta}}{m_r^{\oplus}} = 6 \left(\frac{\ell^{\Delta}}{\ell^{\oplus}}\right)^2 \qquad \text{III. 4-14}$$

By combining Equ. III.4-13 and -14 one obtains:

$$\frac{m_r^{\oplus}}{m^{\oplus}} = \frac{1}{6} \quad \frac{\ell^{\Delta}}{\ell^{\oplus}} \qquad \text{III. 4-15}$$

If $\frac{\ell^{\Delta}}{\ell^{\oplus}} = 6$, no mass reduction is needed as shown before. If $\frac{\ell^{\Delta}}{\ell^{\oplus}} = 1$, all masses of the model have to be reduced to 1/6. Fig. III. 4-6 illustrates equ. III.4-15.

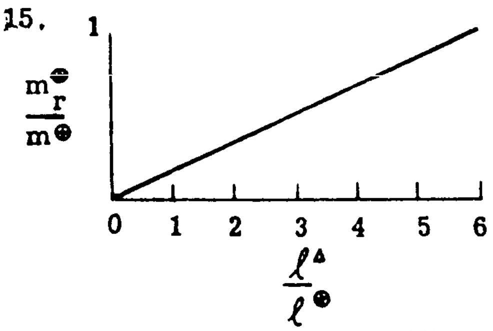

This conception gives free choice of the scale factor of length. Besides Equ. III. 4-15, the condition of Equ. III.4-4 has to be fulfilled:

$$\frac{\nu^{\Delta}}{\nu^{\oplus}} = \sqrt{\frac{1}{6} \frac{\ell^{\Delta}}{\ell^{\oplus}}}$$

Figure III. 4-6

Table III. 4-3 contains all model rules of perfect and imperfect similarity. Table III. 4-4 gives some illustrations for this rule.

[redacted]

[redacted]

Perfect Similarity	Imperfect Similarity Moon vehicle and model are of the same material		
	Weight Reduction	Mass Reduction	Fictive Young's Modulus
$\frac{\ell^\oplus}{\ell^\Delta} = \frac{1}{6}\left(\frac{c^\oplus}{c^\Delta}\right)^2$	$\frac{\ell^\oplus}{\ell^\Delta} = \frac{1}{6}\;\frac{W^\oplus}{W_r^\oplus}$	$\frac{\ell^\oplus}{\ell^\Delta} = \frac{1}{6}\;\frac{m^\oplus}{m_r^\oplus}$	$\frac{\ell^\oplus}{\ell^\Delta} = 6\,\frac{E}{(E)}$
$\frac{\nu^\oplus}{\nu^\Delta} = \sqrt{6\,\frac{\ell^\oplus}{\ell^\Delta}}$	*	*	*
$\frac{a^\oplus}{a^\Delta} = 6$	*	*	*
$\frac{m^\oplus}{m^\Delta} = \frac{\rho^\oplus}{\rho^\Delta}\left(\frac{\ell^\oplus}{\ell^\Delta}\right)^3$	*	$\frac{m_r^\oplus}{m^\Delta} = \frac{1}{6}\left(\frac{\ell^\oplus}{\ell^\Delta}\right)^2$	*
$\frac{W^\oplus}{W^\Delta} = 6\;\frac{m^\oplus}{m^\Delta}$	$\frac{W_r^\oplus}{W^\Delta} = \frac{\ell^\Delta}{\ell^\oplus}\;\frac{m^\oplus}{m^\Delta}$	*	*
$\frac{F^\oplus}{F^\Delta} = 6\;\frac{m^\oplus}{m^\Delta}$	*	*	*
$\frac{P^\oplus}{P^\Delta} = \frac{F^\oplus}{F^\Delta}\;\frac{\nu^\oplus}{\nu^\Delta}$	*	*	*

TABLE III.4-3. MODEL RULES OF PERFECT AND IMPERFECT SIMILARITY.

($W^\oplus$ and $m^\oplus$ are weights and masses of the perfect model.)

* = Same as for perfect similarity

[redacted]

TABLE III. 4-4. SOME EXAMPLES ILLUSTRATING THE MODEL RULES

Lunar roving vehicle on the moon	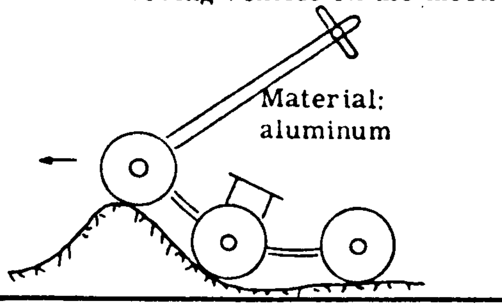							
Model on earth		$l^{\oplus}/l^{\Delta}$	$v^{\oplus}/v^{\Delta}$	$a^{\oplus}/a^{\Delta}$	$m^{\oplus}/m^{\Delta}$	$W^{\oplus}/W^{\Delta}$	$F^{\oplus}/F^{\Delta}$	$P^{\oplus}/P^{\Delta}$
Perfect Similarity	Material: aluminum 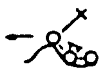	1/6	1	6	1/216	1/36	1/36	1/36
	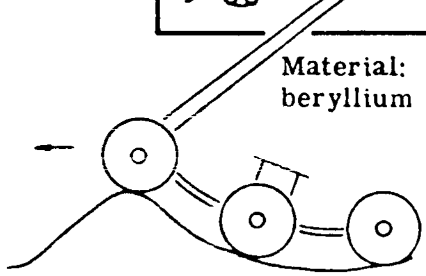	1.12	2.6	6	0.95	5.7	5.7	14.8
Imperfect Similarity for $l^{\oplus}/l^{\Delta} = 1/2$ Material: aluminum	Weight reduction $\frac{W_r^{\oplus}}{W^{\oplus}} = 1/3$ 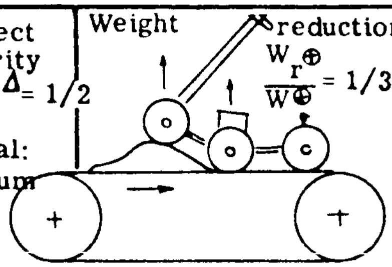	1/2	$\sqrt{3}$	6	1/8	$W_r^{\oplus}/W^{\Delta}$ 1/4	3/4	$3/4\sqrt{3}$
Scale factors of length other than 1/2 are possible	Mass reduction $\frac{m_r^{\oplus}}{m^{\oplus}} = 1/3$ 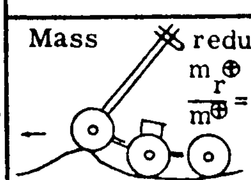	1/2	$\sqrt{3}$	6	$m_r^{\oplus}/m^{\Delta}$ 1/24	1/4	1/4	$\sqrt{3}/4$
	Fictive Young's modulus 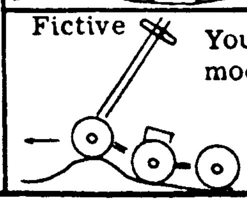	1/2	$\sqrt{3}$	6	1/8	3/4	3/4	$3/4\sqrt{3}$

INFLUENCE OF DAMPING FORCES

If we presume that the friction of damping devices (shock absorbers, plastic members) is proportional to the velocity of deformation and if the magnitude of these damping forces is high, the Reynolds number has to be considered.

$$Re = \frac{\rho \nu \ell}{\eta}$$

where η is the viscosity

Therefore $$\frac{\rho^{\Delta} \nu^{\Delta} \ell^{\Delta}}{\eta^{\Delta}} = \frac{\rho^{\bullet} \nu^{\bullet} \ell^{\bullet}}{\eta^{\bullet}}$$

or $$\frac{\eta^{\oplus}}{\eta^{\Delta}} = \frac{\rho^{\oplus}}{\rho^{\Delta}} \frac{\nu^{\oplus}}{\nu^{\Delta}} \frac{\ell^{\oplus}}{\ell^{\Delta}} \qquad \text{III. 4-16}$$

Hence $$\frac{\nu^{\oplus}}{\nu^{\Delta}} = \sqrt[6]{\frac{\ell^{\oplus}}{\ell^{\Delta}}}$$

and it is also $$\frac{\eta^{\oplus}}{\eta^{\Delta}} = \frac{\rho^{\oplus}}{\rho^{\Delta}} \frac{\ell^{\oplus}}{\ell^{\Delta}} \sqrt[6]{\frac{\ell^{\oplus}}{\ell^{\Delta}}} \qquad \text{III. 4-17}$$

The scale factor of length is determined by one of the equations in Table IV.

PERFECT SIMILARITY ON SOFT SOIL

The interaction on earth between a vehicle and soft soil can be described satisfactorily in terms of Coulomb's equation $\tau = c + p \tan \varphi$ and Bekker's equation $$\tau = \left(\frac{k_c}{b} + k_{\varphi}\right) z^n$$

M. G. Bekker of GM DRL[9] has shown how these two equations furnish a basis for the calculation of sinkage, rolling resistance and thrust of a tracked or wheeled vehicle on a variety of different soils. The agreement between calculation and experiment is generally good.

The properties of moon soil are unknown. However, we may expect that the two equations are applicable on earth as well as on the moon; namely, the soil properties can be measured in terms of cohesion c, angle of internal friction φ and moduli k_c and k_{φ}. Therefore, it is feasible to deduce model rules from these two equations.

Coulomb's equation expresses the resistance of a soil against horizontal shearing

$$F_s = A\left(c + p \tan \varphi\right) \qquad \text{III. 4-18}$$

where A is the shear area and p is the vertical pressure.

This shear resistance can be divided into two parts

$$F_c = A\,c \quad \text{and} \quad F_\varphi = A\,p \tan \varphi$$

The pressure p is caused by the weight of the vehicle

$$p = \frac{m\ g}{A}$$

Therefore, the second force is represented by

$$F_\varphi = mg \tan \varphi \sim \ell^3\ \rho\, g \tan \varphi \qquad \text{III. 4-19}$$

and the first force is represented by

$$F_c \sim \ell^2\ c \qquad \text{III. 4-20}$$

where ℓ is a characteristic height of the vehicle.

Bekker's equation represents the resistance of soil against vertical penetration.

$$F_p = A\left(\frac{k_c}{b} + k_\varphi\right) z^n \qquad \text{III. 4-21}$$

From this we obtain two forces:

$$F_{kc} = A\,\frac{k_c}{b}\ z^n$$

and

$$F_{k\varphi} = A\,k_\varphi\ z^n$$

It has been shown elsewhere (8) that η may vary considerably from 1 without changing the similarity greatly. Therefore, one can simplify the last two terms

$$F_{kc} \sim \ell^2\ k_c \qquad \text{III. 4-22}$$

$$F_{k\varphi} \sim \ell^3\, k_\varphi \qquad \text{III. 4-23}$$

In order to derive the model rules which govern the performance of a vehicle on soft ground, one has to combine the gravitational force, the elastic force and the inertial force of the vehicle and the four soil forces:

Vehicle	Gravitational force	$F_g \sim \rho\, g\, \ell^3$	III. 4-24
	Elastic force	$F_e \sim E\, \ell^2$	III. 4-25
	Inertial force	$F_i \sim \rho\, \dfrac{\ell^4}{t^2}$	III. 4-26
Soil	Shear force	$F_c \sim c\, \ell^2$	III. 4-20
		$F_\varphi \sim \rho\, g \tan\varphi\, \ell^3$	III. 4-19
	Penetration force	$F_{kc} \sim k_c\, \ell^2$	III. 4-22
		$F_{k\varphi} \sim k_\varphi\, \ell^3$	III. 4-23

One obtains 6 dimensionless numbers. The combinations are arbitrary, but they have to fulfill the requirement that each force can be combined with each other force.

$$\frac{F_g}{F_{k\varphi}} = \frac{\rho\, g}{k_\varphi} \qquad \frac{F_g}{F_e} = \frac{\rho\, g\, \ell}{E}$$

$$\frac{F_g}{F_\varphi} = \frac{1}{\tan\varphi} \qquad \frac{F_g}{F_{kc}} = \frac{c}{k_c}$$

$$\frac{F_g}{F_i} = \frac{g\, t^2}{\ell} = \frac{g\, \ell}{v^2} \qquad \frac{F_c}{F_{kc}} = \frac{E}{k_c}$$

The performances of the moon vehicle and the model on earth are similar if

$$\frac{F_g^{\triangle}}{F_{k\varphi}^{\triangle}} = \frac{F_g^{\oplus}}{F_{k\varphi}^{\oplus}} \qquad \text{and so on}$$

Therefore

$$\frac{\rho^{\Delta}}{k_{\varphi}^{\Delta}} = \frac{6\rho^{\oplus}}{k_{\varphi}^{\oplus}} \qquad \frac{\rho^{\Delta}\ell^{\Delta}}{E^{\Delta}} = \frac{6\rho^{\oplus}\ell^{\oplus}}{E^{\oplus}}$$

$$\varphi^{\Delta} = \varphi^{\oplus} \qquad \frac{c^{\Delta}}{k_c^{\Delta}} = \frac{c^{\oplus}}{k_c^{\oplus}}$$

$$\frac{\ell^{\Delta}}{\nu^{\Delta 2}} = \frac{6\ell^{\oplus}}{\nu^{\oplus 2}} \qquad \frac{E^{\Delta}}{k_c^{\Delta}} = \frac{E^{\oplus}}{k_c^{\oplus}}$$

As obtained above, perfect similarity is possible only if

$$\ell^{\Delta} = 6\,\ell^{\oplus}$$
$$E^{\Delta} = E^{\oplus} \qquad \text{(See Equation III. 4-6)}$$
$$\rho^{\Delta} = \rho^{\oplus}$$

Hence

$$\nu^{\oplus} = \nu^{\Delta}$$
$$k_{\varphi}^{\oplus} = 6\,k_{\varphi}^{\Delta}$$
$$\varphi^{\oplus} = \varphi^{\Delta}$$
$$k_c^{\oplus} = k_c^{\Delta}$$
$$c^{\oplus} = c^{\Delta}$$

If the model moves with the same velocity as the moon vehicle, the measured sinkages, forces and powers can be referred to a moon soil with the same c, φ and k_c, but with a module k_{φ} which is six times smaller than the module on earth.

This result corresponds with the formula for bearing capacity (general and local shear failure) as formulated by Terzaghi (6) and others. The bearing capacity of a soil without cohesion can be calculated from

$$Q_D = 2\gamma\ b^2 \ell\ N_{\gamma} \qquad \text{III. 4-24}$$

where γ is the specific weight of the soil, the width of the footing is 2b, ℓ is the length of the (rectangular) footing, and N_{γ} is a soil parameter depending on the angle of internal friction φ. If the soil on the moon has no cohesion, the bearing capacity is 6 times smaller than on earth, according to the above formula, because the specific weight is six times smaller.(7)

If the moon venicle is six times larger than the earth vehicle, it is

$$\frac{b^{\oplus}}{b^{\Delta}} = \frac{\ell^{\oplus}}{\ell^{\Delta}} = \frac{\gamma^{\Delta}}{\gamma^{\oplus}} = \frac{1}{6} \quad \text{and (provided that } N_{\gamma}^{\Delta} = N_{\gamma}^{\oplus})$$

$$\frac{Q_D^{\oplus}}{Q_D^{\Delta}} = \frac{1}{36} .$$

This relationship between bearing capacities is the same in the case of cohesive soil. According to Terzaghi, it is

$$Q_D = 2b\ell c\, N_c \qquad \text{III. 4-25}$$

where N_c is a soil parameter depending on the angle of internal friction φ.

Hence, if $N_c^{\oplus} = N_c^{\Delta}$ and $\dfrac{b^{\oplus}}{b^{\Delta}} = \dfrac{\ell^{\oplus}}{\ell^{\Delta}} = \dfrac{1}{6}$ and $c^{\oplus} = c^{\Delta}$

$$\frac{Q_D^{\oplus}}{Q_D^{\Delta}} = \frac{1}{36}$$

If one compares any other forces, the same figure is obtained. The comparison of the elastic forces provides

$$\frac{F_e^{\oplus}}{F_e^{\Delta}} = \frac{\ell^{\oplus 2}}{\ell^{\Delta 2}} \; \frac{E^{\oplus}}{E^{\Delta}} = \frac{1}{36} \quad \text{with } E^{\oplus} = E^{\Delta}$$

or of the force $F_{k\varphi}$

$$\frac{F_{k\varphi}^{\oplus}}{F_{k\varphi}^{\Delta}} = \frac{k_{\varphi}^{\oplus}}{k_{\varphi}^{\Delta}} \; \frac{\ell^{\oplus 3}}{\ell^{\Delta 3}} = \frac{1}{36} \quad \text{with } k_{\varphi}^{\oplus} = 6k_{\varphi}^{\Delta}$$

HOW TO PERFORM MODEL TESTING

There are two exact solutions of the problem of testing models:

- To conduct experiments with the full-size moon vehicle in an aircraft flying a 1/6 g trajectory
- To conduct experiments on earth with a model similar to the full-scale vehicle, but 1/6 its size.

In both cases one obtains a true picture of the performance of the moon vehicle by measuring velocities, accelerations, powers and forces, and by applying the pertinent model rules. Yet both arrangements have disadvantages. In the first case, the status of low gravity can be maintained at best less than one minute, a time too short for most experiments. In the second case, the small size of the model may degrade the accuracy of the measurement.

Therefore, it is desirable to have a model

- which can move 10 minutes or longer without interruption (for instance, climbing a steep hill of varying slopes)
- whose size is large enough to install motors, gears, pick-ups, antennas, etc.

This can be obtained by applying the laws of imperfect similarity as discussed above. The method of weight reduction is incomplete, because the model is not self-propelled and cannot be steered. The method of spring distortion is restricted to movement with special distributions of tensile and shearing stresses. The method of mass reduction works satisfactorily only if the masses are not elastic and the springs have negligible masses. However, the latter conception seems to be the most promising.

Figure III. 4-7

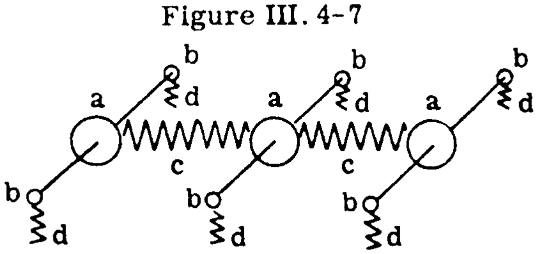

a. masses of payload c. springs of elastic frame

b. masses of wheels d. springs of wheels

Fig. III.4-7 shows how to replace an elastic frame vehicle with a system of unelastic masses and massless springs. The vehicle consists of 3 main masses (holding payload, batteries, electronics, instrumentation, antenna, etc.) connected by 8 springs (elastic frame) and supported

[redacted]

by 6 elastic wheels with small masses. All masses of the vehicle are concentrated in these 9 masses, and all elastic parts of the vehicle are represented by the 8 springs.

This approach leads to the following conclusions: The gravitational forces, the elastic forces, and the inertia forces of the spring-mass system, and the soil force, are represented as follows:

Vehicle
$$\begin{cases} F_g \sim mg \\ F_c \sim K\ell \\ F_i \sim m\dfrac{\nu^2}{\ell} \end{cases}$$

Soil
$$\begin{cases} F_{kc} \sim k_c \ell^2 \\ F_{k\varphi} \sim k_\varphi \ell^3 \\ F_c \sim c\ell^2 \\ F_\varphi \sim mg\tan\varphi \end{cases}$$

K is a spring constant. Again, one obtains 6 dimensionless numbers:

$$\frac{F_g}{F_\varphi} = \frac{1}{\tan\varphi} \qquad \frac{F_g}{F_c} = \frac{mg}{K\ell}$$

$$\frac{F_g}{F_c} = \frac{mg}{c\ell^2} \qquad \frac{F_{kc}}{F_c} = \frac{k_c}{c}$$

$$\frac{F_g}{F_i} = \frac{g\ell}{\nu^2} \qquad \frac{F_{kc}}{F_{k\varphi}} = \frac{k_c}{\ell k_\varphi}$$

and 6 relationships between the vehicle-soil system on the moon and the vehicle-soil system on earth

$$\frac{\nu^\oplus}{\nu^\Delta} = \sqrt{6\,\frac{\ell^\oplus}{\ell^\Delta}} \qquad \frac{k_c^\oplus}{k_c^\Delta} = \frac{c^\oplus}{c^\Delta}$$

$$\frac{m^\oplus}{m^\Delta} = \frac{K^\oplus}{6K^\Delta}\,\frac{\ell^\oplus}{\ell^\Delta} \qquad \frac{k_\varphi^\oplus}{k_\varphi^\Delta} = \frac{k_c^\oplus}{k_c^\Delta}\,\frac{\ell^\Delta}{\ell^\oplus}$$

$$\frac{c^\oplus}{c^\Delta} = 6\,\frac{m^\oplus}{m^\Delta}\left(\frac{\ell^\Delta}{\ell^\oplus}\right)^2 \qquad \frac{\varphi^\oplus}{\varphi^\Delta} = 1$$

The masses and the spring constants of the imperfect model are not equal to the masses and the spring constants of the perfect model. Therefore, they are denoted by a subscript r in the following table, Table III.4-5, which gives some feasible combinations of m_r, K_r and $\ell^\oplus$.

398

[redacted]

$\frac{l^\oplus}{l^\Delta}$	$\frac{K_r^\oplus}{K^\Delta}$	$\frac{K^\oplus}{K^\Delta}$	$\frac{K_r^\oplus}{K^\oplus}$	$\frac{m_r^\oplus}{m^\Delta}$	$\frac{m^\oplus}{m^\Delta}$	$\frac{m_r^\oplus}{m^\oplus}$	$\frac{\varphi^\oplus}{\varphi^\Delta}$	$\frac{c^\oplus}{c^\Delta}$	$\frac{k_c^\oplus}{k_c^\Delta}$	$\frac{k_\varphi^\oplus}{k_\varphi^\Delta}$	$\frac{F^\oplus}{F^\Delta}$	$\frac{P^\oplus}{P^\Delta}$	$\frac{\nu^\oplus}{\nu^\Delta}$
	1		1	1/6		1/6		1	1	1	1	2.45	
1	2	1	2	1/3	1	1/3	1	2	2	2	2	4.9	2.45
	6		6	1		1		6	6	6	6	14.7	
	1/2		1	1/24		1/3		1	1	2	1/4	0.43	
	1 *		2*	1/12*		2/3*		2 *	2 *	4 *	1/2*	0.87*	
1/2	3/2	1/2	3	1/8	1/8	1	1	3	3	6	3/4	1.3	1.73
	2		4	1/6		4/3		4	4	8	1	1.73	
	6		12	1/2		4		12	12	24	3	5.2	
	1/6**		1**	1/216**		1 **		1 **	1**	6 **	1/36**	1/36**	
	1	1/6	6	1/36	1/216	6		6	6	36	1/6	1/6	1
1/6	2		12	1/18		18	1	12	12	72	1/3	1/3	
	6		36	1/6		36		36	36	216	1	1	

TABLE III. 4-5. DATA FOR MODELS WITH REDUCED MASSES AND SPRINGS

* Perfectly similar model
** Imperfect 1:2 model

The most suitable data provides the following model:

$$\ell^{\oplus} = \frac{1}{2}\,\ell^{\Delta}$$

$$K_r^{\oplus} = K^{\Delta} = 2K^{\oplus}$$

$$m_r^{\oplus} = \frac{1}{12}\,m^{\Delta} = \frac{2}{3}\,m^{\oplus}$$

The size of this model is half the size of the moon vehicle. The spring constant has to be twice as high as the spring constant of the perfect model, and the mass has to be 2/3 of the mass of the perfect model.

The model soil corresponds with moon soil, with an angle of internal friction of $\varphi^{\Delta} = \varphi^{\oplus}$, a cohesion of $c^{\Delta} = \frac{1}{2}\,c^{\oplus}$, a modulus $k_c^{\Delta} = \frac{1}{2}\,k_c^{\oplus}$ and a modulus $k_{\varphi} = \frac{1}{4}\,k^{\oplus}$.

The velocity of the perfectly similar model is the same as the velocity of the original moon vehicle. In order to determine the performance of the moon vehicle, the measured acceleration and the frequencies of vibrations must be divided by 6. The measured penetration depth and deflection of the wheel and other geometrical deformations, such as the amplitude of vibrations, must be multiplied by 6. The power of the model must be multiplied by 36 and so must all forces such as thrust, rolling resistance and elastic forces of the frame.

If more accurate quantative data were required an imperfect 1:2 model could be built and evaluated.

The masses of the imperfect 1:2 model must be reduced to 2/3 of the masses of a perfect 1:2 model. If, for instance, the mass of wheel of the moon vehicle is m, then the mass of the imperfect 1:2 model has to be $m_r^{\oplus} = \frac{2}{3} \cdot \frac{m^{\Delta}}{2^3} = \frac{m^{\Delta}}{12}$ (see Table III.4-5). The spring constant of the imperfect 1:2 model must be increased to twice the spring constant of a perfect 1:2 model. If, for instance, the spring constant of the elastic frame of the moon vehicle is K, the spring constant of the imperfect 1:2 model has to be $K_r^{\oplus} = 2\,\frac{K^{\Delta}}{2} = K^{\Delta}$ (see Table III.4-5).

It is important and necessary to double the spring constant in respect to bending as well as in respect to twisting.

In order to determine the performance of the moon vehicle, the velocity of this model must be divided by 1.73; the acceleration must be divided by 6; the frequencies of vibration are 3.46 times higher than the frequencies of the moon vehicle; and all geometrical deformations must be multiplied by 2, all forces by 2, and power by 1.15 (see Table III.4-5).

The parameters c, φ, k_c, and k_φ of the soil on earth vary from the pertinent parameter of the moon soil according to Table III.4-5. In order to cover a large variety of feasible moon soils, at least ten different soils must be tested, such as granular soil with different grain sizes, cohesive soil, firm soils, and stratified soils. The geometrical shape of the terrain must also be varied from a smooth and even surface to a rough surface with different slopes and obstacles.

INSTRUMENTATION

Movie cameras could be used to measure the three-dimensional movements of the model, the evaluation of the films giving the displacement, velocities and acceleration of the model.

Forces, torques, works and power would be measured by strain gauges, by the electric energy output of the propellant motor, and by other standard devices.

B. TEST MODEL DEVELOPMENT

1. DYNAMIC MODEL

The 1/6-scale dynamic model is completed and has been function-tested. Complete performance testing will begin with the completion of the model-testing facility.

Weight, CG, and moment calculations are shown in Table III.4-6. The following general comments in connection with the table show that there is good correlation between the dynamic model and the SLRV. The fact that the model is underweight will permit corrections to be made as the SLRV configuration changes during the study phase.

1. (a) The data on the model is based on measured weights. Component weights are accurate to 1/100 of a gram.

   (b) The I (inertia) values are based on determining appropriate radius of gyration (k) values. On symmetrical parts this was done with conventional handbook formulas. On composite, non-symmetrical parts a little "judgment" was used. An overall accuracy of ±5% is assumed on the I values.

2. The data on the vehicle was gleaned primarily from estimates made on 9/23/63.

3. The first vehicle I values look somewhat realistic (in relationship to the model) and the present weight difference should be sufficient to dynamically balance (I-wise) the model to the full-scale vehicle.

TABLE III.4-6.

WEIGHTS, C. G.'s & MOMENTS FOR INDIRECT LINK VS MODEL

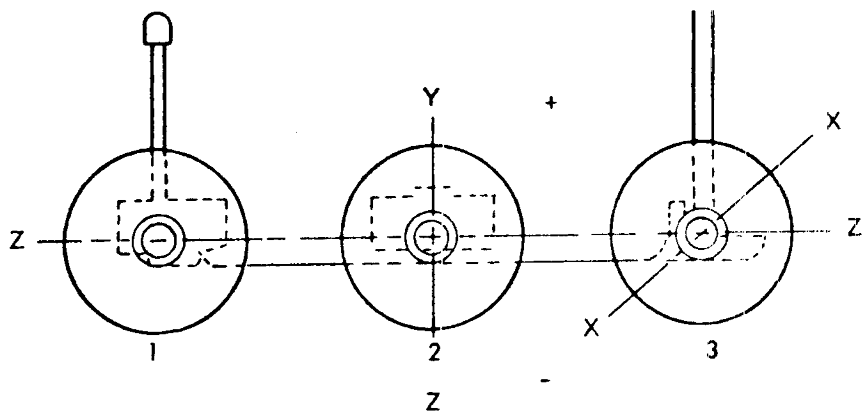

Total Vehicle Weight = 88. 14

Model Weight - X Scale = 61. 43 (underlined); 26. 71 beneath

Δ = 56 Gms

	1		2		3		Frame	
	Model x Scale Factor	Vehicle	M x SF	V	M x SF	V	M x SF	V
Weight (Pounds)	19. 98	31. 01	21. 16	36. 07	17. 95	19. 86	2. 34	1. 20
Y Axis Center of Gravity (+ is up)	+ 1. 68	+ [illegible]42	+ 3. 78	+ 1. 74	+ 2. 64	+ 2. 60		
I_{xx} Slug-$In^2 x 10^{-2}$	1369. 8	2931. 8	9319. 7	4175. 4	1786. 8	2538. 9	958. 9	980. 9
I_{yy} Slug-$In^2 x 10^{-2}$	2870. 4	5855. 1	2774. 1	5824. 1	2484. 6	4191. 1	958. 9	980. 9
I_{zz} Slug-$In^2 x 10^{-2}$	3797. 5	6958. 7	11, 609. 8	8374. 3	3861. 6	6143. 9	32. 9	20. 6

4. The model frame is the only component which is out of line weight-wise.

5. It should be noted that the present axis used for I values are not centroidal and cannot be transferred to any other axis as they are presented here.

6. The lack of a stadia on the vehicle accounts for the small I_{xx} of element 2. The large I_{yy} can be partially blamed on motor gear box placement vs the model with its central motor mount.

2. FULL-SCALE EARTH-WEIGHT CONTROL MODEL

All drawings required for fabrication of the basic vehicle have been signed off and released. Long-lead items such as gear boxes, wheels and spare motors have had procurement action initiated. A review of the design has also been held with representatives from the structures, mobility, and mechanical-subsystem groups.

The Engineering Test Model, or ETM, (see Figure III. 4-8) is a radio-controlled, battery-powered, full-scale, earth-weight model of the GM Surveyor Lunar Roving Vehicle. It is designed to demonstrate the essential performance features of our vehicle concept. The demonstration will include:

1. A test of drawbar pull versus slip in dry, loose sand in an instrumented laboratory soil bin.
2. An obstacle performance test on a hard-surfaced obstacle course consisting of a 30-inch step, a 20-inch-wide crevice, and a 45-degree slope.
3. A maneuverability demonstration among three pylons on 9-foot centers.
4. An overall mobility and maneuverability demonstration on the GM DRL outdoor obstacle course, or Lunarium.

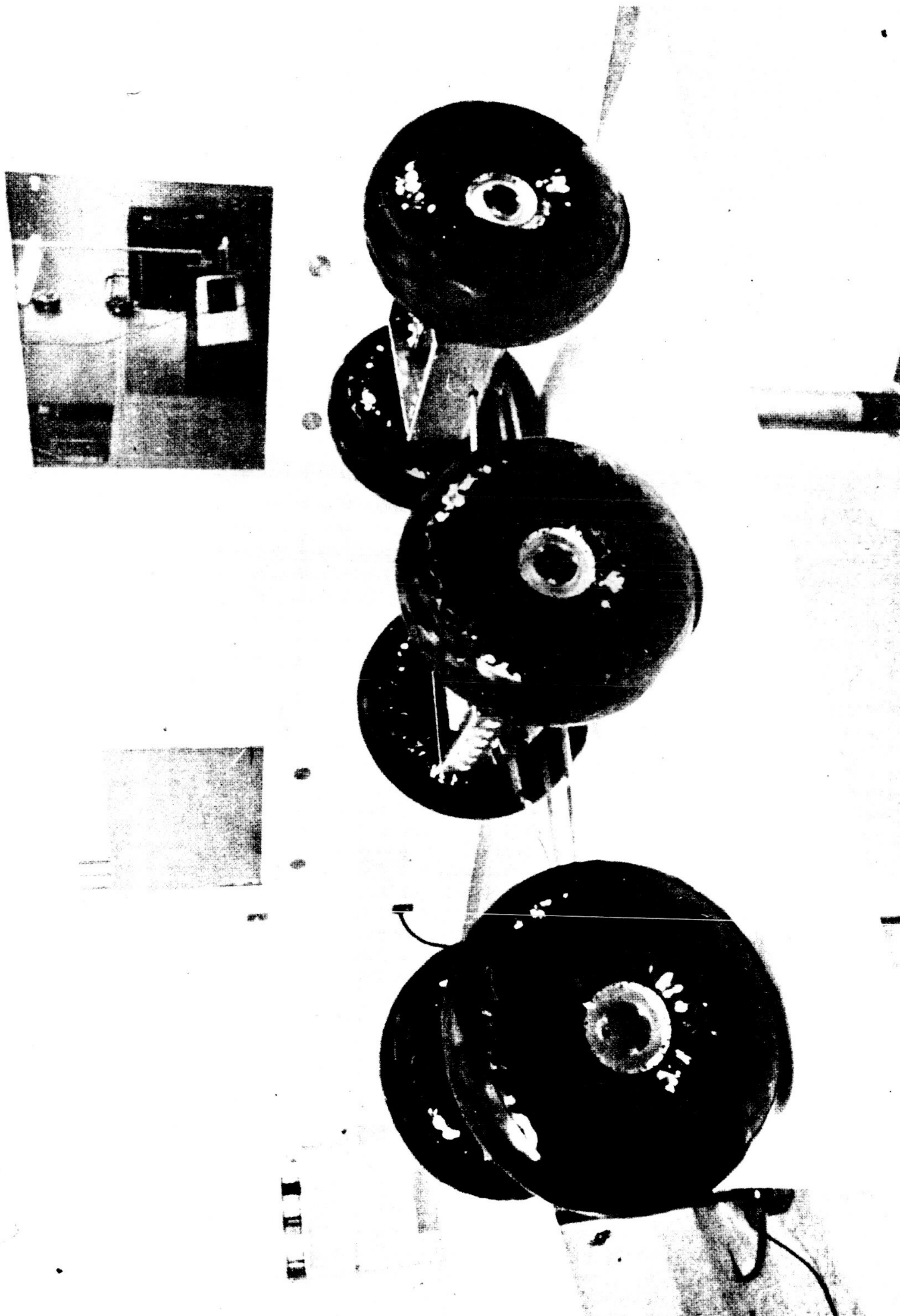

Figure III. 4-8

Shown in addition to mobility and maneuverability will be safety features incorporated into the vehicle design, operation in reverse, start-and-stop operation, and other features.

Another view of the ETM is shown in Figure III.4-9. The all solid state and relay RCA command and control electronics section is visible in the center compartment. The ten commands available to the vehicle are:

1. Locomote one step forward
2. Locomote one step backward
3. Locomote continuously forward
4. Locomote continuously backward
5. Stop continuous locomotion
6. Steer one 7.5-degree step right
7. Steer one 7.5-degree step left
8. Steer to 30 degrees right
9. Steer to 30 degrees left
10. Steer to center

The front and rear compartments house batteries and steering assemblies. The wheels have inner tubes to support the vehicle under conditions of earth gravity and heavy polyurethane tread bands to resist wear. Spring constants and wheel construction are identical to the actual lunar vehicle except for the inner tubes and the covering materials. The lunar wheels will be covered with formed, fine-gauge, stainless steel mesh, prohibited by cost and time from being used on the ETM.

A dummy superstructure, to include DIBSI tubes, a ground plane antenna and mast, and a television mast, will be added to simulate the actual lunar vehicle in appearance and to house weights for properly locating the center of gravity. The solar panel array will not be simulated.

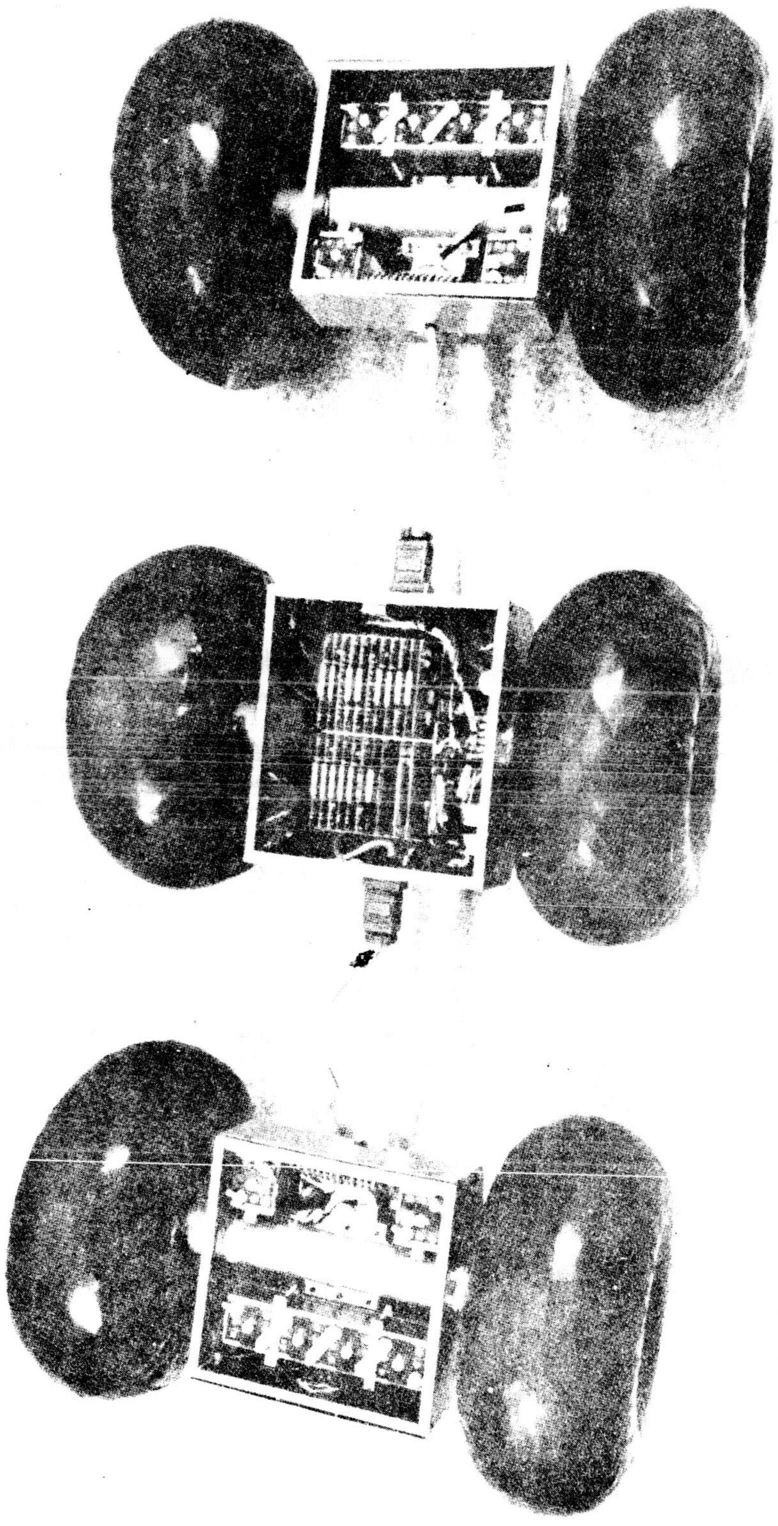

Figure III. 4-9

C. ENGINEERING TEST MODEL DEMONSTRATIONS

1. Purpose

The purpose of this demonstration is to show the essential performance features of the GM DRL three-section, six-wheeled, spring-frame, articulated lunar vehicle design. The following demonstrations will be performed:

1. Drawbar pull vs slip in dry, loose sand in a laboratory soil bin.
2. Obstacle performance on a hard-surface obstacle course consisting of:
   a. A 30-inch step obstacle
   b. A 20-inch-wide crevice
   c. A slope of 45 degrees
3. Maneuverability between three pylons on 9-foot centers.
4. Overall mobility and maneuverability on the GM DRL outdoor obstacle course (Lunarium).

In addition to demonstrating vehicle mobility and maneuverability, several other vehicle features will be shown:

1. Operation of the vehicle in reverse.
2. Operation of vehicle roll tilt switches, which prevent overturning of the vehicle in the roll mode.
3. Operation of vehicle switch bumpers, which shut off the vehicle wheel-drive motors when a tall, narrow obstacle is contacted between either the front or rear wheels.
4. Operation of vehicle under simulated mechanical failure conditions. To be simulated are:

a. Failure of any one of the six wheel-drive motors, resulting in releasing of free-wheeling mechanism, causing affected wheel to free wheel.

b. Failure of one of two steering actuators, leaving one axle locked in any one of nine positions.

5. The effect of removing wheel drive power when the vehicle is ascending or descending a hill.

6. Operation of vehicle pitch tilt switches, which prevent overturning of the vehicle when attempting to climb an obstacle over 30 inches high.

2. Description of Engineering Test Model

The Engineering Test Model is a radio controlled, battery powered, full scale, earth weight model of the GM DRL Surveyor Lunar Roving Vehicle. It has been designed to demonstrate the essential performance features of the GM DRL vehicle concept. These features include high soft ground mobility, high maneuverability, the ability to climb a 30 inch step obstacle and traverse a 20 inch crevice, protection against overturning and getting "hung up" and, the capability of maintaining good mobility and maneuverability in spite of wheel drive or steering actuator failure.

The vehicle weighs 90 pounds and is 32 inches wide and 72 inches long. Fig. III. 4-10 illustrates the vehicle. The spring wire frame, plastic coated fabric covered wheels are 18 inches in diameter and 8 inches wide. A replaceable polyurethane plastic tread strip is added for increased tire life under severe conditions. Vehicle motive power is supplied by silver-zinc storage batteries powering the six wheels by individual electric motors and planetary gear reducers. Steering is of the wagon type; front and back units are turned by mechanisms similar to the wheel drive mechanisms with the addition of a final worm gear reduction.

A citizens band radio control receiver, through solid state and relay logic circuitry, provides the vehicle with the following command capability:

1. Locomote one step forward.
2. Locomote one step backward
3. Locomote continuously forward.
4. Locomote continuously backward.
5. Stop continuous locomotion.
6. Steer one 7. 5 degree step right.

64-406

VOL II APP. SEC III

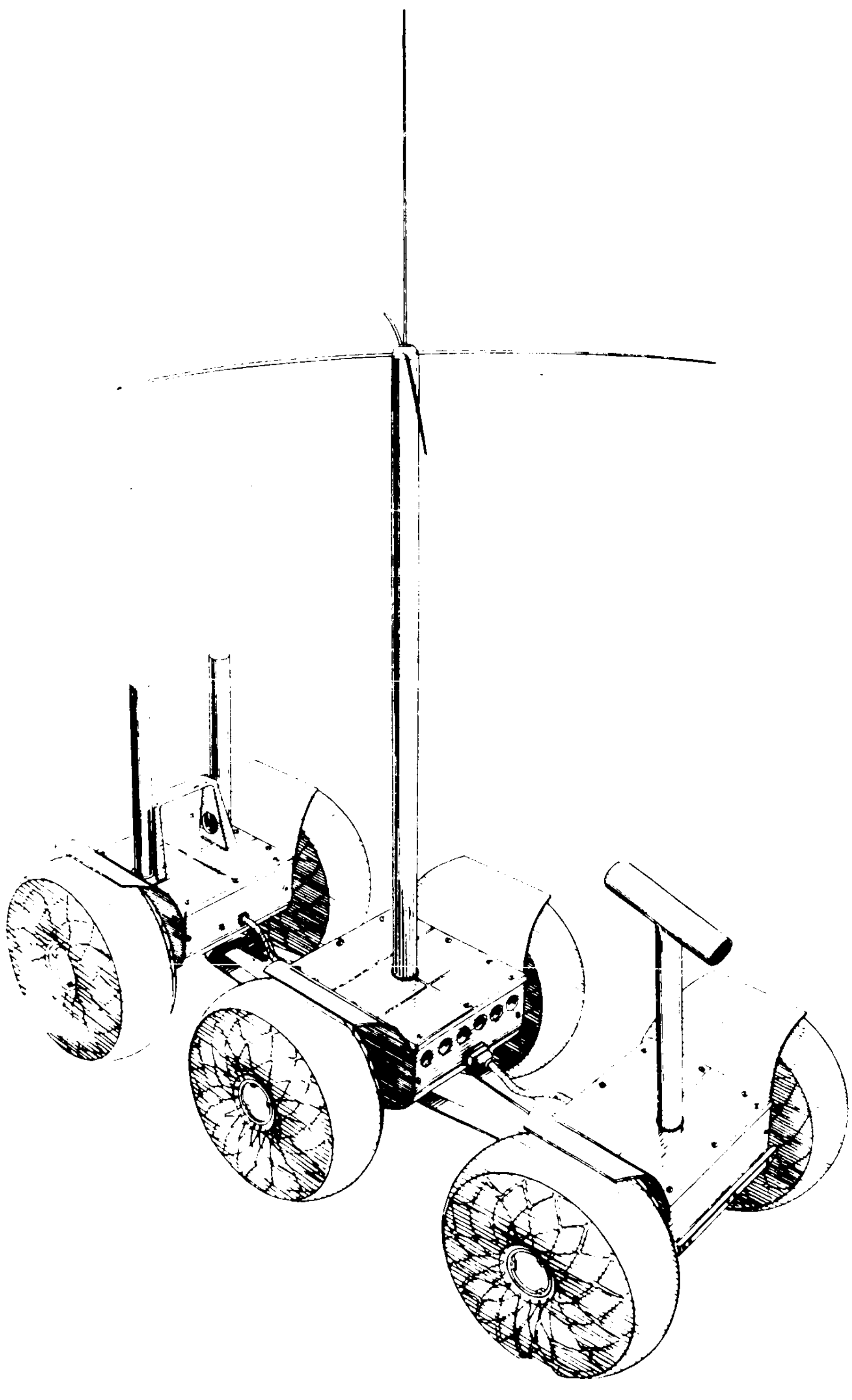

Fig. III. 4-10. Engineering Test Model (ETM)

7. Steer one 7. 5 degree step left.
8. Steer to 30 degrees right.
9. Steer to 30 degrees left.
10. Steer to center.

Vehicle "hanging up" is virtually prevented by bumper switches on the front and rear compartments. These switches automatically shut the wheel-drive motors off when a narrow object of sufficient height is contacted by either end of the vehicle. Such an object might "hang up" the vehicle if an attempt was made to cross it. Wider obstacles up to 30 inches high can be climbed by the vehicle.

Roll safety mercury switches are mounted in all three compartments and are wired to automatically shut the vehicle off when the front and center or the rear and center compartment roll angles both exceed 45 degrees. Inadvertent overturning of the vehicle is thereby prevented.

To preclude overturning of the vehicle along the pitch axis, as when attempting to climb a very high step obstacle, a similar switch arrangement in pitch is provided. When the front or rear compartment starts to fall toward the center of the vehicle, motive power is removed.

Nominal speed of the ETM is . 6 feet per second and minimum steering radius is 72 inches. Dummy DIBSI soil mechanics instruments, a television camera mast and a ground plane antenna and mast are mounted on the vehicle to simulate appearance of the lunar vehicle. Center of gravity locations of each compartment and the overall vehicle simulate those of the lunar vehicle.

[redacted]

3. Description of Test Courses and Equipment

SOIL BIN

The GM DRL Mobility Research Laboratory Large Soil Bin, illustrated in Fig. III. 4-11 is 40 feet long with a soil section 60 inches wide and 30 inches deep. A test carriage is mounted on rails which provide full guidance for loads of 2000 pounds at 1 to 4 feet per second, and 1000-pound loads at up to 10 feet per second. A variable A. C. drive system is used to propel, brake, and control the carriage. The test carriage with its associated dynamometer and wheel-test rig includes means for measuring drawbar pull, sinkage, wheel speed and slip, and torque input to vehicle models. A work car mounted on the rail system contains soil tilling and preparation equipment.

OBSTACLE COURSE

The laboratory obstacle course, shown in Fig. III. 4-12 is composed of built-up wooden blocks appropriately arranged to provide a 30-inch step obstacle, a 20-inch crevice and a 45-degree slope for the purpose of demonstrating vehicle hard-surface mobility.

MANEUVERABILITY COURSE

To demonstrate maneuverability, the vehicle will perform figure eights around pylons spaced 9 feet apart, as shown in Figure III. 4-13.

OUTSIDE TEST COURSE (LUNARIUM)

The Lunarium is a specially constructed outdoor test facility used as a vehicle obstacle course and covers an area approximately 200 by 250 feet. It consists of crater-like bunkers of slopes up to 30 degrees and a large number of boulders

[redacted]

[redacted]

VOL. II APP. SEC. III.

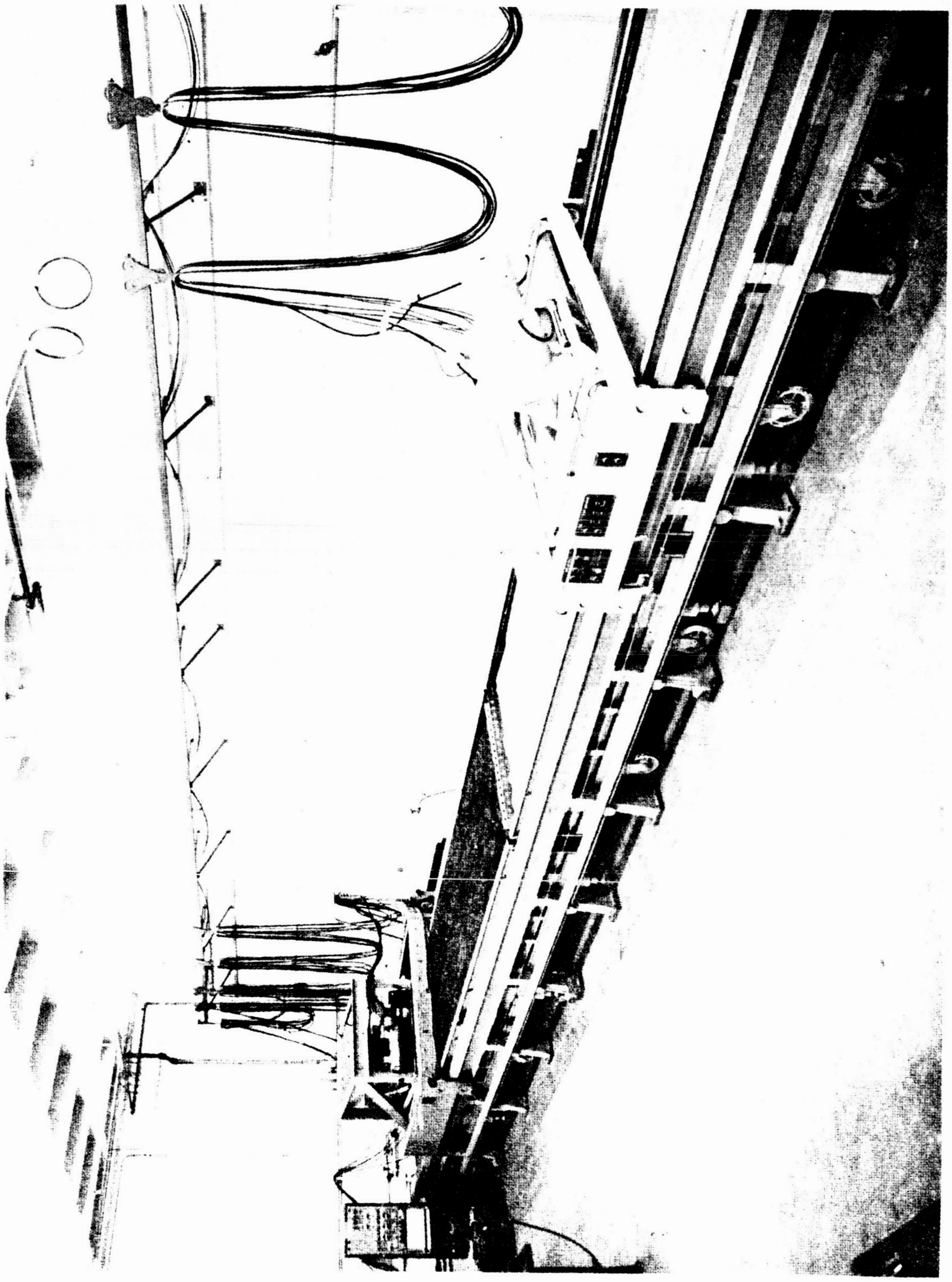

Fig. III. 4-11. Soil Bin

[redacted]

418

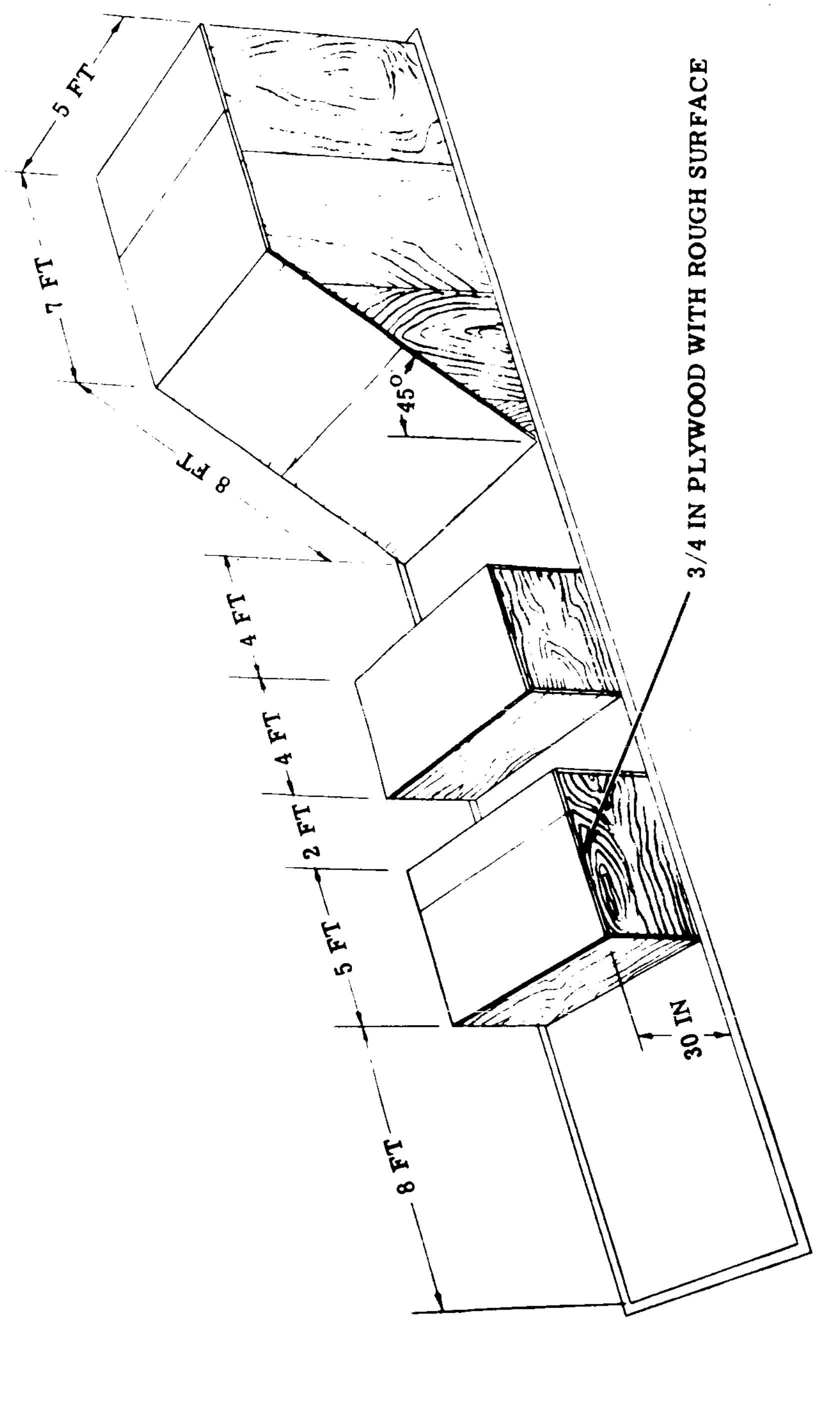

Fig. III. 4-12. Laboratory Obstacle Course

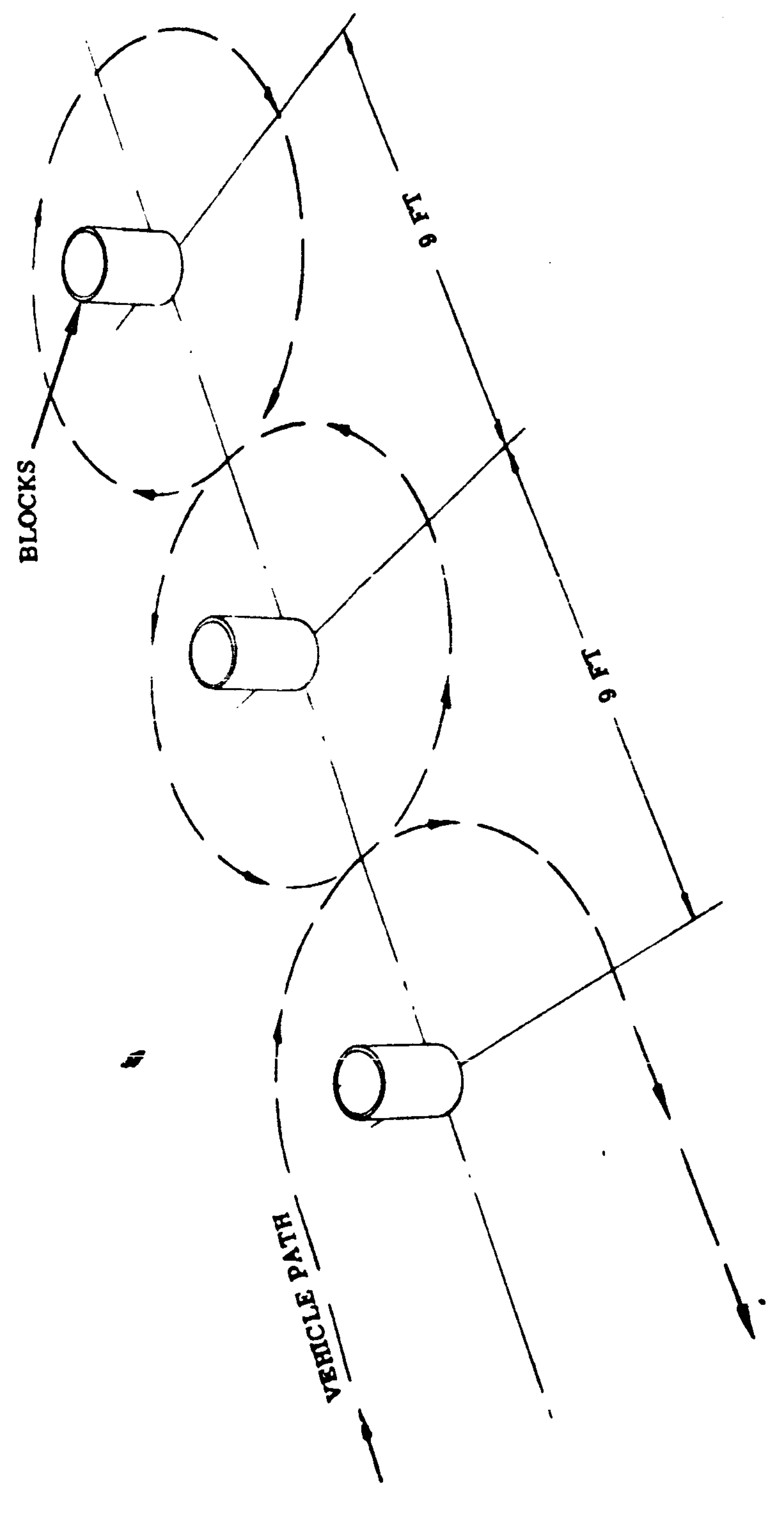

Fig. III.4-13. Laboratory Maneuverability Course in both random and maze-type arrangements which provide navigation problems. A portion of the Lunarium is devoted to step obstacles and crevices composed of appropriately sized rocks arranged in the proper pattern. The portion of the Lunarium to be used for the ETM demonstration is shown in the photo of Fig. III. 4-14. A typical demonstration course is drawn in on the photograph. The course and the significance of the numbered points on the photo will be discussed later.

Vol. II APP. SEC. III

Fig. III. 4-14. Laboratories Outside Test Course (Lunarium)

A10

4. Demonstration Plan

SOFT-SURFACE MOBILITY

A drawbar-pull vs slip test will be demonstrated in the soil bin filled with dry, loose sand. The ETM will be attached to the dynamometer system and will be driven by its own power. The speed of the dynamometer carriage will be gradually reduced during the run, resulting in varying slip in the range of approximately 5 to 90%. The drawbar-pull, as a function of slip, will be directly recorded on an X-Y plotter. The test results will be compared with analytical predictions.

OBSTACLE PERFORMANCE

The obstacle performance will be demonstrated by test runs over the laboratory obstacle course. The coefficient of friction of the wood surfaces in the obstacle course against the vehicle tires is approximately .75. The vehicle will run the course in both directions with the front end and rear end leading, a total of four runs over each obstacle.

MANEUVERABILITY

The steering performance and minimum turning radius will be demonstrated in the laboratory by maneuvering the test model around the obstacles, as illustrated in Fig. III. 4-13. The vehicle will be run through this course backwards as well as in the normal forward direction.

OUTSIDE TEST COURSE (LUNARIUM)

The overall performance of the vehicle will be demonstrated on the Lunarium. Although an infinite number of routes through the course exist, the course illustrated in the photo of Fig. III. 4-14 is suggested as one which will demonstrate all of the performance features of the vehicle. The numbered points on the photo will demonstrate the following vehicle features:

1. Crossing 20-inch rock crevice.
2. Climbing a 30-inch rock step obstacle
3. Backing up with the right vehicle wheels along the side of a high rock. When the tilt angle of both the rear and center compartments exceed 45 degrees, the vehicle will automatically stop and not overturn as it would if it continued.
4. Bumper switch operation. An attempt to climb a high, narrow rock will automatically shut the vehicle off. The vehicle will then be backed away.
5. Climbing steep sand bank. The vehicle will be stopped part way up the slope.
6. Descending steep sand bank followed by operation along side parallel to top of bank. The vehicle will be stopped part way down the slope.
7. Climbing and descending steep sand bank at 45 degrees.
8. Climbing and descending large rock pile.

At appropriate points along the course, single wheel revolution operation in both forward and reverse will be demonstrated.

PERFORMANCE WITH SIMULATED MECHANICAL FAILURES

During any of the previously described demonstrations, operation of the vehicle with any one of the six wheels free-wheeling will be shown at the customer's discretion. Similarly, operation with either steering actuator disabled in any position may be shown. Performance of the vehicle under these conditions will, of course, be degraded.

APPENDIX V

LOCOMOTION EVALUATION AND VEHICLE CONCEPT SELECTION

APPENDIX V

LOCOMOTION EVALUATION AND VEHICLE CONCEPT SELECTION

The basic modes of locomotion such as walking, (running), crawling (sliding), rolling (wheels and tracks) and jumping (leaping) had been investigated long before the problem of lunar surface locomotion became the subject of a programmed effort (M. G. Bekker "Theory of Land Locomotion," Univ. of Mich. Press, 1956; "Mechanics of Locomotion and Lunar Surface Concepts" SAE No. 632 K, 1963.)

It was concluded in these studies that while walking and rolling could be considered as based on a similar kinematic principle, the simplicity and reliability of the rolling mechanisms were unparalleled by anything else.

Furthermore the weight and complexity of a walking device including the necessary feedback-controlled stability and step length adjustment would be unfavorable not only for lunar, but also for terrestrial locomotion.

Moreover, the space requirement for accommodation of a walking system of linkages would be greater than that for a wheel of comparable performance. For equal sizes of wheels and feet, the soft ground performance of the foot was not markedly better (Figure III. 5-1), while obstacle performance was definitely inferior.

Thus walking, running and jumping were dismissed as reliable and economic locomotion modes. Crawling (sliding) also was found impractical because of an exceedingly high propulsive power requirement due to the inevitable Coulomb friction. The danger of "cold welding" and rather poor obstacle crossing ability further disqualified this type of locomotion, and relegated

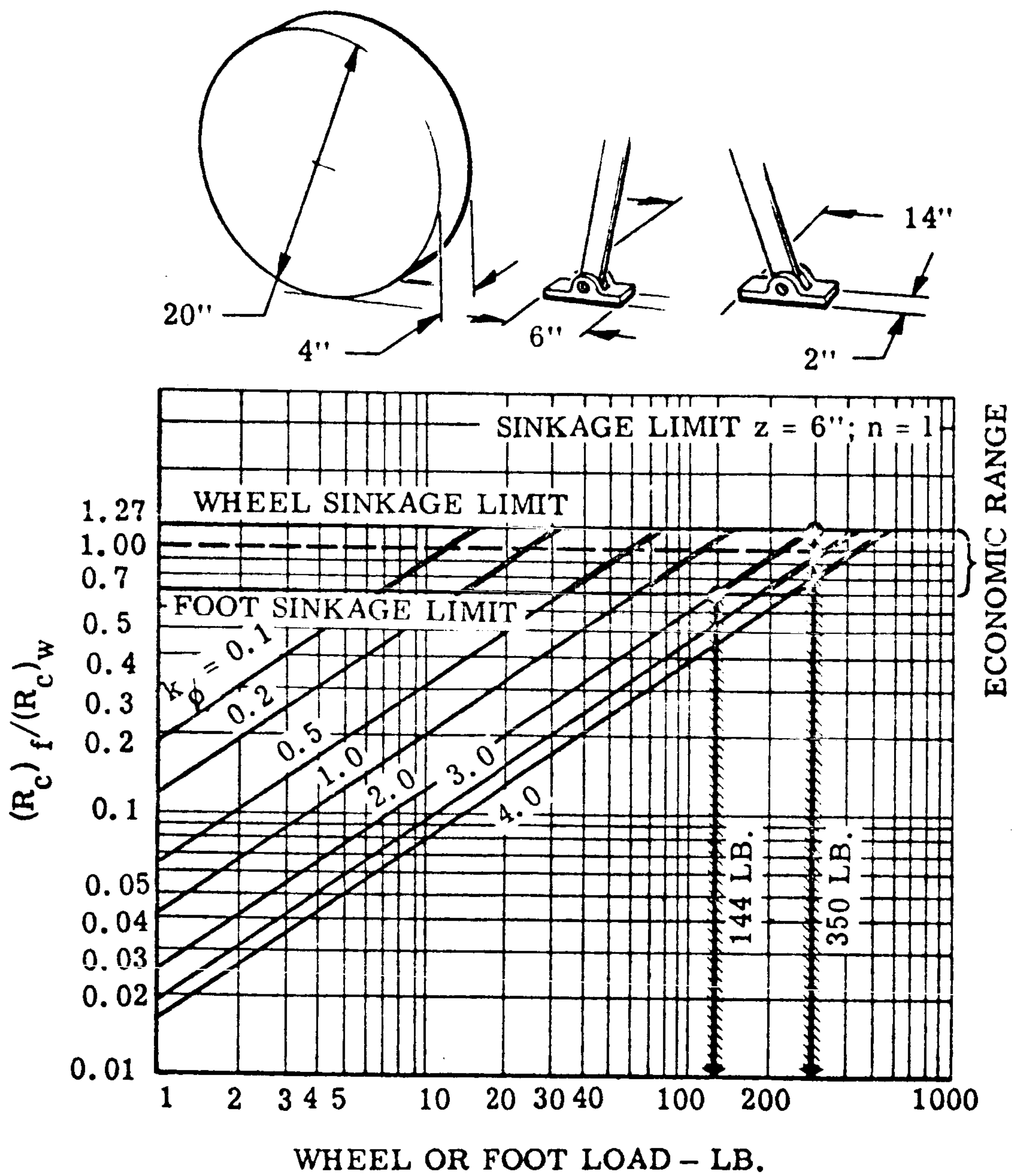

Fig. III.5-1. Ratio of Motion Resistances of a Pair of Feet and a Comparable Wheel it to the rank of highly improbable applications. As a result of the foregoing determinations only wheels and tracks were considered.

Both tracks and wheels have merit. The tracks' advantage lies in the extremely low ground pressure that can be obtained. In the case of heavy, high density vehicles such as combat tanks, wheels cannot provide the required low ground pressure for soft ground crossing. Thus it was necessary to put the wheels on an "artificial road", which would lower the wheel peak loads by spreading them over a larger ground contact area.

For lunar locomotion a tracked vehicle does not appear practical. First, vehicle weights are substantially lower because of limited spacecraft payload capacity. Second, the lunar gravity field reduces all ground loads by a factor of six. Hence no heavy loads acting upon the lunar soil can be envisaged for the time being.

Figure III. 5-2 illustrates the motion resistance-to-weight ratio of various vehicle configurations as a function of soil consistencies. It illustrates that at the k_{ϕ} value of the JPL specified soft soil model the motion resistance-to-weight ratio of the tracked vehicle is approximately 1/4 that of a six wheeled vehicle of comparable size. In the SLRV wheeled configuration the motion resistance accounts for only 20% of the locomotion energy.

Tests on concrete surfaces where the external motion resistance of wheels and tracks are comparable indicate that the internal losses in accelerating inertias, power drive inefficiencies, frictional effects, etc. are several times higher for tracked configurations than wheels. On an absolute scale then the tracked vehicle will require several times the energy per meter of the wheeled vehicle even though the energy to overcome soil motion resistance is lower by a factor of 4.

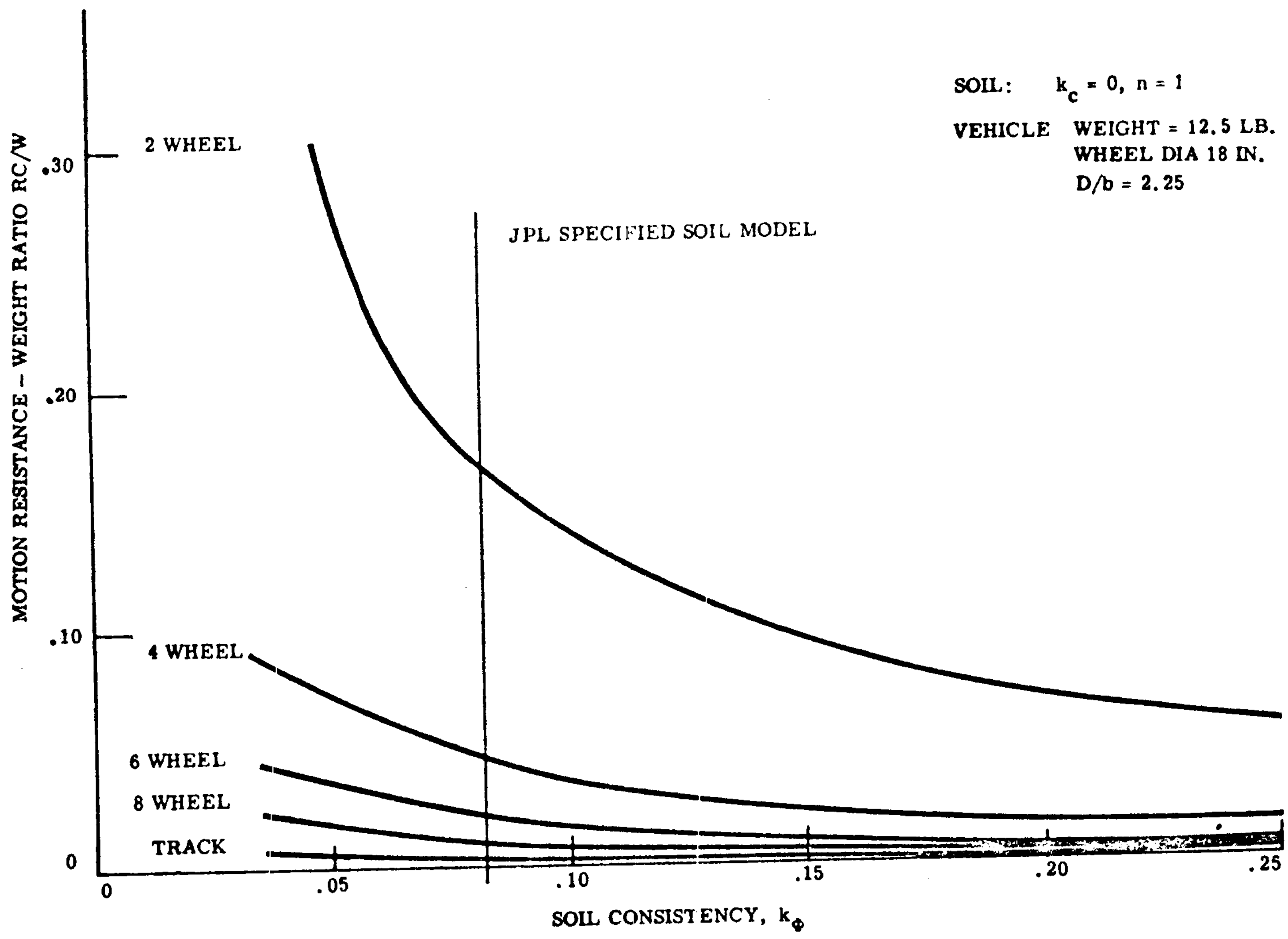

Fig. III. 5-2. Motion Resistance of Various Vehicle Configurations

Tracked vehicles as mentioned previously may be considered basically rigid wheeled fixed frame vehicles which carry their own "road" for the purposes of hard ground comparison. In this respect the obstacle crossing performance of a track is basically limited to the height of the sprocket. Even a two-element articulated tracked vehicle does not do much better.

In summing then, tracks were considered premature, if not impractical for lunar locomotion for the following reasons:

1. available evidence points toward the existence, on the moon, of cohesionless granular masses, or solids;
2. even when assuming the existence of cohesive-frictional mass such as that produced in Gold-Hapke model, it was found that the strength of such "soil" does not warrant the use of tracks although the soil model displayed very low bearing capacity and density;
3. obstacle performance of properly designed wheeled vehicles is much superior to that of tracked vehicles;
4. weight of tracks and suspension is higher than that of wheels;
5. reliability of the wheel is beyond comparison with that of the track particularly if one considers the almost unavoidable "track overthrowing" on obstacles, the danger of "cold welding" on guide pins, sprockets, etc., the "dirt packing", and other dangers inherent in track concept;
6. power required for driving a tracked vehicle is substantially greater than that for a wheeled vehicle, for considered lunar soil models;

7. spaceship packaging ability of a tracked vehicle having mobility equal to that of a wheeled vehicle, under assumed lunar soil models, was much more difficult than that of a properly designed deformed wheel vehicle.

In conclusion, then it was determined with a satisfactory level of confidence, that a wheeled lunar vehicle should fulfill the existing requirements with a much higher probability of success than the tracked one.

A wheeled vehicle was found particularly attractive when designed with elastic wheels. (Figure III. 5-3).

The vehicle concept thus evolved i. e. the one which would produce maximum mobility on one hand, and the optimum packaging ability on the space craft on the other, led directly to the six-by-six wheel configuration linked with an elastic frame.

The soft ground crossing capability of this configuration was superior to that of a conventional rigid frame vehicle configuration (Figure III. 5-4) and the obstacle crossing was unprecedented (Figure III. 5-5).

With this background a mobility tradeoff analysis was conducted.

Figure III. 5-6 shows three alternative vehicle configurations, (compatible with the Surveyor payload envelope) on which the mobility tradeoffs are based. As a ground rule for the evaluations, the vehicle design philosophy was the same for all configurations. For example, inflatable wheels were not considered for any of the configurations.

The basic configurations include 3-, 4-, and 6-wheeled designs. For each configuration, weight-mobility tradeoffs were performed.

426

[redacted]

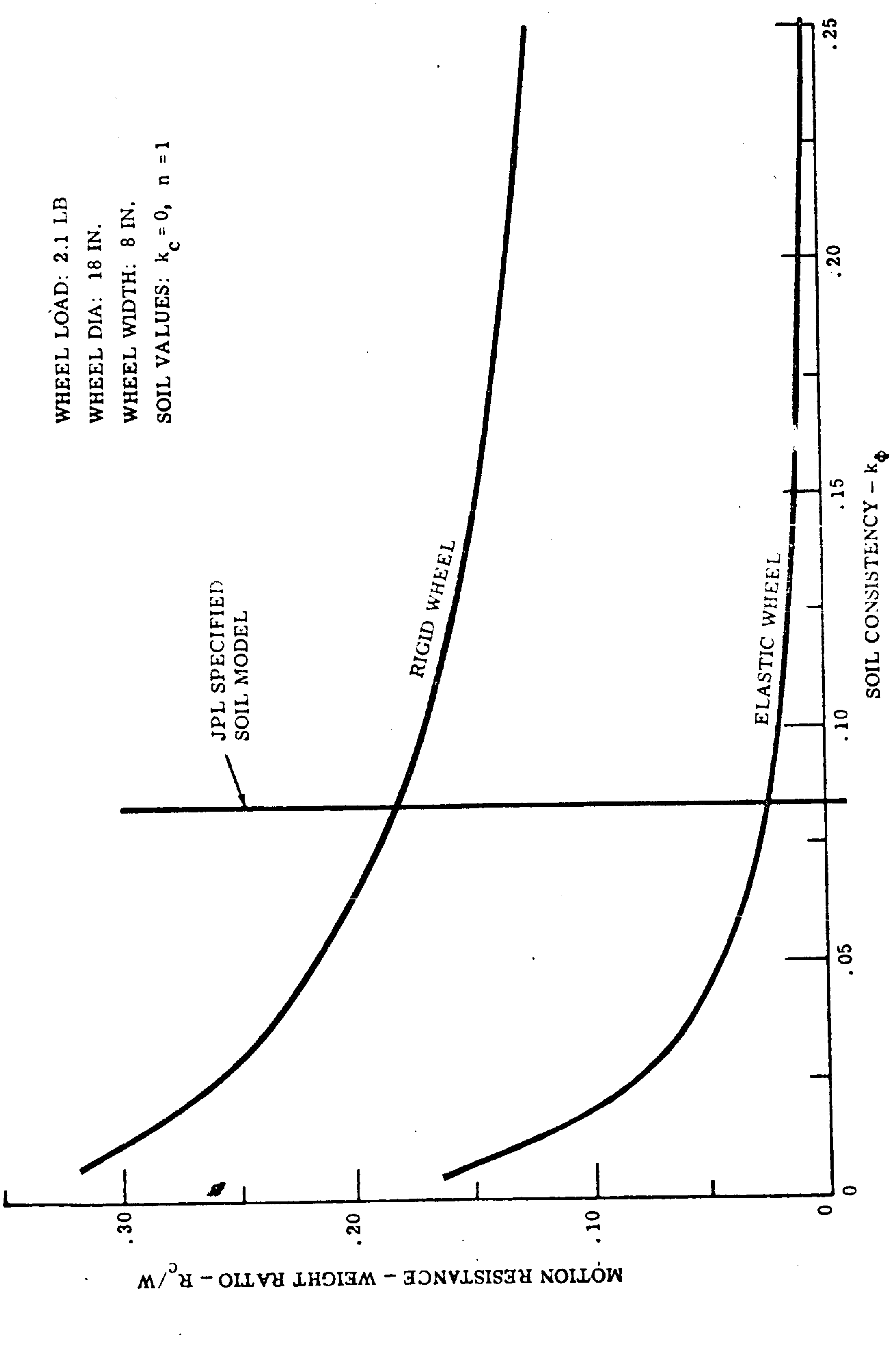

Fig. III.5-3. Comparison of Motion Resistances for Rigid and Elastic Wheels of Equal Size

[redacted]

64-406
VOL II · APP. SEC. III

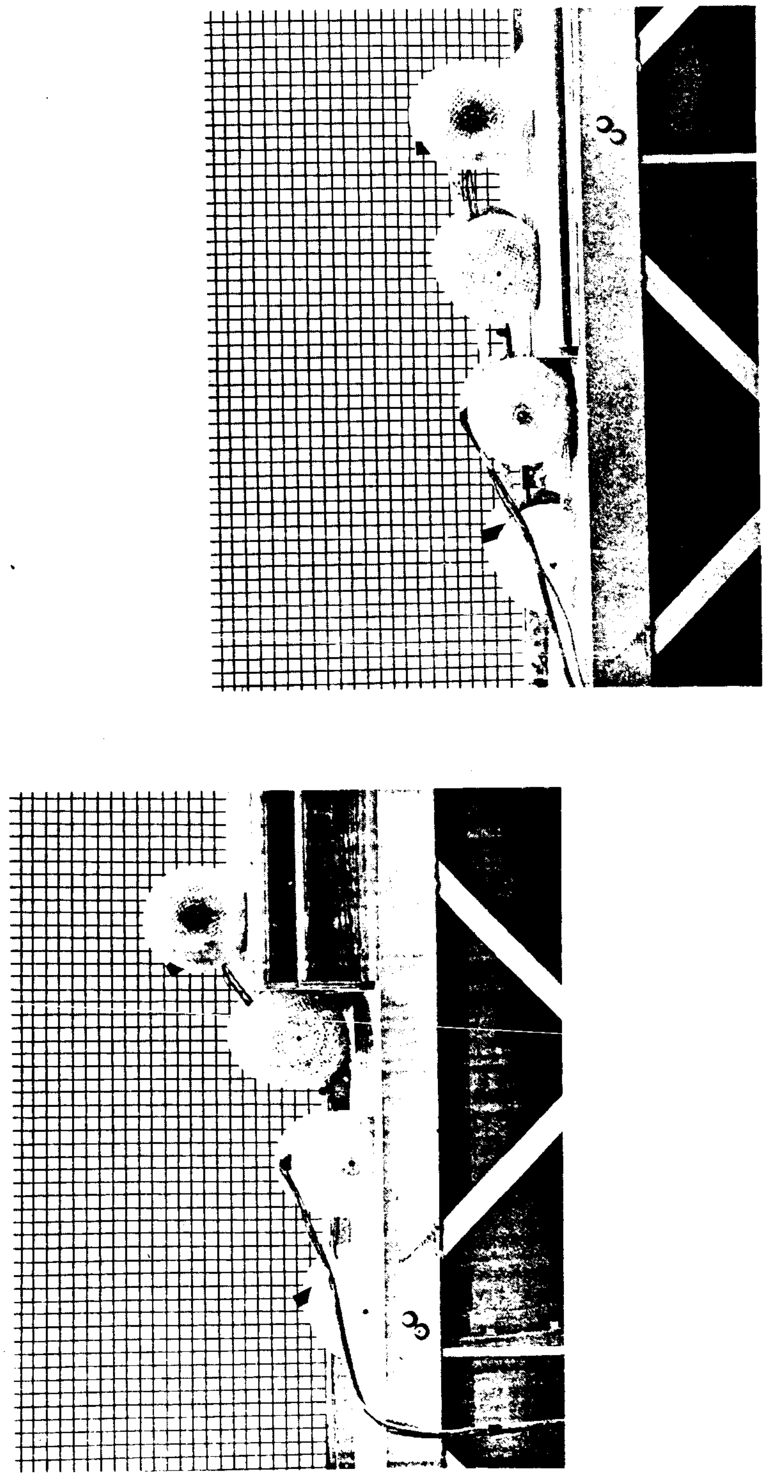

Fig. III.5-4. Comparison of Obstacle Climbing Performance in Soft Soil of a Rigid and Flexible Frame Vehicle

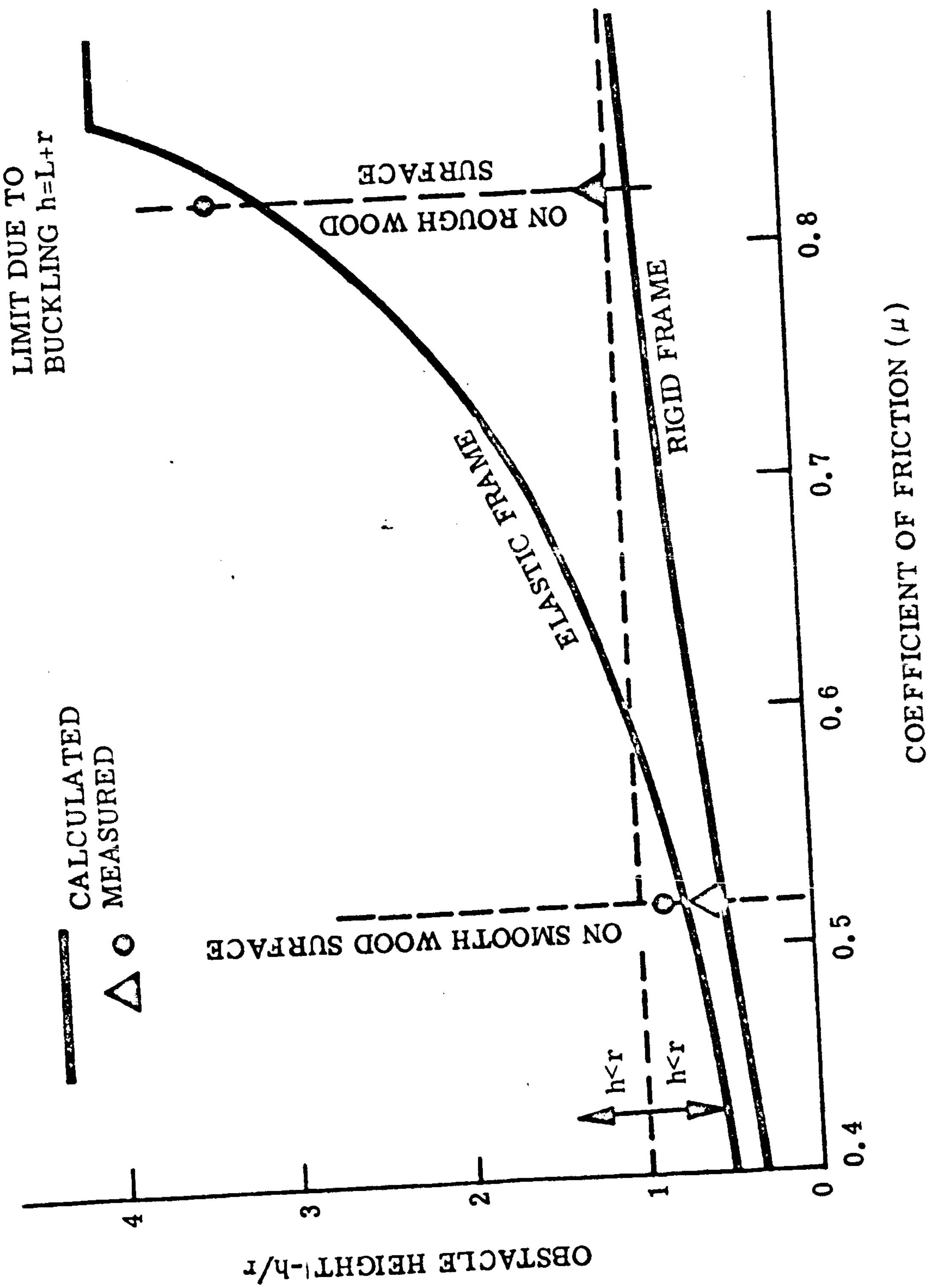

Fig. III. 5-5. Comparison of Abilities of Elastic and Rigid Frame Vehicles in Negotiating Vertical Obstacles

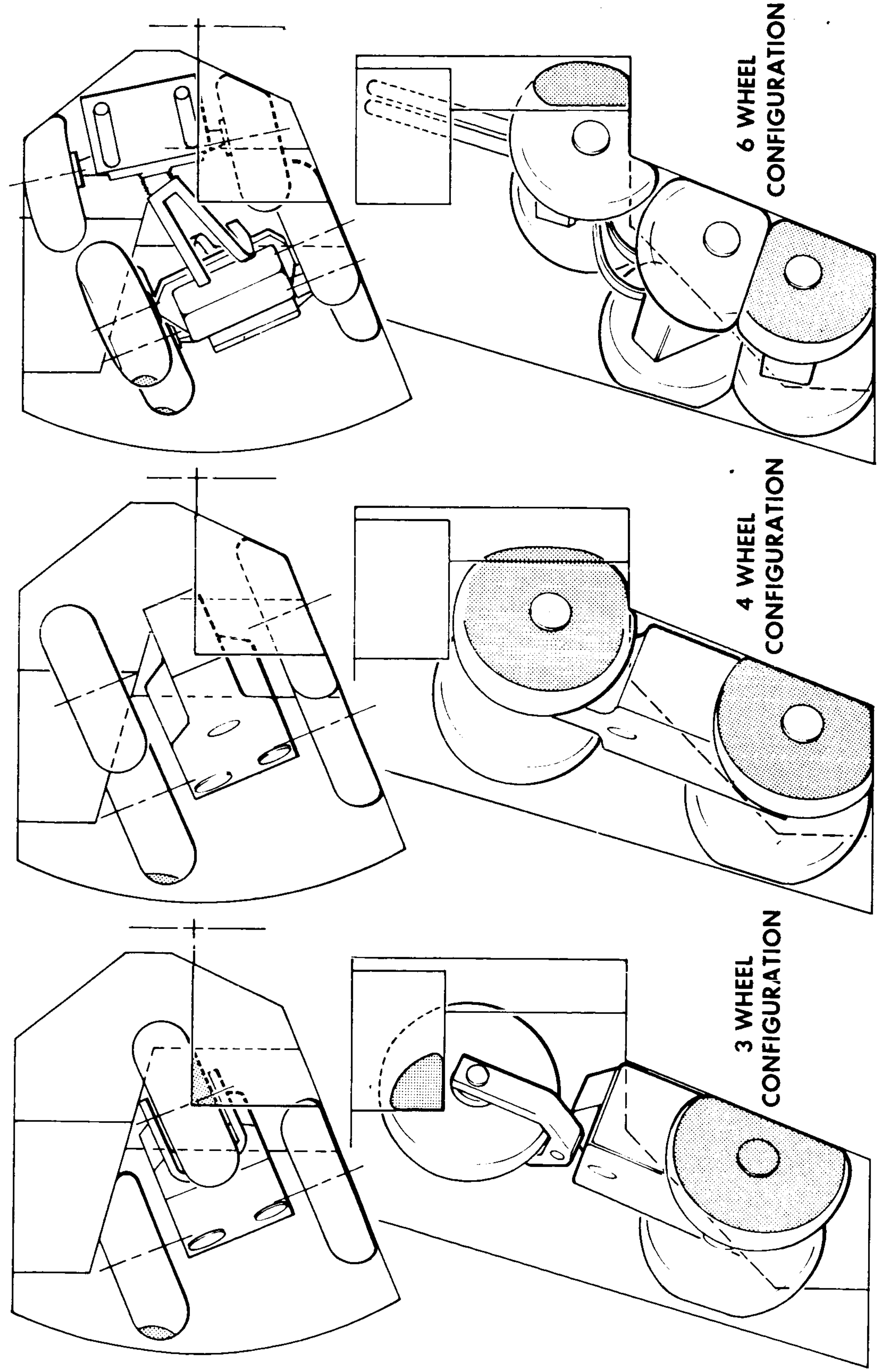

Figure III.5-6. Mobility Trade-Off Configurations

[redacted]

The mobilities of the different vehicles were evaluated as a weighted average of different mobility performance factors. One of these factors — the ability to negotiate obstacles — is shown in Figure III. 5-7.

The vertical scale is the step-obstacle capability, which varies from 14 to 75 centimeters. The horizontal scale is the net vehicle weight, which ranges from 14.4 to 22.3 pounds.

The net vehicle weight includes the basic frame, exclusive of payload compartments, and the wheels, drives, steering mechanisms, axles, fenders, bumpers, and attachments.

The obstacle performances of the 3- and 4-wheeled vehicles are similar except that the 4-wheeled vehicles are about 2 pounds heavier than the 3-wheeled. The smallest 3- and 4-wheeled vehicles, with 12-inch wheel diameters, have step limitations of about 14 centimeters. The largest 3- and 4-wheeled vehicles that are stowable, with 22-inch wheel diameters, have step limitations of 25 centimeters.

The weight of the smallest 6-wheeled vehicle, which has a 12-inch wheel diameter, is 17.6 pounds. Below this point the payload capacity is inadequate for the SLRV. The largest 6-wheeled vehicle, the design choice for the SLRV, weights 22.3 pounds and has a step limitation of 75 centimeters.

The measure of the soft-terrain capability of the vehicles is the ratio of drawbar-pull to weight, which is the ordinate of Figure III. 5-8. The abscissa is the net vehicle weight of the different configurations. The curves shown apply to the soft ground characteristics specified in EPD-98. In particular, $k_c = 0$, $k_\phi = .083$, $n = 1$, $c = 0$, and $\phi = 30$ degrees are the Bekker coefficients.

The ratio of drawbar-pull to weight of the 3-wheeled vehicles is largest for weights less than 19.6 pounds. Above 21.1 pounds the drawbar-pull/weight ratio of the 6-wheeled vehicles is largest.

[redacted]

[redacted]

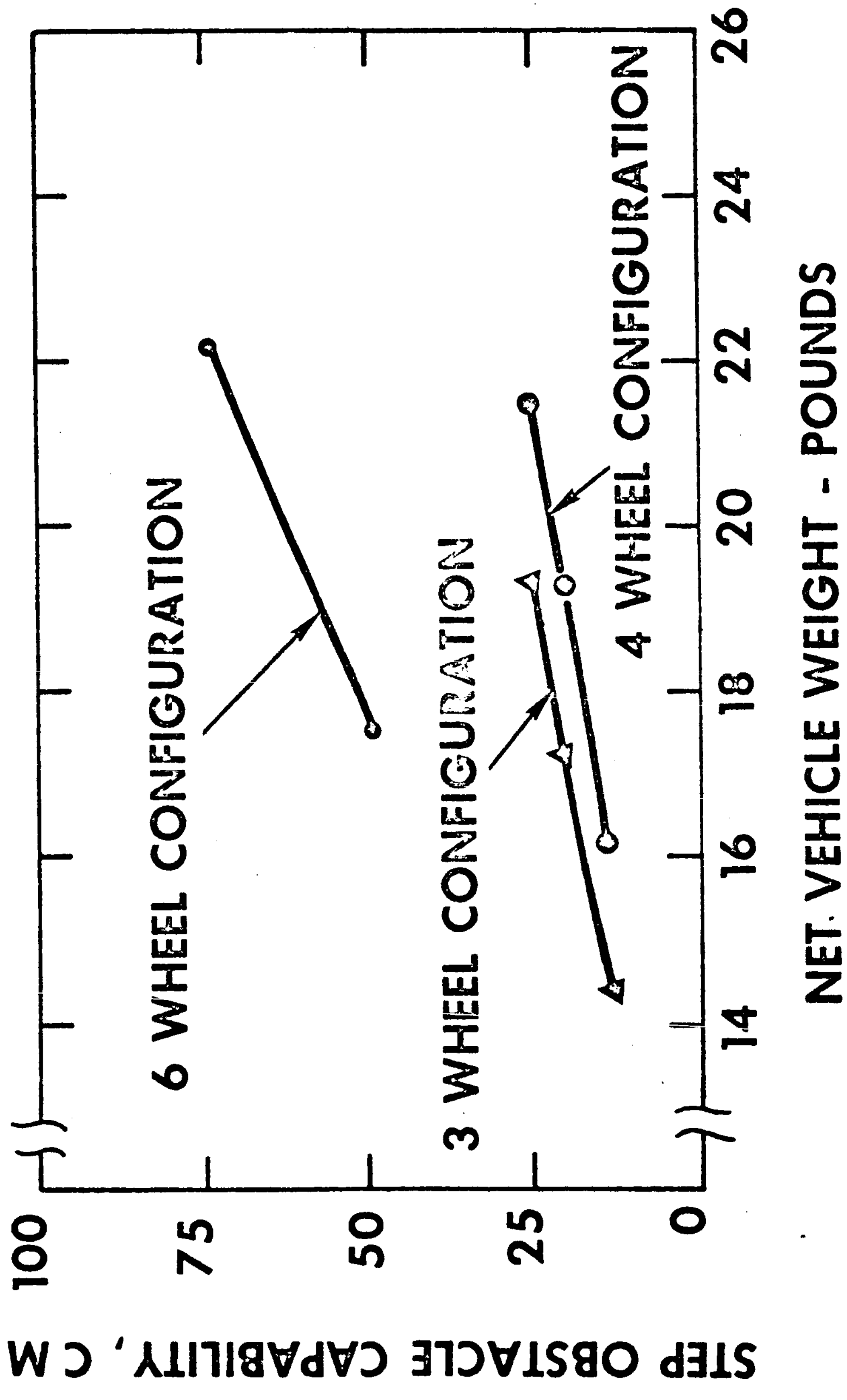

Figure III.5-7. Rough Terrain Mobility vs Net Vehicle Weight

432

[redacted]

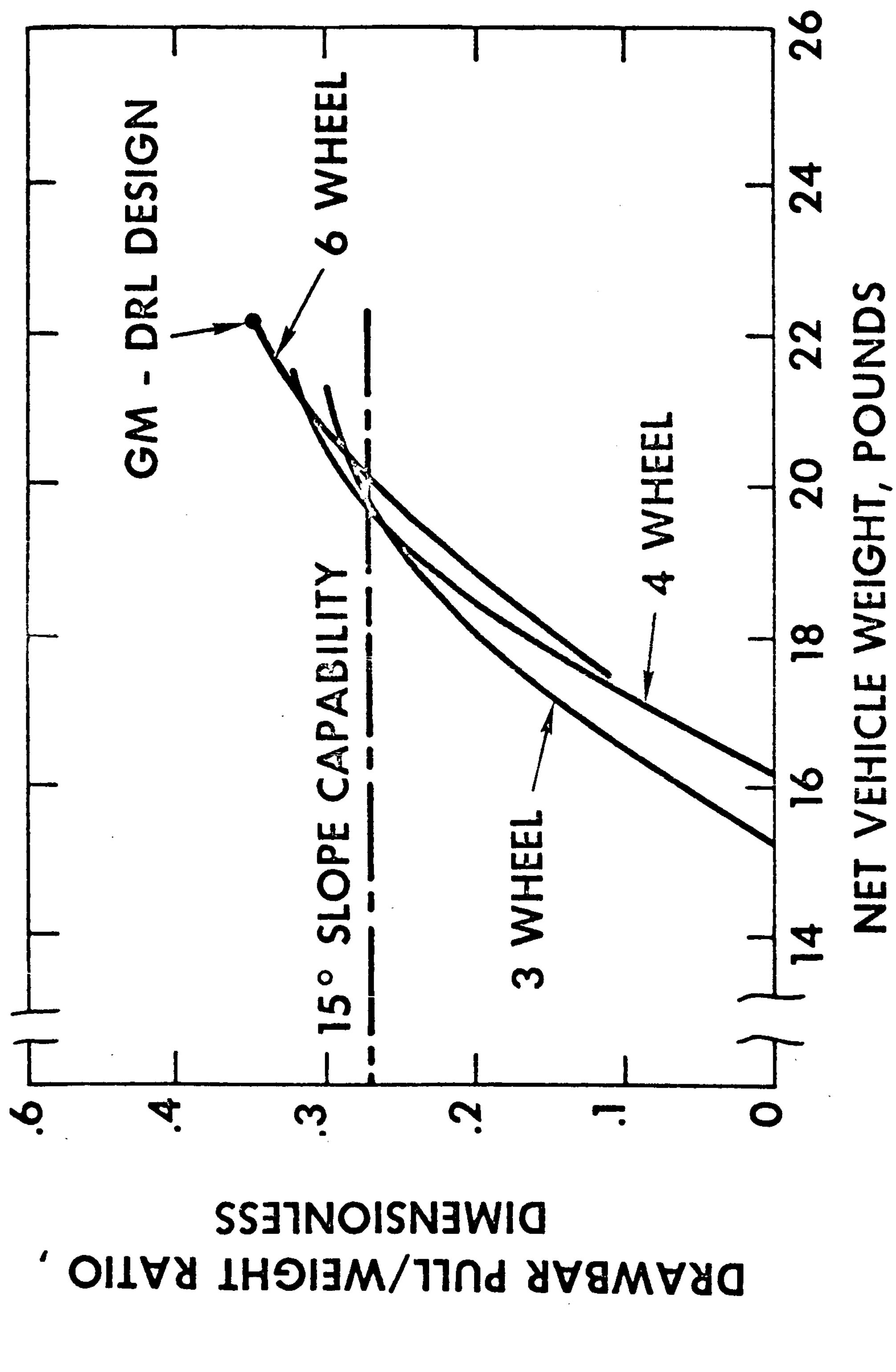

Figure III.5-8. Soft Terrain Performance vs Net Vehicle Weight

To compare all the configurations with respect to mobility for different net vehicle weights, the dimensionless weighted average of mobility, shown graphed in Figure III. 5-9, was computed. The drawer-pull/weight, obstacle performance, crevice-crossing capability, slope climbing capability, lateral stability, and maneuverability were graded for each vehicle on a scale from 0 to 100. These graded factors were weighted as shown in the slide: drawbar-pull/weight, 40 points; obstacle performance, 20 points; crevice crossing, 15 points; slope climbing, 10 points; lateral stability, 10 points; maneuverability, 5 points. This grading, which reflects lack of information about the lunar surface, does not systematically support the 6-wheeled vehicle. In fact, the soft-ground capability, which is weighted most heavily, is the characteristic in which the 3- and 4-wheeled vehicles are most competitive with the 6-wheeled vehicle.

Figure III. 5-9 shows that the 6-wheeled vehicles are preferred above 17.6 pounds, and the 3-wheeled vehicles below 17.6 pounds. The range in which the 3-wheeled vehicles are preferred is only 3.4 pounds.

the limiting obstacle height is found to be

$$\frac{h}{r} = 1 - \frac{1 - 2\mu^2}{\sqrt{1 + 5\mu^2 + 4\mu^4}} \qquad \text{for} \quad \mu^2 \leq \frac{1}{2} \qquad \text{(III. 1-47)}$$

It is interesting to note that below values of $\mu = \sqrt{1/2}$, the obstacle performance of the EFV depends only upon the friction coefficient μ, and there is no difference in the performance of the EFV regardless of the stiffness parameters involved.

Condition $h > r$

Now a vehicle is considered when the obstacle height h is higher than the wheel radius r. In Fig. III. 1-46 a schematic sketch of such a condition is presented with the front wheel of the vehicle climbing the rigid vertical obstacle.

When the conditions of equilibrium are applied to the whole vehicle, we have for the horizontal forces

$$\mu (F_3 + F_2) = N \qquad \text{(III. 1-48)}$$

and for the vertical forces

$$3W = F_3 + F_2 + \mu N \qquad \text{(III. 1-49)}$$

In this case the performance equations cannot be obtained from the principles of statics alone, and it is thus necessary to consider the stiffness of the elastic frame as a parameter. As illustrated in Figure III. 1-47, the elastic frame may be regarded as a simple beam with a concentrated load and a moment at a distance l from the support. For small deflections

Duplicate

88